

**Investigation into the viability of silver-*N*-heterocyclic carbenes as a  
class of chemotherapeutic agents**

Heba Abdulla Mohamed Abuelmaaty Abdelgawad

Submitted in accordance with the requirements for the degree of  
Doctor of Philosophy

The University of Leeds

School of Chemistry

September, 2016

The candidate confirms that the work submitted is her own, except where work which has formed part of jointly-authored publications has been included. The candidate confirms that appropriate credit has been given within the thesis where reference has been made to the work of others.

Jointly-authored publication:

“Silver-*N*-Heterocyclic carbene complexes as promising anticancer compounds”, Mohamed, H. A.; Willans, C. E. In *Organometallic Chemistry*; Royal Society of Chemistry: Specialist Periodical Reports, **2014**; Vol. 39, p 26.

“Synthesis and anticancer activity of silver(I)-*N*-heterocyclic carbene complexes derived from the natural xanthine products caffeine, theophylline and theobromine”, Mohamed, H. A.; Lake, B. R. M.; Laing, T.; Phillips, R. M.; Willans, C. E. *Dalton transactions*, **2015**, *44*, 7563.

Jointly-authored *manuscript in preparation*:

“Synthesis and anticancer activity of silver(I)-*N*-heterocyclic carbene complexes derived from clotrimazole”, Mohamed, H.A.; Shepherd, S.; Mohamadi S.; Blundell, H.A.; Das, M.; Pask, C.M.; Lake, B.R.M.; Nelson A.; Phillips, R.M.; Willans, C.E. *Manuscript in preparation*.

This copy has been supplied on the understanding that it is copyright material and that no quotation from the thesis may be published without proper acknowledgement.

The right of Heba Abdulla Mohamed Abuelmaaty Abdelgawad to be identified as Author of this work has been asserted by her in accordance with the Copyright, Designs and Patents Act 1988.

© 2016 The University of Leeds and Heba Abdulla Mohamed Abuelmaaty Abdelgawad

## Acknowledgements

I would like to start by thanking Dr Charlotte Willans for giving me the opportunity to take up this PhD project which I have utterly enjoyed. Her tremendous supervision and support smoothed the way for a positive experience, in which I have learned a lot in a few years.

I would like to thank Ms. Tanya Marinko-Covell for running my elemental samples, and Mr. Simon Barrett for always keeping the NMR machines up and running, and for granting me access to quickly run my light-sensitive samples. I would also like to thank Mr. Algy Kazlauciusas for running my SEM samples and patiently working with me to get decent results.

I am very grateful to all our collaborators who helped shape my project, starting with Professor Roger Philips and his student Samantha Shepherd for doing the cell line testing. I would like to continue to thank Sam for always being so kind and positive, making sure I got my results when I needed them regardless of the amount, and for training me on MTT assays. I would like to thank Dr. Paul Thornton and his student Mthulisi Mike Khuphe for guiding me with the polymer project, providing some polymers and showing me how to make them, which allowed me to make some my own. I am also thankful to have collaborated with Prof. Andrew Nelson and Shezi, for using their biosensing setup led to innovative results.

Special thanks has to go to Dr. Ben Lake (a.k.a. Benson) for showing me the ropes, for being the funniest after a few pints, and fun to be around in general. I also want to thank the current Willans group, Mike and Jordan, who made the lab and office a great place to be, and whom I have enjoyed the bulk of my PhD with, normally having fun playing games, on occasional nights out and on conferences (and the unforgettable leamington spa). Many thanks to Bank, for being the best lab buddy and for being cool with everything, to Johnny, for being the most genuine person, a sincere friend, and the best neighbour, and to the lovely Frances (Francois), whom I wish had started in our group earlier so we could've spent more time!

More thanks goes to the Hardie group, especially Flo for always being an amazing friend, for being so supportive, someone I know I can always count on and who's got my back (and much much more!). I also want to thank Sam O (stay positive Sam, there is light at the end of the tunnel), Vikki and Hayder. I must also thank Chris Pask for countless things really, one of which is not pointing out how many times I asked the same question on different occasions.

I would like to dedicate the rest of my acknowledgements to the beautiful people of 1.25, moving to your office was a blessing in disguise. I have to start with Laura, whom I am grateful to have spent the last 6 months (and best 6 months) of my PhD with, you really got me through them, by being hilarious (shisha pipes and all), and by listening to my whining, supporting me and constantly making me laugh . Love you habibty. Special thanks goes to Kay, for brightening up each day with her cheerfulness, enthusiasm and positivity, and also being a genuine friend all at the same time, and to Pablito, first and foremost for being Pabulous (obviously) and for adding the spice (and everything nice) that we needed to our days. To Flo, Laura, Kay and Pablo, you are habayby!

I also want to thank Matt, mainly for being cool, and for all the discussions about many random things (some of which were inspired by Pablo), Sam G, for our deep discussions which mostly revolve around Game of Thrones, Raf, our office boss and the voice of reason, Cecilia, the coolest mum, Izar (for being so Spanish) and Iurii.

I would love to thank my friends and family back home, for supporting me and listening to all my whining over the past years and never failing to reassure me. Finally, the biggest thank you goes to my parents, for their unconditional love and support, I love you and couldn't have done this without you.

## Abstract

This thesis details the synthesis of various libraries of silver(I)-*N*-heterocyclic carbenes (Ag(I)-NHCs) that are derived from natural and/or biologically relevant non-toxic precursors. The complexes have been evaluated as potential classes of chemotherapeutic agents. Furthermore, the use of polymers for encapsulating the Ag(I)-NHC complexes was investigated for drug-delivery, and a unique biological membrane has been used to examine the interaction of the complexes with a membrane monolayer.

Ag(I)-NHC complexes derived from the xanthine precursors caffeine, theophylline and theobromine were evaluated for anticancer activity against eight cancerous cell lines, revealing IC<sub>50</sub> values in the micromolar range. Hydrophobicity measurements revealed that a fine balance of steric bulk around the Ag-carbene bond and water solubility of the complex is required for the antiproliferative activity. Complexes derived from the antifungal compound clotrimazole were prepared. Various trends are discussed which relate cytotoxicity to hydrophobicity, N-substitution on the carbene ligand, counteranions, and substitution on the phenyl ring of clotrimazole. Selectivity ratios for these complexes were calculated which revealed that complexes with N-hydroxyethyl substituents on the ligand, which exhibit IC<sub>50</sub> values similar to those obtained for cisplatin, had excellent selectivity. Water-soluble complexes bearing alcohol or carboxylic acid N-substituents on the ligand were prepared from biologically relevant precursors. Hydrophobicity measurements and *in vitro* cytotoxicity studies revealed similar hydrophobicity-cytotoxicity trends to those obtained for the clotrimazole-derived complexes. Overall, the results indicate that intermediate lipophilicity results in high antiproliferative activity.

Encapsulation of the Ag(I)-NHC complexes inside polymers *via* different routes was investigated using non-toxic polyethylene glycol (PEG)-based polymers. Dynamic light scattering (DLS) and scanning electron microscopy (SEM) studies suggested successful encapsulation and/or coordination of the complexes with the particles. In some cases, it was found that the cytotoxicity of the complexes increased upon encapsulation with a polymer. Various Ag(I)-NHCs were screened using a unique biological sensor that detects the interaction of the complexes with a membrane monolayer. The results gave insight into the possible mechanism of action of the complexes through their ability to interact with biological membranes. Further development of this technique may provide a valuable pre-screen for drug molecules, prior to more costly and time-consuming cell work.

## Table of Contents

|  |      |
|--|------|
| <b>Acknowledgments</b> .....   | iii  |
| <b>Abstract</b> .....  | v    |
| <b>Table of Contents</b> .....   | vi   |
| <b>List of Figures</b> .....   | xv   |
| <b>List of Schemes</b> .....   | xxii |
| <b>List of Tables</b> .....  | xxiv |
| <b>List of Abbreviations</b> .....   | xxvi |
| <b>Chapter 1</b> .....   | 1    |
| <i>Introduction</i> .....  | 1    |
| <b>1.1 Overview</b> .....  | 1    |
| <b>1.2 Carbenes</b> .....  | 1    |
| <b>1.3 Metal-carbene bond</b> .....  | 2    |
| <b>1.3.1 Fischer carbenes</b> .....  | 2    |
| <b>1.3.2 Schrock carbenes</b> .....  | 3    |
| <b>1.4 N-Heterocyclic carbenes</b> .....                                     | 3    |
| <b>1.5 Metal-NHCs</b> .....  | 4    |
| <b>1.6 Metal-NHCs as anticancer agents</b> .....                             | 5    |
| <b>1.6.1 Gold-NHCs as anticancer agents</b> .....                            | 6    |
| <b>1.6.2 Platinum-NHCs as anticancer agents</b> .....                        | 8    |
| <b>1.6.3 Palladium, ruthenium and copper-NHCs as anticancer agents</b> ..... | 10   |
| <b>1.7 Silver-NHCs</b> .....   | 12   |
| <b>1.7.1 Preparation of silver(I)-NHCs</b> .....                             | 12   |
| <b>1.7.2 History of silver in medicine</b> .....                             | 15   |
| <b>1.7.3 Silver(I)-NHCs as antibacterial agents</b> .....                    | 16   |
| <b>1.8 Silver(I)-NHCs as anticancer agents</b> .....                         | 18   |
| <b>1.9 Project aims</b> .....  | 25   |
| <b>1.10 References</b> .....   | 26   |

|  |    |
|--|----|
| <b>Chapter 2</b> .....   | 33 |
| <i>Synthesis and anticancer activity of silver(I)-N-heterocyclic carbene complexes derived from the natural xanthine products caffeine, theophylline and theobromine</i> ..... | 33 |
| 2.1 Introduction.....  | 33 |
| 2.2 Ligand synthesis.....  | 34 |
| 2.2.1 Imidazolium salts prepared from caffeine.....  | 35 |
| 2.2.2 Imidazolium salts prepared from theophylline.....  | 38 |
| 2.2.3 Imidazolium salts prepared from theobromine.....   | 45 |
| 2.3 Silver-(I) NHC complexes.....  | 46 |
| 2.4 Hydrophobicity measurements.....   | 51 |
| 2.5 Anticancer testing.....  | 54 |
| 2.6 Conclusions.....   | 56 |
| 2.7 References.....  | 57 |
| <b>Chapter 3</b> .....   | 58 |
| <i>Copper- and ruthenium-N-heterocyclic carbene complexes derived from the natural xanthine precursors caffeine and theophylline</i> .....                                     | 58 |
| 3.1 Introduction.....  | 58 |
| 3.2 Electrochemical synthesis.....   | 59 |
| 3.2.1 Electrochemical synthesis of Cu(I)-NHC complexes.....  | 60 |
| 3.3 Synthesis of Ru(II)-NHC complexes.....   | 63 |
| 3.4 Anticancer Testing.....  | 66 |
| 3.5 Conclusions.....   | 67 |
| 3.6 References.....  | 68 |
| <b>Chapter 4</b> .....   | 70 |
| <i>Synthesis and anticancer activity of silver(I)-N-heterocyclic carbene complexes derived from clotrimazole</i> .....   | 70 |
| 4.1 Introduction.....  | 70 |
| 4.2 Ligand synthesis.....  | 72 |
| 4.2.1 Clotrimazole-derived imidazolium salts.....  | 72 |

|   |            |
|---|------------|
| 4.2.2 Imidazolium salts synthesised from 2-chlorotriyl chloride.....  | 75         |
| 4.2.3 Imidazolium salts synthesised from trityl chloride.....   | 78         |
| 4.3 Silver(I)-NHC complexes.....  | 80         |
| 4.4 Hydrophobicity measurements.....  | 84         |
| 4.5 Anticancer testing.....   | 86         |
| 4.6 Conclusions.....  | 90         |
| 4.7 References.....   | 91         |
| <b>Chapter 5</b> .....  | <b>92</b>  |
| <i>Synthesis and anticancer activity of water soluble hydroxyethyl-substituted and carboxylic acid-substituted silver(I)-N-heterocyclic carbene complexes</i> ..... | 92         |
| 5.1 Introduction.....   | 92         |
| 5.2 Ligand synthesis.....   | 93         |
| 5.2.1 N-Hydroxyethyl-substituted imidazolium salts.....   | 93         |
| 5.2.2 L-Alanine derived imidazolium salt.....   | 94         |
| 5.2.3 Bis-imidazolium salts.....  | 95         |
| 5.2.4 Carboxylic acid N-substituted imidazolium salts.....  | 98         |
| 5.3 Silver(I)-NHC complexes.....  | 99         |
| 5.3.1 Silver(I)-NHC complexes with N-hydroxyethyl substituents.....   | 99         |
| 5.3.2 Two-dimensional polymeric silver(I)-NHC complex.....  | 101        |
| 5.3.3 Silver(I)-NHC complexes from bis-imidazoliums.....  | 103        |
| 5.3.4 N-Carboxylic acid substituted silver(I)-NHCs.....   | 104        |
| 5.4 Hydrophobicity measurements.....  | 105        |
| 5.5 Anticancer Testing.....   | 107        |
| 5.6 Conclusions.....  | 111        |
| 5.7 References.....   | 112        |
| <b>Chapter 6</b> .....  | <b>113</b> |
| <i>Development of polymer-silver-NHC conjugates and micelles for drug delivery</i> .....  | 113        |
| 6.1 Introduction.....   | 113        |

|                  |  |     |
|------------------|--|-----|
| 6.2              | Conjugation of silver-NHCs to polymers.....  | 115 |
| 6.3              | Encapsulation of silver(I)-NHCs into polymers.....   | 122 |
| 6.3.1            | Confocal fluorescence microscopy.....  | 126 |
| 6.4              | Electrostatic attraction between silver(I)-NHCs and polymers.....                              | 128 |
| 6.4.1            | Synthesis of mPEG-poly(lysine) PM5.....  | 130 |
| 6.5              | Anticancer activity of drug-polymer micelles.....  | 135 |
| 6.6              | Conclusions.....   | 136 |
| 6.7              | Future work.....   | 138 |
| 6.8              | References.....  | 139 |
| <b>Chapter 7</b> | .....  | 140 |
|                  | <i>Electrochemical screening of silver(I)-NHC complexes on a unique biological sensor.....</i> | 140 |
| 7.1              | Introduction.....  | 140 |
| 7.2              | Organometallic complexes interactions with DOPC.....   | 143 |
| 7.2.1            | Interaction of Cisplatin with DOPC.....  | 144 |
| 7.2.2            | Interaction of xanthine-derived silver(I)-NHCs with DOPC.....                                  | 145 |
| 7.2.3            | Interaction of water-soluble silver(I)-NHCs with DOPC.....                                     | 146 |
| 7.2.4            | Interaction of clotrimazole-derived silver(I)-NHCs with DOPC.....                              | 148 |
| 7.3              | Limit of detection (LoD).....  | 151 |
| 7.4              | Interaction of imidazolium salts with DOPC.....  | 152 |
| 7.5              | Interaction of silver salts with DOPC.....   | 154 |
| 7.6              | Conclusion.....  | 155 |
| 7.7              | References.....  | 157 |
| <b>Chapter 8</b> | .....  | 158 |
|                  | <i>Experimental.....</i>   | 158 |
| 8.1              | Methods and Instrumentation.....   | 158 |
| 8.1.1            | General.....   | 158 |
| 8.1.2            | NMR spectroscopy.....  | 158 |
| 8.1.3            | Mass spectrometry.....   | 158 |

|  |     |
|--|-----|
| <b>8.1.4</b> Microanalysis.....                            | 158 |
| <b>8.1.5</b> X-Ray crystallography.....                    | 159 |
| <b>8.1.6</b> Hydrophobicity studies.....                   | 159 |
| <b>8.1.7</b> Cytotoxicity studies.....                     | 160 |
| <b>8.1.8</b> Infra-red spectroscopy.....                   | 161 |
| <b>8.1.9</b> Dynamic Light Scattering (DLS).....           | 161 |
| <b>8.1.10</b> Scanning Electron Microscopy (SEM).....      | 161 |
| <b>8.1.11</b> Confocal Fluorescence Microscopy.....        | 162 |
| <b>8.1.12</b> Biomembrane sensing device.....              | 162 |
| <b>8.1.13</b> RCV scans.....                               | 162 |
| <b>8.1.14</b> Limit of Detection (LoD).....                | 163 |
| <b>8.1.15</b> Electrochemical synthesis.....               | 163 |
| <b>8.2</b> Experimental details.....                       | 164 |
| <b>8.2.1</b> Preparation of P2.....                        | 164 |
| <b>8.2.2</b> Preparation of P3.....                        | 164 |
| <b>8.2.3</b> Preparation of P4.....                        | 165 |
| <b>8.2.4</b> Preparation of P5.....                        | 165 |
| <b>8.2.5</b> Preparation of P28A <sup>3</sup> .....        | 166 |
| <b>8.2.6</b> Preparation of P28B <sup>3</sup> .....        | 166 |
| <b>8.2.7</b> Preparation of P29-31 <sup>4</sup> .....      | 166 |
| <b>8.2.8</b> Preparation of P33 <sup>5</sup> .....         | 167 |
| <b>8.2.9</b> Preparation of P(PM5) <sup>6,7</sup> .....    | 167 |
| <b>8.2.10</b> Preparation of P(PM5.A-C) <sup>7</sup> ..... | 168 |
| <b>8.2.11</b> Preparation of PM5.A-C.....                  | 169 |
| <b>8.2.12</b> Preparation of L1 <sup>8</sup> .....         | 170 |
| <b>8.2.13</b> Preparation of L1.1 <sup>9</sup> .....       | 170 |
| <b>8.2.14</b> Preparation of L1.2 <sup>9</sup> .....       | 170 |
| <b>8.2.15</b> Preparation of L2.....                       | 171 |
| <b>8.2.16</b> Preparation of L3.....                       | 171 |

|               |  |     |
|---------------|--|-----|
| <b>8.2.17</b> | Preparation of L3.1.....                   | 172 |
| <b>8.2.18</b> | Preparation of L4.....                     | 172 |
| <b>8.2.19</b> | Preparation of L5 <sup>8</sup> .....       | 173 |
| <b>8.2.20</b> | Preparation of L6.....                     | 173 |
| <b>8.2.21</b> | Preparation of L7.....                     | 174 |
| <b>8.2.22</b> | Preparation of L8.....                     | 174 |
| <b>8.2.23</b> | Preparation of L9.....                     | 175 |
| <b>8.2.24</b> | Preparation of L10.....                    | 175 |
| <b>8.2.25</b> | Preparation of L11.....                    | 176 |
| <b>8.2.26</b> | Preparation of L12.....                    | 176 |
| <b>8.2.27</b> | Preparation of L13.....                    | 177 |
| <b>8.2.28</b> | Preparation of L14.....                    | 177 |
| <b>8.2.29</b> | Preparation of L15.....                    | 178 |
| <b>8.2.30</b> | Preparation of L16.....                    | 178 |
| <b>8.2.31</b> | Preparation of L17.....                    | 179 |
| <b>8.2.32</b> | Preparation of L18.....                    | 179 |
| <b>8.2.33</b> | Preparation of L19.....                    | 180 |
| <b>8.2.34</b> | Preparation of L20 <sup>10, 11</sup> ..... | 180 |
| <b>8.2.35</b> | Preparation of L21.....                    | 181 |
| <b>8.2.36</b> | Preparation of L22.....                    | 181 |
| <b>8.2.37</b> | Preparation of L23 <sup>10</sup> .....     | 182 |
| <b>8.2.38</b> | Preparation of L24 <sup>10</sup> .....     | 182 |
| <b>8.2.39</b> | Preparation of L25.....                    | 183 |
| <b>8.2.40</b> | Preparation of L26.....                    | 183 |
| <b>8.2.41</b> | Preparation of L27.....                    | 184 |
| <b>8.2.42</b> | Preparation of L28.....                    | 184 |
| <b>8.2.43</b> | Preparation of L29.....                    | 185 |
| <b>8.2.44</b> | Preparation of L30.....                    | 185 |
| <b>8.2.45</b> | Preparation of L31.....                    | 186 |

|  |     |
|--|-----|
| <b>8.2.46</b> Preparation of L32.....              | 186 |
| <b>8.2.47</b> Preparation of L33.....              | 187 |
| <b>8.2.48</b> Preparation of L34.....              | 187 |
| <b>8.2.49</b> Preparation of L35.....              | 188 |
| <b>8.2.50</b> Preparation of L36.....              | 188 |
| <b>8.2.51</b> Preparation of L37.....              | 189 |
| <b>8.2.52</b> Preparation of C1 <sup>8</sup> ..... | 189 |
| <b>8.2.53</b> Preparation of C1.Cu.....            | 190 |
| <b>8.2.54</b> Preparation of C1.Ru.....            | 190 |
| <b>8.2.55</b> Preparation of C2.....               | 191 |
| <b>8.2.56</b> Preparation of C2.Cu.....            | 191 |
| <b>8.2.57</b> Preparation of C2.Ru.....            | 192 |
| <b>8.2.58</b> Preparation of C3.....               | 192 |
| <b>8.2.59</b> Preparation of C3.Cu.....            | 193 |
| <b>8.2.60</b> Preparation of C3.Ru.....            | 193 |
| <b>8.2.61</b> Preparation of C4.....               | 194 |
| <b>8.2.62</b> Preparation of C5.....               | 194 |
| <b>8.2.63</b> Preparation of C6.....               | 195 |
| <b>8.2.64</b> Preparation of C7.....               | 195 |
| <b>8.2.65</b> Preparation of C8.....               | 196 |
| <b>8.2.66</b> Preparation of C9.....               | 196 |
| <b>8.2.67</b> Preparation of C10.....              | 197 |
| <b>8.2.68</b> Preparation of C11.....              | 197 |
| <b>8.2.69</b> Preparation of C12.....              | 198 |
| <b>8.2.70</b> Preparation of C13A.....             | 198 |
| <b>8.2.71</b> Preparation of C13B.....             | 199 |
| <b>8.2.72</b> Preparation of C14.....              | 199 |
| <b>8.2.73</b> Preparation of C15.....              | 200 |
| <b>8.2.74</b> Preparation of C16.....              | 200 |

|                |  |     |
|----------------|--|-----|
| <b>8.2.75</b>  | Preparation of C17.....                    | 201 |
| <b>8.2.76</b>  | Preparation of C18A.....                   | 201 |
| <b>8.2.77</b>  | Preparation of C18B.....                   | 202 |
| <b>8.2.78</b>  | Preparation of C19.....                    | 202 |
| <b>8.2.79</b>  | Preparation of C20 <sup>10, 11</sup> ..... | 203 |
| <b>8.2.80</b>  | Preparation of C21.....                    | 203 |
| <b>8.2.81</b>  | Preparation of C22.....                    | 204 |
| <b>8.2.82</b>  | Preparation of C23.....                    | 204 |
| <b>8.2.83</b>  | Preparation of C24 <sup>10</sup> .....     | 205 |
| <b>8.2.84</b>  | Preparation of C25.....                    | 205 |
| <b>8.2.85</b>  | Preparation of C26.....                    | 206 |
| <b>8.2.86</b>  | Preparation of C27.....                    | 206 |
| <b>8.2.87</b>  | Preparation of C28.....                    | 207 |
| <b>8.2.88</b>  | Preparation of C29.....                    | 207 |
| <b>8.2.89</b>  | Preparation of C30.....                    | 208 |
| <b>8.2.90</b>  | Preparation of C31.....                    | 208 |
| <b>8.2.91</b>  | Preparation of C32.....                    | 209 |
| <b>8.2.92</b>  | Preparation of C33.....                    | 210 |
| <b>8.2.93</b>  | Preparation of C34.....                    | 210 |
| <b>8.2.94</b>  | Preparation of C35.....                    | 211 |
| <b>8.2.95</b>  | Preparation of C36.....                    | 211 |
| <b>8.2.96</b>  | Preparation of C37.....                    | 212 |
| <b>8.2.97</b>  | Preparation of PDC1.....                   | 212 |
| <b>8.2.98</b>  | Preparation of PDC2.....                   | 213 |
| <b>8.2.99</b>  | Preparation of PDC3.....                   | 213 |
| <b>8.2.100</b> | Preparation of PDMa.....                   | 214 |
| <b>8.2.101</b> | Preparation of PDM4b.....                  | 214 |
| <b>8.2.102</b> | Preparation of PDM5.....                   | 215 |
| <b>8.3</b>     | References.....                            | 216 |

|   |     |
|---|-----|
| <b>Chapter 9</b> .....                            | 217 |
| <i>Summary, conclusions and future work</i> ..... | 217 |
| <b>9.1</b> References.....                        | 222 |
| <b>Appendix</b> .....                             | 223 |

## List of Figures

### Chapter 1

|  |    |
|--|----|
| <b>Figure 1.1:</b> Correlation between bond angle and orbitals in a carbene <sup>2</sup> .....   | 1  |
| <b>Figure 1.2:</b> Fischer carbene metal-carbon bond <sup>9</sup> .....  | 3  |
| <b>Figure 1.3:</b> Schrock carbene metal-carbon bond <sup>9</sup> .....  | 3  |
| <b>Figure 1.4:</b> Electronic structures of carbenes highlighting singlet state of NHCs <sup>15</sup> .....  | 4  |
| <b>Figure 1.5:</b> Three orbital contributions in M-NHC bond, NHC→M $\sigma$ -donation, M→NHC $\pi^*$ -back donation and NHC→M $\pi$ -donation <sup>9</sup> .....  | 5  |
| <b>Figure 1.6:</b> Structures of cisplatin and auranofin.....  | 6  |
| <b>Figure 1.7:</b> Au-NHC complexes that display chemotherapeutic properties <sup>56, 68-72</sup> .....  | 7  |
| <b>Figure 1.8:</b> Pt(II)-NHC complexes that display chemotherapeutic properties <sup>41, 73, 74</sup> .....   | 8  |
| <b>Figure 1.9:</b> Mechanisms of action of Au-NHCs and Pt-NHCs that lead to apoptosis. <sup>39</sup> Au-NHCs (yellow circles) through mitochondrial accumulation (green route), and Pt-NHCs (white circles) through DNA binding (blue route).... | 9  |
| <b>Figure 1.10:</b> Pd(II)- <sup>75, 76</sup> Ru(II, III)- <sup>57, 58, 60, 61, 77, 78</sup> and Cu(I)-NHC <sup>79, 80</sup> complexes that exhibit cytotoxic behaviour.....   | 11 |
| <b>Figure 1.11:</b> NHCs that have been coordinated to silver <sup>81-88</sup> .....   | 12 |
| <b>Figure 1.12:</b> Structure of silver sulfadiazine.....  | 15 |
| <b>Figure 1.13:</b> Antibacterial pyridine-linked pincer Ag(I)-NHC complexes ( <b>Ag1</b> , <b>Ag2</b> ), <sup>139</sup> and antimicrobial Ag(I)-NHC that has been encapsulated in nanoparticles( <b>Ag3</b> ) <sup>140</sup> .....              | 16 |
| <b>Figure 1.14:</b> Ag(I)-NHC acetate complexes <sup>145, 146, 150</sup> and halide-containing Ag(I)-NHC <sup>152</sup> complexes that display antibacterial properties.....   | 17 |
| <b>Figure 1.15:</b> Ag(I)-NHC complex <b>Ag12</b> reported to inhibit thioredoxin reductase <sup>158</sup> .....   | 18 |
| <b>Figure 1.16:</b> Ag(I)-NHC anticancer complexes with different xylyl spacers <b>Ag13-Ag16</b> <sup>153</sup> .....  | 19 |

**Figure 1.17:** Ag(I)-NHCs with reported anticancer activity against lung cancer cell line H460<sup>154</sup> and breast cancer cell line MCF-7<sup>79</sup> **Error! Bookmark not defined.**

**Figure 1.18:** Ag(I)-NHC acetate,<sup>160</sup> and Ag(I)-bis(NHC) complexes<sup>155</sup> with anticancer properties.....21

**Figure 1.19:** Ag(I)-NHC complexes with antiproliferative properties<sup>153-156, 158-160</sup> .....22

**Figure 1.20:** Ag(I)-NHC acetate complexes, symmetrically and unsymmetrically benzyl- or 4 cyanobenzyl-substituted bromo complexes and benzimidazole-derived Ag(I)-NHCs that exhibit anticancer activity<sup>157</sup> .....23

**Figure 1.21:** Ag(I)-NHC complexes evaluated for their anticancer activity<sup>159</sup> ...24

## Chapter 2

**Figure 2.1:** Metabolism of caffeine with its reported percentages of metabolites<sup>7</sup> .....33

**Figure 2.2:** Overlay of the <sup>1</sup>H-NMR spectra (300 MHz, DMSO-d<sub>6</sub>) of caffeine (top) and its methylated imidazolium iodide (bottom).....36

**Figure 2.3:** <sup>1</sup>H NMR spectra (300 MHz, DMSO-d<sub>6</sub>) of theophylline (top), **P2** (middle) and **L2** (bottom).....40

**Figure 2.4:** Molecular structure of **L3.1**. The molecular structure on the right depicts the π-π stacking interactions between the xanthine ring and the benzene ring of the tosylate. Ellipsoids are drawn at 50% probability and H atoms are omitted for clarity .....41

**Figure 2.5:** Molecular structures of **L2** and **L3**. Ellipsoids are drawn at 50% probability level and H atoms are omitted for clarity.....42

**Figure 2.6:** Molecular structure imidazolium salt **L4**. Ellipsoids are drawn at 50% probability level. Water molecules and H atoms have been omitted for clarity..44

**Figure 2.7:** <sup>1</sup>H NMR spectrum (300MHZ, DMSO-d<sub>6</sub>) of **L5**.....45

**Figure 2.8:** <sup>1</sup>H-NMR spectra (300MHZ, DMSO- d<sub>6</sub>) of Ag(I)-NHC complex **C1** (bottom) and imidazolium salt L1 (top).....46

**Figure 2.9:** Molecular structure of Ag(I)-NHC complex **C1**. Ellipsoids are shown at 50% probability and H atoms (except those on H<sub>2</sub>O) are omitted for clarity...47

|   |    |
|---|----|
| <b>Figure 2.10:</b> Molecular structure of <b>C2</b> . H atoms have been omitted (except for H <sub>2</sub> O) for clarity and ellipsoids are shown at 50% probability.....   | 49 |
| <b>Figure 2.11:</b> Molecular structures of novel xanthine-derived neutral Ag(I)-NHC acetate complexes <b>C3</b> and <b>C4</b> . H atoms have been omitted for clarity and ellipsoids are shown at 50% probability..... | 49 |
| <b>Figure 2.12:</b> <sup>1</sup> H-NMR spectra (300MHz, D <sub>2</sub> O) of <b>C5</b> and DMSO in 1:1 ratio. 1) 0 hours, 2) 4 hours, 3) 7 hours, 4) 12 hours, 5) 24 hours, 6) 48 hours, 7) 72 hours.....               | 50 |
| <b>Figure 2.13:</b> UV/vis spectroscopy measurements of samples with concentration 5, 10, 20, 40 and 60 μM.....   | 52 |
| <b>Figure 2.14:</b> Differences in absorbances of shaken and unshaken samples...  | 52 |
| <b>Figure 2.15:</b> Log <i>P</i> values for Ag(I)-NHC complexes <b>C1-C5</b> .....  | 53 |
| <b>Figure 2.16:</b> IC <sub>50</sub> (μM) values of Ag(I)-NHC complexes <b>C1-C5</b> and cisplatin against eight cancerous cell lines.....  | 55 |

### Chapter 3

|  |    |
|--|----|
| <b>Figure 3.1:</b> Cu(I)-NHC complexes that exhibit anticancer activities <sup>19</sup> .....  | 58 |
| <b>Figure 3.2:</b> Ru(II)-NHC complexes that exhibit anticancer activities <sup>20</sup> .....   | 58 |
| <b>Figure 3.3:</b> Faraday's law - calculation of theoretical reaction time.....   | 59 |
| <b>Figure 3.4:</b> <sup>1</sup> H-NMR (300MHz, DMSO- d <sub>6</sub> ) of (1). the attempted electrochemical synthesis of Ag(NHC)I (unsuccessful) and (2). the successful electrochemical synthesis of <b>C1.Cu</b> (Cu(NHC)I).....   | 61 |
| <b>Figure 3.5:</b> Molecular structure <b>C1.Cu</b> . H atoms have been omitted for clarity and ellipsoids are shown at 50% probability.....   | 61 |
| <b>Figure 3.6:</b> Synthesis of Ru(II)-NHC complexes.....  | 63 |
| <b>Figure 3.7:</b> <sup>1</sup> H-NMR spectra (300MHz, CDCl <sub>3</sub> ) of <b>C1.Ru</b> , <b>C2.Ru</b> and <b>C3.Ru</b> ...   | 64 |
| <b>Figure 3.8:</b> Molecular structures of <b>A. C2.Ru</b> and <b>B. C3.Ru</b> and <b>C.</b> packing diagram of <b>C2.Ru</b> along the <i>b</i> axis. Ellipsoids are shown at 50% probability level and H-atoms (except those on C(6) in <b>C3.Ru</b> ) are omitted for clarity.....   | 65 |
| <b>Figure 3.9:</b> IC <sub>50</sub> (μM) values of Ag(I)-NHC complexes <b>C1.Ag</b> , <b>C2.Ag</b> and <b>C3.Ag</b> (MTT assay) <sup>26</sup> and their analogous Cu(I)-NHC <b>C1.Cu</b> , <b>C2.Cu</b> and <b>C3.Cu</b> and Ru(II)-NHC <b>C1.Ru</b> , <b>C2.Ru</b> and <b>C3.Ru</b> complexes (SRB assay) against three cancerous cell lines..... | 67 |

## Chapter 4

- Figure 4.1:** Molecular structure of clotrimazole, and its metabolites, 2-chlorobenzophenone **A** and (2-chlorophenyl)diphenylmethanol **B**<sup>1</sup>.....70
- Figure 4.2:** Clotrimazole-coordinated silver complex with potent antibacterial properties.....70
- Figure 4.3:** Cu<sup>2+</sup>, Co<sup>2+</sup>, Zn<sup>2+</sup> and Ni<sup>2+</sup> clotrimazole-coordination complexes that exhibit anticancer properties<sup>5</sup> and Mn<sup>+</sup> complex with antibacterial activity<sup>6</sup> ....70
- Figure 4.4:** Molecular structures of imidazolium salts **L6-L8**. Ellipsoids are drawn at 50% probability level and H atoms are omitted for clarity.....73
- Figure 4.5:** Anion- $\pi$  interactions observed in **L7** and **L8**.....74
- Figure 4.6:** Molecular structure of imidazolium chloride salts **L9, L10, L12** and **L13**. Ellipsoids are drawn at the 50% probability level and H atoms (except those on H<sub>2</sub>O) have been omitted for clarity.....76
- Figure 4.7:** **A.** anion- $\pi$  interactions observed in **L9, L10, L12** and **L13**, and **B.** packing diagrams of **L10** and **L13** along the *b* axes.....77
- Figure 4.8:** <sup>13</sup>C{<sup>1</sup>H} NMR spectra (75 MHz, CHCl<sub>3</sub>) of **L11** (top) and **L16** (bottom).....78
- Figure 4.9:** Molecular structure of **L18**. Ellipsoids are shown at 50% probability level and H atoms (except OH) are omitted for clarity.....79
- Figure 4.10:** Clotrimazole-derived imidazolium salts synthesised in this work.79
- Figure 4.11:** Structures of mono(NHC) and bis(NHC) complexes.....81
- Figure 4.12:** Molecular structures of **C7, C13B, C14, C15** and **C17**. Ellipsoids are shown at 50% probability for **C14** and **C15**, 40 % for **C17** and 35% for **C7** and **C13B**. H atoms are omitted for clarity.....82
- Figure 4.13:** Packing diagram of **C13B** along the *c* axis. Ellipsoids are shown at 35% probability and H atoms are omitted for clarity.....83
- Figure 4.14:** Structure-based hydrophobicity trends.....84
- Figure 4.15:** Bar chart of Log *P* values of **C6-C18** and cisplatin.....85

## Chapter 5

- Figure 5.1:** Water soluble Ag(I)-NHC complexes reported in the literature<sup>1,2,492</sup>
- Figure 5.2:** <sup>1</sup>H NMR spectrum (300 MHz, MeOD) of **L28**.....94

|   |     |
|---|-----|
| <b>Figure 5.3:</b> Illustration of glycine amino acid incorporated in <b>L29-L31</b> .....  | 95  |
| <b>Figure 5.4:</b> <sup>1</sup> H-NMR spectrum (300MHz, acetonitrile-d <sub>3</sub> ) of <b>L30</b> .....   | 96  |
| <b>Figure 5.5:</b> HRMS of <b>L30</b> .....   | 96  |
| <b>Figure 5.6:</b> Molecular structure of <b>L30</b> . Ellipsoids are shown at 50% probability and H atoms are omitted for clarity.....   | 97  |
| <b>Figure 5.7:</b> Packing diagram of <b>L30</b> along the <i>b</i> axis.....   | 97  |
| <b>Figure 5.8:</b> <sup>1</sup> H-NMR spectrum (300MHz, CDCl <sub>3</sub> ) of <b>L33</b> .....   | 98  |
| <b>Figure 5.9:</b> <sup>1</sup> H NMR spectra (300MHz, MeOD-d <sub>4</sub> ) of <b>L19</b> (top) and <b>C19</b> (bottom).....   | 100 |
| <b>Figure 5.10:</b> Molecular structure of <b>C28</b> . Ellipsoids are shown at 50% probability and H atoms are omitted for clarity.....  | 102 |
| <b>Figure 5.11:</b> HRMS for <b>C30</b> .....   | 103 |
| <b>Figure 5.12:</b> HRMS of <b>C33</b> .....  | 104 |
| <b>Figure 5.13:</b> Log <i>P</i> values of complexes <b>C19</b> , <b>C20</b> and <b>C22-C33</b> : N-hydroxyethyl substituted (blue), 2D-polymer (green), N-carboxylic acid / ester-substituted silver dimers (red) and N-carboxylic acid substituted silver monomers (purple))..... | 106 |
| <b>Figure 5.14:</b> IC <sub>50</sub> values of complexes <b>C19</b> , <b>C20</b> , and <b>C22-C33</b> and cisplatin against pancreatic adenocarcinoma cell line Panc 10.05.....   | 109 |
| <b>Figure 5.15:</b> IC <sub>50</sub> values of <b>C23</b> , <b>C27</b> and <b>C28</b> and cisplatin against Panc 10.05, Mia-PA-CA-2 and BE and ARPE-19.....   | 110 |

## Chapter 6

|  |     |
|--|-----|
| <b>Figure 6.1:</b> Structural models of polymer-drug conjugate systems ( <b>A-D</b> ) <sup>2</sup> and polymer-drug micelles ( <b>E</b> ) (Cpt = camptothecin, an anticancer drug) <sup>12</sup> ..... | 113 |
| <b>Figure 6.2:</b> Illustration of using PEG for drug conjugation <sup>4</sup> .....   | 114 |
| <b>Figure 6.3:</b> Illustration of EPR effect <sup>2</sup> .....   | 114 |
| <b>Figure 6.4:</b> <sup>1</sup> H NMR spectra (300MHz, CD <sub>3</sub> OD) of <b>PM1</b> (top) and <b>PDC1</b> (bottom).....   | 115 |
| <b>Figure 6.5:</b> Solid-state <sup>13</sup> C NMR spectra (12 kHz) of <b>PM1</b> (top) and <b>PDC1</b> (bottom).....  | 116 |

|   |     |
|---|-----|
| <b>Figure 6.6:</b> Illustration of drug, linker and polymer portions of <b>PDC1</b> and <b>PDC2</b> .....   | 116 |
| <b>Figure 6.7:</b> <sup>1</sup> H NMR spectra (300MHz, DMSO-d <sub>6</sub> ) of the Fischer esterification reaction to give <b>PM3-L20</b> .....  | 119 |
| <b>Figure 6.8:</b> <sup>1</sup> H NMR spectra (300MHz, DMSO-d <sub>6</sub> ) of the reaction of <b>PM3-L20</b> with Ag <sub>2</sub> O over 24 hours.....  | 119 |
| <b>Figure 6.9:</b> <sup>1</sup> H NMR spectra (300MHz, DMSO-d <sub>6</sub> ) of <b>PM3</b> (top), <b>C20</b> (middle) and <b>PDC3</b> (bottom).....   | 120 |
| <b>Figure 6.10:</b> IC <sub>50</sub> values of drug-polymer conjugates <b>PDC1-PDC3</b> and the corresponding Ag(I)-NHC <b>C20</b> and <b>C34</b> .....   | 121 |
| <b>Figure 6.11:</b> SEM image of particles formed from self-assembly of mPEG <sub>5000</sub> P(Phe) <b>PM4</b> in water (10µg/mL).....  | 122 |
| <b>Figure 6.12:</b> Illustration of the encapsulation of Ag(I)-NHC complex <b>C20</b> to give <b>PDM4a</b> .....  | 123 |
| <b>Figure 6.13:</b> SEM images of <b>PDM4a</b> <b>A.</b> individual particles, <b>B.</b> magnification of on a single particle, <b>C.</b> silver ion mapping of image <b>B.</b> .....   | 124 |
| <b>Figure 6.14:</b> SEM-EDX spectrum showing peaks corresponding to silver and chloride ions.....   | 125 |
| <b>Figure 6.15:</b> SEM image of a 1:1 AgOAc: <b>PM4</b> mixture in aqueous solution, showing crystallisation of AgOAc.....   | 125 |
| <b>Figure 6.16:</b> Fluorescent Ag(I)-NHC complexes.....  | 126 |
| <b>Figure 6.17:</b> Images of <b>PDM4b</b> under <b>A.</b> visible light <b>B.</b> fluorescence <b>C.</b> superimposition of images <b>A.</b> and <b>B.</b> .....   | 127 |
| <b>Figure 6.1:</b> Fluorescence emission spectrum of <b>C27</b> .....   | 127 |
| <b>Figure 6.19:</b> Ag(I)-NHC complexes, imidazolium salts and mPEG-polylysine <b>PM5</b> used in micelle formation through electrostatic attraction.....   | 128 |
| <b>Figure 6.20:</b> Illustration of polymer-drug micelle formation through electrostatic attraction of oppositely charged ions.....   | 129 |
| <b>Figure 6.21:</b> Three step synthesis of mPEG <sub>5000</sub> poly(lysine) <b>PM5</b> .....  | 130 |
| <b>Figure 6.22:</b> <sup>1</sup> H NMR spectra (300MHz) of CBZ-NCA (DMSO-d <sub>6</sub> ), mPEG <sub>5000</sub> poly(lysine)CBZ (CF <sub>3</sub> COOD) and mPEG <sub>5000</sub> poly(lysine) <b>PM5</b> (DMSO-d <sub>6</sub> )..... | 131 |
| <b>Figure 6.23:</b> SEM images of <b>PDM5.B.C33</b> .....   | 133 |

|   |     |
|---|-----|
| <b>Figure 6.24:</b> Illustration of <b>A.</b> a solution of <b>PM5</b> and Ag(I)-NHC complex <b>C30</b> , and <b>B.</b> micelles formed upon mixing the solutions, and their corresponding DLS measurement results..... | 134 |
| <b>Figure 6.25:</b> IC <sub>50</sub> values of PDMs versus complexes against Panc 10.05.....  | 135 |
| <b>Figure 6.26:</b> Illustration of nanoparticle engineering for tumour selectivity and toxicity <sup>28</sup> .....  | 138 |

## Chapter 7

|  |     |
|--|-----|
| <b>Figure 7.1:</b> Diagram of electrochemical screening device <sup>22</sup> .....   | 141 |
| <b>Figure 7.2:</b> Diagram of the wafer-like device <sup>19</sup> .....  | 141 |
| <b>Figure 7.3:</b> (a). Typical RCV scan of DOPC monolayer (b). Illustration of predicted phase transitions <sup>18</sup> .....          | 142 |
| <b>Figure 7.4:</b> Phase transitions of DOPC monolayer <sup>15</sup> .....   | 142 |
| <b>Figure 7.5:</b> Characteristic RCV peaks of DOPC at potential range -0.4 V to -1.2V.....  | 143 |
| <b>Figure 7.6:</b> RCV of cisplatin on DOPC.....   | 144 |
| <b>Figure 7.7:</b> Route of entrance of cisplatin into a cell by copper transporters <sup>24</sup> .....                                 | 144 |
| <b>Figure 7.8:</b> Interaction of <b>C5</b> with DOPC.....   | 145 |
| <b>Figure 7.9:</b> RCVs showing interactions of water-soluble Ag(I)-NHC complexes with DOPC <b>C24</b> , <b>C27</b> and <b>C33</b> ..... | 147 |
| <b>Figure 7.10:</b> Interaction of clotrimazole-derived complexes with DOPC.....   | 150 |
| <b>Figure 7.11:</b> Calibration curve for <b>C8</b> used to determine LoD.....   | 151 |
| <b>Figure 7.12:</b> Interaction of clotrimazole-derived imidazolium salts with DOPC.....   | 153 |
| <b>Figure 7.13:</b> Interactions of silver salts with DOPC.....  | 154 |

## Chapter 9

|  |     |
|--|-----|
| <b>Figure 9.2:</b> Summary of Ag(I)-NHC complexes investigated as chemotherapeutic agents..... | 219 |
| <b>Figure 9.3:</b> Xanthine-derived Cu(I)- & Ru(II)-NHCs showed no cytotoxicity.....           | 220 |
| <b>Figure 9.4:</b> Ag(I)-NHCs derived from antifungal agents for future work.....              | 222 |

## List of Schemes

### Chapter 1

|  |    |
|--|----|
| <b>Scheme 1.1:</b> Synthesis of the first free N-heterocyclic carbene (NHC) <sup>6</sup> .....   | 2  |
| <b>Scheme 1.2:</b> Synthesis of Ag(I)-NHC by reacting a free carbene with a silver salt <sup>81</sup> .....  | 12 |
| <b>Scheme 1.3:</b> Synthesis of Ag(I)-NHC complexes by reaction of imidazolium salts with basic silver reagents A. Ag <sub>2</sub> O, <sup>83</sup> B. AgOAc, <sup>75, 80</sup> and C. Ag <sub>2</sub> CO <sub>3</sub> <sup>94</sup> ..... | 13 |
| <b>Scheme 1.4:</b> Synthesis of Ag(I)-NHC by reacting imidazolium salt with a base in the presence of silver salt <sup>83</sup> .....  | 14 |
| <b>Scheme 1.5:</b> Transmetalation from Ag to A. Au and B. Pd <sup>114, 118, 123</sup> .....   | 14 |
| <b>Scheme 1.6:</b> Release of Ag <sup>+</sup> ions from nanoparticles under aerobic conditions <sup>138</sup> .....  | 15 |

### Chapter 2

|   |    |
|---|----|
| <b>Scheme 2.1:</b> Mesomeric effect of caffeine <sup>9</sup> .....  | 34 |
| <b>Scheme 2.2:</b> Mesomeric effects of xanthinium salts <sup>9</sup> .....   | 34 |
| <b>Scheme 2.3:</b> Alkylation of theophylline with benzyl bromide and butyl iodide...38   |    |
| <b>Scheme 2.4:</b> Synthesis of imidazolium salts <b>L2</b> and <b>L3</b> .....   | 39 |
| <b>Scheme 2.5:</b> Synthesis of phenyl substituted ligand precursor <b>P4</b> from theophylline using the Ullmann reaction..... | 43 |
| <b>Scheme 2.6:</b> Synthesis imidazolium salt <b>L4</b> .....   | 44 |
| <b>Scheme 2.7:</b> Hydroxylation of theobromine to <b>P5</b> and synthesis of <b>L5</b> <sup>10</sup> .....                     | 45 |
| <b>Scheme 2.8:</b> Synthesis of Ag(I)-NHC complex <b>C1</b> using AgOAc <sup>1</sup> .....                                      | 46 |
| <b>Scheme 2.9:</b> Synthesis of neutral Ag(I)-NHC acetate complexes <b>C1-C5</b> .....  | 48 |

### Chapter 3

|  |    |
|--|----|
| <b>Scheme 3.1:</b> Attempted electrochemical synthesis of a Ag(I)-NHC complex from <b>L1</b> ..... | 59 |
| <b>Scheme 3.2:</b> Electrochemical synthesis of Cu(I)-NHC complexes.....                           | 60 |
| <b>Scheme 3.3:</b> Copper catalysed arylation reaction.....  | 62 |

## Chapter 4

|  |     |
|--|-----|
| <b>Scheme 4.1:</b> Synthesis of imidazolium iodide salts <b>L6-L8</b> from clotrimazole...   | 72  |
| <b>Scheme 4.2:</b> Synthesis of imidazolium chloride salts <b>L9-L13</b> from 2-chlorotriptyl chloride.....  | 75  |
| <b>Scheme 4.3:</b> Synthesis of imidazolium chloride salts <b>L14-L18</b> from triptyl chloride.....   | 78  |
| <b>Scheme 4.4:</b> Synthesis of Ag(I)-NHC complexes <b>C6-C18</b> . *Elemental analysis reveals a mixture of Ag(NHC)X and [Ag(NHC) <sub>2</sub> ]X, where X = I or Cl..... | 80  |
| <b>Scheme 5.1:</b> Synthesis of imidazolium salts <b>L19-L27</b> .....   | 93  |
| <b>Scheme 5.2:</b> Synthesis of imidazolium salt <b>L28</b> from L-alanine.....  | 94  |
| <b>Scheme 5.3:</b> Attempted synthesis of bis-imidazolium salt from L-alanine <sup>7</sup> .....   | 95  |
| <b>Scheme 5.4:</b> Synthesis of bis-imidazolium salts <b>L29-L31</b> starting with <sup>1</sup> H-imidazole.....   | 95  |
| <b>Scheme 5.5:</b> Synthesis of dicarboxylic acid imidazolium salt <b>L32</b> .....  | 98  |
| <b>Scheme 5.6:</b> Synthesis of <b>L33</b> .....   | 98  |
| <b>Scheme 5.7:</b> Synthesis of water soluble Ag(I)-NHC complexes <b>C19-C27</b> .....   | 99  |
| <b>Scheme 5.8:</b> Synthesis of 2-dimensional Ag(I)-NHC polymer <b>C28</b> .....   | 101 |
| <b>Scheme 5.9:</b> Synthesis of Ag(I)-NHC complexes <b>C29-C31</b> .....   | 103 |
| <b>Scheme 5.10:</b> Synthesis of carboxylic acid N-substituted Ag(I)-NHC complexes <b>C32</b> and <b>C33</b> .....   | 104 |

## Chapter 6

|  |     |
|--|-----|
| <b>Scheme 6.1:</b> Synthesis of polymer-Ag(I)-NHC conjugates <b>PDC1</b> and <b>PDC2</b> .....   | 115 |
| <b>Scheme 6.2:</b> Fischer esterification of <b>PM3</b> and <b>L20</b> to form <b>PM3-L20</b> and reaction with Ag <sub>2</sub> O..... | 118 |
| <b>Scheme 6.3:</b> Synthesis of <b>PDC3</b> through a Steglich esterification reaction...  | 120 |

## List of Tables

### Chapter 1

- Table 1.1:** IC<sub>50</sub> values of complexes **Ag19-Ag23** against MCF-7 compared to cisplatin<sup>79</sup>.....20
- Table 1.2:** IC<sub>50</sub> values (μM) of five Ag(I)-NHC complexes against KB cells<sup>159</sup>...24

### Chapter 2

- Table 2.1:** Methylation of caffeine under different reaction conditions.....35
- Table 2.2:** Methylation of caffeine using different reagents to form imidazolium salts **L1**, **L1.1** and **L1.2**.....37
- Table 2.3:** Microwave reactions to synthesise imidazolium iodide **L2**.....39
- Table 2.4:** Selected bond lengths and angles for **L2**, **L3** and **L3.1** derived from theophylline .....42
- Table 2.5:** Selected bond distances, bond angles and torsion angles for Ag(I)-NHC complexes **C2-C4**.....49

### Chapter 3

- Table 3.1:** Reaction conditions: 1.2 mmol 3,5-dimethylphenol, 1.0 mmol 4-iodoanisole, 2.0 mmol Cs<sub>2</sub>CO<sub>3</sub>, 0.1 mmol catalyst, 5 mL MeCN, 90°C, 24h....62
- Table 3.2:** IC<sub>50</sub> values of Cu(I)-NHC complexes and Ru(II)-NHC complexes against ten cancerous cell lines.....66

### Chapter 4

- Table 4.1:** Reaction conditions tested for the synthesis of methyl substituted imidazolium salt **L6**.....72
- Table 4.2:** Selected bond lengths and angles for imidazolium salts **L6-L8**.....74
- Table 4.3:** Selected bond lengths and angles for **L9**, **L10**, **L12** and **L13**.....76

## Chapter 5

|   |     |
|---|-----|
| <b>Table 5.1:</b> Log <i>P</i> values of <b>C22</b> , <b>C23</b> and <b>C25-C36</b> , and cisplatin.....  | 105 |
| <b>Table 5.2:</b> IC <sub>50</sub> values for complexes <b>C19</b> , <b>C20</b> , <b>C22-C33</b> and cisplatin on Panc 10.05.....   | 108 |
| <b>Table 5.3:</b> Responses of Panc 10.05, Mia-PA-CA-2 and BE cancerous cell lines and ARPE-19 non-cancerous cell line to Ag(I)-NHC complexes <b>C23</b> , <b>C27</b> , <b>C28</b> and <b>C33</b> . Values presented are IC <sub>50</sub> (μM) ±SD for three independent experiments..... | 110 |

## Chapter 6

|  |     |
|--|-----|
| <b>Table 6.1:</b> Micelle formation <i>via</i> electrostatic attraction (reactions referred to as polymer-drug micelles <i>e.g.</i> <b>PDM5.A.L30</b> )..... | 132 |
| <b>Table 6.2:</b> Cytotoxicity data on PDMs versus complexes.....  | 135 |

## Chapter 7

|   |     |
|---|-----|
| <b>Table 7.1:</b> Summary of potential routes for cell entry for water-soluble Ag(I)-NHC complexes..... | 146 |
| <b>Table 7.2:</b> Limit of detection (LoD) values.....  | 151 |
| <b>Table 7.3:</b> Summary of DOPC recovery.....   | 154 |
| <b>Table 7.4:</b> Conclusions from membrane biosensing technique.....                                   | 156 |

## List of Abbreviations

|                               |   |
|-------------------------------|---|
| Å                             | Angstrom, $1 \times 10^{-10}$ m                     |
| AIF                           | Apoptosis inducing factor                           |
| arom                          | Protons attached to an aromatic ring                |
| C                             | Complex   |
| CBZ                           | Carbobenzyloxy                                      |
| $^{13}\text{C}\{^1\text{H}\}$ | Proton-decoupled carbon (NMR)                       |
| Cpt                           | Camptothecin  |
| Ctr1                          | Copper transporter                                  |
| d                             | Doublet resonance                                   |
| DCC                           | N, N'- Dicyclohexylcarbodiimide                     |
| dept                          | Distortionless enhancement by polarisation transfer |
| DLS                           | Dynamic light scattering                            |
| DMAP                          | 4-Dimethylaminopyridine                             |
| DMF                           | Dimethylformamide                                   |
| DMSO                          | Dimethylsulfoxide                                   |
| DNA                           | Deoxyribonucleic acid                               |
| DOPC                          | Dioleoylphosphatidylcholine                         |
| EDX                           | Energy-dispersive X-ray spectroscopy                |
| EPR                           | Enhanced permeability and retention                 |
| ESI                           | Electrospray ionisation                             |
| <i>et al.</i>                 | <i>et alia</i> (and others)                         |
| FDA                           | Food and Drug Administration                        |
| GR                            | Glutathione reductase                               |
| HOMO                          | Highest occupied molecular orbital                  |
| HRMS                          | High resolution mass spectrometry                   |

|                       |  |
|-----------------------|--|
| IC <sub>50</sub>      | Inhibitory concentration 50%                       |
| <i>i</i> <sub>c</sub> | Capacitance current                                |
| <i>i.e.</i>           | <i>id est</i> (that is)                            |
| Hz                    | Hertz  |
| <i>J</i>              | NMR coupling constant                              |
| L                     | Ligand   |
| Log <i>P</i>          | Log partition-coefficient                          |
| LoD                   | Limit of detection                                 |
| LUMO                  | Lowest unoccupied molecular orbital                |
| m                     | Multiplet resonance                                |
| mA                    | Milliamps  |
| mes                   | Mesityl aromatic ring                              |
| MHz                   | Megahertz  |
| MMP                   | Mitochondrial membrane potential                   |
| mPEG                  | Methoxy-polyethylene glycol                        |
| MRSA                  | Methicillin-resistant <i>Staphylococcus aureus</i> |
| MS                    | Mass spectrometry                                  |
| MTT                   | Microculture tetrazolium assay                     |
| m/z                   | Mass to charge ratio                               |
| NAMI                  | New antitumour metastasis inhibitor                |
| NCA                   | N-Carboxyanhydride                                 |
| NHC                   | <i>N</i> -Heterocyclic carbene                     |
| NMR                   | Nuclear magnetic resonance                         |
| NP                    | Nanoparticle                                       |
| P                     | Precursor  |
| PDC                   | Polymer-drug conjugate                             |
| PDI                   | Polydispersity index                               |

|        |                                    |
|--------|------------------------------------|
| PDM    | Polymer-drug micelle               |
| PEG    | Polyethylene glycol                |
| PM     | Polymer                            |
| P(Phe) | Poly-phenylalanine                 |
| ppm    | Parts per million                  |
| Q      | Total charge, C or A s             |
| RCV    | Rapid cyclic voltammetry           |
| RT     | Room temperature                   |
| s      | Singlet resonance                  |
| SAR    | Structure-activity relationship    |
| SD     | Standard deviation                 |
| SEM    | Scanning electron microscopy       |
| sept   | Septet resonance                   |
| siRNA  | Small interfering Ribonucleic acid |
| SRB    | Sulforhodamine B assay             |
| t      | Triplet resonance                  |
| TFA    | Trifluoroacetic acid               |
| THF    | Tetrahydrofuran                    |
| TrxR   | Thioredoxin reductase              |

## Chapter 1 Introduction

### 1.1 Overview

This thesis is focussed on the synthesis and *in vitro* anticancer activity of silver(I)-*N* heterocyclic carbene (Ag(I)-NHC) complexes, the use of polymers for the encapsulation of these complexes with the purpose of targeted delivery to cancerous cells, and the use of a novel biosensing device to detect the potential effects of Ag(I)-NHCs on a biological membrane. This chapter introduces the field of NHCs, with a focus on Ag(I)-NHCs, discussing biological applications and reviewing reported anticancer properties.

### 1.2 Carbenes

Carbenes are uncharged compounds with a divalent carbon atom that has only six electrons in its valence shell.<sup>1</sup> Two of the electrons are uninvolved in bonding and can be assigned to two nonbonding orbitals. The carbon atom of a carbene can be either linear or bent, depending on the hybridisation at the carbenic centre.<sup>1, 2</sup> A linear geometry indicates an  $sp$ -hybridised carbene centre with two nonbonding degenerate orbitals ( $p_x$  and  $p_y$ ). The bent molecule breaks this degeneracy and the carbon atom adopts  $sp^2$ -type hybridisation, with the  $p_y$  orbital remaining almost unchanged (it is usually called  $p_\pi$ ), and the  $p_x$  orbital being stabilised since it acquires some  $s$  character (it is therefore called  $\sigma$ ). Most carbenes are bent and their frontier orbitals are called  $\sigma$  and  $p_\pi$ , whilst the linear geometry is a rare case (**Figure 1.1**).<sup>2</sup>

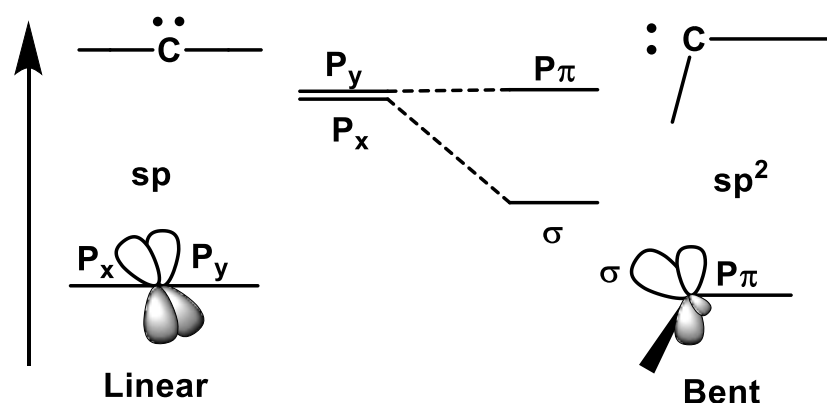
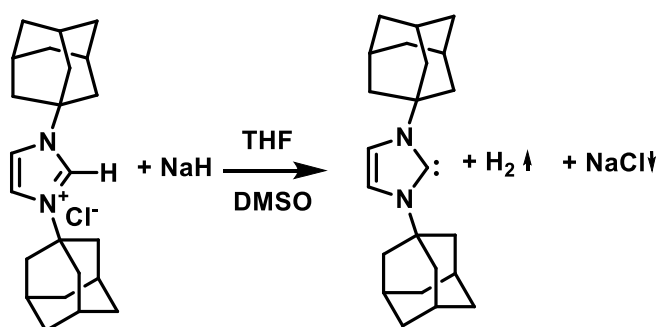


**Figure 1.1:** Correlation between bond angle and orbitals in a carbene<sup>2</sup>

Free carbenes are characteristically unstable due to their incomplete electron octet and coordinative unsaturation. Preparation of the first isolable carbene was reported by Bertrand and co-workers,<sup>3</sup> by stabilisation through interactions with neighbouring phosphorus and silicon atoms. Inspired by the structures of metal-carbene complexes by Öfele<sup>4</sup> and Wanzlick<sup>5</sup>, Arduengo<sup>6</sup> succeeded in isolating the first free NHC. 1,3-Di(adamantyl)imidazol-2-ylidene was isolated through the deprotonation of an imidazolium salt bearing bulky adamantyl N-substituents using NaH and catalytic amounts of the dimsyl anion (**Scheme 1.1**).<sup>6</sup>



**Scheme 1.1:** Synthesis of the first free N-heterocyclic carbene (NHC)<sup>6</sup>

### 1.3 Metal-carbene bond

Metal-carbenes are categorised into Fischer and Schrock carbenes. Fischer carbene complexes are compounds that have a heteroatom linked to the carbenic carbon, and are usually associated with a metal in a low oxidation state,  $\pi$ -acceptor ligands, and electrophilic character at the carbenic carbon. Schrock carbene complexes (also referred to as alkylidenes) are compounds with alkyl groups or hydrogen atoms adjacent to the carbene centre, and are usually associated with higher oxidation state metal atoms, a variety of ligands (usually free molecules that are not closed shell species), and nucleophilic character at the carbenic carbon.<sup>7</sup>

#### 1.3.1 Fischer carbenes

Fischer carbene complexes such as aminocarbenes and alkoxy-carbenes have a substantial energy gap between their singlet and triplet ground states and are therefore well-stabilised singlet carbenes.<sup>2</sup> These compounds form a metal carbon bond by mutually exchanging electrons (donor-acceptor interaction) from singlet closed shell orbitals found in both the carbene and the metal. The main interaction in this bond is the carbene-metal  $\sigma$ -donation (**Figure 1.2**). The

other interaction is the metal-carbene  $\pi$ -back donation, where the  $\pi$ -electrons are generally polarised toward the metal. This character is diminished by the stabilisation of the carbene through its donating  $\alpha$ -groups.<sup>8, 9</sup> The  $\pi$ -back donation from the metal in diaminocarbenes (including NHCs) is weak since the carbenic carbon is already stabilised by  $\pi$ -donation from its  $\alpha$ -amino-groups. Fischer carbene complexes are electrophilic at the metal-carbon bond and are therefore susceptible to nucleophilic attack at the carbene centre.<sup>10, 11</sup> The early synthesis of carbenes was first established by Skell in the 1950s, and they were introduced into inorganic and organometallic chemistry by Fischer and his students in 1964.<sup>12, 13</sup>

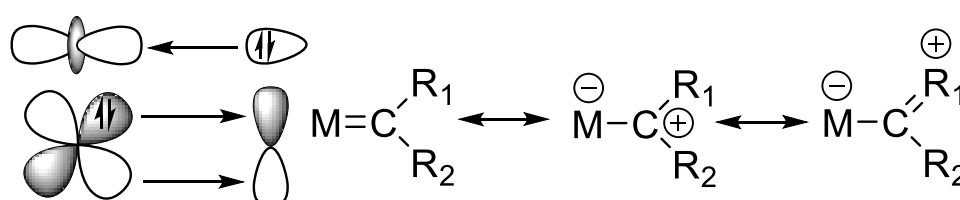


**Figure 1.2:** Fischer carbene metal-carbon bond<sup>9</sup>

### 1.3.2 Schrock carbenes

Schrock carbenes such as dialkylcarbenes or alkylidenes have a small gap between their singlet and triplet ground states and are therefore weakly stabilised carbenes. Their metal-carbene bond is formed through the interaction of triplet orbitals of both the carbene and metal (**Figure 1.3**). Their metal-carbon bond is viewed as a double bond as the  $\pi$ -electrons are equally distributed between the carbon and the metal. They are nucleophilic at the carbene centre which is susceptible to reaction with an electrophile.<sup>7, 9, 14</sup>

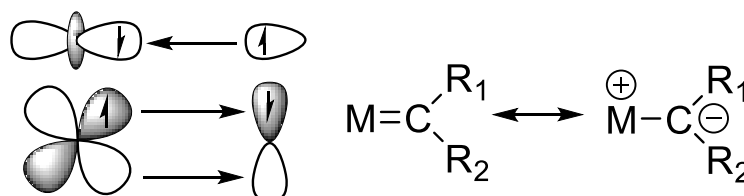


**Figure 1.3:** Schrock carbene metal-carbon bond<sup>9</sup>

## 1.4 N-Heterocyclic carbenes

NHCs are heterocycles with a bent carbene centre and at least one adjacent nitrogen atom.<sup>2, 9</sup> The  $\sigma$ -withdrawing effect (inductive) of the two  $\alpha$ -amino substituents stabilises the  $sp^2$ -hybridised  $\sigma$  orbital containing a lone pair of electrons. The  $\alpha$ -amino lone pairs are meanwhile donated into the vacant  $p$ -orbital (mesomeric effect), destabilising it. The electroneutrality at the carbene centre is maintained by this 'push-pull' effect and the singlet state is preserved (Figure 1.4).<sup>15</sup>

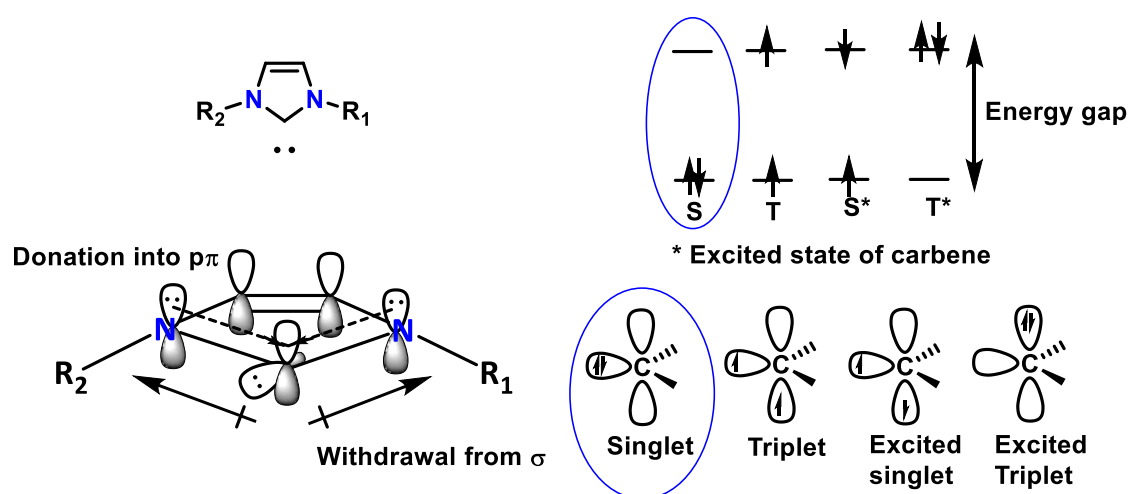


**Figure 1.4:** Electronic structures of carbenes highlighting singlet state of NHCs<sup>15</sup>

## 1.5 Metal-NHCs

Transition metals-NHCs are used as catalysts in cross coupling reactions,<sup>16-21</sup> olefin metathesis<sup>22, 23</sup> and hydrogenation reactions<sup>24</sup> among many other catalytic processes.<sup>1, 25, 26</sup> Metal-NHCs are also used as substrates for the development of organometallic materials<sup>27-29</sup> including polymers<sup>30</sup> and photoactive materials.<sup>31</sup> Medicinal applications of metal-NHCs include antibacterial and anticancer properties.<sup>32,33</sup>

Co-ordination of NHCs to transition metals is owed to their strong  $\sigma$ -donor ability. However,  $\sigma$ -donation is not the only orbital contribution in the metal-NHC bond, both  $d \rightarrow \pi^*$  (metal to NHC) back donation as well as  $\pi \rightarrow d$  (NHC to metal) donation are also present (**Figure 1.5**).<sup>9, 34, 35</sup> Since  $\sigma$ -donation is the major orbital contribution, the metal-NHC bond is depicted as a single rather than a double bond. NHCs are therefore strong  $\sigma$ -donors and weak  $\pi$ -acceptors, with coordination properties similar to those of phosphines to which they are usually compared to in the literature.<sup>36</sup>

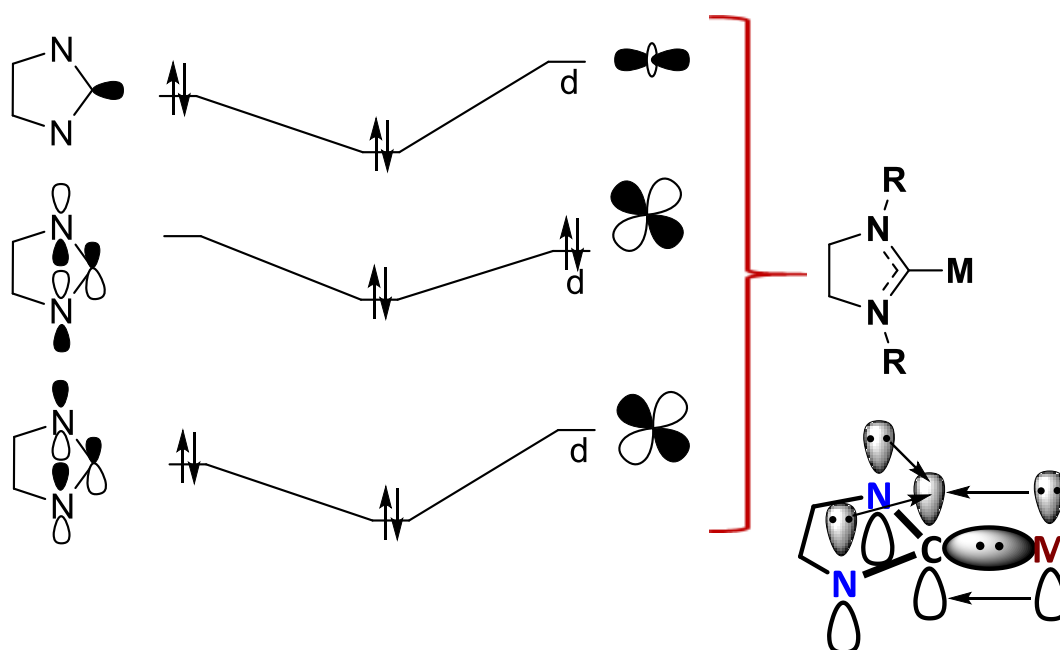


**Figure 1.5:** Three orbital contributions in M-NHC bond, NHC $\rightarrow$ M  $\sigma$ -donation, M $\rightarrow$ NHC  $\pi^*$ -back donation and NHC $\rightarrow$ M  $\pi$ -donation<sup>9</sup>

## 1.6 Metal-NHCs as anticancer agents

Since the discovery of cisplatin in 1965 (**Figure 1.6**),<sup>37</sup> metallo-based drugs have gained significant attention for the treatment of cancer. Auranofin, a Au-based anti-rheumatic drug, was recently reported effective against a cisplatin-resistant ovarian cancer cell line.<sup>38</sup> Metal-NHCs have shown potential as anticancer agents and are a fast growing field of research.<sup>39</sup> Although Pt-NHCs<sup>40-42</sup> and Au-NHCs<sup>43-54</sup> have been the main focus in this area, Ag-NHCs are rapidly emerging.<sup>55</sup> Ag-NHCs with anticancer properties possibly bind to the same biological targets as Au-NHCs, in particular Se-containing enzymes e.g. Thioredoxin reductase (TrxR).<sup>56</sup> Ru-NHCs,<sup>57-61</sup> Pd-NHCs,<sup>62-64</sup> and Cu-NHCs<sup>65</sup> have also been reported for their potential use as anticancer agents.

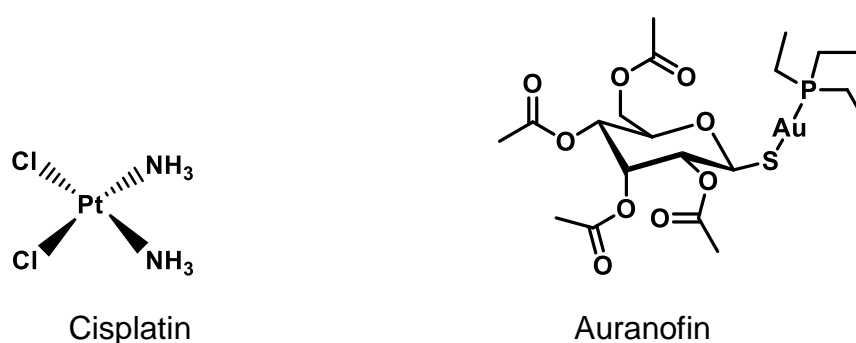


**Figure 1.6:** Structures of cisplatin and auranofin

### 1.6.1. Gold-NHCs as anticancer agents

Barnard *et al.* reported Au(I)-bis(NHC) complexes that induce Ca<sup>2+</sup> sensitive Mitochondrial Membrane Permeation (MMP) causing mitochondrial swelling and subsequent cell death.<sup>66</sup> Baker and co-workers reported simple cationic Au(I)-bis(NHC) (**Au1**, **Figure 1.7**) that also caused mitochondrial swelling, and correlated the antitumor activity to the lipophilicity (calculated as Log *P*) of the complexes.<sup>67</sup> Hickey *et al.* studied cationic Au(I)-bis(NHC) complexes with the same general structure as **Au1** that also target mitochondria by selectively binding to selenol-over thiol-containing proteins. This is reflected in one of the complexes which selectively inhibits 50% activity of TrxR (a selenoenzyme) at 5 μM concentration while showing no effect on glutathione reductase (GR, a thiol based enzyme).<sup>56</sup> Inhibition of TrxR leads to apoptosis of cancer cells, and as these complexes do not do not inhibit GR, normal cells are not affected.<sup>56</sup> Hovarth and co-workers suggested the selective cytotoxicity towards cancerous cells of Au(I)-NHC complex **Au2** is due to the incorporation of the ferrocene moiety.<sup>68</sup> Recently, Bertrand *et al.* reported caffeine based Au(I)-NHC

complexes, including one neutral complex, **Au3** and cationic Au(I)-bis(NHC) complexes, with the general structure **Au4**, (**Figure 1.7**). Although they were less active than cisplatin, one complex (R = H) was 2-fold more potent than cisplatin against the cancerous cell line A2780/R.<sup>69</sup> Two Au(I)-NHC complexes, **Au5** and **Au6** (**Figure 1.7**), one containing 2,3,4,6-tetra-O-acetyl-1-thio- $\beta$ -D-pyranosatothiolato and the other a saccharin ligand, were reported as potential anticancer agents by Fremont *et al.*<sup>70</sup> Tacke and co-workers more recently tested saccharine containing complexes **Au7-Au9** against breast cancer cell line MCF-7, revealing higher potency compared to cisplatin.<sup>71</sup> Lemke *et al.* reported two amino acid containing Au-NHC complexes, **Au10** and **Au11**, that show good antitumor activity compared to the non-amino acid derivatives.<sup>72</sup>

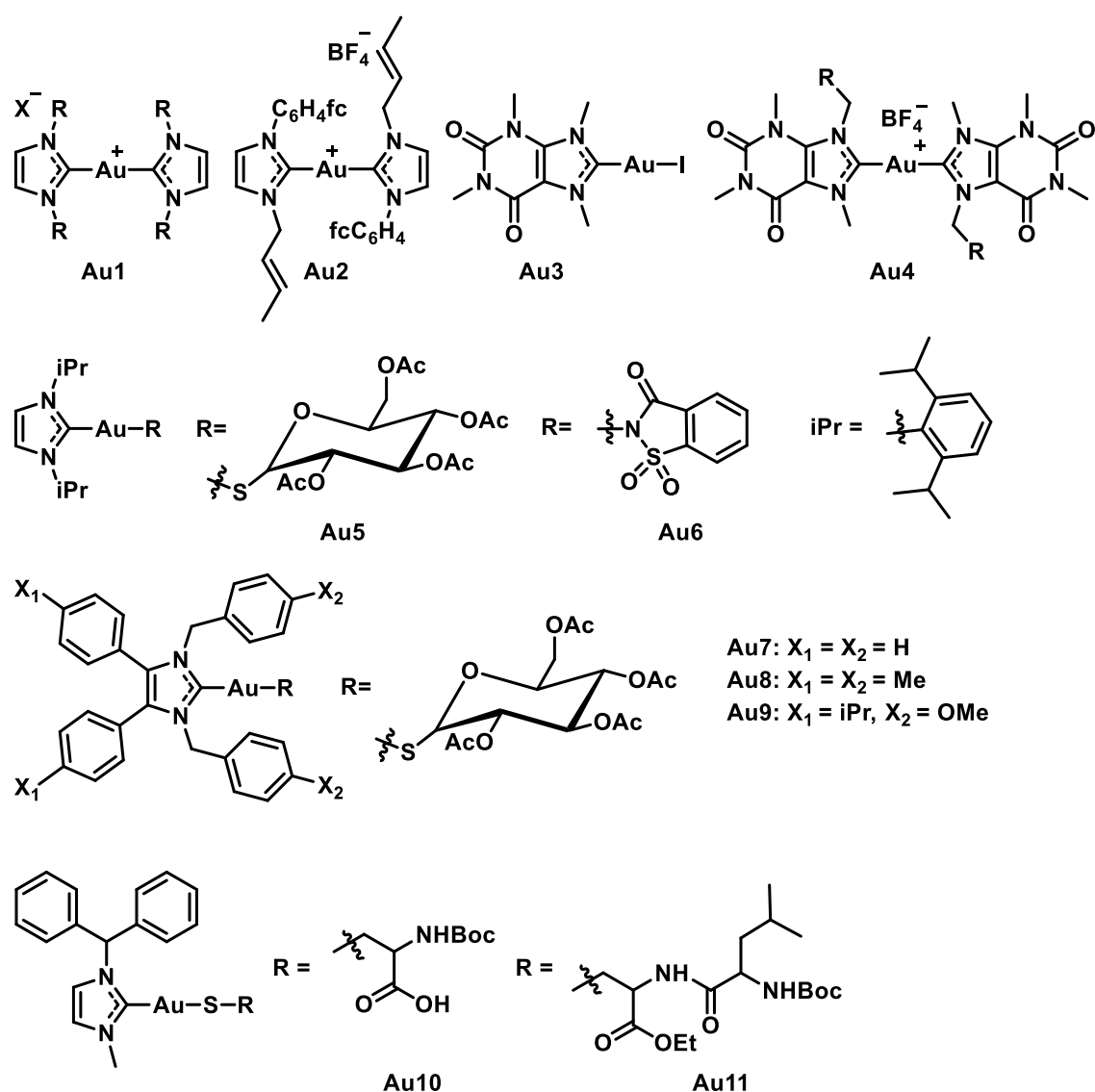


**Figure 1.7:** Au-NHC complexes that display chemotherapeutic properties<sup>56, 68-72</sup>

### 1.6.2 Platinum-NHCs as anticancer agents

Skander *et al.* explored the anticancer activity of twelve Pt(II)-NHC complexes with the general structures **Pt1-Pt5** (Figure 1.8).<sup>40</sup> Most complexes were reported to be significantly more potent than cisplatin, and a few showed activity against cisplatin resistant cell lines.<sup>40</sup> Sun and co-workers revealed the ability of cyclometalated Pt complexes to accumulate in the cytoplasm, with **Pt6** showing 200 fold higher affinity towards human carcinoma cell line HeLa than the non-cancerous human lung fibroblast cell line CCD-19Lu.<sup>41</sup> A library of amino Pt-bis(NHC)s with general structure **Pt7** that are all more potent than cisplatin against many cancerous cell lines (KB3-1, SK-OV3, OVCAR-8, MV-4-11, and A2780) were reported by Chtchigrovsky and co-workers.<sup>73</sup> Caffeine-based Pt-NHC, **Pt8**, reportedly exhibits antitumor properties.<sup>74</sup> The mechanism of action of Pt-NHC complexes in general has been found to be similar to that of cisplatin, where the complex intercalates with the two strands of DNA, inhibiting DNA growth and inducing cell apoptosis. The difference in mechanism between Pt-NHC complexes and Au-NHC complexes is illustrated in Figure 1.9,<sup>39</sup> displaying the accumulation of Au-NHC in the mitochondria, leading to mitochondrial disruption through inhibiting mitochondrial enzymes.

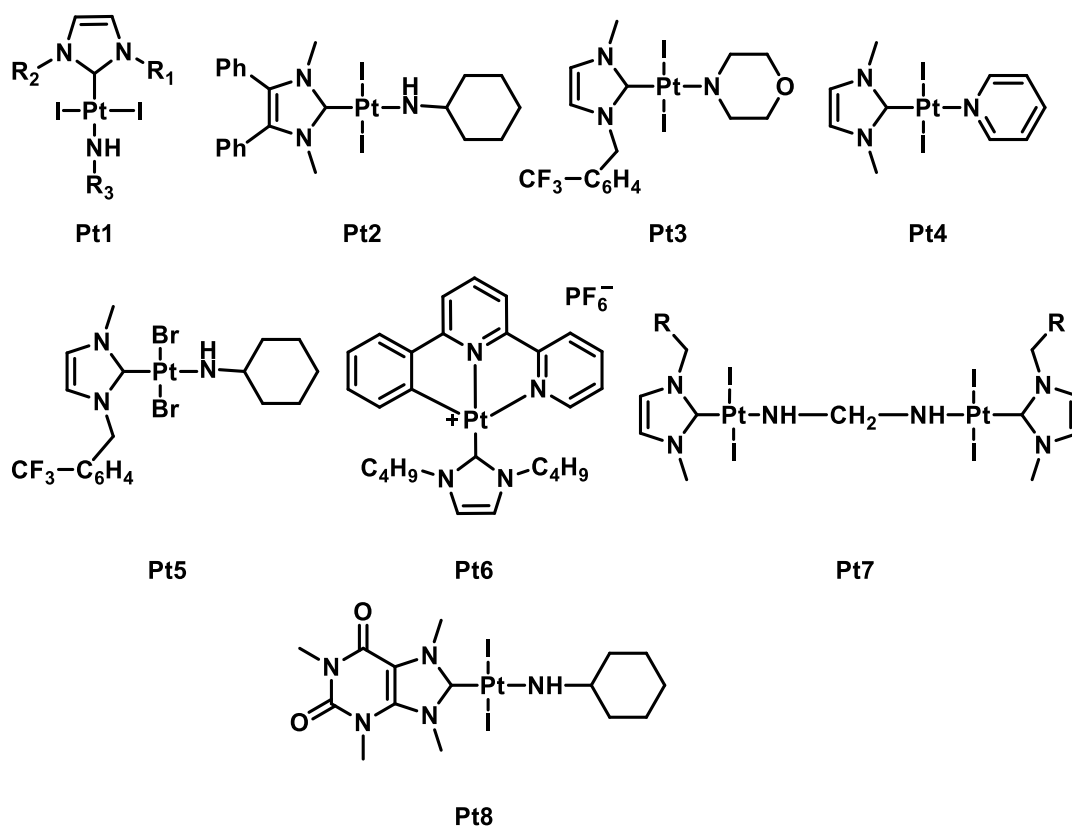
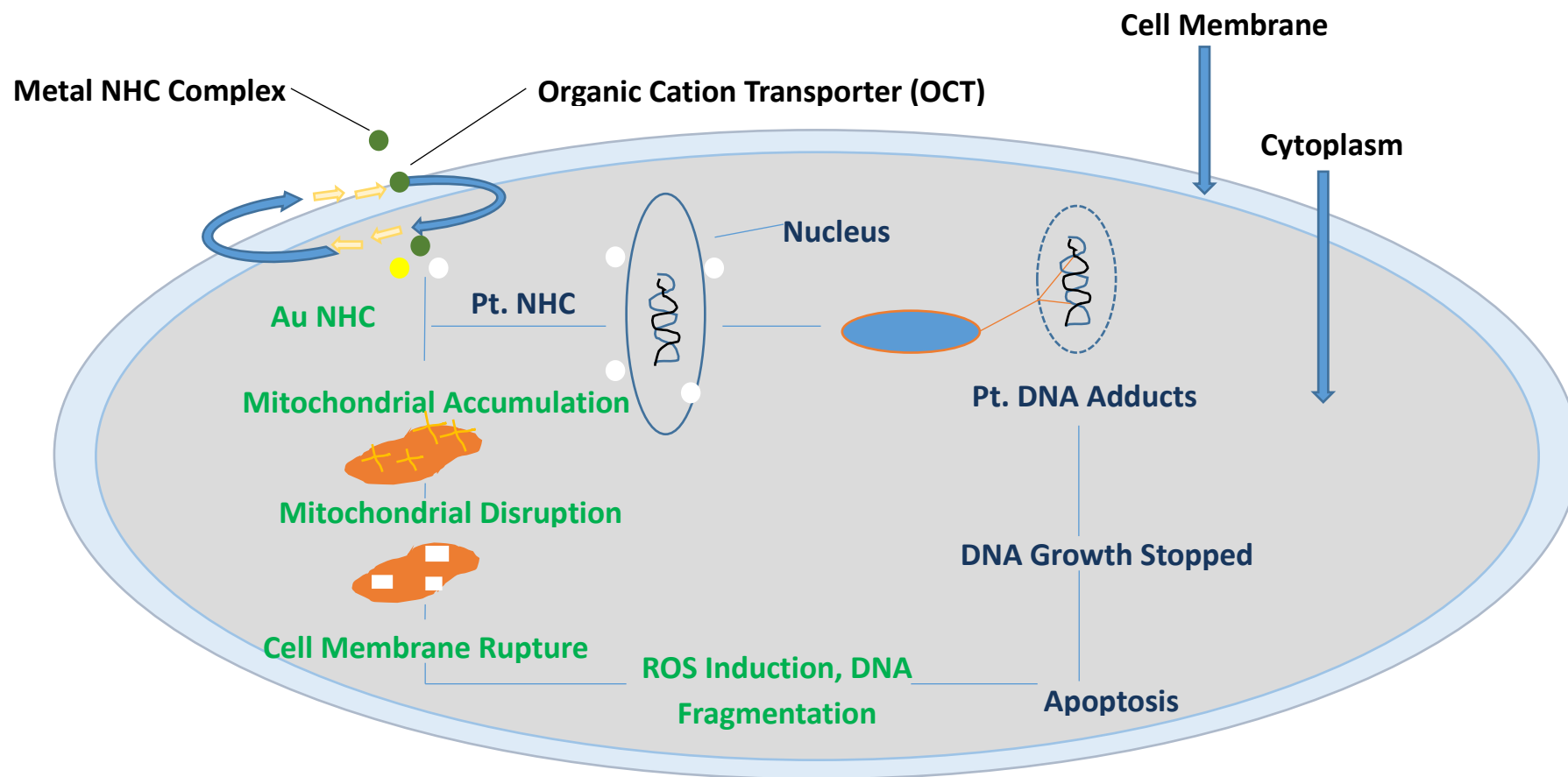


Figure 1.8: Pt(II)-NHC complexes that display chemotherapeutic properties<sup>41, 73, 74</sup>



**Figure 1.9:** Mechanisms of action of Au-NHCs and Pt-NHCs that lead to apoptosis.<sup>39</sup> Au-NHCs (yellow circles) through mitochondrial accumulation (green route), and Pt-NHCs (white circles) through DNA binding (blue route)

### 1.6.3 Palladium, ruthenium and copper-NHCs as anticancer agents

Two Pd(II)-NHC complexes, **Pd1** and **Pd2** (Figure 1.10), were tested for antitumor activity.<sup>75</sup> **Pd2** showed potent anticancer activity against cervical cancer HeLa cells, being more potent than cisplatin, as well as its corresponding Au and Ag complexes. Haque *et al.* compared the anticancer activities of two Pd(II) NHC complexes, **Pd3** and **Pd4**, to that of 5-fluorouracil (5-FU) and reported that only the *trans* geometry of these complexes exhibited cytotoxicity.<sup>76</sup>

Various Ru(II)- and Ru(III)-NHC complexes have revealed promising anticancer properties.<sup>57, 58, 60, 61, 77, 78</sup> For example, Oehninger *et al.* reported Ru(II)-NHC complex **Ru1** to show good cytotoxicity, by reported inhibition of selenol containing enzymes such as TrxR.<sup>61</sup> Tacke and co-workers also reported six Ru(II)-NHC complexes of general structures **Ru2** and **Ru3** that showed higher potency than their corresponding Au(I)-NHC complexes against Caki-1 and MCF-7.<sup>65</sup> Four Ru(II)  $\eta^6$ -arene imidazole complexes **Ru1** and **Ru4-Ru6** were reported to have anticancer properties, with complex **Ru4** having 3 fold more toxicity towards cancer cells compared to non-cancerous cells.<sup>78</sup> Gallori *et al.* report the DNA binding ability of NAMI-A **Ru5**, thus providing a potential mode of action to explain its potent cytotoxicity.<sup>57</sup> Further investigation into complex **Ru5** and **Ru6** revealed their ability to induce DNA unwinding, and revealed the role of **Ru5** in selective metastatic cell targeting and binding to collagen.<sup>77</sup> Two bis-imidazole DMSO containing complexes **Ru7** and **Ru8** displayed antiproliferative and antimetastatic activity by arresting the cell cycle in G0/G1 phase, thus inducing apoptosis.<sup>60</sup>

Teyssot *et al.* investigated the anticancer properties of seven Cu(I)-NHC complexes including **Cu1** and **Cu2** and their saturated imidazole analogues, which were all more potent ( $IC_{50} = 0.04 - 4.4 \mu M$ ) than the activity of cisplatin ( $IC_{50} = 10.4 \mu M$ ) against the breast cancer cell-line MCF-7.<sup>79</sup> Tacke and co-workers reported the synthesis of ten biologically active symmetrically and non-symmetrically *p*-benzyl substituted Cu(I)-NHC bromide complexes of general structure **Cu3** and **Cu4**.<sup>80</sup> The *iso*-propyl substituted Cu(I)-NHC complexes showed better cytotoxicity than the remainder of the complexes against both breast cancer cell-line MCF-7 and renal cancer cell-line Caki-1. One Cu(I)-NHC complex with *iso*-propyl and methoxy substituents on the benzyl groups revealed superior cytotoxicity to cisplatin.

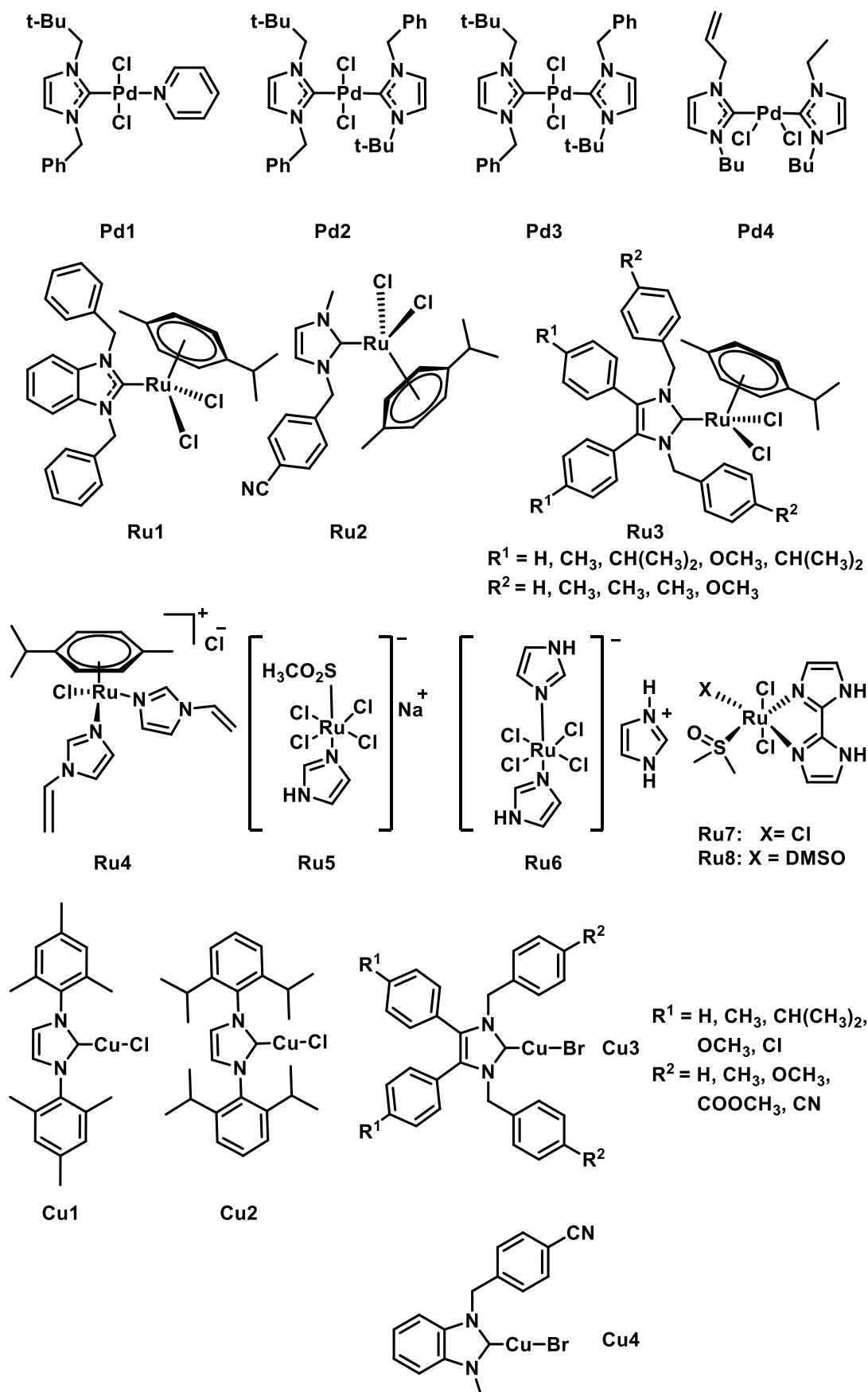


**Figure 1.10:** Pd(II)-<sup>75, 76</sup> Ru(II, III)-<sup>57, 58, 60, 61, 77, 78</sup> and Cu(I)-NHC<sup>79, 80</sup> complexes that exhibit cytotoxic behaviour

## 1.7 Silver-NHCs

Various NHC-type ligands have been used to complex silver, including imidazolin-2-ylidene (**A**), benzimidazol-2-ylidenes (**B**), imidazolidin-2-ylidenes (**C**), tetrahydropyrimid-2-ylidenes (**D**), 1,2,4-triazolin-5-ylidenes (**E**) and imidazolin-4(5)-ylidenes (**F**) (**Figure 1.11**).<sup>81-88</sup> Transmetalation reactions of NHCs from silver to other metals have been reported for the synthesis of a broad range of transition metals: Au(I), Cu(I), Cu(II), Ni(II), Pd(II), Pt(II), Rh(I), Rh(III), Ir(I), Ir(III), Ru(II), Ru(III), and Ru(IV).<sup>89</sup>

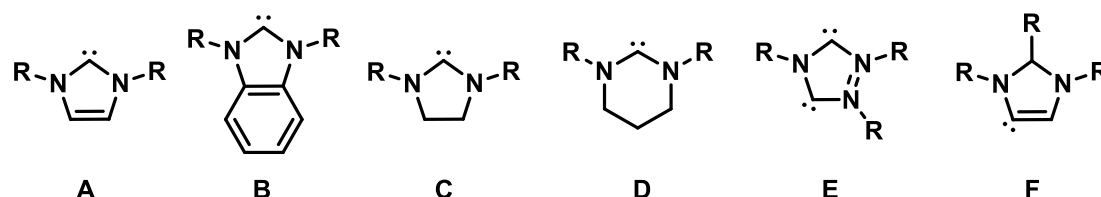
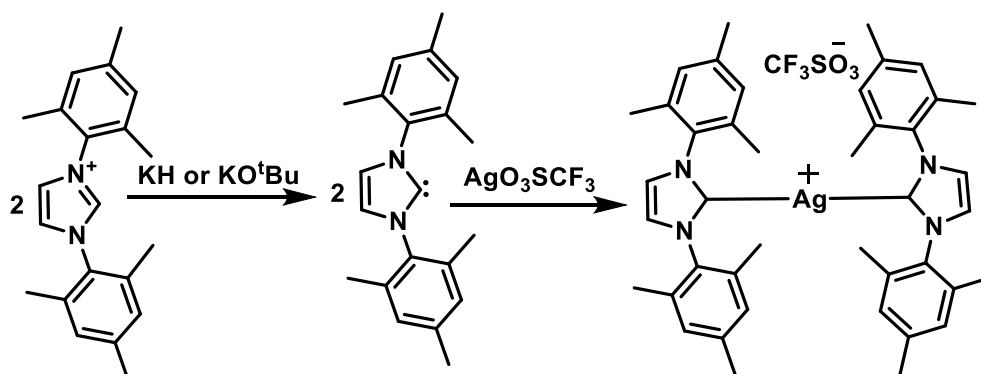


**Figure 1.11:** NHCs that have been coordinated to silver<sup>81-88</sup>

### 1.7.1 Preparation of silver(I)-NHCs

The first Ag(I)-NHC complex to be structurally characterised was prepared by reaction of a free carbene with a silver salt.<sup>81</sup> In 1997, the formation of a Ag(I)-NHC complex formed by reaction of a triazolium salt with silver acetate was reported.<sup>82</sup> The most popular current method for the preparation of Ag(I)-NHCs was reported in 1998 by Lin and Wang, using Ag<sub>2</sub>O as both the base and metallating reagent.<sup>83</sup> Ag(I)-NHCs can be synthesised from imidazolium salts in several different ways, with four common methods highlighted below:

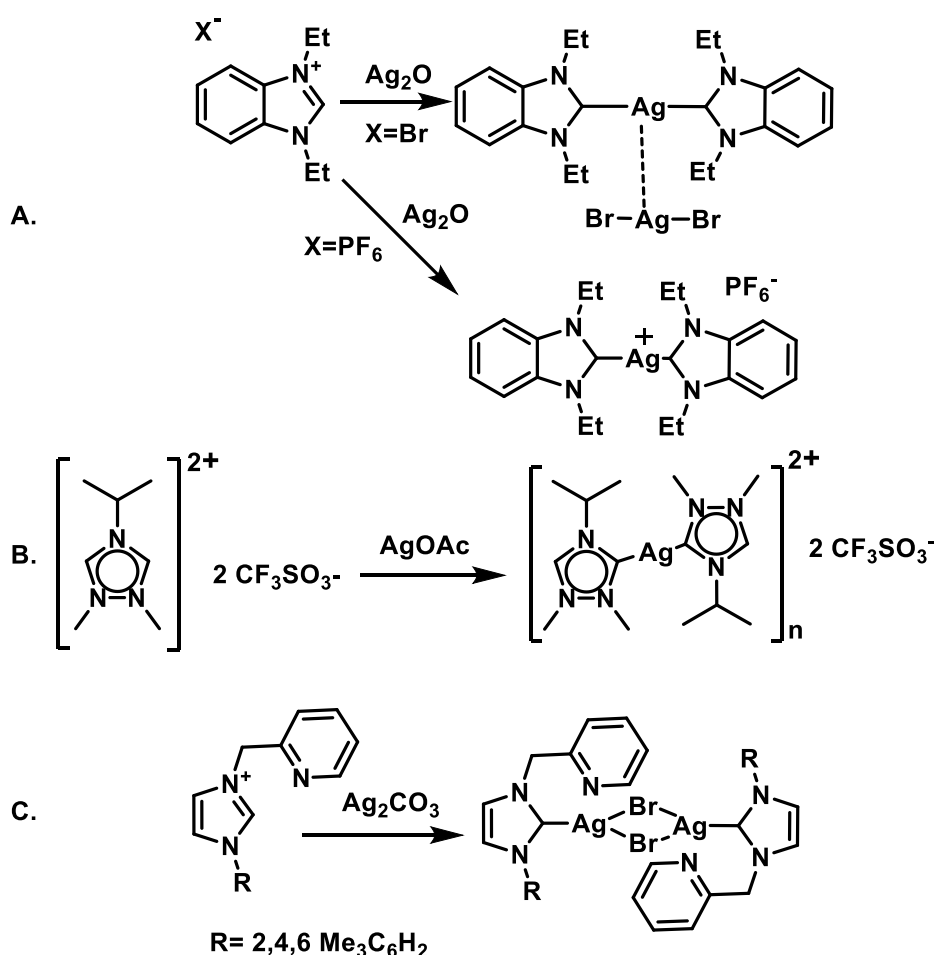
1. Preparation of a free carbene followed by reaction with a silver salt e.g. silver triflate (**Scheme 1.2**).<sup>81, 90-92</sup>



**Scheme 1.2:** Synthesis of Ag(I)-NHC by reacting a free carbene with a silver salt<sup>81</sup>

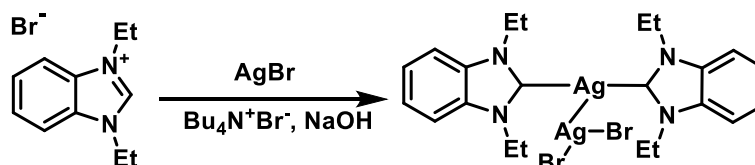
2. Reaction of imidazolium salts with basic silver reagents *in situ* e.g.  $\text{Ag}_2\text{O}$ ,  $\text{AgOAc}$ , or  $\text{Ag}_2\text{CO}_3$  (**Scheme 1.3**).<sup>82, 83, 85-88, 93, 94</sup>

Silver oxide is the most commonly used basic metal to prepare NHCs, as the reaction time is relatively short and can be monitored by the uptake of the insoluble  $\text{Ag}_2\text{O}$ . A range of solvents have been used with  $\text{Ag}_2\text{O}$  in the synthesis of Ag-NHCs, including  $\text{CH}_2\text{Cl}_2$ , 1,2- $(\text{CH}_2)_2\text{Cl}_2$ , DMSO,  $(\text{CH}_3)_2\text{CO}$ , MeOH, MeCN, DMF,  $\text{H}_2\text{O}$  and also solvent mixtures. Most of these reactions proceed at room temperature, however, it was found that silver oxide reactions with bulky imidazolium salts often require heating. This suggests that steric bulk around the imidazolium cation affects the ability of the silver oxide to effectively deprotonate the imidazolium salt. Molecular sieves were reportedly used in some such reactions as they speed up the rate of the reaction ( $\text{H}_2\text{O}$  is generated) and may increase the purity of some products.<sup>82, 83, 87, 94-109</sup>



**Scheme 1.3:** Synthesis of Ag(I)-NHC complexes by reaction of imidazolium salts with basic silver reagents **A.**  $\text{Ag}_2\text{O}$ ,<sup>83</sup> **B.**  $\text{AgOAc}$ ,<sup>75, 80</sup> and **C.**  $\text{Ag}_2\text{CO}_3$ <sup>94</sup>

3. Reaction of an imidazolium salt with a base in the presence of silver salt.<sup>83</sup> A method using a phase transfer catalyst to synthesise a Ag(I)-NHC from the benzimidazolium salt in the presence of AgBr is shown in **Scheme 1.4**. This provides the same products as the silver oxide route (**Scheme 1.3A**). However, this method did not work with other imidazolium salts.<sup>83, 94</sup>

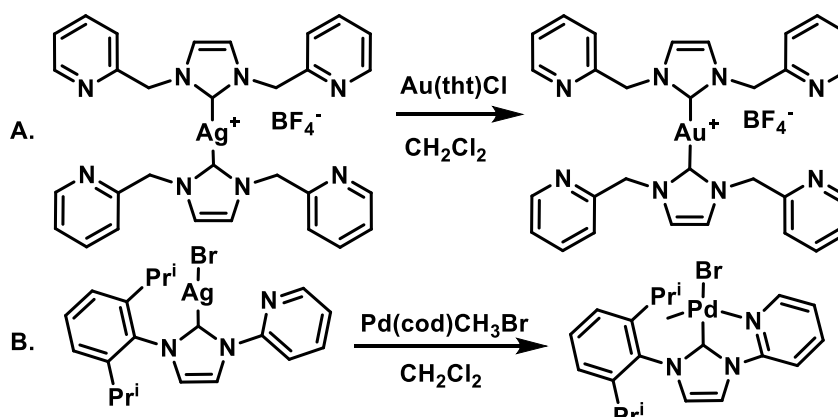


**Scheme 1.4:** Synthesis of Ag(I)-NHC by reacting imidazolium salt with a base in the presence of silver salt<sup>83</sup>

4. Transmetallation from W-NHC on to silver.<sup>84</sup>

The Ag(I)-NHC complexes synthesised from this method were moisture sensitive and quickly decomposed to the imidazolium salt when exposed to air. This method has been discarded due to the success of silver oxide.<sup>84, 110, 111</sup>

One main purpose of synthesising Ag(I)-NHCs is to transfer the NHC ligand to other transition metals. Some metal-NHC complexes can be synthesised by deprotonation of the imidazolium salt using a strong base, and then reaction with the desired metal. However, many compounds do not metalate due to degradation under the required harsh conditions. As mentioned previously, Ag(I)-NHC complexes has been successful at transferring to a variety of other metals (**Scheme 1.5**). Transmetallation reactions are generally carried out under aerobic conditions and can occur in the presence of water. Since synthesising Ag(I)-NHC complexes and transferring them to other transition metals is reasonably facile, this route is more commonly used than other routes which require anaerobic conditions.<sup>93, 101, 103, 106, 112-122</sup>



**Scheme 1.5:** Transmetallation from Ag to **A.** Au and **B.** Pd<sup>114, 118, 123</sup>

### 1.7.2 History of silver in medicine

For centuries, metallic silver was used as an antimicrobial agent to purify drinking water and used medicinally to cure ailments.<sup>124-130</sup> Wounds and infectious diseases were treated with silver nitrate, even before the discovery of bacteria. Following the discovery of bacteria, silver nitrate was used to minimise bacterial growth on burns patients. Later on, dilute solutions of silver nitrate were dropped into the eyes of new-born babies to prevent conjunctivitis and other bacterial infections that might be contracted during birth. Silver sulfadiazine (**Figure 1.12**), discovered in the 1960s, was found to be more effective and safer than silver nitrate in treating burn wounds and is currently the most widely used remedy in American burn centres. Since silver-based therapeutics can be used for the treatment of burns, open wounds and chronic ulcers, the interest in developing silver-based NHCs from this area was initiated. Silver is considered nontoxic to mammalian cells within the determined exposure limits (0.01-0.1 mg/m<sup>3</sup>),<sup>131, 132</sup> due to however, silver compounds may cause skin discoloration, known as Argyria.<sup>133</sup> Therefore, the ideal silver compound is one that slowly releases silver into the wound and traps it in the wound without discoloration, thus maintaining a constant source of antimicrobial agents to prevent re-infection.<sup>89</sup> Recently, the interest in silver as an antibacterial re-emerged in the form of silver nanoparticles,<sup>134-136</sup> introduced in various forms, including silver-based dressings, silver-coated textile fabrics and silver-coated medicinal devices such as nanogels and nanolotions.<sup>134, 137</sup> The mechanism of action of silver as an antimicrobial, and the role of 'Ag<sup>+</sup> ions release' is under debate, and in an attempt to resolve it, Liu *et al.* evaluated the release of Ag<sup>+</sup> ions under aerobic and anaerobic conditions, concluding the release of Ag<sup>+</sup> ions from nanoparticles occurs exclusively in the presence of oxygen (**Scheme 1.6**).<sup>138</sup> Further research is required to end the ongoing debate and to determine the role of silver in bacterial cells as well as cancerous cells.

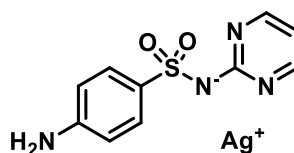


**Figure 1.12:** Structure of silver sulfadiazine



**Scheme 1.6:** Release of Ag<sup>+</sup> ions from nanoparticles under aerobic conditions<sup>138</sup>

### 1.7.3 Silver(I)-NHCs as antibacterial agents

Currently, Ag(I)-NHC complexes are the most widely studied type of metal-NHCs in the field of anti-infectives. Two pyridine-linked pincer Ag(I)-NHC complexes **Ag1** and **Ag2** (**Figure 1.13**) were found to be active against *E. coli*, *S. aureus* and *P. aeruginosa*, with minimum inhibitory concentration values lower than that of AgNO<sub>3</sub>.<sup>139</sup> It is thought that the complexes slowly release Ag<sup>+</sup> ions into the culture medium, however, the distribution of the bioavailable active species responsible for the antimicrobial properties is unknown. The encapsulation of Ag(I)-NHC complexes in nanoparticles or nanofibres has been reported.<sup>140-143</sup> One example is **Ag3** (**Figure 1.13**), which has been encapsulated into an electro-spun polymer and the antimicrobial properties of this polymer were studied.<sup>140</sup> It was found that the encapsulation of Ag(I)-NHC complexes into fibre mats resulted in improved antimicrobial activity, faster kill rate, and increased bioavailability of the active silver species when compared to silver sulfadiazine or silver nitrate. However, the decomposition of the Ag(I)-NHC complex not only releases cationic silver but also the imidazolium salt, which was found to be relatively toxic in this case.<sup>140-143</sup> This highlights the importance of utilising non-toxic imidazolium salts as ligand precursors.

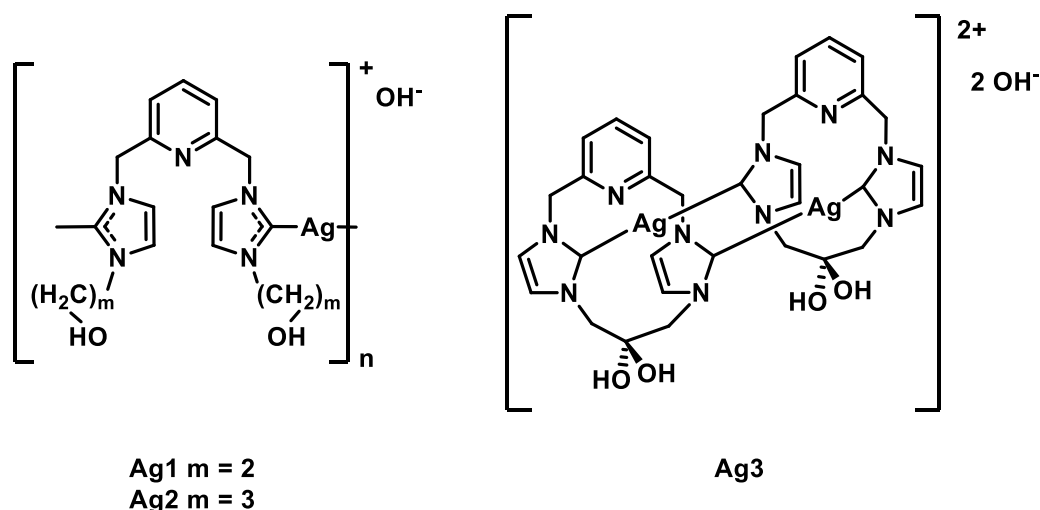


**Figure 1.13:** Antibacterial pyridine-linked pincer Ag(I)-NHC complexes (**Ag1**, **Ag2**),<sup>139</sup> and antimicrobial Ag(I)-NHC that has been encapsulated in nanoparticles(**Ag3**)<sup>140</sup>

Biologically benign precursors such as the xanthine derivatives caffeine and theobromine, that are commonly found in the body, have been utilised for the synthesis of **Ag4** and **Ag5** (Figure 1.14).<sup>98</sup> Complexes **Ag4-Ag8** were effective against highly resistant opportunistic pathogens recovered from the respiratory tract of patients with cystic fibrosis as well as against *E. coli* J53.<sup>144-151</sup> Symmetric and non-symmetric Ag(I)-NHC complexes including **Ag4-Ag8** were evaluated against both Gram-positive bacteria *S. aureus* and the Gram-negative bacteria *E. coli*. It was observed that the more lipophilic the compound is, the more it is able to penetrate the cell membrane effectively leading to better antibacterial activity.<sup>144-151</sup> 14 Halide containing Ag(I)-NHC complexes including **Ag9-Ag11** were reported,<sup>152</sup> and found to be active against *E. coli*, *S. aureus* and the resistant strains *S. aureus* *NorA* and *S. aureus* *MRSA*.<sup>152</sup>

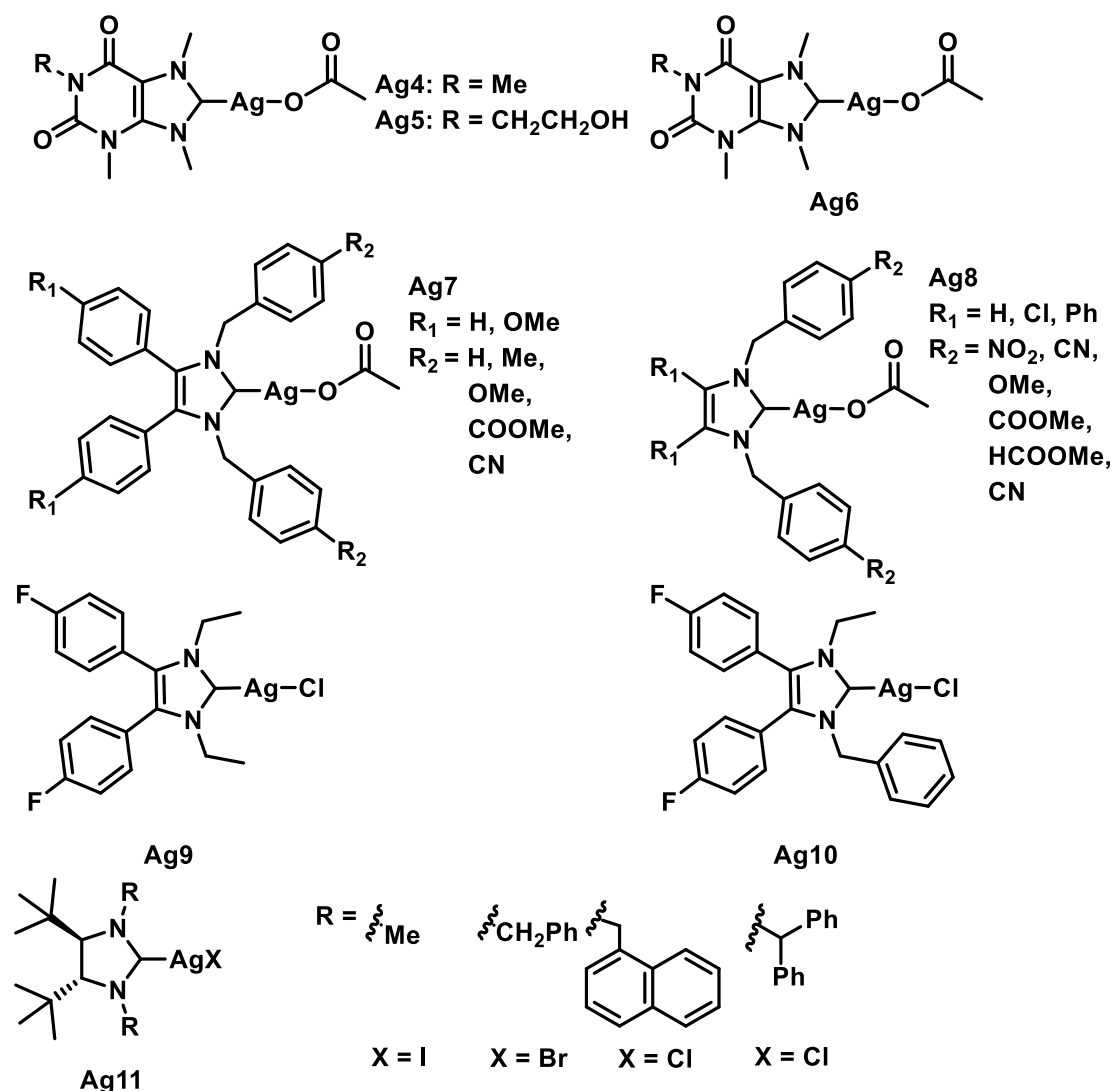


**Figure 1.14:** Ag(I)-NHC acetate complexes<sup>145, 146, 150</sup> and halide-containing Ag(I)-NHC<sup>152</sup> complexes that display antibacterial properties

## 1.8 Silver(I)-NHCs as anticancer agents

The medicinal applications investigated for Ag(I)-NHC complexes has mainly involved their use as anti-infectives (section 1.7.3). However, more recently, a number of groups have reported cytotoxic effects of Ag(I)-NHCs against cancer cells.<sup>79, 129, 146-150, 152-161</sup> The mechanism of action of Ag(I)-NHC complexes in cancer remains unknown, however, their cellular targets appear to be similar to those of Au(I)-NHC complexes, *i.e.* target mitochondrial enzymes (**Figure 1.9**). This is possibly due to the affinity of both Ag and Au to sulfur-containing enzymes such as thioredoxin reductase and glutathione reductase which are overexpressed in cancerous cells. For example, TrxR, a sulfur-containing enzyme found in both the cytoplasm (TrxR1) and the mitochondria (TrxR2), has been reported to be inhibited by Ag(I)-NHC complex **Ag12** (**Figure 1.15**).<sup>158</sup> Youngs and co-workers described the benefits of encapsulation of Ag(I)-NHC complexes into polymeric nanoparticles (NPs).<sup>129</sup> Water-soluble complexes seemingly improved the encapsulation into nanoparticles (NPs) as the encapsulation is performed in water, therefore the higher the water-solubility of the complex the higher the encapsulation. The NPs were reported to provide good resistance against biological inactivation of the Ag(I)-NHC complex from sulphur containing enzymes such as glutathione reductase. The NPs also make use of the 'leaky' blood vessels near the tumour, referred to as enhanced permeability and retention, or EPR effect of tumour tissue.<sup>129</sup> The enhanced permeability part of the cancerous tissue EPR effect allows the entrance of macromolecules such as NPs, while the reduced retention through the decreased lymphatic drainage keeps the NPs in the cancerous tissue for a prolonged time.

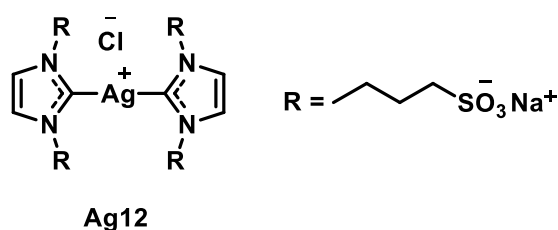


**Figure 1.15:** Ag(I)-NHC complex **Ag12** reported to inhibit thioredoxin reductase<sup>158</sup>

A series of mono- and binuclear Ag(I)-NHC complexes with different xylyl spacers have been synthesised and their anticancer activity reported (**Figure 1.16**).<sup>153</sup> **Ag14-Ag16** showed good anticancer activity against human colorectal HT116, with IC<sub>50</sub> values (**Ag14** = 1.3μM, **Ag15** = 1.1μM, **Ag16** = 0.9μM) five times lower than 5-fluorouracil (5μM) while the value for complex **Ag13** (5.4μM) was almost equal to 5-fluorouracil.<sup>153</sup>

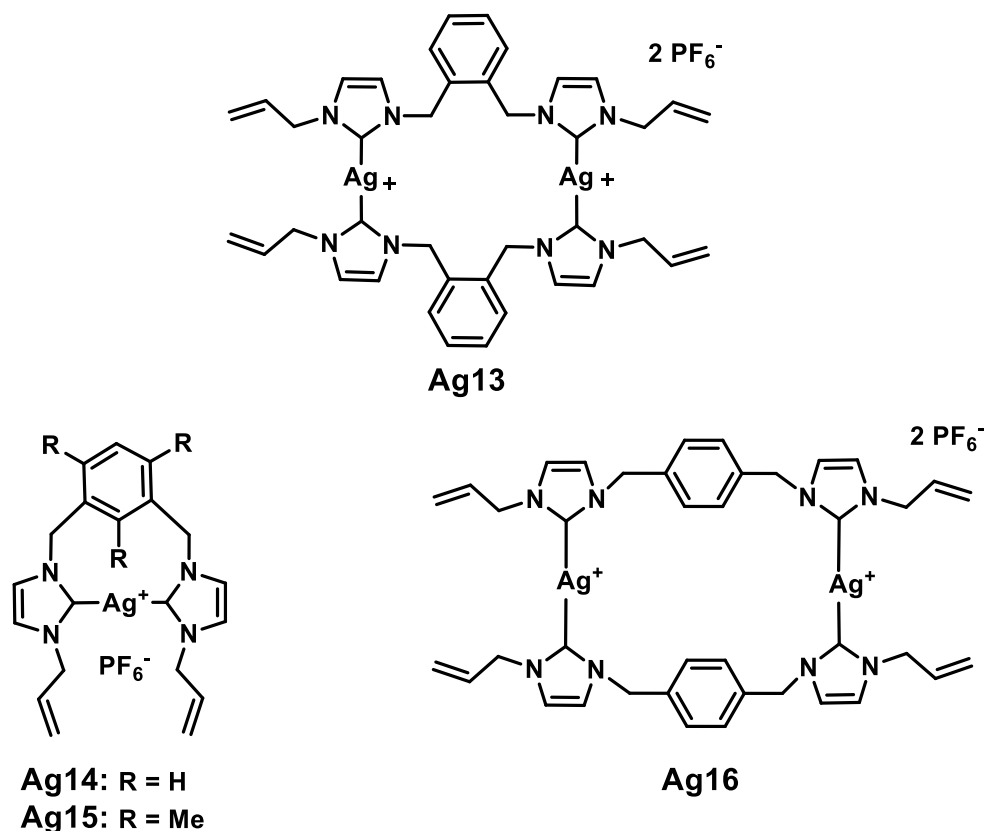


**Figure 1.16:** Ag(I)-NHC anticancer complexes with different xylyl spacers  
**Ag13-Ag16**<sup>153</sup>

Two simple Ag(I)-NHCs **Ag17** and **Ag18** were synthesised (**Figure 1.17**), and their anticancer activities were tested on H460, a lung cancer cell line, revealing anticancer efficacies comparable to that of cisplatin.<sup>154</sup> The cytotoxicity of Ag(I)-NHC **Ag19** was tested on 6 different human cancerous cell lines (KB: oral carcinoma, HL60: promyelocytic leukaemia, HL60R: resistant HL60, MCF-7: breast cancer, MCF-7R: resistant MCF-7, T47D: breast cancer), revealing higher cytotoxicity than cisplatin on all the cell lines.<sup>79</sup> **Ag19-Ag23** were evaluated against MCF-7, a breast cell line, to study the effect of the ligand. Increasing the stability of the ligand by either increasing the steric hindrance around the metal (**Ag19** versus **Ag21**) or by decreasing its saturation (**Ag19** versus **Ag20**) increased the cytotoxicity ten-fold. Another observation was that having a large substituent on the imidazole ring (**Ag23**) exhibits lower IC<sub>50</sub> than that of cisplatin (**Table 1.1**).<sup>79</sup> This is possibly due to the bulkiness of the substituent, which may lead to a slow and prolonged release of Ag<sup>+</sup> ions.

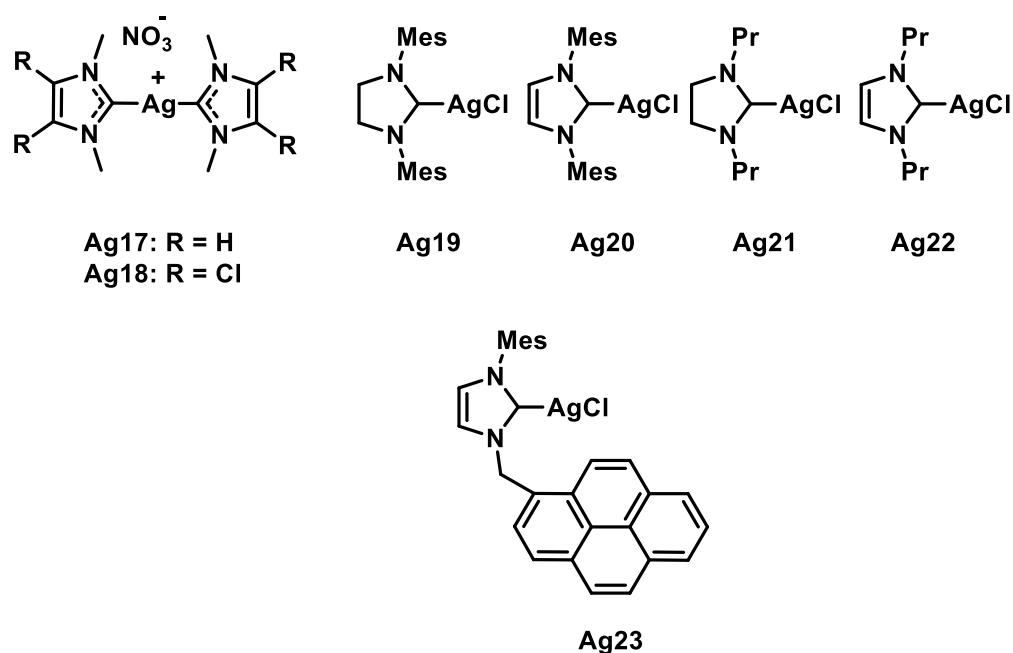


**Figure 1.17:** Ag(I)-NHCs with reported anticancer activity against lung cancer cell line H460<sup>154</sup> and breast cancer cell line MCF-7<sup>79</sup>

**Table 1.1:** IC<sub>50</sub> values of complexes **Ag19-Ag23** against MCF-7 compared to cisplatin<sup>79</sup>

| Complex               | cisplatin | Ag19          | Ag20          | Ag21          | Ag22          | Ag23          |
|-----------------------|-----------|---------------|---------------|---------------|---------------|---------------|
| IC <sub>50</sub> (μM) | 10.4±0.1  | 0.25<br>±0.01 | 0.08<br>±0.01 | 0.06<br>±0.01 | 0.03<br>±0.01 | 0.42<br>±0.01 |

Three Ag(I)-NHC acetate complexes (**Ag24-Ag26**, **Figure 1.18**),<sup>145</sup> silver nitrate, and silver acetate were reported to exhibit anticancer activity against the cancer cell lines OVCAR-3 (ovarian), MB157 (breast), and Hela (cervical). However, their anticancer activity was found to be less potent than cisplatin. All three complexes showed higher activity against the breast cancer cell line over the ovarian cell line.<sup>160</sup> A series of monodentate, bidentate and macrocyclic cationic Ag(I)-bis(NHC) complexes **Ag27-Ag30** were synthesised and their cytotoxicities tested against human breast adenocarcinoma MCF7 and the colon adenocarcinoma DLD1 cell lines. The complexes exhibited higher cytotoxicity than simple silver salts (AgBr, AgBF<sub>4</sub>), which exhibited negligible cytotoxicity.<sup>155</sup>

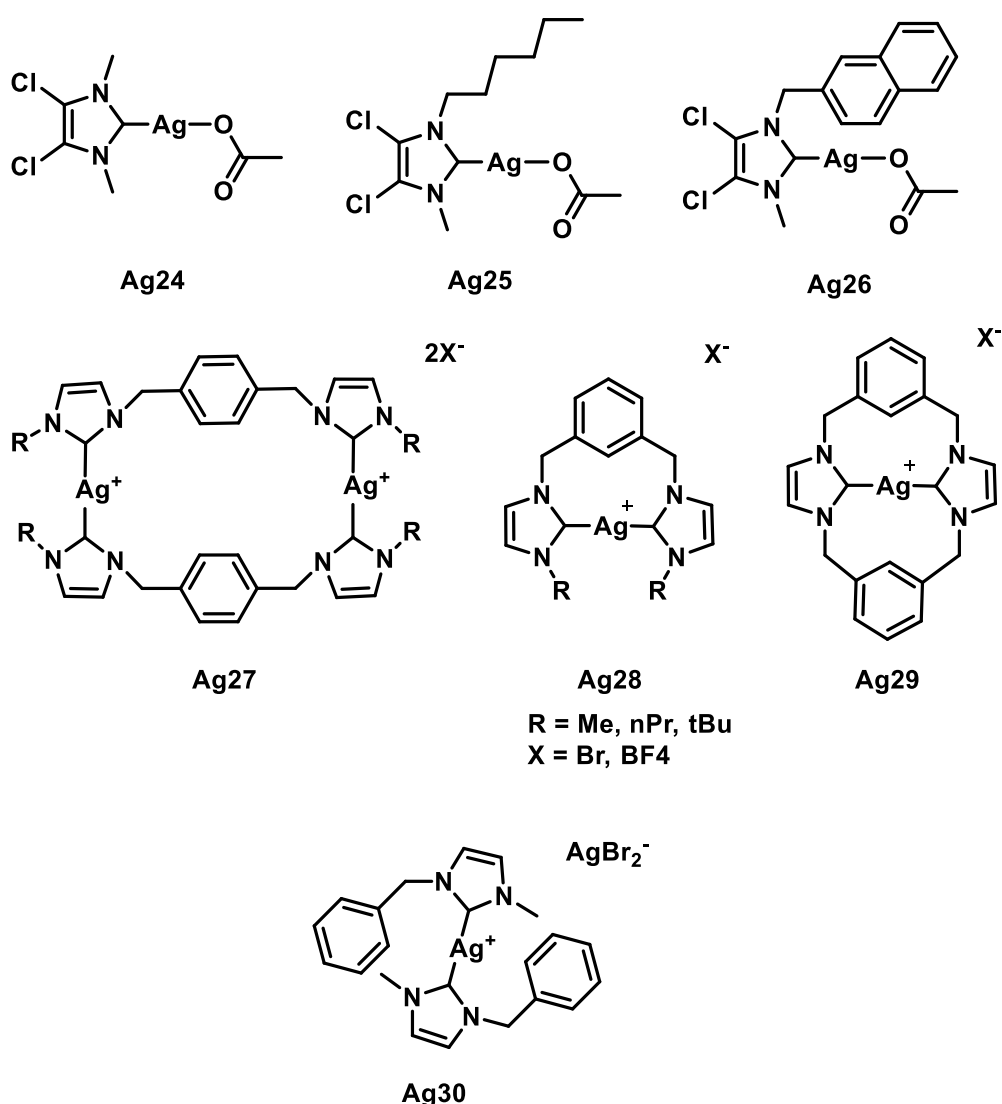


**Figure 1.18:** Ag(I)-NHC acetate,<sup>160</sup> and Ag(I)-bis(NHC) complexes<sup>155</sup> with anticancer properties

A number of Ag(I)-NHC complexes (general structures **Ag31**-**Ag33**, **Figure 1.19**) displayed IC<sub>50</sub> values similar to those obtained for analogous Au or Pt-NHC complexes, and lower than those obtained for established cytotoxic drugs such as 5-fluorouracil.<sup>153-156, 160</sup> Molecular studies revealed the ability of three complexes with general structure **Ag34** to accumulate in the mitochondria and depolarise the mitochondrial membrane.<sup>159</sup> This induces apoptosis through damage of the endoplasmic reticulum and cytosolic translocation of the apoptotic inducing factor (AIF) from the internal part of the mitochondrial membrane.<sup>159</sup> Moreover, the potential of **Ag32** to strongly inhibit TrxR activity was recently confirmed.<sup>158</sup>

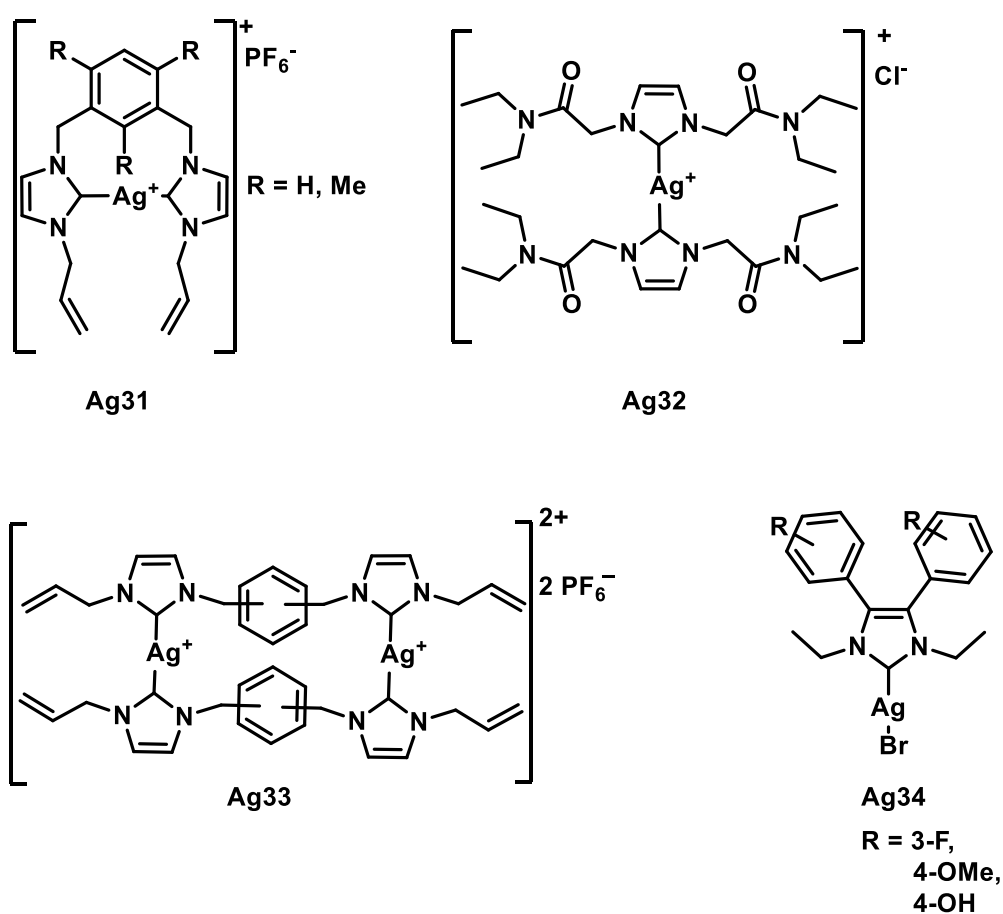


**Figure 1.19:** Ag(I)-NHC complexes with antiproliferative properties<sup>153-156, 158-160</sup>

The cytotoxicity of Ag(I)-NHC acetate complexes **Ag35** and **Ag36** (Figure 1.20) were evaluated against the human cancerous renal-cell line Caki-1. Symmetric and asymmetric Ag(I)-NHC bromide complexes **Ag37** and **Ag38** were reported and their cytotoxicity evaluated against the human cancerous renal cell line Caki-1. For **Ag35**, the complex R = H ( $IC_{50} = 13.5\mu M \pm 2.0$ ), showed superior anticancer activity to its corresponding R = Cl ( $IC_{50} = 68.3\mu M \pm 1.0$ ) complex, while for **Ag38**, the complex R = H ( $3.3\mu M \pm 0.4$ ) revealed the highest cytotoxicity with  $IC_{50}$  value similar to that obtained for cisplatin ( $3.3\mu M$ ), higher than its corresponding R = Bn ( $IC_{50} = 13.2\mu M \pm 1.0$ ) and comparable to its Au(I) counterpart.<sup>149</sup> These results show the importance of hydrophobic substituents such as benzyl groups in anticancer activity, however additional hydrophobic groups (e.g. Cl or Bn) leads to a decrease in cytotoxicity, and therefore suggesting that a balance in hydrophobic substituents is ideal for anticancer activity. Based on the success of previously reported benzimidazole-derived Ag(I)-NHCs as anticancer agents,<sup>146</sup> two more were synthesised (general structure **Ag39**) by Haque *et al.*<sup>157</sup>  $IC_{50}$  values of **Ag39** ( $13.9$ - $14.6\mu M$ ) although higher, were comparable to those obtained for 5-fluorouracil ( $5\mu M$ ) against HCT 116 cell line.

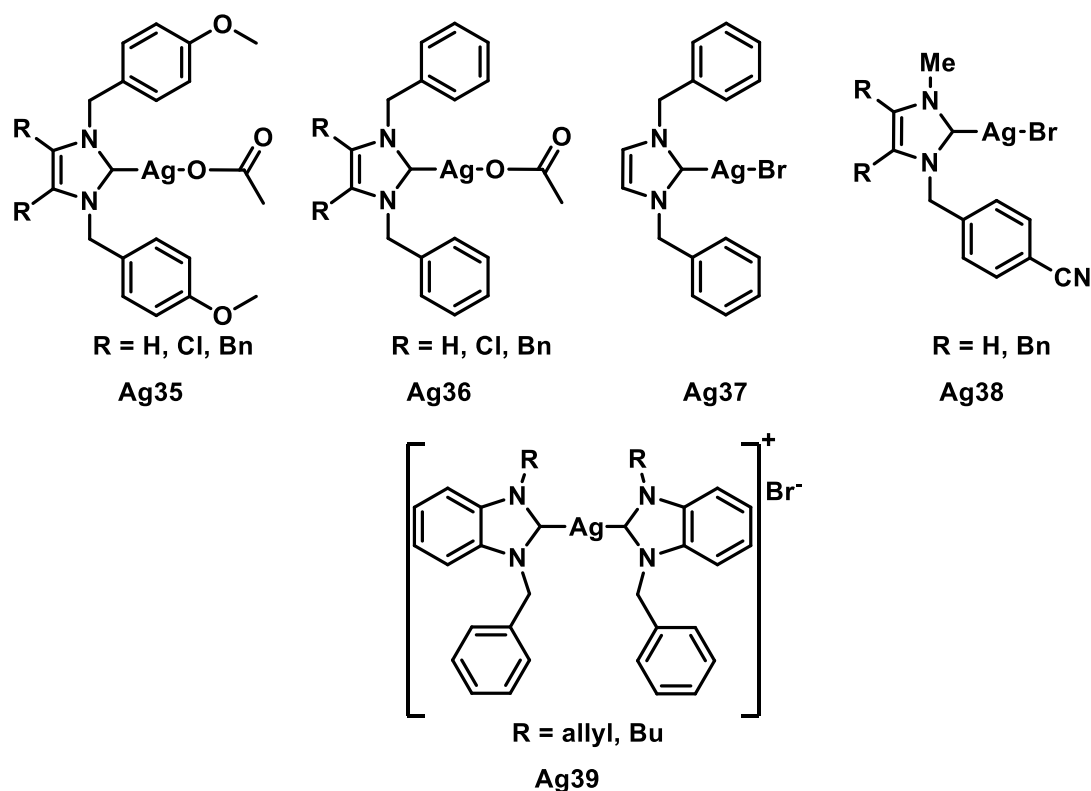


**Figure 1.20:** Ag(I)-NHC acetate complexes, symmetrically and unsymmetrically benzyl- or 4 cyanobenzyl-substituted bromo complexes and benzimidazole-derived Ag(I)-NHCs that exhibit anticancer activity<sup>157</sup>

Fourteen Ag(I)-NHC complexes, **Ag11** and **Ag40-Ag42** (**Figure 1.21**) were previously reported for their antibacterial properties against *E. coli* and *S. aureus*, and for their *in vitro* cytotoxicity against MRC5 cells, which are human noncancerous cells in rapid proliferation (secondary human lung fibroblasts).<sup>152</sup> Promising cytotoxicity against MRC5 cells in bactericidal concentrations encouraged Roland *et al.* to further investigate the anticancer activity of these complexes against different cancerous cell lines.<sup>159</sup> Initially the complexes were tested against KB cells (human carcinoma of the nasopharynx) at two concentrations, 10  $\mu\text{M}$  and 1  $\mu\text{M}$ . The  $\text{IC}_{50}$  values of the 5 most active Ag(I)-NHC complexes **Ag11a**, **Ag11b**, **Ag40d**, **Ag41a** and **Ag41b** were subsequently evaluated against KB cells, all showing superior cytotoxicity compared to cisplatin (**Table 1.2**).<sup>159</sup>

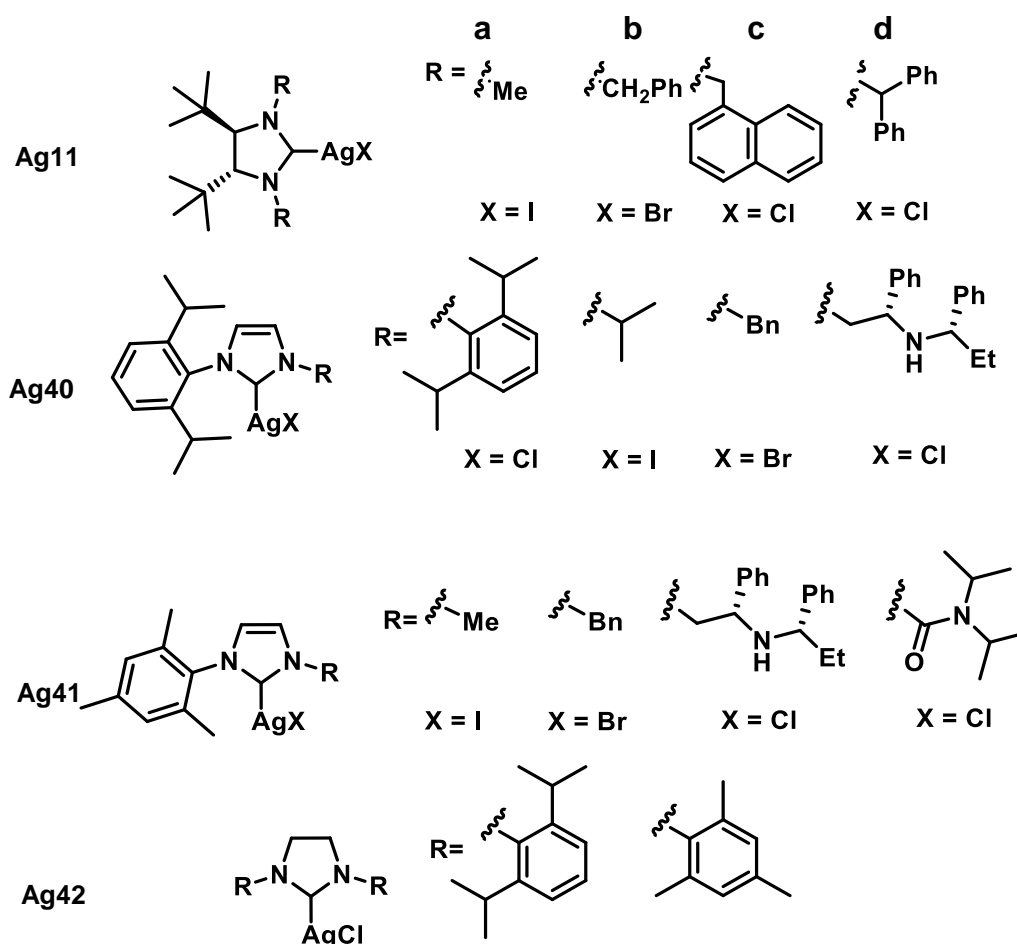


**Figure 1.21:** Ag(I)-NHC complexes evaluated for their anticancer activity<sup>159</sup>

**Table 1.2:**  $\text{IC}_{50}$  values ( $\mu\text{M}$ ) of five Ag(I)-NHC complexes against KB cells<sup>159</sup>

| Complex               | <b>Ag11a</b> | <b>Ag11b</b> | <b>Ag40d</b> | <b>Ag41a</b> | <b>Ag41b</b> | cisplatin |
|-----------------------|--------------|--------------|--------------|--------------|--------------|-----------|
| $\text{IC}_{50}$ (nM) | 165 $\pm$ 25 | 35 $\pm$ 5   | 145 $\pm$ 15 | 45 $\pm$ 5   | 130 $\pm$ 10 | 2200      |

## 1.9 Project aims

The aim of this project is to synthesise libraries of Ag(I)-NHC complexes from a variety of non-toxic, naturally-derived and/or biologically relevant ligand precursors. Examples of naturally-derived precursors include xanthine derivatives, caffeine, theophylline and theobromine, and amino acid L-alanine. An example of a biologically benign precursor is the non-toxic, imidazole-based antifungal compound clotrimazole. The cytotoxicity of the complexes against various cell lines will be evaluated using MTT-based assays, with the aim of establishing structure-activity relationships (SAR). Studies conducted on both cancerous and non-cancerous cell lines can give insight to the selectivity of these complexes. Hydrophobicity measurements will be conducted on the complexes to determine their Log *P* values, which will aid in the understanding of how they are likely to be distributed inside the body, since a Log *P* value is a measure of how the complex partitions between aqueous and organic layers.

Drug delivery is a major concern in pharmaceuticals, however, it has been rarely been addressed for organometallic drugs. Therefore, developing carriers that can selectively deliver the Ag(I)-NHC complexes to cancerous cells will be a focus in this work. The use of polymers as carriers or delivery vehicles for the Ag(I)-NHC complexes will be investigated, with the aim being to acquire maximum potency with minimal toxicity. Either chemical conjugation of the Ag(I)-NHC complexes to various polymers to form polymer-complex conjugates, or physical encapsulation of the Ag(I)-NHC complexes into polymeric micelles will be considered. Furthermore, screening of Ag(I)-NHC complexes and imidazolium salts using a unique electrochemical biosensing device, to evaluate their effect on a phospholipid monolayer, may help understand their mechanism of action, since the phospholipid monolayer mimics biological membranes. Determination of limit of detection (LoD) of complexes using this biosensing device may help predict their corresponding anticancer activity.

## 1.10 References

1. W. A. Herrmann, *Angewandte Chemie-International Edition*, 2002, **41**, 1290-1309.
2. D. Bourissou, O. Guerret, F. P. Gabbai and G. Bertrand, *Chemical Reviews*, 2000, **100**, 39-91.
3. A. Igau, H. Grützmacher, A. Baceiredo and G. Bertrand, *Journal of the American Chemical Society*, 1988, **110**, 6463-6466.
4. K. Öfele, *Journal of Organometallic Chemistry*, 1968, **12**, P42-&.
5. H. W. Wanzlick and H.J. Schonher, *Angewandte Chemie-International Edition*, 1968, **7**, 141-&.
6. A. J. Arduengo, R. L. Harlow and M. Kline, *Journal of the American Chemical Society*, 1991, **113**, 361-363.
7. S. F. Vyboishchikov and G. Frenking, *Chemistry-a European Journal*, 1998, **4**, 1428-1438.
8. T. E. Taylor and M. B. Hall, *Journal of the American Chemical Society*, 1984, **106**, 1576-1584.
9. P. de Fremont, N. Marion and S. P. Nolan, *Coordination Chemistry Reviews*, 2009, **253**, 862-892.
10. G. Frenking, M. Sola and S. F. Vyboishchikov, *Journal of Organometallic Chemistry*, 2005, **690**, 6178-6204.
11. W. W. Schoeller, D. Eisner, S. Grigoleit, A. B. Rozhenko and A. Alijah, *Journal of the American Chemical Society*, 2000, **122**, 10115-10120.
12. P. S. Skell and S. R. Sandler, *Journal of the American Chemical Society*, 1958, **80**, 2024-2025.
13. E. O. Fischer and A. Maasbol, *Angewandte Chemie-International Edition*, 1964, **3**, 580-&.
14. Y. Canac, M. Soleilhavoup, S. Conejero and G. Bertrand, *Journal of Organometallic Chemistry*, 2004, **689**, 3857-3865.
15. S. T. Liddle, I. S. Edworthy and P. L. Arnold, *Chemical Society Reviews*, 2007, **36**, 1732-1744.
16. C. Valente, S. Calimsiz, K. H. Hoi, D. Mallik, M. Sayah and M. G. Organ, *Angewandte Chemie-International Edition*, 2012, **51**, 3314-3332.
17. S. Wuertz and F. Glorius, *Accounts of Chemical Research*, 2008, **41**, 1523-1533.
18. D. S. McGuinness and K. J. Cavell, *Organometallics*, 2000, **19**, 741-748.
19. M. S. Viciu, R. F. Germaneau, O. Navarro-Fernandez, E. D. Stevens and S. P. Nolan, *Organometallics*, 2002, **21**, 5470-5472.
20. E. A. B. Kantchev, C. J. O'Brien and M. G. Organ, *Angewandte Chemie-International Edition*, 2007, **46**, 2768-2813.
21. W. A. Herrmann, M. Elison, J. Fischer, C. Kocher and G. R. J. Artus, *Angewandte Chemie-International Edition in English*, 1995, **34**, 2371-2374.
22. G. C. Vougioukalakis and R. H. Grubbs, *Chemical Reviews*, 2010, **110**, 1746-1787.
23. F. C. Courchay, J. C. Sworen and K. B. Wagener, *Macromolecules*, 2003, **36**, 8231-8239.
24. U. L. Dharmasena, H. M. Foucault, E. N. dos Santos, D. E. Fogg and S. P. Nolan, *Organometallics*, 2005, **24**, 1056-1058.
25. S. Diez-Gonzalez, N. Marion and S. P. Nolan, *Chemical Reviews*, 2009, **109**, 3612-3676.

26. in *N-Heterocyclic Carbenes in Transition Metal Catalysis*, ed. F. Glorius, Editon edn., 2007, vol. 21, pp. 1-231.
27. L. Mercks and M. Albrecht, *Chemical Society Reviews*, **2010**, **39**, 1903-1912.
28. K. Oisaki, Q. Li, H. Furukawa, A. U. Czaja and O. M. Yaghi, *Journal of the American Chemical Society*, 2010, **132**, 9262-9264.
29. K. M. Lee, C. K. Lee and I. J. B. Lin, *Angewandte Chemie-International Edition in English*, 1997, **36**, 1850-1852.
30. A. J. Boydston, K. A. Williams and C. W. Bielawski, *Journal of the American Chemical Society*, 2005, **127**, 12496-12497.
31. R. Visbal and M. Concepcion Gimeno, *Chemical Society Reviews*, 2014, **43**, 3551-3574.
32. S. A. Patil, S. A. Patil, R. Patil, R. S. Keri, S. Budagumpi, G. R. Balakrishna and M. Tacke, *Future Medicinal Chemistry*, 2015, **7**, 1305-1333.
33. K. M. Hindi, M. J. Panzner, C. A. Tessier, C. L. Cannon and W. J. Youngs, *Chemical Reviews*, 2009, **109**, 3859-3884.
34. S. Diez-Gonzalez and S. P. Nolan, *Coordination Chemistry Reviews*, 2007, **251**, 874-883.
35. H. Jacobsen, A. Correa, A. Poater, C. Costabile and L. Cavallo, *Coordination Chemistry Reviews*, 2009, **253**, 687-703.
36. R. H. Crabtree, *Journal of Organometallic Chemistry*, 2005, **690**, 5451-5457.
37. S. J. Lippard, *Science*, 1982, **218**, 1075-1082.
38. C. Marzano, V. Gandin, A. Folda, G. Scutari, A. Bindoli and M. P. Rigobello, *Free Radical Biology and Medicine*, 2007, **42**, 872-881.
39. S. B. Aher, P. N. Muskawar, K. Thenmozhi and P. R. Bhagat, *European Journal of Medicinal Chemistry*, 2014, **81**, 408-419.
40. M. Skander, P. Retailleau, B. Bourrie, L. Schio, P. Mailliet and A. Marinetti, *Journal of Medicinal Chemistry*, 2010, **53**, 2146-2154.
41. R. W.-Y. Sun, A. L.-F. Chow, X.-H. Li, J. J. Yan, S. S.-Y. Chui and C.-M. Che, *Chemical Science*, 2011, **2**, 728-736.
42. G. Dahm, E. Borre, G. Guichard and S. Bellemin-Lapponnaz, *European Journal of Inorganic Chemistry*, 2015, 1665-1668.
43. R. Rubbiani, I. Kitanovic, H. Alborzinia, S. Can, A. Kitanovic, L. A. Onambele, M. Stefanopoulou, Y. Geldmacher, W. S. Sheldrick, G. Wolber, A. Prokop, S. Woelfl and I. Ott, *Journal of Medicinal Chemistry*, 2010, **53**, 8608-8618.
44. R. Rubbiani, S. Can, I. Kitanovic, H. Alborzinia, M. Stefanopoulou, M. Kokoschka, S. Moenchgesang, W. S. Sheldrick, S. Woelfl and I. Ott, *Journal of Medicinal Chemistry*, 2011, **54**, 8646-8657.
45. W. Liu, K. Bendorf, M. Proetto, U. Abram, A. Hagenbach and R. Gust, *Journal of Medicinal Chemistry*, 2011, **54**, 8605-8615.
46. W. Liu, K. Bendorf, M. Proetto, A. Hagenbach, U. Abram and R. Gust, *Journal of Medicinal Chemistry*, 2012, **55**, 3713-3724.
47. P. C. Kunz, C. Wetzel, S. Koegel, M. U. Kassack and B. Spingler, *Dalton Transactions*, 2011, **40**, 35-37.
48. J. Weaver, S. Gaillard, C. Toye, S. Macpherson, S. P. Nolan and A. Riches, *Chemistry-a European Journal*, 2011, **17**, 6620-6624.
49. H. Sivaram, J. Tan and H. Han Vinh, *Dalton Transactions*, 2013, **42**, 12421-12428.

50. E. Schuh, C. Pflueger, A. Citta, A. Folda, M. P. Rigobello, A. Bindoli, A. Casini and F. Mohr, *Journal of Medicinal Chemistry*, 2012, **55**, 5518-5528.
51. L. Kaps, B. Biersack, H. Müller-Bunz, K. Mahal, J. Muenzner, M. Tacke, T. Müller and R. Schobert, *Journal of Inorganic Biochemistry*, 2012, **106**, 52-58.
52. J. Fernandez-Gallardo, B. T. Elie, M. Sanau and M. Contel, *Chemical Communications*, 2016, **52**, 3155-3158.
53. R. B. Bostancioglu, M. Kaya, A. T. Koparal and K. Benkli, *Anti-Cancer Drugs*, 2016, **27**, 225-234.
54. B. Bertrand, E. Bodio, P. Richard, M. Picquet, P. Le Gendre and A. Casini, *Journal of Organometallic Chemistry*, 2015, **775**, 124-129.
55. H. A. Mohamed and C. E. Willans, in *Organometallic Chemistry*, Specialist Periodical Reports, **2014**, vol. 39, pp. 26-50.
56. J. L. Hickey, R. A. Ruhayel, P. J. Barnard, M. V. Baker, S. J. Berners-Price and A. Filipovska, *Journal of the American Chemical Society*, 2008, **130**, 12570-12571.
57. E. Gallori, C. Vettori, E. Alessio, F. G. Vilchez, R. Vilaplana, P. Orioli, A. Casini and L. Messori, *Archives of Biochemistry and Biophysics*, 2000, **376**, 156-162.
58. J. Malina, O. Novakova, B. K. Keppler, E. Alessio and V. Brabec, *Journal of Biological Inorganic Chemistry*, 2001, **6**, 435-445.
59. N. Cetinbas, M. I. Webb, J. A. Dubland and C. J. Walsby, *Journal of Biological Inorganic Chemistry*, 2010, **15**, 131-145.
60. C. Tan, S. Hu, J. Liu and L. Ji, *European Journal of Medicinal Chemistry*, 2011, **46**, 1555-1563.
61. L. Oehninger, M. Stefanopoulou, H. Alborzinia, J. Schur, S. Ludewig, K. Namikawa, A. Munoz-Castro, R. W. Koester, K. Baumann, S. Woelfl, W. S. Sheldrick and I. Ott, *Dalton Transactions*, 2013, **42**, 1657-1666.
62. C.-H. Wang, W.-C. Shih, H. C. Chang, Y.-Y. Kuo, W.-C. Hung, T.-G. Ong and W.-S. Li, *Journal of Medicinal Chemistry*, 2011, **54**, 5245-5249.
63. S. Budagumpi, R. A. Haque and A. W. Salman, *Coordination Chemistry Reviews*, 2012, **256**, 1787-1830.
64. J.-Y. Lee, J.-Y. Lee, Y.-Y. Chang, C.-H. Hu, N. M. Wang and H. M. Lee, *Organometallics*, 2015, **34**, 4359-4368.
65. F. Hackenberg and M. Tacke, *Dalton Transactions*, 2014, **43**, 8144-8153.
66. P. J. Barnard, M. V. Baker, S. J. Berners-Price and D. A. Day, *Journal of Inorganic Biochemistry*, 2004, **98**, 1642-1647.
67. M. V. Baker, P. J. Barnard, S. J. Berners-Price, S. K. Brayshaw, J. L. Hickey, B. W. Skelton and A. H. White, *Dalton Transactions*, 2006, 3708-3715.
68. U. E. I. Horvath, G. Bentivoglio, M. Hummel, H. Schottenberger, K. Wurst, M. J. Nell, C. E. J. van Rensburg, S. Cronje and H. G. Raubenheimer, *New Journal of Chemistry*, 2008, **32**, 533-539.
69. B. Bertrand, L. Stefan, M. Pirrotta, D. Monchaud, E. Bodio, P. Richard, P. Le Gendre, E. Warmerdam, M. H. de Jager, G. M. M. Groothuis, M. Picquet and A. Casini, *Inorganic Chemistry*, 2014, **53**, 2296-2303.
70. P. de Fremont, E. D. Stevens, M. D. Eelman, D. E. Fogg and S. P. Nolan, *Organometallics*, 2006, **25**, 5824-5828.
71. F. Hackenberg, H. Mueller-Bunz, R. Smith, W. Streciwilk, X. Zhu and M. Tacke, *Organometallics*, 2014, **32**, 5551-5560.
72. J. Lemke, A. Pinto, P. Niehoff, V. Vasylyeva and N. Metzler-Nolte, *Dalton Transactions*, 2009, 7063-7070.

73. M. Chtchigrovsky, L. Eloy, H. Jullien, L. Saker, E. Segal-Bendirdjian, J. Poupon, S. Bombard, T. Cresteil, P. Retailleau and A. Marinetti, *Journal of Medicinal Chemistry*, 2013, **56**, 2074-2086.
74. A. Gautier and F. Cisnetti, *Metallomics*, 2011, **4**, 23-32.
75. S. Ray, R. Mohan, J. K. Singh, M. K. Samantaray, M. M. Shaikh, D. Panda and P. Ghosh, *Journal of the American Chemical Society*, 2007, **129**, 15042-15053.
76. R. A. Haque, A. W. Salman, S. Budagumpi, A. A.-A. Abdullah and A. M. S. A. Majid, *Metallomics*, 2013, **5**, 760-769.
77. G. Sava, S. Zorzet, C. Turrin, F. Vita, M. Soranzo, G. Zabucchi, M. Cocchietto, A. Bergamo, S. DiGiovine, G. Pezzoni, L. Sartor and S. Garbisa, *Clinical Cancer Research*, 2003, **9**, 1898-1905.
78. C. A. Vock, C. Scolaro, A. D. Phillips, R. Scopelliti, G. Sava and P. J. Dyson, *Journal of Medicinal Chemistry*, 2006, **49**, 5552-5561.
79. M.-L. Teyssot, A.-S. Jarrousse, M. Manin, A. Chevy, S. Roche, F. Norre, C. Beaudoin, L. Morel, D. Boyer, R. Mahiou and A. Gautier, *Dalton Transactions*, 2009, 6894-6902.
80. R. A. Bassani, J. W. M. Bassani and D. M. Bers, *Journal of Physiology-London*, 1992, **453**, 591-608.
81. A. J. Arduengo, H. V. R. Dias, J. C. Calabrese and F. Davidson, *Organometallics*, 1993, **12**, 3405-3409.
82. O. Guerret, S. Sole, H. Gornitzka, M. Teichert, G. Trinquier and G. Bertrand, *Journal of the American Chemical Society*, 1997, **119**, 6668-6669.
83. H. M. J. Wang and I. J. B. Lin, *Organometallics*, 1998, **17**, 972-975.
84. R. Z. Ku, J. C. Huang, J. Y. Cho, F. M. Kiang, K. R. Reddy, Y. C. Chen, K. J. Lee, J. H. Lee, G. H. Lee, S. M. Peng and S. T. Liu, *Organometallics*, 1999, **18**, 2145-2154.
85. W. A. Herrmann, S. K. Schneider, K. Öfele, M. Sakamoto and E. Herdtweck, *Journal of Organometallic Chemistry*, 2004, **689**, 2441-2449.
86. M. Mayr, K. Wurst, K. H. Ongania and M. R. Buchmeiser, *Chemistry-a European Journal*, 2004, **10**, 1256-1266.
87. O. Guerret, S. Sole, H. Gornitzka, G. Trinquier and G. Bertrand, *Journal of Organometallic Chemistry*, 2000, **600**, 112-117.
88. A. R. Chianese, A. Kovacevic, B. M. Zeglis, J. W. Faller and R. H. Crabtree, *Organometallics*, 2004, **23**, 2461-2468.
89. J. C. Garrison and W. J. Youngs, *Chemical Reviews*, 2005, **105**, 3978-4008.
90. A. Caballero, E. Diez-Barra, F. A. Jalon, S. Merino and J. Tejada, *Journal of Organometallic Chemistry*, 2001, **617**, 395-398.
91. A. Caballero, E. Diez-Barra, F. A. Jalon, S. Merino, A. M. Rodriguez and J. Tejada, *Journal of Organometallic Chemistry*, 2001, **627**, 263-264.
92. M. A. Fox, M. F. Mahon, N. J. Patmore and A. S. Weller, *Inorganic Chemistry*, 2002, **41**, 4567-4573.
93. X. L. Hu, I. Castro-Rodriguez, K. Olsen and K. Meyer, *Organometallics*, 2004, **23**, 755-764.
94. A. A. D. Tulloch, A. A. Danopoulos, S. Winston, S. Kleinhenz and G. Eastham, *Journal of the Chemical Society-Dalton Transactions*, 2000, 4499-4506.
95. J. J. Van Veldhuizen, S. B. Garber, J. S. Kingsbury and A. H. Hoveyda, *Journal of the American Chemical Society*, 2002, **124**, 4954-4955.

96. B. Bildstein, M. Malaun, H. Kopacka, K. Wurst, M. Mitterbock, K. H. Ongania, G. Opromolla and P. Zanello, *Organometallics*, 1999, **18**, 4325-4336.
97. J. C. Garrison, R. S. Simons, C. A. Tessier and W. J. Youngs, *Journal of Organometallic Chemistry*, 2003, **673**, 1-4.
98. A. Kascatan-Nebioglu, M. J. Panzner, J. C. Garrison, C. A. Tessier and W. J. Youngs, *Organometallics*, 2004, **23**, 1928-1931.
99. C. A. Quezada, J. C. Garrison, M. J. Panzner, C. A. Tessier and W. J. Youngs, *Organometallics*, 2004, **23**, 4846-4848.
100. P. L. Arnold, A. C. Scarisbrick, A. J. Blake and C. Wilson, *Chemical Communications*, 2001, 2340-2341.
101. A. A. Danopoulos, A. A. D. Tulloch, S. Winston, G. Eastham and M. B. Hursthouse, *Dalton Transactions*, 2003, 1009-1015.
102. L. G. Bonnet, R. E. Douthwaite and R. Hodgson, *Organometallics*, 2003, **22**, 4384-4386.
103. K. S. Coleman, H. T. Chamberlayne, S. Turberville, M. L. H. Green and A. R. Cowley, *Dalton Transactions*, 2003, 2917-2922.
104. L. G. Bonnet, R. E. Douthwaite and B. M. Kariuki, *Organometallics*, 2003, **22**, 4187-4189.
105. A. O. Larsen, W. Leu, C. N. Oberhuber, J. E. Campbell and A. H. Hoveyda, *Journal of the American Chemical Society*, 2004, **126**, 11130-11131.
106. L. G. Bonnet, R. E. Douthwaite, R. Hodgson, J. Houghton, B. M. Kariuki and S. Simonovic, *Dalton Transactions*, 2004, 3528-3535.
107. J. J. Van Veldhuizen, J. E. Campbell, R. E. Giudici and A. H. Hoveyda, *Journal of the American Chemical Society*, 2005, **127**, 6877-6882.
108. P. L. Chiu, C. Y. Chen, J. Y. Zeng, C. Y. Lu and H. M. Lee, *Journal of Organometallic Chemistry*, 2005, **690**, 1682-1687.
109. A. R. Chianese, B. M. Zeglis and R. H. Crabtree, *Chemical Communications*, 2004, 2176-2177.
110. H. P. Chen, R. Z. Ku and S. T. Liu, *Journal of the Chinese Chemical Society*, 2001, **48**, 13-16.
111. S. T. Liu and K. R. Reddy, *Chemical Society Reviews*, 1999, **28**, 315-322.
112. A. M. Magill, D. S. McGuinness, K. J. Cavell, G. J. P. Britovsek, V. C. Gibson, A. J. P. White, D. J. Williams, A. H. White and B. W. Skelton, *Journal of Organometallic Chemistry*, 2001, **617**, 546-560.
113. D. J. Nielsen, K. J. Cavell, B. W. Skelton and A. H. White, *Inorganica Chimica Acta*, 2002, **327**, 116-125.
114. A. A. D. Tulloch, S. Winston, A. A. Danopoulos, G. Eastham and M. B. Hursthouse, *Dalton Transactions*, 2003, 699-708.
115. R. E. Douthwaite, J. Houghton and B. M. Kariuki, *Chemical Communications*, 2004, 698-699.
116. E. Mas-Marza, M. Poyatos, M. Sanau and E. Peris, *Inorganic Chemistry*, 2004, **43**, 2213-2219.
117. A. Alexakis, C. L. Winn, F. Guillen, J. Pytkowicz, S. Roland and P. Mangeney, *Advanced Synthesis & Catalysis*, 2003, **345**, 345-348.
118. S. K. Schneider, W. A. Herrmann and E. Herdtweck, *Zeitschrift Fur Anorganische Und Allgemeine Chemie*, 2003, **629**, 2363-2370.
119. X. L. Hu, I. Castro-Rodriguez and K. Meyer, *Journal of the American Chemical Society*, 2003, **125**, 12237-12245.
120. Y. A. Wanniarachchi, M. A. Khan and L. M. Slaughter, *Organometallics*, 2004, **23**, 5881-5884.

121. P. de Fremont, N. M. Scott, E. D. Stevens and S. P. Nolan, *Organometallics*, 2005, **24**, 2411-2418.
122. H. M. Lee, P. L. Chiu, C. H. Hu, C. L. Lai and Y. C. Chou, *Journal of Organometallic Chemistry*, 2005, **690**, 403-414.
123. V. J. Catalano, M. A. Malwitz and A. O. Etogo, *Inorganic Chemistry*, 2004, **43**, 5714-5724.
124. H. J. Klasen, *Burns*, 2000, **26**, 131-138.
125. A. B. G. Lansdown and A. Williams, *Journal of wound care*, 2004, **13**, 131-136.
126. H. J. Klasen, *Burns*, 2000, **26**, 117-130.
127. A. B. G. Lansdown, *Journal of wound care*, 2002, **11**, 125-130.
128. A. Melaiye and W. J. Youngs, *Expert Opinion on Therapeutic Patents*, 2005, **15**, 125-130.
129. W. J. Youngs, A. R. Knapp, P. O. Wagers and C. A. Tessier, *Dalton Transactions*, 2012, **41**, 327-336.
130. A. Kascatan-Nebioglu, M. J. Panzner, C. A. Tessier, C. L. Cannon and W. J. Youngs, *Coordination Chemistry Reviews*, 2007, **251**, 884-895.
131. A. B. G. Lansdown, *Current problems in dermatology*, 2006, **33**, 17-34.
132. P. L. Drake and K. J. Hazelwood, *Ann. Occup. Hyg.*, 2005, **49**, 575-585.
133. Y. Kim, H. S. Suh, H. J. Cha, S. H. Kim, K. S. Jeong and D. H. Kim, *American Journal of Industrial Medicine*, 2009, **52**, 246-250.
134. M. Rai, A. Yadav and A. Gade, *Biotechnology Advances*, 2009, **27**, 76-83.
135. J. S. Kim, E. Kuk, K. N. Yu, J.-H. Kim, S. J. Park, H. J. Lee, S. H. Kim, Y. K. Park, Y. H. Park, C.-Y. Hwang, Y.-K. Kim, Y.-S. Lee, D. H. Jeong and M.-H. Cho, *Nanomedicine-Nanotechnology Biology and Medicine*, 2007, **3**, 95-101.
136. V. K. Sharma, R. A. Yngard and Y. Lin, *Advances in Colloid and Interface Science*, 2009, **145**, 83-96.
137. L. Rizzello and P. P. Pompa, *Chemical Society Reviews*, 2014, **43**, 1501-1518.
138. J. Liu, D. A. Sonshine, S. Shervani and R. H. Hurt, *Acs Nano*, 2010, **4**, 6903-6913.
139. A. Melaiye, R. S. Simons, A. Milsted, F. Pingitore, C. Wesdemiotis, C. A. Tessier and W. J. Youngs, *Journal of Medicinal Chemistry*, 2004, **47**, 973-977.
140. A. Melaiye, Z. H. Sun, K. Hindi, A. Milsted, D. Ely, D. H. Reneker, C. A. Tessier and W. J. Youngs, *Journal of the American Chemical Society*, 2005, **127**, 2285-2291.
141. A. A. Elzatahry, A. M. Al-Enizi, E. A. Elsayed, R. R. Butorac, S. S. Al-Deyab, M. A. M. Wadaan and A. H. Cowley, *International Journal of Nanomedicine*, **7**, 2829-2832.
142. J. G. Leid, A. J. Ditto, A. Knapp, P. N. Shah, B. D. Wright, R. Blust, L. Christensen, C. B. Clemons, J. P. Wilber, G. W. Young, A. G. Kang, M. J. Panzner, C. L. Cannon, Y. H. Yun, W. J. Youngs, N. M. Seckinger and E. K. Cope, *Journal of Antimicrobial Chemotherapy*, **67**, 138-148.
143. K. M. Hindi, A. J. Ditto, M. J. Panzner, D. A. Medvetz, D. S. Han, C. E. Hovis, J. K. Hilliard, J. B. Taylor, Y. H. Yun, C. L. Cannon and W. J. Youngs, *Biomaterials*, 2009, **30**, 3771-3779.
144. A. Kascatan-Nebioglu, A. Melaiye, K. Hindi, S. Durmus, M. J. Panzner, L. A. Hogue, R. J. Mallett, C. E. Hovis, M. Coughenour, S. D. Crosby, A. Milsted, D. L. Ely, C. A. Tessier, C. L. Cannon and W. J. Youngs, *Journal of Medicinal Chemistry*, 2006, **49**, 6811-6818.

145. K. M. Hindi, T. J. Siciliano, S. Durmus, M. J. Panzner, D. A. Medvetz, D. V. Reddy, L. A. Hogue, C. E. Hovis, J. K. Hilliard, R. J. Mallet, C. A. Tessier, C. L. Cannon and W. J. Youngs, *Journal of Medicinal Chemistry*, 2008, **51**, 1577-1583.
146. S. Patil, K. Dietrich, A. Deally, B. Gleeson, H. Mueller-Bunz, F. Paradisi and M. Tacke, *Helvetica Chimica Acta*, 2010, **93**, 2347-2364.
147. S. Patil, J. Claffey, A. Deally, M. Hogan, B. Gleeson, L. M. M. Mendez, H. Mueller-Bunz, F. Paradisi and M. Tacke, *European Journal of Inorganic Chemistry*, 2010, 1020-1031.
148. S. Patil, A. Deally, B. Gleeson, H. Mueller-Bunz, F. Paradisi and M. Tacke, *Applied Organometallic Chemistry*, 2010, **24**, 781-793.
149. S. Patil, A. Deally, F. Hackenberg, L. Kaps, H. Mueller-Bunz, R. Schobert and M. Tacke, *Helvetica Chimica Acta*, 2011, **94**, 1551-1562.
150. S. Patil, A. Deally, B. Gleeson, H. Mueller-Bunz, F. Paradisi and M. Tacke, *Metallomics*, 2011, **3**, 74-88.
151. F. Hackenberg, G. Lally, H. Mueller-Bunz, F. Paradisi, D. Quaglia, W. Streciwilk and M. Tacke, *Journal of Organometallic Chemistry*, 2012, **717**, 123-134.
152. S. Roland, C. Jolivalt, T. Cresteil, L. Eloy, P. Bouhours, A. Hequet, V. Mansuy, C. Vanucci and J.-M. Paris, *Chemistry-a European Journal*, 2011, **17**, 1442-1446.
153. R. A. Haque, M. Z. Ghdayeb, A. W. Salman, S. Budagumpi, M. B. K. Ahamed and A. M. S. A. Majid, *Inorganic Chemistry Communications*, 2012, **22**, 113-119.
154. T. J. Siciliano, M. C. Deblock, K. M. Hindi, S. Durmus, M. J. Panzner, C. A. Tessier and W. J. Youngs, *Journal of Organometallic Chemistry*, 2011, **696**, 1066-1071.
155. D. C. F. Monteiro, R. M. Phillips, B. D. Crossley, J. Fielden and C. E. Willans, *Dalton Transactions*, 2012, **41**, 3720-3725.
156. L. Oehninger, R. Rubbiani and I. Ott, *Dalton Transactions*, 2013, **42**, 3269-3284.
157. R. A. Haque, M. Z. Ghdayeb, S. Budagumpi, A. W. Salman, M. B. K. Ahamed and A. M. S. A. Majid, *Inorganica Chimica Acta*, 2013, **394**, 519-525.
158. M. Pellei, V. Gandin, M. Marinelli, C. Marzano, M. Yousufuddin, H. V. R. Dias and C. Santini, *Inorganic Chemistry*, 2012, **51**, 9873-9882.
159. L. Eloy, A.-S. Jarrousse, M.-L. Teyssot, A. Gautier, L. Morel, C. Jolivalt, T. Cresteil and S. Roland, *Chemmedchem*, 2012, **7**, 805-814.
160. D. A. Medvetz, K. M. Hindi, M. J. Panzner, A. J. Ditto, Y. H. Yun and W. J. Youngs, *Metal-based drugs*, 2008, **2008**.
161. S. Roland, C. Jolivalt, T. Cresteil, L. Eloy, P. Bouhours, A. Hequet, V. Mansuy, C. Vanucci and J. M. Paris, *Chemistry-a European Journal*, 2011, **17**, 1442-1446.

## Chapter 2

### Synthesis and anticancer activity of silver(I)-*N*-heterocyclic carbene complexes derived from the natural xanthine products caffeine, theophylline and theobromine

#### 2.1 Introduction

Natural xanthine derivatives caffeine, theophylline and theobromine are found in cocoa beans and tea leaves, are readily available and have low toxicity.<sup>1</sup> Medicinally, xanthines have been used as central nervous system stimulants,<sup>2</sup> diuretics<sup>3</sup> and smooth muscle relaxants.<sup>4-6</sup> Caffeine has been consumed for centuries in different beverages, and its pharmacokinetics such as absorption and metabolism, including its demethylation to paraxanthine, theophylline and theobromine, are well studied (**Figure 2.1**).<sup>7, 8</sup>

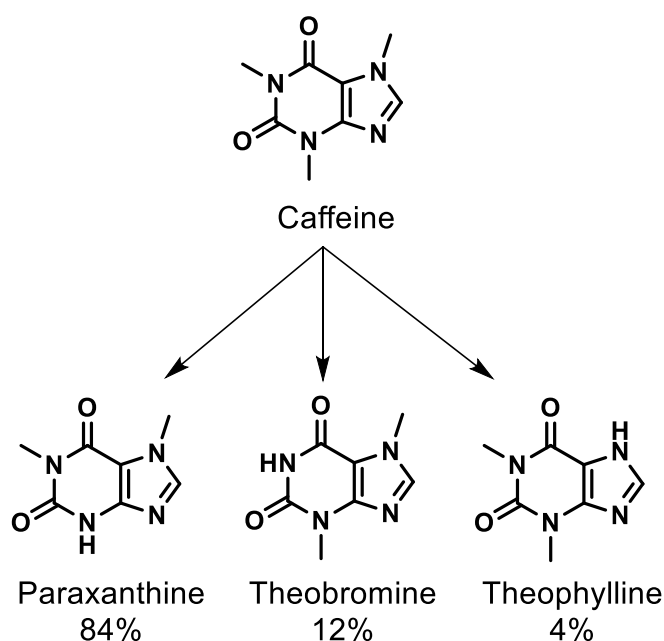
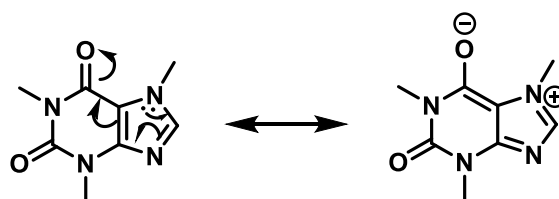


**Figure 2.1:** Metabolism of caffeine with its reported percentages of metabolites<sup>7</sup>

As the aim of this project is to use natural precursors to synthesise Ag(I)-NHC complexes with non-toxic metabolites, caffeine theophylline and theobromine were used in the synthesis of imidazolium salts, which were subsequently deprotonated and coordinated to silver for cancer therapy.

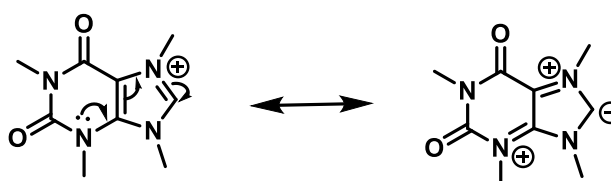
## 2.2 Ligand synthesis

Caffeine, theophylline and theobromine were used as precursors for the synthesis of imidazolium salts. Substitution on the second nitrogen of these xanthines was anticipated to be challenging due to the delocalisation (electron withdrawing) of electrons into the backbone dioxypyrimidine ring. This negative mesomeric effect (-M, **Scheme 2.1**) renders the unsubstituted nitrogen atom on the imidazole ring weakly basic and a poor nucleophile, constraining a normally simple alkylation.



**Scheme 2.1:** Mesomeric effect of caffeine<sup>9</sup>

Contrary to caffeine, N-substituted imidazolium salts have a positive mesomeric effect (+M effect), where electrons are released from the dioxypyrimidine to the imidazolium ring (**Scheme 2.2**). This effect stabilises a subsequent metal-carbene bond as it permits the donation of the electrons from the carbene to metal d orbitals.



**Scheme 2.2:** Mesomeric effects of xanthinium salts<sup>9</sup>

### 2.2.1 Imidazolium salts prepared from caffeine

Caffeine was used to synthesise imidazolium salt **L1**, and according to a literature procedure by Youngs *et al.*, heating caffeine at reflux with excess methyl iodide in DMF yields the desired 1,3,7,9-tetramethylxanthinium iodide.<sup>1</sup> Several attempts to prepare the desired methylated imidazolium salt were made using Youngs procedure and modified conditions, including changes of solvent, temperature, reaction time, and equivalents of methyl iodide (**Table 2.1**).

Reaction in acetonitrile yields the imidazolium salt after 48 hours of heating in a sealed vessel with 20 equivalents of methyl iodide (**Table 2.1**, entry 4). Since methyl iodide is volatile and has a boiling point of 40°C, using a sealed system prevents its escape and increases pressure. Changing the solvent to DMF and heating to 145°C resulted in an increase in yield slightly, even with less equivalents of methyl iodide (entry 5). This could be attributed to the higher solubility of caffeine in DMF though is likely due to the higher reaction temperature. Doubling the equivalents of methyl iodide in DMF increased the yield further to 61% (entry 6). Using a sealed system significantly increased the yield to 78% in DMF (entry 7).

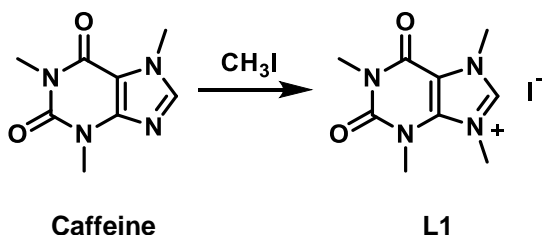
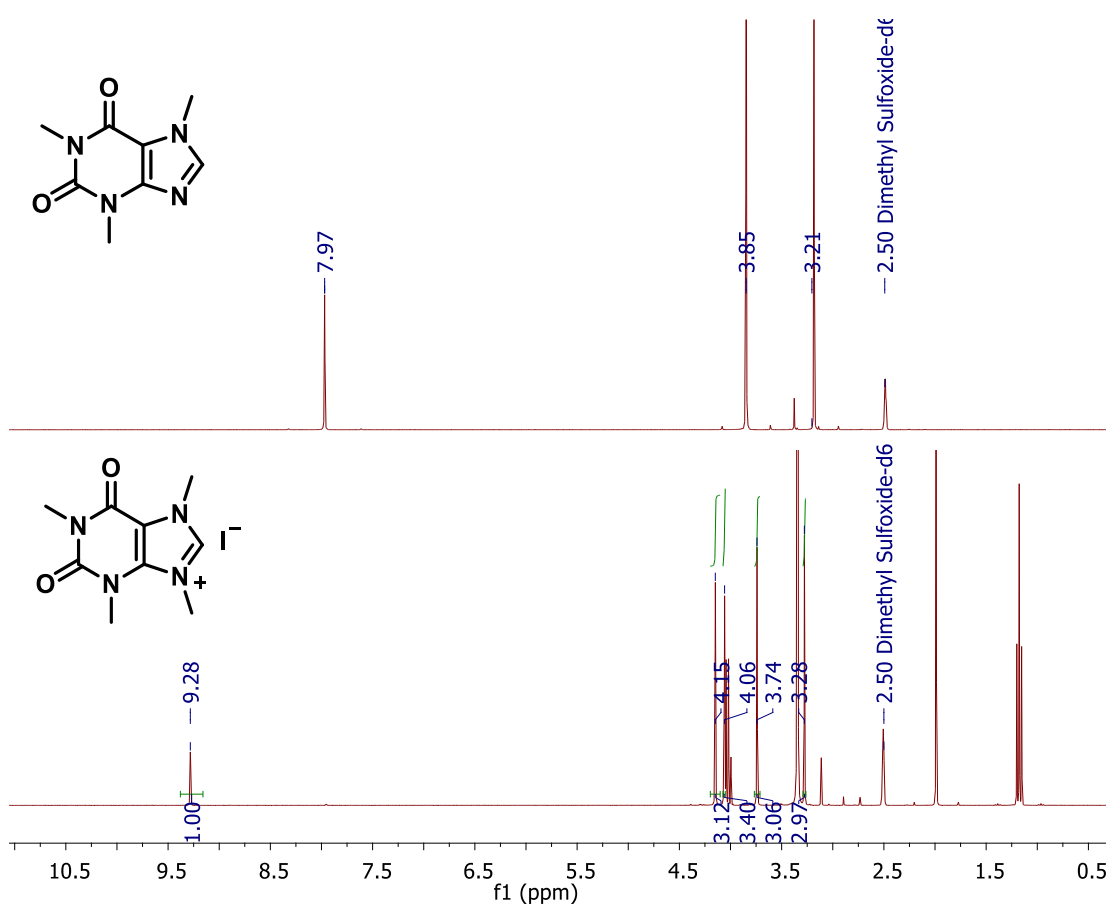


**Table 2.1:** Methylation of caffeine under different reaction conditions

|   | Solvent | Eq. of CH <sub>3</sub> I | Temp (°C)        | Time (hours) | Yield (%) <sup>b</sup> |
|---|---------|--------------------------|------------------|--------------|------------------------|
| 1 | MeCN    | 10                       | 90               | 24           | 0                      |
| 2 | MeCN    | 20                       | 90               | 24           | 0                      |
| 3 | MeCN    | 20                       | 90               | 48           | 0                      |
| 4 | MeCN    | 20                       | 90 <sup>a</sup>  | 48           | 46                     |
| 5 | DMF     | 10                       | 145              | 24           | 51                     |
| 6 | DMF     | 20                       | 145              | 24           | 61                     |
| 7 | DMF     | 20                       | 145 <sup>a</sup> | 24           | 78                     |

<sup>a</sup> sealed reaction vessel <sup>b</sup> determined using isolated yield

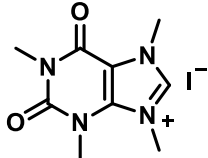
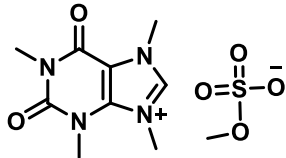
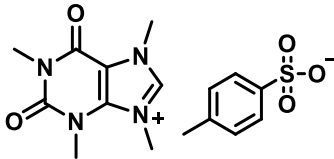
The formation of imidazolium iodide **L1** can be observed in the  $^1\text{H}$  NMR spectrum by the downfield shift of the carbon atom between the two nitrogen atoms of the imidazole / imidazolium ring (C1) (**Figure 2.2**). The C1 proton in caffeine, which appears at 8 ppm is shifted to 9.28 ppm in the imidazolium iodide, along with the presence of four singlet peaks between 4.2-3.2 ppm that correspond to the four methyl groups. **L1** was further characterised using  $^{13}\text{C}\{^1\text{H}\}$  NMR spectroscopy and HRMS. A peak corresponding to  $[\text{M}-\text{I}]^+$  is observed at  $m/z$  209.1038 in the mass spectrum (ESI+).



**Figure 2.2:** Overlay of the  $^1\text{H}$ -NMR spectra (300 MHz,  $\text{DMSO}-d_6$ ) of caffeine (top) and its methylated imidazolium iodide (bottom). Suppression of the  $\text{H}_2\text{O}$  peak was performed, therefore peaks in the same region are correspondingly suppressed

Investigation into the use of other methylating agents in place of methyl iodide was carried out. The reaction of caffeine with 1.2 equivalents of dimethyl sulphate and methyl tosylate led to similar yields as 20 equivalents of methyl iodide (**Table 2.2**). Imidazolium salts **L1.1** and **L1.2** were successfully synthesised, however the products were sticky and challenging to purify and isolate, even after extraction of the product into CH<sub>2</sub>Cl<sub>2</sub> and several re-crystallisations. Conversely, excess methyl iodide is easily removed from the solution by heating *in vacuo* to yield a white solid. Methyl iodide was therefore used going forward.

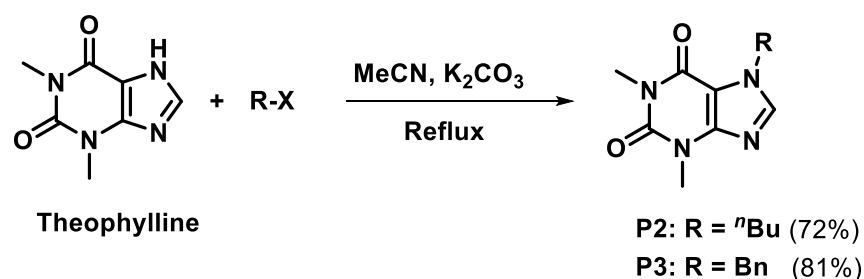
**Table 2.2** : Methylation of caffeine using different reagents to form imidazolium salts **L1**, **L1.1** and **L1.2**

|   | Methylating Agent | Equivalents | Imidazolium salt   | Yield (%) <sup>a</sup> |
|---|-------------------|-------------|--|------------------------|
| 1 | Methyl iodide     | 20          | <br>L1    | 78                     |
| 2 | Dimethyl sulfate  | 1.2         | <br>L1.1 | 75                     |
| 3 | Methyl tosylate   | 1.2         | <br>L1.2 | 71                     |

<sup>a</sup> determined using isolated yield

### 2.2.2 Imidazolium salts prepared from theophylline

To synthesise imidazolium salts with a variety of N-substituents other than methyl, it was necessary to use theophylline as the precursor as opposed to caffeine. Efforts were made to alkylate caffeine using benzyl bromide and butyl iodide, including reactions in a sealed vessel in DMF and microwave reactions under pressure. These led to very poor yields of the desired imidazolium salts, which is likely due to the relatively low basicity of the nitrogen atom as shown in **Scheme 2.1**. The two nitrogen atoms on the imidazole ring of theophylline are unsubstituted, with one bearing an acidic proton. This can be deprotonated to render a nucleophilic nitrogen atom for substitution. It was possible to alkylate theophylline with both a benzyl and a butyl group, in the presence of a base, furnishing white solids **P1** and **P2** with yields in excess of 70% (**Scheme 2.3**). Following the substitution of the first nitrogen atom, the theophylline based ligand precursors **P2** and **P3** are similar to caffeine as three of the nitrogens of the xanthine backbone are substituted and thus have the same mesomeric effect.



**Scheme 2.3:** Alkylation of theophylline with benzyl bromide and butyl iodide

Methylation of **P1** using methyl iodide under microwave conditions (17.5 bar) gave imidazolium salt **L2** (**Table 2.3**). All microwave reactions were prepared with 3 mL of DMF in microwave vessels fitted with a rubber seal. This rubber fitting allows pressure release in order to maintain the set pressure, and possibly results in loss of volatile methyl iodide. Increasing the reaction time from 20 to 30 minutes at 100°C (Entries 1 and 2, **Table 2.3**) has minimal effect on the yield of **L2** while increasing the temperature to 145°C does have a positive effect. Increasing the equivalents of methyl iodide from 20 to 30 (Entries 3 and 4) at 145°C increases the yield from 36% to 54%. 30 equivalents of methyl iodide and a reaction time of 30 minutes furnishes 77% yield (entry 5). Treating **P2** in the same manner as caffeine by heating in a sealed vessel in DMF with excess methyl iodide gave **L2** in a yield of 87% (**Scheme 2.4**), while reaction with **P3** gave **L3** in 20% yield.

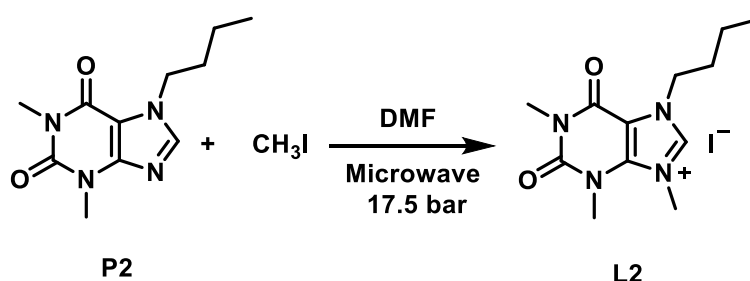
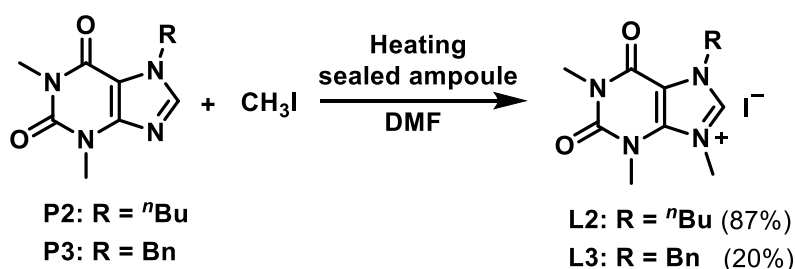


**Table 2.3:** Microwave reactions to synthesise imidazolium iodide **L2**

|   | Temp (°C) | Eq. CH <sub>3</sub> I | Time (minutes) | Yield (%) <sup>a</sup> |
|---|-----------|-----------------------|----------------|------------------------|
| 1 | 100       | 30                    | 20             | 6                      |
| 2 | 100       | 30                    | 30             | 7                      |
| 3 | 145       | 20                    | 20             | 36                     |
| 4 | 145       | 30                    | 20             | 54                     |
| 5 | 145       | 30                    | 30             | 77                     |

<sup>a</sup> determined by peak integrations in <sup>1</sup>H NMR spectrum.



**Scheme 2.4:** Synthesis of imidazolium salts **L2** and **L3**

Alkylation of theophylline using benzyl bromide or butyl iodide, followed by methylation to form the imidazolium iodide can be monitored using  $^1\text{H}$  NMR spectroscopy (**Figure 2.3**). Upon alkylation, the resonances (4.23, 1.74, 1.21 and 0.88 ppm) corresponding to the  $n$ -butyl protons in **P2** (**Figure 2.3**, middle) display the most substantial shift from theophylline (top). The proton on the C1 carbon and the methyl proton peaks only shift by 0.02-0.05 ppm. Significant shifts in the  $^1\text{H}$ -NMR spectrum between **P2** (middle) and **L2** (bottom) can be observed; the proton on the C1 carbon shifts downfield from 8.09 ppm to 9.41 ppm in **L2**. The singlet peaks corresponding to the backbone methyl groups also shift downfield significantly, while the  $\text{CH}_3$  (0.88 ppm) and  $\text{CH}_2$  (4.23, 1.74 and 1.21 ppm) peaks of the  $n$ -butyl group only shift slightly.

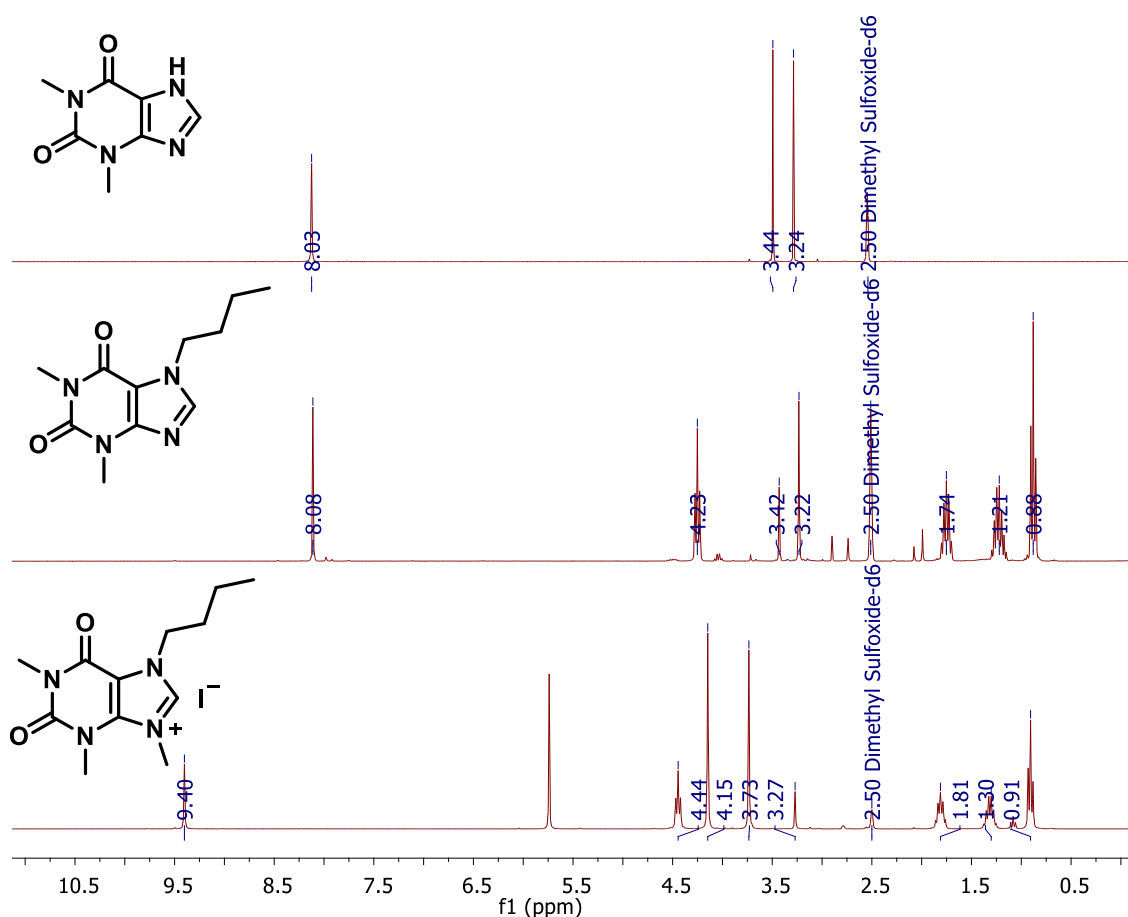


**Figure 2.3:**  $^1\text{H}$  NMR spectra (300 MHz,  $\text{DMSO-d}_6$ ) of **theophylline** (top), **P2** (middle) and **L2** (bottom). Suppression of the  $\text{H}_2\text{O}$  peak was performed, therefore peaks in the same region are correspondingly suppressed.

Attempts to synthesise further imidazolium salts through reaction of **P1** or **P2** with benzyl bromide or  $n$ -butyl iodide were unsuccessful, likely due to the weak basicity of the nitrogen atom of the imidazole as discussed previously.

Heating **P3** at reflux with methyl tosylate results in imidazolium **L3.1** (**Figure 2.4**) in 35% yield. **P2** was unreactive under the same reaction conditions, demonstrating that methyl iodide as a more effective and general methylating agent. Single crystals of **L3.1** suitable for X-ray diffraction analysis were grown by the vapour diffusion of pentane into a concentrated solution of the ligand in  $\text{CH}_2\text{Cl}_2$ . It was found to crystallise in the triclinic crystal system, with the structural solution being performed in the space group  $P1$ . Inspection of the extended structure reveals the presence of  $\pi$ - $\pi$  stacking between the benzene ring of the tosylate and the xanthine ring of the ligand (**Figure 2.4**). The xanthine ring and the tosylate are coplanar, while the benzyl group is significantly bent out of plane due to the neighbouring bulky tosylate counterion. Two molecules of **L3.1** are present in the asymmetric unit.

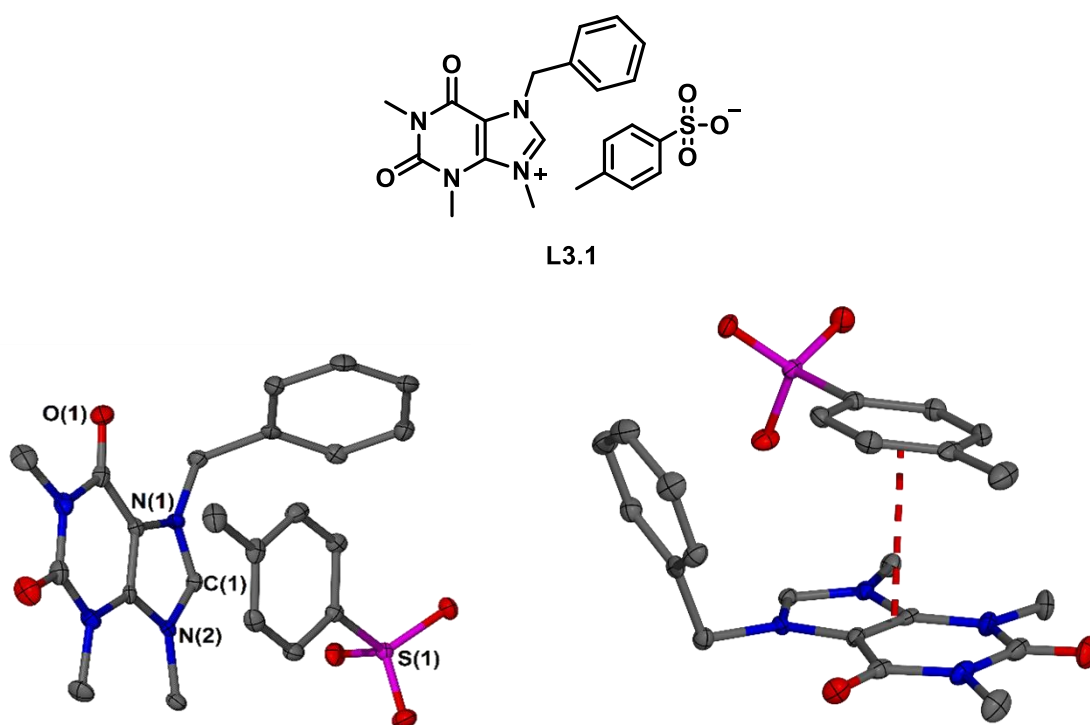


**Figure 2.4:** Molecular structure of **L3.1**. The molecular structure on the right depicts the  $\pi$ - $\pi$  stacking interactions between the xanthine ring and the benzene ring of the tosylate. Ellipsoids are drawn at 50% probability and H atoms are omitted for clarity

Single crystals of imidazolium salts **L2** and **L3** (**Figure 2.5**) were grown by vapour diffusion of n-pentane into concentration solutions of the ligands in CH<sub>2</sub>Cl<sub>2</sub>. While **L2** was found to crystallise in the monoclinic crystal system with the structural solution performed in the space group *Cc*, **L3** crystallised in the orthorhombic crystal system and the structural solution was performed in the space group *Pna2*<sub>1</sub>. The trimethyl xanthine ring system in both ligands exhibit a planar geometry with both the benzyl in **L3** and the butyl in **L2** groups oriented out of the defined planes (**Table 2.4**).

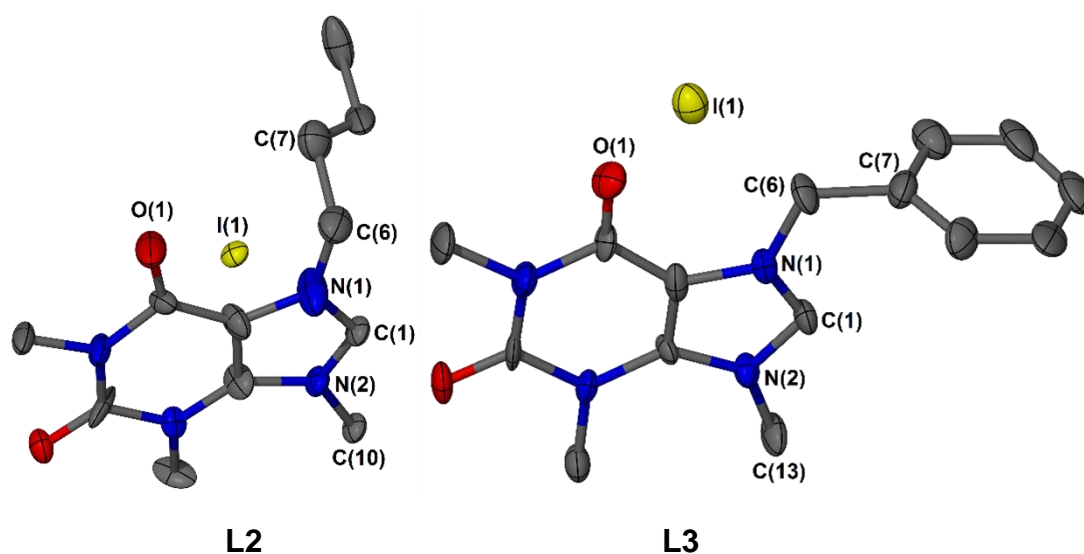
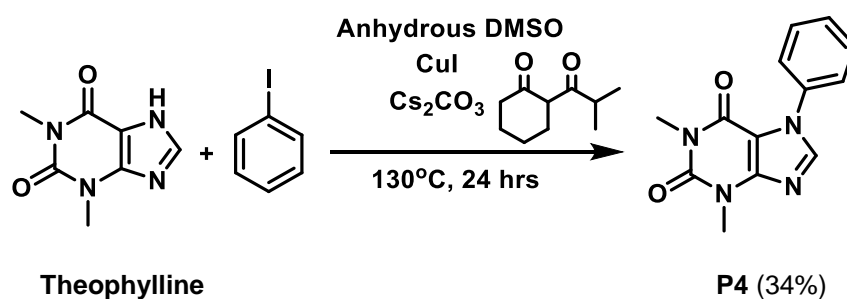


**Figure 2.5:** Molecular structures of **L2** and **L3**. Ellipsoids are drawn at 50% probability level and H atoms are omitted for clarity

**Table 2.4:** Selected bond lengths and angles for **L2**, **L3** and **L3.1** derived from theophylline

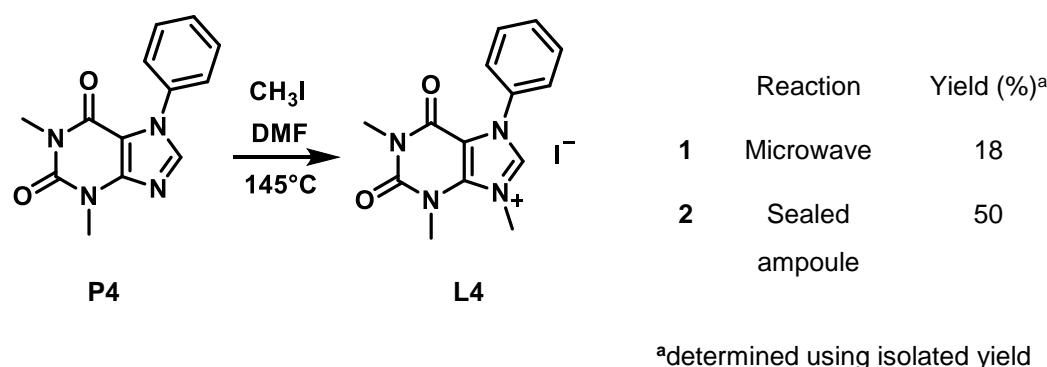
| Bond lengths (Å) and angles (°) | <b>L2</b> | <b>L3</b>  | <b>L3.1</b> |
|---------------------------------|-----------|------------|-------------|
| N1-C1-N2                        | 113.4(11) | 108.8(8)   | 110.2(3)    |
| N1-C6-C7                        | 113.6(13) | 108.2(9)   | 112.0(3)    |
| C1-N1-C6                        | 129.0(12) | 125.5(8)   | 123.0(3)    |
| N1-C1                           | 1.344(16) | 1.285 (14) | 1.313(5)    |
| N1-C6                           | 1.484(18) | 1.513(13)  | 1.487(5)    |

Although the benzyl group is seemingly slightly more restricted than the butyl group in the solid state structure, due to its flexibility it is not considered a bulky group hence will not in theory hinder the release rate of silver in solution. An aromatic ring that is directly attached to the imidazole would provide more steric protection and kinetic stabilisation of the Ag(I)-NHC bond, which may lead to a prolonged release of silver *in vivo*. Therefore, a phenyl derivative was synthesised using an Ullmann coupling reaction (**Scheme 2.5**). The reaction was initially performed with DL-proline as the ligand though no product was formed. Modification of the reaction by replacing DL-proline with isobutyryl cyclohexanone rendered the desired product **P4** in DMSO at 130°C.



**Scheme 2.5:** Synthesis of phenyl substituted ligand precursor **P4** from theophylline using the Ullmann reaction

Methylation of **P4** to form **L4** was performed in both a sealed vessel and in a microwave (**Scheme 2.6**). The yield obtained in a sealed vessel was over double that obtained in the microwave, demonstrating again the higher efficiency of a sealed system. Single crystals of **L4** were grown by slow evaporation of MeCN. **L4** crystallised in the monoclinic crystal system with the structural solution performed in the space group  $P2_1/n$ . The imidazolium crystallised with two molecules of water though there is no evidence of hydrogen bonding between the water and the iodide counterion. The direct attachment of an aromatic phenyl ring to the imidazole renders it almost coplanar in the solid state, increasing the intermolecular  $\pi$  overlap between the two aromatic systems and significantly shortening the N1-C6 bond length to 1.438 Å (5) versus N1-C6 bond length in **L2**, **L3** and **L3.1** which are between 1.48-1.51 Å.



**Scheme 2.6:** Synthesis imidazolium salt **L4**.

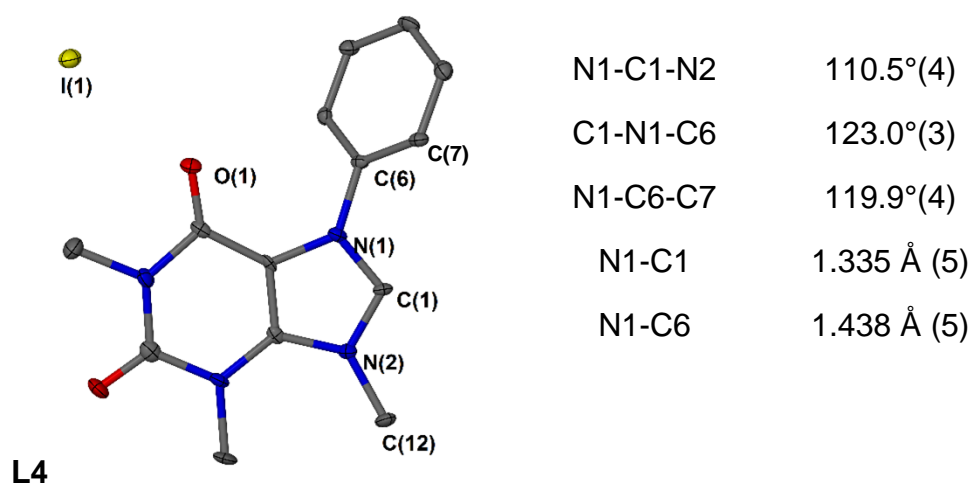
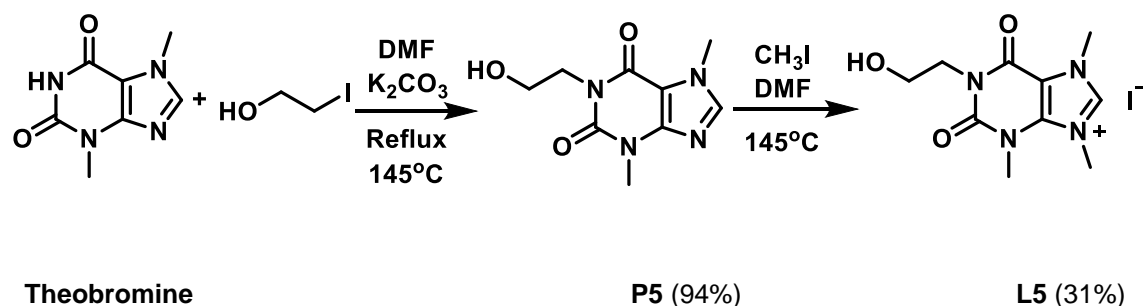


**Figure 2.6:** Molecular structure imidazolium salt **L4**. Ellipsoids are drawn at 50% probability level. Water molecules and H atoms have been omitted for clarity

### 2.2.3 Imidazolium salts prepared from theobromine

To investigate the effect of water solubility on anticancer activity, a hydroxylated ligand precursor **P5** was synthesised from theobromine following a method reported by Youngs *et al.* (**Scheme 2.7**).<sup>10</sup> The presence of the hydroxyethyl group on **P5** retains the water solubility of theophylline, as opposed to **P2-P4** which are insoluble in water. **L5** was prepared through reaction of **P4** with methyl iodide at 145°C in a sealed vessel. The characteristic imidazolium proton peak appears at 9.27 ppm in the <sup>1</sup>H NMR spectrum of **L5** (**Figure 2.7**).



**Scheme 2.7:** Hydroxylation of theobromine to **P5** and synthesis of **L5**<sup>10</sup>

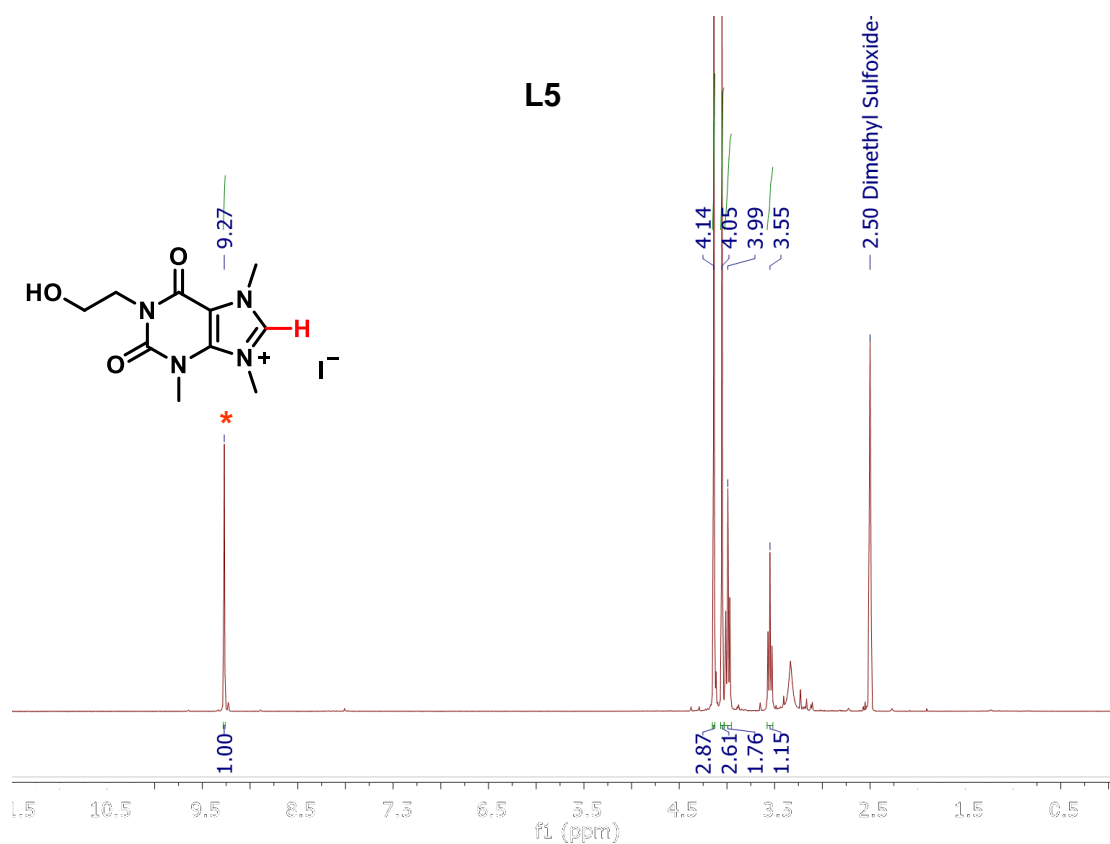
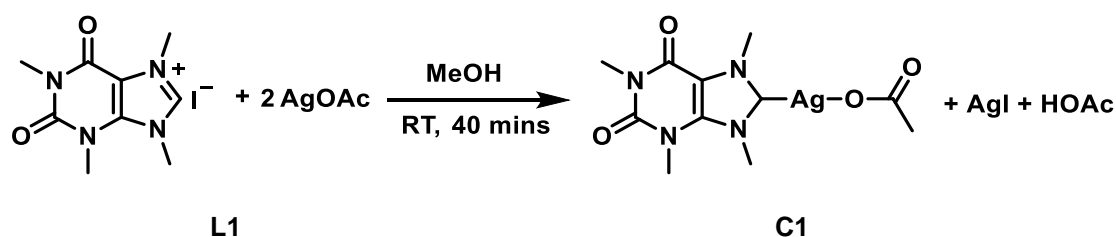


**Figure 2.7:** <sup>1</sup>H NMR spectrum (300MHz, DMSO-d<sub>6</sub>) of **L5**

## 2.3 Silver-(I) NHC complexes

Coordination of silver to xanthine-derived imidazolium salts **L1-L5** was initially attempted *via* reaction with  $\text{Ag}_2\text{O}$  under different reaction conditions, with varying solvents (MeCN,  $\text{CH}_2\text{Cl}_2$ , MeOH and  $\text{H}_2\text{O}$ ) and temperatures ranging from room temperature to  $90^\circ\text{C}$ . Although the characteristic imidazolium proton peak at  $\approx 9$  ppm disappears following these reactions, several peaks at  $\approx 8$  ppm appear. This indicates the presence of imidazolium salts with different counter anions (e.g.  $\text{AgX}_2^-$ ), which may be a result of  $\text{Ag(I)-NHC}$  decomposition. A different route using  $\text{AgOAc}$  in methanol at room temperature reported by Youngs *et al.* was used (**Scheme 2.8**).<sup>1</sup> **C1** was prepared at room temperature in 1 hour, and isolated as a stable solid in 56% yield. The reaction can be easily monitored by observing the disappearance of the imidazolium proton peak in the  $^1\text{H}$  NMR spectrum (**Figure 2.8**). The complex is very stable and does not decompose when stored as a dry solid.



**Scheme 2.8:** Synthesis of  $\text{Ag(I)-NHC}$  complex **C1** using  $\text{AgOAc}$ <sup>1</sup>

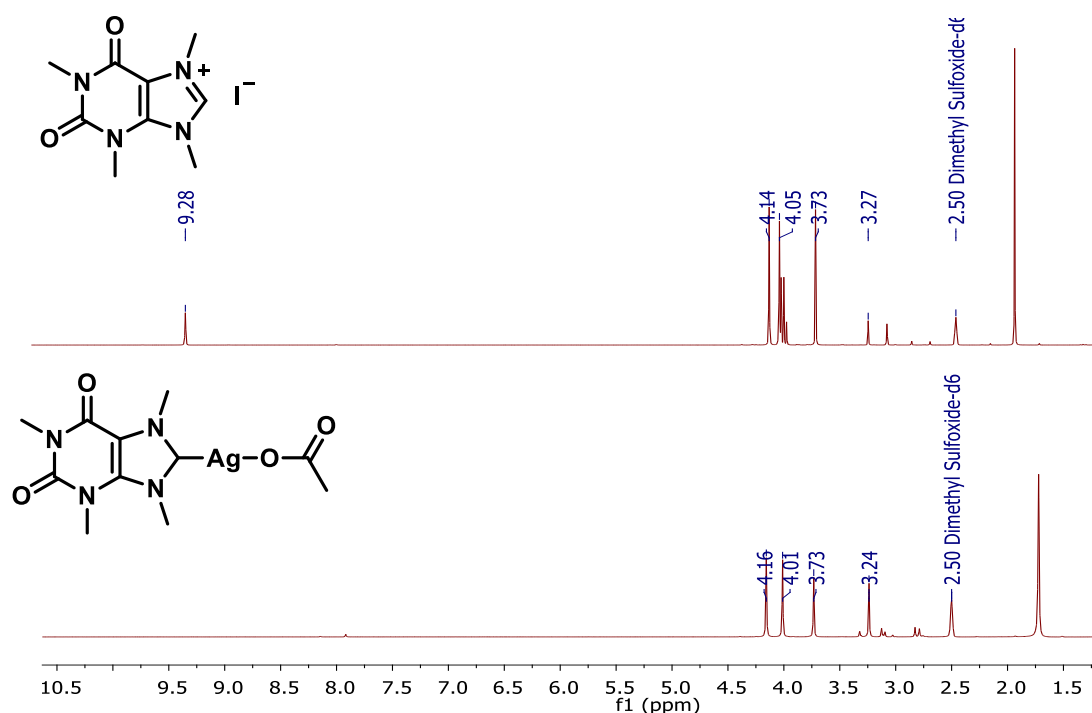


**Figure 2.8:**  $^1\text{H}$ -NMR spectra (300MHz,  $\text{DMSO-d}_6$ ) of  $\text{Ag(I)-NHC}$  complex **C1** (bottom) and imidazolium salt **L1** (top)

Single crystals of **C1** were grown by slow evaporation of a solution in MeOH. The molecular structure obtained (**Figure 2.9**) shows the bond length between the carbenic carbon and silver atom is 2.068(3) Å and the N1-C1-N2 bond angle 105.7°(3) is within error to the solid state structure reported by Youngs *et al.*<sup>1</sup> The Ag(I)-NHC complex is almost linear at the silver centre with an C1-Ag1-O3 angle of 168.21°(10). **C1** crystallises in the monoclinic crystal system with the structural solution being performed in the space group *P21/n*. The xanthine group is perfectly planar and co-crystallises with two water molecules which form H-bonds with the acetate group.

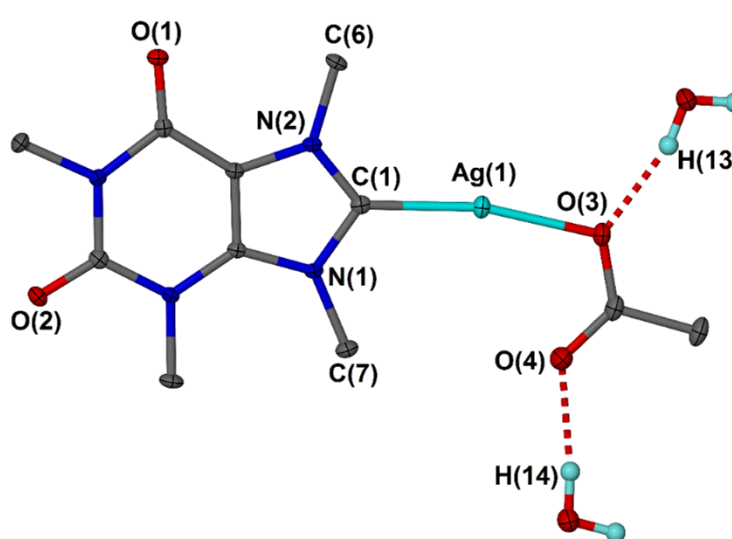
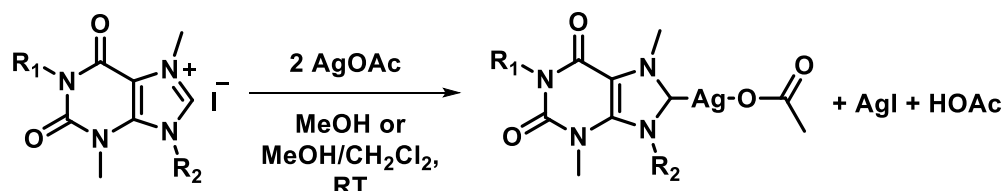


**Figure 2.9:** Molecular structure of Ag(I)-NHC complex **C1**. Ellipsoids are shown at 50% probability and H atoms (except those on H<sub>2</sub>O) are omitted for clarity

A library of four further neutral Ag(I)-NHC complexes **C2-C5** were synthesised using two equivalents of silver acetate in either MeOH or a solvent mixture of CH<sub>2</sub>Cl<sub>2</sub> and MeOH to improve the solubility of the ligands (**Scheme 2.9**). The complexes were fully characterised using <sup>1</sup>H and <sup>13</sup>C{<sup>1</sup>H} NMR spectroscopy, HRMS and elemental analysis, and the molecular structures of the novel complexes were obtained using X-ray diffraction analysis.



**C1:** R<sub>1</sub> = Me, R<sub>2</sub> = Me (54%)

**C2:** R<sub>1</sub> = Me, R<sub>2</sub> = <sup>n</sup>Bu (55%)

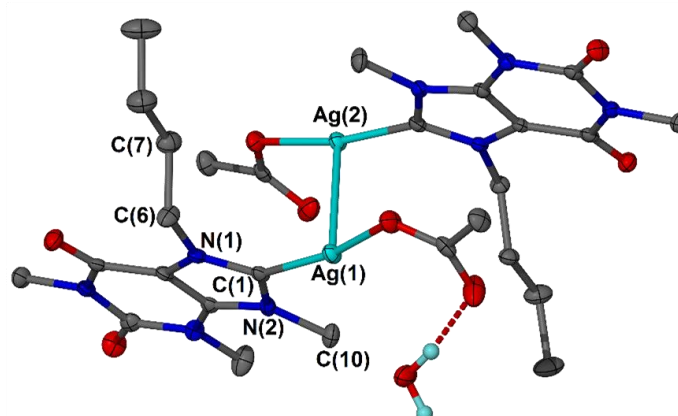
**C3:** R<sub>1</sub> = Me, R<sub>2</sub> = Bn (40%)

**C4:** R<sub>1</sub> = Me, R<sub>2</sub> = Ph (69%)

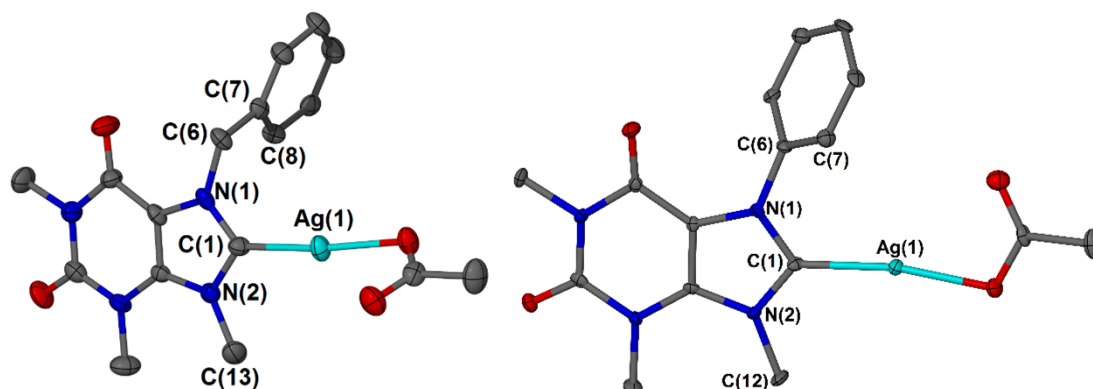
**C5:** R<sub>1</sub> = (CH<sub>2</sub>)<sub>2</sub>OH, R<sub>2</sub> = Me (28%)

**Scheme 2.9:** Synthesis of neutral Ag(I)-NHC acetate complexes **C1-C5**

Single crystals of complexes **C2-C4** were grown by vapour diffusion of pentane into concentrated solutions of the complexes in CH<sub>2</sub>Cl<sub>2</sub>. All three complexes crystallise in the triclinic crystal system and all three were solved in the *P*-1 space group (**Figure 2.10** and **Figure 2.11**). Upon coordination to silver, the C1-N1-C6 angle decreases for all three complexes from their corresponding imidazoliums, which is a common feature of NHC formation. Unlike **C3** and **C4**, **C2** crystallises as a dimer with a ligand-unsupported argentophilic interaction (Ag---Ag = 3.19 Å, **Figure 2.10**, **Table 2.5**) which is in agreement with previously reported binuclear Ag(I)-NHC complexes.<sup>11, 12</sup> **C2** also crystallises with one molecule of water which forms a hydrogen bond with the acetate group.

**C2**

**Figure 2.10:** Molecular structure of **C2**. H atoms have been omitted (except for water) for clarity and ellipsoids are shown at 50% probability

**C3****C4**

**Figure 2.11:** Molecular structures of Novel xanthine based neutral Ag(I)-NHC acetate complexes **C3** and **C4**. H atoms have been omitted for clarity and ellipsoids are shown at 50% probability

**Table 2.5:** Selected bond distances, bond angles and torsion angles for Ag(I)-NHC complexes **C2-4**

| Bond lengths (Å) and angles (°) | <b>C2</b>  | <b>C3</b> | <b>C4</b> |
|---------------------------------|------------|-----------|-----------|
| Ag1-C1-N1                       | 126.68(11) | 127.8(4)  | 125.3(2)  |
| N1-C6-C7                        | 111.08(12) | 113.4(5)  | 119.2(3)  |
| C1-N1-C6                        | 123.66(12) | 123.4(5)  | 122.4(3)  |
| Ag1-C1                          | 2.078(3)   | 2.052(7)  | 2.068(4)  |
| Ag1-Ag2                         | 3.1931(3)  | -         | -         |
| C1-N1-C6-C7                     | 94.14(18)  | 85.4      | -55.7(5)  |

The stability of the silver complexes in water was investigated to enable prediction of how they might behave in a biological system. A  $^1\text{H}$  NMR experiment containing equal equivalents of the silver complex and DMSO (internal standard) in  $\text{D}_2\text{O}$  was conducted to measure the rate of decomposition. **C1-C5** were found to be stable for 24 hours with minimal decomposition. **Figure 2.12** shows the  $^1\text{H}$  NMR spectrum of **C5** as an example. Decomposition of the complex was monitored by first determining the ratio of the integration of the  $\text{CH}_3$  peak of the complex (red) to the integration of the  $\text{CH}_3$  peaks of DMSO (green) at 0 hours, after which the ratios at different hours is compared to. The decrease in ratio is the % decomposition since the integration of complex peaks (e.g.  $\text{CH}_3$  peak) decrease upon decomposition as new peaks appear. After 48 hours, 16 % decomposition was observed, and increases to 23 % decomposition after 72 hours. The stability of **C1-C5** in  $\text{H}_2\text{O}$  for at least 24 hours indicates the possibility of high bioavailability and long half-life of the intact complexes *in vivo*.

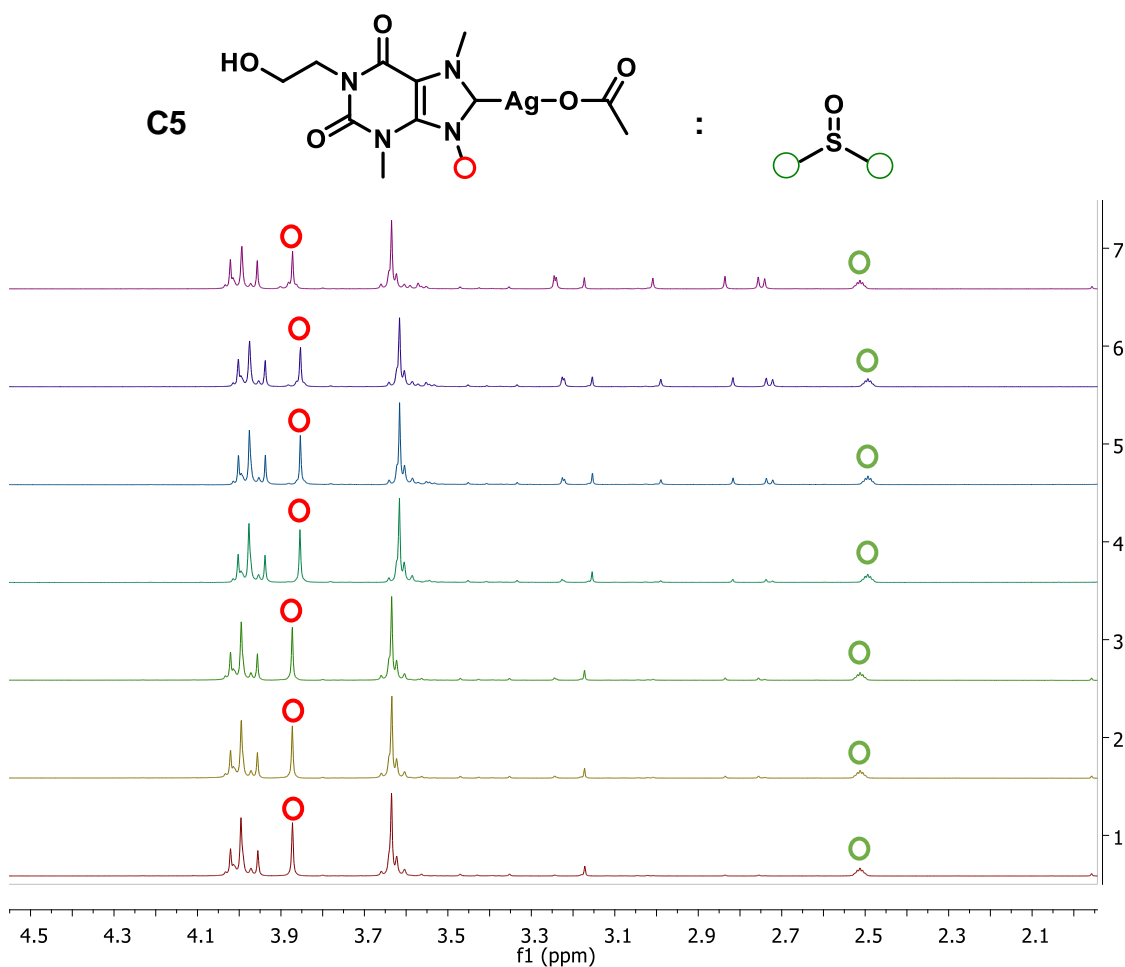


**Figure 2.12:**  $^1\text{H}$ -NMR spectra (300MHz,  $\text{D}_2\text{O}$ ) of **C5** and DMSO in 1:1 ratio.  
1) 0 hours, 2) 4 hours, 3) 7 hours, 4) 12 hours, 5) 24 hours, 6) 48 hours, 7) 72 hours

## 2.4 Hydrophobicity measurements

The hydrophobicity of complexes **C1-C5** was measured by partitioning these complexes between octanol and water, hence predicting how they would partition between the blood and lipid bi-layers inside the body. A correlation between Log  $P$  and cytotoxicity has frequently been made.<sup>13</sup> Hickey *et al.* reported that 'tuning' the Log  $P$  to achieve intermediate hydrophobicity/hydrophilicity gave the optimal potency, as a complex that they developed with intermediate lipophilicity (Log  $P$  = -0.29) was the most active against tumorigenic breast cancer cell lines MDA-MB-231 and MDA-MB-468 in addition to possessing higher selectivity to these cancerous cell lines over the non-cancerous human mammary epithelial cells HMEC.<sup>14</sup> The importance of determining the lipophilicity of a drug as a predictor of its activity is highlighted in Lipinski's 'rule of 5'.<sup>15</sup> This rule predicts that poor absorption (in bloodstream) or permeation (through membranes) of a drug is more probable when there are more than 5 H-bond donors, 10 H-bond acceptors, the molecular weight is greater than 500 and the calculated Log  $P$  is greater than 5.<sup>15, 16</sup> Although this rule applies to organic compounds, aiming to follow the rule for our organometallic complexes may improve their absorption *i.e.* their oral activity.

Equal volumes of octanol and NaCl-saturated water were stirred at room temperature for 24 hours, and separated to give octanol-saturated water and water-saturated octanol. The water layer represents the bloodstream while the octanol represents the lipid bi-layers. Five standard concentrations (5, 10, 20, 40 and 60  $\mu$ M) of the complexes were prepared from the octanol-saturated water. Analysis by UV/vis spectroscopy was used to determine the wavelength at which the maximum absorbance of each sample is reached. An example is shown in **Figure 2.13A** where the maximum absorbance for 5 samples with different concentrations of complex appear to be reached at the same wavelength of 274nm. A calibration curve of absorbance vs. concentration at this wavelength was calculated (**Figure 2.13B**), and the formula for the curve was obtained. Following calibration, seven samples of concentration 50  $\mu$ M were made up from one stock solution in the octanol-saturated water. 3 mL of octanol-saturated water containing the complex was placed in a centrifuge tube and 3 mL of water-saturated octanol was layered on top. Six samples were shaken for 4 hours using a vibrax machine at 500 g/min, and the last one was left unshaken. The absorbances of the seven samples were measured using UV/vis spectroscopy (**Figure 2.14**).

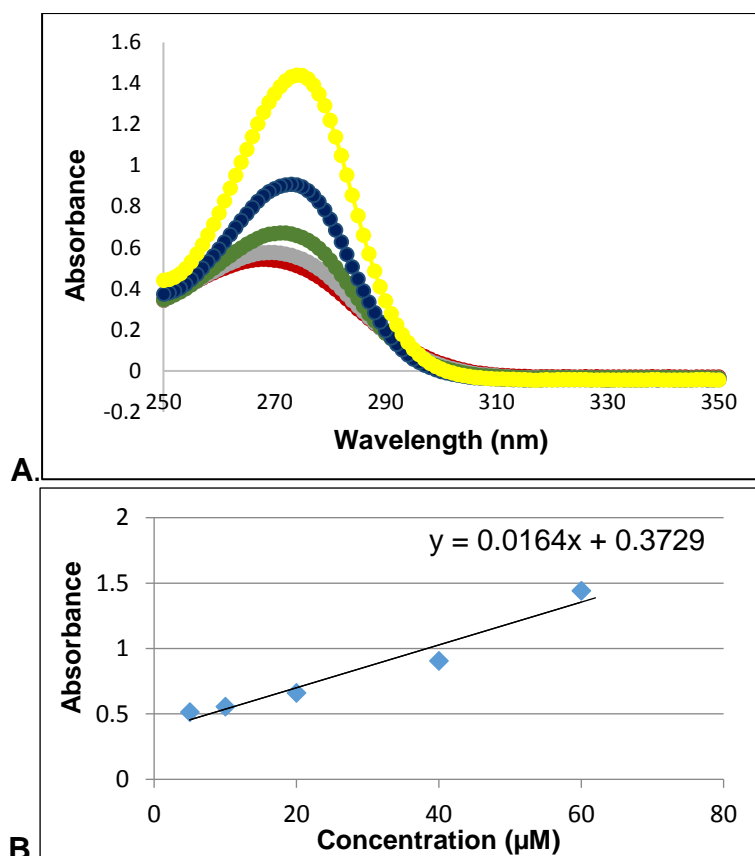


**Figure 2.13:** UV/vis spectroscopy measurements of samples with concentration 5, 10, 20, 40 and 60 uM, example graph **A.** displays the wavelength at which the maximum absorption for each concentration is reached and **B.** is an example of a calibration curve of concentration vs. absorbance

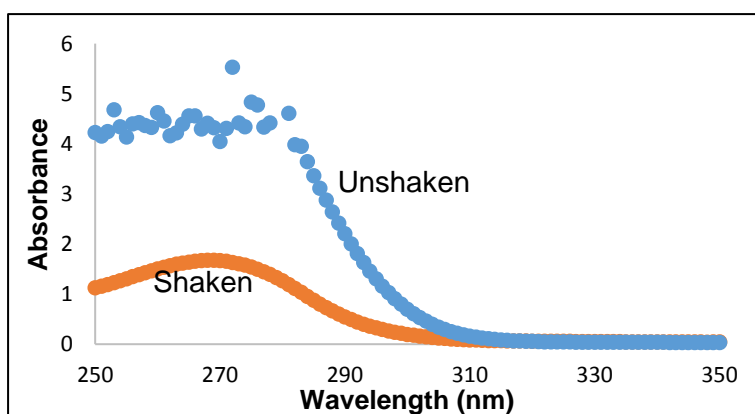


**Figure 2.14:** Differences in absorbances of shaken and unshaken samples

The concentration of the six shaken samples and the unshaken sample were calculated by converting the maximum absorbance at the same wavelength

274nm using the equation generated from the calibration curve. The average of the concentrations of the six shaken samples represents the concentration of the complex in the aqueous phase. The concentration of the complex in octanol is calculated by subtracting the average concentration of the shaken samples (conc. in aqueous phase) from the concentration of the unshaken sample. The partition coefficient ( $\text{Log } P$ ) of the complex is calculated as  $\text{Log } P = \text{Log} ([\text{conc. in octanol}]/[\text{conc. in aqueous}])$ . A positive  $\text{Log } P$  value indicates a hydrophobic complex and a negative  $\text{Log } P$  is an indication that the complex is hydrophilic.

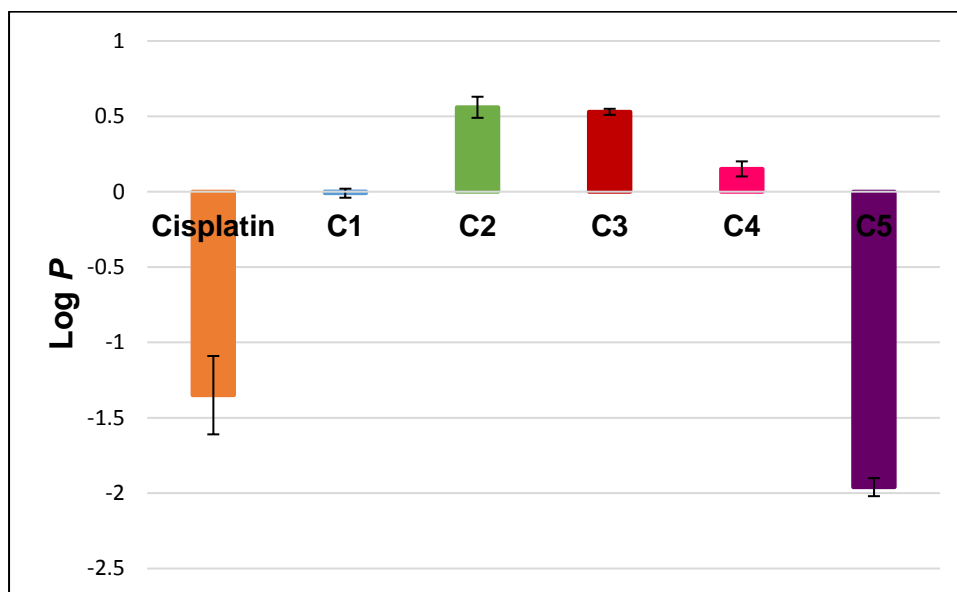


**Figure 2.15:**  $\text{Log } P$  values for Ag(I)-NHC complexes **C1-C5**.

Unsurprisingly, the N-hydroxyethyl substituted complex **C5** is the most hydrophilic ( $\text{Log } P = -1.96$ ), followed by the N-methyl substituted complex **C1** ( $\text{Log } P = -0.01$ ) while all three N-butyl, N-benzyl and N-phenyl substituted complexes **C2-C4** are hydrophobic (positive  $\text{Log } P$ ). It is clear that adding the N-hydroxyethyl group onto the xanthine complexes significantly increases the hydrophilicity, though is not as hydrophilic as cisplatin which has frequently been reported with a  $\text{Log } P$  of  $-2.36$ .<sup>17</sup> However, hydrophobicity measurements using the same method as for **C1-C5** obtained a  $\text{Log } P$  value of  $-1.35$  for cisplatin, making **C5** more hydrophilic than cisplatin when measured under the same conditions (**Figure 2.15**).

## 2.5 Anticancer testing

Antiproliferative studies were conducted by Prof. Roger Philips (University of Huddersfield) using MTT-based assays. The Ag(I)-NHC complexes were tested against eight cancerous cell lines, colorectal carcinoma HCT116 and human colorectal adenocarcinoma HT-29 (colon cancer), glioblastoma LN229, glioblastoma astrocytoma U-87MG and glioblastoma astrocytoma grade III-IV malignant tumor U-251 (brain), human pancreatic carcinoma Panc 1, cervical cancer SiHa and malignant melanoma A375 (skin cancer). Results are shown in **Figure 2.16** including values obtained for cisplatin against the same cell lines. Cisplatin was found to be more cytotoxic than **C1-C5** against all cell lines.

From the five xanthine-derived complexes the most hydrophilic **C5** showed enhanced cytotoxicity against most cell lines in comparison to **C1-C3**, except against U-87MG and Panc 1 where **C2** shows greater cytotoxicity than **C5**, and on U-251 where **C3** shows better cytotoxicity than **C5**. The general increased activity of **C5** against most of the cell lines may be attributed to its improved water solubility due to the presence of the hydroxyethyl group. Although hydrophilicity appears to play a role in cytotoxicity, complex **C4** showed overall similar potency to **C5**, with higher potency in some of the cell lines including Panc 1, U-251 and U-87MG. **C4** displays superior anticancer activity compared to **C1-C3** on all eight cell lines except for U-87MG where **C2** shows better potency. **C4** can therefore be considered the most cytotoxic complex on average out of the Ag(I)-NHC complexes **C1-C5**. This could be attributed to the steric bulk provided by the phenyl substituent which stabilises the Ag-NHC bond and results in its slow release into solution, and hence slow release in biological media.

The general superior cytotoxicity of both **C4** and **C5**, which are attributed to steric bulk and hydrophilicity respectively, suggests that a combination of both water solubility and substituents providing steric bulk may lead to the optimum anticancer Ag(I)-NHC complex.<sup>18</sup> It is also important to point out the anticancer activity of **C2** on the glioblastoma astrocytoma U-87MG cell line, which is superior to the activities of both **C4** and **C5**. This implies that the anticancer activity of **C2** is tumour specific and may be worthy of further investigation against more cancerous cell lines in the future.

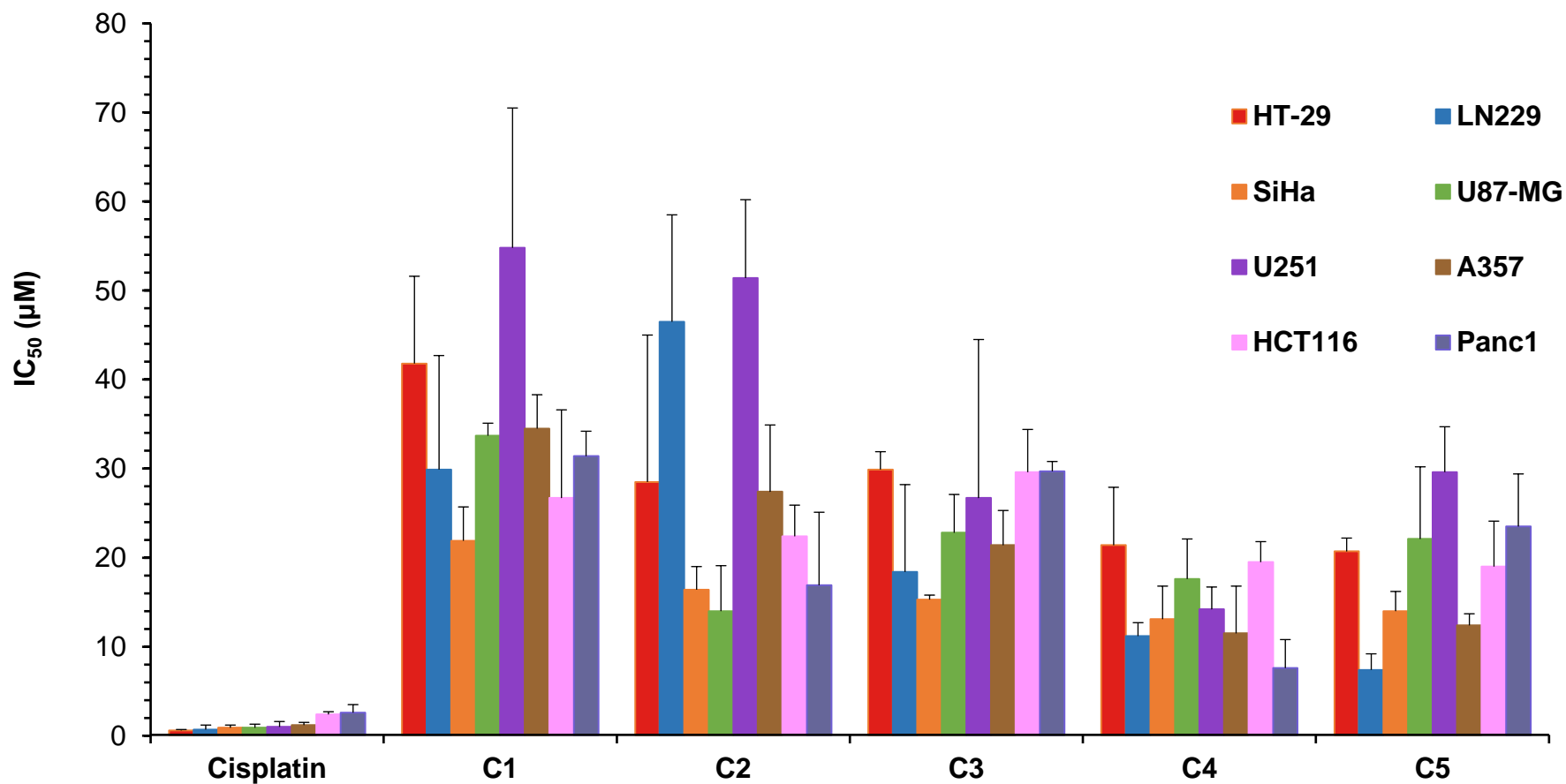


**Figure 2.16:**  $IC_{50}$  ( $\mu\text{M}$ ) values of Ag(I)-NHC complexes **C1-C5** and cisplatin against eight cancerous cell lines

## 2.6 Conclusions

Different routes to synthesise imidazolium salts from caffeine were attempted, leading to the development of a successful route for the methylation of caffeine with good yield. Other alkyl groups could not be added to caffeine due the low basicity of the nitrogen atom, therefore theophylline and theobromine were used as the starting precursors to alkylate with varying groups before methylation and the formation of imidazolium iodides.

Neutral monodentate Ag(I)-NHC complexes were synthesised by reaction of the imidazolium salts with silver acetate, and full characterisation was obtained including X-ray diffraction analysis. The stability of all complexes in water was examined with minimal decomposition after 24 hours. Hydrophobicity/hydrophilicity profiles were determined with the utility of UV/vis spectroscopy and Log *P* values were calculated. The Log *P* values indicate how well these complexes will go through the bloodstream and cross the biological membranes. The presence of a hydroxyethyl group on the ligand backbone rendered complex **C5** hydrophilic as opposed to the complexes with *n*-butyl, benzyl and phenyl N-substituents (**C2**, **C3** and **C4**), which were hydrophobic.

The cytotoxicity of **C1-C5** against 8 different cancerous cell lines was measured and compared to cisplatin. All five complexes show promising antiproliferative activity as IC<sub>50</sub> values were in the micromolar range, however not as cytotoxic as cisplatin. It is evident that increased steric effects of the ligand enhances cytotoxicity as the most cytotoxic Ag(I)-NHC complex **C4** is hydrophobic and contains a bulky phenyl group. It is also clear that water solubility enhances cytotoxicity, as **C5**, which contains a hydroxyethyl group and is the most hydrophilic complex, shows superior cytotoxicity compared to **C1**.

A combination of steric bulk and water solubility in a Ag(I)-NHC complex will potentially optimise anticancer activity. This combines the benefits of the steric effects that lead to slow release of silver into the cells, and the improved solubility in water that will improve its transport through the bloodstream, increasing its infiltration into tumours through their “leaky” blood vessels<sup>19-21</sup>. This combination can also maintain an “intermediate lipophilicity”, a property suggested by Hickey *et al.* that acquires the optimum anticancer activity.<sup>14</sup>

## 2.7 References

1. A. Kascatan-Nebioglu, A. Melaiye, K. Hindi, S. Durmus, M. J. Panzner, L. A. Hogue, R. J. Mallett, C. E. Hovis, M. Coughenour, S. D. Crosby, A. Milsted, D. L. Ely, C. A. Tessier, C. L. Cannon and W. J. Youngs, *Journal of Medicinal Chemistry*, 2006, **49**, 6811-6818.
2. D. D. P. Ferreira, B. Stutz, F. G. De Mello, R. A. M. Reis and R. C. C. Kubrusly, *Neuroscience*, 2014, **281**, 208-215.
3. D. Bolignano, G. Coppolino, A. Barilla, S. Campo, M. Criseo, D. Tripodo and M. Buemi, *Journal of Renal Nutrition*, 2007, **17**, 225-234.
4. L. E. Brackett, M. T. Shamim and J. W. Daly, *Biochemical Pharmacology*, 1990, **39**, 1897-1904.
5. J. W. Daly, *Cellular and Molecular Life Sciences*, 2007, **64**, 2153-2169.
6. G. J. Cropp, *American Journal of Medicine*, 1996, **100**, S19-S29.
7. M. A. Heckman, J. Weil and E. G. de Mejia, *Journal of Food Science*, 2010, **75**, R77-R87.
8. D. M. Grant, B. K. Tang and W. Kalow, *Clinical Pharmacology & Therapeutics*, 1983, **33**, 591-602.
9. B. Bertrand, L. Stefan, M. Pirrotta, D. Monchaud, E. Bodio, P. Richard, P. Le Gendre, E. Warmerdam, M. H. de Jager, G. M. M. Groothuis, M. Picquet and A. Casini, *Inorganic Chemistry*, 2014, **53**, 2296-2303.
10. M. J. Panzner, K. M. Hindi, B. D. Wright, J. B. Taylor, D. S. Han, W. J. Youngs and C. L. Cannon, *Dalton Transactions*, 2009, 7308-7313.
11. X. Liu, G. C. Guo, M. L. Fu, X. H. Liu, M. S. Wang and J. S. Huang, *Inorganic Chemistry*, 2006, **45**, 3679-3685.
12. C. M. Che, M. C. Tse, M. C. W. Chan, K. K. Cheung, D. L. Phillips and K. H. Leung, *Journal of the American Chemical Society*, 2000, **122**, 2464-2468.
13. S. Trapp and R. W. Horobin, *European Biophysics Journal with Biophysics Letters*, 2005, **34**, 959-966.
14. J. L. Hickey, R. A. Ruhayel, P. J. Barnard, M. V. Baker, S. J. Berners-Price and A. Filipovska, *Journal of the American Chemical Society*, 2008, **130**, 12570-12571.
15. C. A. Lipinski, F. Lombardo, B. W. Dominy and P. J. Feeney, *Advanced Drug Delivery Reviews*, 1997, **23**, 3-25.
16. C. A. Lipinski, F. Lombardo, B. W. Dominy and P. J. Feeney, *Advanced Drug Delivery Reviews*, 2001, **46**, 3-26.
17. D. Screnci, M. J. McKeage, P. Galettis, T. W. Hambley, B. D. Palmer and B. C. Baguley, *British Journal of Cancer*, 2000, **82**, 966-972.
18. H. A. Mohamed, B. R. M. Lake, T. Laing, R. M. Phillips and C. E. Willans, *Dalton transactions*, 2015, **44**, 7563-7569.
19. S. K. Hobbs, W. L. Monsky, F. Yuan, W. G. Roberts, L. Griffith, V. P. Torchilin and R. K. Jain, *Proceedings of the National Academy of Sciences of the United States of America*, 1998, **95**, 4607-4612.
20. J. A. Nagy, A. M. Dvorak and H. F. Dvorak, in *Annual Review of Pathology-Mechanisms of Disease*, 2007, vol. 2, pp. 251-275.
21. F. Yuan, M. Leunig, S. K. Huang, D. A. Berk, D. Papahadjopoulos and R. K. Jain, *Cancer Research*, 1994, **54**, 3352-3356.

## Chapter 3

### Copper- and ruthenium-N-heterocyclic carbene complexes derived from the natural xanthine precursors caffeine and theophylline

#### 3.1 Introduction

Metal-NHCs have shown potential as anticancer agents and are a fast growing field of research.<sup>1</sup> Although Pt-<sup>2, 3</sup> and Au-NHCs<sup>4-12</sup> have been the main focus in this area, Ru-<sup>13-17</sup> and Cu-NHCs<sup>18, 19</sup> have also been reported for their potential use as anticancer agents. These were discussed in detail in section 1.6.3, and examples of Cu(I)-NHC<sup>19</sup> and Ru(II)-NHC<sup>20</sup> complexes with reported anticancer activities are shown in **Figure 3.1** and **Figure 3.2**. The promising anticancer activity of Cu(I)- and Ru(II)-NHC complexes reported in the literature,<sup>21</sup> inspired us to synthesise and study xanthine-derived Cu(I)-NHC and Ru(II)-NHC complexes.

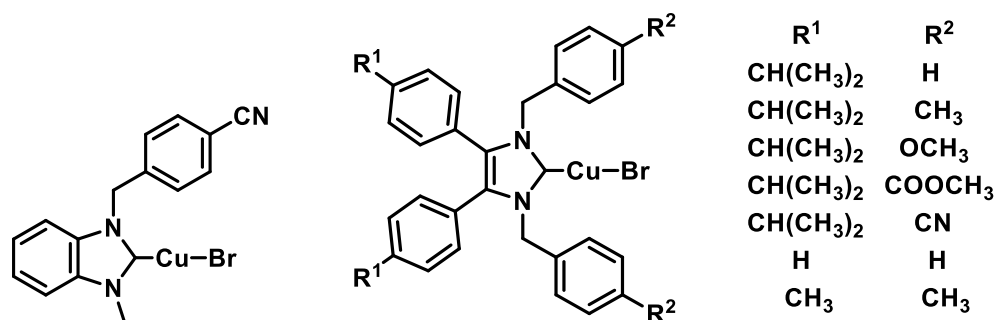


**Figure 3.1:** Cu(I)-NHC complexes that exhibit anticancer activities<sup>19</sup>

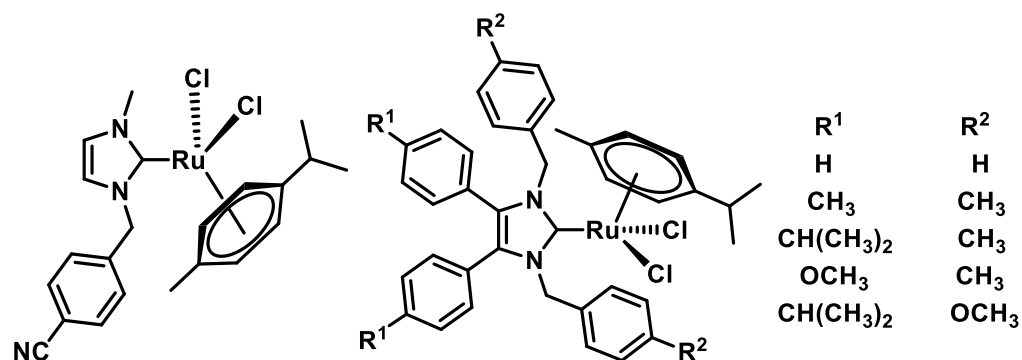


**Figure 3.2:** Ru(II)-NHC complexes that exhibit anticancer activities<sup>20</sup>

### 3.2 Electrochemical synthesis

The electrochemical synthesis of metal-NHCs is a well-established technique in the Willans group.<sup>22-25</sup> Attempts were made to electrochemically synthesise a Ag(I)-NHC complex starting from **L1**, using a silver anode and a copper cathode, under anhydrous conditions. The theoretical reaction time was calculated to be 32 minutes using Faraday's law (**Figure 3.3**) with 0.2g (0.6mmol) of **L1**. However, after 2 hours at 30 mA, a mixture of Ag(I)-NHC and **L1** were observed by <sup>1</sup>H NMR spectroscopy (**Figure 3.4** (1)).

$$Q = nFN$$

$Q$  = total charge [C or A s]

$$t = Q/I$$

$n$  = number of electrons transferred

$F$  = Faraday's constant [C mol<sup>-1</sup>]

$N$  = moles of starting material [mol]

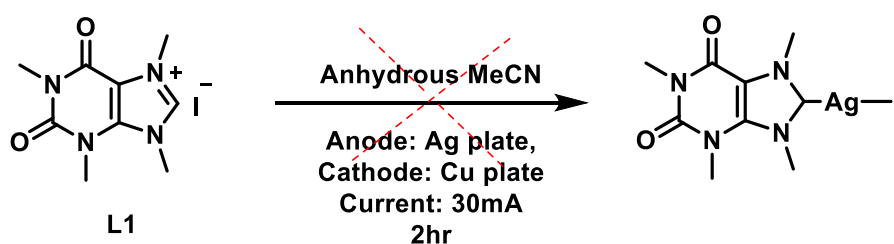
$$t = nFN/I$$

$I$  = current [A]

$t$  = time [s]

$$\text{E.g. } t = \frac{1 \times F \times 0.0006 \text{ mol}}{0.03 \text{ A}} = 1914 \text{ seconds or 32 minutes}$$

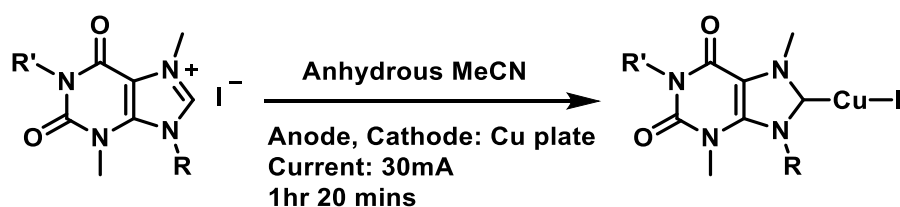
**Figure 3.3:** Faraday's law - calculation of theoretical reaction time



**Scheme 3.1:** Attempted electrochemical synthesis of a Ag(I)-NHC complex from **L1**

### 3.2.1 Electrochemical synthesis of Cu(I)-NHC complexes

For the electrochemical synthesis of xanthine-derived Cu(I)-NHC complexes a copper anode was utilised, in addition to the copper cathode. The method was successful in furnishing Cu(I)-NHC complexes starting from ligands **L1**, **L2** and **L3** (**Scheme 3.2**) to give Cu(I)-NHC complexes **C1.Cu**, **C2.Cu** and **C3.Cu**. The Cu(I) complexes are insoluble in MeCN and precipitate out of solution when formed. Interestingly, **C1.Cu**, **C2.Cu** and **C3.Cu** are unusually stable in air in the solid state, and only begin to oxidise to Cu(II) after six hours in DMSO- $d_6$  following exposure to air. This observation regarding their stability is unlike literature examples of Cu(I)-NHC complexes, which oxidise to Cu(II) upon exposure to low levels of oxygen.<sup>22, 23, 25</sup> This stability may be due to the electron withdrawing effect of the xanthine backbone, leading to a ‘softer’ NHC ligand (carbon donor), strengthening the ‘soft-soft’ interaction with Cu(I). The relatively ‘soft’ iodide anion may also be contributing to the stability of the complex. The same synthetic route was applied to **L4** and **L5** in order to complete a library of five Cu(I) complexes, however, these did not form the desired Cu(NHC)I complexes **C4.Cu** or **C5.Cu** (**Scheme 3.2**). Comparison of the  $^1\text{H}$  NMR spectra of the electrochemical product from **Scheme 3.1** and the Cu(NHC)I product from **Scheme 3.2(1.)** are shown in **Figure 3.4**. The  $^1\text{H}$  NMR spectra display the successful facile synthesis of pure **C1.Cu** unlike its corresponding Ag(I) complex.



- |    |  |   |   |
|----|--|---|---|
| 1. | <b>L1:</b> R = Me, R' = Me                                 | <b>C1.Cu:</b> R = Me, R' = Me                                 | ✓ |
| 2. | <b>L2:</b> R = <sup>n</sup> Bu, R' = Me                    | <b>C2.Cu:</b> R = <sup>n</sup> Bu, R' = Me                    | ✓ |
| 3. | <b>L3:</b> R = Bn, R' = Me                                 | <b>C3.Cu:</b> R = Bn, R' = Me                                 | ✓ |
| 4. | <b>L4:</b> R = Ph, R' = Me                                 | <b>C4.Cu:</b> R = Ph, R' = Me                                 | ✗ |
| 5. | <b>L5:</b> R = Me, R' = (CH <sub>2</sub> ) <sub>2</sub> OH | <b>C5.Cu:</b> R = Me, R' = (CH <sub>2</sub> ) <sub>2</sub> OH | ✗ |

**Scheme 3.2:** Electrochemical synthesis of Cu(I)-NHC complexes

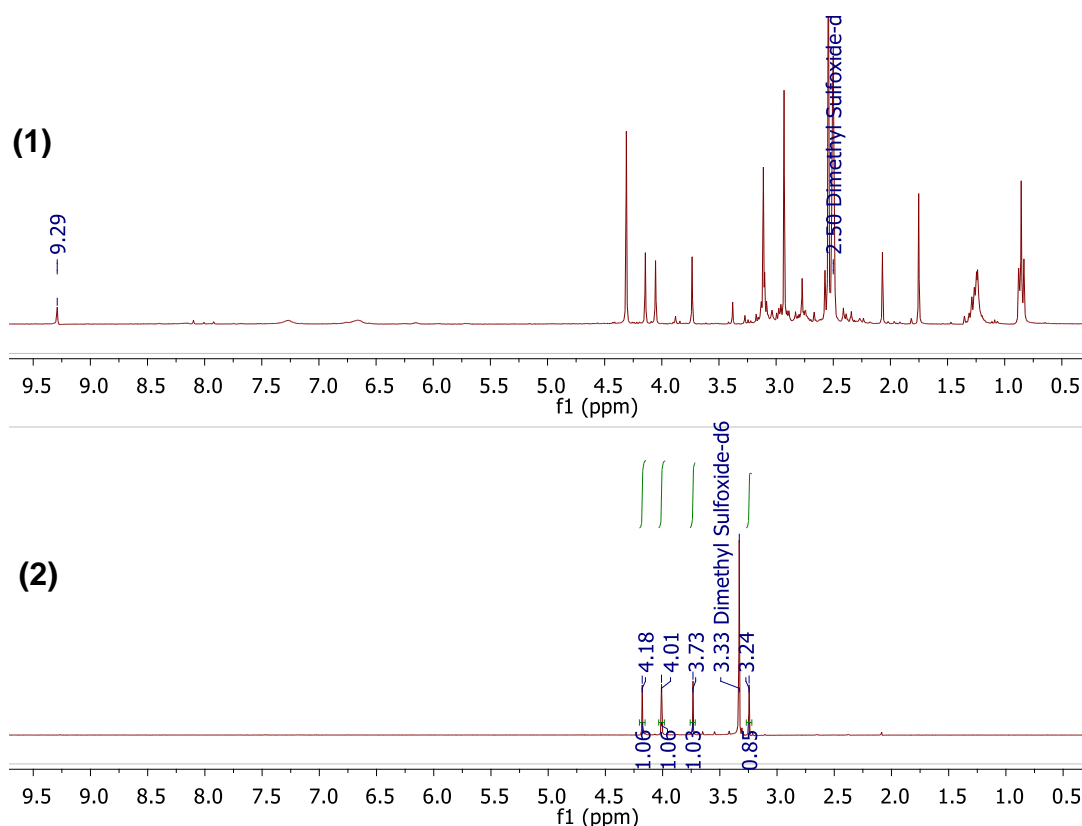


**Figure 3.4:**  $^1\text{H-NMR}$  (300MHz,  $\text{DMSO-d}_6$ ) of **(1)**. the attempted electrochemical synthesis of  $\text{Ag(NHC)I}$  (unsuccessful) and **(2)**. the successful electrochemical synthesis of **C1.Cu** ( $\text{Cu(NHC)I}$ )

Single crystals of complex **C1.Cu** were grown by vapour diffusion of diethyl ether into concentrated solution of the complex in DMSO. **C1.Cu** crystallises in the triclinic crystal system and was solved in the  $P-1$  space group (**Figure 3.5**). The bent geometry around the Cu atom is due to the formation of a halide-bridged dimer in the solid state. The bond length between the carbenic carbon and copper atom is  $1.928(5)$  Å and the bond angle  $\text{N1-C1-N2}$  is  $105.3(4)^\circ$  which are similar to those found for the corresponding silver acetate complex **C1** (Chapter 2).

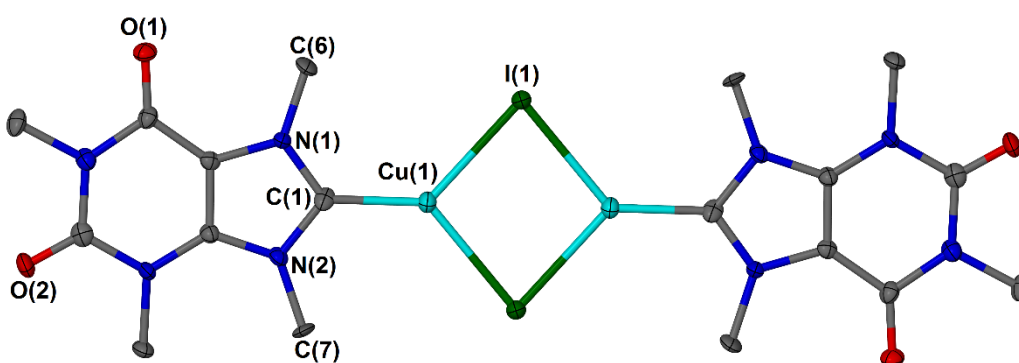


**Figure 3.5:** Molecular structure **C1.Cu**. H atoms have been omitted for clarity and ellipsoids are shown at 50% probability

The unusual stability of these Cu(I)-NHC complexes may be advantageous in catalysis, therefore, they were examined in a copper catalysed Ullmann reaction. Cu(I)-NHC complexes have been previously reported by the Willans group to exhibit reasonable activity in the etherification reaction of 3,5-dimethylphenol.<sup>22</sup> Therefore, complexes **C1.Cu**, **C2.Cu** and **C3.Cu** were investigated as catalysts in the same reaction (**Scheme 3.3**). *In situ* generated catalysts were examined, using 10 mol% of the ligand precursors **L1**, **L2**, **L3** and **L4** and 10 mol% of CuI and the results were compared to those obtained using ligand 1,3-bis(2,4,6-trimethylphenyl)imidazolium chloride (IMes). Electrochemically preformed Cu(I)-NHC complexes **C1.Cu**, **C2.Cu** and **C3.Cu** were also tested with a 10 mol% loading and the results were compared to both mono-substituted Cu(IMes)Cl and bis-substituted Cu(IMes)<sub>2</sub>PF<sub>6</sub>. The yields of the coupled product, which are presented in **Table 3.1**, show that these Cu(I)-NHC complexes are not effective in the Ullmann reaction, with yields less than 20%.



**Scheme 3.3:** Copper catalysed arylation reaction

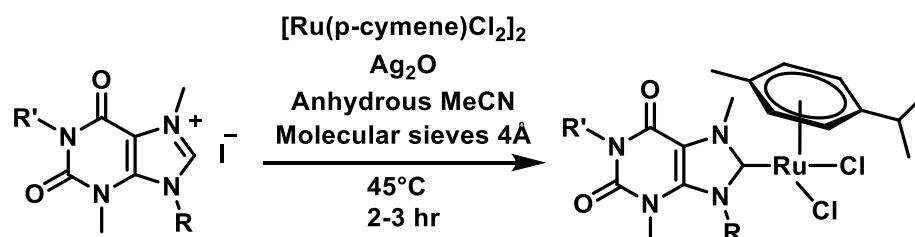
**Table 3.1:** Reaction conditions: 1.2 mmol 3,5-dimethylphenol, 1.0 mmol 4-iodoanisole, 2.0 mmol Cs<sub>2</sub>CO<sub>3</sub>, 0.1 mmol catalyst, 5 mL MeCN, 90°C, 24h

| Entry | Catalyst (10 mol%) | GC yield (%) <sup>a</sup> |
|-------|--------------------|---------------------------|
| 1     | CuI                | 5                         |
| 2     | CuI + IMes.Cl      | 28                        |
| 3     | Cu(IMes)Cl         | 11                        |
| 4     | <b>C1.Cu</b>       | 3                         |
| 5     | <b>C2.Cu</b>       | 11                        |
| 6     | <b>C3.Cu</b>       | 6                         |
| 7     | CuI + <b>L1</b>    | 4                         |
| 8     | CuI + <b>L2</b>    | 5                         |
| 9     | CuI+ <b>L3</b>     | 3                         |
| 10    | CuI+ <b>L4</b>     | 17                        |

<sup>a</sup> Yields were determined by GC using *p*-cymene as an internal standard

### 3.3 Synthesis of Ru(II)-NHC complexes

Xanthine-derived Ru(II)-NHC complexes **C1.Ru**, **C2.Ru** and **C3.Ru** were synthesised by transmetallation from Ag(I)-NHC complexes formed *in situ*, utilising Ag<sub>2</sub>O and [Ru(*p*-cymene)Cl<sub>2</sub>]<sub>2</sub> (**Figure 3.6**). Visual monitoring of the reaction was possible by observing the precipitation of silver salt. Reaction times of 2 hours gave the desired complexes, with longer reaction times (> 3 hours) resulting in the decomposition of the complex, observed by a change in the solution colour from red/orange to dark green. **C1.Ru**, **C2.Ru** and **C3.Ru** are stable orange/red powders when stored as dry solids for several months. Reaction of **L4** under similar conditions to **L1**, **L2** and **L3** required longer time (3 hours) to form the desired product, however, **C4.Ru** decomposes to a green solid in a few hours when stored as a dry solid, so was not taken forward to cell-line testing. Although reaction with **L5** furnishes a red solid, the product analysed was not the desired Ru(II)-NHC complex **C5.Ru**.



- |    |  |   |   |
|----|--|---|---|
| 1. | <b>L1:</b> R = Me, R' = Me                                 | <b>C1.Ru:</b> R = Me, R' = Me                                 | ✓ |
| 2. | <b>L2:</b> R = <sup>n</sup> Bu, R' = Me                    | <b>C2.Ru:</b> R = <sup>n</sup> Bu, R' = Me                    | ✓ |
| 3. | <b>L3:</b> R = Bn, R' = Me                                 | <b>C3.Ru:</b> R = Bn, R' = Me                                 | ✓ |
| 4. | <b>L4:</b> R = Ph, R' = Me                                 | <b>C4.Ru:</b> R = Ph, R' = Me                                 | ✓ |
| 5. | <b>L5:</b> R = Me, R' = (CH <sub>2</sub> ) <sub>2</sub> OH | <b>C5.Ru:</b> R = Me, R' = (CH <sub>2</sub> ) <sub>2</sub> OH | ✗ |

**Figure 3.6:** Synthesis of Ru(II)-NHC complexes

A comparison of the  $^1\text{H}$  NMR spectra of **C1.Ru**, **C2.Ru** and **C3.Ru** (Figure 3.7) reveals an interesting shift in the doublet resonance corresponding to two of the *p*-cymene protons which are shifted downfield from  $\approx 5.45$  ppm (**C1.Ru** / **C2.Ru**) to 7.03 ppm in **C3.Ru**. This downfield shift is likely due to a deshielding effect caused by the close proximity of the aromatic benzyl substituent to the *p*-cymene.

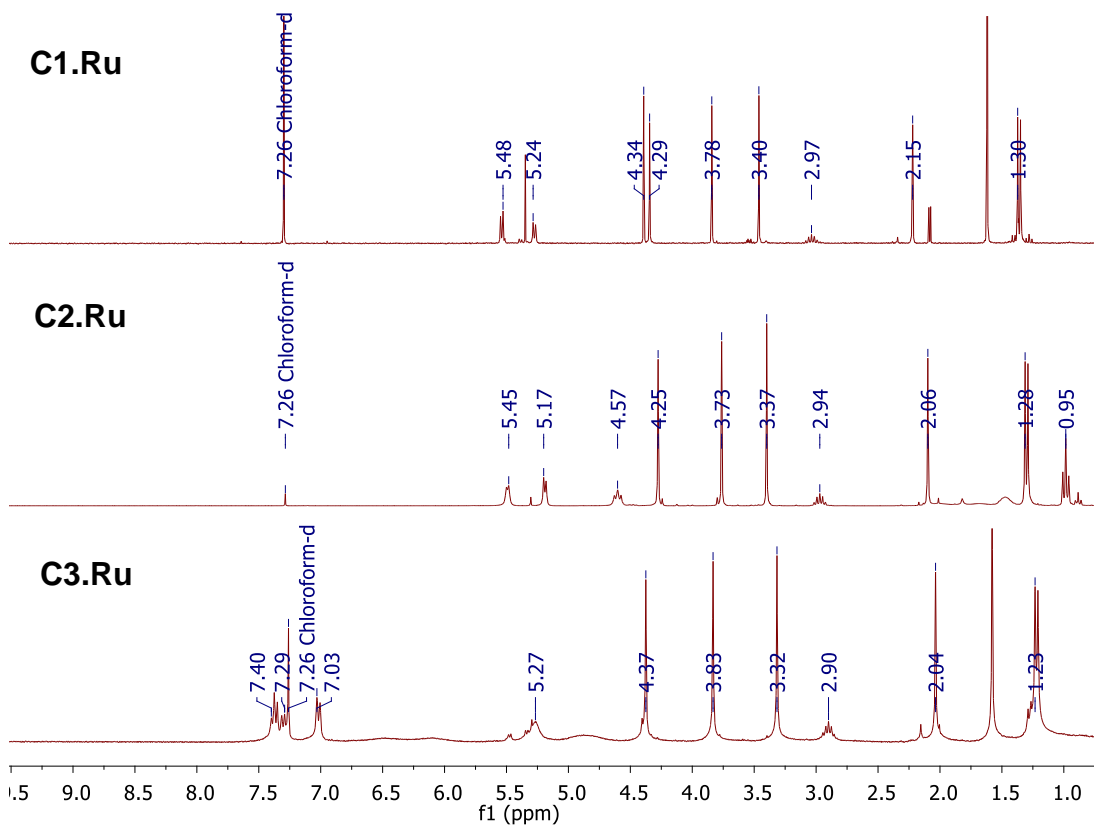
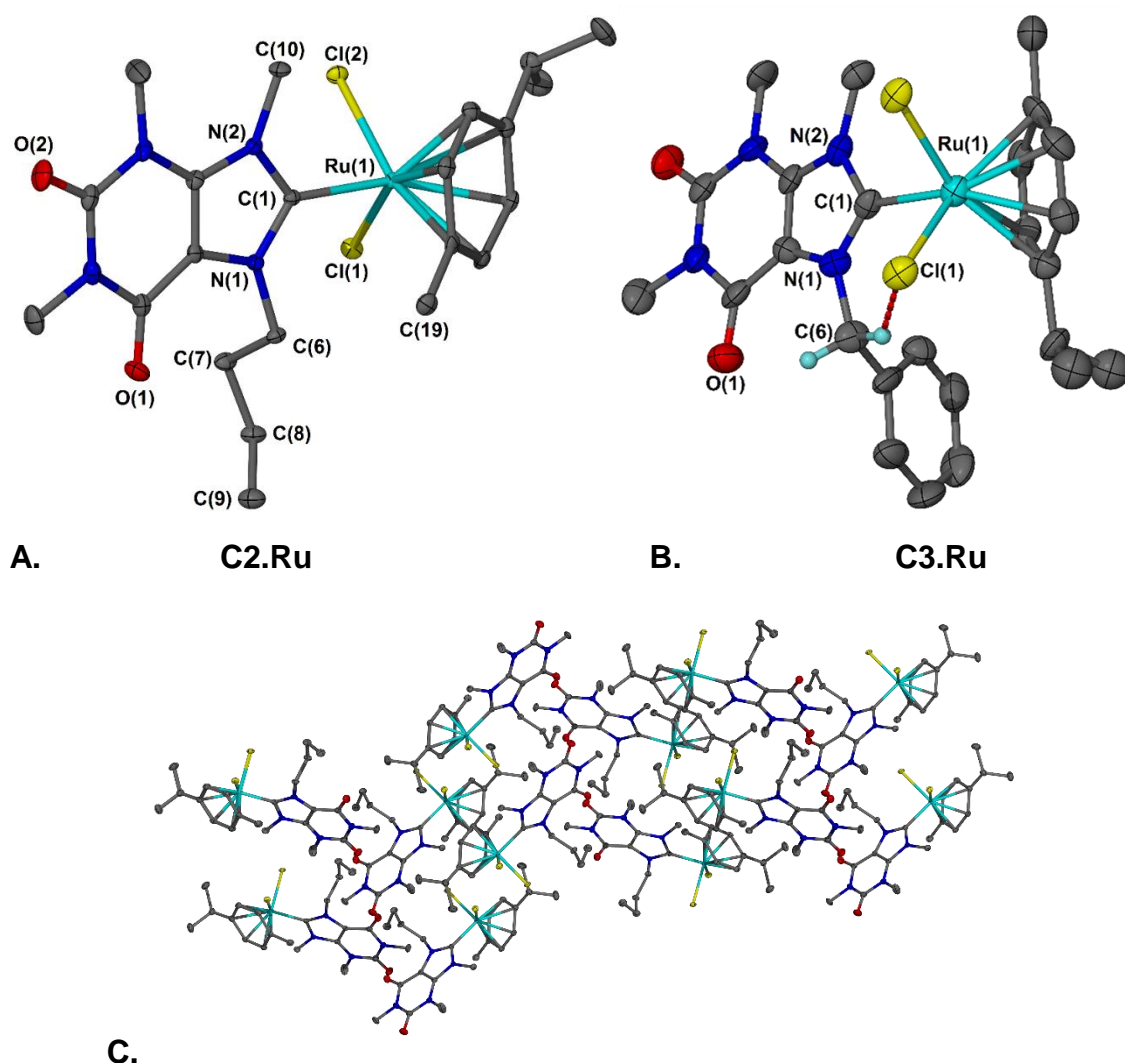


Figure 3.7:  $^1\text{H}$ -NMR spectra (300MHz,  $\text{CDCl}_3$ ) of **C1.Ru**, **C2.Ru** and **C3.Ru**

Single crystals of complexes **C2.Ru** and **C3.Ru** were grown by vapour diffusion of Et<sub>2</sub>O into concentrated solutions of the complexes in CHCl<sub>3</sub>. **C2.Ru** and **C3.Ru** both crystallise in the orthorhombic crystal system and structural solutions are solved in the  $P2_12_12_1$  space group. The molecular structures of are displayed in **Figure 3.8**. **C3.Ru** shows a hydrogen bond between a methylene proton of the benzyl substituent and a chloride. The packing diagram of **C2.Ru** displays intermolecular T-stacking interactions between the aromatic xanthine rings, holding planes of molecules together, which is not observed in the packing of **C3.Ru**.



**Figure 3.8:** Molecular structures of **A. C2.Ru** and **B. C3.Ru** and **C.** packing diagram of **C2.Ru** along the *b* axis. Ellipsoids are shown at 50% probability level and H-atoms (except those on C(6) in **C3.Ru**) are omitted for clarity

### 3.4 Anticancer Testing

Xanthine-derived Cu(I)-NHC complexes **C1.Cu**, **C2.Cu** and **C3.Cu** and Ru(II)-NHC complexes **C1.Ru**, **C2.Ru** and **C3.Ru** were evaluated for their anticancer activity. Cytotoxicity studies (MTT-based assays conducted at the University of Huddersfield) against pancreatic adenocarcinoma cell line Panc 10.05 revealed poor or negligible cytotoxicity of all six complexes (**Table 3.2**). Further studies using SRB assays were conducted at the University of Heidelberg against nine cell lines including colorectal carcinoma cell lines HT116 wt and HT116 p53<sup>-/-</sup>, human colorectal adenocarcinoma HT29, prostate adenocarcinoma LNCaP, prostate carcinoma DU145, grade IV prostate adenocarcinoma PC3, mammary gland adenocarcinoma MDA-MB-231 and pancreatic adenocarcinoma cell lines MiaPaca and Panc1. Surprisingly, all six complexes showed no or poor anticancer activity against the nine cell lines, despite their corresponding Ag(I)-acetate complexes **C1.Ag**, **C2.Ag** and **C3.Ag** having shown good anticancer activity against various cancerous cell lines (Chapter 2).<sup>26</sup> Comparison of the anticancer activity of nine Ag(I), Cu(I) and Ru(II)-NHC complexes against three cell lines, HT29, HTC116 and Panc 1 (**Figure 3.10**), illustrates the superior antiproliferative activity of Ag over Cu and Ru.

| <b>Table 3.2:</b> IC <sub>50</sub> values of Cu(I)-NHC complexes and Ru(II)-NHC complexes against ten cancerous cell lines, <sup>a</sup> MTT-based assay and <sup>b</sup> SRB-based assay |              |              |              |              |              |              |
|---|--------------|--------------|--------------|--------------|--------------|--------------|
|   | <b>C1.Cu</b> | <b>C2.Cu</b> | <b>C3.Cu</b> | <b>C1.Ru</b> | <b>C2.Ru</b> | <b>C3.Ru</b> |
| <sup>a</sup> <b>Panc 10.05</b>  | >100         | >100         | 51±25        | 94 ±5        | >100         | >100         |
| <sup>b</sup> <b>HT116</b>   | >100         | >100         | >100         | >100         | >100         | >100         |
| <sup>b</sup> <b>HT116 p53<sup>-/-</sup></b>   | >100         | >100         | >100         | >100         | >100         | >100         |
| <sup>b</sup> <b>HT29</b>  | >100         | >100         | >100         | >100         | >100         | >100         |
| <sup>b</sup> <b>LNCaP</b>   | >100         | >100         | >100         | >100         | >100         | >100         |
| <sup>b</sup> <b>DU145</b>   | >100         | >100         | >100         | >100         | >100         | >100         |
| <sup>b</sup> <b>MiaPaca</b>   | >100         | >100         | >100         | >100         | >100         | >100         |
| <sup>b</sup> <b>MDA-MB-231</b>  | >100         | >100         | >100         | >100         | >100         | >100         |
| <sup>b</sup> <b>Panc1</b>   | >100         | >100         | >100         | >100         | >100         | >100         |
| <sup>b</sup> <b>PC3</b>   | >100         | >100         | >100         | >100         | >100         | >100         |

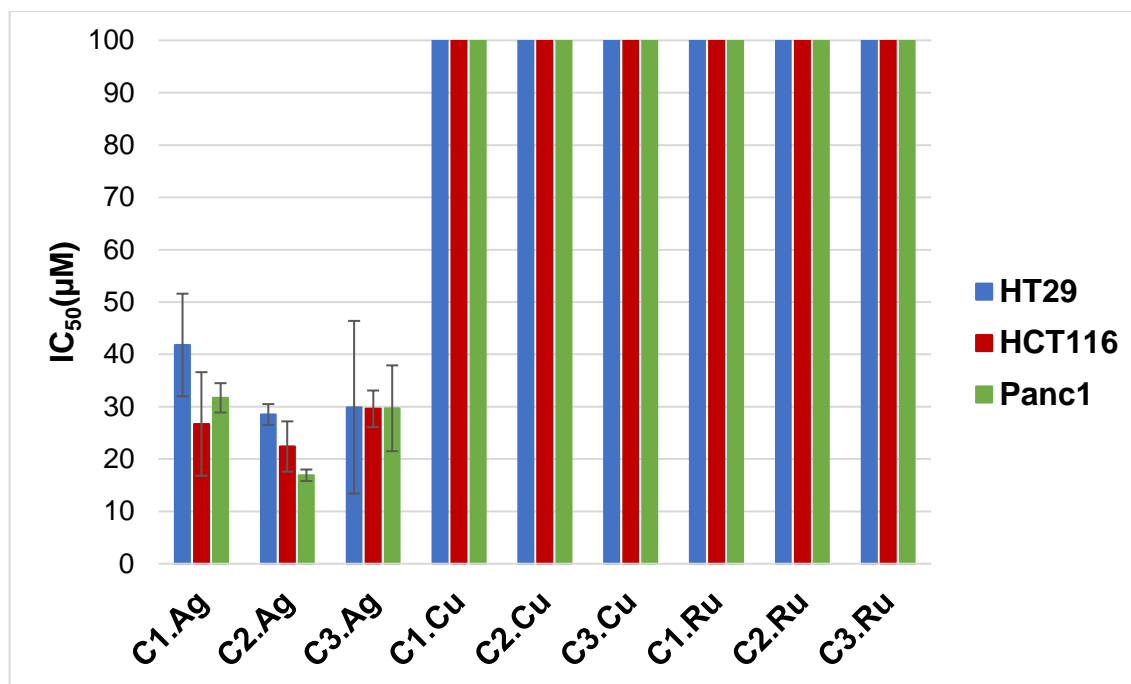


**Figure 3.9:**  $IC_{50}$  ( $\mu\text{M}$ ) values of Ag(I)-NHC complexes **C1.Ag**, **C2.Ag** and **C3.Ag**<sup>26</sup> and their analogous Cu(I)-NHC **C1.Cu**, **C2.Cu** and **C3.Cu** and Ru(II)-NHC **C1.Ru**, **C2.Ru** and **C3.Ru** complexes against three cancerous cell lines

### 3.5 Conclusions

Xanthine-derived imidazolium iodides **L1**, **L2** and **L3** were used in the electrochemical synthesis of three Cu(I)-NHC complexes, **C1.Cu**, **C2.Cu** and **C3.Cu**, and the synthesis of three Ru(II)-NHC complexes **C1.Ru**, **C2.Ru** and **C3.Ru** *via* transmetallation using  $\text{Ag}_2\text{O}$  and Ru *p*-cymene dimer. Synthesis of xanthine-derived Pt(II)-NHC complexes proved challenging as mixtures of products appear to form. The antiproliferative activity of the six Cu(I)-NHC and Ru(II)-NHC complexes was evaluated against ten cancerous cell lines, showing little or no cytotoxicity.<sup>27</sup> Comparison of the antiproliferative activity with those of three previously reported Ag(I) complexes, **C1.Ag**, **C2.Ag** and **C3.Ag**,<sup>26</sup> displays the superior activity of the Ag(I)-NHC complexes. This may be due to a stronger Cu-carbene and a Ru-carbene bond that hinders the release of the metal ions required for the anticancer activity, while the Ag-carbene is a weaker bond. Another possible reason is that the redox potential of these complexes required to form the active species is not in the redox potential window of their biological target, e.g. mitochondrial redox potential window.<sup>19</sup> These interesting findings suggest that Ag(I)-NHC complexes have greater potential as anticancer agents over either Cu(I)-NHC or Ru(II)-NHC complexes, when coordinated by xanthine-derived NHC ligands.

### 3.7 References

1. S. B. Aher, P. N. Muskawar, K. Thenmozhi and P. R. Bhagat, *European Journal of Medicinal Chemistry*, 2014, **81**, 408-419.
2. M. Skander, P. Retailleau, B. Bourrie, L. Schio, P. Mailliet and A. Marinetti, *Journal of Medicinal Chemistry*, 2010, **53**, 2146-2154.
3. R. W.-Y. Sun, A. L.-F. Chow, X.-H. Li, J. J. Yan, S. S.-Y. Chui and C.-M. Che, *Chemical Science*, 2011, **2**, 728-736.
4. R. Rubbiani, I. Kitanovic, H. Alborzina, S. Can, A. Kitanovic, L. A. Onambele, M. Stefanopoulou, Y. Geldmacher, W. S. Sheldrick, G. Wolber, A. Prokop, S. Woelfl and I. Ott, *Journal of Medicinal Chemistry*, 2010, **53**, 8608-8618.
5. R. Rubbiani, S. Can, I. Kitanovic, H. Alborzina, M. Stefanopoulou, M. Kokoschka, S. Moenchgesang, W. S. Sheldrick, S. Woelfl and I. Ott, *Journal of Medicinal Chemistry*, 2011, **54**, 8646-8657.
6. W. Liu, K. Bendorf, M. Proetto, U. Abram, A. Hagenbach and R. Gust, *Journal of Medicinal Chemistry*, 2011, **54**, 8605-8615.
7. W. Liu, K. Bendorf, M. Proetto, A. Hagenbach, U. Abram and R. Gust, *Journal of Medicinal Chemistry*, 2012, **55**, 3713-3724.
8. P. C. Kunz, C. Wetzels, S. Koegel, M. U. Kassack and B. Spingler, *Dalton Transactions*, 2011, **40**, 35-37.
9. J. Weaver, S. Gaillard, C. Toye, S. Macpherson, S. P. Nolan and A. Riches, *Chemistry-a European Journal*, 2011, **17**, 6620-6624.
10. H. Sivaram, J. Tan and H. Han Vinh, *Dalton Transactions*, 2013, **42**, 12421-12428.
11. E. Schuh, C. Pflueger, A. Citta, A. Folda, M. P. Rigobello, A. Bindoli, A. Casini and F. Mohr, *Journal of Medicinal Chemistry*, 2012, **55**, 5518-5528.
12. L. Kaps, B. Biersack, H. Mueller-Bunz, K. Mahal, J. Muenzner, M. Tacke, T. Mueller and R. Schobert, *Journal of Inorganic Biochemistry*, 2012, **106**, 52-58.
13. E. Gallori, C. Vettori, E. Alessio, F. G. Vilchez, R. Vilaplana, P. Orioli, A. Casini and L. Messori, *Archives of Biochemistry and Biophysics*, 2000, **376**, 156-162.
14. J. Malina, O. Novakova, B. K. Keppler, E. Alessio and V. Brabec, *Journal of Biological Inorganic Chemistry*, 2001, **6**, 435-445.
15. N. Cetinbas, M. I. Webb, J. A. Dubland and C. J. Walsby, *Journal of Biological Inorganic Chemistry*, 2010, **15**, 131-145.
16. C. Tan, S. Hu, J. Liu and L. Ji, *European Journal of Medicinal Chemistry*, 2011, **46**, 1555-1563.
17. L. Oehninger, M. Stefanopoulou, H. Alborzina, J. Schur, S. Ludewig, K. Namikawa, A. Munoz-Castro, R. W. Koester, K. Baumann, S. Woelfl, W. S. Sheldrick and I. Ott, *Dalton Transactions*, 2013, **42**, 1657-1666.
18. R. A. Bassani, J. W. M. Bassani and D. M. Bers, *Journal of Physiology-London*, 1992, **453**, 591-608.
19. F. Hackenberg and M. Tacke, *Dalton Transactions*, 2014, **43**, 8144-8153.
20. F. Hackenberg, H. Mueller-Bunz, R. Smith, W. Streciwilk, X. Zhu and M. Tacke, *Organometallics*, 2014, **32**, 5551-5560.
21. M.-L. Teysot, A.-S. Jarrousse, M. Manin, A. Chevy, S. Roche, F. Norre, C. Beaudoin, L. Morel, D. Boyer, R. Mahiou and A. Gautier, *Dalton Transactions*, 2009, 6894-6902.

22. B. R. M. Lake and C. E. Willans, *Organometallics*, 2014, **33**, 2027-2038.
23. M. R. Chapman, Y. M. Shafi, N. Kapur, B. N. Nguyen and C. E. Willans, *Chemical Communications*, 2015.
24. E. K. Bullough, M. A. Little and C. E. Willans, *Organometallics*, 2013, **32**, 570-577.
25. B. R. M. Lake, E. K. Bullough, T. J. Williams, A. C. Whitwood, M. A. Little and C. E. Willans, *Chemical Communications*, 2012, **48**, 4887-4889.
26. H. A. Mohamed, B. R. M. Lake, T. Laing, R. M. Phillips and C. E. Willans, *Dalton transactions*, 2015, **44**, 7563-7569.
27. J.-J. Zhang, J. Munzner, M. A. Abu el Maaty, B. Karge, R. Schobert, S. Wolf and I. Ott, *Dalton Transactions*, 2016.

## Chapter 4

### Synthesis and anticancer activity of silver(I)-N-heterocyclic carbene complexes derived from clotrimazole

#### 4.1 Introduction

Clotrimazole (**Figure 4.1**) is an imidazole containing compound that is predominantly used topically as an antifungal agent. It is widely used and highly effective in the treatment of fungal diseases in plants, humans and animals.<sup>1</sup> Clotrimazole is known to be of low toxicity, with its metabolism being well studied and understood.<sup>1</sup> Regarding its biosafety, it was found to be non-toxic towards mammalian cells when tested on cell line HepG2, with reported cell viability in excess of 80%.<sup>2</sup> Recently, a clotrimazole-coordinated silver complex (**Figure 4.2**) was reported by Govender *et al.* to be effective against *Staphylococcus aureus* and MRSA.<sup>2</sup>

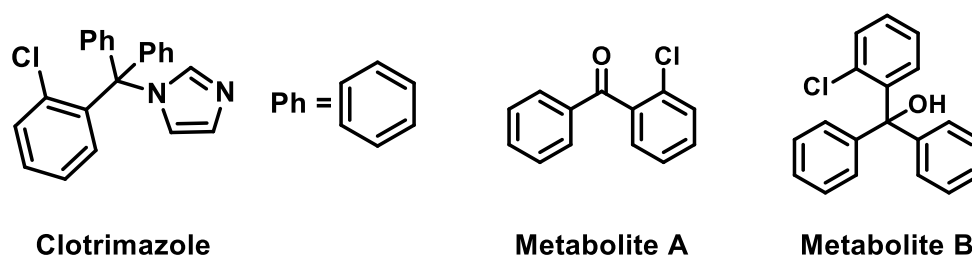


**Figure 4.1:** Molecular structure of clotrimazole, and its metabolites, 2-chlorobenzophenone **A** and (2-chlorophenyl)diphenylmethanol **B**<sup>1</sup>

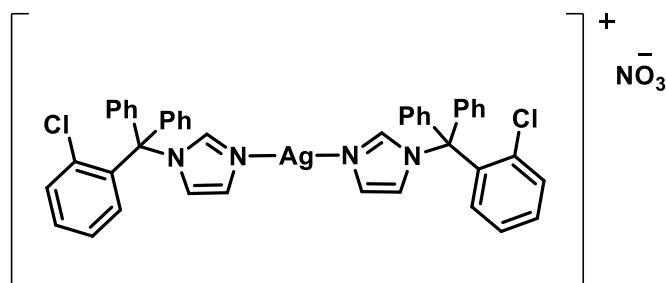


**Figure 4.2:** Clotrimazole-coordinated silver complex with potent antibacterial properties

Antitumor activity in lung metastases has also been reported for clotrimazole, including inhibition of cell proliferation both *in vitro* and *in vivo*.<sup>3</sup> Its *in vitro* activity is attributed to its cellular effect of depleting intracellular  $\text{Ca}^{2+}$  stores, interfering with the cellular homeostasis and contributing to the inhibition of cell proliferation in a dose-dependent manner. In addition, *in vivo* studies show the inhibitory effect of clotrimazole on lung metastases produced in mice, demonstrating its potential as an antiproliferative agent. Halperin *et al.* further investigated the intracellular role of clotrimazole resulting from  $\text{Ca}^{2+}$  depletion, and concluded that it has an effect on the activation of protein kinase R (PKR) followed by phosphorylation of translation initiation factor eIF2 $\alpha$ , thereby inhibiting protein synthesis at the translation initiation level leading to blockage of the cell cycle in G<sub>1</sub>.<sup>4</sup>

$\text{Cu}^{2+}$ ,  $\text{Co}^{2+}$ ,  $\text{Zn}^{2+}$  and  $\text{Ni}^{2+}$  coordination complexes of clotrimazole have recently been synthesised by Barba-Behrens *et al.*, with reported oxidative DNA damage (**Figure 4.3**).<sup>5</sup> The reduction of  $\text{Cu}^{2+}$  to  $\text{Cu}^+$ , which was studied electrochemically in one complex, appears to be the source of oxidative DNA damage properties. Mn(I) complexes of clotrimazole and related antifungals such as ketoconazole have been synthesised and tested against different strains of bacteria, showing good antiparasitic activity.<sup>6</sup>

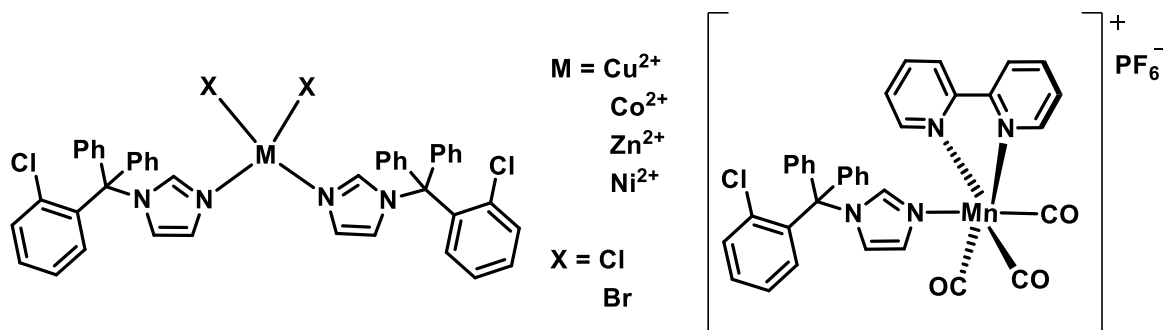


**Figure 4.3:**  $\text{Cu}^{2+}$ ,  $\text{Co}^{2+}$ ,  $\text{Zn}^{2+}$  and  $\text{Ni}^{2+}$  clotrimazole-coordination complexes that exhibit anticancer properties<sup>5</sup> and  $\text{Mn}^+$  complex with antibacterial activity<sup>6</sup>

As clotrimazole has low toxicity and has exhibited anticancer activities, it was used in the synthesis of imidazolium salts, followed by coordination to silver to give novel Ag(I)-NHC complexes. These were examined against a range of cancerous and non-cancerous cell lines to determine IC<sub>50</sub> values and selectivity indices.

## 4.2 Ligand synthesis

### 4.2.1 Clotrimazole-derived imidazolium salts

Only a small number of imidazolium salts prepared from clotrimazole have been reported to date.<sup>7,8</sup> In this study, clotrimazole was initially used for the synthesis of imidazolium iodide salts through reaction with alkyl halides such as methyl iodide. Reaction at RT gave 45% yield after 24 hours (**Table 4.1**, entry 1), therefore the reaction was heated at reflux in CH<sub>2</sub>Cl<sub>2</sub> (entry 2). A higher yield of 67% was obtained, which could be increased further to 74% after only 15 minutes by using microwave conditions (entry 3).

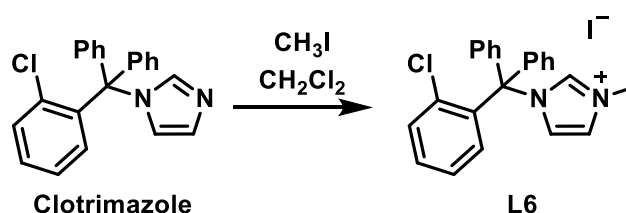
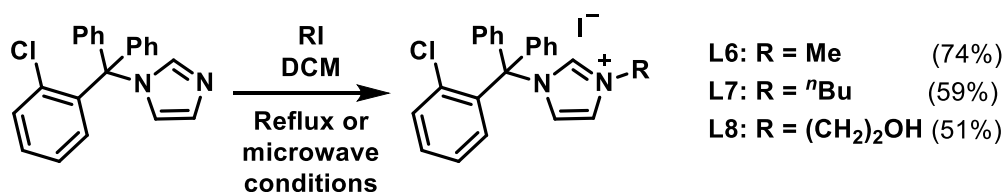


**Table 4.1:** Reaction conditions tested for the synthesis of methyl substituted imidazolium salt **L6**

|   | Temperature                              | Time (hours) | Yield % |
|---|--|--------------|---------|
| 1 | Room temperature                         | 24           | 45      |
| 2 | Reflux                                   | 24           | 67      |
| 3 | Microwave conditions<br>(45°C, 17.5 bar) | 0.25         | 74      |

Reactions were also performed with *n*-butyl iodide under microwave conditions and with 2-iodoethanol under reflux to synthesise imidazolium iodides **L7** and **L8** (**Scheme 4.1**). Ligands **L6-L8** were fully characterised using <sup>1</sup>H and <sup>13</sup>C{<sup>1</sup>H} NMR spectroscopy, HRMS and elemental analysis.



**Scheme 4.1:** Synthesis of imidazolium iodide salts **L6-L8** from clotrimazole

Single crystals of **L6-L8** suitable for X-ray diffraction analysis were grown by the vapour diffusion of Et<sub>2</sub>O into concentrated solutions of the ligands in CH<sub>2</sub>Cl<sub>2</sub>. The solid state structures (**Figure 4.4**) show the expected imidazolium salts with no evidence of hydrogen bonding between the iodide anions and the electron deficient imidazolium N-C-N rings. A C-H...I hydrogen bond might be expected to occur from a combination of electrostatic, charge transfer, polarization and dispersion between N-CH-N (proton donor) and the iodide (acceptor).<sup>9</sup> **L6** crystallised in the orthorhombic crystal system and was solved in the space group *Pbca*, while **L7** and **L8** both crystallised in the triclinic crystal system and their structural solutions were performed in the space group *P-1*. The tetrahedral geometry at **C4** of the triphenyl group is consistent in all three ligands in which all four angles around **C4** are  $\approx 109^\circ$  (**Table 4.2**). Although there is no evidence of anion- $\pi$  interactions between the iodide anion and the imidazolium ring in any of the ligands, anion- $\pi$  interactions appear to be present in both **L7** and **L8** between the aryl chloride and the imidazolium ring centroid, indicated by the short aryl chloride...imidazolium centroid distances of 3.278 Å and 3.331 Å respectively, which fall below the sum of the Van der Waals radii (**Figure 4.5**).

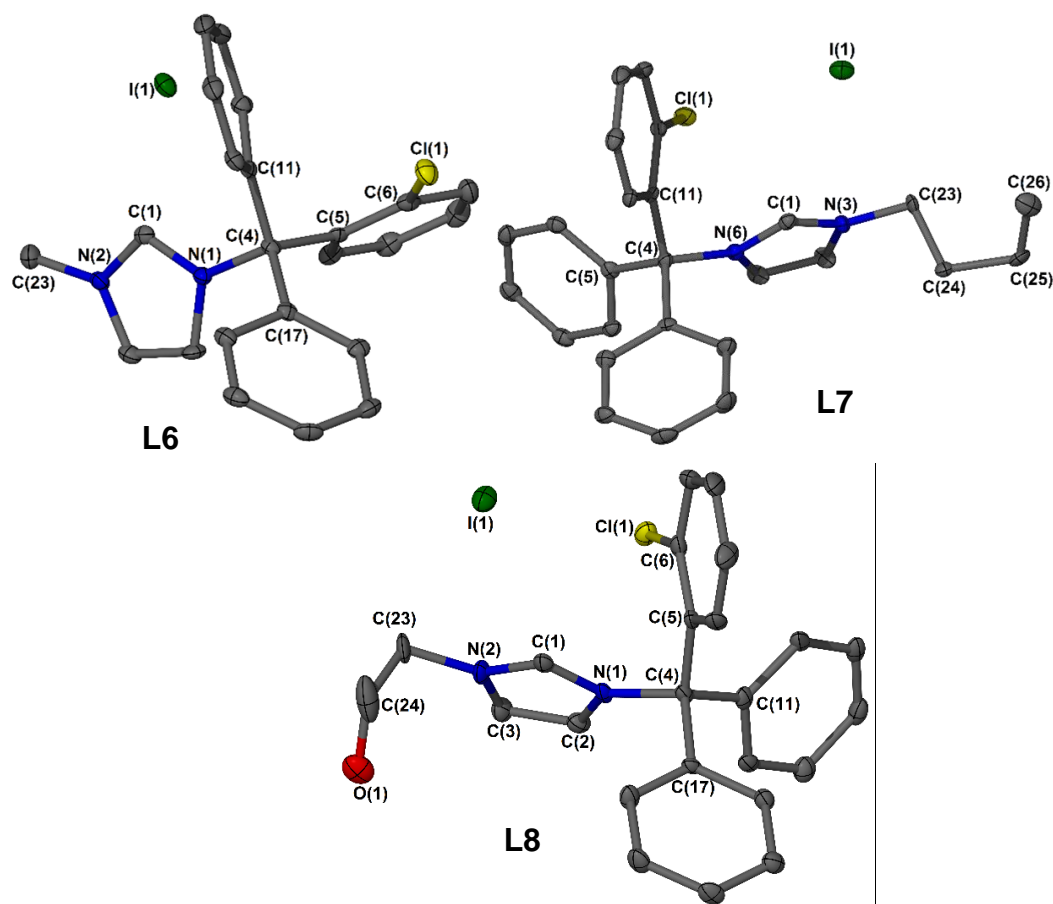


**Figure 4.4:** Molecular structures of imidazolium salts **L6-L8**. Ellipsoids are drawn at 50% probability level and H atoms are omitted for clarity

An interesting finding in the solid state structure of **L8** is the substitutional disorder between the chloride of the trityl group and the iodide counterion, most likely due to an exchange between the two. This results in a mixture of 97% Cl(1) and 3% I(2) on the phenyl, and a mixture of 29% Cl(2) and 71% I(1) as the counterion.

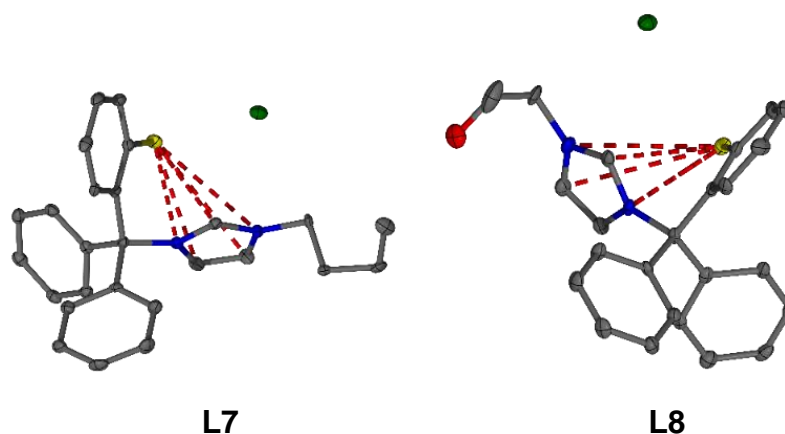
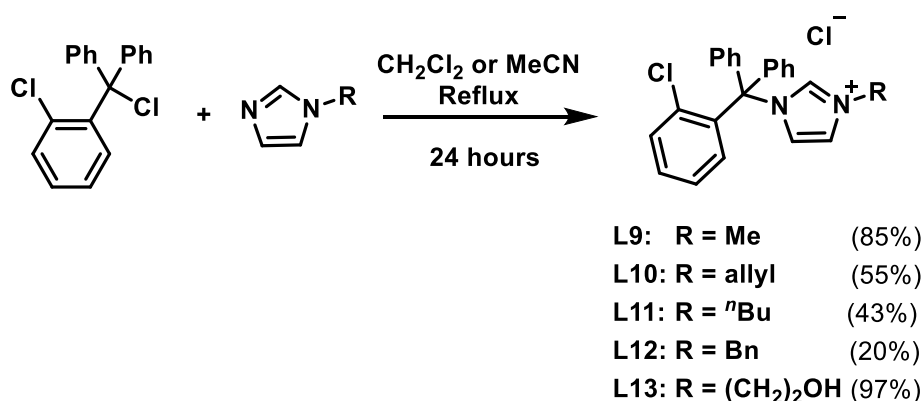


**Figure 4.5:** Anion- $\pi$  interactions observed in **L7** and **L8**

| <b>Table 4.2:</b> Selected bond lengths and angles for imidazolium salts <b>L6-L8</b> |           |            |           |
|---|-----------|------------|-----------|
| Bond Lengths (Å) and angles (°)   | <b>L6</b> | <b>L7</b>  | <b>L8</b> |
| N1-C1-N2  | 108.9(2)  | 109.2(2)   | 109.0(4)  |
| N1-C4-C5  | 107.1(3)  | 106.31(19) | 106.0(3)  |
| N1-C4-C17   | 108.3(3)  | 110.4(2)   | 108.0(3)  |
| N1-C4-C11   | 104.4(3)  | 107.8(2)   | 110.6(3)  |
| C5-C4-C11   | 112.8(3)  | 113.2(2)   | 111.9(3)  |
| C17-C4-C11  | 114.0(3)  | 109.6(2)   | 109.1(3)  |
| C17-C4-C5   | 109.8(3)  | 113.2(2)   | 111.1(3)  |
| C6-Cl1  | 1.741(4)  | 1.745(3)   | 1.747(5)  |
| N1-C4   | 1.508(4)  | 1.513(3)   | 1.519(5)  |
| N2-C23  | 1.465(4)  | 1.478(3)   | 1.469(5)  |
| Cl1.....C1  | 5.511     | 3.188      | 3.201     |
| I1.....C1   | 3.729     | 3.815      | 3.630     |
| Cl1.....I1  | 6.864     | 4.771      | 4.443     |

### 4.2.2 Imidazolium salts synthesised from 2-chlorotrityl chloride

In order to prevent mixed halides between the phenyl group and the counterion, a second route was developed for the synthesis of the desired imidazolium salts. Substituted imidazoles were reacted with 2-chlorotrityl chloride in either  $\text{CH}_2\text{Cl}_2$  or MeCN at reflux to give imidazolium chloride salts **L9-L13** (Scheme 4.2), which were fully characterised using  $^1\text{H}$  and  $^{13}\text{C}\{^1\text{H}\}$  NMR spectroscopy, HRMS and elemental analysis.



**Scheme 4.2:** Synthesis of imidazolium chloride salts **L9-L13** from 2-chlorotrityl chloride

Single crystals of **L9**, **L10**, **L12** and **L13** suitable for X-ray diffraction analysis were grown by vapour diffusion of  $\text{Et}_2\text{O}$  into concentrated solutions of the ligands in either  $\text{CH}_2\text{Cl}_2$  (**L9**, **L10** and **L12**) or MeOH (**L13**). **L9** and **L12** crystallised in the monoclinic crystal system with the structural solution of **L9** solved in the space group  $P2_1$  and **L12** solved in the space group  $P2_1/c$ . **L10** crystallised in the orthorhombic crystal system and the structural solution solved in the space group  $Pbca$ , while **L13** crystallised in the triclinic crystal system and its structural solution solved in the space group  $P-1$ . Both **L10** and **L12** crystallised with a molecule of  $\text{H}_2\text{O}$  which forms hydrogen bonds with the chloride counterion (Figure 4.6). Hydrogen bonding of the chloride counterion with the imidazolium N-CH-N is only observed in the molecular structure of **L9**.

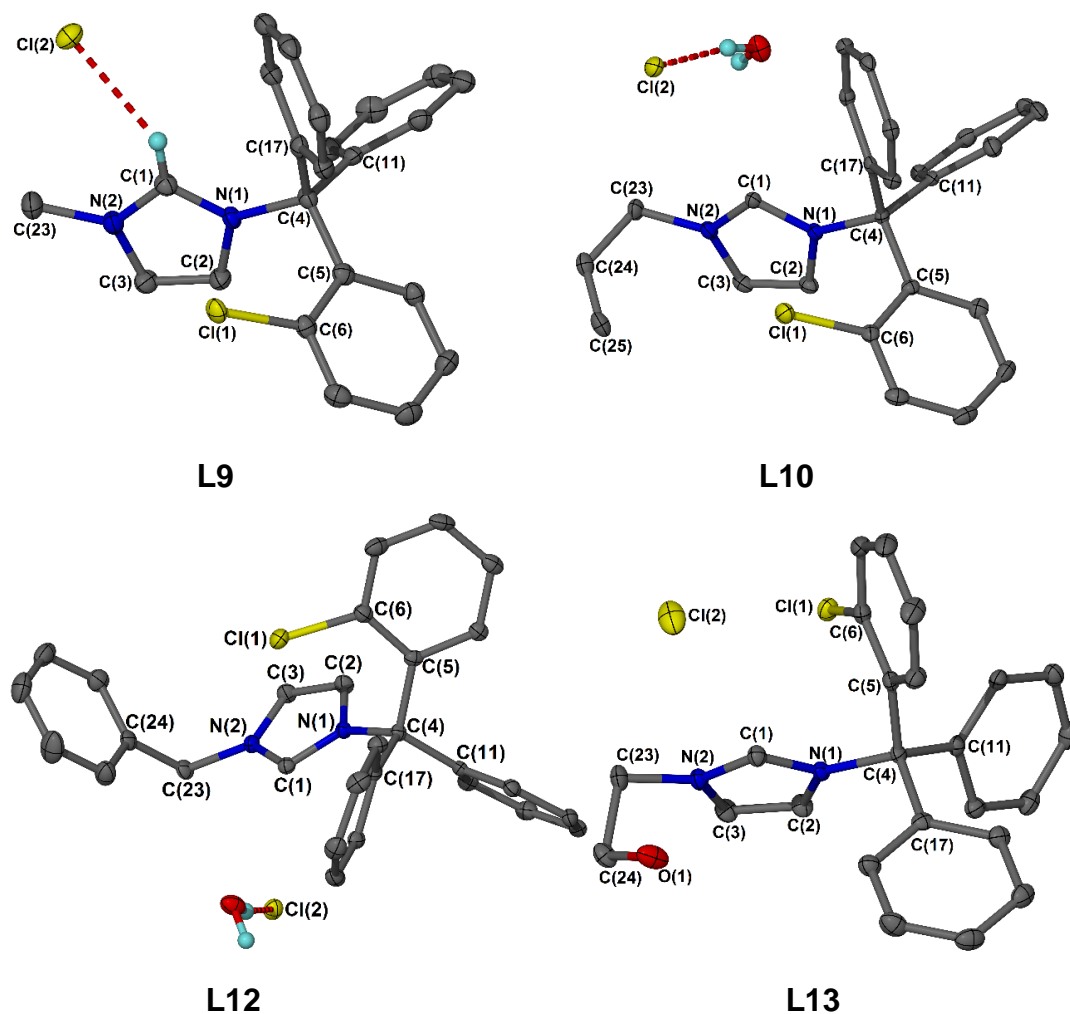


**Figure 4.6:** Molecular structure of imidazolium chloride salts **L9**, **L10**, **L12** and **L13**. Ellipsoids are drawn at the 50% probability level and H atoms (except those on H<sub>2</sub>O) have been omitted for clarity

| <b>Table 4.3:</b> Selected bond lengths and angles for <b>L9</b> , <b>L10</b> , <b>L12</b> and <b>L13</b> . |           |             |             |             |
|---|-----------|-------------|-------------|-------------|
| Bond Lengths (Å)<br>and angles (°)  | <b>L9</b> | <b>L10</b>  | <b>L12</b>  | <b>L13</b>  |
| N(1)-C(1)-N(2)  | 108.1 (3) | 108.53 (17) | 108.21 (16) | 108.99 (14) |
| N(1)-C(4)   | 1.514 (4) | 1.503 (2)   | 1.516 (2)   | 1.509 (2)   |
| N(2)-C(23)  | 1.478 (4) | 1.467 (2)   | 1.485 (2)   | 1.470 (2)   |
| Cl(1)-C(6)  | 1.755 (3) | 1.745 (2)   | 1.752 (2)   | 1.7471 (17) |
| Cl(1)·····C(1)  | 3.271     | 3.255       | 3.256       | 3.230       |
| Cl(2)·····C(1)  | 3.323     | 3.432       | 3.782       | 3.371       |
| Cl(1)·····Cl(2)   | 5.661     | 5.415       | 7.026       | 4.247       |

Similarly to **L7** and **L8**, anion- $\pi$  interactions between the chloride on the trityl group (labelled Cl(1) in the molecular structures) and the N-C-N carbon atom (labelled C(1)) are present in **L10**, **L12** and **L13**, indicated by the short distances between them (**Table 4.3**). Intermolecular hydrogen bonds between the protons in the H<sub>2</sub>O molecules and the chloride counterion are observed in the packing of **L10** and **L13** (**Figure 4.7**). The packing diagrams of **L10** and **L13** show that the molecules pack head-tail-tail-head on all axes, with intermolecular hydrogen bonds between the OH of one molecule and chloride counterion of another in the centre of the planes.

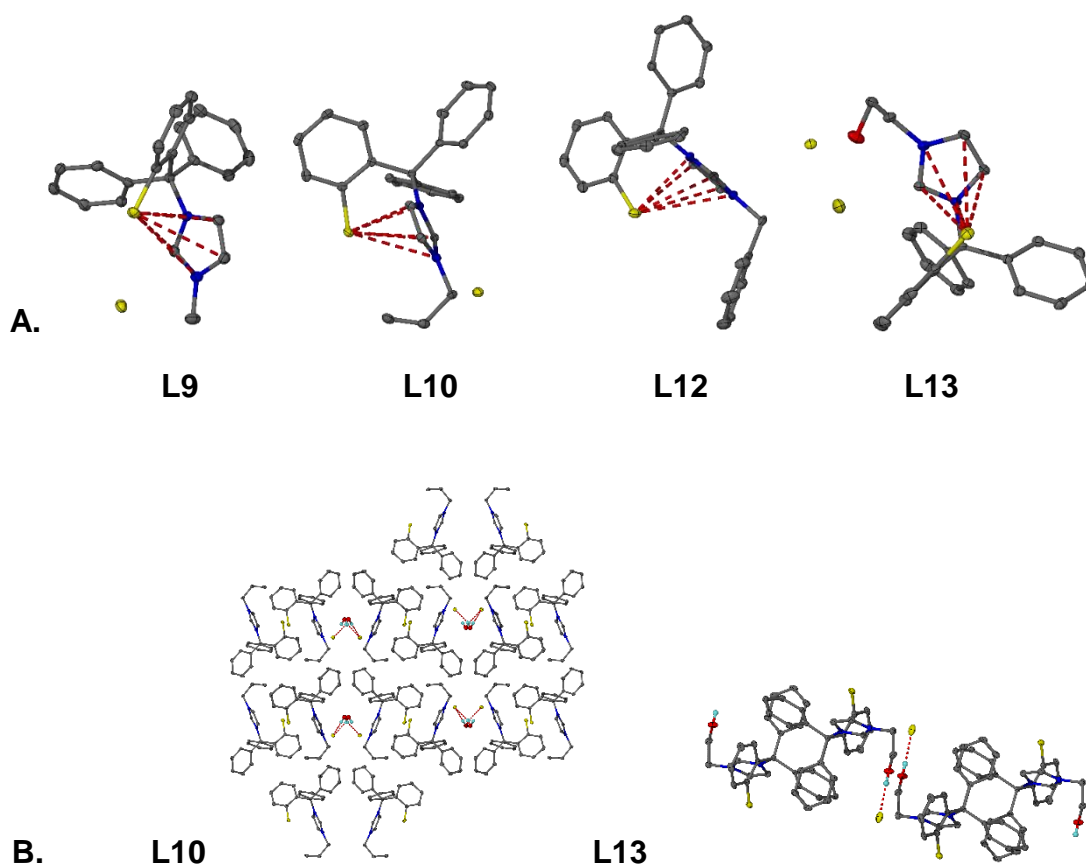
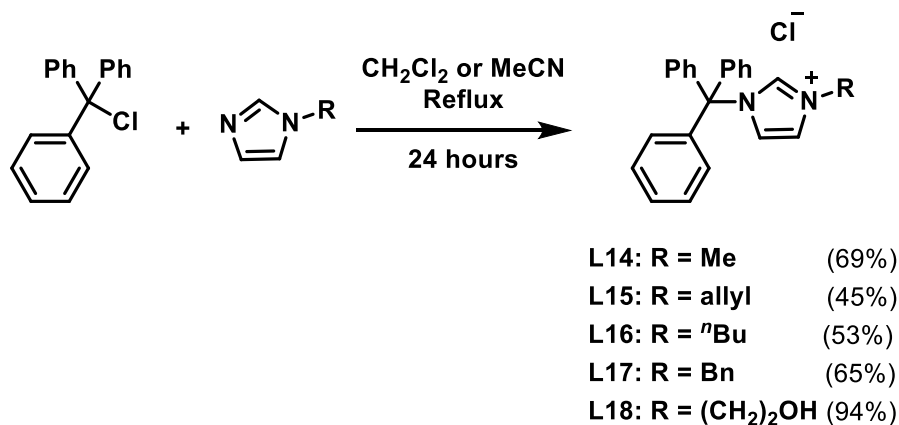


**Figure 4.7:** **A.** anion- $\pi$  interactions observed in **L9**, **L10**, **L12** and **L13**, and **B.** packing diagrams of **L10** and **L13** along the *b* axes

### 4.2.3 Imidazolium salts synthesised from trityl chloride

Imidazolium salts **L17-L21** were prepared from trityl chloride in order to examine the effect of removing the chloride from the trityl group (**Scheme 4.3**) on anticancer activity. Slight shifts in the  $^1\text{H}$  NMR spectra are observed between the chloride-containing ligands **L9-L13** and their non-chloride analogous **L14-L18**. Bigger shifts are observed in the  $^{13}\text{C}\{^1\text{H}\}$  spectra where the loss of Cl generates a symmetrical trityl group as shown in **Figure 4.8**.



**Scheme 4.3:** Synthesis of imidazolium chloride salts **L14-L18** from trityl chloride

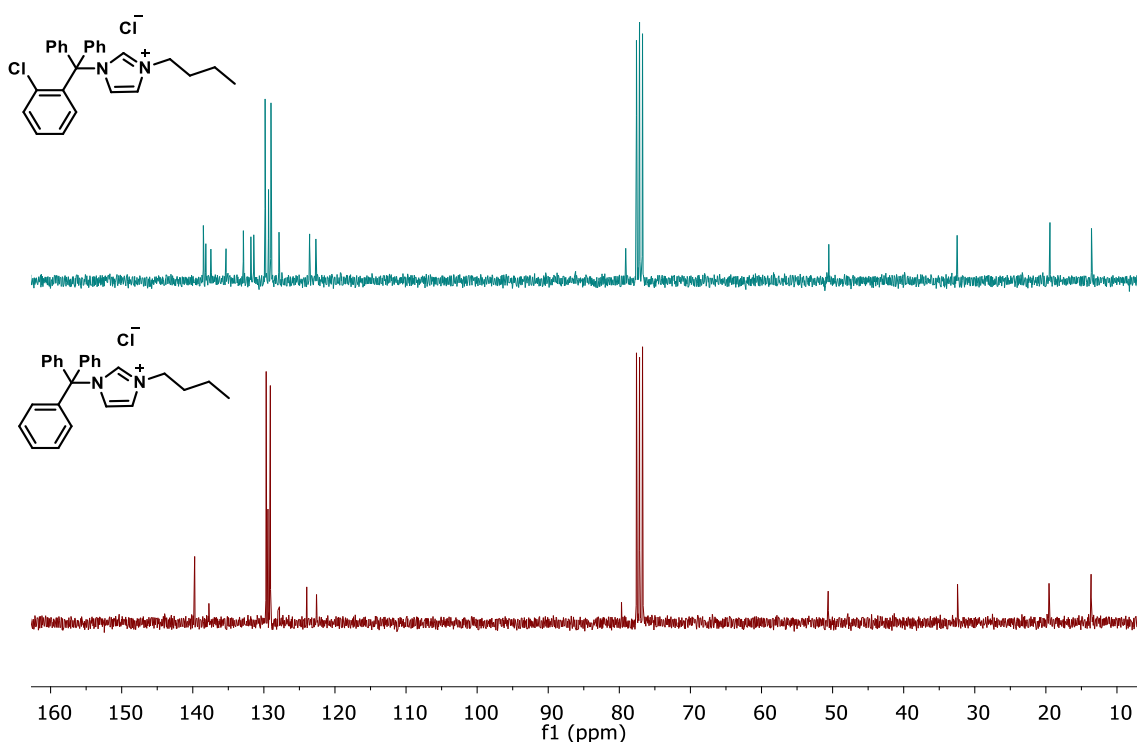


**Figure 4.8:**  $^{13}\text{C}\{^1\text{H}\}$  NMR spectra (75 MHz,  $\text{CHCl}_3$ ) of **L11** (top) and **L16** (bottom)

Single crystals of **L18** suitable for X-ray diffraction analysis were grown by vapour diffusion of Et<sub>2</sub>O into a concentrated solution in MeOH. **L18** crystallises in the monoclinic crystal system and the structural solution was performed in the *P2<sub>1</sub>/c* space group. A hydrogen bond between the chloride counterion and the terminal OH group can be seen in the solid state structure (**Figure 4.9**), which is not observed in other OH containing imidazolium salts **L8** and **L13**.

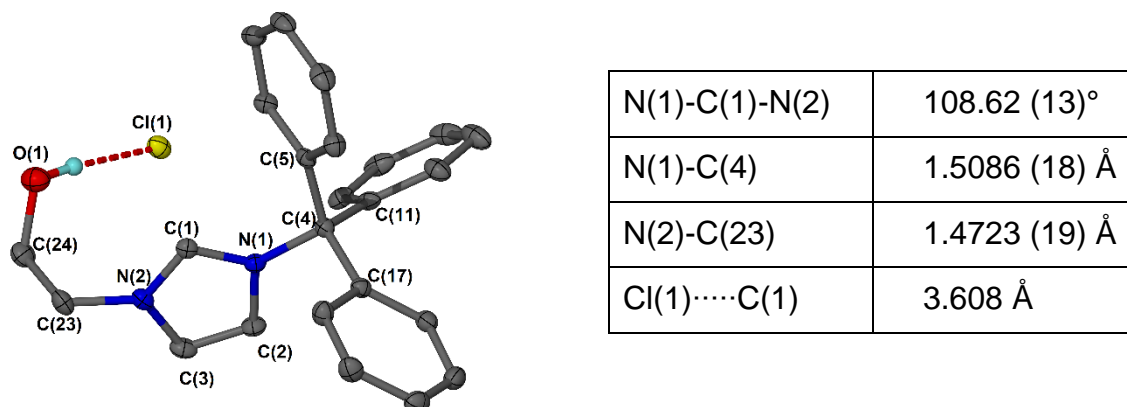
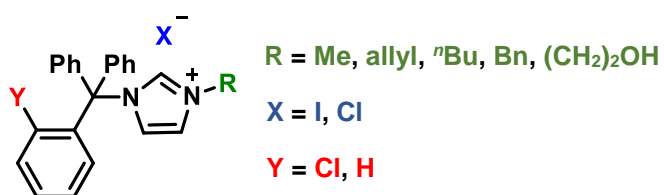


**Figure 4.9:** Molecular structure of **L18**. Ellipsoids are shown at 50% probability level and H atoms (except OH) are omitted for clarity

Thirteen clotrimazole-derived ligand precursors **L6-L18** have been synthesised and are categorised into three groups: 1) those containing an iodide counterion and 2-chlorotriptyl group (**L6-L8**), 2) those containing a chloride counterion and 2 chlorotriptyl group (**L9-L13**), and 3) those containing a chloride counterion and triptyl group (**L14-L18**) (**Figure 4.10**).

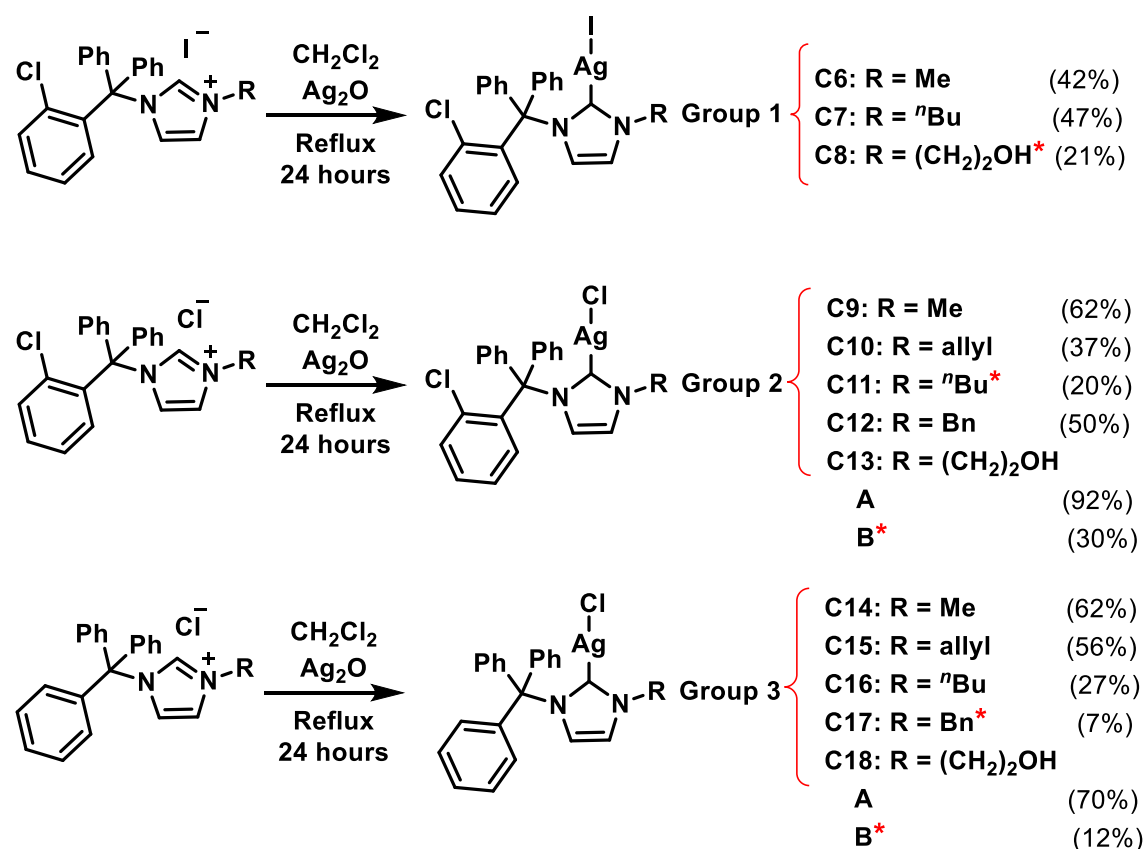


| Group | X  | Me  | allyl | <sup>n</sup> Bu | Bn  | (CH <sub>2</sub> ) <sub>2</sub> OH | Y  |
|-------|----|-----|-------|-----------------|-----|------------------------------------|----|
| 1     | I  | L6  | -     | L7              | -   | L8                                 | Cl |
| 2     | Cl | L9  | L10   | L11             | L12 | L13                                | Cl |
| 3     | Cl | L14 | L15   | L16             | L17 | L18                                | H  |

**Figure 4.10:** Clotrimazole-derived imidazolium salts synthesised in this work

### 4.3 Silver(I)-NHC complexes

Silver(I)-NHC complexes were synthesised by reaction of the thirteen ligand precursors with  $\text{Ag}_2\text{O}$  in  $\text{CH}_2\text{Cl}_2$  at reflux (**Scheme 4.4**). The thirteen complexes **C6-C18** were fully characterised using  $^1\text{H}$  and  $^{13}\text{C}\{^1\text{H}\}$  NMR spectroscopy, HRMS and elemental analysis. Both mono(NHC) and bis(NHC) complexes are observed in the HRMS data, which is not uncommon for  $\text{Ag}(\text{I})$ -NHC complexes (**Figure 4.11**).<sup>10-12</sup> The elemental analysis reveals the formation of mono(NHC) in each case except **C8**, **C11** and **C17** which revealed a mixture of mono(NHCs) and bis(NHCs) (see experimental). In the case of **C13** and **C18**, increasing the amount of  $\text{Ag}_2\text{O}$  in the reactions gave only mono(NHC) complexes. Therefore the complexes are numbered **C13A** and **C18A** (purely mono(NHCs)), and **C13B** and **C18B** (mixture of mono(NHCs) and bis(NHCs)).



**Scheme 4.4:** Synthesis of silver(I)-NHC complexes **C6-C18**. \*Elemental analysis reveals a mixture of  $\text{Ag}(\text{NHC})\text{X}$  and  $[\text{Ag}(\text{NHC})_2]\text{X}$ , where  $\text{X} = \text{I}$  or  $\text{Cl}$

Single crystals suitable for X-ray diffraction analysis of **C7**, **C13B**, **C14**, **C15** and **C17** were obtained by vapour diffusion of Et<sub>2</sub>O (**C13**, **C14**, **C15** and **C17**) or C<sub>5</sub>H<sub>12</sub> (**C7**) into concentrated solutions of the complexes in either CH<sub>2</sub>Cl<sub>2</sub> (**C7**, **C14**, **C15** and **C17**) or MeOH (**C13B**). All five complexes crystallise in the monoclinic crystal system, with their structural solutions performed in different space groups; **C7**, **C14** and **C17** were solved in *P2<sub>1</sub>/n*, **C13B** in *C2/c* and **C15** in *P2<sub>1</sub>* space groups. While complexes **C14** and **C15** crystallise as mono(NHC) complexes, **C7**, **C13B** and **C17** crystallise as the bis(NHC) complex (**Figure 4.12**). Interestingly, two bis(NHC) molecules of **C7** are present in one unit cell, and co-crystallise with a molecule of n-pentane and [AgCl]<sub>2</sub> as shown in **Figure 4.12**, in addition halide exchange can be observed between the Cl<sup>-</sup> on the triphenyl and the I<sup>-</sup> counterion. **C17** Co-crystallises with a molecule of H<sub>2</sub>O and two molecules of CH<sub>2</sub>Cl<sub>2</sub>, one of which it forms hydrogen bonds with an aromatic hydrogen. The silver centres in each solid-state structure deviate slightly from linearity (**Table 4.4**). Similar to the packing of its ligand precursor **L13**, the molecules in **C13B** pack head-tail-tail-head (**Figure 4.13**).

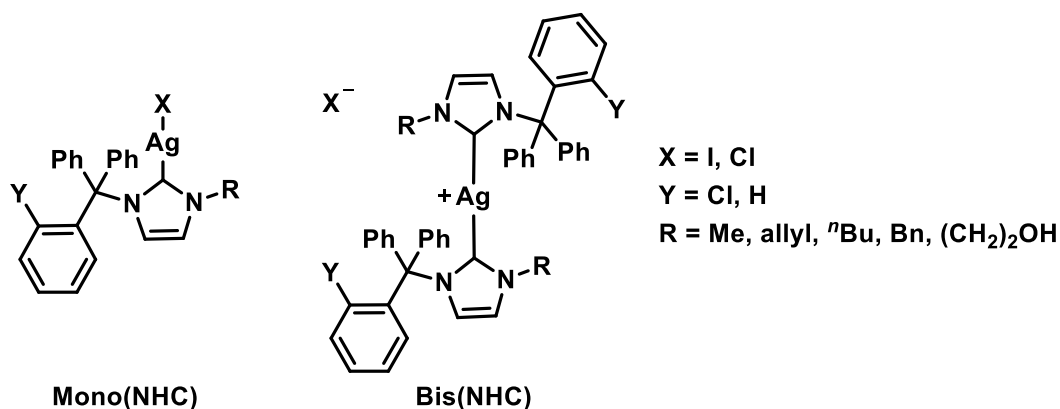


**Figure 4.11:** Structures of mono(NHC) and bis(NHC) complexes

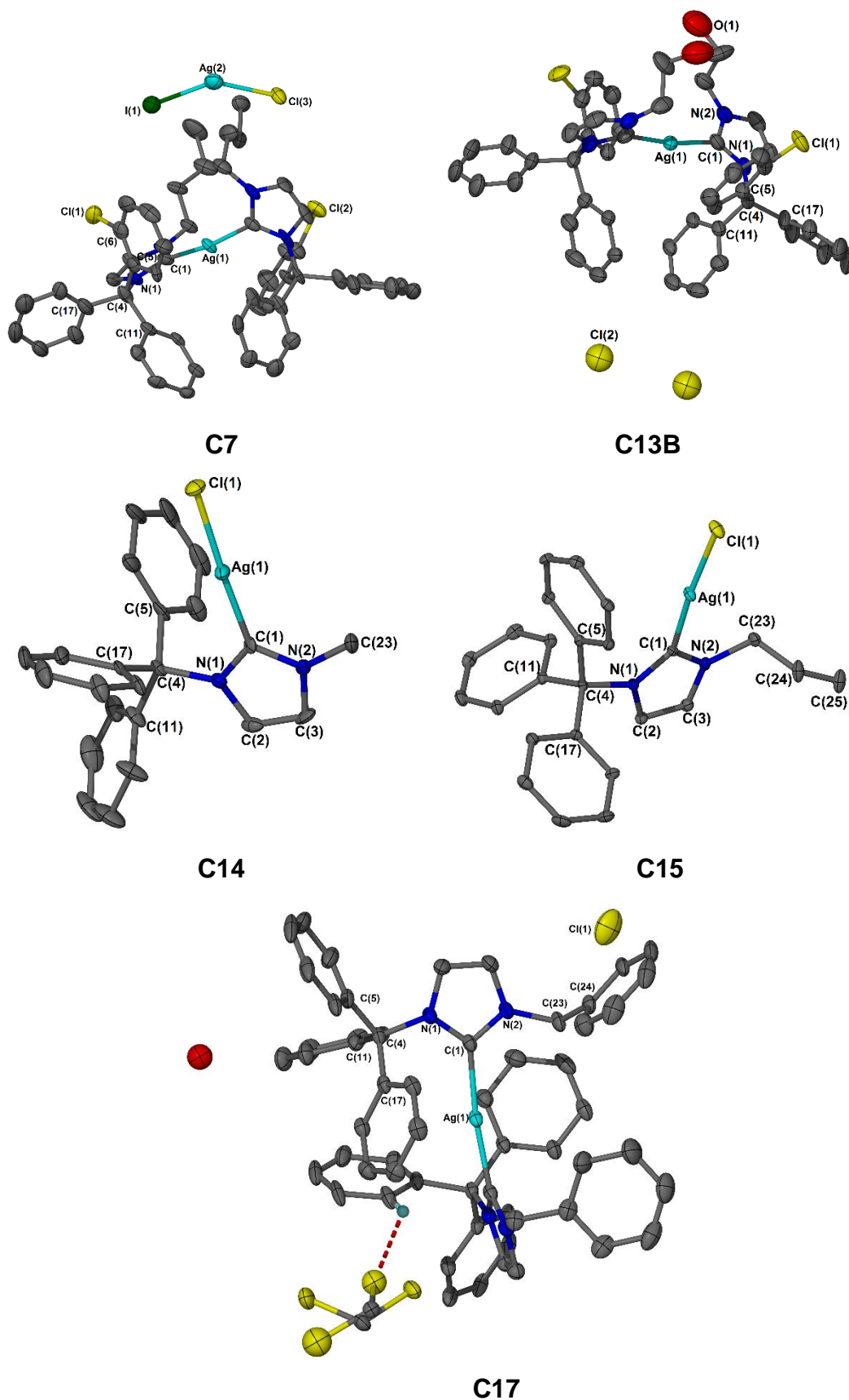


**Figure 4.12:** Molecular structures of **C7**, **C13B**, **C14**, **C15** and **C17**. Ellipsoids are shown at 50% probability for **C14** and **C15**, 40 % for **C17** and 35% for **C7** and **C13B**. H atoms are omitted for clarity

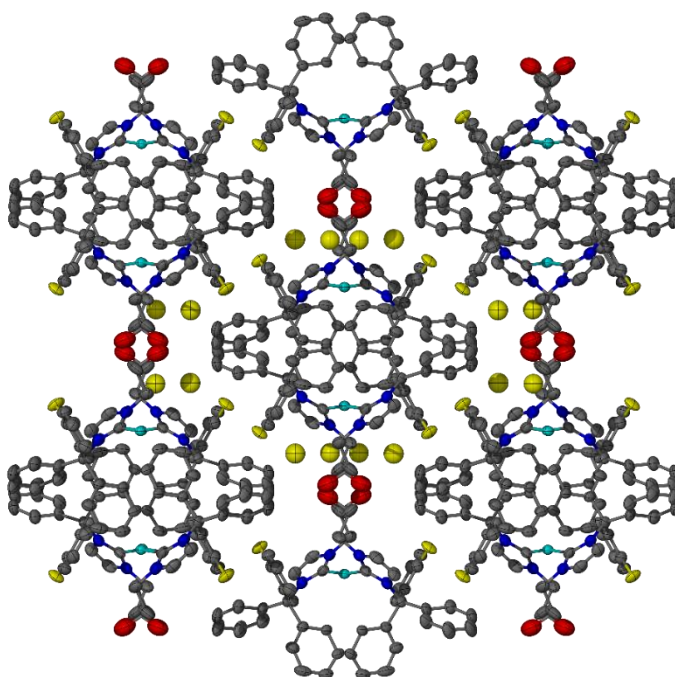


**Figure 4.13:** Packing diagram of **C13B** along the *c* axis. Ellipsoids are shown at 35% probability and H atoms are omitted for clarity

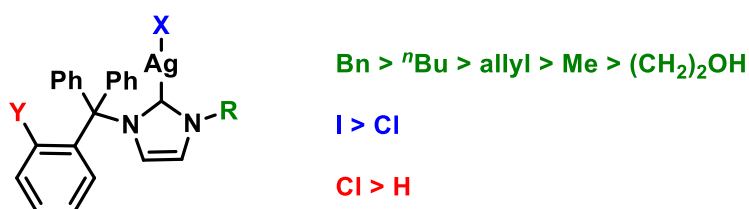
**Table 4.4:** Selected bond lengths and angles for **C7**, **C13B**, **C14**, **C15** and **C17**

| Selected bond lengths (Å) and angles (°) | <b>C7</b>  | <b>C13B</b> | <b>C14</b>  | <b>C15</b>  | <b>C17</b>  |
|--|------------|-------------|-------------|-------------|-------------|
| <b>Ag1-C1</b>                            | 2.08 (2)   | 2.109 (10)  | 2.091 (5)   | 2.102 (4)   | 2.121 (3)   |
| <b>Ag1-Cl1</b>                           | -          | -           | 2.3216 (14) | 2.3633 (12) | -           |
| <b>N1-C1-N2</b>                          | 104.9 (17) | 106.0 (9)   | 105.9 (5)   | 103.9 (3)   | 104.1 (3)   |
| <b>Ag1-C1-N1</b>                         | 130.4 (15) | 131.8 (7)   | 127.3 (4)   | 132.9 (3)   | 127.8 (3)   |
| <b>C1-Ag1-C1</b>                         | 171.2 (7)  | 171.3 (5)   | -           | -           | 173.66 (12) |
| <b>C1-Ag1-Cl1</b>                        | -          | -           | 176.42 (14) | 174.45 (11) | -           |

## 4.4 Hydrophobicity measurements

The hydrophobicity of complexes **C6-C18** was measured in a similar fashion as previously reported for xanthine-derived complexes (section 2.4). Unlike xanthine-derived complexes **C1-C5** which were more soluble in the aqueous layer, clotrimazole derived complexes were found to be more soluble in the octanol layer, and hence measurements for **C6-C18** were conducted in the octanol layer. As discussed in chapter 2, a negative Log *P* value indicates a hydrophilic complex, and a positive Log *P* indicates a lipophilic complex which is more likely to cross biological membranes through passive diffusion.

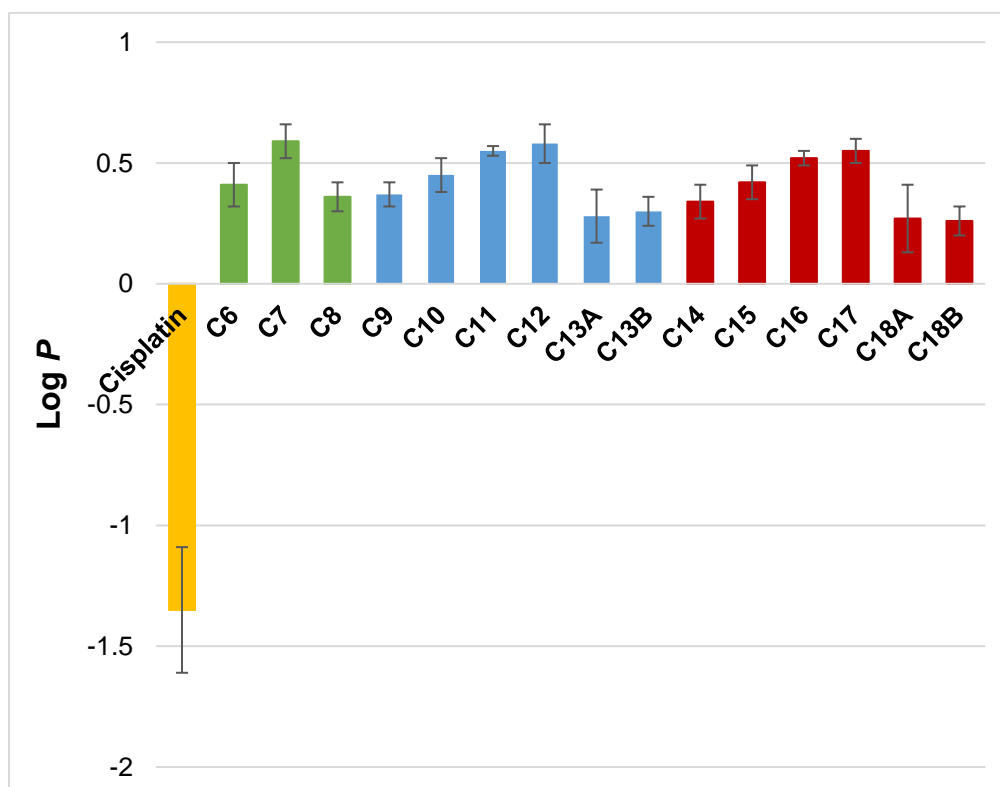
Due to the triphenyl group, all thirteen complexes **C6-C18** showed positive Log *P* values indicating that they are all hydrophobic (**Table 4.5**). In general, hydrophobicity increases where R = hydroxyethyl < methyl < allyl < butyl < benzyl, across the three groups of complexes. The 2-chlorotriptyl complexes **C9-C13** are slightly more hydrophobic than their triptyl derivatives **C14-18**. Exchanging the counterion from I<sup>-</sup> to Cl<sup>-</sup> decreases the hydrophobicity *i.e.* **C6-C8** are more hydrophobic than **C9, C11** and **C13**. The Log *P* of cisplatin was measured using the same method. Cisplatin was more soluble in the aqueous layer and a value of -1.35 was obtained, which is less negative than the literature value of -2.35, though the complex is clearly hydrophilic.



**Figure 4.14:** Structure-based hydrophobicity trends

**Table 4.5:** Log *P* values of **C6-C18** and cisplatin

| <b>Complex</b>          | <b>Log <i>P</i></b> | <b>±SD</b> |
|-------------------------|---------------------|------------|
| <b><i>Cisplatin</i></b> | -1.35               | 0.26       |
| <b>C6</b>               | 0.41                | 0.09       |
| <b>C7</b>               | 0.59                | 0.07       |
| <b>C8</b>               | 0.36                | 0.06       |
| <b>C9</b>               | 0.37                | 0.05       |
| <b>C10</b>              | 0.45                | 0.07       |
| <b>C11</b>              | 0.55                | 0.02       |
| <b>C12</b>              | 0.58                | 0.08       |
| <b>C13A</b>             | 0.28                | 0.11       |
| <b>C13B</b>             | 0.30                | 0.06       |
| <b>C14</b>              | 0.34                | 0.07       |
| <b>C15</b>              | 0.42                | 0.07       |
| <b>C16</b>              | 0.52                | 0.03       |
| <b>C17</b>              | 0.55                | 0.05       |
| <b>C18A</b>             | 0.25                | 0.14       |
| <b>C18B</b>             | 0.26                | 0.06       |

**Figure 4.15:** Bar chart of Log *P* values of **C6-C18** and cisplatin

## 4.5 Anticancer testing

The *in vitro* cytotoxicity of complexes **C6-C18** was measured using MTT-based assays against cancerous cell line Panc 10.05, a pancreatic adenocarcinoma cell line, in addition to non-cancerous ARPE-19, a retinal epithelial cell line. Complexes that exhibited promising cytotoxicity and/or selectivity were further tested against the cancerous cell lines Mia-PA-CA-2 (pancreatic carcinoma) and BE (colorectal carcinoma). The results are summarised in **Table 4.6** and **Figure 4.16**. It is evident that the 2-chlorotrityl complexes (**C9-C13**) are consistently more cytotoxic than their trityl analogues (**C14-C18**) against Panc 10.05. This indicates a positive effect of having a 2-chloro substituent on the trityl which may be attributed to increased hydrophobicity, improving the complexes ability to cross cellular membranes.<sup>13</sup>

Interestingly, the N-hydroxyethyl substituted complexes **C13** and **C18** (including mono-NHCs (**C13A** and **C18A**) and mixed mono/bis(NHCs) (**C13B** and **C18B**)) are the most cytotoxic in their groupings (highlighted in red, **Table 4.6**). These are followed by the N-benzyl containing complexes **C12** and **C17** (highlighted in green), possibly attributed to their lipophilicity which allows them to cross cell membranes. Improved water solubility allows a drug to flow more freely through the bloodstream and reach its site of action, which is beneficial *in vivo*.<sup>14, 15</sup> In addition, improved water solubility (increased relative hydrophilicity and lower Log *P*) leads to a drug with a more “intermediate lipophilicity”, which is reportedly optimum for anticancer activity.<sup>16</sup>

N-hydroxyethyl substituted complexes **C13B** and **C18B** are significantly more selective towards Panc 10.05 over ARPE-19 than other complexes in their groups. **C13B** has similar cytotoxicity to cisplatin, with an IC<sub>50</sub> value of 1.3 (± 0.5), compared to cisplatin's 1.7 (± 0.4) against Panc 10.05. Furthermore, **C13B** displays much improved selectivity over cisplatin, with an ARPE-19 / Panc 10.05 selectivity ratio of 17.5 (cisplatin = 3.8) an ARPE-19 / Mia-PA-CA2 selectivity ratio of 6.62 (cisplatin = 2.3). The selectivity ratios represent the selectivity of the drug towards cancerous over non-cancerous cell lines, and is presented as a value of IC<sub>50</sub> non-cancerous / IC<sub>50</sub> cancerous e.g. IC<sub>50</sub> ARPE-19 / IC<sub>50</sub> Panc10.05, where a higher value indicates higher selectivity towards cancerous cell line. It is worthy to note that **C18A**, **C13A**, and **C9** display no toxicity towards the non-cancerous cell line at the highest concentration (50µM) indicating that these complexes may be selective towards cancer cell lines.

Iodide-containing complexes **C6-C8** were evaluated against the 3 cancerous cell lines Panc 10.05, Mia-PA-CA2 and BE and the non-cancerous ARPE-19. The results on the colorectal carcinoma BE indicate that the same trends observed above for **C9-C18** also apply to **C6-C8** on this specific cell line, with hydroxyethyl substituted complex **C8** showing the lowest IC<sub>50</sub> value ( $2.0 \pm 0.3$ ). In particular, **C8** appears selective towards BE over the other cell lines, and has significantly improved cytotoxicity compared to the analogous complexes with chloride counterions. This indicates that the presence of the iodide counter anion increases cytotoxicity against BE (highlighted in red, **Table 4.6**).

**Table 4.6:** Responses of Panc 10.05, Mia-PA-CA-2 and BE cancerous cell lines and ARPE-19 non-cancerous cell line to silver(I)-NHC complexes **C6-C18**. Values presented are IC<sub>50</sub> (μM) ±SD for three independent experiments. \*minimum value if IC<sub>50</sub> for ARPE-19 is 50 μM.

| Cell Line        | Panc 10.05 | Selectivity ratio<br>(ARPE-19/Panc10.05) | Mia-PA-CA2 | Selectivity ratio<br>(ARPE-19/MIA-PA-CA2) | BE         | Selectivity ratio<br>(ARPE-19/BE) | ARPE-19    |
|------------------|------------|--|------------|---|------------|-----------------------------------|------------|
| <b>Cisplatin</b> | 1.7 ± 0.4  | 3.8                                      | 2.8 ± 2.1  | 2.3                                       | 0.7 ± 0.3  | 9.7                               | 6.4 ± 1.0  |
| <b>C6</b>        | 10.0 ± 7.0 | 2.4                                      | 5.7 ± 2.3  | 4.2                                       | 3.3 ± 1.2  | 7.3                               | 24.2 ± 2.6 |
| <b>C7</b>        | 3.9 ± 2.0  | 2.3                                      | 4.6 ± 3.9  | 1.9                                       | 3.6 ± 0.9  | 2.4                               | 8.7 ± 1.5  |
| <b>C8</b>        | 13.3 ± 8.0 | 1.2                                      | 6.9 ± 2.1  | 2.3                                       | 2.0 ± 0.3  | 8.5                               | 26.0 ± 1.7 |
| <b>C9</b>        | 7.1 ± 3.7  | 7.0*                                     | 11.7 ± 1.6 | 4.3*                                      | 18.0 ± 4.4 | 2.8*                              | > 50       |
| <b>C10</b>       | 9.4 ± 5.6  | 1.2                                      | 6.3 ± 4.8  | 1.8                                       | 6.7 ± 1.1  | 1.7                               | 11.5 ± 3.0 |
| <b>C11</b>       | 10.1 ± 4.6 | 1.6                                      | -          | -   | -          | -                                 | 16.3 ± 3.2 |
| <b>C12</b>       | 5.8 ± 1.4  | 1.8                                      | 7.0 ± 1.6  | 1.5                                       | 8.4 ± 1.3  | 1.2                               | 10.3 ± 0.8 |
| <b>C13A</b>      | -          | -  | 3.3 ± 0.9  | 15.2*                                     | -          | -                                 | > 50       |
| <b>C13B</b>      | 1.3 ± 0.5  | 17.5                                     | 3.3 ± 1.2  | 6.6                                       | 5.8 ± 4.6  | 3.8                               | 21.9 ± 4.4 |
| <b>C14</b>       | 16.1 ± 0.9 | 1.7                                      | -          | -   | -          | -                                 | 26.7 ± 7.8 |
| <b>C15</b>       | 16.1 ± 2.0 | 1.7                                      | -          | -   | -          | -                                 | 27.5 ± 7.5 |
| <b>C16</b>       | 16.8 ± 1.9 | 0.8                                      | -          | -   | -          | -                                 | 13.8 ± 6.5 |
| <b>C17</b>       | 9.6 ± 1.2  | 3.4                                      | -          | -   | -          | -                                 | 32.1 ± 3.3 |
| <b>C18A</b>      | -          | -  | 2.7 ± 0.3  | 18.3*                                     | -          | -                                 | > 50       |
| <b>C18B</b>      | 5.3 ± 1.7  | 5.3                                      | 5.9 ± 1.3  | 4.8                                       | 6.1 ± 3.0  | 4.6                               | 28.0 ± 4.2 |

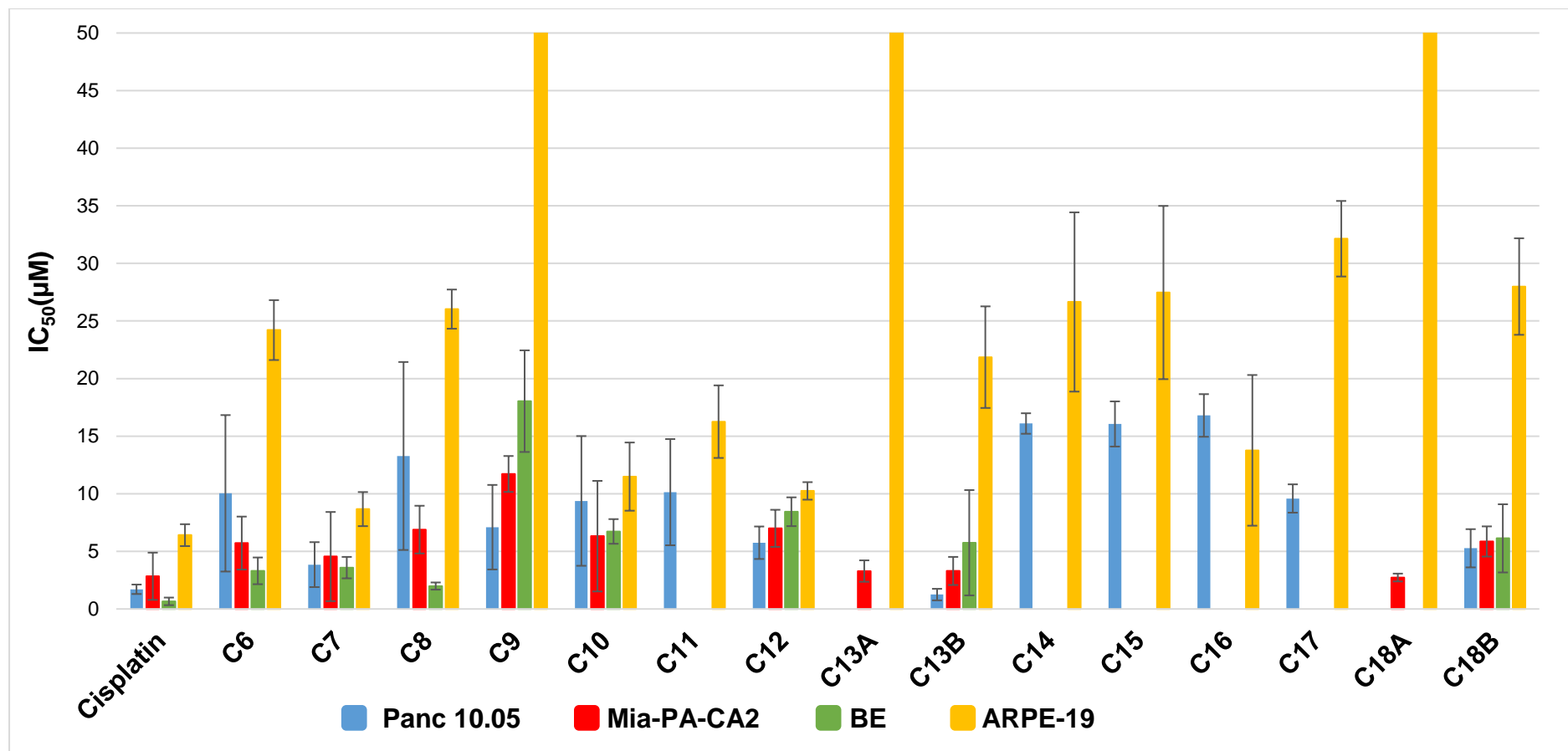


**Figure 4.16:** Bar chart to show IC<sub>50</sub> values for complexes **C6-C18** in comparison to cisplatin against Panc 10.05, Mia-PA-CA-2 and BE cancerous cell lines and ARPE-19 non-cancerous cell line

## 4.6 Conclusions

Thirteen imidazolium salts derived from clotrimazole (Group 1), 2-chlorotriptyl (Group 2) and triptyl (Group 3) were synthesised with varying counterions, N-substituents and triphenyl substituents. All thirteen imidazolium salts were used as ligand precursors for the synthesis of thirteen silver(I)-NHC complexes **C6-C18**. The ligand precursors **L6-L18** and silver(I)-NHC complexes **C6-C18** were fully characterised using  $^1\text{H}$  and  $^{13}\text{C}\{^1\text{H}\}$  NMR spectroscopy, HRMS and elemental analysis; molecular structures for most of the ligands were obtained using X-ray diffraction analysis. Solid-state structures of five complexes were obtained indicating the presence of both mono and bis(NHC) complexes. Hydrophobicity measurements conducted in octanol provided positive Log *P* values for all complexes, pointing to their lipophilic nature attributed to the bulky triphenyl substituent. Cisplatin, which is hydrophilic, had a measured Log *P* value of -1.35.

Cytotoxicity studies were conducted using **C6-C18** against the cancerous cell line Panc 10.05 and the non-cancerous cell line ARPE-19, and selectivity ratios were calculated. Complexes with promising cytotoxicity or selectivity values were further tested against cancerous cell lines Mia-PA-CA2 and BE. The antiproliferative results show that a hydroxyethyl substituent has a positive effect on cytotoxicity, with **C13** having a similar  $\text{IC}_{50}$  value to cisplatin against Panc 10.05, and significantly higher selectivity for the cancerous cell line over the non-cancerous cell line ARPE-19 (selectivity ratio for **C13B** = 17.5 and cisplatin = 3.8). **C13** and **C18** have the lowest Log *P* values of this class and are therefore of “intermediate lipophilicity”, which has previously been reported to be ideal for cytotoxicity.<sup>16</sup>

## 4.7 References

1. P. R. Sawyer, R. N. Brogden, R. M. Pinder, T. M. Speight and G. S. Avery, *Drugs*, 1975, **9**, 424-447.
2. R. S. Kalhapure, S. J. Sonawane, D. R. Sikwal, M. Jadhav, S. Rambharose, C. Mocktar and T. Govender, *Colloids and surfaces. B, Biointerfaces*, 2015, **136**, 651-658.
3. L. R. Benzaquen, C. Brugnara, H. R. Byers, S. Gattonicelli and J. A. Halperin, *Nature Medicine*, 1995, **1**, 534-540.
4. H. Aktas, R. Flückiger, J. A. Acosta, J. M. Savage, S. S. Palakurthi and J. A. Halperin, *Proceedings of the National Academy of Sciences of the United States of America*, 1998, **95**, 8280-8285.
5. S. Betanzos-Lara, N. P. Chmel, M. T. Zimmerman, L. R. Barron-Sosa, C. Garino, L. Salassa, A. Rodger, J. L. Brumaghim, I. Gracia-Mora and N. Barba-Behrens, *Dalton Transactions*, 2015, **44**, 3673-3685.
6. P. V. Simpson, C. Nagel, H. Bruhn and U. Schatzschneider, *Organometallics*, 2015, **34**, 3809-3815.
7. Z. Oláh, K. Józsvay, L. Pecze, T. Letoha, N. Babai, D. Budai, F. Ötvös, S. Szalma and C. Vizler, *PLoS ONE*, 2007, **2**, e545.
8. J. L. Harper and J. W. Daly, *Biochemical Pharmacology*, 2000, **60**, 317-324.
9. K. M. Lee, H. C. Chang, J. C. Jiang, L. C. Lu, C. J. Hsiao, Y. T. Lee, S. H. Lin and I. J. B. Lin, *Journal of Chemical Physics*, 2004, **120**, 8645-8650.
10. M. V. Baker, D. H. Brown, R. A. Haque, B. W. Skelton and A. H. White, *Dalton Transactions*, 2004, 3756-3764.
11. D. C. F. Monteiro, R. M. Phillips, B. D. Crossley, J. Fielden and C. E. Willans, *Dalton Transactions*, 2012, **41**, 3720-3725.
12. A. Melaiye, R. S. Simons, A. Milsted, F. Pingitore, C. Wesdemiotis, C. A. Tessier and W. J. Youngs, *Journal of Medicinal Chemistry*, 2004, **47**, 973-977.
13. S. Trapp and R. W. Horobin, *European Biophysics Journal with Biophysics Letters*, 2005, **34**, 959-966.
14. C. A. Lipinski, F. Lombardo, B. W. Dominy and P. J. Feeney, *Advanced Drug Delivery Reviews*, 2001, **46**, 3-26.
15. C. A. Lipinski, F. Lombardo, B. W. Dominy and P. J. Feeney, *Advanced Drug Delivery Reviews*, 2012, **64**, 4-17.
16. J. L. Hickey, R. A. Ruhayel, P. J. Barnard, M. V. Baker, S. J. Berners-Price and A. Filipovska, *Journal of the American Chemical Society*, 2008, **130**, 12570-12571.

## Chapter 5

### Synthesis and anticancer activity of water soluble hydroxyethyl-substituted and carboxylic acid-substituted silver(I)-N-heterocyclic carbene complexes

#### 5.1 Introduction

The synthesis of water-soluble Ag(I)-NHC complexes has been previously reported in the literature.<sup>1-3</sup> The improved water solubility was achieved by the addition of alcohol or ether groups to the NHC ligands, resulting in improved biological availability of these complexes.<sup>1,2</sup> Youngs *et al.* reported the synthesis of Ag(I)-bis(NHC) complexes with alcohol N-substituents of different chain lengths (**Figure 5.1A**).<sup>4</sup> Braunstein *et al.* reported simple alcohol and ether N-substituted Ag(I)-bis(NHC) complexes (**Figure 5.1B** and **C**), and Napoli *et al.* also report Ag(I)-bis(NHC) complexes with varying alcohol N-substituents (**Figure 5.1D**). These complexes have shown promising antibacterial properties when tested against bacterial strains of *Escherichia coli* and *Bacillus subtilis*. Therefore, with the aim of improving the bioavailability of Ag(I)-NHCs for cancer therapeutics through the formation of water soluble complexes, alcohol, carboxylic acid and ester N-substituted NHCs were synthesised.

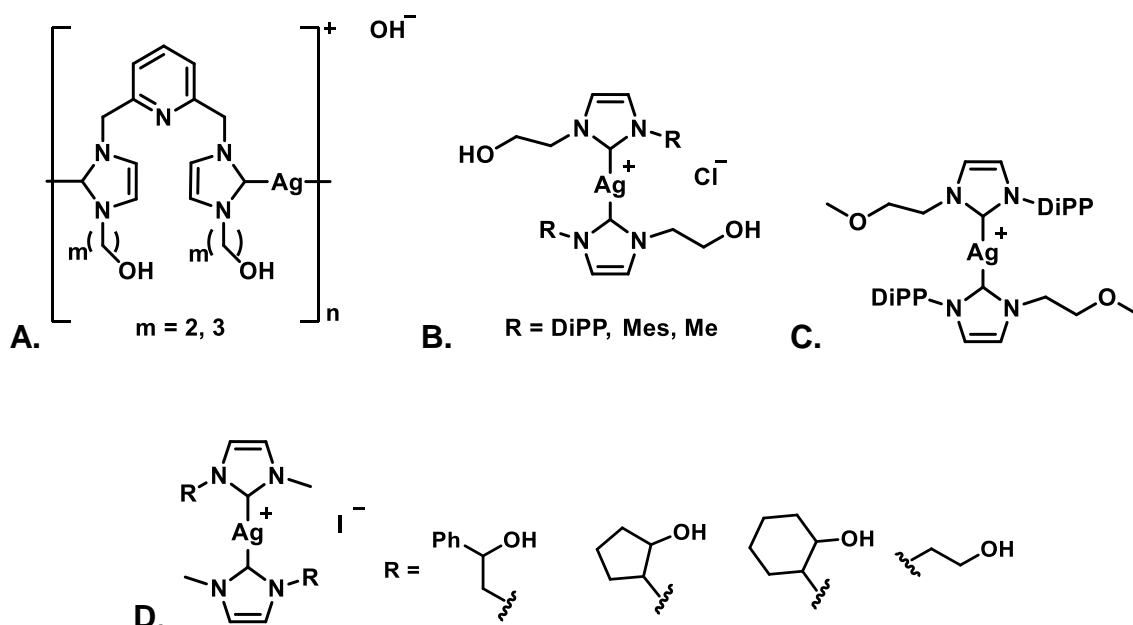
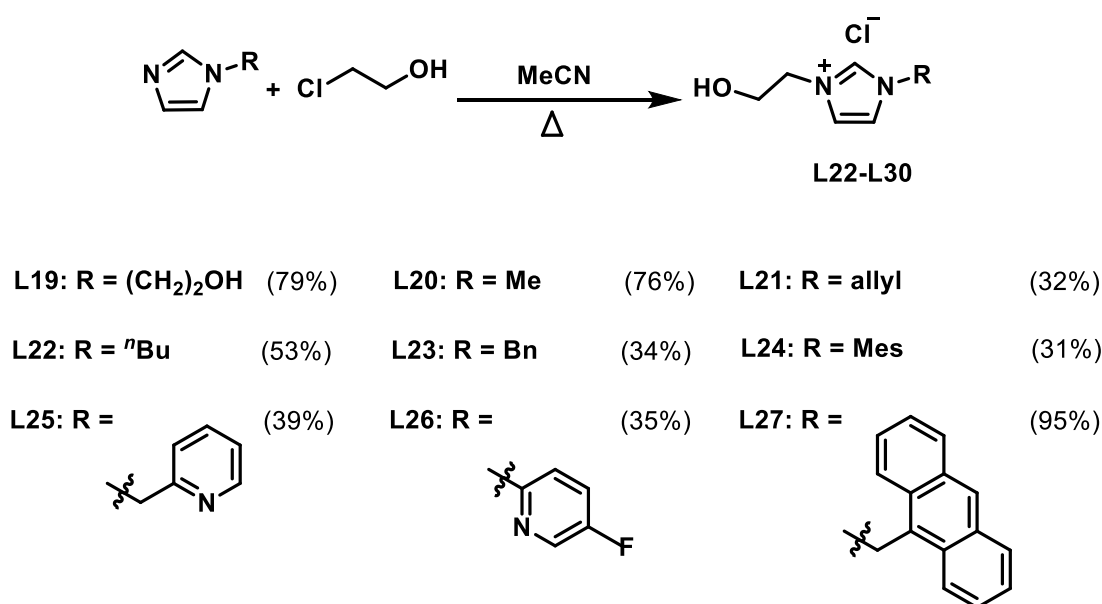


**Figure 5.1:** Water soluble Ag(I)-NHC complexes reported in the literature<sup>1, 2, 4</sup>

## 5.2 Ligand synthesis

### 5.2.1 N-Hydroxyethyl-substituted imidazolium salts

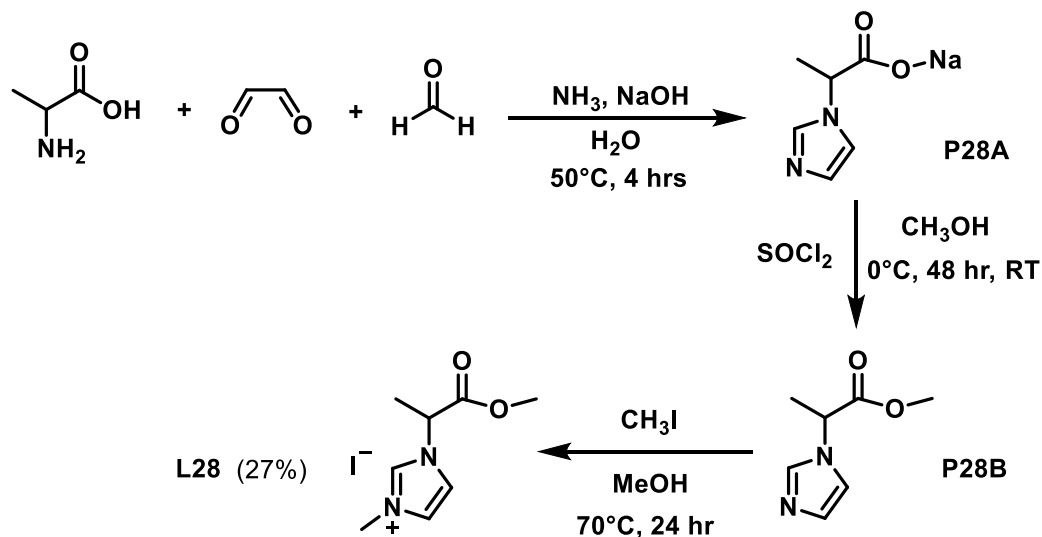
Nine imidazolium salts **L19-L27** were synthesised using modified methods reported by Braunstein *et al.*, starting with an N-substituted imidazole which is reacted with 2-chloroethanol (**Scheme 5.1**).<sup>3</sup> The reagents were heated in MeCN in a sealed vessel at 90°C for 24-72 hours. Commercially available substituted imidazoles were used for the synthesis of **L19-L23**, while for **L24-L27** the starting imidazoles were synthesised following methods reported in the literature.<sup>5, 6</sup> **L19-L27** were fully characterised using <sup>1</sup>H and <sup>13</sup>C{<sup>1</sup>H} NMR spectroscopy, HRMS and elemental analysis. Facile purification of **L20-L27** through recrystallisation from MeOH and Et<sub>2</sub>O furnished the products with yields shown in **Scheme 5.1**. On the other hand, purification of **L19** was more challenging as both the starting 1-(2-hydroxyethyl) imidazole and the resulting imidazolium salt have similar solubility's in a number of solvents including MeOH, (CH<sub>3</sub>)<sub>2</sub>CO, H<sub>2</sub>O, MeCN, CH<sub>2</sub>Cl<sub>2</sub> and CHCl<sub>3</sub>. Therefore optimum conversion was essential in this reaction, which required heating the reagents in MeCN in a sealed vessel at 90°C for 6 days, resulting in no remaining imidazole, and an isolated product in 79% yield.



**Scheme 5.1:** Synthesis of imidazolium salts **L19-L27**

### 5.2.2 L-Alanine derived imidazolium salt

Following methods reported by Meyer *et al.*,<sup>7</sup> L-alanine was reacted with glyoxal and formaldehyde, resulting in its cyclisation to form the imidazole **P28A**. Addition of thionyl chloride to the imidazole in MeOH forms methyl ester **P28B** (Scheme 5.2). Reaction with excess methyl iodide in a sealed vessel was performed to give **L28**. The <sup>1</sup>H NMR spectrum performed in MeOD is shown in Figure 5.2.



Scheme 5.2: Synthesis of imidazolium salt **L28** from L-alanine

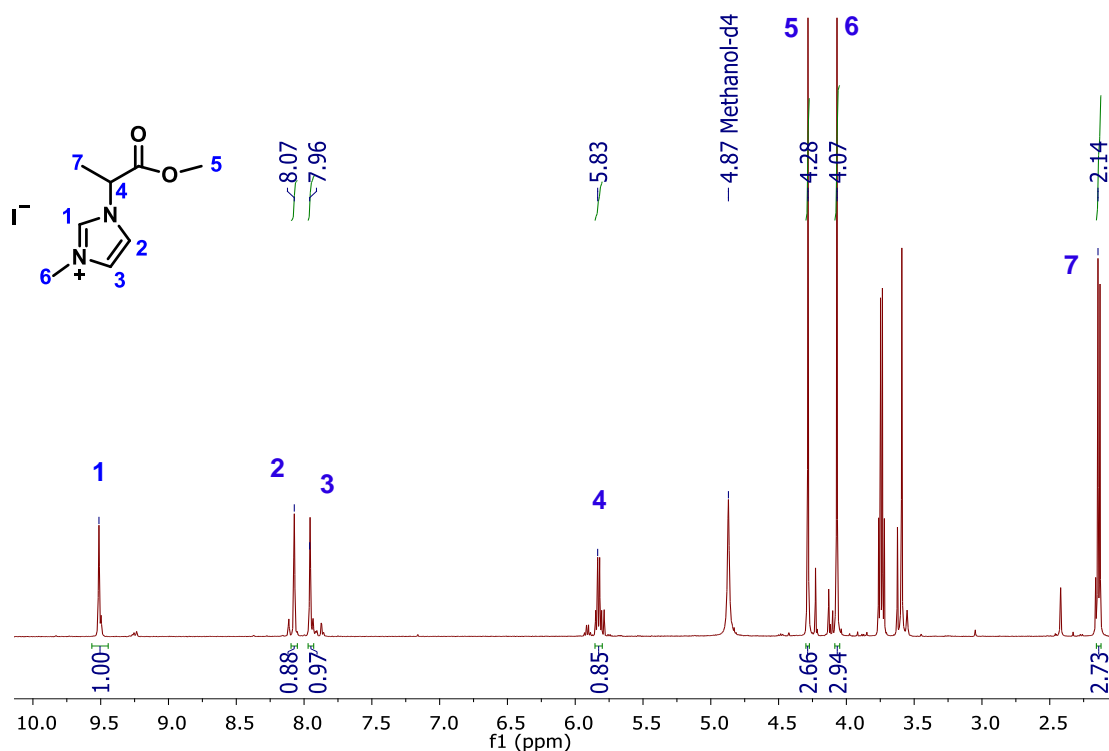
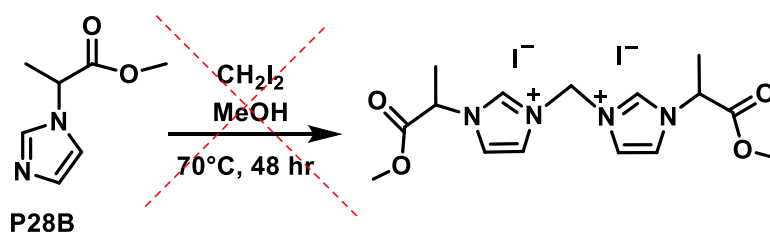


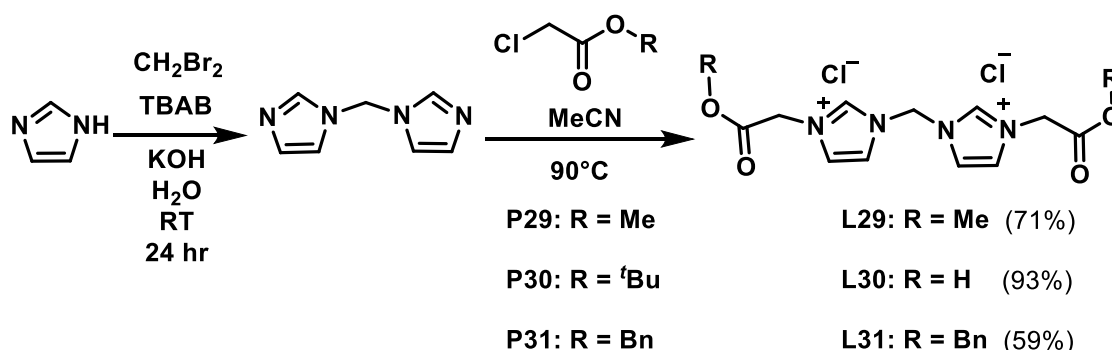
Figure 5.2: <sup>1</sup>H NMR spectrum (300 MHz, MeOD) of **L28**

### 5.2.3 Bis-imidazolium salts

The initial aim was to synthesise a bis-imidazolium salt from L-alanine following methods reported by Meyer *et al.*,<sup>7</sup> through reaction of **P28B** with diiodomethane (**Scheme 5.3**). However, the desired product was not synthesised, possibly due to polymerisation of diiodomethane. Instead, carboxylic acid N-substituted bis-imidazolium salts were prepared. Reaction of imidazole with dibromomethane in a minimum amount of H<sub>2</sub>O, in the presence of KOH and a phase transfer agent (tetrabutylammonium bromide), yields bis-imidazole (**Scheme 5.4**). Further reaction with two equivalents of a chloroacetate (methyl, *tert*-butyl and benzyl chloroacetate) rendered bis-imidazolium salts **L29-L31**. **Figure 5.3** illustrates the amino acid glycine as an integrated portion of **L29-L31**, which can arguably categorise them as 'biologically relevant'.



**Scheme 5.3:** Attempted synthesis of bis-imidazolium salt from L-alanine<sup>7</sup>



**Scheme 5.4:** Synthesis of bis-imidazolium salts **L29-L31** starting with 1H-imidazole

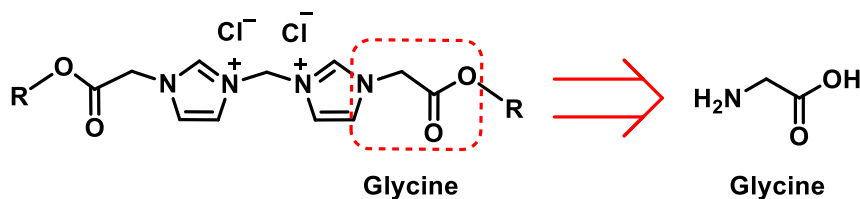


**Figure 5.3:** Illustration of glycine amino acid incorporated in **L29-L31**

The exact nature of **L30** was challenging to identify, as the cleavage of the *tert*-butyl to form carboxylic acid may have occurred. This is likely due to the stability of the *tert*-butyl carbocation, which can be cleaved under the reaction conditions. The  $^1\text{H-NMR}$  spectrum of **L30** shows the *tert*-butyl group or carbocation as a singlet at 1.47 ppm (**Figure 5.4**), while HRMS (**Figure 5.5**), X-ray diffraction analysis (**Figure 5.6**), and elemental analysis indicate presence of terminal carboxylic acid groups.

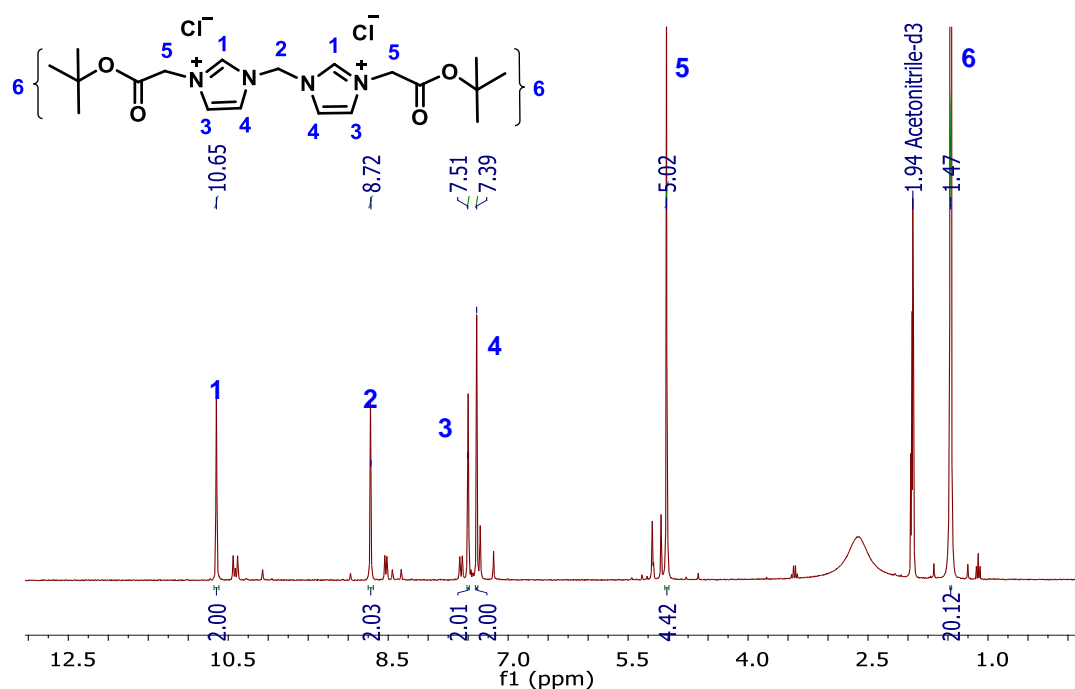


**Figure 5.4:**  $^1\text{H-NMR}$  spectrum (300MHz, acetonitrile- $\text{d}_3$ ) of **L30**

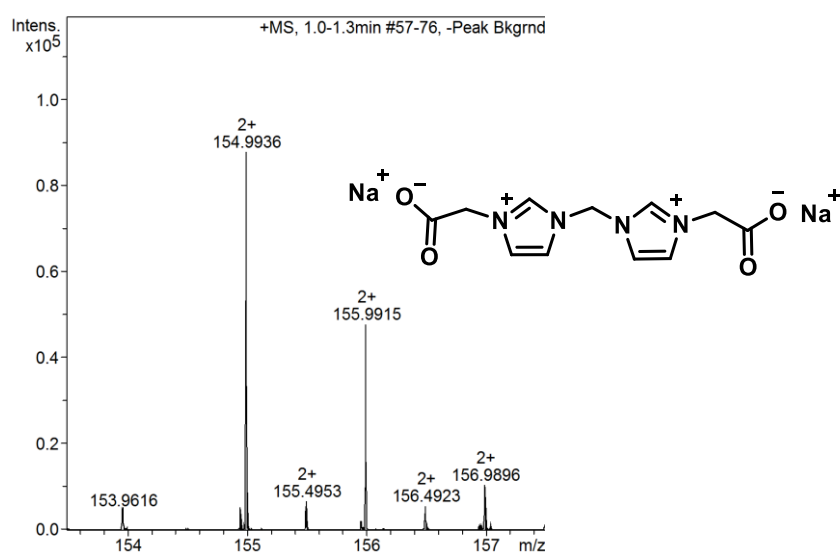


**Figure 5.5:** HRMS of **L30**

Single crystals of **L30** suitable for X-ray diffraction analysis were grown by vapour diffusion of Et<sub>2</sub>O into a concentrated solution of the ligand in MeOH. **L30** crystallises in the monoclinic crystal system and the structural solution solved in the space group *I*2/a. **L30** co-crystallises with a molecule of H<sub>2</sub>O as shown in **Figure 5.6**, with no evidence of hydrogen bonding between the water molecule and the carboxylic acid terminals. The packing structure of **L30** along the *b* axis is shown in **Figure 5.7**. The imidazolium counterion was found to be 50% Cl and 50% OH.

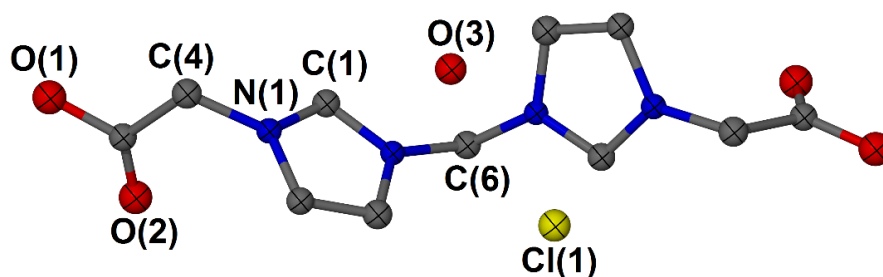


**Figure 5.6:** Molecular structure of **L30**. Ellipsoids are shown at 50% probability and H atoms are omitted for clarity

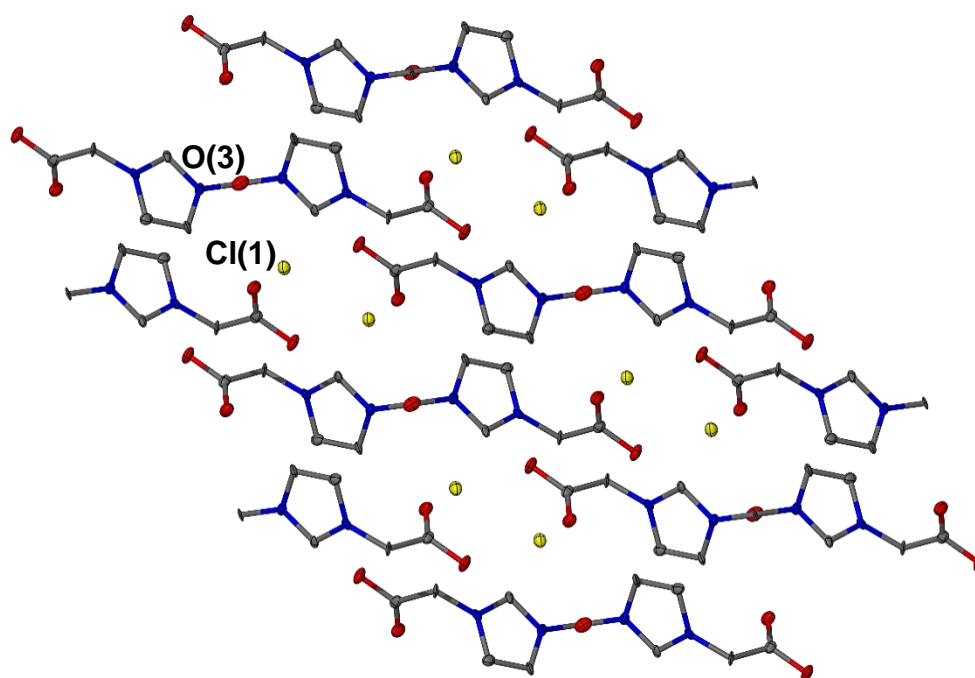
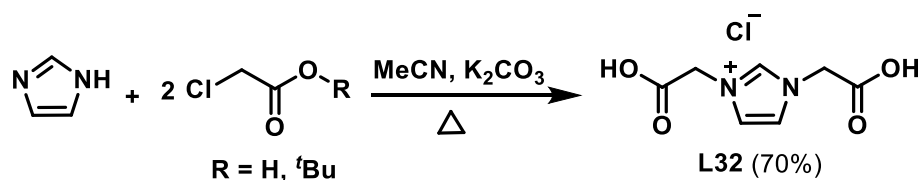


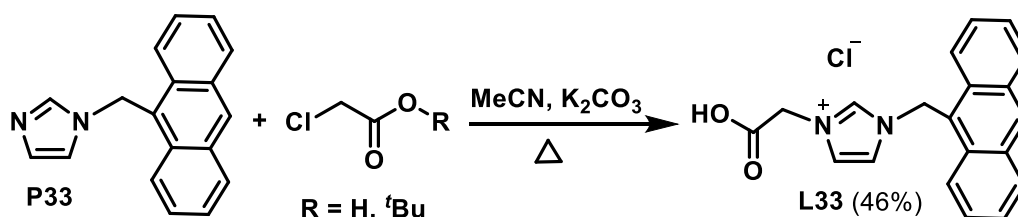
**Figure 5.7:** Packing diagram of **L30** along the *b* axis

### 5.2.4 Carboxylic acid N-substituted imidazolium salts

Following results obtained in the synthesis of **L30** to give carboxylic acid N-substituted imidazolium salts, the synthesis of additional N-carboxylic acid substituted ligand precursors for coordination to silver was pursued. An imidazolium salt with carboxylic acid groups on both nitrogen atoms (**L32**) was synthesised through reaction of imidazole with either chloroacetic acid or with *tert*-butyl chloroacetate (**Scheme 5.5**). The synthesis of an imidazolium salt with a carboxylic acid N-substituent and an anthracene N-substituent (**L33**) is shown in **Scheme 5.6**. As with **L32**, reaction of **P33** with either chloroacetic acid or with *tert*-butyl chloroacetate renders the desired product **L33**. The <sup>1</sup>H NMR spectrum shows the imidazolium proton downfield shift to 11.30 ppm, which is particularly deshielded due to the anthracene electron withdrawing effect (**Figure 5.8**).



**Scheme 5.5:** Synthesis of dicarboxylic acid imidazolium salt **L32**



**Scheme 5.6:** Synthesis of **L33**

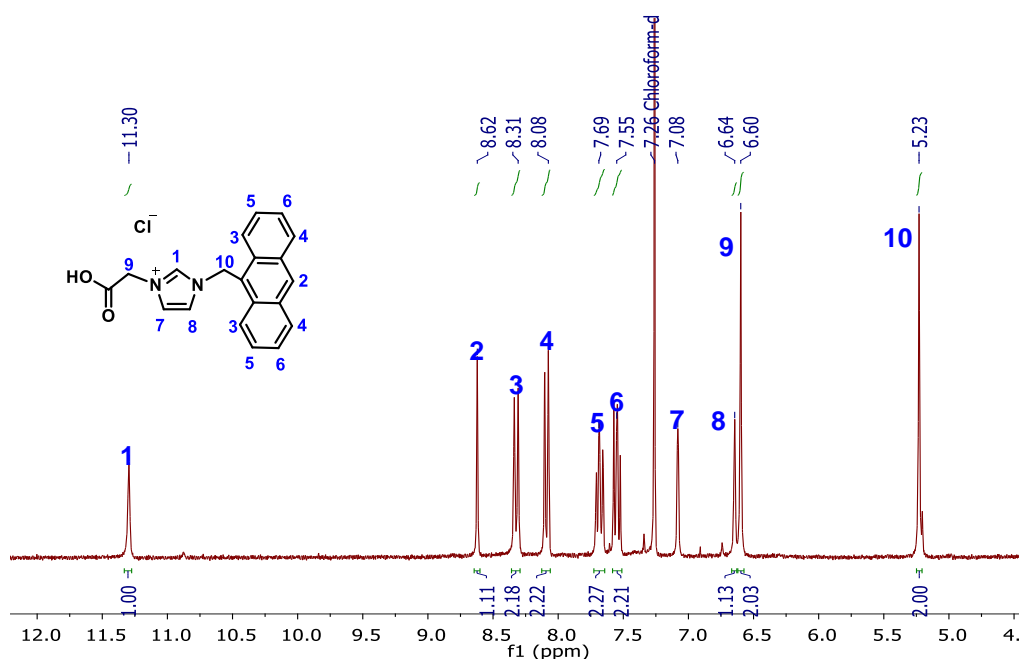
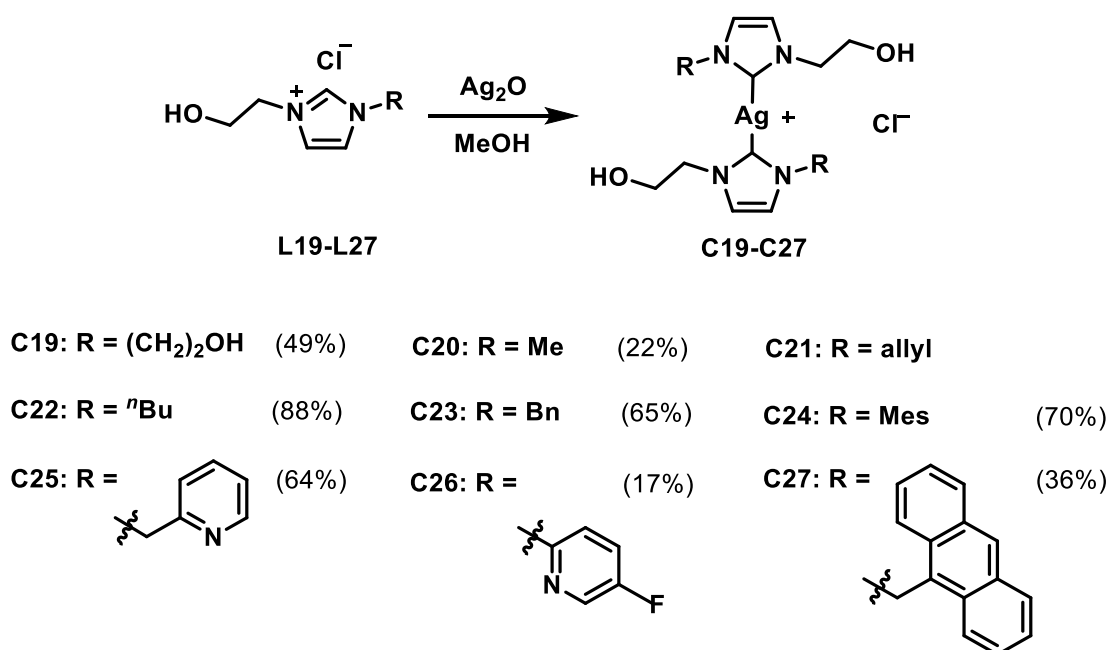


**Figure 5.8:** <sup>1</sup>H-NMR spectrum (300MHz, CDCl<sub>3</sub>) of **L33**

## 5.3 Silver(I)-NHC complexes

### 5.3.1 Silver(I)-NHC complexes with N-hydroxyethyl substituents

Reaction of **L19-L27** with  $\text{Ag}_2\text{O}$  in MeOH gives Ag(I)-bis(NHC) complexes **C19-C27** of the type  $[\text{Ag}(\text{NHC})_2]^+\text{Cl}^-$  (**Scheme 5.7**). The formation of the Ag(I)-NHC complexes can be monitored using  $^1\text{H}$  NMR spectroscopy, with disappearance of the imidazolium proton peak at  $\approx 9$  ppm (**Figure 5.9**). The formation of the Ag(I)-bis(NHC) cation is also observed through the HRMS data. Purification of **C19-C27** was performed by filtration through celite followed by recrystallisation from MeOH and  $\text{Et}_2\text{O}$ . Complexes **C19-C27** were fully characterised using  $^1\text{H}$  and  $^{13}\text{C}\{^1\text{H}\}$  NMR spectroscopy, HRMS and elemental analysis. The complexes are stable as solids and can be stored for several months when kept away from atmospheric moisture. However, **C21** appears to be an exception, as it decomposes during recrystallisation, which is detected by the colour change of the complex to a dark grey colour. Although successful synthesis and analysis were conducted on **C21**, it was not considered for cytotoxicity testing due to its instability.



**Scheme 5.7:** Synthesis of water soluble Ag(I)-NHC complexes **C19-C27**

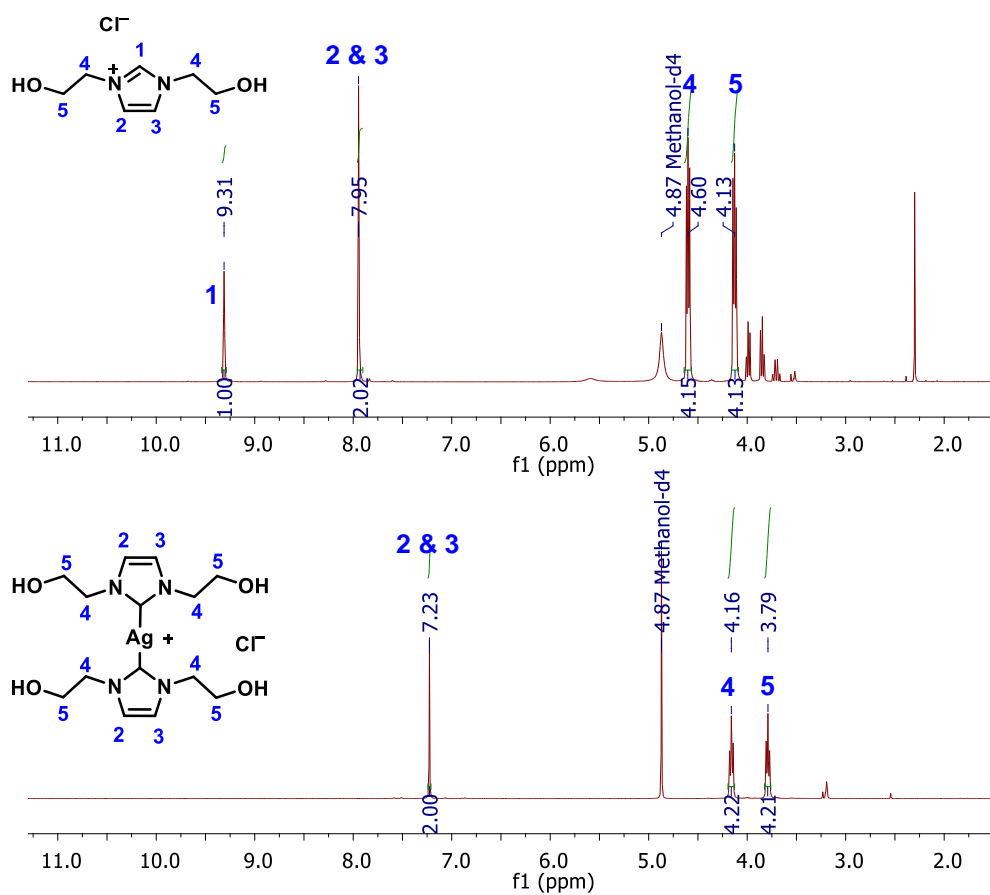
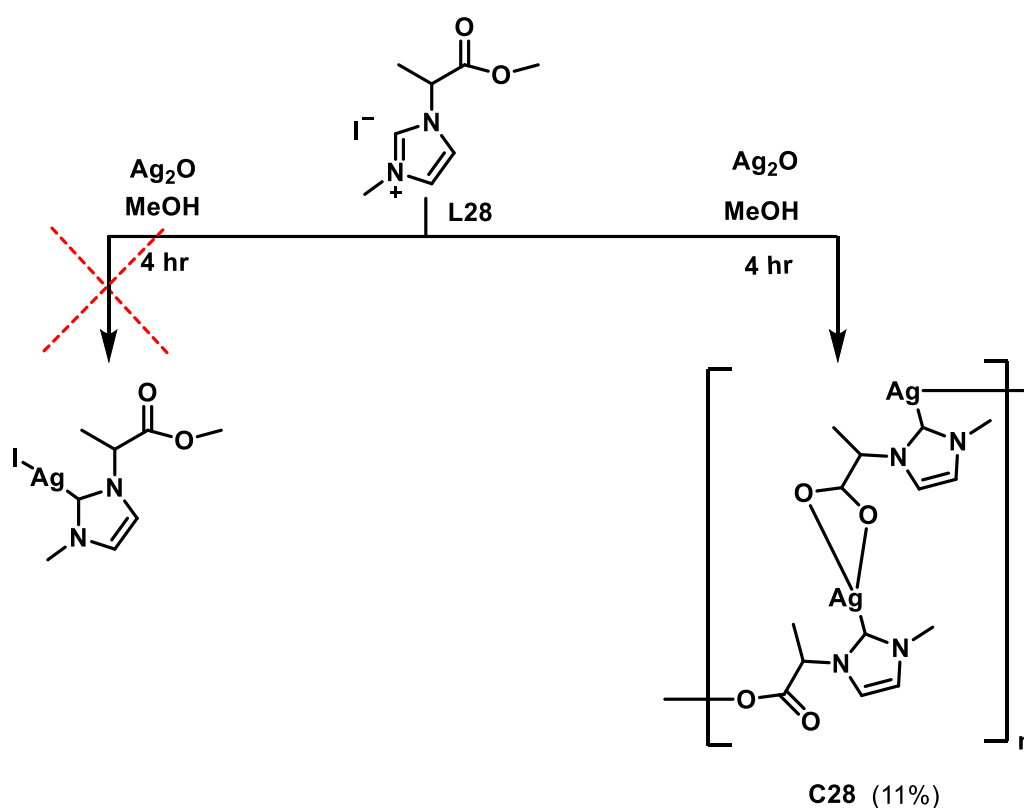


**Figure 5.9:** <sup>1</sup>H NMR spectra (300MHz, MeOD-d<sub>4</sub>) of **L19** (top) and **C19** (bottom)

### 5.3.2 Two-dimensional polymeric silver(I)-NHC complex

L-Alanine-derived imidazolium salt **L28** was reacted with  $\text{Ag}_2\text{O}$  in MeOH (**Scheme 5.8**). However, the basicity of  $\text{Ag}_2\text{O}$  was found to hydrolyse the ester, allowing the silver to coordinate to the two oxygen atoms, in addition to its coordination to the carbene centre. Full analysis of the product, including HRMS, NMR spectroscopy, elemental analysis and X-ray diffraction analysis, validates the formation of the Ag(I)-NHC complex **C28**, which is a 2-dimensional polymer in the solid state (**Figure 5.10**). Single crystals of **C28** suitable for X-ray diffraction analysis were grown by vapour diffusion of  $\text{Et}_2\text{O}$  into a concentrated solution of the complex in MeOH. **C28** crystallises in the monoclinic crystal system and the structural solution was solved in the space group  $P2_1/n$  (**Figure 5.10**). The silver atoms display argentophilic interactions, with each coordinating another silver atom, two oxygen molecules of the formal ester and the carbenic carbon. This coordination has previously been reported in the literature as a dimeric dianion.<sup>8</sup> The Ag-Ag bond length is 3.1039(17) Å, while the Ag-O bond lengths are 2.335(8) Å and 2.499(11) Å, and the Ag-C bond length is 2.057(9) Å, all of which are in close agreement with the literature.<sup>8</sup>



**Scheme 5.8:** Synthesis of 2-dimensional Ag(I)-NHC polymer **C28**

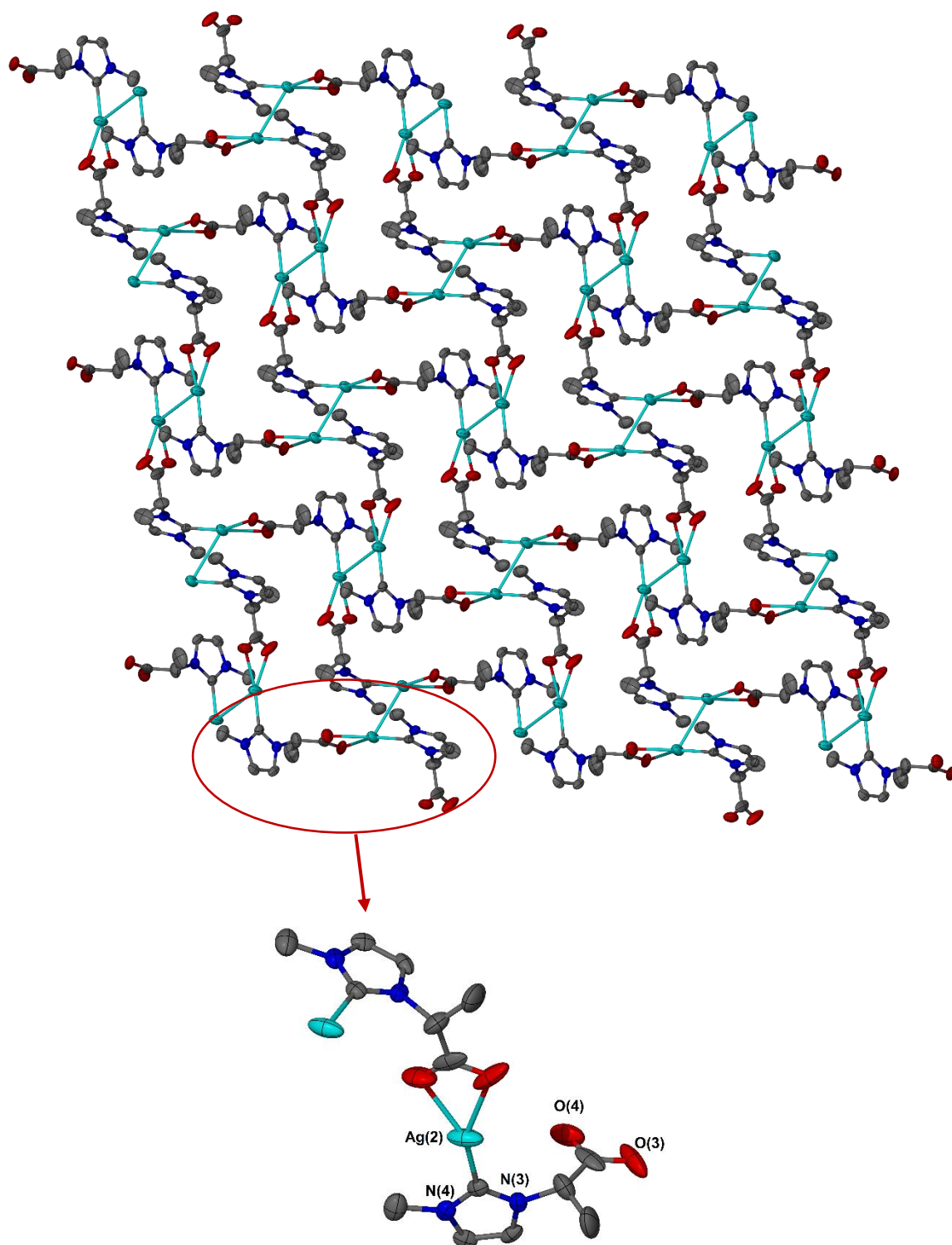
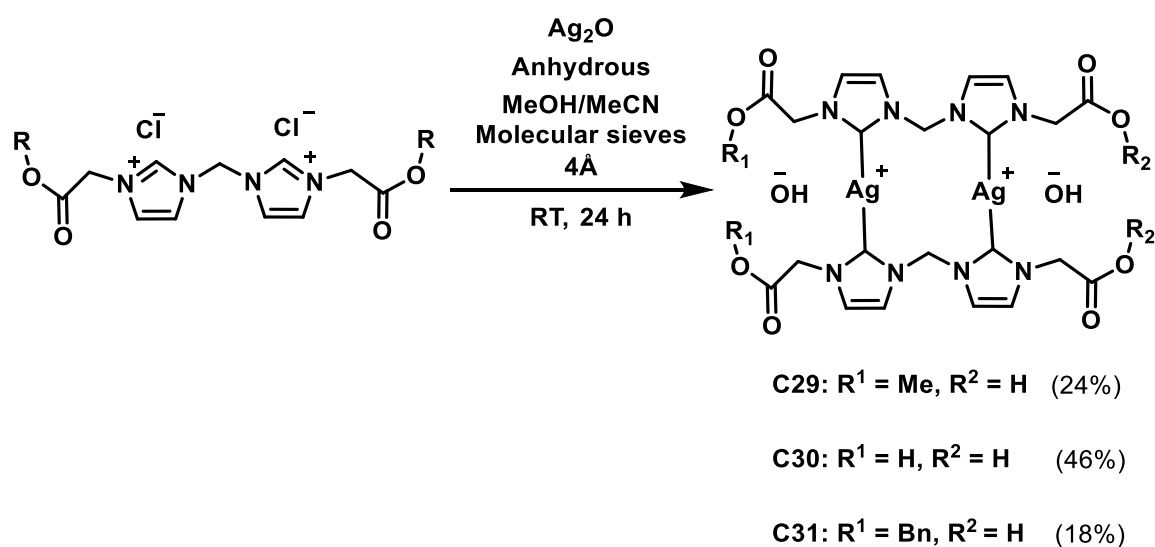


**Figure 5.10:** Molecular structure of **C28**. Ellipsoids are shown at 50% probability and H atoms are omitted for clarity

### 5.3.3 Silver(I)-NHC complexes from bis-imidazoliums

Reaction of imidazolium salts **L29-L31** with  $\text{Ag}_2\text{O}$  in a solvent mixture of MeOH and MeCN under anhydrous conditions, furnished Ag(I)-bis(NHC) complexes with two OH counterions (**Scheme 5.9**). Complexes **C29-C31** are isolated as white solids, which are stable and very soluble in water. Full characterisation of the complexes including HRMS, NMR spectroscopy, and elemental analysis suggest that complex **C30** has 4 terminal carboxylic acid groups (**Figure 5.11**) and both **C29** and **C31** have a mixture of carboxylic acids and esters in a 1:1 ratio.



**Scheme 5.9:** Synthesis of Ag(I)-NHC complexes **C29-C31**

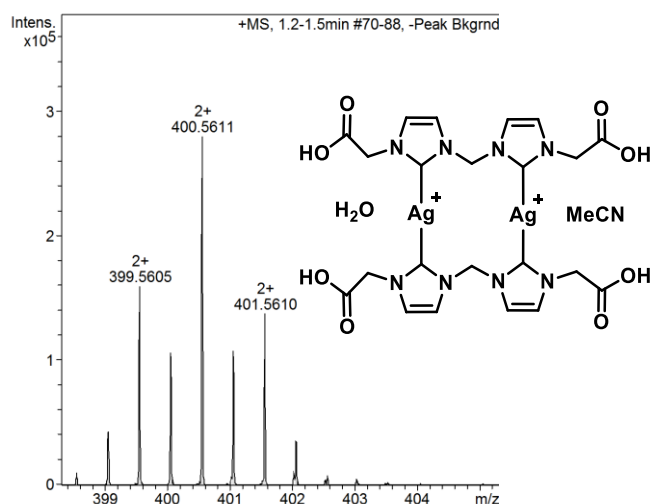
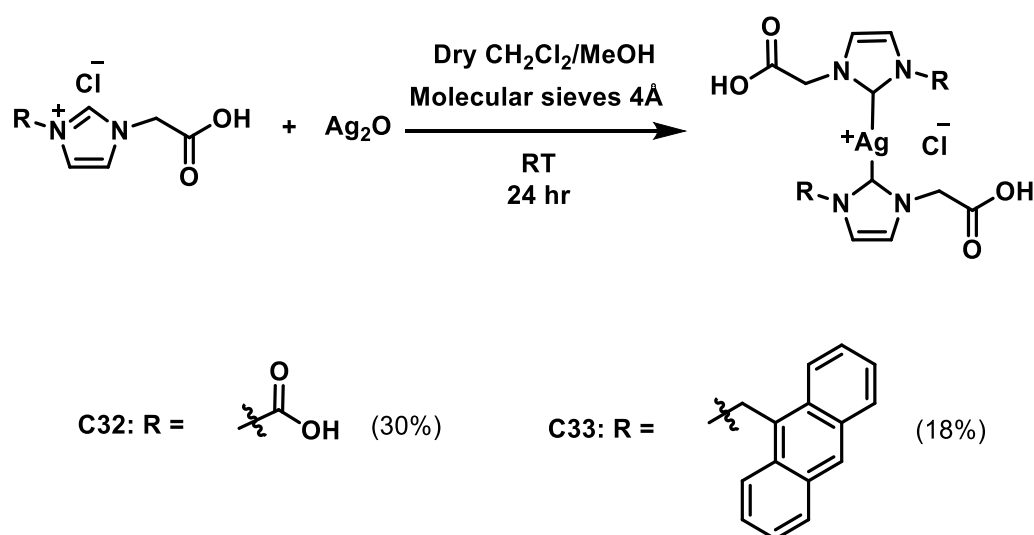


**Figure 5.11:** HRMS for **C30**

### 5.3.4 N-Carboxylic acid substituted silver(I)-NHCs

Reaction of **L35** and **L36** with  $\text{Ag}_2\text{O}$  in a solvent mixture of MeOH and  $\text{CH}_2\text{Cl}_2$  under anhydrous conditions furnished Ag(I)-bis(NHC) complexes **C32** and **C33** (**Scheme 5.10**). Complexes were characterised using NMR spectroscopy, elemental analysis and HRMS (**Figure 5.12**).



**Scheme 5.10:** Synthesis of carboxylic acid N-substituted Ag(I)-NHC complexes **C32** and **C33**

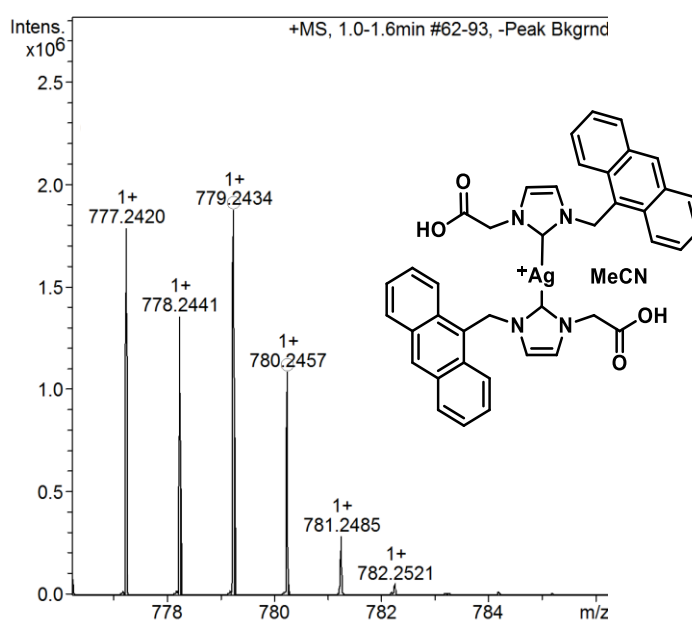


**Figure 5.12:** HRMS of **C33**

## 5.4 Hydrophobicity measurements

Hydrophobicity measurements were conducted using UV/vis spectroscopy on **C19**, **C20** and **C22-C33** and Log *P* values obtained (**Table 5.1**, **Figure 5.13**). All complexes are water-soluble and therefore the hydrophobicity measurements were conducted in the aqueous layer. The Log *P* values of the fourteen complexes vary from -0.35 to 0.496. N-Hydroxyethyl substituted complexes **C19**, **C20**, **C22**, the two dimensional Ag(I)-NHC polymer **C28**, the N-carboxylic acid substituted silver dimer **C30** and monomer **C33** are hydrophilic with negative Log *P* values. N-Anthracene substituted complexes **C27** and **C33** and N-benzyl substituted silver dimer **C31** have a more “intermediate lipophilicity” with Log *P* values  $\approx$  0.3-0.5.

**Table 5.1:** Log *P* values of **C19**, **C20** and **C22-C33**, and cisplatin

| Complex          | Log <i>P</i> | SD( $\pm$ ) |
|------------------|--------------|-------------|
| <b>Cisplatin</b> | -1.35        | 0.26        |
| <b>C19</b>       | -0.35        | 0.20        |
| <b>C20</b>       | -0.14        | 0.16        |
| <b>C22</b>       | -0.07        | 0.13        |
| <b>C23</b>       | 0.02         | 0.07        |
| <b>C24</b>       | 0.11         | 0.13        |
| <b>C25</b>       | 0.005        | 0.08        |
| <b>C26</b>       | 0.08         | 0.16        |
| <b>C27</b>       | 0.29         | 0.01        |
| <b>C28</b>       | -0.17        | 0.02        |
| <b>C29</b>       | 0.086        | 0.13        |
| <b>C30</b>       | -0.05        | 0.07        |
| <b>C31</b>       | 0.496        | 0.21        |
| <b>C32</b>       | -0.21        | 0.15        |
| <b>C33</b>       | 0.33         | 0.11        |

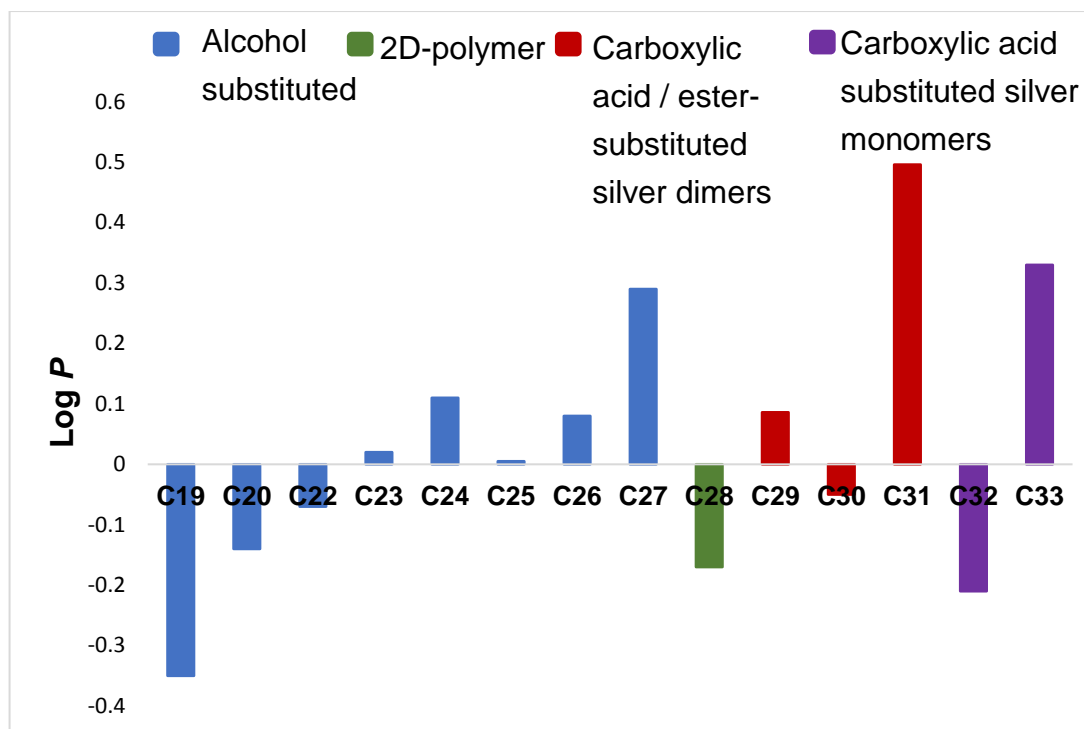


**Figure 5.13:** Log  $P$  values of complexes **C19**, **C20** and **C22-C33**: N-hydroxyethyl substituted (blue), 2D-polymer (green), N-carboxylic acid / ester- substituted silver dimers (red) and N-carboxylic acid substituted silver monomers (purple)

## 5.5 Anticancer Testing

The cytotoxicity of **C19**, **C20** and **C22-C33** were evaluated against pancreatic adenocarcinoma cancerous cell line Panc 10.05 (**Table 5.2**, **Figure 5.14**). Complexes that displayed promising anticancer activity (*i.e.* IC<sub>50</sub> values below 10 (**C23**, **C27** and **C28**)), were further tested against pancreatic carcinoma Mia-PA-CA-2 and colorectal carcinoma BE cancerous cell lines. The selectivity of **C23**, **C27** and **C28** towards cancerous cell lines was evaluated by comparison of their cytotoxicity with toxicity on non-cancerous retinal epithelial ARPE-19 (**Figure 5.15**)

Alcohol substituted complexes appear more cytotoxic than the corresponding carboxylic acid substituted complexes. For example, **C19** with two N-hydroxyethyl substituents has a significantly lower IC<sub>50</sub> value ( $14.7 \pm 3.4$ ) against Panc 10.05 than **C32** with two N-carboxylic acid substituents (IC<sub>50</sub> > 100 $\mu$ M). Other examples include the N-hydroxyethyl and N-anthracene substituted complex **C27**, which is more cytotoxic than the corresponding N-carboxylic acid and N-anthracene substituted **C33**, and the N-hydroxyethyl and N-benzyl substituted complex **C23**, which is more cytotoxic than N-hydroxyethyl and N-benzyl substituted bis-imidazole complex **C31**. Within the bis-imidazole complexes, the N-carboxylic acid substituted **C30** and **C31** are more cytotoxic than **C29**.

**C23** exhibits the lowest IC<sub>50</sub> value ( $3.0\mu\text{M} \pm 0.5$ ) close to that displayed by cisplatin ( $1.7\mu\text{M} \pm 0.4$ ) while also having superior selectivity towards cancerous cells (selectivity ratio of 7.3 compared to 3.8 for cisplatin, **Table 5.2**). The “intermediate lipophilicity” of **C23** and **C27** may contribute to their superior cytotoxicity, as they contain both hydrophilic (hydroxyethyl) and hydrophobic (benzyl or anthracene) N-substituents. Complexes bearing both hydrophilic and hydrophobic N-substituents appear to be more cytotoxic than their corresponding complexes with only hydrophilic N-substituents. For example, the N-benzyl and N-carboxylic acid substituted complex **C31** is more cytotoxic than N-carboxylic acid substituted complex **C30**, and N-hydroxyethyl and N-benzyl substituted complex **C23** is more cytotoxic than N-hydroxyethyl substituted complex **C19**. However, lipophilicity does not appear to be the only factor in determining the anticancer activity of water-soluble Ag(I)-NHC complexes, as there are other examples of complexes with “intermediate lipophilicity” *e.g.* **C24-C26**, which do not display good cytotoxicity.

The promising cytotoxicity of **C28** ( $7.5\mu\text{M} \pm 0.3$ ) may be due to its polymeric nature that leads to a prolonged exposure<sup>9</sup> of the cancerous cells to the cytotoxic portion of the complex. **C28** displays superior cytotoxicity against cancerous cell lines Mia-PA-CA-2 and BE over both **C23** and **C27**, with the highest selectivity ratio to Mia-PA-CA2 (**Figure 5.14**).

**Table 5.2:** IC<sub>50</sub> values for complexes **C19**, **C20**, **C22-C33** and cisplatin on Panc 10.05

| <b>Complex</b>   | <b>IC<sub>50</sub> (<math>\mu\text{M}</math>) <math>\pm</math>SD</b> |
|------------------|--|
| <b>Cisplatin</b> | 1.7 $\pm$ 0.4  |
| <b>C19</b>       | 14.7 $\pm$ 3.4   |
| <b>C20</b>       | 30.6 $\pm$ 3.4   |
| <b>C22</b>       | 17.0 $\pm$ 4.1   |
| <b>C23</b>       | 3.0 $\pm$ 0.5  |
| <b>C24</b>       | 24.0 $\pm$ 3.4   |
| <b>C25</b>       | 15.8 $\pm$ 1.0   |
| <b>C26</b>       | 33.2 $\pm$ 3.5   |
| <b>C27</b>       | 8.3 $\pm$ 2.1  |
| <b>C28</b>       | 7.5 $\pm$ 0.3  |
| <b>C29</b>       | 17.1 $\pm$ 6.7   |
| <b>C30</b>       | 12.27 $\pm$ 3.20   |
| <b>C31</b>       | 10.44 $\pm$ 1.86   |
| <b>C32</b>       | > 100  |
| <b>C33</b>       | 26.3 $\pm$ 11.5  |

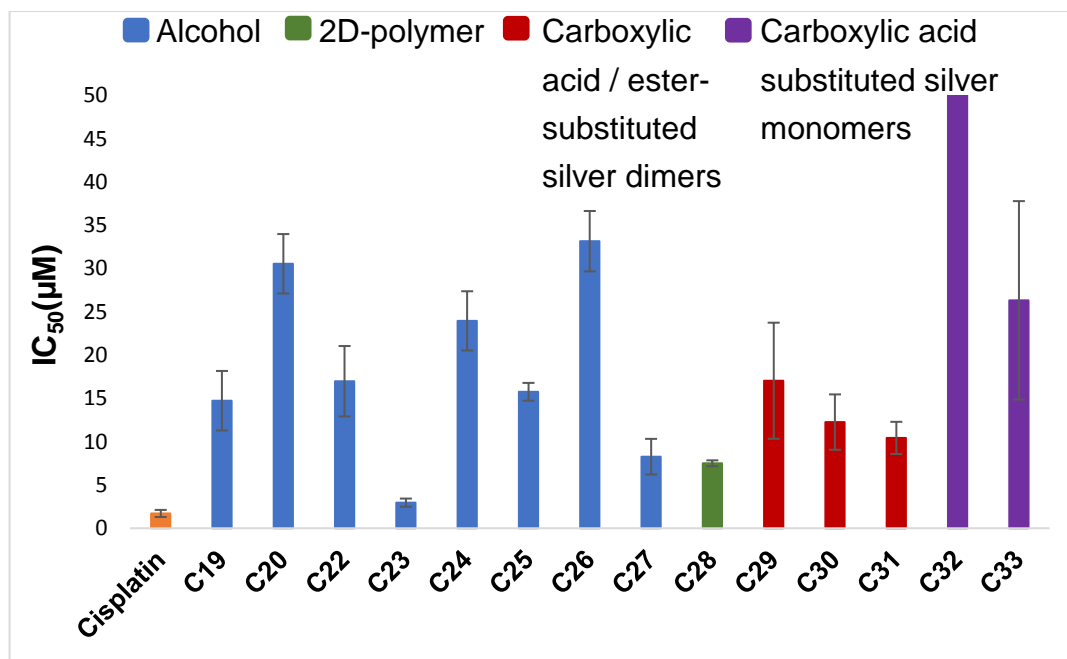


**Figure 5.14:** IC<sub>50</sub> values of complexes **C19**, **C20**, and **C22-C33** and cisplatin against pancreatic adenocarcinoma cell line Panc 10.05

**Table 5.3:** Responses of Panc 10.05, Mia-PA-CA-2 and BE cancerous cell lines and ARPE-19 non-cancerous cell line to Ag(I)-NHC complexes **C23**, **C27**, **C28** and **C33**. Values presented are  $IC_{50}$  ( $\mu M$ )  $\pm$ SD for three independent experiments

| Cell Line        | <b>Panc 10.05</b> | Selectivity ratio<br>(ARPE-19 /Panc10.05) | <b>MIA-PA-CA2</b> | Selectivity ratio<br>(ARPE-19 /MIA-PA-CA2) | <b>BE</b>      | Selectivity ratio<br>(ARPE-19 /BE) | <b>ARPE-19</b> |
|------------------|-------------------|---|-------------------|--|----------------|------------------------------------|----------------|
| <b>Cisplatin</b> | 1.7 $\pm$ 0.4     | 3.8                                       | 2.8 $\pm$ 2.1     | 2.3  | 0.7 $\pm$ 0.3  | 9.7                                | 6.4 $\pm$ 1.0  |
| <b>C23</b>       | 3.0 $\pm$ 0.5     | 7.3                                       | 5.7 $\pm$ 1.8     | 3.8  | 7.0 $\pm$ 2.6  | 3.1                                | 21.4 $\pm$ 2.9 |
| <b>C27</b>       | 8.3 $\pm$ 2.1     | 1.7                                       | 6.2 $\pm$ 3.6     | 2.2  | 12.0 $\pm$ 3.6 | 1.1                                | 13.7 $\pm$ 2.9 |
| <b>C28</b>       | 7.5 $\pm$ 0.3     | 2.5                                       | 4.9 $\pm$ 2.6     | 3.9  | 5.4 $\pm$ 3.6  | 3.5                                | 19.0 $\pm$ 5.1 |
| <b>C33</b>       | 26.3 $\pm$ 11.5   | 2.6                                       | -                 | -  | -              | -                                  | 68.7 $\pm$ 7.2 |

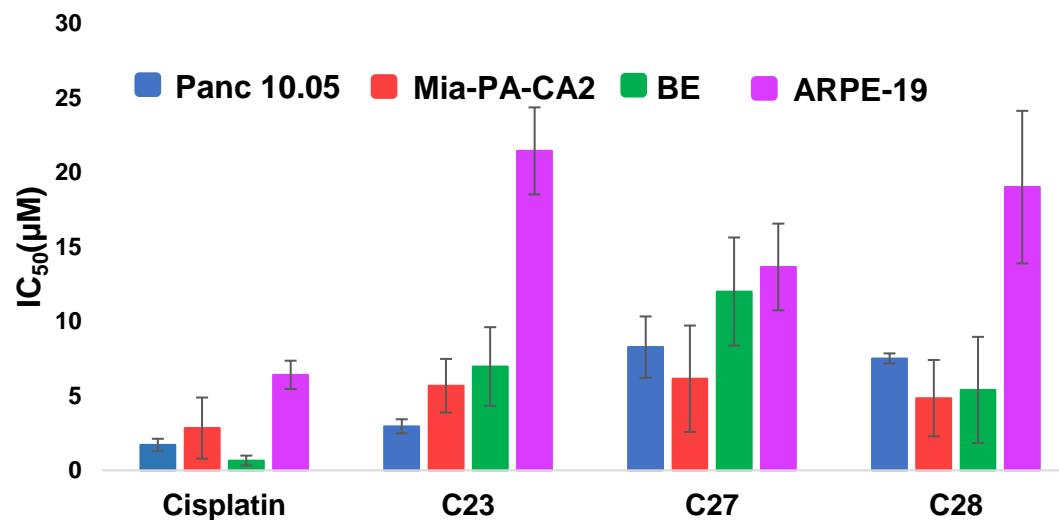


**Figure 5.15:**  $IC_{50}$  values of **C23**, **C27** and **C28** and cisplatin against Panc 10.05, Mia-PA-CA-2 and BE and ARPE-19

## 5.6 Conclusions

Fifteen water-soluble imidazolium salts **L19-L33** have been synthesised from which Ag(I)-NHC complexes **C19-C33** were prepared. N-Hydroxyethyl-substituted ligands formed Ag(I)-bis(NHC) complexes **C19-C27**; L-alanine-derived ligand precursor formed a two-dimensional Ag(I)-NHC complex **C28**; Bis-imidazolium salts formed N-carboxylic acid-substituted Ag(I)-bis(NHC) dimers **C29-C31**; and the N-carboxylic acid-substituted imidazoliums formed Ag(I)-bis(NHC) monomers **C32** and **C33**. All ligand precursors and complexes have been fully characterised using  $^1\text{H}$  and  $^{13}\text{C}\{^1\text{H}\}$  NMR spectroscopy, HRMS and elemental analysis.

Hydrophobicity measurements were conducted and, as expected, the Log  $P$  values were small ( $< 0.5$ ) due to the presence of the hydrophilic side chains, with six complexes (**C19**, **C20**, **C22**, **C28**, **C30** and **C32**) showing negative Log  $P$  values. Cytotoxicity studies were performed against pancreatic adenocarcinoma cell line Panc 10.05 using all the complexes (except **C21**) reported in this chapter. Complexes bearing both N-hydrophilic and N-hydrophobic substituents (e.g. **C23** and **C27**) tended to be more cytotoxic than complexes with solely N-hydrophilic substituents (e.g. **C19** and **C32**). This finding supports previous conclusions drawn in Chapters 2 and 4, where “intermediate lipophilicity” appears to be a contributing factor for superior antiproliferative activity. Lipophilicity of a complex however does not appear to be the only factor affecting the cytotoxicity of these complexes, as some that also bear both N-hydrophilic and N-hydrophobic substituents do not exhibit high antiproliferative activity (e.g. **C24-C26**).

**C28** exhibited good antiproliferative activity, possibly due to its polymeric structure, which suggest the use polymers with Ag(I)-NHC complexes in cancer therapy may improve anticancer activity (see Chapter 6). The three complexes **C23**, **C27** and **C28** with superior cytotoxicity values were further tested against pancreatic carcinoma Mia-PA-CA-2 and colorectal carcinoma BE cancerous cell lines. Their selectivities were evaluated through testing against non-cancerous retinal epithelial ARPE-19 and compared to cisplatin, revealing a higher selectivity of **C23** over cisplatin on both Panc 10.05 and Mia-PA-CA-2. **C23** is therefore a promising complex with antiproliferative activity close to cisplatin, while showing superior selectivity towards cancerous cell lines Panc 10.05 and Mia-PA-CA-2.

## 5.7 References

1. A. Melaiye, R. S. Simons, A. Milsted, F. Pingitore, C. Wesdemiotis, C. A. Tessier and W. J. Youngs, *Journal of Medicinal Chemistry*, 2004, **47**, 973-977.
2. M. Napoli, C. Saturnino, E. I. Cianciulli, M. Varcamonti, A. Zanfardino, G. Tommonaro and P. Longo, *Journal of Organometallic Chemistry*, 2013, **725**, 46-53.
3. S. Hameury, P. de Fremont, P.-A. R. Breuil, H. Olivier-Bourbigou and P. Braunstein, *Dalton Transactions*, 2014, **43**, 4700-4710.
4. J. C. Garrison and W. J. Youngs, *Chemical Reviews*, 2005, **105**, 3978-4008.
5. Q. Li, X. Li, J. Yang, H.-B. Song and L.-F. Tang, *Polyhedron*, 2013, **59**, 29-37.
6. G. Occhipinti, V. R. Jensen, K. W. Tornroos, N. A. Froystein and H.-R. Bjorsvik, *Tetrahedron*, 2009, **65**, 7186-7194.
7. A. Meyer, M. A. Taige and T. Strassner, *Journal of Organometallic Chemistry*, 2009, **694**, 1861-1868.
8. R. Della Pergola, M. Bruschi, A. Sironi, V. Colombo and A. Sironi, *Organometallics*, 2014, **33**, 5610-5613.
9. B. B. Fredholm, K. Battig, J. Holmen, A. Nehlig and E. E. Zvartau, *Pharmacological Reviews*, 1999, **51**, 83-133.

## Chapter 6

### Development of polymer-silver-NHC conjugates and micelles for drug delivery

#### 6.1 Introduction

Polymer-drug conjugates (PDCs) have been investigated as drug delivery systems,<sup>1-8</sup> and are reported to improve the therapeutic index of low molecular weight drugs in different therapeutic areas, including cancer, and infectious and inflammatory diseases. Small-molecule drugs have a small therapeutic index *i.e.* a small concentration window where they are effective and non-toxic, due to a high clearance rate, and to non-selectivity to their site of action, leading to toxicity and a small 'effective dose'. Since the establishment of Ringsdorf's model<sup>9, 10</sup> (**Figure 6.1A**) of a general drug delivery system over three decades ago, variations from the original mononuclear model were developed, including polynuclear, starlike and dendritic systems (**Figure 6.1B-D**). Several polymer-drug systems have been approved and released to the market that including treatments for hepatitis C and leukemia,<sup>7</sup> while others have gone through clinical trials including a system that involves cisplatin.<sup>8</sup> Encapsulation of a drug inside a polymer in the form of a polymer-drug micelle (PDM) is a more recent development for drug-delivery.<sup>11</sup> PDMs are referred to in the literature as micelles, polymeric micelles or polymeric nanoparticles (NP), when their diameters are in the nanomolar range. Encapsulation of drugs has many advantages, including protection from enzymatic degradation and hepatic inactivation *in vivo*, and the possibility of controlled drug release. An example of drug encapsulation into micelles is shown in **Figure 6.1E**, with the anticancer drug camptothecin (Cpt), *via* co-precipitation with polymers.<sup>12</sup>

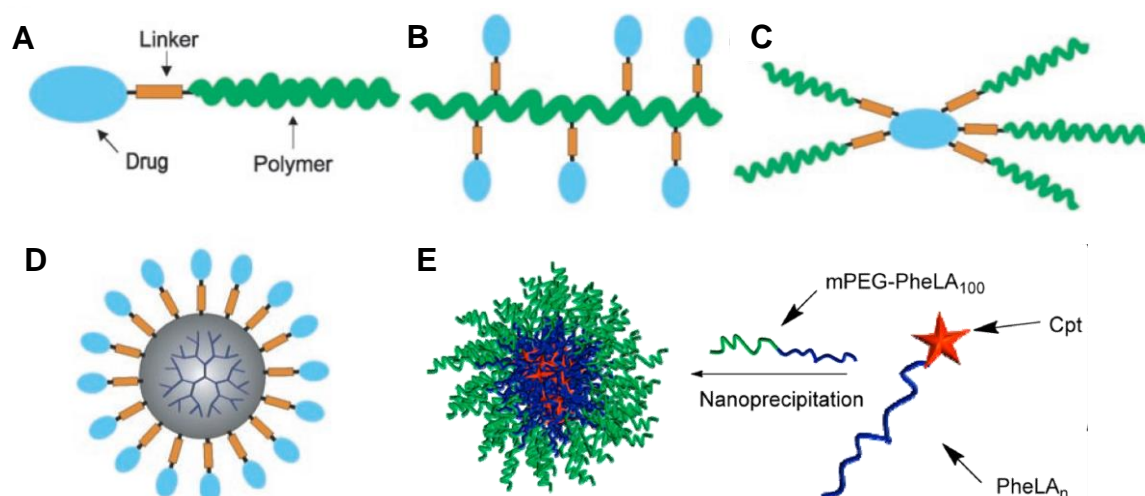


**Figure 6.1:** Structural models of polymer-drug conjugate systems (**A-D**)<sup>2</sup> and polymer-drug micelles (**E**) (Cpt = camptothecin, an anticancer drug)<sup>12</sup>

Polyethylene-glycol (PEG) is one of the most used polymers in drug delivery systems because it is non-toxic, and is FDA approved.<sup>4, 5</sup> The non-ionic, hydrophilic nature of PEG prevents opsonisation (interaction with blood components), and improves water solubility. This prevents aggregation, leading to formulations with enhanced stability, in addition to preventing enzymatic cleavage (**Figure 6.2**). Targeting of the PDCs or PDMs in cancer therapeutics can be achieved passively due to the enhanced permeability and retention of the cancerous tissues known as the EPR effect.<sup>13, 14</sup> The use of macromolecules for targeting antitumor drugs without cell-specific targeting, and solely based on the biochemical and physiological differences of healthy and malignant tissues (**Figure 6.3**), has been introduced by Maeda *et al.*<sup>13, 15</sup> and Jain *et al.*<sup>16, 17</sup> Their work opened a new area of polymer-based drug formulations without the use of receptor-recognisable groups such as antibodies, oligosaccharides and proteins on the surface of the micelle.<sup>18, 19</sup> This chapter describes the use of polymers for Ag(I)-NHC conjugation or encapsulation, with the aim of utilising the EPR effect to target cancerous cells, reduce their renal clearance rates and to increase shelf-life.

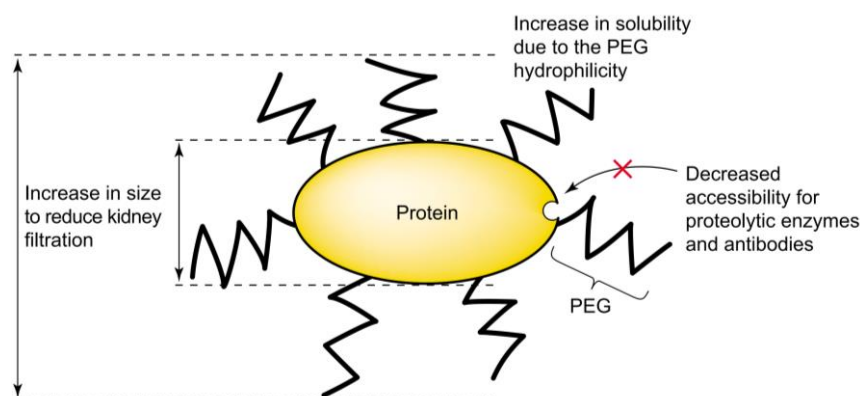


**Figure 6.2:** Illustration of using PEG for drug conjugation<sup>4</sup>

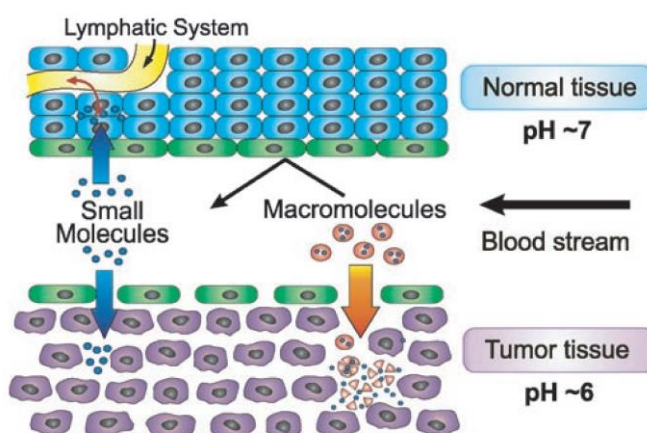
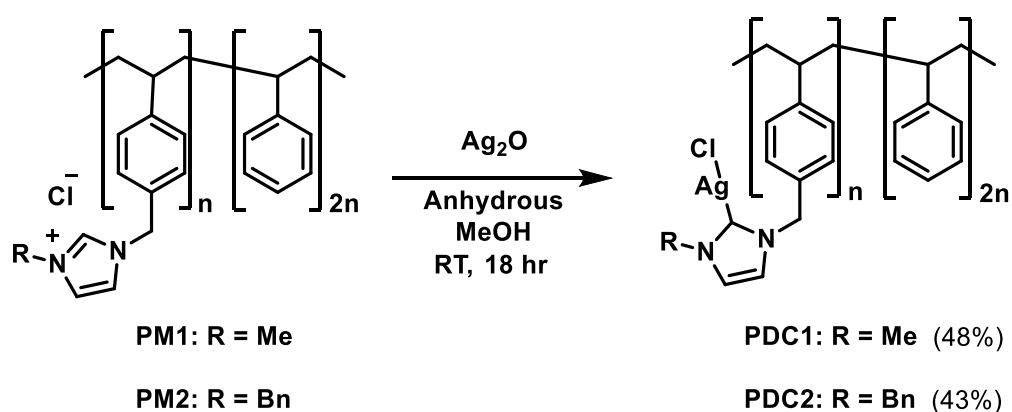


**Figure 6.3:** Illustration of EPR effect<sup>2</sup>

## 6.2 Conjugation of silver-NHCs to polymers

The synthesis of polymer-Ag(I)-NHC conjugates was attempted using block copolymers **PM1** and **PM2** bearing imidazolium salts. Reaction of **PM1** and **PM2** with silver oxide in MeOH under anhydrous conditions successfully forms the polymer-silver conjugates **PDC1** and **PDC2** (**Scheme 6.1**). Coordination of silver is observed in the  $^1\text{H}$  NMR spectra through the loss of the imidazolium proton peak that usually appears at  $\approx 9.30$  ppm (**Figure 6.4**).



**Scheme 6.1:** Synthesis of polymer-Ag(I)-NHC conjugates **PDC1** and **PDC2**

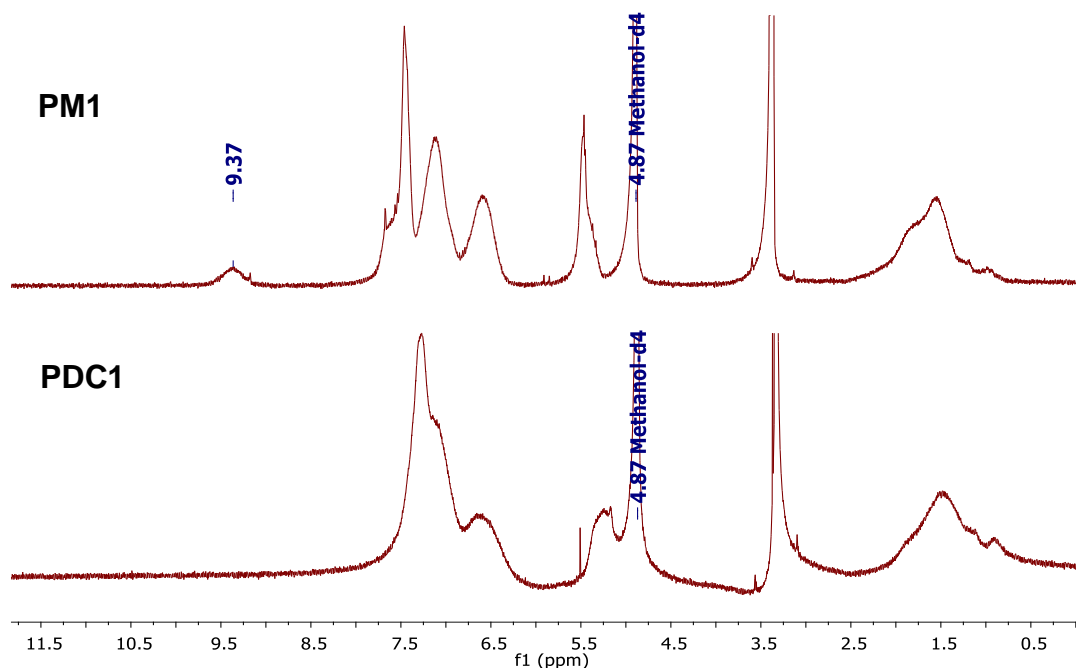


**Figure 6.4:**  $^1\text{H}$  NMR spectra (300MHz,  $\text{CD}_3\text{OD}$ ) of **PM1** (top) and **PDC1** (bottom)

Solid state  $^{13}\text{C}$  NMR spectroscopy is consistent with of silver coordination to the polymers (**Figure 6.5**). This is presented by the appearance of the Ag-C shift at  $\approx 180$  ppm and 168 ppm for both conjugates **PDC1** and **PDC2** which is not present in the solid state  $^{13}\text{C}$  NMR spectra of **PM1** and **PM2**. Following Ringsdorf's model,<sup>9, 10</sup> the drug in this PDC is the Ag(I)-NHC, the linker is the methylene bridge and the polymer is the block copolymer (**Figure 6.6**).

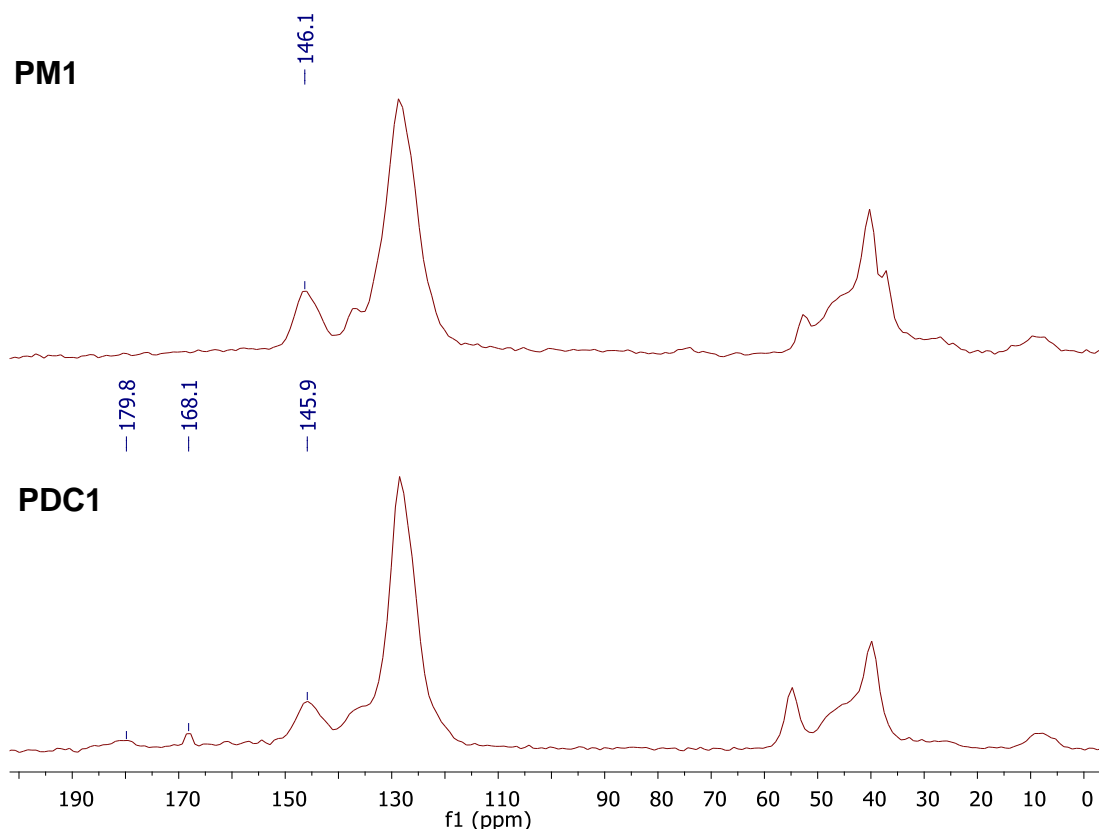


**Figure 6.5:** Solid-state  $^{13}\text{C}$  NMR spectra (12 kHz) of **PM1** (top) and **PDC1** (bottom)

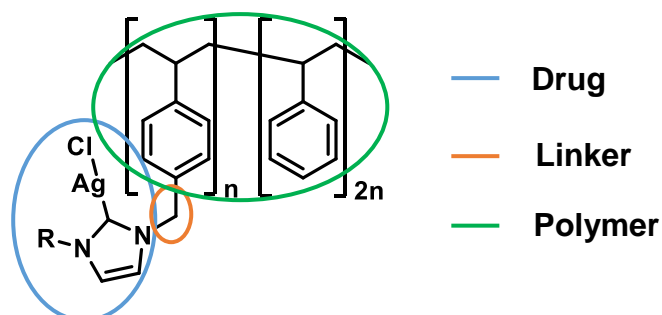
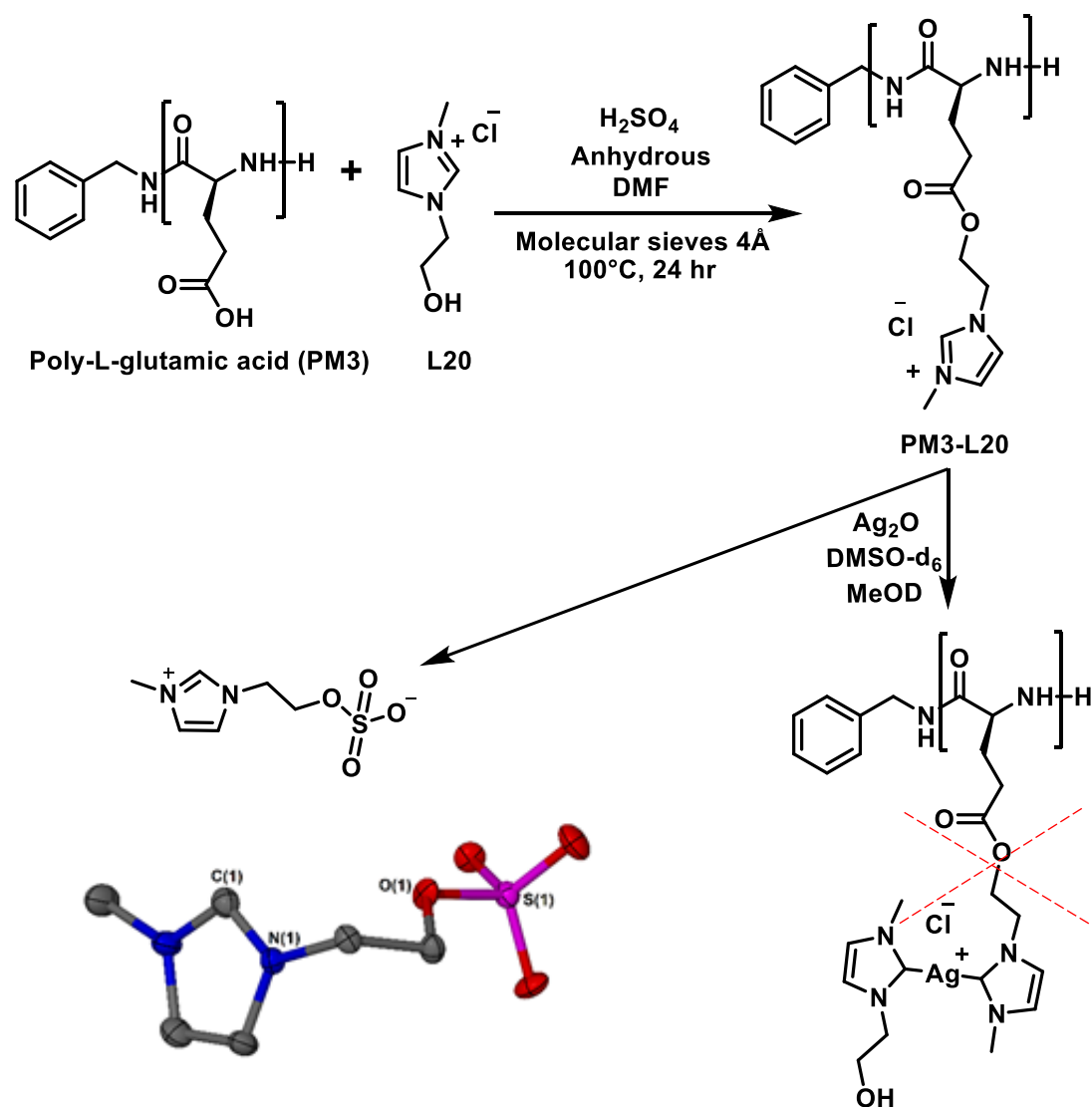


**Figure 6.6 :** Illustration of drug, linker and polymer portions of **PDC1** and **PDC2**

With the aim to use naturally-derived polymers, poly (L)-glutamic acid (**PM3**) was reacted with imidazolium salt **L20** to form an ester linking **PM3** and **L20** (**Scheme 6.2**). The Fischer esterification was conducted in DMF to solubilise **PM3**, and under anhydrous conditions with molecular sieves to remove any water generated from the reaction that may possibly hydrolyse the resulting ester bond.  $^1\text{H}$  NMR spectra suggest successful esterification with the appearance of the imidazolium proton peak at  $\approx 9$  ppm and a broad peak  $\approx 5$  ppm corresponding to  $\text{CH}_2$  groups (**Figure 6.7**). The **PM3-L20** conjugate  $^1\text{H}$  NMR spectrum is broader than that of **PM3**, due to more signal overlap, and a slower relaxation time as the molecular mass increases.

Reaction with silver oxide in a solvent mixture of DMSO and MeOH did not yield the desired product **PDC3**. The imidazolium proton peak was still present in the  $^1\text{H}$  NMR spectrum after 24 hours of slowly increasing the temperature from 40 to 120°C (**Figure 6.8**). However, there is a shift in the proton peaks attributable to the  $\text{CH}_2$  groups of **PM3-L20**, from 3.5-5.5 ppm to 2.0-3.5 ppm. This indicates that hydrolysis of the ester may have occurred, which was confirmed through a single crystal suitable for X-ray diffraction analysis obtained from vapour diffusion of  $\text{Et}_2\text{O}$  into the reaction solution. The molecular structure shows that **PM3-L20** has reacted with DMSO to form an ether link. **PM3-L20** crystallised in the orthorhombic crystal system and structural solution was solved in the *Pbca* space group.



**Scheme 6.2:** Fischer esterification of **PM3** and **L20** to form **PM3-L20** and reaction with  $\text{Ag}_2\text{O}$

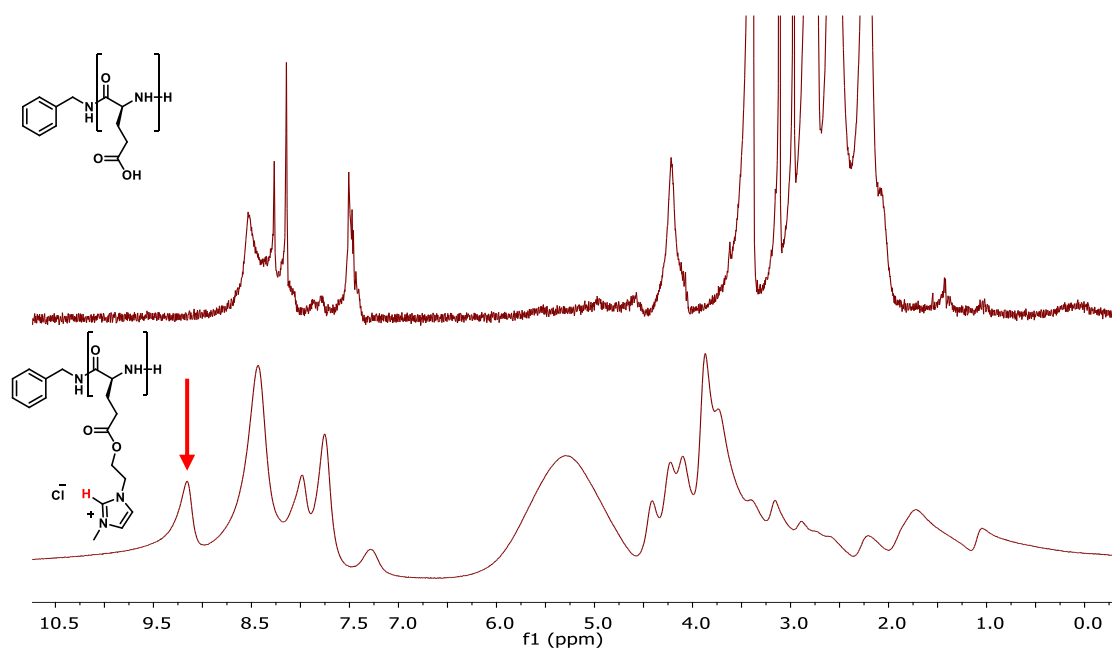


**Figure 6.7:** <sup>1</sup>H NMR spectra (300MHz, DMSO-d<sub>6</sub>) of the Fischer esterification reaction to give **PM3-L20**.

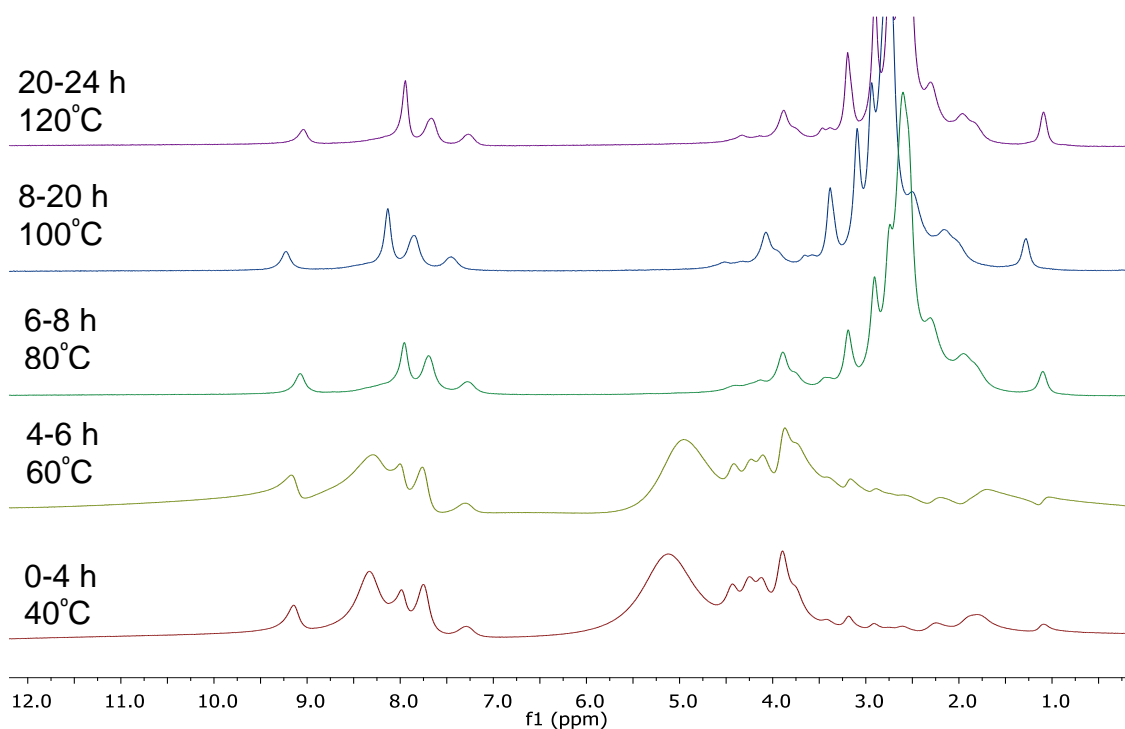
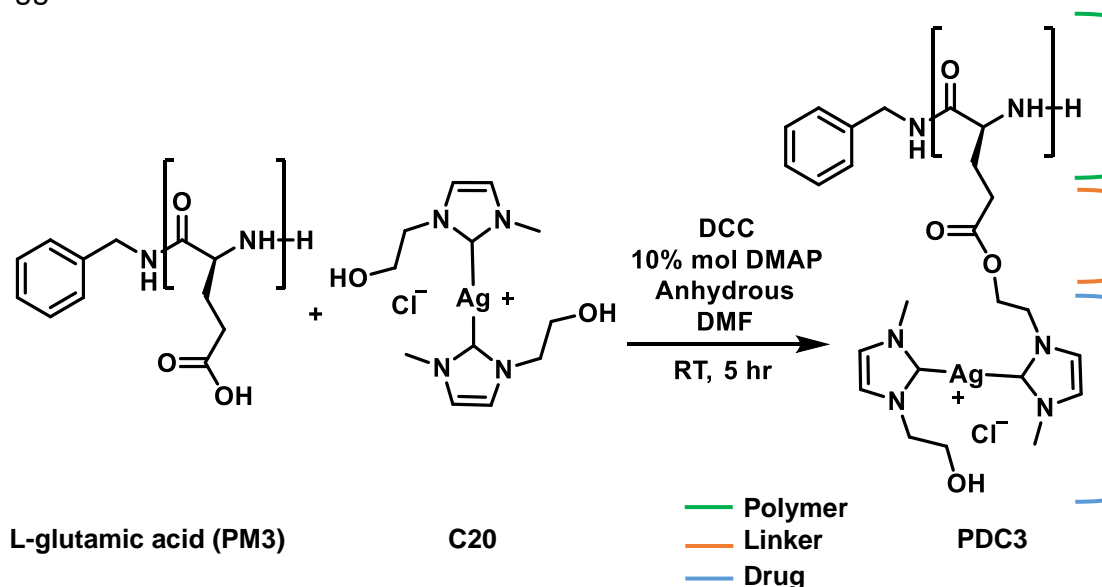


**Figure 6.8:** <sup>1</sup>H NMR spectra (300MHz, DMSO-d<sub>6</sub>) of the reaction of **PM3-L20** with Ag<sub>2</sub>O over 24 hours

An alternative route was explored which involved reaction of the preformed silver complex **C20** with **PM3** via a Steglich esterification reaction (**Scheme 6.3**), avoiding the use of  $\text{Ag}_2\text{O}$  and  $\text{MeOH}$ . The reaction uses 4-dimethylaminopyridine (DMAP) as a catalyst and dicyclohexylcarbodiimide (DCC) as a coupling reagent. HRMS, IR spectroscopy, NMR spectroscopy (**Figure 6.9**) and elemental analysis suggest successful esterification and formation of **PDC3**.



**Scheme 6.3:** Synthesis of **PDC3** through a Steglich esterification reaction

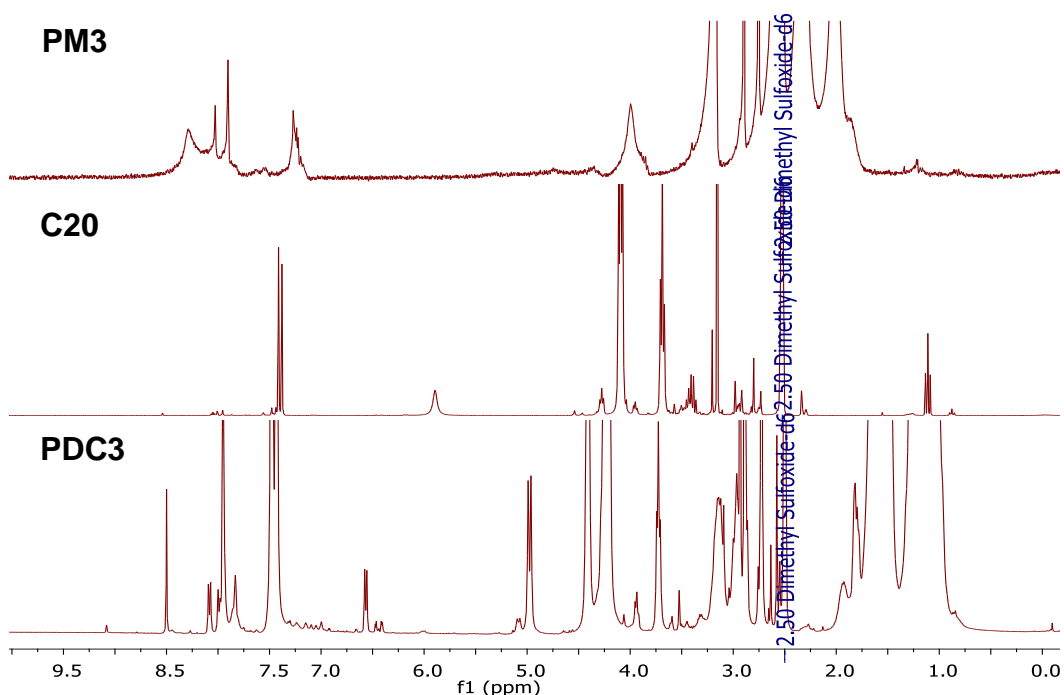


**Figure 6.9:**  $^1\text{H}$  NMR spectra (300MHz,  $\text{DMSO-d}_6$ ) of **PM3** (top), **C20** (middle) and **PDC3** (bottom)

The anticancer activity of the polymer-Ag(I)-NHC conjugates **PDC1-PDC3** were evaluated against pancreatic adenocarcinoma cell line Panc 10.05. The results were compared to the corresponding Ag(I)-NHC complex on its own (**Figure 6.10**). The molecular weights of PDCs used for the MTT-assays were calculated as a single unit with one Ag atom as shown in **Figure 6.10**. The ester linked drug-polymer conjugate **PDC3** showed superior anticancer activity to its corresponding drug **C20**, and the methylene linked drug-polymer conjugate **PDC2** is also more cytotoxic than its corresponding drug **C34** previously reported by Willans *et al.*<sup>20</sup> These results display the potential of Ag(I)-NHC-polymer conjugates as a strategy for enhancing the anticancer activity, possibly through the slow release of the silver from the polymer. Further possibility of protecting the drug *in vivo*, ability to tune the polymer for targeting.

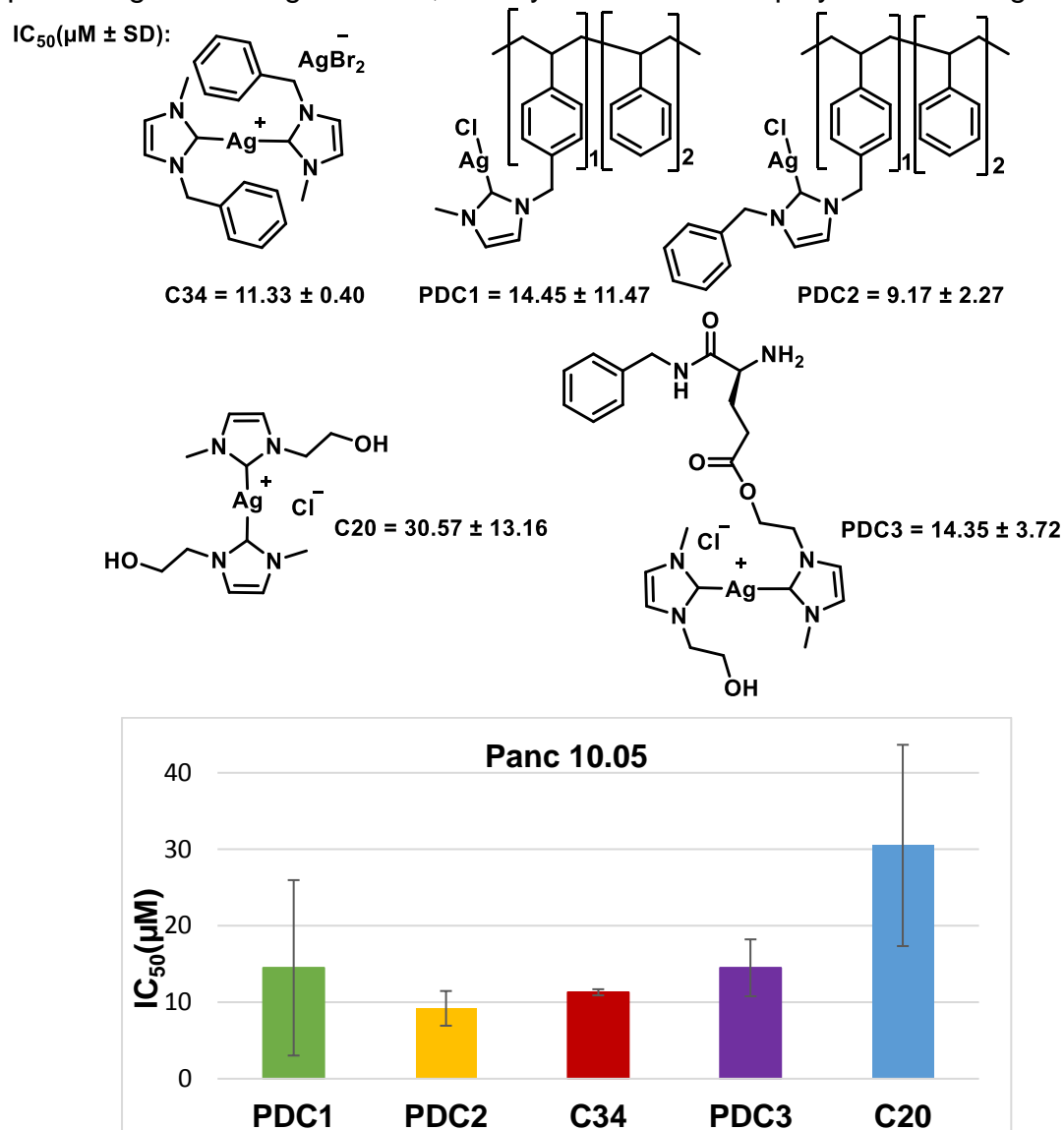
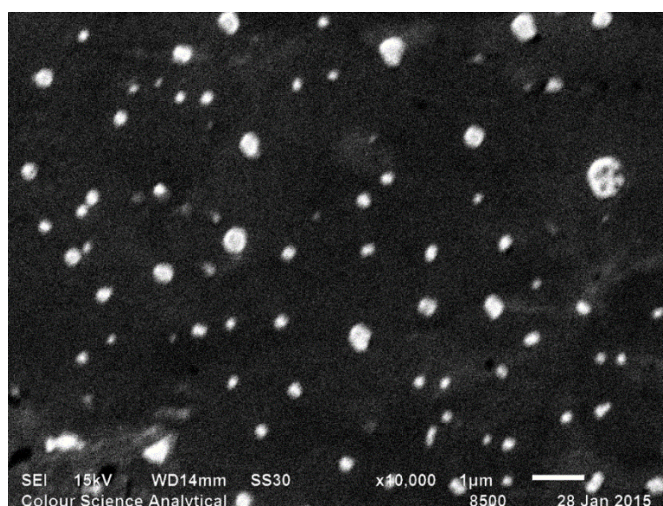


**Figure 6.10:** IC<sub>50</sub> values of drug-polymer conjugates **PDC1-PDC3** and the corresponding Ag(I)-NHC **C20** and **C34**

### 6.3 Encapsulation of silver(I)-NHCs into polymers

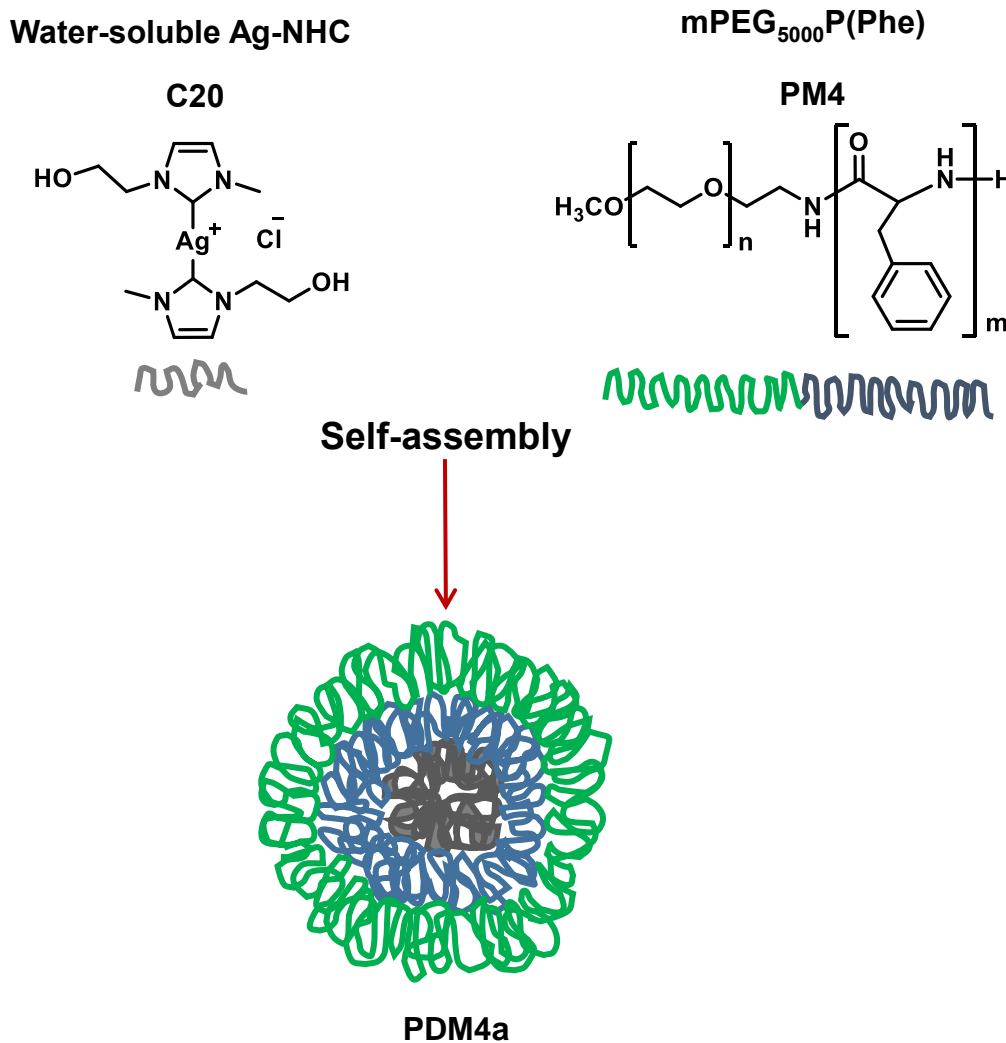
Although **PDC1-PDC3** may improve targeting of the silver-based drugs through the EPR effect, the linearity of the conjugates exposes the Ag(I)-NHCs to enzymes. Encapsulation of the Ag(I)-NHCs by polymers which can self-assemble under specific conditions to form polymer-drug micelles (PDMs), may protect the complexes from enzyme interactions before reaching their target.

Methoxy-poly(ethylene glycol)-poly(phenyl-alanine) (mPEG<sub>5000</sub>P(Phe)) **PM4** was considered for the encapsulation of the complexes due to the non-toxic properties of PEG.<sup>21</sup> Initially, the ability of mPEG<sub>5000</sub>P(Phe) to self-assemble in aqueous medium to form micelles was investigated. Dynamic light scattering (DLS) revealed self-aggregation of **PM4** to particles with an average particle size of 121.4 nm. This was also in agreement with the scanning electron microscopy (SEM) images (**Figure 6.11**). The polydispersity index (PDI) of the formed particles had a value of 0.26, suggesting successful self-assembly into relatively uniformly sized particles. Although a typical nanoparticle delivery system size ranges from 10-100 nm, while some groups report larger sized nanoparticles.<sup>22</sup> Differences in particle size translates to different pharmacokinetic and distribution parameters.



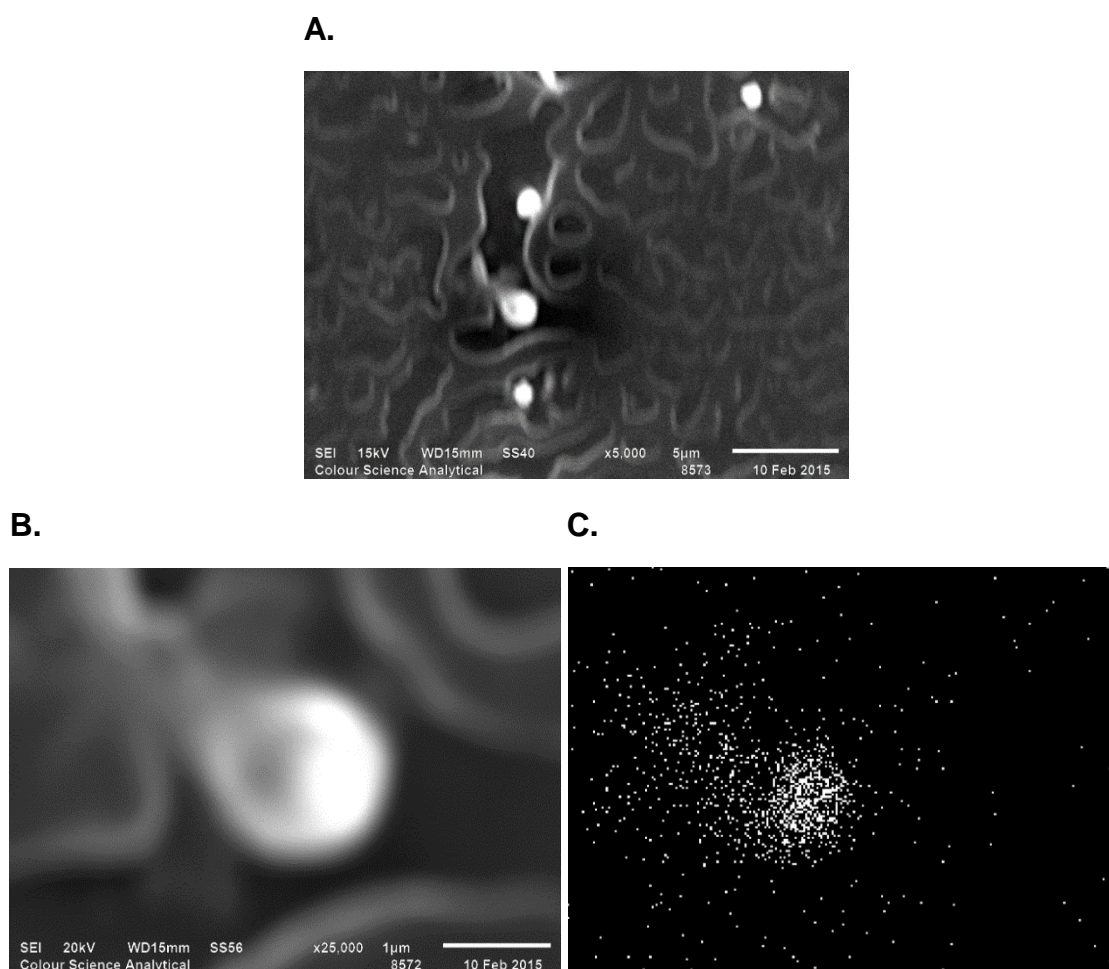
**Figure 6.11:** SEM image of particles formed from self-assembly of mPEG<sub>5000</sub>P(Phe) **PM4** in water (10µg/mL)

The particles formed constitute an inner lining with the hydrophobic block (P(Phe)) surrounded by the outer hydrophilic block (mPEG). Encapsulation was investigated using a water-soluble Ag(I)-NHC (**C20**), with varying ratios of **C20:PM4**. DLS analysis revealed the formation of **PDM4a** with an average particle size of 151.7 nm and PDI of 0.307, when using 1:1 ratio of Ag(I)-NHC complex to polymer (**Figure 6.12**). The driving force for the particle formation is mainly the interaction of the polar hydrophilic mPEG with the H<sub>2</sub>O through hydrogen bonds, and the non-polar hydrophobic P(Phe) migration to the organic solvent (DMF), causing a microphase separation. This is due to the disruption of the cohesive energy at the interface of the amphiphile and water, leading to formation of micelle-like aggregates. The Ag(I)-NHC may be embedded inside the micelle possibly through interactions (van der Waals' forces) with the hydrophobic block P(Phe).

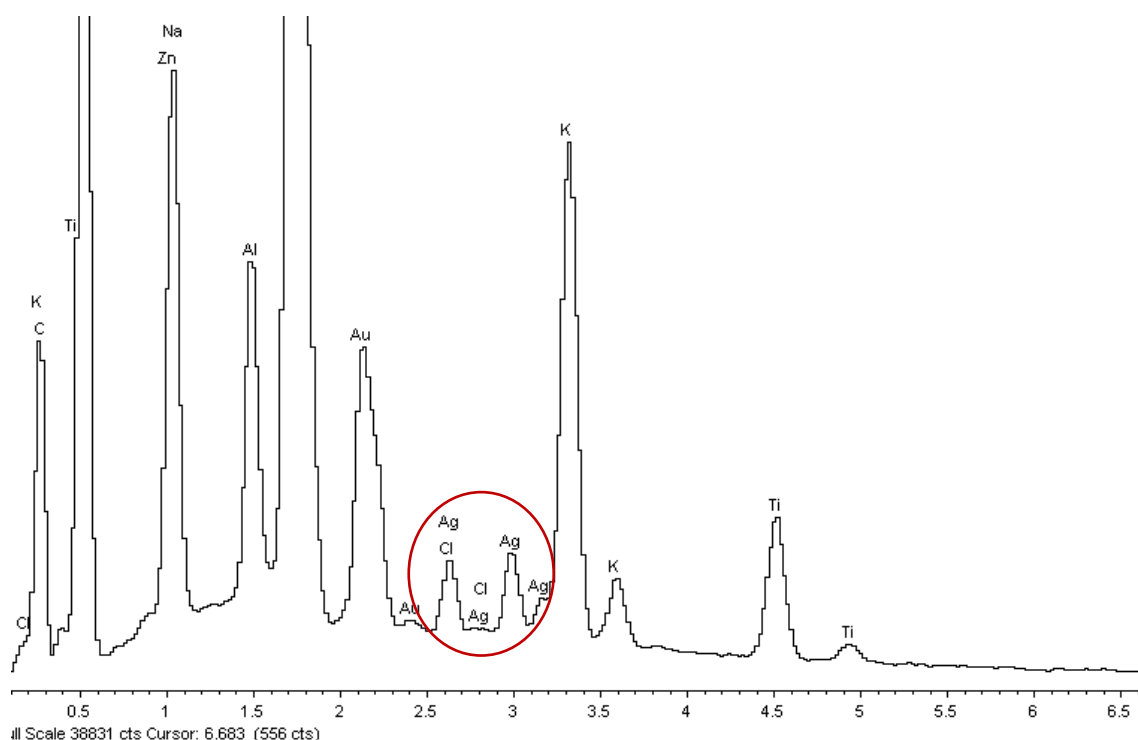


**Figure 6.12:** Illustration of the encapsulation of Ag(I)-NHC complex **C20** to give **PDM4a**

SEM analysis of **PDM4a** revealed the formation of discrete particles (**Figure 6.13A** and **B**). Energy-dispersive X-ray spectroscopy (EDX) was performed on the sample to map the location of silver ions (**Figure 6.13C**). SEM-EDX reveals that the silver ions are located within the particle region, shown when images **B** and **C** in **Figure 6.13** are superimposed, suggesting the successful encapsulation of Ag(I)-NHC complex **C20**. The EDX spectrum shows peaks corresponding to silver and chloride ions found in the sample, supporting the presence of the complex within the particle region (**Figure 6.14**).

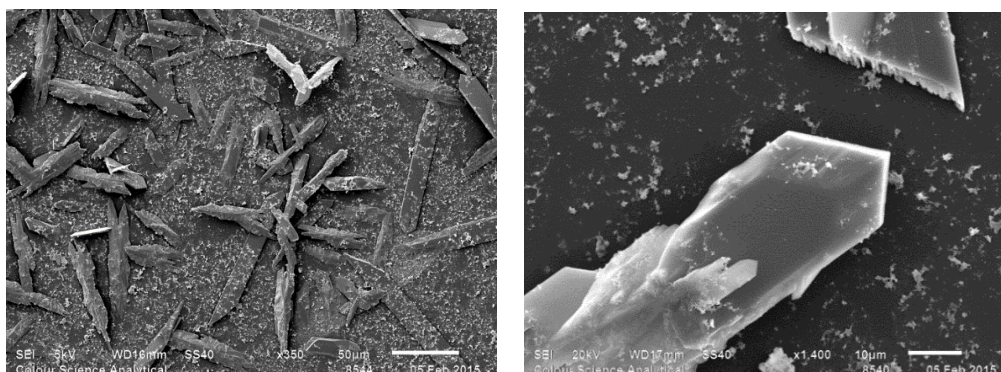


**Figure 6.13:** SEM images of **PDM4a** **A.** individual particles, **B.** magnification of on a single particle, **C.** silver ion mapping of image **B.**



**Figure 6.14:** SEM-EDX spectrum showing peaks corresponding to silver and chloride ions

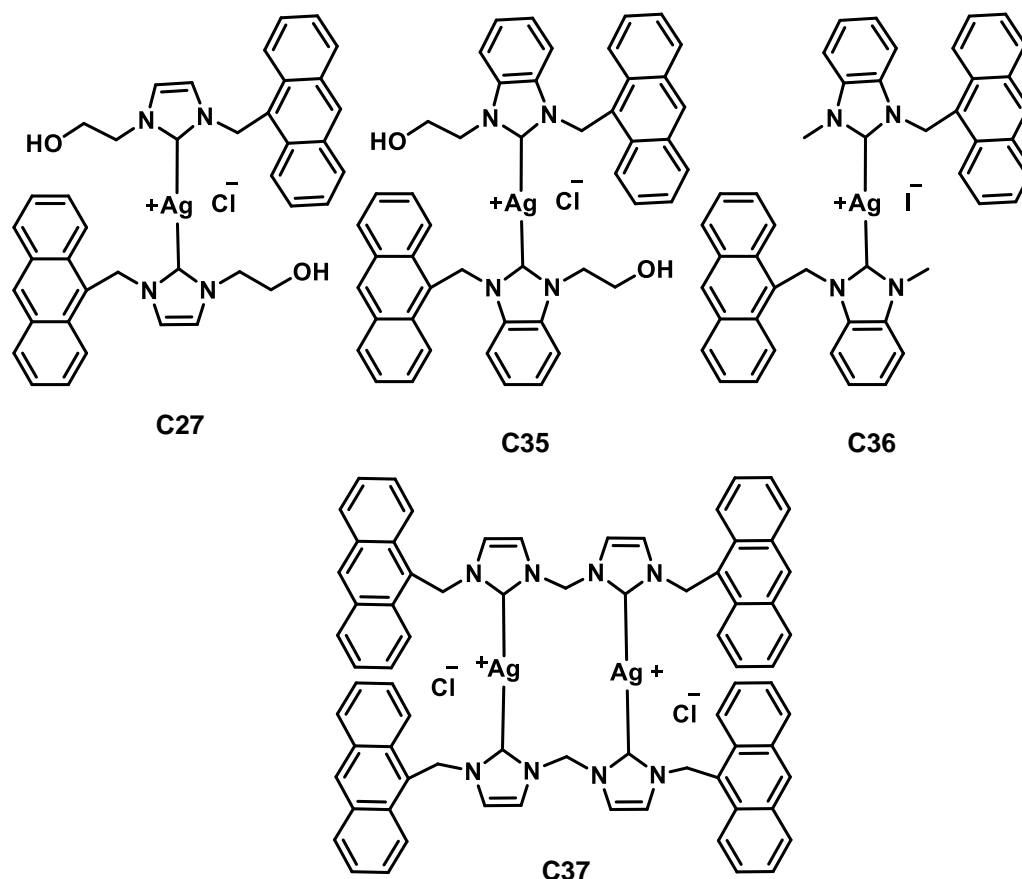
To further understand the role of the NHC in the encapsulation process, encapsulation of a silver salt was attempted by employing the same procedure with AgOAc. Equivalent amounts of AgOAc and polymer were utilised, with DLS results showing PDI values above 0.7, indicating a polydisperse sample. SEM images reveal crystallisation of silver salt with no indication of encapsulation or micelle formation (**Figure 6.15**). This result suggests that the NHC ligand plays an important role in the encapsulation process.



**Figure 6.15:** SEM image of a 1:1 AgOAc:PM4 mixture in aqueous solution, showing crystallisation of AgOAc

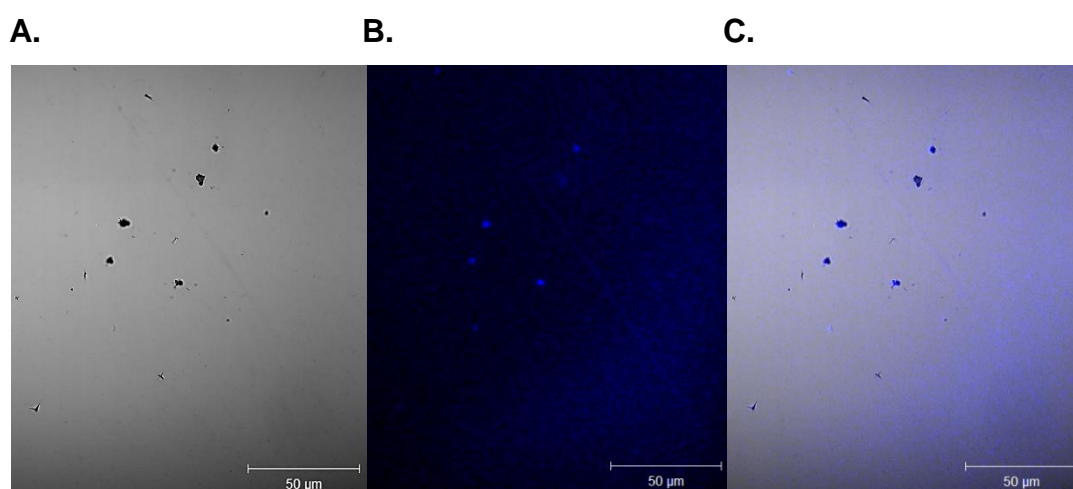
### 6.3.1 Confocal fluorescence microscopy

Fluorescence microscopy may be used to detect the encapsulation of compounds bearing a fluorescent moiety. Therefore, various complexes, that contain a fluorescent anthracene N-substituent were designed and synthesised (**C27**, **C35-C37**, **Figure 6.16**). **C37** was found to be insoluble in water and was therefore not considered further, while the solubility in water of **C27**, **C35** and **C39** were estimated. **C27** was found to be significantly more soluble than **C35** and **C36** ( $\text{C27} \gg \text{C35} > \text{C36}$ ). Encapsulation of **C27**, **C35** and **C36** were performed in a similar manner as **PDM4a**. **C35** and **C36** yielded particles with PDI values above 0.7, therefore were not further investigated using fluorescent imaging. Encapsulation of **C27** resulted in particles **PDM4b** with an average particle size of 134.3 nm and a PDI value of 0.668.

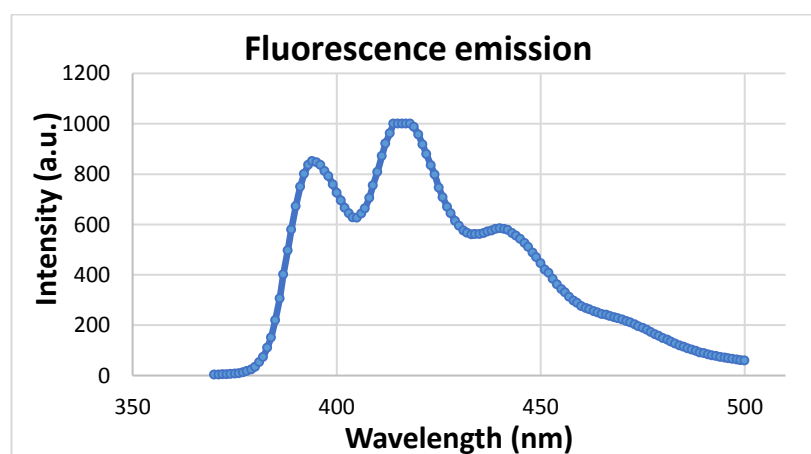


**Figure 6.16** : Fluorescent Ag(I)-NHC complexes

Encapsulation of **C27** into **PM4** was performed by adding equal volumes of equal concentrations of **C27** and **PM4** solutions together in  $\text{CH}_2\text{Cl}_2$ . An equal volume of water was subsequently added to the sample with constant agitation.  $\text{CH}_2\text{Cl}_2$  was removed *in vacuo* leaving the aqueous medium that contained the particles. Confocal microscopy was used to image particles **PDM4b**, by employing an excitation at 405 nm and detection at 370-500 nm. The images taken under visible light (**Figure 6.17A**) and under fluorescence (**B**), were superimposed (**C**). These images show the fluorescence in the sample, *i.e.* the Ag(I)-NHC complex located in the same region as the particles. Since **C27** emits fluorescence in the range 370-500 nm (**Figure 6.18**), the results indicate either encapsulation of silver inside micelles, or conjugation to micellar surface.



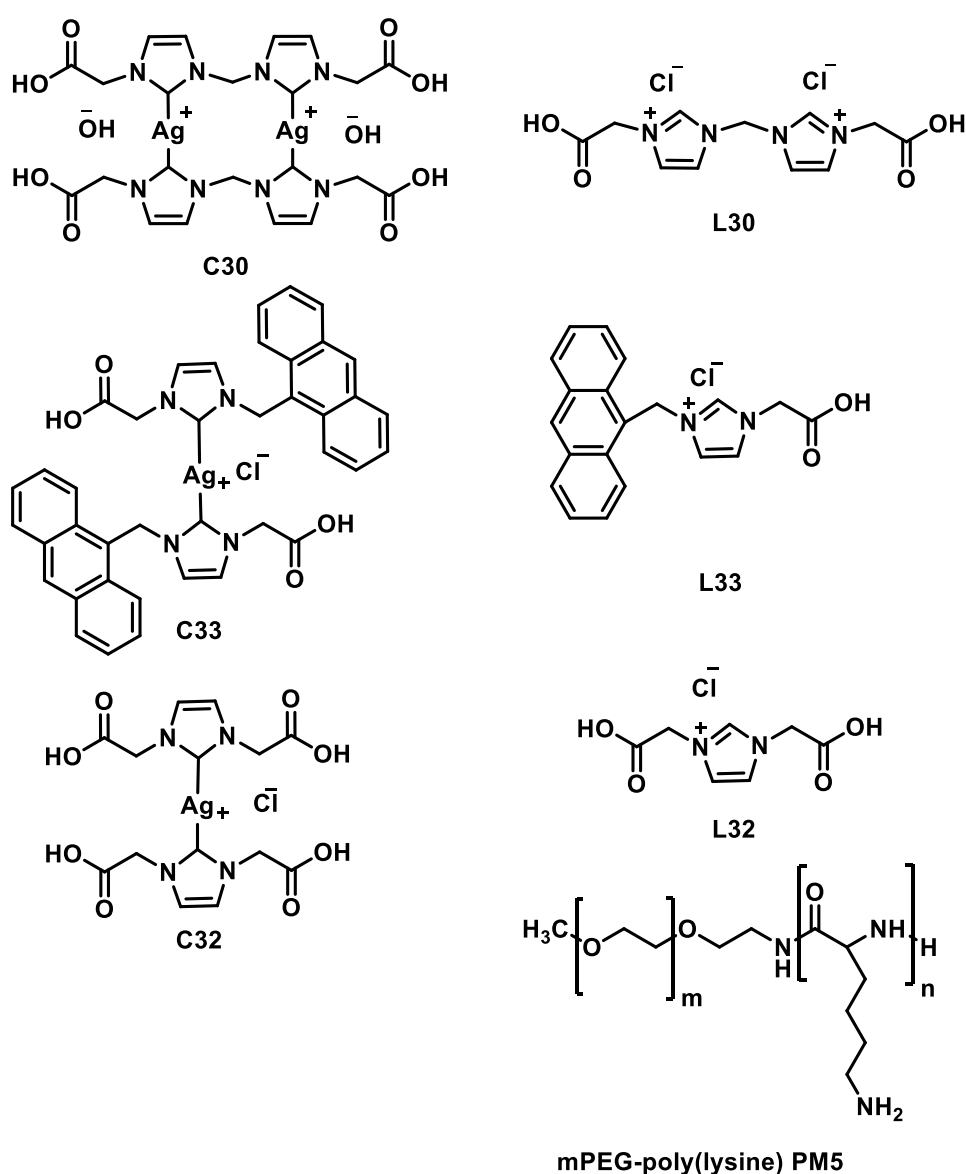
**Figure 6.17** : Images of **PDM4b** under **A.** visible light **B.** fluorescence **C.** superimposition of images **A.** and **B.**



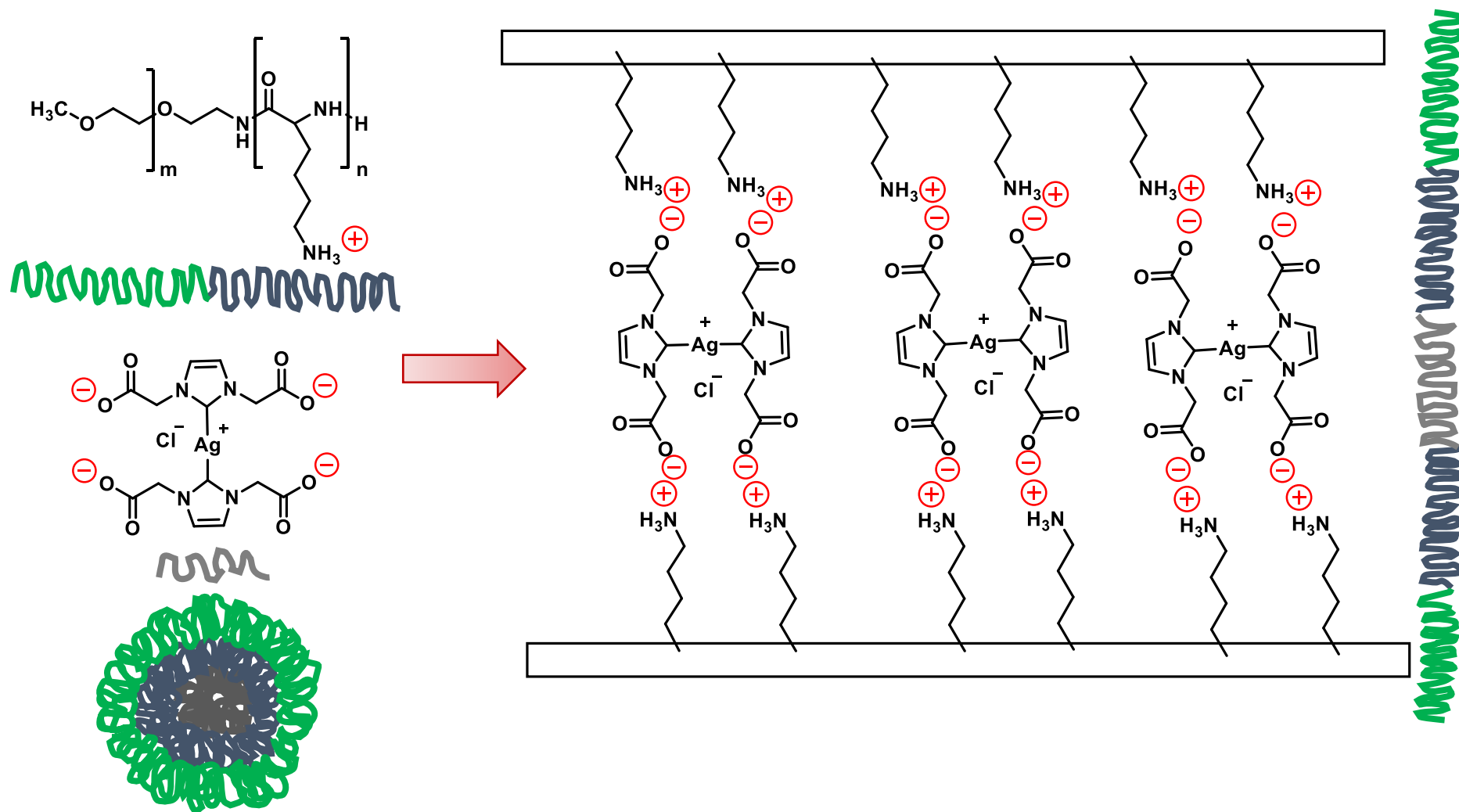
**Figure 6.18**: Fluorescence emission spectrum of **C27**

### 6.4 Electrostatic attraction between silver(I)-NHCs and polymers

Electrostatic attraction as a method of drug-polymer conjugation and subsequent micelle formation was investigated. This method is frequently performed with poly(lysine) as the cationic polymer for drug-conjugation and delivery.<sup>23-27</sup> Therefore, in this work, mPEG<sub>5000</sub>poly(lysine) **PM5** was used as the cationic polymer, while carboxylic acid N-substituted complexes **C30**, **C32** and **C33**, and the corresponding imidazolium salts **L30**, **L32** and **L33** were used as anionic drugs (**Figure 6.19**). This technique ensures that micelles are only formed when contact between the drug and the polymer occurs, thereby eliminating the possibility of conjugation of the drug to the surface of pre-formed polymeric micelles (**Figure 6.20**).



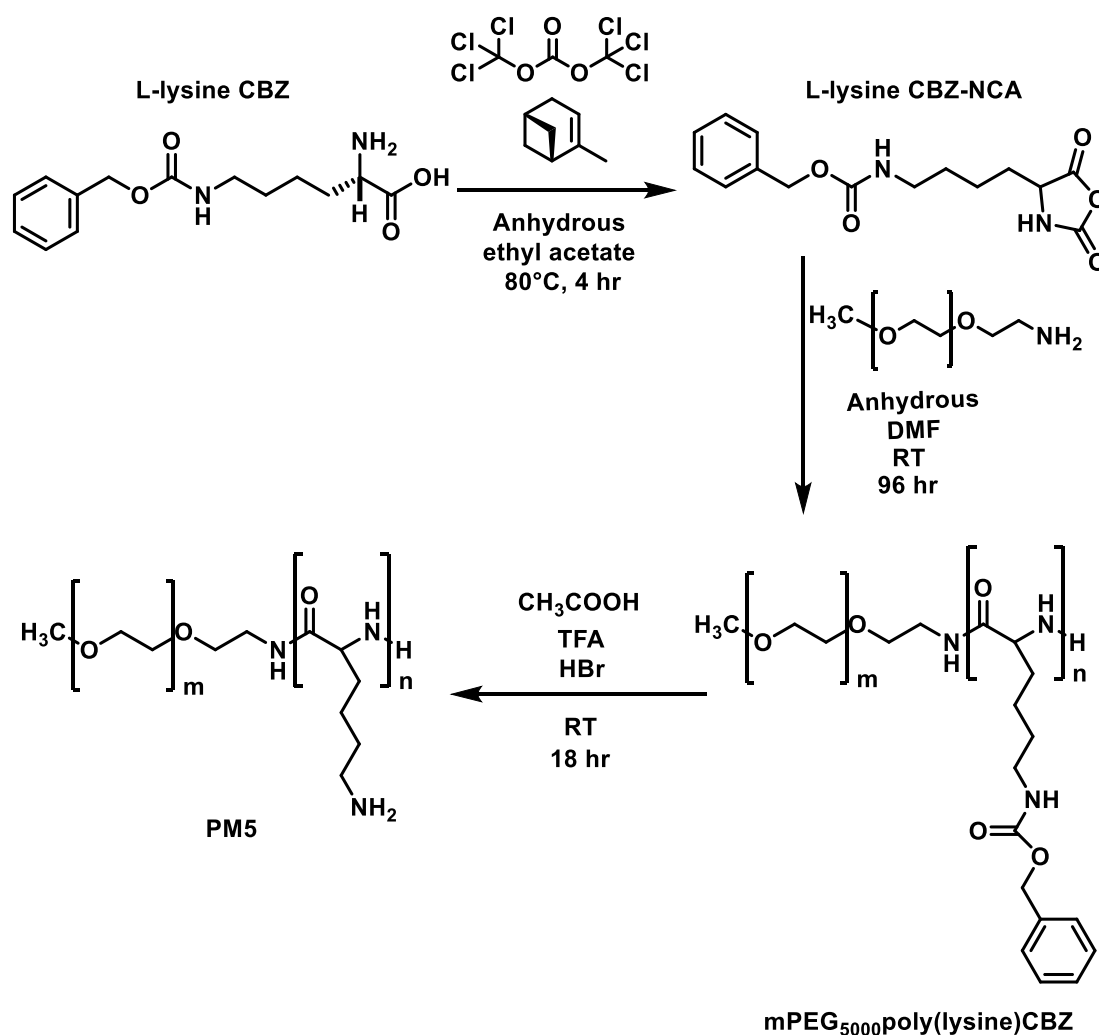
**Figure 6.19:** Ag(I)-NHC complexes, imidazolium salts and mPEG-polylysine **PM5** used in micelle formation through electrostatic attraction



**Figure 6.20:** Illustration of polymer-drug micelle formation through electrostatic attraction of oppositely charged ions

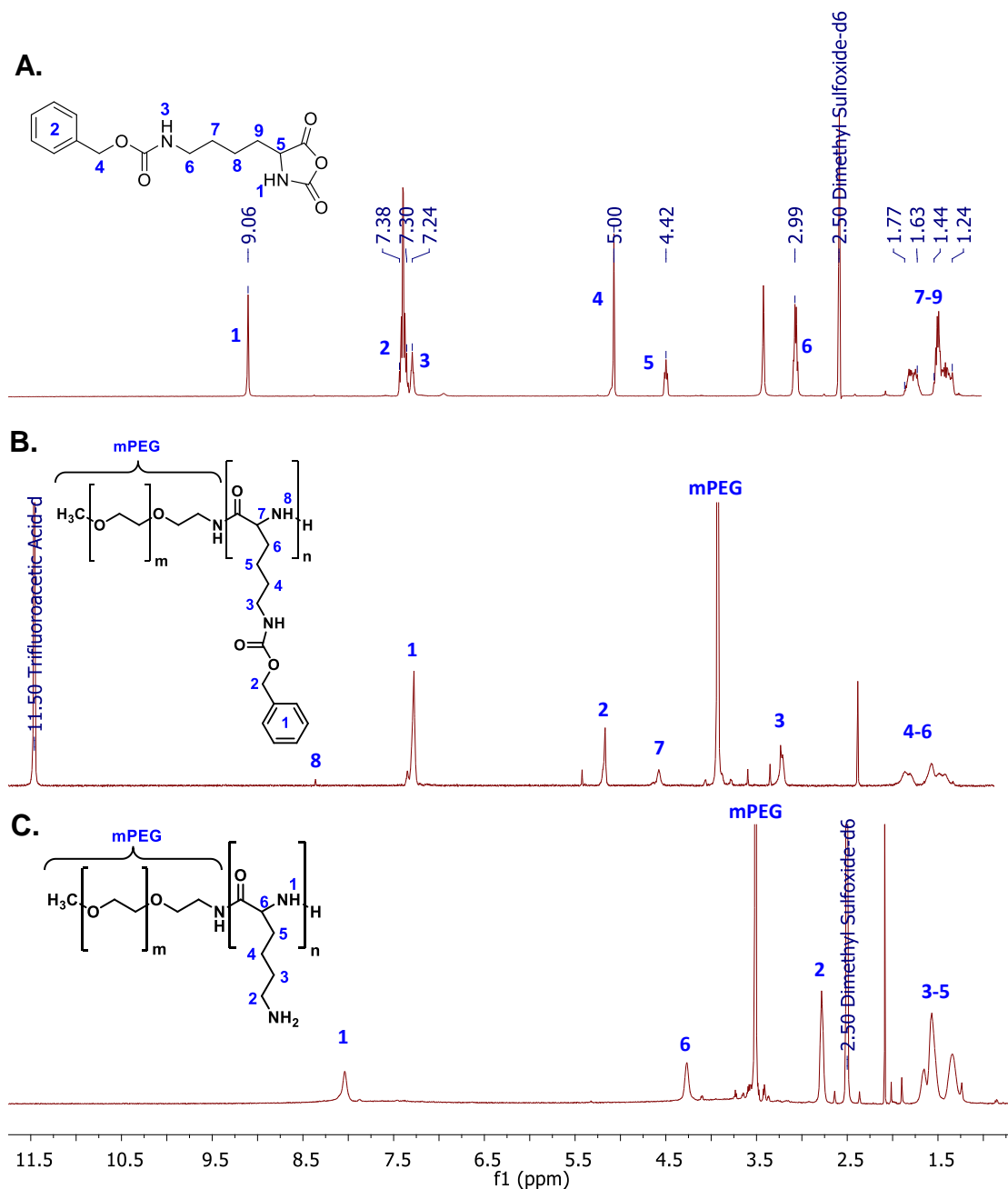
### 6.4.1 Synthesis of mPEG-poly(lysine) PM5

Methoxy-poly(ethylene glycol)-poly(lysine) (mPEG<sub>5000</sub>poly(lysine)), **PM5**, was synthesised with three different lengths of the poly(lysine), to furnish three polymers of varying mPEG to poly(lysine) ratios. The aim was to examine the effect of polymer chain length on the size of the micelle formed. The three step synthesis of **PM5** involves synthesis of L-Lysine carbobenzyloxy N-carboxyanhydride (L-lysine CBZ-NCA) from L-lysine carbobenzyloxy (L-lysine CBZ), *via* the reaction of L-lysine CBZ with triphosgene in ethyl acetate, in the presence of a proton scavenger  $\alpha$ -pinene (**Figure 6.21**). The synthesis of L-lysine CBZ-NCA was followed by ring opening polymerisation from an mPEG<sub>5000</sub> amine. Various ratios of NCA to amine (20, 40 and 75) were reacted in DMF, furnishing mPEG<sub>5000</sub>poly(lysine CBZ). Deprotection of poly(lysine CBZ) occurs through hydrolysis of CBZ groups in hydroboromic acid (33%), in acetic acid solution.



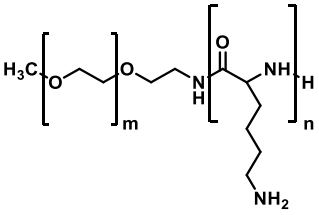
**Figure 6.21:** Three step synthesis of mPEG<sub>5000</sub>poly(lysine) **PM5**

$^1\text{H}$  NMR spectroscopy was used to monitor the reaction steps, showing the formation of CBZ-NCA with the resonance corresponding to the amine proton in NCA at 9.06 ppm (labelled 1 in **Figure 6.22A**). This peak shifts upfield to 8.30 ppm upon ring opening polymerisation (labelled 8 in **B**). The aromatic protons from the mPEG<sub>5000</sub>poly(lysine CBZ) (labelled 1 in **B**) disappear upon deprotection to form mPEG<sub>5000</sub>poly(lysine) **PM5** (**Figure 6.22C**).



**Figure 6.22:**  $^1\text{H}$  NMR spectra (300MHz) of **A.** CBZ-NCA (DMSO- $d_6$ ), **B.** mPEG<sub>5000</sub>poly(lysine)CBZ ( $\text{CF}_3\text{COOD}$ ) and **C.** mPEG<sub>5000</sub>poly(lysine) **PM5** (DMSO- $d_6$ )

Solutions of the three polymers **PM5.A-C** with varying polylysine to mPEG ratios (**Table 6.1**), and solutions of **L30**, **C30**, **L32**, **C32**, **L33** and **C33**, at a concentration of 1 mg/mL were prepared in HPLC grade water. All solutions were filtered through a 0.45  $\mu\text{m}$  followed by a 0.2 $\mu\text{m}$  PTFE syringe filter, with DLS analysis indicating no particles present after filtration of the solutions. Filtered solutions of 1:1 molar ratios of polymer to ligand/complex were subsequently prepared and analysed using DLS at 37°C to mimic the body temperature. It was found that particles generally increase in diameter with an increase in polymer length. However, **PDM5.B.C33** had a larger average particle diameter than expected of 452.7nm, suggesting vesicle formation. Unlike **PM5.A**, particles formed using **PM5.B** and **PM5.C** possessed PDI values below 0.7 upon interaction with all six complexes and ligands. Imidazolium salts and the corresponding Ag(I)-NHC complexes seem to behave in a similar manner to each other with regards electrostatic interaction, suggesting that the presence of Ag(I) neither hinders nor promotes encapsulation.

| <b>Table 6.1: Micelle formation via electrostatic attraction (reactions referred to as polymer-drug micelles e.g. PDM5.A.L30)</b>                                 |                                   |                                   |                            |
|---|-----------------------------------|-----------------------------------|----------------------------|
|  <p style="text-align: center;"><b>mPEG<sub>5000</sub>poly(lysine) PM5</b></p> |                                   |                                   | <b>Ligand/<br/>Complex</b> |
| <b>A</b><br><b>n = 39m</b>  | <b>B</b><br><b>n = 50m</b>        | <b>C</b><br><b>n = 140m</b>       |                            |
| PDI: 1.000<br>APS: <b>146.0nm</b>   | PDI: 0.754<br>APS: <b>173.1nm</b> | PDI: 0.292<br>APS: <b>224.2nm</b> | <b>L30</b>                 |
| PDI: 0.188<br>APS: <b>159.7nm</b>   | PDI: 0.173<br>APS: <b>175.6nm</b> | PDI: 0.153<br>APS: <b>176.5nm</b> | <b>C30</b>                 |
| PDI: 0.545<br>APS: <b>130.0nm</b>   | PDI: 0.632<br>APS: <b>162.2nm</b> | PDI: 0.270<br>APS: <b>252.1nm</b> | <b>L32</b>                 |
| PDI: 0.769<br>APS: <b>101.1nm</b>   | PDI: 0.277<br>APS: <b>178.2nm</b> | PDI: 0.378<br>APS: <b>199.5nm</b> | <b>C32</b>                 |
| PDI: 1.000<br>APS: <b>121.8nm</b>   | -                                 | PDI: 0.484<br>APS: <b>253.2nm</b> | <b>L33</b>                 |
| PDI: 0.249<br>APS: <b>160.8nm</b>   | PDI: 0.173<br>APS: <b>452.7nm</b> | PDI: 0.449<br>APS: <b>221.8nm</b> | <b>C33</b>                 |

SEM images of the particles were obtained and all the results appear to be in agreement with the DLS results. PDC **PDM5.B.C33** particles appear to be vesicles having an 'outer shell' (**Figure 6.23**), possibly the polymer outer lining or the mPEG portion, while the Ag(I)-NHC is likely to be encapsulated inside this shell, surrounded by the poly(lysine) portion, and stabilised by electrostatic attraction. **Figure 6.24** illustrates the behaviour of **PM5**, and the Ag(I)-NHC complex **C30** where no particles are observed (**A**). Upon mixing of the solutions, electrostatic attraction between the opposite charges begin to form micelles and a particle size curve is observed in the DLS (**B**).

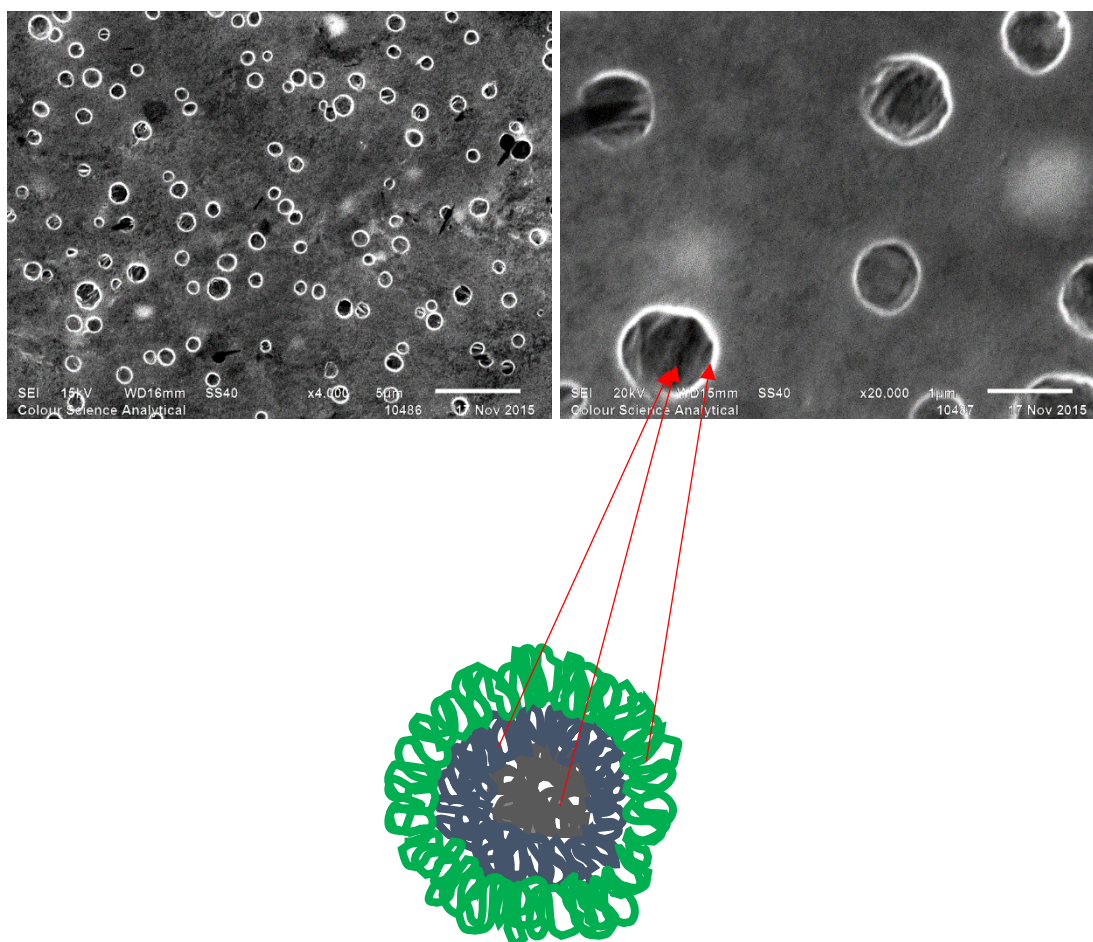
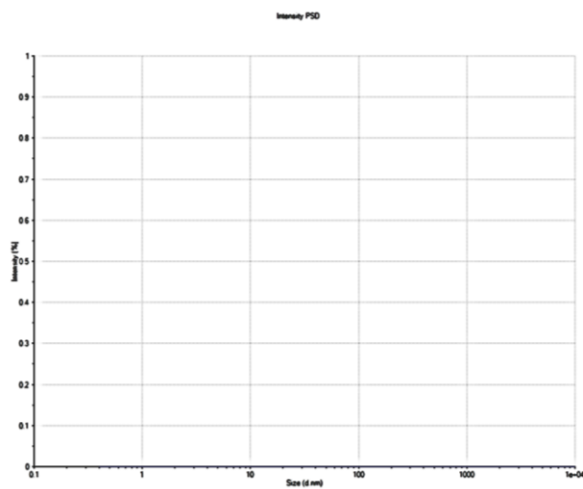
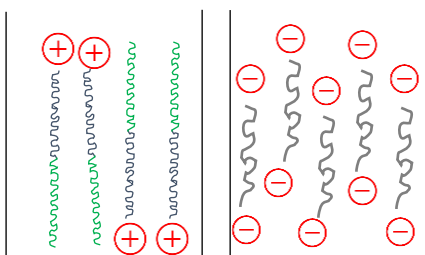


**Figure 6.23:** SEM images of **PDM5.B.C33**

A.



B.

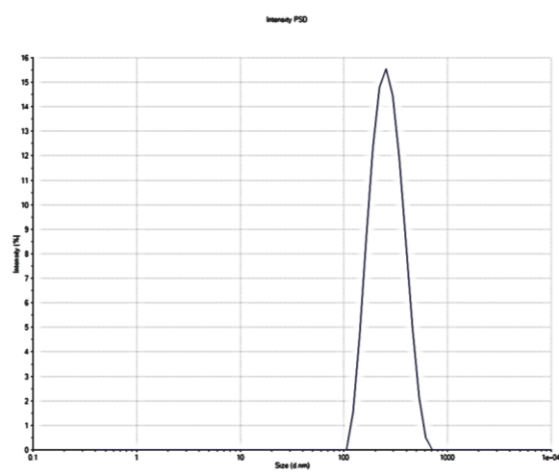
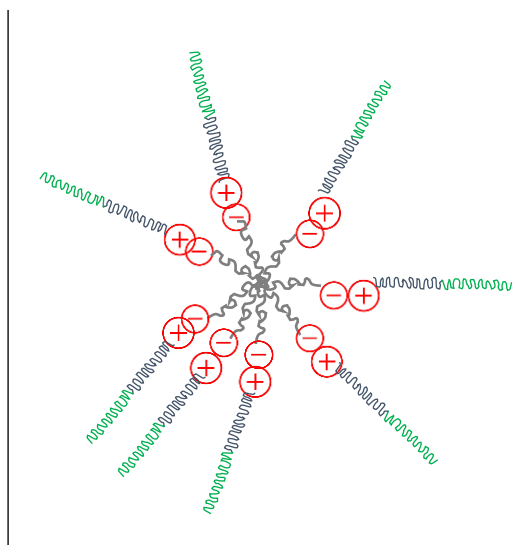


**Figure 6.24:** Illustration of **A.** a solution of **PM5** and **Ag(I)-NHC complex C30**, and **B.** micelles formed upon mixing the solutions, and their corresponding DLS measurement results

## 6.5 Anticancer activity of drug-polymer micelles

The anticancer activity of the particles **PDM4a**, **PDM5.B.C30** and **PDM5.B.C33** were evaluated against the pancreatic adenocarcinoma cell line Panc 10.05 (**Table 6.2** and **Figure 6.25**). The results were compared to those previously obtained for the non-conjugated Ag(I)-NHC complexes **C20**, **C30** and **C33**. The particles consistently displayed higher potency against the cancerous cell line when compared to the Ag(I)-NHC. This indicates that the polymer coating whether mPEG<sub>5000</sub>P(Phe) (e.g. in **PDM4a**) or mPEG<sub>5000</sub>poly(lysine) (e.g. in **PDM5.B.C30** and **PDM5.B.C33**) either exhibits toxicity against the cells, adding to the existing cytotoxicity of the drug or leads to slow release of Ag ions by protecting the Ag(I)-NHC. The selectivity of the particles towards cancerous cells was evaluated by determining cytotoxicity values against the non-cancerous cell line ARPE-19. In general, the non-encapsulated Ag(I)-NHC complexes appear to be more selective towards Panc 10.05 than the PDMs. However, *in vivo* studies are required to determine the benefits of EPR effect on the polymeric nanoparticles in comparison to the Ag(I)-NHC complexes.

**Table 6.2:** Cytotoxicity data on PDMs versus complexes

| Compound          | Panc 10.05  | ARPE-19     | Selectivity ratio |
|-------------------|-------------|-------------|-------------------|
| <b>C20</b>        | 30.6 ± 13.2 | >100        | 3.3               |
| <b>PDM4a</b>      | 25.8 ± 4.3  | 83.4 ± 17.1 | 3.2               |
| <b>C30</b>        | 12.3 ± 3.2  | >100        | 8.2               |
| <b>PDM5.B.C30</b> | 8.2 ± 1.8   | 23.6 ± 6.9  | 2.9               |
| <b>C33</b>        | 26.3 ± 11.5 | 68.7 ± 7.2  | 2.6               |
| <b>PDM5.B.C33</b> | 16.0 ± 5.5  | 22.7 ± 2.7  | 1.4               |

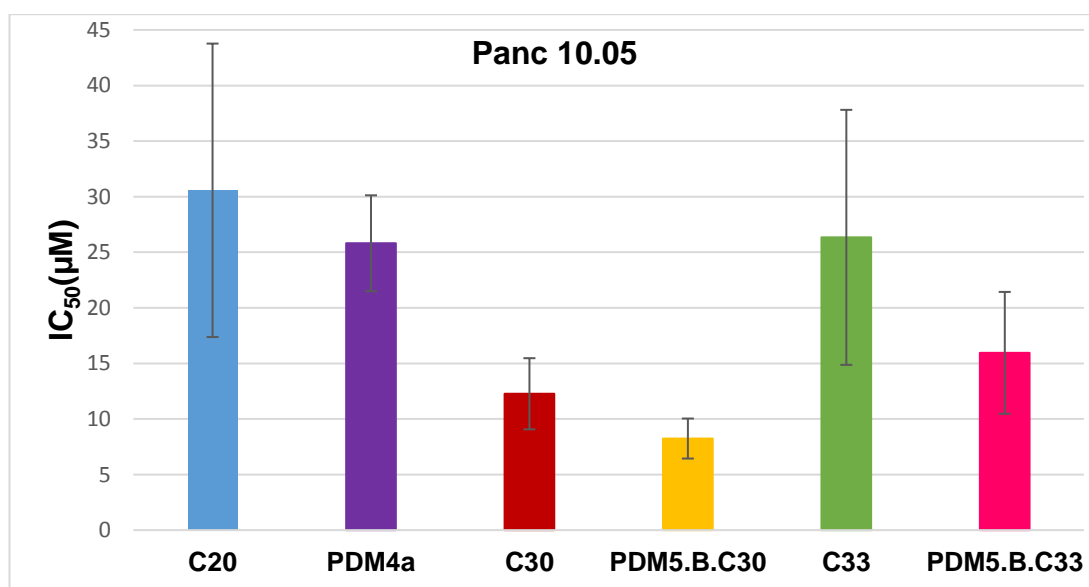


**Figure 6.25:** IC<sub>50</sub> values of PDMs versus complexes against Panc 10.05

## 6.6 Conclusions

The examination of possible delivery vehicles for Ag(I)-NHC complexes as drug molecules by the use of polymers, either through forming linear polymer-Ag(I)-NHC conjugates (PDCs), or through encapsulating the Ag(I)-NHC within polymeric micelles (PDMs) has been reported. Encapsulation and/or conjugation to polymers increases the size and molecular weight of the compound, which is more likely to selectively pass through the cancerous tissues due to enhanced permeability and retention (EPR). This EPR effect may also result in longer retention of the drug in cancerous tissues, thereby enhancing the anticancer effect. Linear polymer-drug conjugates were synthesised using imidazolium salt containing block copolymers **PM1** and **PM2**, with silver being coordinated to form **PDC1** and **PDC2**. Ag(I)-NHCs were chemically coordinated to poly-(L-glutamic acid) **PM3**, through formation of an ester bond to form **PDC3**. The anticancer activities of **PDC1-PDC3** were determined against the cancerous cell line Panc 10.05. The results revealed higher potency than the corresponding non-polymer-containing Ag(I)-NHC complexes **C20** and **C34**. This indicates improved activity due to polymer conjugation which, combined with the *in vivo* EPR effect, provides significant potential for these complexes in the treatment of cancer.

Encapsulation of Ag(I)-NHCs into self-assembled polymeric micelles was also investigated as an alternative approach to delivering the complexes to the site of action. mPEG<sub>5000</sub>-poly-(phenylalanine) **PM4** was used to encapsulate **C20** in water to form **PDM4a**. DLS studies revealed an average particle size and particle size distribution that were in agreement with SEM findings. SEM-EDX revealed that **C20** was more concentrated within the regions of the particles, suggesting successful encapsulation. The encapsulation of fluorescent Ag(I)-NHC **C27** into mPEG<sub>5000</sub>P(Phe) **PM4** to form **PDM4b** was performed. Confocal fluorescent microscopy showed fluorescence in the area within the particle, also suggesting the success of the encapsulation process.

Encapsulation was also explored using electrostatic interaction between the Ag(I)-NHC drug and the polymer mPEG<sub>5000</sub>poly(lysine) **PM5**. In water, the terminal secondary amine groups are protonated to bear a positive charge, and the carboxylic acid substituents of the NHC ligand are deprotonated to give a negative charge. Addition of polymer solutions and Ag(I)-NHCs solutions in water resulted in the formation of particles, which is likely due to electrostatic attraction. This is supported by the fact that no particles were observed in solutions of either the complex or the polymer prior to adding them together.

The anticancer activity of the particles **PDM4a**, **PDM5.B.C30** and **PDM5.B.C33** were determined against Panc 10.05. Results show superior activity (1.1-1.6 fold increase in anticancer activity) of the PDMs compared to the corresponding non-encapsulated Ag(I)-NHC complexes **C20**, **C30** and **C33**, again showing the potential benefits of encapsulation on improving the anticancer activity of Ag(I)-NHCs. The improved cytotoxicity may be due to the slow release of Ag<sup>+</sup> ions from the polymeric particles, leading to a prolonged exposure of the cells to the cytotoxic effects. These benefits may improve further *in vivo* due to the EPR effect.

Both encapsulation and conjugation of Ag(I)-NHC complexes to polymers were successful and produced a range of preliminary results that are worthy of further investigation. Both PDCs and PDMs appear to be promising delivery vehicles for delivering the Ag(I)-NHC complexes to their site of action, where silver is believed will be slowly released leading to a prolonged anticancer activity. The use of PDCs and PDMs may improve the bioavailability of the drug, by acting as a prodrug that releases the active drug into cancerous cells.

## 6.7 Future work

Future work should focus on *in vivo* testing, to evaluate the efficiency of the polymer-Ag(I)-NHC conjugates and micelles in delivering the Ag(I)-NHC complexes to the cancerous tissue. This will involve animal studies that will determine their safety or toxicity, and whether the polymers improve the selectivity of the complexes. *In vitro* mechanistic studies are currently in progress (at the University of Huddersfield) to determine the molecular targets e.g. receptors, proteins or enzyme that affect, are affected by or interact with the Ag(I)-NHC complexes. Combined *in vitro* and *in vivo* results will determine future molecular engineering or drug-delivery strategies for selective delivery of the complexes to cancerous tissues.

Recent developments in molecular engineering of an anticancer drug-delivery system include engineering of a nanomaterial that can target multi-drug resistant cancers.<sup>28</sup> This nanomaterial involves adding additional coatings to PDMs, the first being siRNA (yellow), followed by positively charged polymer (red) and finally a hydrated polysaccharide layer (purple, **Figure 6.26**). The siRNA acts as the gene blocker that prevents the resistant tumour cells from dividing, and due to its negative charge, it can be protected by a positively charged polymer. To target this nanoparticle material, it is disguised by adding a negatively charged natural hydrated polysaccharide that is found in the body and creates a veil of water molecules around the nanoparticle, allowing it to travel in the blood stream without elimination by blood enzymes. Tumor-specific molecules such as protein, antigens or receptors could be added on its surface for tumour-targeting of the Ag(I)-NHC anticancer drug.

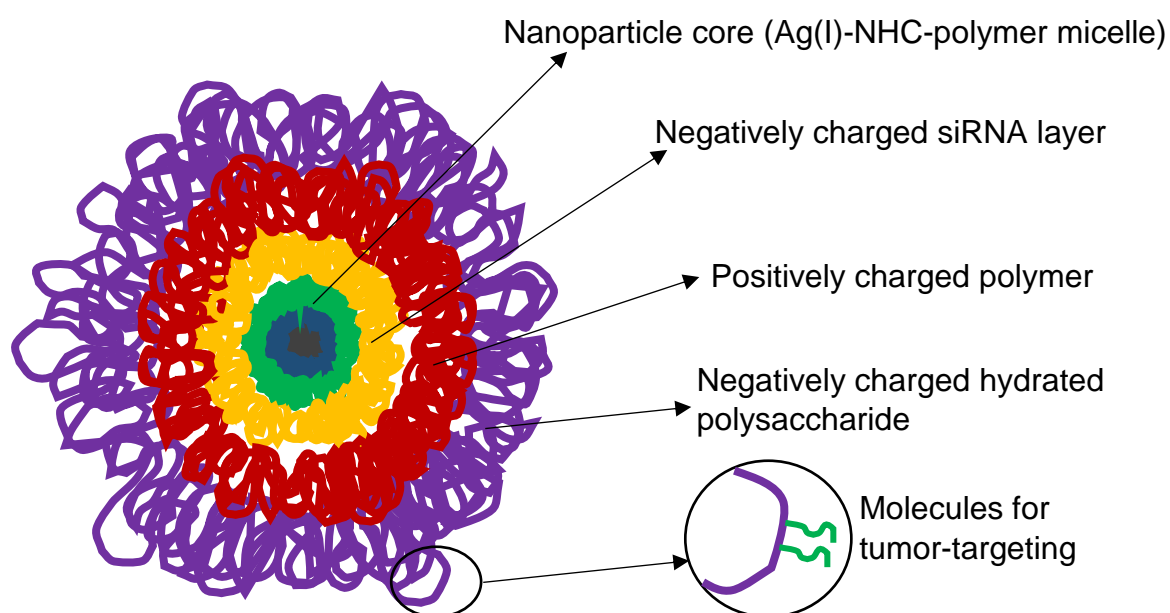


**Figure 6.26:** Illustration of nanoparticle engineering for tumour selectivity and toxicity<sup>28</sup>

## 6.8 References

1. C. G. Palivan, R. Goers, A. Najer, X. Zhang, A. Car and W. Meier, *Chemical Society Reviews*, **45**, 377-411.
2. R. Haag and F. Kratz, *Angewandte Chemie-International Edition*, 2006, **45**, 1198-1215.
3. T. M. Allen and P. R. Cullis, *Science*, 2004, **303**, 1818-1822.
4. F. M. Veronese and G. Pasut, *Drug Discovery Today*, 2005, **10**, 1451-1458.
5. K. Knop, R. Hoogenboom, D. Fischer and U. S. Schubert, *Angewandte Chemie-International Edition*, **49**, 6288-6308.
6. D. E. Discher and A. Eisenberg, *Science*, 2002, **297**, 967-973.
7. R. Duncan, *Nature Reviews Drug Discovery*, 2003, **2**, 347-360.
8. X. Wang and Z. Guo, *Chemical Society Reviews*, **42**, 202-224.
9. L. Gros, H. Ringsdorf and H. Schupp, *Angewandte Chemie-International Edition in English*, 1981, **20**, 305-325.
10. H. Ringsdorf, *Journal of Polymer Science Part C-Polymer Symposium*, 1975, 135-153.
11. N. Kamaly, Z. Xiao, P. M. Valencia, A. F. Radovic-Moreno and O. C. Farokhzad, *Chemical Society Reviews*, **41**, 2971-3010.
12. Q. Yin, R. Tong, Y. Xu, K. Baek, L. W. Dobrucki, T. M. Fan and J. Cheng, *Biomacromolecules*, 2013, **14**, 920-929.
13. H. Maeda, J. Wu, T. Sawa, Y. Matsumura and K. Hori, *Journal of Controlled Release*, 2000, **65**, 271-284.
14. H. Maeda and Y. Matsumura, *Critical Reviews in Therapeutic Drug Carrier Systems*, 1989, **6**, 193-210.
15. Y. Matsumura and H. Maeda, *Cancer Research*, 1986, **46**, 6387-6392.
16. R. K. Jain, *Cancer Research*, 1987, **47**, 3039-3051.
17. R. K. Jain, *Cancer and Metastasis Reviews*, 1987, **6**, 559-593.
18. R. Duncan, *Current Opinion in Biotechnology*, **22**, 492-501.
19. R. Langer, *Nature*, 1998, **392**, 5-10.
20. D. C. F. Monteiro, R. M. Phillips, B. D. Crossley, J. Fielden and C. E. Willans, *Dalton Transactions*, 2012, **41**, 3720-3725.
21. A. Lavasanifar, J. Samuel and G. S. Kwon, *Advanced Drug Delivery Reviews*, 2002, **54**, 169-190.
22. E. C. Dreaden, L. A. Austin, M. A. Mackey and M. A. El-Sayed, *Therapeutic delivery*, 2012, **3**, 457-478.
23. D. W. Pack, A. S. Hoffman, S. Pun and P. S. Stayton, *Nature Reviews Drug Discovery*, 2005, **4**, 581-593.
24. W. Zauner, M. Ogris and E. Wagner, *Advanced Drug Delivery Reviews*, 1998, **30**, 97-113.
25. K. Zatloukal, E. Wagner, M. Cotten, S. Phillips, C. Plank, P. Steinlein, D. T. Curiel and M. L. Birnstiel, *Annals of the New York Academy of Sciences*, 1992, **660**, 136-153.
26. W. H. Suh, J. K. Chung, S. H. Park and S. W. Kim, *Journal of Controlled Release*, 2001, **72**, 171-178.
27. C. P. Leamon, D. Weigl and R. W. Hendren, *Bioconjugate Chemistry*, 1999, **10**, 947-957.
28. Z. J. Deng, S. W. Morton, E. Ben-Akiva, E. C. Dreaden, K. E. Shopsowitz and P. T. Hammond, *Acs Nano*, 2013, **7**, 9571-9584.

## Chapter 7

### Electrochemical screening of silver(I)-NHC complexes on a unique biological sensor

#### 7.1 Introduction

Electrochemical biosensors are a subclass of chemical sensors, which consist of a molecular sensing device that combines a biological recognition component to an electrode transducer. The electrode transducer converts the biological recognition event into a measurable electrical signal.<sup>1, 2</sup> The past three decades have observed an abundance of research on biosensors. This is owed to their speed, specificity, low cost, and portability, which allow them to act as alternatives to some clinical testing, including home-use devices such as diabetes monitoring.<sup>3</sup> Electrochemical biosensors are categorised into two classes, biocatalytic devices and affinity receptors.<sup>2</sup> Biocatalytic devices use enzymes, whole cells or tissue slides to produce electroactive species when contacted with a target.<sup>4</sup> Examples include glucose sensors,<sup>5</sup> xanthine sensors<sup>6</sup> and lactate sensors.<sup>7</sup> Affinity biosensors depend on selective binding or interaction of the target with a biological component such as an antibody, a protein or a receptor, which could assist in detection and monitoring of cancers.<sup>2, 8</sup> Examples of affinity biosensors include Immunoassays and Immunosensors,<sup>9-11</sup> DNA hybridisation biosensors<sup>12, 13</sup> and receptor-based biosensors.<sup>14</sup>

A unique electrochemical biosensor has been developed over the last decade by Nelson *et al.*, to detect interactions of compounds with a membrane.<sup>15-23</sup> The sensing electrode consists of a mercury coated platinum contact (**Figure 7.1**), onto which a phospholipid monolayer (membrane) is deposited. The sensing electrode is connected to an on-line high throughput flow system, which utilises rapid cyclic voltammograms (RCVs) to display changes in capacitance current peaks when a voltage of 40 V s<sup>-1</sup> is applied. The electrodes electrochemically detect the damage caused to the membrane when in contact with a membrane-active compound. This unique setup has been used in drug screening of membrane-active pharmaceuticals, and in detection of toxins in water supplies.<sup>19, 20, 22</sup> In this study, monolayers of dioleoyl phosphatidylcholine (DOPC) were used as the biological membrane, and Ag(I)-NHC complexes were tested as potential membrane-active compounds. A correlation between the limit of detection (LoD) values of Ag(I)-NHC complexes obtained from this setup and the IC<sub>50</sub> values obtained from MTT assays, will determine the possible use of this biosensing device as a fast, cheap and easy tool for screening of biologically-active complexes, prior to or instead of widely-known and more costly biological testing.

The biosensor consists of a flow cell with a merged wafer-like device that contains eight mercury coated “on chip” Pt disc working electrodes, a Pt auxiliary electrode and a Ag/AgCl (**Figure 7.2**, also labelled 4 in **Figure 7.1**).<sup>22</sup> This device was attuned to achieve optimum deposition and removal of the phospholipid monolayer and compound-interaction response signals. This was achieved by minimising the dimensions of the Pt/Hg electrodes using rapid cyclic voltammetry to facilitate the deposition of DOPC on the electrode from the DOPC dispersion.<sup>19</sup>

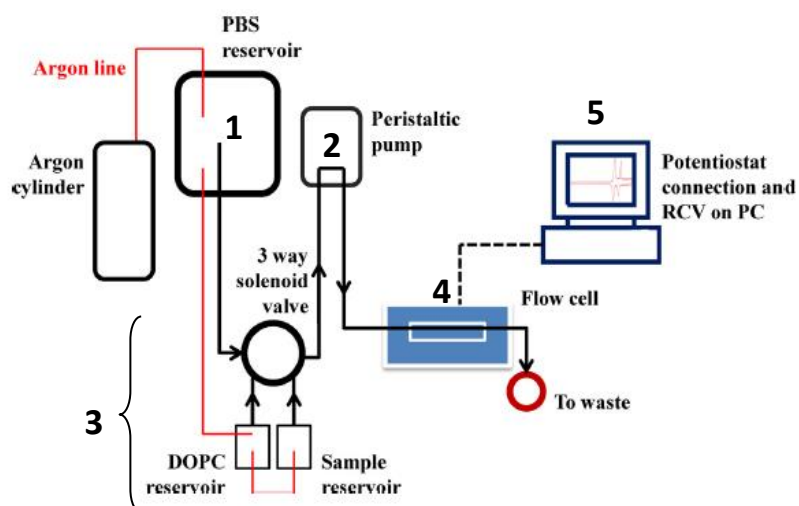
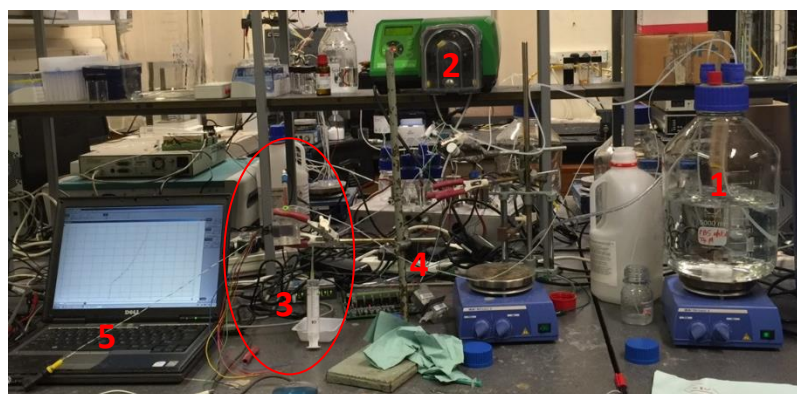


**Figure 7.1:**Diagram of electrochemical screening device<sup>22</sup>

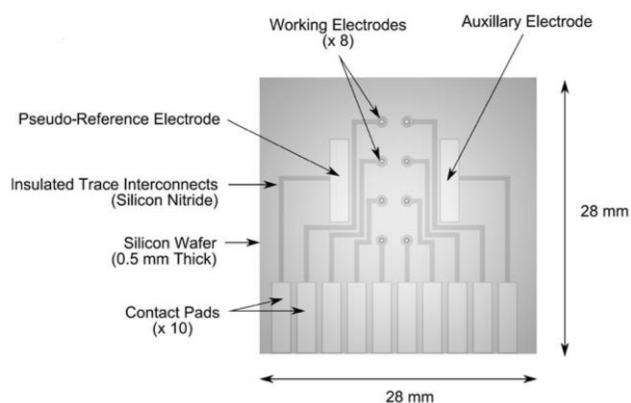


**Figure 7.2:** Diagram of the wafer-like device<sup>19</sup>

The DOPC monolayer undergoes two potential induced phase transitions, translated into two characteristic sharp capacitance current peaks when a potential is applied between -0.2 and -1.8 V (**Figure 7.3 (a)**).<sup>18</sup> The two peaks correspond to the permeation of the layer to ions, and the re-organisation of the layer to form bilayer areas, respectively (**Figure 7.3 (b)**). Direct measurements of structural changes of the DOPC monolayer were later reported using atomic force-distance techniques to illustrate the precise changes in the monolayer structure (**Figure 7.4**).<sup>15</sup> Interaction of a compound/toxin with the layer is detected by changes in the characteristic peak configurations.

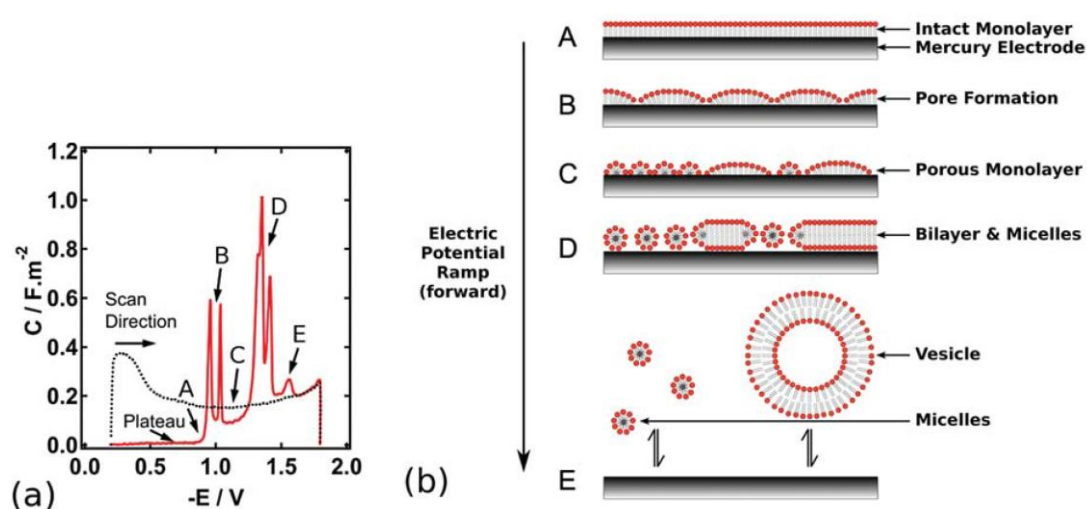


**Figure 7.3:** (a). Typical RCV scan of DOPC monolayer (b). Illustration of predicted phase transitions<sup>18</sup>

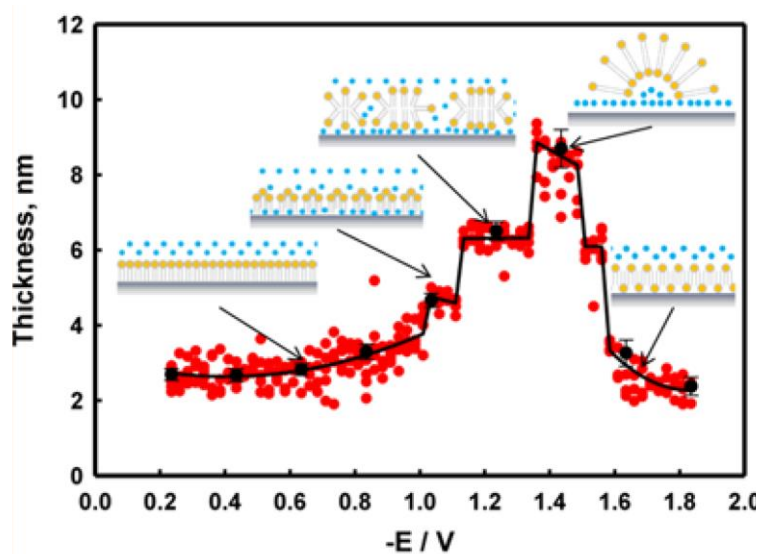


**Figure 7.4:** Phase transitions of DOPC monolayer<sup>15</sup>

## 7.2 Organometallic complexes interactions with DOPC

In this work, Ag(I)-NHC complexes from the xanthine-derived (Chapter 2), clotrimazole-derived (Chapter 4) and water-soluble (Chapter 5) groups were screened on this electrochemical biosensor using DOPC as the biological monolayer. Deposition of dioleoyl phosphatidylcholine (DOPC) on the Pt/Hg is performed before the introduction of a complex, and a potential excursion is applied from -0.4 V to -3.0 V at  $100 \text{ V s}^{-1}$  scan rate. 100-200  $\mu\text{L}$  of DOPC is inserted into the flow cell through the solenoid valve, after which the characteristic RCV peaks corresponding to phase transitions appear. The potential excursion is then changed to -0.4 V to -1.2 V, and the RCV profile of DOPC after repetitive cycling in this range is shown in **Figure 7.5**. Changes to the characteristic RCV peaks when subjected to a particular compound are an indication of the interaction of the compound with the DOPC. Recovery, or failure of recovery, of the characteristic RCV peaks to their normal state after exposure to a compound specifies the extent of permanent membrane damage. Results obtained from this technique are compared to cytotoxicity data from MTT-based assays, to evaluate the ability of the technique in predicting the anticancer activity of organometallic complexes.

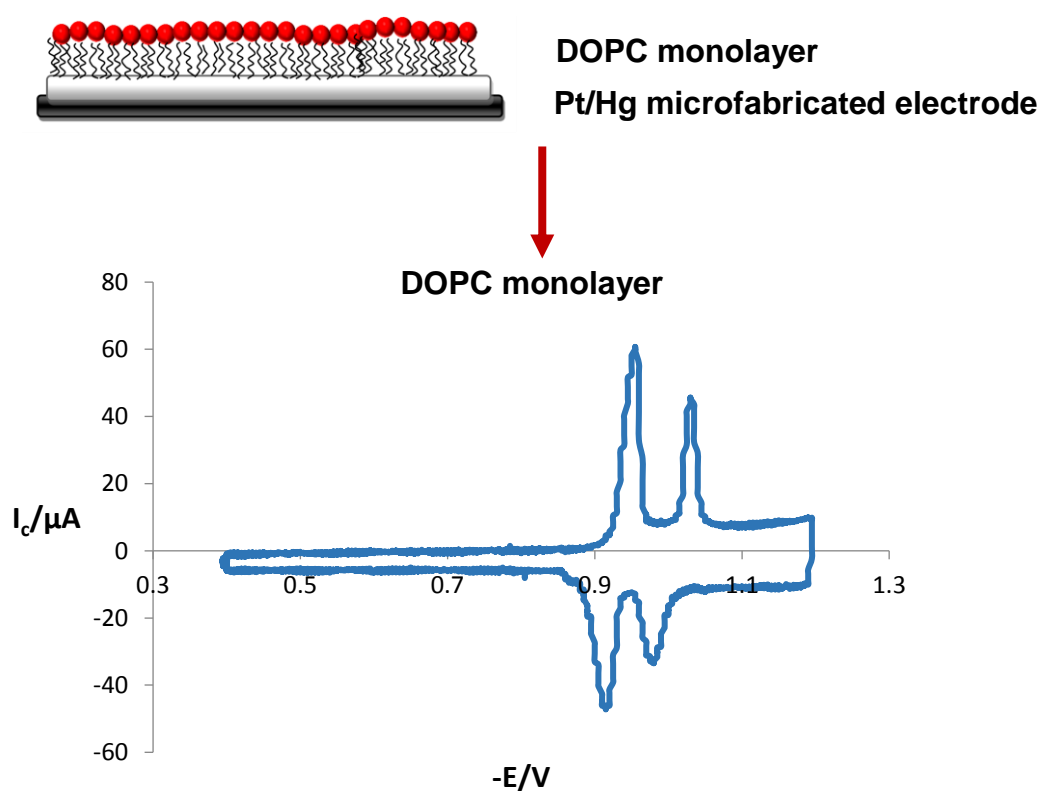


**Figure 7.5:** Characteristic RCV peaks of DOPC at potential range -0.4 V to -1.2V

### 7.2.1 Interaction of Cisplatin with DOPC

Cisplatin was initially screened on the electrochemical biosensor at a concentration of  $10 \mu\text{mol dm}^{-3}$  showing no change in the RCV. Higher concentrations were subsequently tested, gradually increasing from  $10 \mu\text{mol dm}^{-3}$  to  $2 \text{ mmol dm}^{-3}$ . The results show that cisplatin exhibits no effect on DOPC monolayer, indicating no interaction with the membrane is observed including at the highest concentration of  $2 \text{ mmol dm}^{-3}$  (**Figure 7.6**). This result is in agreement with the mechanism of action of cisplatin reported in the literature,<sup>24</sup> in which the drug enters the cell *via* copper transporter Ctr1 as opposed to passive diffusion (**Figure 7.7**).

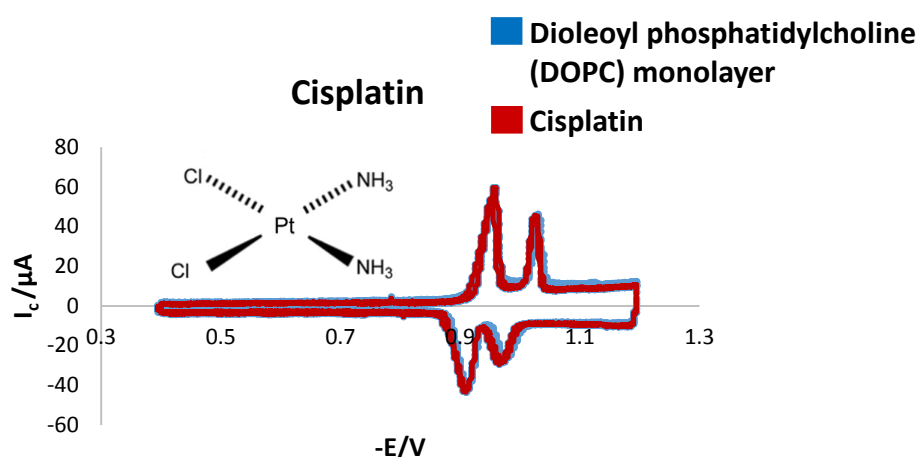


**Figure 7.6:** RCV of cisplatin on DOPC

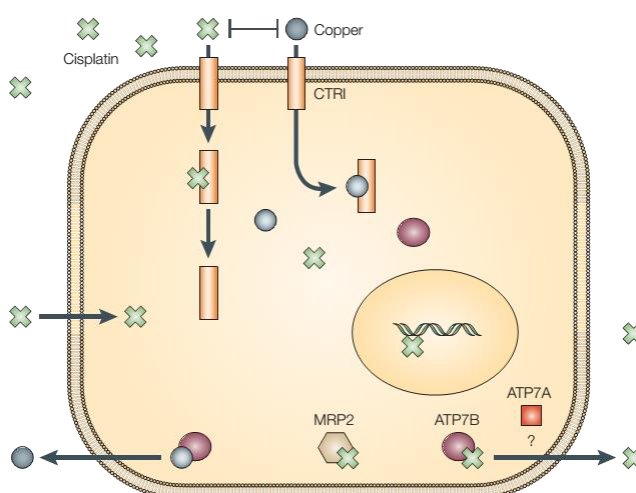


**Figure 7.7:** Route of entrance of cisplatin into a cell by copper transporters<sup>24</sup>

### 7.2.2 Interaction of xanthine-derived silver(I)-NHCs with DOPC

Water soluble xanthine-derived Ag(I)-NHC complex **C5** was screened for its interaction with DOPC, using varying concentrations of the complex. Results display no interaction with DOPC, including at a high concentration of  $2 \text{ mmol dm}^{-3}$  (**Figure 7.8**). We have reported that **C5** exhibits anticancer activity against a range of cell lines, strongly indicating that it is able to cross a cell membrane.<sup>25</sup> The results from the biomembrane-sensing device suggest that cell entrance of **C5** is through an alternative mechanism to passive diffusion, *i.e.* are actively transported *via* channels or transporters across the cell wall. **C1**, **C2**, **C3** and **C4** were also screened, and similar to **C5**, displayed no interaction with DOPC. Results indicate that xanthine-derived complexes generally have an alternative active-transport method to cross cell membranes. This mechanism may be similar to that reported for caffeine and its metabolites.<sup>1-4, 26</sup>

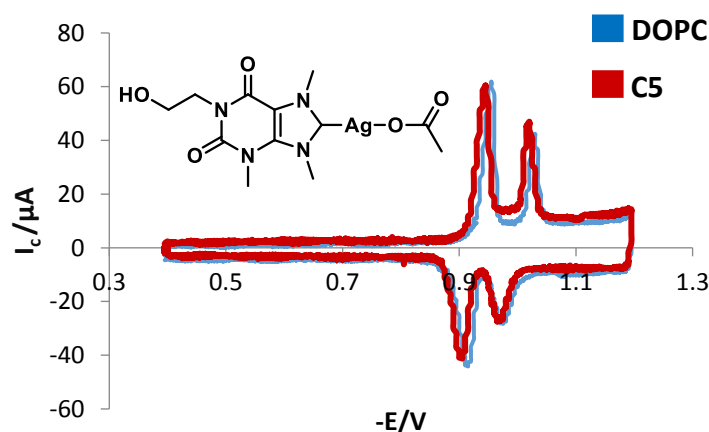


**Figure 7.8:** Interaction of **C5** with DOPC

### 7.2.3 Interaction of water-soluble silver(I)-NHCs with DOPC

Water-soluble Ag(I)-bis(NHC) complexes **C19**, **C20** and **C22-C33** (Chapter 5) were screened at a concentration of 50  $\mu\text{mol dm}^{-3}$  against DOPC. The RCVs of the complexes displayed no interaction with DOPC, with the exception of **C24**, **C27** and **C33** (Figure 7.9). The three complexes displayed varying degrees of interaction with DOPC, with **C27** exhibiting the strongest interaction. **C27** and **C33** both contain an anthracene N-substituent, increasing the aromaticity of the complex, to which the interaction with DOPC may be attributed.<sup>22</sup> The N-hydroxyethyl substituent in **C27** is replaced by a N-carboxylic acid substituent in **C33**, indicating that the N-alcohol substituent improves the interaction with DOPC when combined with an aromatic group. The ability of **C24** to interact with DOPC may be attributed to having both the aromaticity of the N-mesityl substituent and the N-alcohol substituent. A relation between Log *P* values and DOPC interaction may be made as **C24**, **C27** and **C33** are in the highest four most hydrophobic complexes in this group. This suggests that increased hydrophobicity increases binding to the DOPC monolayer. The inability of **C19**, **C20**, **C22**, **C23** and **C25-C32** to interact with DOPC, regardless of their positive Log *P* values, and the presence of aromatic benzyl rings in complexes **C23** and **C31**, suggests that benzyl N-substituents as the aromatic components are not sufficient to enable binding to the monolayer. A correlation between membrane activity and cytotoxicity was not found for this group of complexes. However, the biomembrane sensing results for complexes **C19**, **C20**, **C22**, **C23** and **C25-C31** which show no interaction with DOPC, but show potential anticancer activity, indicates that active transport may be a route for cell entry. For complexes **C24**, **C27** and **C33** which exhibited both membrane interaction and anticancer activity, a combination of passive diffusion and active transport may together be routes to cross the membranes (Table 7.1).

**Table 7.1:** Summary of potential routes for cell entry for water-soluble Ag(I)-NHC complexes

|                                    | DOPC interaction | Cell Entry                           |
|------------------------------------|------------------|--------------------------------------|
| <b>C19, C20, C22, C23, C25-C32</b> | No               | Active transport                     |
| <b>C24, C27, C33</b>               | Yes              | Passive diffusion + Active transport |

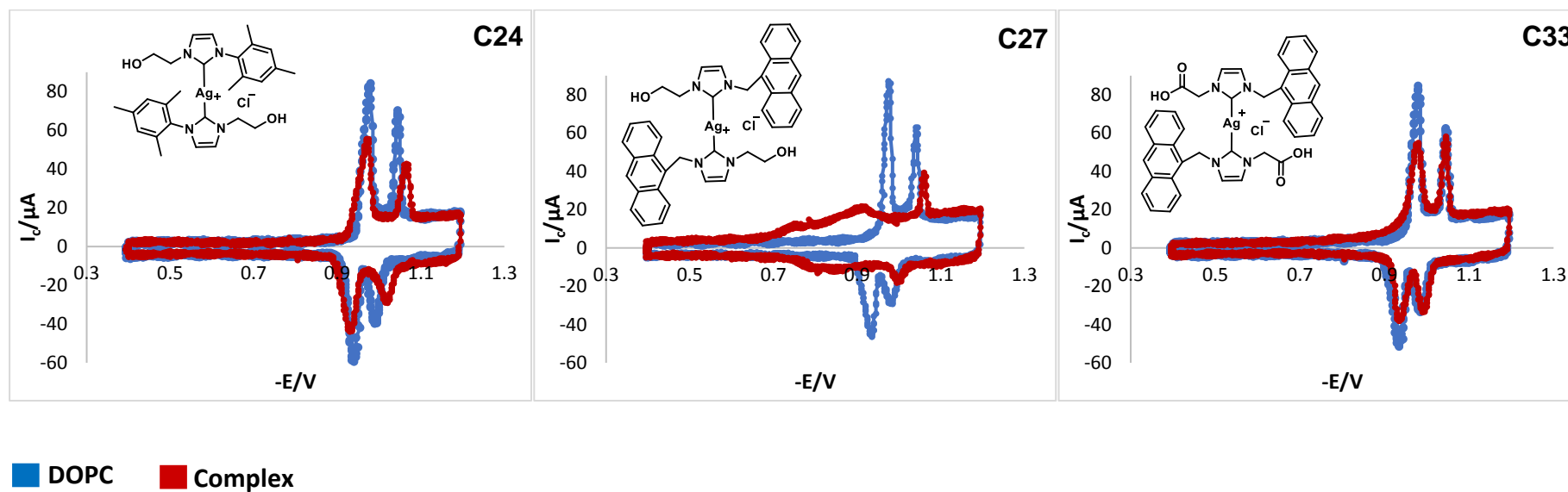
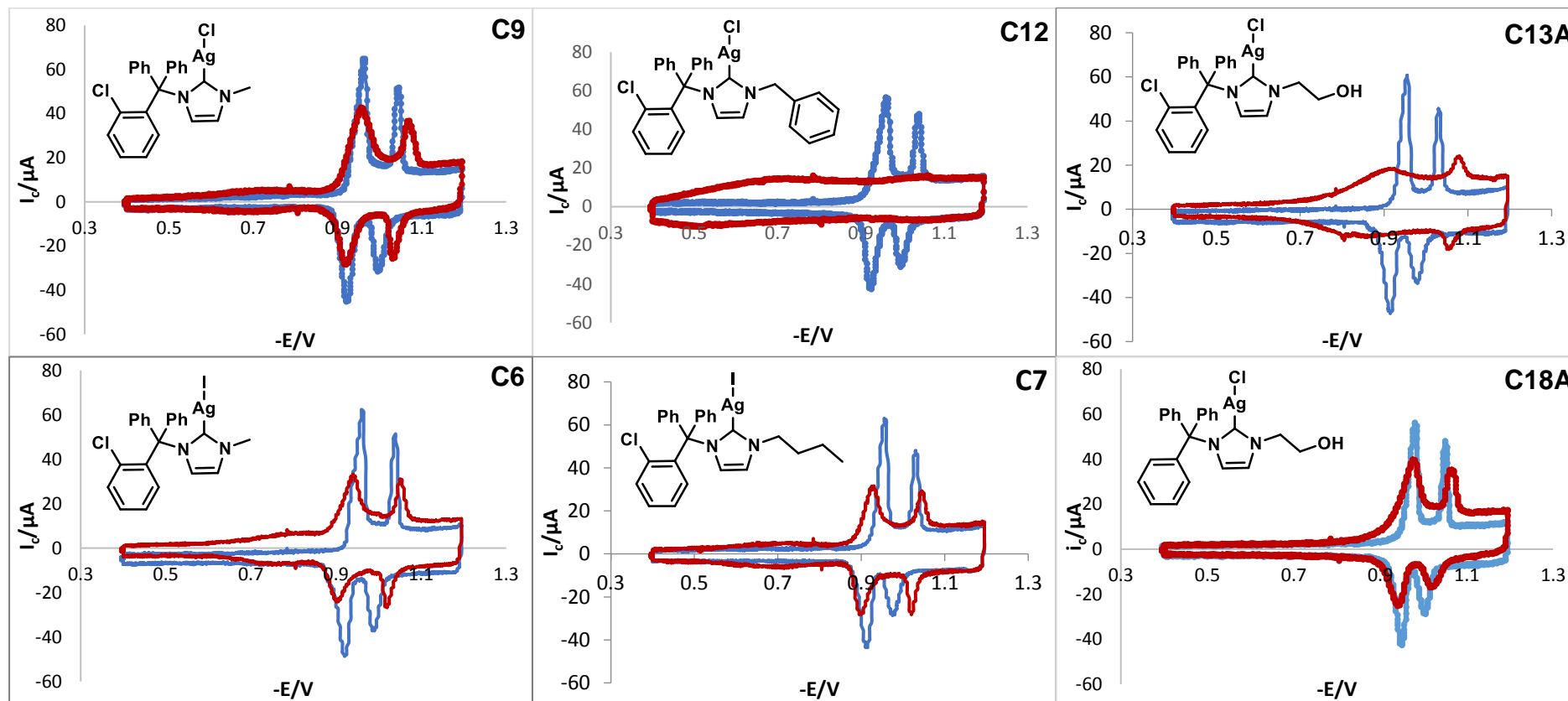


**Figure 7.9:** RCVs showing interactions of water-soluble Ag(I)-NHC complexes with DOPC **C24**, **C27** and **C33**

#### 7.2.4 Interaction of clotrimazole-derived silver(I)-NHCs with DOPC

Clotrimazole-derived complexes are the most promising group of Ag(I)-NHC complexes as potential anticancer agents in this work (Chapter 4). A correlation between Log *P* values and cytotoxicity of these complexes has been observed. Ten complexes in this group of varying cytotoxicity, N-substituents and counterions were screened on the biomembrane sensor at a concentration of 50  $\mu\text{mol dm}^{-3}$  (**Figure 7.10**). The RCVs show that these complexes have varying degrees of interaction with DOPC according to their structural features. The ability of these complexes to interact with DOPC suggests that passive diffusion is most likely the main route of cell entry for this class of complexes, which is mainly attributed to their bulky aromatic triphenyl N-substituents.

**C13A** interacts strongly with DOPC, and substituting the Cl on the triphenyl group with H in **C18A**, results in a decrease in interaction. This indicates that Cl has an important role in membrane binding. Substituting the alcohol N-substituent in **C13A** for a benzyl group in **C12** leads to an increase in interaction, suggesting that the aromaticity of the benzyl group when added to the aromaticity of the triphenyl group potentiates its effect in membrane interaction. A change of counterion from Cl in **C13B** to I in **C8** slightly increases the interaction with the DOPC monolayer. Changing the alcohol N-substituent in **C13A** for a methyl group in **C9** noticeably decreases the interaction with the membrane. This suggests that the alcohol group has an effect in maintaining a strong interaction with DOPC, with hydrophobicity measurements showing that this complex has intermediate lipophilicity, which is ideal for optimum anticancer activity.



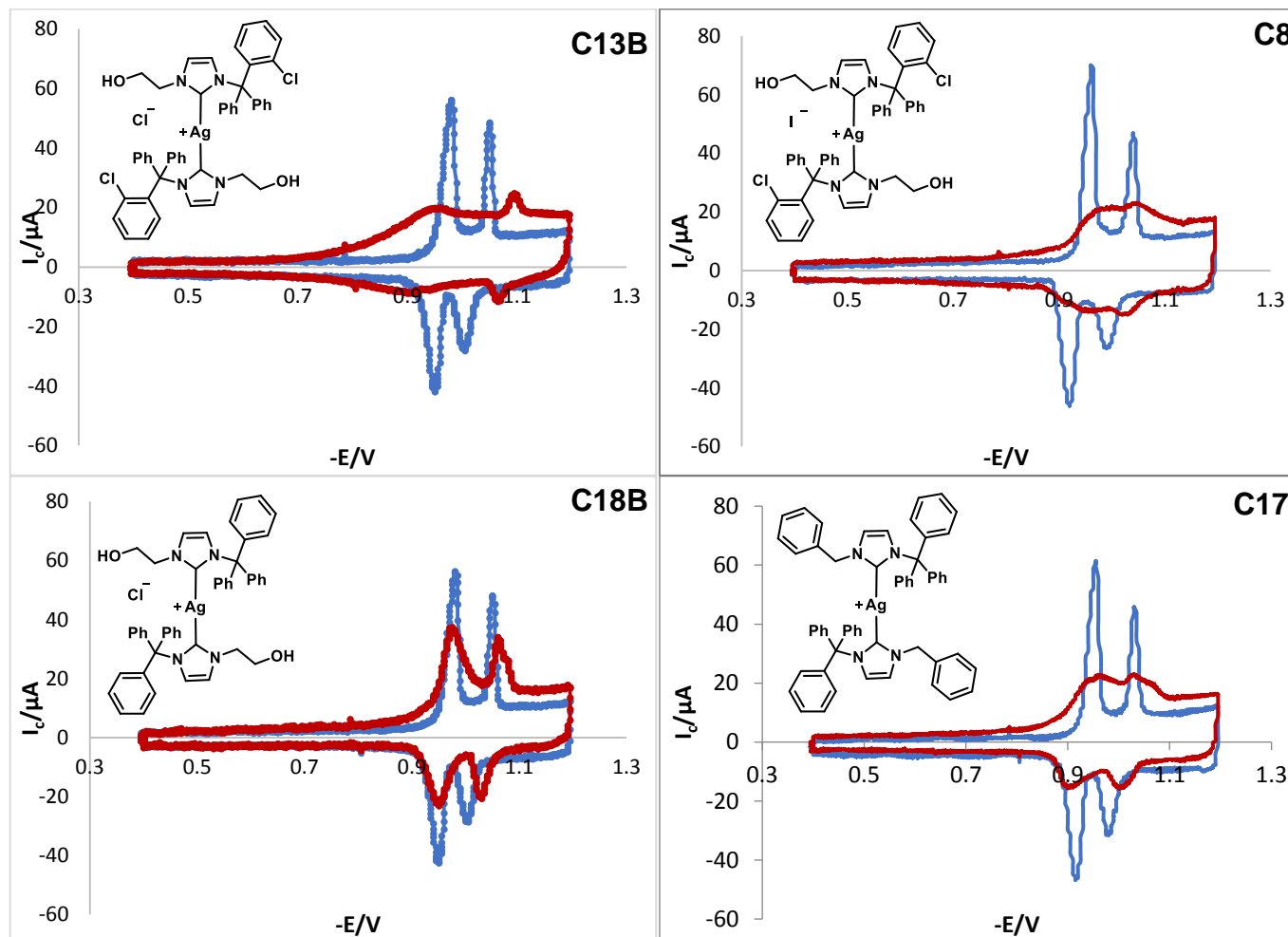


Figure 7.10: Interaction of clotrimazole-derived complexes with DOPC

### 7.3 Limit of detection (LoD)

The limit of detection (LoD) of seven clotrimazole-derived complexes was calculated. LoD is the lowest concentration of the complex that is detectable by the biosensor, which produces a recognisable comparison to the control measurement. This is measured by extrapolating the average capacitance current ( $i_c$ ) of ten control measurements of DOPC from a calibration curve (capacitance current versus concentration of the complex, example shown in **Figure 7.11**), of which the standard deviation (SD) is also calculated. The effect relating to three times the SD of the control was read from the calibration curve to estimate the detection limit values. The results show that **C13B** has the lowest LoD value, therefore it is considered the most membrane active complex (**Table 7.2**). **C13B** also shows the most promising cytotoxicity and selectivity results with an  $IC_{50}$  value against Panc 10.05, lower than that obtained for cisplatin. This result implies that it may be possible to use the electrochemical biosensing device as a forecasting tool, to determine the most promising anticancer complex within a particular class.

**Table 7.2:** Limit of detection (LoD) values

| Complex | LoD ( $\mu\text{M}$ ) |
|---------|-----------------------|
| C13B    | 0.002                 |
| C18B    | 0.0125                |
| C8      | 0.035                 |
| C17     | 0.3                   |
| C12     | 0.15                  |
| C6      | 0.05                  |
| C7      | 0.02                  |

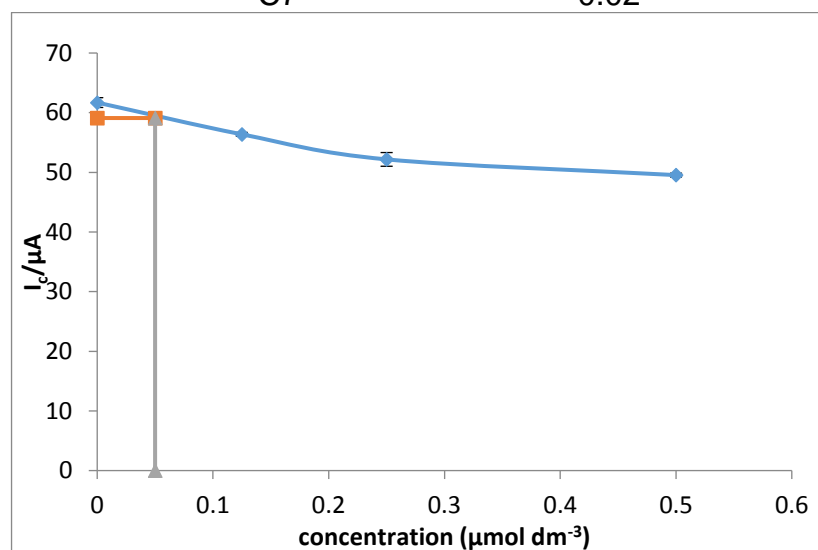


**Figure 7.11:** Calibration curve for **C8** used to determine LoD

### 7.4 Interaction of imidazolium salts with DOPC

The role of the carbene moiety in the anticancer activity of Ag(I)-NHC complexes is unknown. They may be involved in damaging the cancerous cells, acting as 'carriers' that transport silver ions into the cells. Screening imidazolium salts against DOPC may help in understanding the ability of these compounds to bind to cell membranes. Six clotrimazole-derived imidazolium salts were screened at  $50 \mu\text{mol dm}^{-3}$  (**Figure 7.12**), with the results showing strong interactions with the monolayer, similar to those observed for the clotrimazole-derived silver complexes. Changes to N-substituents, counterions and Cl on the triphenyl N-substituent result in the same changes in DOPC interactions as those observed for the silver complexes. These include increase in membrane interaction upon either addition of a Cl on the triphenyl group, an N-benzyl or N-alcohol-substituent and/or changing the counterion ion to I. This suggests that the carbene moiety in the Ag(I)-NHCs is responsible for membrane binding.

Screening clotrimazole-derived Ag(I)-NHC on DOPC membrane resulted in an irreversible change i.e. the membrane did not revert back to its original state as the compound is flushed out. Interestingly, the change following exposure to imidazolium salts was found to be reversible. This suggest that of silver damages the DOPC monolayer, and may translate into its ability to damage cancerous cell membranes *in vivo*. The fact that the DOPC membrane recovers following exposure to imidazolium salts indicates that the carbene acts as a carrier for the drug across the cell membrane.

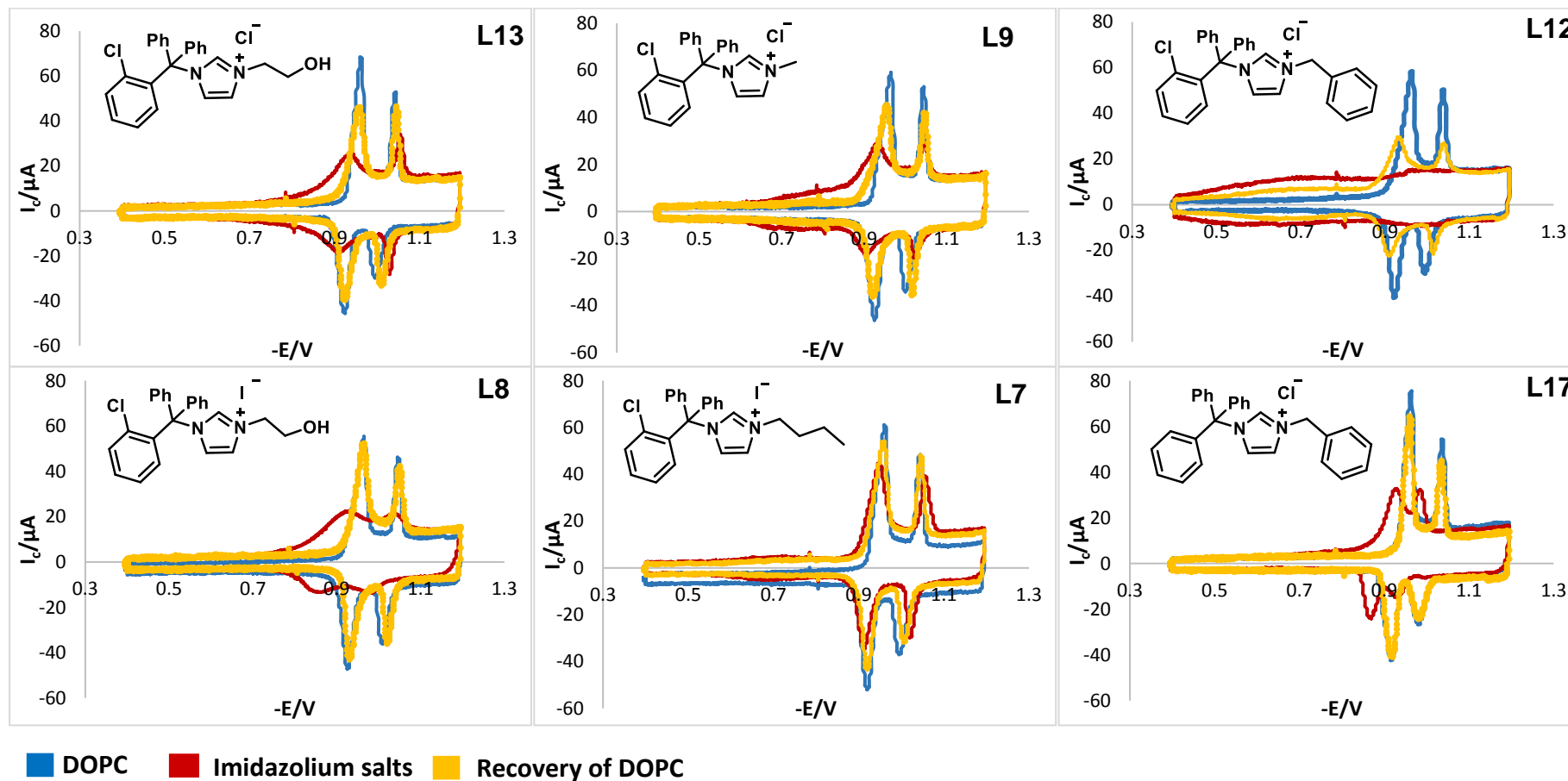
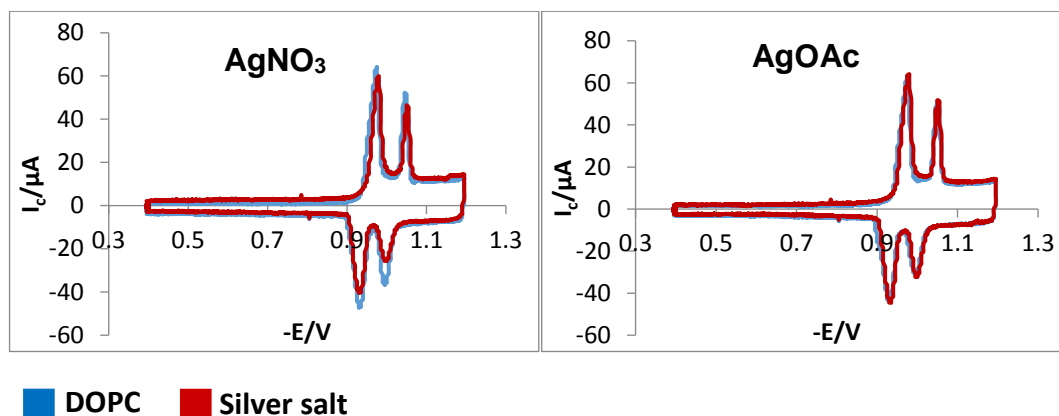


Figure 7.12: Interaction of clotrimazole-derived imidazolium salts with DOPC

### 7.5 Interaction of silver salts with DOPC

Silver salts  $\text{AgNO}_3$  and  $\text{AgOAc}$  were screened at increasing concentrations to  $2\text{mmol dm}^{-3}$ , showing no effect on DOPC (**Figure 7.13**). This shows the necessity of the carbene for membrane interaction, and supports the suggestion that the carbene carries the silver ions to the cell membrane (**Table 7.3**).



**Figure 7.13:** Interactions of silver salts with DOPC

**Table 7.3:** Summary of DOPC recovery

|  | DOPC interaction | DOPC recovery |
|--|------------------|---------------|
| Clotrimazole-derived Ag(I)-NHC complexes | Yes              | No            |
| Clotrimazole-derived Imidazolium salts   | Yes              | Yes           |
| Silver salts                             | No               | N/A           |

## 7.6 Conclusions

A unique electrochemical biosensing device developed by Nelson *et al.* was used to monitor the effects of cisplatin, Ag(I)-NHC complexes, imidazolium salts and silver salts on a phospholipid monolayer (DOPC). The measured interactions with DOPC can help predict how each complex/salt might behave when it comes into contact with a cell membrane *in vivo*. Comparison of DOPC interactions and IC<sub>50</sub> values revealed the potential application of this technique as a pre-screening device for anticancer complexes. DOPC-interaction potentially translates into passive diffusion across cell membranes *in vivo*, and since cisplatin actively enters cells *via* copper transporters, no interaction was observed with DOPC at high concentrations. Xanthine-derived complexes also revealed no DOPC-interaction, with these complexes having exhibited anticancer activity against eight cancerous lines, suggesting 'active transport' *via* a channel or transporter as the mechanism of cell entry. Screening of water-soluble complexes generally displayed no effect on DOPC, with the exception of N-anthracene or N-mesityl substituted complexes. This highlights the importance of N-bulky aromatics in membrane interactions and possibly a combination of passive diffusion and active transport is possible.

Clotrimazole-derived complexes exhibited strong DOPC interactions, indicating that the main route of cell entry for this group of complexes is *via* passive diffusion. Changes in N-substituents affected the degree of interaction, where an N-benzyl substituent increases the interaction with DOPC, followed by the N-alcohol substituent, which appears more effective than N-alkyl substituents in membrane interaction. Changes in halide counterions had a minor effect on DOPC interaction, however replacing the Cl on the N-triphenyl substituent with H decreased DOPC interaction. Determination of the limit of detection (LoD) revealed that complex **C13B**, which displayed the lowest IC<sub>50</sub> value, also had the lowest LoD value. Further development is required for this device as a prescreening tool for anticancer activity, with these preliminary findings providing significant promise. Since the imidazolium salts screened revealed strong DOPC interactions similar to those of the analogous Ag(I)-NHC complexes, suggests that the carbene moiety is responsible for the membrane-interactions of the complexes. This further implies that Ag(I) is responsible for damaging the membrane, which is supported by the inability of the DOPC to recover after exposure to Ag(I)-NHC complexes. The hypothesis is that silver ions are responsible for the anticancer activity of the complexes, since they irreversibly damage the cell membrane, while carbene moiety carries them to the cell, and binds to the cell membrane (**Table 7.4**).

**Table 7.4:** Conclusions from membrane biosensing technique

|   | <b>DOPC<br/>interaction</b> | <b>Suggested<br/>Cell Entry</b>              | <b>DOPC<br/>recovery</b> |
|---|-----------------------------|--|--------------------------|
| <b>Cisplatin</b>                                  | No                          | Copper transporters                          | -                        |
| <b>Xanthine-derived<br/>Ag(I)-NHC</b>             | No                          | Active transport                             | -                        |
| <b>Water-soluble<br/>Ag(I)-NHC</b>                | No                          | Active transport                             | -                        |
| <b>Clotrimazole-derived<br/>Ag(I)-NHC</b>         | Yes                         | Passive diffusion                            | No                       |
| <b>Clotrimazole-derived<br/>Imidazolium salts</b> | Yes                         | Passive diffusion                            | Yes                      |
| <b>Ag salts</b>                                   | No                          | Imidazolium<br>NHC salts<br>(carbene moiety) | -                        |

## 7.7 References

1. J. Wang, *Biosensors & Bioelectronics*, 2006, **21**, 1887-1892.
2. N. J. Ronkainen, H. B. Halsall and W. R. Heineman, *Chemical Society Reviews*, 2010, **39**, 1747-1763.
3. J. D. Newman and A. P. F. Turner, *Biosensors & Bioelectronics*, 2005, **20**, 2435-2453.
4. D. Grieshaber, R. MacKenzie, J. Voeroes and E. Reimhult, *Sensors*, 2008, **8**, 1400-1458.
5. J. Wang, *Analytical Chemistry*, 1995, **67**, 487-492.
6. I. Karube and E. Tamiya, *Food Biotechnology (New York)*, 1987, **1**, 147-166.
7. M. Mascini, F. Mazzei, D. Moscone, G. Calabrese and M. M. Benedetti, *Clinical chemistry*, 1987, **33**, 591-593.
8. J. F. Rusling, C. V. Kumar, J. S. Gutkind and V. Patel, *Analyst*, 2010, **135**, 2496-2511.
9. M. Seydack, *Biosensors & Bioelectronics*, 2005, **20**, 2454-2469.
10. K. Graumann and A. Premstaller, *Biotechnology journal*, 2006, **1**, 164-186.
11. S. A. Kellermann and L. L. Green, *Current opinion in biotechnology*, 2002, **13**, 593-597.
12. S. Takenaka, K. Yamashita, M. Takagi, Y. Uto and H. Kondo, *Analytical Chemistry*, 2000, **72**, 1334-1341.
13. A. D. Ellington and J. W. Szostak, *Nature*, 1990, **346**, 818-822.
14. N. Matsuno, M. Murawsky, J. Ridgeway and J. Cuppoletti, *Biochimica et Biophysica Acta (BBA) - Biomembranes*, 2004, **1665**, 184-190.
15. A. Vakurov, M. Galluzzi, A. Podesta, N. Gamper, A. L. Nelson and S. D. A. Connell, *Acs Nano*, 2014, **8**, 3242-3250.
16. A. Vakurov, R. Brydson and A. Nelson, *Langmuir*, 2012, **28**, 1246-1255.
17. D. Bizzotto and A. Nelson, *Langmuir*, 1998, **14**, 6269-6273.
18. A. V. Brukhno, A. Akinshina, Z. Coldrick, A. Nelson and S. Auer, *Soft Matter*, 2011, **7**, 1006-1017.
19. Z. Coldrick, A. Penezić, B. Gašparović, P. Steenson, J. Merrifield and A. Nelson, *J Appl Electrochem*, 2011, **41**, 939-949.
20. Z. Coldrick, P. Steenson, P. Millner, M. Davies and A. Nelson, *Electrochimica Acta*, 2009, **54**, 4954-4962.
21. A. Nelson, *Journal of Electroanalytical Chemistry*, 2007, **601**, 83-93.
22. S. Mohamadi, D. J. Tate, A. Vakurov and A. Nelson, *Analytica Chimica Acta*, 2014, **813**, 83-89.
23. A. Nelson, *Current Opinion in Colloid & Interface Science*, 2010, **15**, 455-466.
24. D. Wang and S. J. Lippard, *Nat Rev Drug Discov*, 2005, **4**, 307-320.
25. H. A. Mohamed, B. R. M. Lake, T. Laing, R. M. Phillips and C. E. Willans, *Dalton transactions*, 2015, **44**, 7563-7569.
26. W. Streciwilk, F. Hackenberg, H. Muller-Bunz and M. Tacke, *Polyhedron*, 2014, **80**, 3-9.

## Chapter 8 Experimental

### 8.1 Methods and Instrumentation

#### 8.1.1 General

All reagents were prepared as outlined or used as supplied without need for further purification. Compounds previously reported were prepared according to literature procedure and fully characterised using NMR spectroscopy and mass spectrometry unless otherwise stated. Manipulations were performed using standard Schlenk line and Glovebox techniques. Argon and nitrogen were passed through a twin-column drying apparatus containing molecular sieves (4Å) and phosphorus pentoxide. Anhydrous solvents were passed over activated alumina to remove water, copper catalyst to remove oxygen and molecular sieves to remove any remaining water *via* the Dow-Grubbs solvent system.

#### 8.1.2 NMR spectroscopy

$^1\text{H}$  and  $^{13}\text{C}\{^1\text{H}\}$  NMR spectra were recorded on either a Bruker DPX300 spectrometer (operating frequency 300.1 MHz for  $^1\text{H}$  and 75.48 MHz for  $^{13}\text{C}\{^1\text{H}\}$ ), a Bruker Avance 500 spectrometer or a Bruker DRX500 spectrometer (both with an operating frequency of 500.13 MHz for  $^1\text{H}$  and 125.80 MHz for  $^{13}\text{C}\{^1\text{H}\}$ ). All spectra were recorded at 298K (unless otherwise stated) in deuterated solvent. Chemical shift values are quoted in parts per million (ppm,  $\delta$ ), coupling constants,  $J$ , are quoted in Hertz (Hz) and assignment of  $^{13}\text{C}\{^1\text{H}\}$  NMR spectra was aided by  $^{13}\text{C}\{^1\text{H}\}$  DEPT135 experiments when necessary.

#### 8.1.3 Mass spectrometry

High-resolution mass spectra were collected on a Bruker Daltonics (micro TOF) instrument operating in the positive ion electrospray mode. Samples were injected directly from feed solutions and acquired over the range  $m/z$  50 – 4000. All spectra were recorded using an acetonitrile/water mix as the eluent and a sodium formate solution as a calibrant.

#### 8.1.4 Microanalysis

Microanalyses were performed in the School of Chemistry, University of Leeds by Ms. Tanya Marinko-Covell using a Carlo Erba Elemental Analyser MOD 1106 spectrometer.

### 8.1.5 X-Ray crystallography

X-ray diffraction data were collected on an Agilent SuperNova diffractometer fitted with an Atlas CCD detector with Mo-K $\alpha$  radiation ( $\lambda = 0.71073 \text{ \AA}$ ) or Cu-K $\alpha$  radiation ( $\lambda = 1.54184 \text{ \AA}$ ). Crystals were mounted under Fomblin on nylon loops. Crystals were held at either 120 or 100 K using an Oxford Cryosystem low temperature device during unit cell determination and data collection. Data sets were corrected for absorption effects using a multiscan method, and the structures were solved either by direct methods using SHELXS-97 or charge flipping (Superflip) interfaced through the program Olex2. Refinement was by full-matrix least squares on F2 using ShelXL-97, interfaced through either the program X-Seed or Olex2. All hydrogen atoms were included at geometrically estimated positions using a riding model unless otherwise stated. Graphics of the crystal structures outlined in this report were generated using X-seed.

### 8.1.6 Hydrophobicity studies

Equal volumes of octanol and NaCl-saturated water were stirred at room temperature for 24 hours, and separated to give octanol-saturated water and water-saturated octanol. Five standard concentrations (5, 10, 20, 40 and 60  $\mu\text{M}$ ) of the complexes were prepared from the octanol-saturated water. Analysis by UV / vis spectroscopy was used to obtain a calibration curve of absorbance versus concentration for each complex at its maximum absorbance. Accurate amounts of the complexes were dissolved in the octanol-saturated water (25 mL) to make up a concentration of 50  $\mu\text{M}$ . 3 mL of octanol-saturated water containing the complex was placed in a centrifuge tube and 3 mL of water-saturated octanol was layered on top. Six samples prepared in this manner were shaken for 4 hours using a vibrax machine at 500  $\text{gmin}^{-1}$ . The layers were separated and the octanol-saturated water layer was retained for analysis using UV / vis spectroscopy. The average concentration of the six runs was calculated using the calibration graph and maximum absorbance for each complex. Subtraction of the average concentration obtained from the concentration of an unshaken sample in octanol-saturated water gave the final [C]<sub>org</sub>. The [C]<sub>org</sub> and [C]<sub>aq</sub> were used to determine the partition coefficient Log *P*. Studies for complexes that are more soluble in water-saturated octanol layer were performed in that layer.

### 8.1.7 Cytotoxicity studies

#### MTT-assay

*In vitro* cell tests for all compounds were performed at the Department of Pharmacy, University of Huddersfield. Cells were incubated in 96-well plates, at  $2 \times 10^3$  cells per well in 200  $\mu\text{L}$  of growth media (RPMI 1640 supplemented with 10 % foetal calf serum, sodium pyruvate (1mM) and L-glutamine (2mM)). Cells were incubated for 24 hours at 37 °C in an atmosphere of 5 %  $\text{CO}_2$  prior to drug exposure. Silver compounds, imidazolium salts and cisplatin were dissolved in dimethylsulfoxide at a concentration of 25 mM and diluted with medium to obtain drug solutions ranging from 25  $\mu\text{M}$  to 0.049  $\mu\text{M}$ . The final dimethylsulfoxide concentration was 0.1% (v/v) which is non-toxic to cells. Drug solutions were applied to cells and incubated for 96 hours at 37 °C in an atmosphere of 5 %  $\text{CO}_2$ . The solutions were removed from the wells and fresh medium added to each well along with 20  $\mu\text{L}$  MTT (5 mg/ml), and incubated for 4 hours at 37 °C in an atmosphere of 5 %  $\text{CO}_2$ . The solutions were removed and 150  $\mu\text{L}$  dimethylsulfoxide was added to each well to dissolve the purple formazan crystals. A plate reader was used to measure the absorbance at 540 nm. Lanes containing medium only, and cells in medium only (no drug), were used as blanks for the spectrophotometer and 100 % cell survival respectively. Cell survival was determined as the absorbance of treated cells divided by the absorbance of controls and expressed as a percentage. The concentration required to kill 50 % of cells ( $\text{IC}_{50}$ ) was determined from plots of percent survival against drug concentration. Each experiment was repeated 3 times and a mean value obtained.

#### SRB-assay

*In vitro* cell tests for Cu(I)-NHC and Ru(II)-NHC complexes were performed at the Institute of Pharmacy and Molecular Biotechnology, University of Heidelberg, following a literature procedure.<sup>1</sup> Cells were seeded in 100  $\mu\text{L}$  aliquots into 96-well plates with a density of 5,000 cells/well, and incubated overnight. Different concentrations of complexes or respective amounts of DMF were added to the cells after incubation, which were further incubated for different time periods. Following treatment, 50  $\mu\text{L}$  of ice cold 10 % trichloroacetic acid (TCA) in  $\text{H}_2\text{O}$  were added to each well, and the plates were kept at 0 °C for 1 h. Subsequently, the solution in the plates was discarded, and the plates were washed twice with  $\text{H}_2\text{O}$  and dried. 100  $\mu\text{L}$  of 1% acetic acid solution containing 0.054 % of sulforhodamine B sodium salt (SRB) were then added. The solution was discarded 30 min later, and the plates were washed

twice with 200  $\mu\text{L}$  of acetic acid (1 %) into each well. The washing solution of acetic acid was quickly discarded after washing. The plates were further dried followed by adding 200  $\mu\text{L}$  of 10 mM Tris (pH 10.5) to each well to dissolve the SRB dye. The plates were shaken for 15 min, after which time the dye was quantified with a plate reader by determining the absorption at 535 nm. The  $\text{IC}_{50}$  values were calculated as the concentrations of the compounds required to inhibit 50 % of cell growth.

### **8.1.8 Infra-red spectroscopy**

FTIR spectra were recorded using a Spectrum One spectrophotometer (PerkinElmer) fitted with diffuse reflectance probe with zinc-selenide window. IR Spectra were recorded using a globular light source through KBr beamsplitter for the range 4000-400  $\text{cm}^{-1}$  using DLATGS detector with KBr window. 32 scans were recorded for each averaged spectrum with a new background recorded after each sample. IR spectra were analysed using the spectroscopy software package *OPUS* (v 6.5, Bruker Optiks GmbH).

### **8.1.9 Dynamic Light Scattering (DLS)**

Particle size and particle size distribution analyses were obtained by performing Dynamic Light Scattering (DLS) with three repeats of each sample using a Zetasizer Nano ZS series instrument at 37°C, using disposable polystyrene cuvettes.

### **8.1.10 Scanning Electron Microscopy (SEM)**

Scanning Electron Microscopy (SEM) experiments were performed using a Pasteur pipette to extract a drop of the solution and deposit it onto an SEM glass cover slip. The sample was allowed to dry in a fume cupboard, after which the cover slip was mounted on an SEM stub using conductive tape. The SEM stub containing the dried sample was sputter-coated with a thin layer of gold using a current of 20 mA for 2 minutes, in a quorum Q150RS sputter-coater. The coated samples were analysed for particle size and morphology using a JOEL JSM-6610LV microscope (Oxford Instruments) equipped with a field emission electron gun as an electron source, using a working distance of 11 mm. Accelerated voltage was applied between 5 and 15 kV.

### 8.1.11 Confocal Fluorescence Microscopy

Fluorescence imaging of was performed using a confocal microscope Zeiss LSM880 inverted with Airyscan microscope that consists of Axio Observer.Z1, Nano Focusing Piezo Stage and ZImulti S1 incubator box. The images were taken at 63 x objective. Lasers include diode 405nm, Argon 458, 488, 514 nm, DPSS 561 nm and HeNe 633 nm. Excitation was performed with 405 nm laser and detection was in the range 370-500 nm.

### 8.1.12 Biomembrane sensing device

The microfabricated Pt/Hg electrode coated with DOPC lipid was contained in a closed flow cell. A constant flow of pH 7.4 PBS was passed over the electrode using a peristaltic pump. The flow cell was connected to a potentiostat interfaced to a Powerlab signal generator and controlled by Scope(c) software. RCVs were obtained by applying a saw-tooth waveform from -0.4 to -1.2 V (vs Ag/AgCl) with ramp rate 40 Vs<sup>-1</sup> applied to the electrode surface. In the absence of faradaic reactions, the current on the RCV plot was directly proportional to the capacitance of the surface and is displayed as a function of voltage. In response to the applied voltage ramp, the DOPC monolayers undergo two pronounced phase transitions characterised by two capacitance current peaks. These peaks correspond to the redistribution of charges and polar groups on the monolayer interface. All assays were carried out in 0.1 mol dm<sup>-3</sup> PBS. The compounds are sampled for 400 seconds after which PBS is flushed through for 400 seconds to allow for any recovery of the DOPC layer initial structure to take place.

### 8.1.13 RCV scans

Increasing the concentration of the compounds in test media increases the response following compound interaction with the DOPC layer. This is shown as enhanced peak suppression. The effect of compound dose on the RCV plot emphasises the effect of compound type on the nature of and sensitivity of interaction with the DOPC coated electrode. When the DOPC coated electrode is exposed to a finite concentration of test compound without silver in PBS and then flushed for 400 seconds with control PBS, the RCV scan of the lipid layer shows a full or partial recovery. The degree of RCV scan recovery is related to the degree of DOPC structure restoration which in turn is related to the degree of reversibility of the interaction.

#### 8.1.14 Limit of Detection (LoD)

LoD is the minimum concentration of the compound in PBS which has a statistically significant effect on the properties of the monolayer. This is measured by plotting a calibration graph of capacitance current peak height versus compound solution concentration following interaction with the respective compound. Subsequently the reproducibility of the capacitance current peak height from the RCVs of the DOPC coated Hg electrode in PBS was estimated by taking ten replicate measurements. The three times standard deviation (SD) of this capacitance peak height was calculated as a control. Accordingly the concentration of test compound which has an equivalent suppressive effect on the capacitance current peak height relating to three times the SD of the control was obtained from the calibration curve to estimate the detection limit values. The detection limits are estimated and quoted as the minimum concentration of compound in water to elicit a response. The LoD is the minimum concentration of the compound in PBS which has a statistically significant effect on the properties of the monolayer and is inversely proportional to the affinity of the compound for the layer.

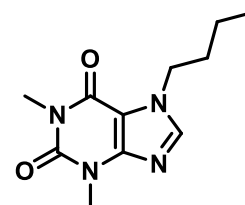
#### 8.1.15 Electrochemical synthesis

The ligand (**L1-L3**) was added to a flame-dried three-necked round-bottomed flask with a magnetic stirrer bar. The solid was further dried under high vacuum for 1 hour, followed by the addition of anhydrous/degassed MeCN (30 mL) was added to the flask. Two copper foils (99.98 % purity, 14 × 11 × 0.025 mm) were connected to an external power supply (positive and negative terminals), introduced to the solution and a potential range applied (25 – 27 V) to maintain a constant current of 30 mA (measured by an in-series ammeter) for 80 minutes. Solid that had precipitated out of solution was filtered and dried *in vacuo* and further recrystallised from MeCN/Et<sub>2</sub>O, washed with Et<sub>2</sub>O (3 × 30 mL) and filtered under N<sub>2</sub> (g) to give the Cu(I) complexes as solids.

## 8.2 Experimental details

### 8.2.1 Preparation of P2

Theophylline (5.0 g, 27.8 mmol) was dissolved in MeCN (70 mL), and potassium carbonate (4.25 g, 30.8 mmol) and butyl iodide (12.0 mL, 105.5 mmol) were added. The mixture was heated at reflux for 48 hours, filtered and washed with MeCN (30 mL x 3) to ensure the dissolution of all the product into the filtrate. The filtrate is dried *in vacuo* to yield the product as a white solid.

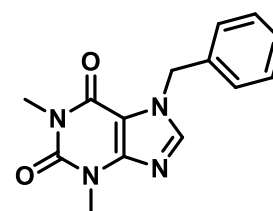


Yield: 4.7 g, 19.9 mmol (72%)

$^1\text{H}$  NMR (300 MHz, DMSO- $d_6$ ):  $\delta$  8.09 (s, 1H, NCHN), 4.26 (t,  $J$  = 7.2 Hz, 2H, CH<sub>2</sub>), 3.42 (s, 3H, CH<sub>3</sub>), 3.19 (s, 3H, CH<sub>3</sub>), 1.74 (quin,  $J$  = 7.2 Hz, 2H, CH<sub>2</sub>), 1.24 (sext,  $J$  = 7.2 Hz, 2H, CH<sub>2</sub>), 0.85 (t,  $J$  = 7.2 Hz, 2H, CH<sub>3</sub>).  $^{13}\text{C}\{^1\text{H}\}$  NMR (75 MHz, DMSO- $d_6$ ):  $\delta$  155.1 (C=O), 151.7 (C=O), 148.9 (C), 140.8 (NCHN), 106.9 (C), 47.0 (CH<sub>2</sub>), 32.8 (CH<sub>2</sub>), 29.7 (CH<sub>2</sub>), 27.9 (CH<sub>3</sub>), 19.5 (CH<sub>3</sub>), 13.4 (CH<sub>3</sub>). HRMS (ESI<sup>+</sup>): Calcd for C<sub>11</sub>H<sub>17</sub>N<sub>4</sub>O<sub>2</sub> [M + H]<sup>+</sup>: 237.1351. Found: 237.1345. Anal. Calcd for C<sub>11</sub>H<sub>16</sub>N<sub>4</sub>O<sub>2</sub>· $\frac{1}{5}$  H<sub>2</sub>O: C, 55.08; H, 6.89; N, 23.36. Found: C, 55.40; H, 6.85; N, 23.30.

### 8.2.2 Preparation of P3

Theophylline (5.0 g, 27.8 mmol) was dissolved in MeCN (80 mL), and potassium carbonate (4.25 g, 30.8 mmol) and benzyl bromide (16.5 mL, 138.7 mmol) were added. The mixture was heated at reflux for 24 hours, filtered and washed with MeCN (30 mL x 3) to ensure the dissolution of all the product into the filtrate. The filtrate was dried *in vacuo* to yield the product as a white solid, which was further recrystallized from MeCN / Et<sub>2</sub>O.



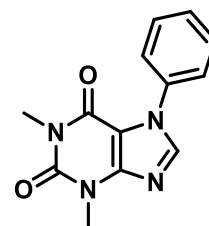
Yield: 6.1g, 22.6 mmol (81%).

$^1\text{H}$  NMR (300 MHz, CDCl<sub>3</sub>)  $\delta$ : 7.58 (s, 1H, NCHN), 7.43–7.32 (m, 5H, aromatic), 5.52 (s, 2H, CH<sub>2</sub>), 3.60 (s, 3H, CH<sub>3</sub>), 3.13 (s, 3H, CH<sub>3</sub>).  $^{13}\text{C}\{^1\text{H}\}$  NMR (75 MHz, CDCl<sub>3</sub>):  $\delta$  153.4 (C=O), 150.1 (C=O), 139.4 (C), 136.1 (NCHN), 133.6 (C), 127.2, 126.9, 126.6 (CH), 105.1 (C), 48.3 (CH<sub>3</sub>), 31.8 (CH<sub>3</sub>), 27.9 (CH<sub>2</sub>). HRMS (ESI<sup>+</sup>): Calcd for C<sub>14</sub>H<sub>15</sub>N<sub>4</sub>O<sub>2</sub> [M + H]<sup>+</sup>: 271.1195. Found: 271.1188. Anal. Calcd for C<sub>14</sub>H<sub>14</sub>N<sub>4</sub>O<sub>2</sub>· $\frac{1}{3}$  Et<sub>2</sub>O: C, 62.43; H, 5.92; N, 18.99. Found: C, 62.00; H, 5.50; N, 19.40.

### 8.2.3 Preparation of P4

Theophylline (4.0 g, 22.2 mmol), copper (I) iodide (1.9 g, 10.0 mmol), cesium carbonate (6.52 g, 20.0 mmol) and 2-isobutyrylcyclohexanone (2.2 mL, 13.1 mmol) were added to a Schlenk flask and degassed. Anhydrous DMSO (17 mL) and iodobenzene (3.5 mL, 31.3 mmol) were added to the Schlenk flask. The mixture was heated at 130 °C for 24 hours. The solution, which had turned dark brown, was dissolved in CH<sub>2</sub>Cl<sub>2</sub> and extracted with H<sub>2</sub>O (x3). The aqueous layers were combined and washed with CH<sub>2</sub>Cl<sub>2</sub> (x3). All the organic layers were combined and dried *in vacuo* to give a dark brown solid. Recrystallisation from CH<sub>2</sub>Cl<sub>2</sub> / Et<sub>2</sub>O furnished the product as a white solid.

To ensure no copper remained in the product, the solid was dissolved in CH<sub>2</sub>Cl<sub>2</sub> and any residual copper was separated by addition of a saturated solution of EDTA (50 mL x2). The organic layer was extracted and dried *in vacuo* to give a white solid.

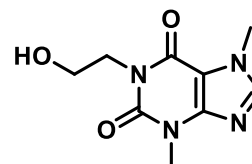


Yield: 1.78 g, 7.0 mmol (32%).

<sup>1</sup>H NMR (300 MHz, DMSO-d<sub>6</sub>): δ 8.31 (s, 1H, NCHN), 7.71–7.14 (m, *J* = 7.5 Hz, 5H, aromatic), 3.46 (s, 3H, CH<sub>3</sub>), 3.18 (s, 3H, CH<sub>3</sub>). <sup>13</sup>C{<sup>1</sup>H} NMR (75 MHz, DMSO-d<sub>6</sub>): δ 153.7 (C=O), 150.9 (C=O), 149.2 (C), 142.7 (NCHN), 134.8 (C), 128.9 (CH), 128.5 (CH), 125.1 (CH), 106.1 (C), 29.6 (CH<sub>3</sub>), 27.8 (CH<sub>3</sub>). HRMS (ESI<sup>+</sup>): Calcd for C<sub>13</sub>H<sub>13</sub>N<sub>4</sub>O<sub>2</sub> [M + H]<sup>+</sup>: 257.1039. Found: 257.1031. Anal. Calcd for C<sub>13</sub>H<sub>12</sub>N<sub>4</sub>O<sub>2</sub>: C, 60.93; H, 4.72; N, 21.86. Found: C, 60.60; H, 4.85; N, 21.80.

### 8.2.4 Preparation of P5<sup>2</sup>

Theobromine (1.0 g, 5.0 mmol) was dissolved in DMF (15 mL), and iodoethanol (0.78 mL, 10.0 mmol) and potassium carbonate (0.84 g, 6.1 mmol) were added. The mixture was heated at reflux for 24 hours, filtered and washed with Et<sub>2</sub>O and dried *in vacuo* to yield a pale brown solid.

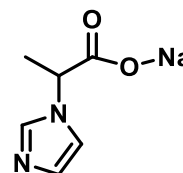


Yield: 1.05 g, 4.7 mmol (94%)

<sup>1</sup>H NMR (300 MHz, DMSO-d<sub>6</sub>): δ 8.00 (s, 1H, NCHN), 4.74 (t, 1H *J* = 5.0 Hz, OH), 3.95 (t, 2H *J* = 5.0 Hz, CH<sub>2</sub>), 3.88 (s, 3H, CH<sub>3</sub>), 3.52 (q, 2H *J* = 5.0 Hz, CH<sub>2</sub>), 3.41 (s, 3H, CH<sub>3</sub>). <sup>13</sup>C{<sup>1</sup>H} NMR (75 MHz, DMSO-d<sub>6</sub>): δ 154.5 (C=O), 151.1 (C=O), 148.3 (C), 143.0 (CH), 106.5 (C), 58.1 (CH<sub>2</sub>), 42.3 (CH<sub>2</sub>), 33.0 (CH<sub>3</sub>), 29.4 (CH<sub>3</sub>). HRMS (ESI<sup>+</sup>): Calcd for C<sub>9</sub>H<sub>12</sub>N<sub>4</sub>NaO<sub>3</sub> [M + Na]<sup>+</sup>: 247.0807. Found: 247.0802.

### 8.2.5 Preparation of P28A<sup>3</sup>

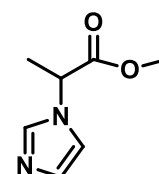
Glyoxal (1.07 mL, 22.44 mmol) and formaldehyde (0.82 mL, 22.44 mmol) were heated to 50 °C in a round-bottomed flask. At the same time, in another round bottomed flask, a mixture of L-alanine (2.0 g, 22.44 mmol), sodium hydroxide (0.90g, 22.44 mmol) and ammonium acetate (1.72 g, 22.44 mmol) were stirred in water (10 mL) until all components were dissolved. This solution was added dropwise to the glyoxal and formaldehyde mixture over 30 minutes, and the reaction mixture was heated for 24 hours at 50 °C. The solution which had turned yellow was dried *in vacuo* to furnish orange crystals.



<sup>1</sup>H NMR (300 MHz, DMSO-d<sub>6</sub>): δ 7.71 (s, 1H, NCHN), 7.02 (s, 1H, C=CH), 6.93 (s, 1H, C=CH), 4.60 (q, 1H *J* = 7.2 Hz, CH), 1.55 (d, 3H *J* = 7.2 Hz, CH<sub>3</sub>). HRMS (ESI<sup>+</sup>): Calcd for C<sub>6</sub>H<sub>8</sub>N<sub>4</sub>NaO<sub>3</sub> [M – Na + H]<sup>+</sup>: 141.0619. Found: 141.0658.

### 8.2.6 Preparation of P28B<sup>3</sup>

The orange crystals of **P5** (4.7 g, 29.0 mmol), were dissolved in MeOH (50 mL) and cooled to 0 °C, and thionyl chloride (2.1 mL, 29.0 mmol) was added dropwise to the cold solution over 90 minutes. The mixture was warmed to room temperature and stirred for 48 hours. The solution, which turned a light yellow colour, was dried *in vacuo* to yield a sticky yellow solid that was dissolved in a saturated solution of NaHCO<sub>3</sub> (70 mL), and the product extracted with ethyl acetate (50 mL x 3), CH<sub>2</sub>Cl<sub>2</sub> (50 mL x 3) and Et<sub>2</sub>O (50 mL x 3). The organic layers were combined and dried over magnesium sulfate and further dried *in vacuo* to yield a brown oil.

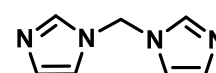


Yield: 0.4 g, 2.6 mmol (9%)

<sup>1</sup>H NMR (300 MHz, CDCl<sub>3</sub>): δ 7.51(s, 1H, NCHN), 6.95 (s, 2H, HC=CH), 4.86 (q, *J* = 7.2 Hz, 1H, CH), 3.64 (s, 3H, O-CH<sub>3</sub>), 1.66 (d, *J* = 7.2 Hz, 3H, CH<sub>3</sub>). HRMS (ESI<sup>+</sup>): Calcd for C<sub>7</sub>H<sub>11</sub>N<sub>2</sub>O<sub>2</sub> [M + H]<sup>+</sup>: 155.0776. Found: 155.0783.

### 8.2.7 Preparation of P29-31<sup>4</sup>

1H-Imidazole (2.0 g, 29.4 mmol), potassium hydroxide (3.29 g, 58.8 mmol) and tetra-n-butyl ammonium bromide (0.284 g, 0.882 mmol) were suspended in water (2 mL) and dissolved by aid of sonication. CH<sub>2</sub>Br<sub>2</sub> (2.06 mL, 29.4 mmol) was added dropwise *via* syringe and the reaction mixture stirred overnight, during which time a white crystalline precipitate formed. The crude solid was collected and



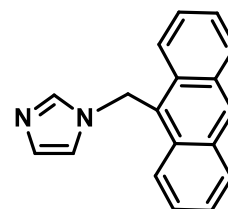
purified by column chromatography (SiO<sub>2</sub>, ethyl acetate) to give the title product as a colourless crystalline solid.

Yield: 1.8 g, 12.2 mmol (41%)

<sup>1</sup>H NMR (300 MHz, DMSO-d<sub>6</sub>): δ 7.96 (s, 1H, NCHN), 7.40 (s, 1H, C=CH), 6.93 (s, 1H, C=CH), 6.23 (s, 2H, N-CH<sub>2</sub>-N). <sup>13</sup>C{<sup>1</sup>H} NMR (75 MHz, DMSO-d<sub>6</sub>): δ 137.3 (NCHN), 129.0 (C=CH), 119.1 (C=CH), 54.7 (CH<sub>2</sub>). HRMS (ESI<sup>+</sup>): Calcd for C<sub>7</sub>H<sub>9</sub>N<sub>4</sub> [M + H]<sup>+</sup>: 149.0827. Found: 149.0821.

### 8.2.8 Preparation of P33<sup>5</sup>

1H-Imidazole (0.2 g, 2.9 mmol), potassium hydroxide (0.33 g, 5.9 mmol) and 9-chloromethyl anthracene (0.66 g, 2.9 mmol) were added to an ampoule. MeCN (30 mL) was added and the mixture was heated at 90°C for 24 hours in a sealed vessel. The solution, which had turned a dark brown colour, was dried *in vacuo*, washed with distilled H<sub>2</sub>O (50 mL) and extracted into Et<sub>2</sub>O (3 x 50 mL) and CH<sub>2</sub>Cl<sub>2</sub> (3 x 50 mL). The organic layers were combined and dried over magnesium sulfate and dried *in vacuo* to yield a brown solid.



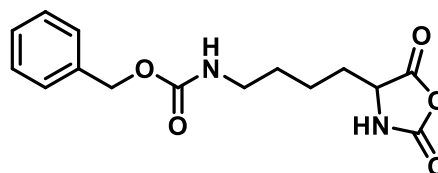
Yield: 0.7 g, 2.7 mmol (92%)

<sup>1</sup>H NMR (300 MHz, CDCl<sub>3</sub>): δ 8.52 (s, 1H, NCHN), 8.17 (d, 2H, *J* = 8.1 Hz, aromatic), 8.03 (d, 2H, *J* = 8.1 Hz, aromatic), 7.56-7.44 (m, 5H, aromatic), 6.96 (s, 2H, CH<sub>2</sub>). <sup>13</sup>C{<sup>1</sup>H} NMR (75 MHz, CDCl<sub>3</sub>): δ 135.8 (N=CH-N), 130.5, 129.8 (C, aromatic), 128.5, 128.2, 126.4 (CH, aromatic), 124.3, 123.7 (N-HC=CH-N), 121.9 (CH, aromatic), 42.3 (CH<sub>2</sub>). HRMS (ESI<sup>+</sup>): Calcd for C<sub>18</sub>H<sub>14</sub>N<sub>2</sub> [M + H]<sup>+</sup>: 259.1191, Found: 259.1247

### 8.2.9 Preparation of P(PM5)<sup>6, 7</sup>

L-Lysine (Z) amino acid (5.02 g, 17.9 mmol) was weighed into a three neck round bottomed flask and dried *in vacuo*.

Anhydrous ethyl acetate (50 mL) and α-pinene (4.23 g, 31.1 mmol) were added to the amino acid and the mixture was heated at reflux for 30 minutes.



Triphosgene (6.78 g, 22.9 mmol) was dissolved in anhydrous ethyl acetate (20 mL) and added into the solution dropwise using a dropping funnel. The solution was heated at reflux for 4 hours until the initial suspension cleared into a gold colour solution. The solution was concentrated by reducing its volume to a third *in vacuo*, after which it was added

dropwise to C<sub>7</sub>H<sub>16</sub> (300 mL) at 0 °C to precipitate the N-carboxy anhydride product as a white solid. The product was filtered and washed with C<sub>7</sub>H<sub>16</sub> (3 x 50 mL) and dried *in vacuo* to yield a white solid.

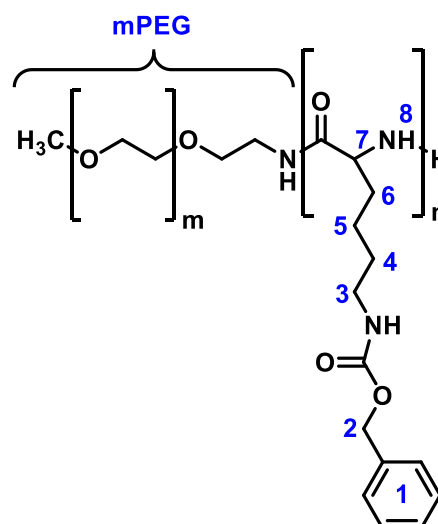
Yield: 4.85 g, 15.8 mmol (89%).

<sup>1</sup>H NMR (300MHz, DMSO-d<sub>6</sub>) : δ 9.07(s, 1H, NH), 7.39-7.30 (m, 5H, aromatic), 7.24 (NH-C=O), 5.00 (s, 2H, O-CH<sub>2</sub>-aromatic), 4.42 (t, 1H, *J* = 6.1 Hz, CH), 2.98 (q, 2H, *J* = 6.1 Hz, CH<sub>2</sub>-NH), 1.77-1.63 (m, 2H, CH<sub>2</sub>), 1.44-1.25 (m, 4H, CH<sub>2</sub>). HRMS (ESI<sup>+</sup>): calcd for C<sub>15</sub>H<sub>18</sub>N<sub>2</sub>NaO<sub>5</sub> [M + Na]<sup>+</sup>: 329.1113. Found: 329.1114. Anal. Calcd for C<sub>15</sub>H<sub>18</sub>N<sub>2</sub>O<sub>5</sub>: C, 58.82; H, 5.92; N, 9.15. Found: C, 58.80; H, 5.90; N, 9.10.

### 8.2.10 Preparation of P(PM5.A-C)<sup>7</sup>

#### Synthesis of methoxy-poly(polyethylene glycol)-b-poly(L-lysine(Cbz))

N(epsilon)-Benzyloxycarbonyl-L-lysine NCA (380.2 mg, 1.24 mmol) was dissolved in anhydrous CH<sub>2</sub>Cl<sub>2</sub> (10 mL). This solution was injected into a dry and nitrogen-purged Schlenk tube sealed with a rubber septum and equipped with a magnetic stirrer bar. O-(2-aminoethyl)-O'-methylpolyethylene glycol (155 mg, 0.031 mmol) was dissolved in anhydrous CH<sub>2</sub>Cl<sub>2</sub> (10 mL) and injected into the Schlenk tube under a constant flow of nitrogen and with constant stirring. The reaction mass



was degassed by bubbling N<sub>2</sub> through the solution and left to stir at room temperature for 120 hours, under a constant stream of nitrogen. The resultant polymer was precipitated in cold Et<sub>2</sub>O (100 mL) for 5 hours. The precipitated polymer was isolated from the supernatant by centrifugation (6000 rpm, 20 min, -5 °C). The polymer was washed three times using cold Et<sub>2</sub>O (100 mL) and dried in a vacuum oven maintained at 40 °C for 24 hours.

| Entry        | mPEG <sub>5000</sub><br>amine (mg) | L-lysine(Cbz)<br>NCA | [M/I] | Yield<br>(mg) |
|--------------|------------------------------------|----------------------|-------|---------------|
| 1 (P(PM5 A)) | 250                                | 306.3                | 20    | 418.0         |

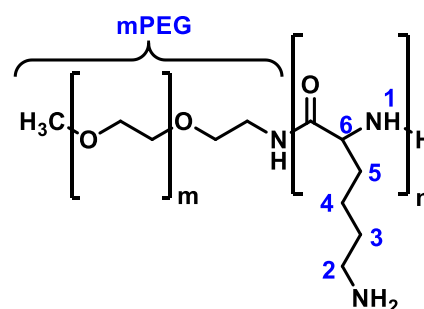
|                     |     |       |    |       |
|---------------------|-----|-------|----|-------|
| <b>2 (P(PM5 B))</b> | 155 | 380.2 | 40 | 487.1 |
| <b>3 (P(PM5 C))</b> | 155 | 712.2 | 75 | 691.0 |

$^1\text{H}$  NMR (300 MHz, Trifluoroacetic acid-d):  $\delta$  8.37 (s, **8**, NH), 7.36-7.28 (broad s, aromatic **1**), 5.15 (broad s, O-CH<sub>2</sub>-aromatic **2**), 4.56 (broad s, CH **7**), 3.90 (broad s, mPEG), 1.87-1.73 (m, CH<sub>2</sub> **4**), 1.56-1.37 (m, CH<sub>2</sub> **5 & 6**).

### 8.2.11 Preparation of PM5.A-C

Synthesis of **methoxy-Poly(polyethylene glycol)-b-Poly(L-lysine)** mPEG<sub>5000</sub>-b-

Poly(L-lysine(Cbz)) (480 mg) was dissolved in CF<sub>3</sub>COOH (5 mL). The polymer solution was added to a 33 wt.% solution of HBr in CH<sub>3</sub>COOH (1.5 mL). The mixture was stirred at room temperature for 24 hours, then added dropwise into cold Et<sub>2</sub>O (150



mL) to induce the precipitation of the deprotected polymer. The precipitate was isolated by centrifugation (3000 rpm, 10 min). The polymer was re-suspended in fresh Et<sub>2</sub>O, stirred for 30 min and centrifuged. This was repeated several times until a clear supernatant was obtained. The polymer was dissolved in de-ionised H<sub>2</sub>O and dialysed against de-ionised water for 96 hours, with the dialysate being substituted with a fresh supply after every 8 hours. The polymer was isolated by freeze-drying.

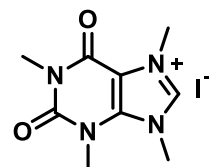
| Entry/Polymer    | Yield (mg) | Yield (wt.%) | M <sub>w</sub> (g/mol)* | m:n* |
|------------------|------------|--------------|-------------------------|------|
| <b>1 (PM5 A)</b> | 171.0      | 43.8         | 10055.6                 | 1:20 |
| <b>2 (PM5 B)</b> | 369.9      | 77.1         | 11464.5                 | 1:40 |
| <b>3 (PM5 C)</b> | 547.8      | 88.4         | 22992.6                 | 1:75 |

\*Estimated from  $^1\text{H}$  NMR by normalising to mPEG<sub>5000</sub> integrals and comparing the mPEG signal (3.40 ppm - 3.52 ppm) to the proton signal from  $\alpha$ -CH groups of poly(L-lysine) (3.25 ppm).

$^1\text{H}$  NMR (300 MHz, DMSO-d<sub>6</sub>):  $\delta$  8.03 (broad s, NH **1**), 4.27 (broad s, CH **6**), 3.51 (broad s, mPEG), 2.78 (broad s, CH<sub>2</sub>-NH<sub>2</sub> **2**), 1.66-1.57 (broad m, CH<sub>2</sub> **3 & 4**), 1.35 (broad s, CH<sub>2</sub> **5**).

**8.2.12 Preparation of L1<sup>8</sup>**

Caffeine (5.0 g, 33.0 mmol) was dissolved in DMF (40 mL), and methyl iodide (9.51 mL, 330.0 mmol) was added. The mixture was heated at reflux for 48 hours. Ethyl acetate (200 mL) was added to the solution to induce precipitation. Most of the solvent was decanted from the precipitate and ethyl acetate (200 mL) was added to the solid. This was decanted and washed a third time with ethyl acetate. The solid was filtered and washed with ethyl acetate (300 mL), and dried *in vacuo* to yield the product as a white solid.

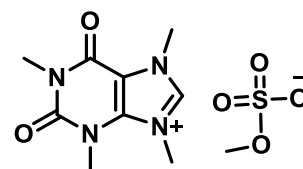


Yield: 5.4 g, 16.0 mmol (49%)

<sup>1</sup>H NMR (300 MHz, DMSO-d<sub>6</sub>): δ 9.27 (s, 1H, NCHN), 4.14 (s, 3H, CH<sub>3</sub>), 4.05 (s, 3H, CH<sub>3</sub>), 3.73 (s, 3H, CH<sub>3</sub>), 3.27 (s, 3H, CH<sub>3</sub>). <sup>13</sup>C{<sup>1</sup>H} NMR (75 MHz, DMSO-d<sub>6</sub>): 153.3 (C=O), 150.2 (C=O), 141.1 (C=C), 138.1 (NCHN), 107.8 (C=C), 36.6, 35.9, 30.4, 25.5 (NCH<sub>3</sub>). HRMS (ESI<sup>+</sup>): Calcd for C<sub>9</sub>H<sub>13</sub>N<sub>4</sub>O<sub>2</sub> [M - I]<sup>+</sup>: 209.1033. Found: 209.1029. M.P: 186.4-188.1°C

**8.2.13 Preparation of L1.1<sup>9</sup>**

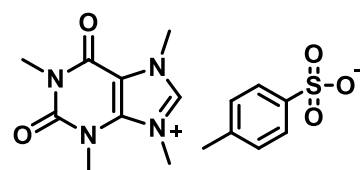
Caffeine (1.0 g, 5.0 mmol) was dissolved in toluene (15 mL) and (CH<sub>3</sub>)<sub>2</sub>SO<sub>4</sub> (0.5 mL, 5.3 mmol) was added. The mixture was heated at reflux for 48 hours. Excess Et<sub>2</sub>O (150 mL) was added to the solution which had turned a brown colour, and the brown oil that precipitated out of solution was filtered and washed with Et<sub>2</sub>O, and dried *in vacuo*. The sticky product was not used in subsequent reactions.



<sup>1</sup>H NMR (300 MHz, D<sub>2</sub>O): δ 8.89 (s, 1H, NCHN), 4.11 (s, 6H, CH<sub>3</sub>), 3.78 (s, 3H, CH<sub>3</sub>), 3.73 (s, 3H, CH<sub>3</sub>), 3.33 (s, 3H, CH<sub>3</sub>). HRMS (ESI<sup>+</sup>): calcd for C<sub>9</sub>H<sub>13</sub>N<sub>4</sub>O<sub>2</sub> [M - OSO<sub>3</sub>CH<sub>3</sub>]<sup>+</sup>: 209.1033. Found: 209.1038.

**8.2.14 Preparation of L1.2<sup>9</sup>**

Caffeine (2.0 g, 10.0 mmol) was dissolved in toluene (30 mL), and *p*-SO<sub>3</sub>CH<sub>3</sub> (C<sub>6</sub>H<sub>5</sub>)CH<sub>3</sub> (7.8 mL, 50.0 mmol) was added. The mixture was heated to reflux for 48 hours. Excess Et<sub>2</sub>O (300 mL) was added to the solution which had turned a yellow colour, and the yellow solid that precipitated out of solution, was filtered and washed with Et<sub>2</sub>O,



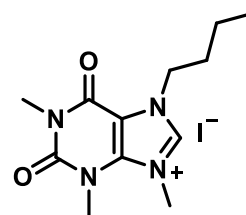
and dried *in vacuo*. The product was not used in subsequent reactions.

Yield: 1.48 g, 3.9 mmol (39%)

$^1\text{H}$  NMR (300 MHz, DMSO- $d_6$ ):  $\delta$  9.25 (s, 1H, NCHN), 7.44 (d,  $J = 7.2$  Hz, 2H, aromatic), 7.09 (d,  $J = 7.2$  Hz, 2H, aromatic), 4.12 (s, 3H,  $\text{CH}_3$ ), 4.03 (s, 3H,  $\text{CH}_3$ ), 3.72 (s, 3H,  $\text{CH}_3$ ), 3.26 (s, 3H,  $\text{CH}_3$ ), 2.28 (s, 3H,  $\text{CH}_3$ ). HRMS (ESI $^+$ ): Calcd for  $\text{C}_9\text{H}_{13}\text{N}_4\text{O}_2$  [M – toISO $_3$ ] $^+$ : 209.1033. Found: 209.1050.

### 8.2.15 Preparation of L2

**P2** (4.5 g, 19.1 mmol), was dissolved in DMF (10 mL) and  $\text{CH}_3\text{I}$  (23.7 mL, 381.0 mmol) was added. The mixture was heated at 70°C for 24 hours in a sealed ampoule. Excess  $\text{Et}_2\text{O}$  (150 mL) was added to the solution resulting in the precipitation of a yellow solid. The solid was recrystallised from  $\text{CH}_2\text{Cl}_2/\text{Et}_2\text{O}$  and dried *in vacuo* to yield a bright yellow solid.

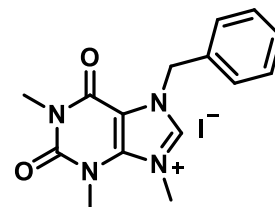


Yield: 6.3 g, 16.7 mmol (87%)

$^1\text{H}$  NMR (300 MHz, DMSO- $d_6$ ):  $\delta$  9.41 (s, 1H, NCHN), 4.45 (t,  $J = 7.3$  Hz, 2H,  $\text{CH}_2$ ), 4.16 (s, 3H,  $\text{CH}_3$ ), 3.76 (s, 3H,  $\text{CH}_3$ ), 3.26 (s, 3H,  $\text{CH}_3$ ), 1.82 (quin,  $J = 7.3$  Hz, 2H,  $\text{CH}_2$ ), 1.31 (sext,  $J = 7.3$  Hz, 2H,  $\text{CH}_2$ ), 0.91 (t,  $J = 7.3$  Hz, 3H,  $\text{CH}_3$ ).  $^1\text{H}$  NMR (300 MHz,  $\text{CDCl}_3$ ):  $\delta$  10.50 (s, 1H, NCHN), 4.58 (t,  $J = 7.3$  Hz, 2H,  $\text{CH}_2$ ), 4.48 (s, 3H,  $\text{CH}_3$ ), 3.87 (s, 3H,  $\text{CH}_3$ ), 3.40 (s, 3H,  $\text{CH}_3$ ), 1.99 (quin,  $J = 7.3$  Hz, 2H,  $\text{CH}_2$ ), 1.45 (sext,  $J = 7.3$  Hz, 2H,  $\text{CH}_2$ ), 0.98 (t,  $J = 7.3$  Hz, 3H,  $\text{CH}_3$ ).  $^{13}\text{C}\{^1\text{H}\}$  NMR (75 MHz,  $\text{CDCl}_3$ ):  $\delta$  153.1 (C=O), 149.9 (C=O), 139.5 (C), 138.6 (CH), 107.8 (C), 49.7 ( $\text{CH}_3$ ), 38.9 ( $\text{CH}_2$ ), 32.3 ( $\text{CH}_2$ ), 32.1 ( $\text{CH}_3$ ), 28.7 ( $\text{CH}_2$ ), 19.4 ( $\text{CH}_3$ ), 13.3 ( $\text{CH}_3$ ). HRMS (ESI $^+$ ): Calcd for  $\text{C}_{12}\text{H}_{19}\text{N}_4\text{O}_2$  [M – I] $^+$ : 251.1503. Found: 251.1589. Anal. Calcd for  $\text{C}_{12}\text{H}_{19}\text{IN}_4\text{O}_2$ : C, 38.11; H, 5.06; N, 14.81. Found: C, 37.80; H, 5.00; N, 14.60. M.P: 142.4-144.7°C

### 8.2.16 Preparation of L3

**P3** (2.6 g, 9.6 mmol), was dissolved in DMF (3 mL) and  $\text{CH}_3\text{I}$  (11.9 mL, 191.0 mmol) was added. The mixture was heated at 70 °C for 24 hours in a sealed ampoule. Excess  $\text{Et}_2\text{O}$  (150mL) was added to the solution which had turned an orange colour resulting in the precipitation of an orange powder. The powder was recrystallised from  $\text{CH}_2\text{Cl}_2/\text{Et}_2\text{O}$  and dried *in vacuo* to yield the product as a yellow solid.

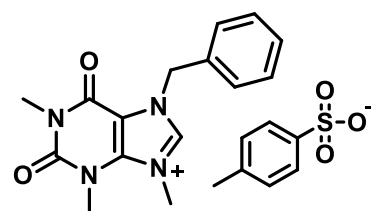


Yield: 0.8 g, 1.9 mmol (20%)

$^1\text{H}$  NMR (300 MHz, DMSO- $d_6$ ):  $\delta$  9.49 (s, 1H, NCHN), 7.46-7.37 (m, 5H, aromatic), 5.75 (s, 2H, CH<sub>2</sub>), 4.16 (s, 3H, CH<sub>3</sub>), 3.73 (s, 3H, CH<sub>3</sub>), 3.26 (s, 3H, CH<sub>3</sub>).  $^{13}\text{C}\{^1\text{H}\}$  NMR (75 MHz, DMSO- $d_6$ ):  $\delta$  153.1(C=O), 150.1 (C=O), 139.8 (C), 139.4 (CH), 134.4 (C-arom), 128.8, 128.7, 128.2 (CH, aromatic), 106.9 (C), 51.1(CH<sub>3</sub>), 37.2 (CH<sub>3</sub>), 31.3 (CH<sub>3</sub>), 28.4(CH<sub>2</sub>). HRMS (ESI<sup>+</sup>): Calcd for C<sub>30</sub>H<sub>33</sub>N<sub>8</sub>O<sub>4</sub> [2M - I]<sup>+</sup>: 569.2614. Found: 569.2619. Anal. Calcd for C<sub>15</sub>H<sub>17</sub>N<sub>4</sub>O<sub>2</sub> · 1/4 Et<sub>2</sub>O: C, 44.61; H, 4.56; N, 13.01. Found: C, 44.80; H, 4.30; N, 12.70. M.P: 200.2-203.4 °C

### 8.2.17 Preparation of L3.1

**P3** (0.85 g, 3.2 mmol) was dissolved in DMF (15 mL) and *p*-SO<sub>3</sub>CH<sub>3</sub>(C<sub>6</sub>H<sub>5</sub>)CH<sub>3</sub> (4.74 mL, 31.5 mmol) was added. The mixture was heated at reflux for 24 hours. Excess ethyl acetate (150 mL) was added to the solution which had turned a reddish-brown clear colour to precipitate a yellow solid. The yellow solid was filtered and washed with ethyl acetate (200 mL) and dried *in vacuo*. The product was not used in subsequent reactions.

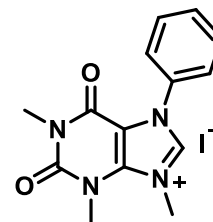


Yield: 0.3 g, 0.7 mmol (21%)

$^1\text{H}$  NMR (300 MHz, DMSO- $d_6$ ):  $\delta$  9.47 (s, 1H, NCHN), 7.68-7.12 (m, 9H, aromatic), 5.69 (s, 2H, CH<sub>2</sub>), 4.13 (s, 3H, CH<sub>3</sub>), 3.70 (s, 3H, CH<sub>3</sub>), 3.09 (s, 3H, CH<sub>3</sub>), 2.28 (s, 3H, CH<sub>3</sub>).  $^{13}\text{C}\{^1\text{H}\}$  NMR (75 MHz, CDCl<sub>3</sub>):  $\delta$  171.3, 156.4, 143.4, 139.8, 129.8, 127.8, 126.6, 124.2, 122.3 (CH, aromatic), 103.8 (C), 60.6(CH<sub>3</sub>), 55.7 (CH<sub>3</sub>), 21.6 (CH<sub>3</sub>), 14.3(CH<sub>2</sub>). HRMS (ESI<sup>+</sup>): Calcd for C<sub>15</sub>H<sub>17</sub>N<sub>4</sub>O<sub>2</sub> [M - tosyl]<sup>+</sup>: 285.3265. Found: 285.3211.

### 8.2.18 Preparation of L4

**P4** (0.2 g, 0.8 mmol) was dissolved in DMF (4 mL), and CH<sub>3</sub>I (0.91 mL, 15.6 mmol) was added. The mixture was heated at 70 °C in a sealed ampoule for 24 hours. Excess Et<sub>2</sub>O (90 mL) was added to the solution, which had turned an orange colour, to furnish the product as a yellow solid that was filtered and dried *in vacuo*.



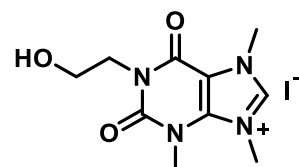
Yield: 0.15 g, 0.4 mmol (50%)

$^1\text{H}$  NMR (300 MHz, DMSO- $d_6$ ):  $\delta$  9.75 (s, 1H, NCHN), 8.17 (broad s, 5H, aromatic), 4.25 (s, 3H, CH<sub>3</sub>), 3.82 (s, 3H, CH<sub>3</sub>), 3.40 (s, 3H, CH<sub>3</sub>).  $^{13}\text{C}\{^1\text{H}\}$  NMR (75 MHz, DMSO- $d_6$ ):  $\delta$  154.1(C), 151.9(C), 140.3(C), 132.7(C), 130.7(CH),

129.3(CH), 125.8(CH), 109.5(CH), 54.4(C), 35.7(CH<sub>3</sub>), 28.5(CH<sub>3</sub>), 26.3(CH<sub>3</sub>). HRMS (ESI<sup>+</sup>): Calcd for C<sub>14</sub>H<sub>15</sub>N<sub>4</sub>O<sub>2</sub> [M - I]<sup>+</sup>: 271.1190. Found: 271.1188. Anal. Calcd for C<sub>14</sub>H<sub>15</sub>IN<sub>4</sub>O<sub>2</sub> · 3H<sub>2</sub>O: C, 37.18; H, 4.68; N, 12.39. Found: C, 36.80; H, 4.20; N, 12.20. M.P: 168.1-169.4 °C

### 8.2.19 Preparation of L5<sup>8</sup>

**P5** (0.3 g, 1.3 mmol) was dissolved in DMF (3 mL) and CH<sub>3</sub>I (5.1 mL, 80.1 mmol) was added. The mixture was heated at 70°C for 48 hours in a sealed ampoule. Excess Et<sub>2</sub>O (90 mL) was added to the solution which had turned turbid yellow to yield a yellow solid. Recrystallisation from MeOH / ethyl acetate furnished the product as a light yellow solid.

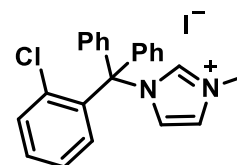


Yield: 0.15 g, 0.4 mmol (31%)

<sup>1</sup>H NMR (300 MHz, DMSO-d<sub>6</sub>): δ 9.27 (s, 1H, NCHN), 4.15 (s, 3H, CH<sub>3</sub>), 4.06 (s, 3H, CH<sub>3</sub>), 3.99 (t, *J* = 6.4 Hz, 2H, CH<sub>2</sub>), 3.55 (t, *J* = 6.4 Hz, 2H, CH<sub>2</sub>). <sup>13</sup>C{<sup>1</sup>H} NMR (125 MHz, DMSO-d<sub>6</sub>): δ 153.3(C=O), 150.2(C=O), 139.7(CH), 139.2(C), 107.7(C), 57.2(CH<sub>2</sub>), 43.5(CH<sub>2</sub>), 36.9(CH<sub>3</sub>), 35.6(CH<sub>3</sub>), 31.1(CH<sub>3</sub>). HRMS (ESI<sup>+</sup>): calcd for C<sub>10</sub>H<sub>15</sub>N<sub>4</sub>O<sub>3</sub> [M - I]<sup>+</sup>: 239.1139. Found: 239.1180 M.P: 180.1-181.7 °C

### 8.2.20 Preparation of L6

Clotrimazole (0.20 g, 0.58 mmol) was dissolved in CH<sub>2</sub>Cl<sub>2</sub> (3 mL) and methyl iodide (0.72 mL, 11.60 mmol) was added. The mixture was heated at 45 °C in the microwave for 15 minutes. Excess Et<sub>2</sub>O (30 mL) was added to the pale yellow solution, prompting precipitation of the product as an off-white solid. The product was filtered, washed with Et<sub>2</sub>O (100 mL), and dried *in vacuo*.

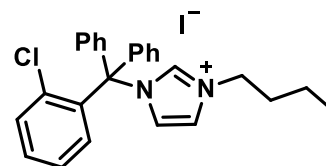


Yield: 0.21 g, 0.4 mmol (74%).

<sup>1</sup>H NMR (300 MHz, CDCl<sub>3</sub>): δ 9.10 (s, 1H, NCHN), 7.75 (s, 1H, NCH), 7.50-7.11 (m, 14H, aromatic), 6.95 (s, 1H, NCH), 4.25 (s, 3H, CH<sub>3</sub>). <sup>13</sup>C{<sup>1</sup>H} NMR (75 MHz, CDCl<sub>3</sub>): δ 138.0 (CH), 137.9 (C), 137.4 (C), 135.1 (C), 132.9 (CH), 131.7 (CH), 131.5 (CH), 130.1 (CH), 192.5 (CH), 129.2 (CH), 128.1 (CH), 124.1 (CH), 123.6 (CH), 79.5 (C), 38.8 (CH<sub>3</sub>). HRMS (ESI<sup>+</sup>): Calcd. for C<sub>23</sub>H<sub>20</sub>ClN<sub>2</sub> [M - I]<sup>+</sup>: 359.1310. Found: 359.1311. C<sub>23</sub>H<sub>26</sub>ClIN<sub>2</sub> · 1/3 H<sub>2</sub>O: C, 56.75; H, 4.14; N, 5.75; found: C, 57.00; H, 4.10; N, 5.70

### 8.2.21 Preparation of L7

Clotrimazole (0.20 g, 0.58 mmol) was dissolved in CH<sub>2</sub>Cl<sub>2</sub> (3 mL) and butyl iodide (0.67 mL, 5.80 mmol) was added. The mixture was heated to 45 °C in the microwave for 15 minutes. Excess Et<sub>2</sub>O (30 mL) was added to the pale yellow solution, inducing precipitation of the product as a white solid. The product was filtered, washed with Et<sub>2</sub>O, and dried *in vacuo*.

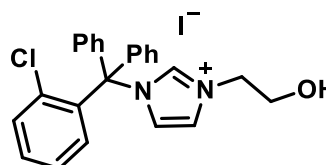


Yield: 0.18 g, 0.34 mmol (59%).

<sup>1</sup>H NMR (300 MHz, CDCl<sub>3</sub>): δ 9.18 (s, 1H, NCHN), 7.71 (s, 1H, NCH), 7.51-6.91 (m, 14H, aromatic), 6.74 (s, 1H, NCH), 4.63 (t, *J* = 7.3 Hz, 2H, CH<sub>2</sub>), 1.86 (m, 2H, CH<sub>2</sub>), 1.37 (m, 2H, CH<sub>2</sub>), 0.93 (t, *J* = 7.3 Hz, 3H, CH<sub>3</sub>). <sup>13</sup>C NMR (CDCl<sub>3</sub>, 75 MHz): δ 140.3 (C), 138.1 (C), 137.1 (CH), 135.5 (C), 132.1 (CH), 131.4 (CH), 130.0 (CH), 129.7 (CH), 129.0 (CH), 127.9 (CH), 127.0 (CH), 123.6 (CH), 121.5 (CH), 79.1 (C), 50.9 (CH<sub>2</sub>), 32.3 (CH<sub>2</sub>), 19.2 (CH<sub>2</sub>), 13.5 (CH<sub>3</sub>). HRMS (ESI<sup>+</sup>): Calcd. for C<sub>26</sub>H<sub>26</sub>ClN<sub>2</sub> [M - I]<sup>+</sup>: 401.1785. Found: 401.1778. M.P.: 103.1-104.9 °C. Anal. Calcd for C<sub>26</sub>H<sub>24</sub>ClIN<sub>2</sub>·<sup>1</sup>/<sub>2</sub>H<sub>2</sub>O: C, 58.06; H, 5.06; N, 5.21; found: C, 58.30; H, 4.90; N, 5.30.

### 8.2.22 Preparation of L8

Clotrimazole (0.50 g, 1.45 mmol) was dissolved in CH<sub>2</sub>Cl<sub>2</sub> (3 mL) and 2-iodoethanol (0.23 mL, 2.9 mmol) was added. The mixture was heated at reflux for 48 hours. Ethyl acetate (30 mL) was added to the resulting brown solution which induced precipitation of a yellow solid. This was filtered and washed with ethyl acetate. Trituration with (CH<sub>3</sub>)<sub>2</sub>CO gave the product as a white solid.

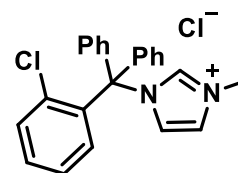


Yield: 0.38 g, 0.74 mmol (51%).

<sup>1</sup>H NMR (300 MHz, CDCl<sub>3</sub>): δ 9.04 (s, 1H, NCHN), 7.75 (s, 1H, NCH), 7.52-7.10 (m, 14H, aromatic), 7.02 (s, 1H, NCH), 4.64 (t, *J* = 4.9 Hz, 2H, CH<sub>2</sub>), 3.99 (t, *J* = 4.9 Hz, 2H, CH<sub>2</sub>), 2.82 (broad s, 1H, OH). <sup>13</sup>C{<sup>1</sup>H} NMR (75 MHz, CDCl<sub>3</sub>): δ 138.1 (C), 137.8 (CH), 137.4 (C), 135.3 (C), 133.0 (CH), 131.5 (CH), 131.4 (CH), 130.0 (CH), 129.5 (CH), 129.2 (CH), 128.1 (CH), 123.5 (CH), 123.4 (CH) 79.3 (C), 59.9 (CH<sub>2</sub>), 52.8 (CH<sub>2</sub>). HRMS (ESI<sup>+</sup>): Calcd. for C<sub>24</sub>H<sub>22</sub>ClN<sub>2</sub>O [M - I]<sup>+</sup>: 389.1421. Found: 389.1419. M.P.: 155.6-156.2 °C. Anal. Calcd for C<sub>24</sub>H<sub>22</sub>ClIN<sub>2</sub>O: C, 55.78; H, 4.29; N, 5.42; found: C, 56.00; H, 4.40; N, 5.80.

**8.2.23 Preparation of L9**

2-Chlorotrityl chloride (0.50 g, 1.60 mmol) and 1-methylimidazole (0.50 mL, 6.27 mmol) were dissolved in MeCN (10 mL) and heated at reflux for 24 hours. The solution was cooled to room temperature and Et<sub>2</sub>O (90 mL) was used to precipitate the product as a white solid.

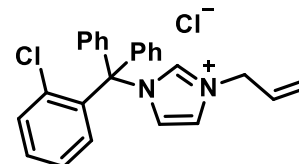


Yield: 0.53 g, 1.35 mmol (85%).

<sup>1</sup>H NMR (300 MHz, CDCl<sub>3</sub>): δ 9.10 (s, 1H, NCHN), 7.75 (s, 1H, NCH), 7.50-7.11 (m, 14H, aromatic), 6.95 (s, 1H, NCH), 4.25 (s, 3H, CH<sub>3</sub>). <sup>13</sup>C{<sup>1</sup>H} NMR (75 MHz, CDCl<sub>3</sub>): δ 139.1 (CH), 138.4 (C), 137.6 (C), 135.4 (C), 133.0 (CH), 131.7 (CH), 131.4 (CH), 130.0 (CH), 129.5 (CH), 129.1 (CH), 127.9 (CH), 123.7 (CH), 123.4 (CH), 79.3 (C), 37.8 (CH<sub>3</sub>). HRMS (ESI<sup>+</sup>): Calcd. for C<sub>23</sub>H<sub>20</sub>ClN<sub>2</sub> [M - Cl]<sup>+</sup>: 359.1310. Found: 359.1311. M.P.: 190.1-190.8 °C. Anal. Calcd for C<sub>23</sub>H<sub>20</sub>Cl<sub>2</sub>N<sub>2</sub>: C, 69.88; H, 5.10; N, 7.09; found: C, 69.80; H, 5.10; N, 7.20.

**8.2.24 Preparation of L10**

2-Chlorotrityl chloride (0.50 g, 1.60 mmol) and 1-allylimidazole (0.48 mL, 4.40 mmol) were dissolved in MeCN (10 mL) and heated at reflux for 24 hours. The yellow solution was allowed to cool to room temperature and addition of Et<sub>2</sub>O (90 mL) was used to precipitate a yellow oil. The solution was decanted from the oil which was washed with ethyl acetate. Trituration in (CH<sub>3</sub>)<sub>2</sub>CO yields the product as a white solid that was dried *in vacuo*.

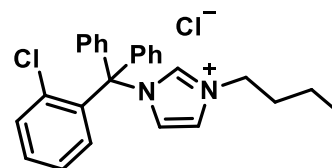


Yield: 0.37 g, 0.9 mmol (55%).

<sup>1</sup>H NMR (CDCl<sub>3</sub>, 300 MHz): δ 9.84 (s, 1H, NCHN), 7.71 (s, 1H, NCH), 7.51-7.06 (m, 14H, aromatic), 6.96 (s, 1H, NCH), 6.08-5.95 (m, 1H, CH), 5.41-5.35 (m, 4H, N-CH<sub>2</sub>CHCH<sub>2</sub>). <sup>13</sup>C{<sup>1</sup>H} NMR (CDCl<sub>3</sub>, 75 MHz): δ 138.8 (CH), 138.4 (C), 137.5 (C), 135.4 (C), 132.9 (CH), 131.8 (CH), 131.5 (CH), 130.8 (CH), 130.0 (CH), 129.5 (CH), 129.1 (CH), 127.9 (CH), 123.5 (CH), 122.2 (CH), 121.9 (CH<sub>2</sub>) 79.4 (C), 52.9 (CH<sub>2</sub>). HRMS (ESI<sup>+</sup>): Calcd. for C<sub>25</sub>H<sub>22</sub>ClN<sub>2</sub> [M - Cl]<sup>+</sup>: 385.1466. Found: 385.1471. M.P.: 157.8-159.1 °C. Anal. Calcd for C<sub>25</sub>H<sub>22</sub>Cl<sub>2</sub>N<sub>2</sub>·<sup>1</sup>/<sub>4</sub> H<sub>2</sub>O: C, 70.26; H, 5.35; N, 6.55; found: C, 70.20; H, 5.30; N, 6.80.

### 8.2.25 Preparation of L11

2-Chlorotrityl chloride (0.50 g, 1.60 mmol) dissolved in CH<sub>2</sub>Cl<sub>2</sub> (5 mL) and 1-butylimidazole (0.21 mL, 1.60 mmol) was added. The mixture was heated at 45 °C for 24 hours in a sealed ampoule. Excess Et<sub>2</sub>O (60 mL) was added to the solution which had turned a yellow colour to obtain the product as a white solid.

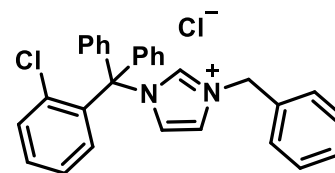


Yield: 0.3 g, 0.7 mmol (43%).

<sup>1</sup>H NMR (300 MHz, CDCl<sub>3</sub>): δ 9.60 (s, 1H, NCHN), 8.19 (s, 1H, HC=C), 7.47-6.98 (m, 15H, aromatic + C=CH), 4.63 (t, *J* = 7.3 Hz, 2H, CH<sub>2</sub>), 1.85-1.74 (m, 2H, CH<sub>2</sub>), 1.28 (dt, *J* = 17.4, 7.3 Hz, 2H, CH<sub>2</sub>), 0.86 (t, *J* = 7.3 Hz, 3H, CH<sub>3</sub>). <sup>13</sup>C{<sup>1</sup>H} NMR (CDCl<sub>3</sub>, 75 MHz): δ 138.5 (C-arom), 138.2 (CH), 137.5, 135.3 (C-arom), 132.9, 131.8, 131.4, 129.8, 129.3, 129.0, 127.9 (CH-arom), 123.6, 122.7 (CH), 79.1 (C), 50.5, 32.5, 19.4 (CH<sub>2</sub>), 13.6 (CH<sub>3</sub>). HRMS (ESI<sup>+</sup>): Calcd. for C<sub>26</sub>H<sub>26</sub>ClN<sub>2</sub> [M - Cl]<sup>+</sup>: 401.1779. Found: 401.1764. M.P.: 161.3-162.9 °C. Anal. Calcd for C<sub>26</sub>H<sub>26</sub>Cl<sub>2</sub>N<sub>2</sub>: C, 71.39; H, 5.99; N, 6.90; found: C, 71.10; H, 6.20; N, 6.60.

### 8.2.26 Preparation of L12

2-Chlorotrityl chloride (0.50 g, 1.60 mmol) and 1-benzylimidazole (0.25 mL, 1.93 mmol) were dissolved in MeCN (10 mL). The mixture was heated at reflux for 24 hours. The solution was allowed to cool to room temperature and excess Et<sub>2</sub>O (90 mL) was added to precipitate a yellow solid. This was filtered and washed with ethyl acetate (100 mL) and (CH<sub>3</sub>)<sub>2</sub>CO (50 mL) to give the product as a white solid which was dried *in vacuo*.

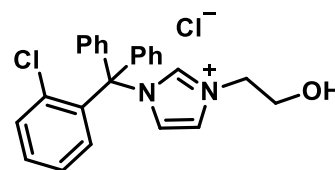


Yield: 0.14 g, 0.3 mmol (20%).

<sup>1</sup>H NMR (300 MHz, CDCl<sub>3</sub>): δ 9.92 (s, 1H, NCHN), 7.49 (s, 1H, NCH), 7.44-7.02 (m, 19H, aromatic), 6.88 (s, 1H, NCH), 5.90 (s, 2H, CH<sub>2</sub>). <sup>13</sup>C{<sup>1</sup>H} NMR (CDCl<sub>3</sub>, 75 MHz): δ 157.7 (C), 138.9 (CH), 138.5 (C), 137.5 (C), 135.4 (C), 133.7 (CH), 132.9 (CH), 131.9 (CH), 131.4 (CH), 129.9 (CH), 129.4 (CH), 129.3 (CH), 129.1 (CH), 129.1 (CH), 127.9 (CH), 123.5 (CH), 122.1 (C), 79.3 (C), 54.1 (CH<sub>2</sub>). HRMS (ESI<sup>+</sup>): Calcd. for C<sub>29</sub>H<sub>24</sub>ClN<sub>2</sub> [M - Cl]<sup>+</sup>: 435.1623. Found: 435.1630. M.P.: 125.8-127.6 °C. Anal. Calcd for C<sub>25</sub>H<sub>22</sub>Cl<sub>2</sub>N<sub>2</sub>·<sup>3</sup>/<sub>5</sub>H<sub>2</sub>O: C, 69.74; H, 5.65; N, 5.61; found: C, 69.90; H, 5.30; N, 6.00.

**8.2.27 Preparation of L13**

2-Chlorotrityl chloride (1.0 g, 3.20 mmol) was dissolved in CH<sub>2</sub>Cl<sub>2</sub> (5 mL) and 1-(2-hydroxyethyl)imidazole (0.30 mL, 3.20 mmol) was added. The solution was heated at 45 °C for 24 hours in a sealed ampoule. Excess C<sub>5</sub>H<sub>12</sub> (100 mL) was added to the solution which had turned yellow, yielding a yellow oil. This was recrystallised from MeOH / C<sub>5</sub>H<sub>12</sub> to obtain the product as a yellow solid.

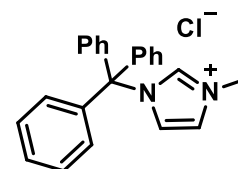


Yield: 1.32 g, 3.1 mmol (97%).

<sup>1</sup>H NMR (300 MHz, acetone-d<sub>6</sub>): δ 8.98 (s, 1H, NCHN), 7.68, 6.91 (s, 1H, HC=CH), 7.87-7.12 (m, 14H, aromatic), 4.41 (t, *J* = 5.1 Hz, 2H, CH<sub>2</sub>), 3.87 (t, *J* = 5.1 Hz, 2H, CH<sub>2</sub>). <sup>1</sup>H NMR (300 MHz, MeOD): δ 9.00 (s, 1H, NCHN), 7.83 (s, 1H, C=CH), 7.64-7.20 (m, 15H, Ar + HC=C), 4.41 (t, *J* = 5.1 Hz, 2H, CH<sub>2</sub>), 3.89 (t, *J* = 5.1 Hz, 2H, CH<sub>2</sub>). <sup>13</sup>C{<sup>1</sup>H} NMR (125 MHz, acetone-d<sub>6</sub>): δ 139.0 (C), 138.2 (CH), 135.4, 133.2 (C-arom), 132.1, 131.8, 130.4, 129.8, 129.3, 128.5, 127.8 (CH-arom), 124.6, 123.8 (CH=CH), 120.6 (C), 79.2 (C), 61.6 (CH<sub>2</sub>), 60.2 (CH<sub>2</sub>). HRMS (ESI<sup>+</sup>): Calcd. for C<sub>24</sub>H<sub>22</sub>ClN<sub>2</sub>O [M - Cl]<sup>+</sup>: 389.1421. Found: 389.1425. M.P.: 172.2-174.6°C. Anal. Calcd for C<sub>24</sub>H<sub>22</sub>Cl<sub>2</sub>N<sub>2</sub>O·<sup>1</sup>/<sub>3</sub> H<sub>2</sub>O: C, 66.83; H, 5.30; N, 6.49. Found: C, 67.20; H, 5.25; N, 6.70.

**8.2.28 Preparation of L14**

Trityl chloride (6.80 g, 24.40 mmol) and 1-methylimidazole (2.0 g, 24.40 mmol) were dissolved in MeCN (20 mL). The mixture was heated at reflux for 24 hours. The white solution was allowed to cool and addition of excess Et<sub>2</sub>O (150 mL) furnished the product as a white solid.

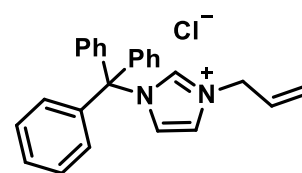


Yield: 6.1 g, 16.9 mmol (69%).

<sup>1</sup>H NMR (300 MHz, CDCl<sub>3</sub>): δ 9.50 (s, 1H, imH), 7.90 (s, 1H, N-CH), 7.42-7.12 (m, 15H, aromatic), 6.97 (s, 1H, N-CH), 4.29 (s, 3H, CH<sub>3</sub>). <sup>13</sup>C{<sup>1</sup>H} NMR (125 MHz, CDCl<sub>3</sub>): δ 147.0(CH), 139.6, 138.0, 135.9 (C-arom), 129.7, 129.3, 129.0, 128.0, 127.9, 127.2, 124.1, 123.8, (CH-arom), 122.1 (CH), 119.9 (CH), 79.5(C), 36.2 (CH<sub>3</sub>). HRMS (ESI<sup>+</sup>): Calcd. For C<sub>23</sub>H<sub>21</sub>N<sub>2</sub> [M - Cl]<sup>+</sup>: 325.1699. Found: 325.1701. M.P.: 162.3-164.5°C. Anal. Calcd for C<sub>23</sub>H<sub>21</sub>ClN<sub>2</sub>·2H<sub>2</sub>O: C, 69.60; H, 6.35; N, 7.06; found: C, 69.80; H, 6.30; N, 7.40.

**8.2.29 Preparation of L15**

Trityl chloride (5.15 g, 18.50 mmol) and 1-allyl-1H-imidazole (0.58 g, 1.49 mmol) were dissolved in CH<sub>2</sub>Cl<sub>2</sub> (20 mL) and heated at reflux for 24 hours. Addition of excess Et<sub>2</sub>O (150 mL) yields the product as a white solid that was dried *in vacuo*.

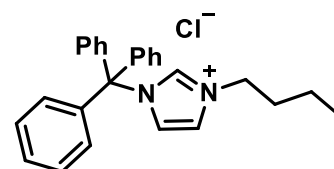


Yield: 3.0 g, 8.4 mmol (45%).

<sup>1</sup>H NMR (300 MHz, CDCl<sub>3</sub>): δ 9.62 (s, 1H, NCHN), 7.81 (s, 1H, N-CH), 7.41-7.11 (m, 15H, aromatic), 6.98 (s, 1H, N-CH), 6.10-5.97 (m, 1H, C=CHallyl), 5.43-5.35 (m, 4H, CH<sub>2</sub>=CH=CH<sub>2</sub>). <sup>13</sup>C{<sup>1</sup>H} NMR (125 MHz, CDCl<sub>3</sub>): δ 139.6 (CH), 138.5 (C), 138.0 (CH), 130.6 (CH), 130.3, 129.6, 129.6, 129.1, 128.9, 128.6, 127.9, 127.6, 126.6, 126.4, 125.7 (C-arom), 123.8 (CH=CH<sub>2</sub>), 122.2 (CH<sub>2</sub>), 52.8 (CH=CH<sub>2</sub>). HRMS (ESI<sup>+</sup>): Calcd. For C<sub>25</sub>H<sub>23</sub>N<sub>2</sub> [M - Cl]<sup>+</sup>: 351.1856. Found: 351.4187. M.P.: 104.8-106.1 °C. Anal. Calcd for C<sub>25</sub>H<sub>23</sub>ClN<sub>2</sub>: C, 72.02; H, 6.37; N, 6.72; found: C, 71.80; H, 6.30; N, 6.90.

**8.2.30 Preparation of L16**

Trityl chloride (4.50 g, 16.12 mmol) and 1-butylimidazole (2.0 g, 16.12 mmol) were dissolved in CH<sub>2</sub>Cl<sub>2</sub> (20 mL) and heated at reflux for 24 hours. Excess Et<sub>2</sub>O was added to the solution to furnish an off white solid. A saturated solution of NaHCO<sub>3</sub> (20 mL) was added to the solid and the product was extracted into CH<sub>2</sub>Cl<sub>2</sub> (20 mL x 3). The organic layers were combined and filtered over magnesium sulfate. Recrystallisation from CH<sub>2</sub>Cl<sub>2</sub> / Et<sub>2</sub>O yielded the product as a white solid which was dried *in vacuo*.

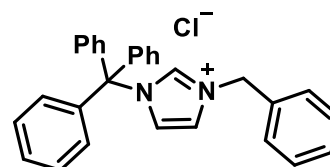


Yield: 3.41 g, 8.5 mmol (53%).

<sup>1</sup>H NMR (300 MHz, CDCl<sub>3</sub>): δ 9.46 (s, 1H, NCHN), 7.99 (s, 1H, HC=C), 7.43-7.03 (m, 15H, aromatic), 7.01 (s, 1H, C=CH), 4.69 (t, *J* = 7.3 Hz, 2H, CH<sub>2</sub>), 1.85 (pent, *J* = 7.3 Hz, 2H, CH<sub>2</sub>), 1.31 (sext, *J* = 7.3 Hz, 2H, CH<sub>2</sub>), 0.97 (t, *J* = 7.3 Hz, 3H, CH<sub>3</sub>). <sup>13</sup>C NMR (75 MHz, CDCl<sub>3</sub>): δ 139.6(CH), 138.1(C), 137.6(CH), 136.3, 135.3, 133.5, 131.3, 130.4, 129.6, 129.3, 128.9, 127.7, 126.3, 125.7, 124.3 (Ar), 123.9, (CH), 50.5, 32.3, 19.5 (CH<sub>2</sub>), 13.5 (CH<sub>3</sub>). HRMS (ESI<sup>+</sup>): Calcd. For C<sub>26</sub>H<sub>27</sub>N<sub>2</sub> [M - Cl]<sup>+</sup>: 367.2169. Found: 367.2119. M.P.: 109.1-111.3 °C. Anal. Calcd for C<sub>26</sub>H<sub>27</sub>ClN<sub>2</sub>·<sup>4</sup>/<sub>3</sub> H<sub>2</sub>O: C, 73.14; H, 7.00; N, 6.56; found: C, 73.10; H, 6.90; N, 6.80.

**8.2.31 Preparation of L17**

Trityl chloride (0.50 g, 1.78 mmol) and 1-benzylimidazole (0.28 g, 1.78 mmol) were dissolved in CH<sub>2</sub>Cl<sub>2</sub> (5 mL). The solution was heated at 45 °C for 24 hours in a sealed ampoule. Excess Et<sub>2</sub>O (60 mL) was added to the solution to give an off white solid which was dried *in vacuo*. A saturated solution of NaHCO<sub>3</sub> (20 mL) was added to the solid and the product was extracted into CH<sub>2</sub>Cl<sub>2</sub> (20 mL x 3). The organic layers were combined and filtered over magnesium sulfate, and excess Et<sub>2</sub>O was added to the solution furnishing the product as a white solid, which was dried *in vacuo*.

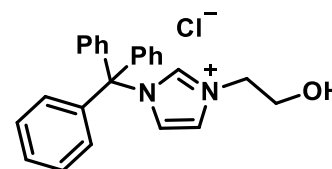


Yield: 0.51 g, 1.2 mmol (65%).

<sup>1</sup>H NMR (500 MHz, CDCl<sub>3</sub>): δ 9.82 (s, 1H, NCHN), 7.71, 6.93 (s, 1H, HC=CH), 7.46-7.11 (m, 20H, aromatic), 5.94 (s, 2H, CH<sub>2</sub>). <sup>13</sup>C{<sup>1</sup>H} NMR (75 MHz, CDCl<sub>3</sub>): δ 138.2(CH), 135.5(C), 129.6, 129.5, 129.4, 129.3, 129.2, 128.9, 127.9, 127.2, 123.7 (Ar), 122.0 (CH), 121.0 (CH), 52.93(CH<sub>2</sub>). HRMS (ESI<sup>+</sup>): Calcd for C<sub>29</sub>H<sub>25</sub>N<sub>2</sub> [M - Cl]<sup>+</sup>: 401.2012. Found: 401.2016. M.P.: 108.4-110.2°C. Anal. Calcd for C<sub>29</sub>H<sub>25</sub>ClN<sub>2</sub>·<sup>5</sup>/<sub>4</sub>H<sub>2</sub>O: C, 75.80; H, 6.03; N, 6.10; found: C, 76.10; H, 5.90; N, 6.50.

**8.2.32 Preparation of L18**

Trityl chloride (0.5 g, 1.8 mmol) was dissolved in CH<sub>2</sub>Cl<sub>2</sub> (5 mL) and 1-(2-hydroxyethyl) imidazole (0.17 mL, 1.80 mmol) was added. The solution was heated at 45°C for 72 hours in a sealed ampoule. A white solid precipitated out of solution, which was filtered off and recrystallised from MeOH / C<sub>5</sub>H<sub>12</sub> (5 mL / 50 mL) furnishing the product as a white solid, which was dried *in vacuo*.

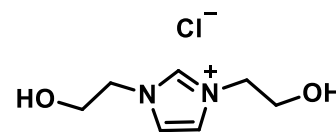


Yield: 0.66 g, 1.7 mmol (94%).

<sup>1</sup>H NMR (300 MHz, MeOD): δ 8.89 (s, 1H, NCHN), 8.24, 7.79 (s, 1H, HC=CH), 7.50-7.24 (m, 15H, Ar), 4.37 (t, 2H, *J* = 5.1 Hz, CH<sub>2</sub>), 4.24 (t, 2H, *J* = 5.1 Hz, CH<sub>2</sub>). <sup>13</sup>C{<sup>1</sup>H} NMR (75 MHz, MeOD): δ 141.4 (C), 139.4 (C), 130.8, 130.3, 129.9 (CH-Ar), 125.5, 123.9 (NCH=CHN), 60.9 (CH<sub>2</sub>), 53.5 (CH<sub>2</sub>). HRMS (ESI<sup>+</sup>): Calcd for C<sub>24</sub>H<sub>23</sub>N<sub>2</sub>O [M - Cl]<sup>+</sup>: 355.1810. Found: 355.1813. M.P.: 156.9-159.1°C. Anal. Calcd for C<sub>24</sub>H<sub>23</sub>ClN<sub>2</sub>O·<sup>1</sup>/<sub>3</sub>H<sub>2</sub>O·<sup>1</sup>/<sub>3</sub>CH<sub>2</sub>Cl<sub>2</sub>: C, 68.73; H, 5.77; N, 6.59; found: C, 69.00; H, 6.00; N, 6.36.

**8.2.33 Preparation of L19**

2-Hydroxyethyl imidazole (0.17 mL, 1.78 mmol) was dissolved in MeCN (2 mL), and 2-chloroethanol (1.0 mL, 14.90 mmol) was added. The mixture was heated at 90 °C for 144 hours in a sealed ampoule. Et<sub>2</sub>O was added to precipitate the product as a yellow oil which was dried *in vacuo*.



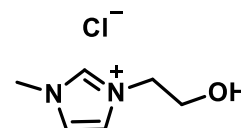
Yield: 0.27 g, 1.4 mmol (79%)

<sup>1</sup>H NMR (300 MHz, MeOD): δ 9.31 (s, 1H, NCHN), 7.95 (s, 1H, HC=C), 7.94 (s, 1H, C=CH), 4.60 (t, *J* = 5.0 Hz, 4H, CH<sub>2</sub>), 4.13 (t, *J* = 5.0 Hz, 4H, CH<sub>2</sub>). <sup>13</sup>C{<sup>1</sup>H} NMR (75 MHz, MeOD): δ 138.0 (NHCN), 124.0 (HC=CH), 61.1, 53.3 (CH<sub>2</sub>). HRMS (ESI<sup>+</sup>): Calcd for C<sub>7</sub>H<sub>13</sub>N<sub>2</sub>O<sub>2</sub> [M - Cl]<sup>+</sup>: 157.0972. Found: 157.0993. IR *v*<sub>max</sub>/ cm<sup>-1</sup> 3289 (OH), 2957, 1157, 1060.

Ligands **L19-L25** are hygroscopic and are mostly oils, hence elemental analysis was not obtained.

**8.2.34 Preparation of L20<sup>10, 11</sup>**

1-Methyl imidazole (1.84 mL, 24.4 mmol) and 2-chloroethanol (1.63 mL, 24.4 mmol) were heated at 100°C in a sealed ampoule for 72 hours. The clear mixture turned dark brown after 24 hours. Excess Et<sub>2</sub>O (30 mL) was added to the mixture and precipitation of the product as a brown oil was aided by sonication. The Et<sub>2</sub>O was decanted and the product was subsequently dried *in vacuo*.

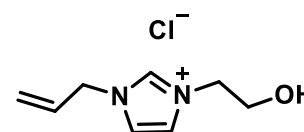


Yield: 3.0 g, 18.5 mmol (76%)

<sup>1</sup>H NMR (300 MHz, D<sub>2</sub>O): δ 8.81 (s, 1H, NCHN), 7.57 (s, 1H, C=CH), 7.51 (s, 1H, C=CH), 4.37 (t, *J* = 5.0 Hz, 2H, CH<sub>2</sub>), 3.98 (t, *J* = 5.0 Hz, 2H, CH<sub>2</sub>), 3.96 (s, 3H, CH<sub>3</sub>). <sup>13</sup>C{<sup>1</sup>H} NMR (75 MHz, D<sub>2</sub>O): δ 136.2 (NCHN), 123.6 (C=C), 122.1 (C=C), 59.8 (CH<sub>2</sub>), 51.6 (CH<sub>2</sub>), 35.9 (CH<sub>3</sub>). HRMS (ESI<sup>+</sup>): Calcd for C<sub>6</sub>H<sub>11</sub>N<sub>2</sub>O [M - Cl]<sup>+</sup>: 127.0866. Found: 127.0866.

**8.2.35 Preparation of L21**

1-(Prop-2-enyl) imidazole (0.48 mL, 5.31 mmol) was dissolved in MeCN (2 mL), and 2-chloroethanol (0.31 mL, 4.62 mmol) was added. The mixture was heated to 90 °C for 24 hours in a sealed ampoule. Addition of Et<sub>2</sub>O (30 mL) precipitates the product as a yellow oil. which was subsequently dried *in vacuo*.

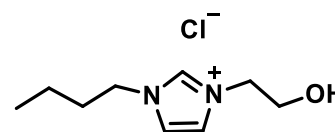


Yield: 0.32 g, 1.7 mmol (32%)

<sup>1</sup>H NMR (300 MHz, MeOD): δ 9.15 (s, 1H, NCHN), 7.76 (s, 1H, HC=C), 7.70 (s, 1H, C=CH), 6.20-6.09 (m, 1H, C=CH,CH<sub>2</sub>), 5.51-5.45 (m, 2H, HC=CH<sub>2</sub>), 4.96 (d, *J* = 6.2 Hz, 2H, CH<sub>2</sub>), 4.40 (t, *J* = 5.0 Hz, 2H, CH<sub>2</sub>), 3.92 (t, *J* = 5.0 Hz, 2H, CH<sub>2</sub>). <sup>13</sup>C{<sup>1</sup>H} NMR (75 MHz, MeOD): δ 137.8 (NHCN), 132.3 (HC=CH<sub>3</sub>), 124.4, 123.7 (HC=CH), 122.0 (N-CH<sub>2</sub>), 61.2, 53.5 (CH<sub>2</sub>), 52.9 (C=CH<sub>2</sub>). HRMS (ESI<sup>+</sup>): Calcd for C<sub>8</sub>H<sub>13</sub>N<sub>2</sub>O [M – Cl + MeOH]<sup>+</sup>: 185.1285. Found: 185.1254. IR *v*<sub>max</sub> / cm<sup>-1</sup> 3333 (OH), 2878, 1645, 1159, 1068.

**8.2.36 Preparation of L22**

1-Butyl imidazole (0.32 mL, 2.4 mmol) was dissolved in MeCN (2 mL), and 2-chloroethanol (0.16 mL, 2.4 mmol) was added. The mixture was heated at 90 °C for 24 hours in a sealed ampoule. Addition of Et<sub>2</sub>O (30 mL) precipitates the product as a yellow oil. The Et<sub>2</sub>O was decanted and the product was subsequently dried *in vacuo*.

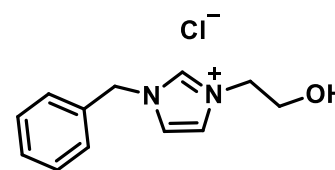


Yield: 0.26 g, 1.3 mmol (53%)

<sup>1</sup>H NMR (300 MHz, MeOD): δ 9.34 (s, 1H, NCHN), 7.92-7.89 (m, 2H, HC=CH), 4.55 (t, *J* = 5.0 Hz, 2H, CH<sub>2</sub>), 4.46 (t, *J* = 7.4 Hz, 2H, CH<sub>2</sub>), 4.06 (t, *J* = 5.0 Hz, 2H, CH<sub>2</sub>), 2.06 (quin, *J* = 7.4 Hz, 2H, CH<sub>2</sub>), 1.53 (sext, *J* = 7.4 Hz, 2H, CH<sub>2</sub>), 1.44 (t, *J* = 7.4 Hz, 3H, CH<sub>3</sub>). <sup>13</sup>C{<sup>1</sup>H} NMR (75 MHz, MeOD): δ 137.6 (NHCN), 124.3, 123.7 (HC=CH), 61.2, 53.4 (CH<sub>2</sub>), 50.7 (CH<sub>2</sub>), 33.2 (CH<sub>2</sub>), 20.5 (CH<sub>2</sub>), 14.0 (CH<sub>3</sub>). HRMS (ESI<sup>+</sup>): Calcd for C<sub>9</sub>H<sub>17</sub>N<sub>2</sub>O [M – Cl]<sup>+</sup>: 169.1335. Found: 169.1339. IR *v*<sub>max</sub> / cm<sup>-1</sup> 3356 (OH), 2962, 1162, 1068.

**8.2.37 Preparation of L23<sup>10</sup>**

1-Benzyl imidazole (0.5 g, 3.2 mmol) dissolved in MeCN (2 mL) and 2-chloroethanol (0.21 mL, 3.2 mmol). The mixture is at 90 °C for 24 hours in a sealed ampoule. Excess Et<sub>2</sub>O (30 mL) was added to the solution to yield the product as a colourless oil. The Et<sub>2</sub>O was decanted and the product was dried *in vacuo*.

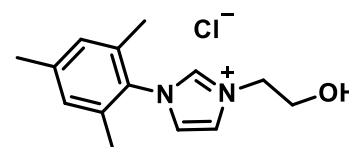


Yield: 0.26 g, 1.1 mmol (34%)

<sup>1</sup>H NMR (300 MHz, MeOD): δ 9.26 (s, 1H, NCHN), 7.74 (s, 1H, C=CH), 7.70 (s, 1H, C=CH), 7.53-7.41 (m, 5H, aromatic), 5.52 (s, 2H, benzyl-CH<sub>2</sub>), 4.39 (t, *J* = 5.0 Hz, 2H, CH<sub>2</sub>), 3.93 (t, *J* = 5.0 Hz, 2H, CH<sub>2</sub>). <sup>13</sup>C{<sup>1</sup>H} NMR (75 MHz, MeOD): δ 137.7 (NCHN), 135.3 (C-arom), 130.3, 130.2, 129.7 (CH-arom), 124.4, 123.5 (HC=CH), 61.0 (CH<sub>2</sub>-benzyl), 54.0, 53.3 (CH<sub>2</sub>). HRMS (ESI<sup>+</sup>): Calcd for C<sub>12</sub>H<sub>15</sub>N<sub>2</sub>O [M – Cl]<sup>+</sup>: 203.1184. Found: 203.1184.

**8.2.38 Preparation of L24<sup>10</sup>**

1-Mesityl imidazole (0.5 g, 2.7 mmol) was dissolved in MeCN (7 mL) and 2-chloroethanol (0.18 mL, 2.7 mmol) added. The mixture was heated at 90°C for 48 hours in a sealed ampoule. Excess Et<sub>2</sub>O (100 mL) was added to the solution which had turned brown yielding a brown solid. The Et<sub>2</sub>O was decanted and the brown solid was dried *in vacuo*.

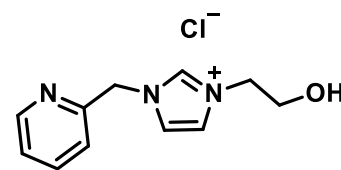


Yield: 0.22 g, 0.8 mmol (31%)

<sup>1</sup>H NMR (300 MHz, DMSO-d<sub>6</sub>): δ 9.42(s, 1H,NCHN), 8.05 (s, 1H, C=CH), 7.92 (s, 1H, C=CH), 7.14 (s, 2H, aromatic), 4.33 (t, 2H, CH<sub>2</sub>), 3.80 (broad s, 2H, CH<sub>2</sub>), 2.33 (s, 3H, CH<sub>3</sub>), 2.02 (s, 6H, CH<sub>3</sub>). <sup>1</sup>H NMR (300 MHz, MeOD): δ 9.27 (s, 1H, NCHN), 7.99 (s, 1H, HC=C), 7.75 (s, 1H, C=CH), 7.15 (s, 2H, Ar), 4.51 (t, *J* = 5.0 Hz, 2H, CH<sub>2</sub>), 3.98 (t, *J* = 5.0 Hz, 2H, CH<sub>2</sub>), 2.38 (s, 3H, CH<sub>3</sub>), 2.12 (s, 6H, CH<sub>3</sub>). <sup>13</sup>C{<sup>1</sup>H} NMR (75 MHz, MeOD): δ 139.1 (NHCN), 130.7 (HC-Ar), 125.3, 124.7 (HC=CH), 60.9, 53.6 (CH<sub>2</sub>), 21.2 (Ar-CH<sub>3</sub>), 17.4 (Ar-CH<sub>3</sub>). HRMS (ESI<sup>+</sup>): calcd for C<sub>14</sub>H<sub>19</sub>N<sub>2</sub>O [M – Cl]<sup>+</sup>: 231.1497. Found: 231.1492.

**8.2.39 Preparation of L25**

2-(1H-imidazol-1-ylmethyl)pyridine (0.5 g, 3.1 mmol) was dissolved in MeCN (2 mL), and 2-chloroethanol (0.20 mL, 3.1 mmol) was added. The mixture was heated at 90 °C for 72 hours in a sealed ampoule. Addition of Et<sub>2</sub>O (50 mL) precipitates the product as a brown oil. The Et<sub>2</sub>O was decanted and the brown oil was dried in *vacuo*.

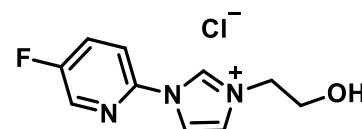


Yield: 0.29 g, 1.2 mmol (39%)

<sup>1</sup>H NMR (300 MHz, MeOD): δ 9.27 (s, 1H, NCHN), 9.02-8.98 (m, 1H, HC=C), 8.58-8.55 (m, 1H, C=CH), 7.93-7.87 (m, 1H, HCN-Ar), 7.76-7.71 (m, 1H, Ar), 7.63-7.58 (m, 1H, Ar), 7.45-7.40 (m, 1H, Ar), 5.64 (s, 2H, CH<sub>2</sub>), 5.05 (s, 1H, OH), 4.42-4.36 (m, 2H, CH<sub>2</sub>), 3.94-3.90 (m, 2H, CH<sub>2</sub>). <sup>13</sup>C{<sup>1</sup>H} NMR (75 MHz, MeOD): δ 154.4 (CN-Ar), 150.9 (HCN-Ar), 139.2 (HC-Ar), 138.5 (NCHN), 125.3, 124.3 (HC=CH), 123.7 (HC-Ar), 120.8 (HC-Ar), 54.8 (CH<sub>2</sub>), 53.5 (CH<sub>2</sub>). HRMS (ESI<sup>+</sup>): Calcd for C<sub>11</sub>H<sub>14</sub>N<sub>3</sub>O [M – Cl]<sup>+</sup>: 204.1131. Found: 204.1131. IR  $\nu_{\max}$  / cm<sup>-1</sup> 3319(OH), 2952, 1476, 1289, 1158, 1065.

**8.2.40 Preparation of L26**

5-fluoro-2-(1H-imidazol-1-yl)pyridine (0.25 g, 1.53 mmol) was dissolved in MeCN (4 mL), and 2-chloroethanol (0.41 mL, 4.24 mmol) was added. The mixture was heated to 90 °C for 144 hours in a sealed ampoule. Addition of Et<sub>2</sub>O (60 mL) precipitates a green oil. The Et<sub>2</sub>O was decanted and the green oil was recrystallised from MeOH / Et<sub>2</sub>O to furnish the product as a pale green solid that was dried in *vacuo*.

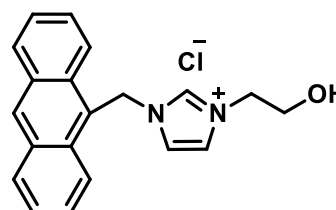


Yield: 0.13 g, 0.5 mmol (35%)

<sup>1</sup>H NMR (300 MHz, MeOD): δ 9.79 (s, 1H, NCHN), 8.47 (d, *J* = 6.0 Hz, 1H, HC=C), 8.30 (d, *J* = 6.0 Hz, 1H, C=CH), 7.99-7.89 (m, 3H, Ar), 4.39 (t, *J* = 5.1 Hz, 2H, CH<sub>2</sub>), 3.90 (t, *J* = 5.1 Hz, 2H, CH<sub>2</sub>). <sup>13</sup>C{<sup>1</sup>H} NMR (75 MHz, MeOD): δ 138.8 (FCCHN), 138.4 (NHCHN), 136.4 (NCN), 128.5, 128.2 (HC=CH), 125.2 (C-F), 120.8 (HC-Ar), 117.1 (HC-Ar), 60.9, 54.0 (CH<sub>2</sub>). HRMS (ESI<sup>+</sup>): calcd for C<sub>10</sub>H<sub>11</sub>FN<sub>3</sub>O [M – Cl]<sup>+</sup>: 208.0881. Found: 208.0888. IR  $\nu_{\max}$  / cm<sup>-1</sup> 3355(OH), 2835, 1546, 1483, 1271, 1078, 1020. Anal. Calcd for C<sub>10</sub>H<sub>11</sub>ClFN<sub>3</sub>O·½ MeCN: C, 46.82; H, 5.18; N, 17.37; found: C, 46.80; H, 4.80; N, 17.70.

### 8.2.41 Preparation of L27

9-(Chloromethyl) anthracene **P8** (0.5 g, 2.2 mmol) was dissolved in MeCN (30 mL) and transferred to an ampoule. 1-(2-hydroxyethyl) imidazole (0.21 mL, 2.2 mmol) was added. The mixture was heated at 90 °C for 24 hours. Excess Et<sub>2</sub>O (200 mL) was added to the orange solution to yield the product as an orange solid. The Et<sub>2</sub>O was decanted and the solid was dried *in vacuo*.

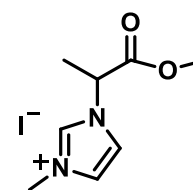


Yield: 0.71 g, 2.1 mmol (95%)

<sup>1</sup>H NMR (300 MHz, CDCl<sub>3</sub>): δ 10.23 (s, 1H, NCHN), 8.61 (s, 1H, aromatic), 8.39 (d, 2H, *J* = 5.3 Hz, aromatic), 8.08 (d, 2H, *J* = 5.3 Hz, aromatic), 7.66 (t, 2H, *J* = 4.7 Hz, aromatic), 7.53 (t, 2H, *J* = 4.7 Hz, aromatic), 7.14 (s, 1H, C=CH), 6.77 (s, 1H, HC=C), 6.55 (s, 2H, CH<sub>2</sub>), 4.41 (t, 2H, *J* = 5.6 Hz, CH<sub>2</sub>), 4.04 (t, 2H, *J* = 5.6 Hz, CH<sub>2</sub>). <sup>13</sup>C{<sup>1</sup>H} NMR (75 MHz, CDCl<sub>3</sub>): δ 137.5 (C), 131.4 (C), 131.1 (C), 130.7 (CH), 129.5 (CH), 128.5 (CH), 125.7 (CH), 122.9 (CH), 122.0 (CH), 121.0 (CH), 59.9 (CH<sub>2</sub>), 52.9 (CH<sub>2</sub>), 46.0 (CH<sub>2</sub>). HRMS (ESI<sup>+</sup>): Calcd for C<sub>20</sub>H<sub>19</sub>N<sub>2</sub>O [M – Cl]<sup>+</sup>: 303.1492. Found: 303.1483. IR ν<sub>max</sub> / cm<sup>-1</sup>: 3233 (OH), 1548-1402 (C-C arom). Anal. Calcd for C<sub>20</sub>H<sub>19</sub>ClN<sub>2</sub>O·<sup>4</sup>/<sub>3</sub> H<sub>2</sub>O·<sup>1</sup>/<sub>3</sub> MeCN: C, 65.92; H, 6.07; N, 8.68; found: C, 66.25; H, 5.90; N, 8.40.

### 8.2.42 Preparation of L28

2-(1-imidazolyl)-propionic acid methyl ester **P28B** (0.4 g, 2.6 mmol) was dissolved in MeOH (5 mL) and methyl iodide (1.0 mL, 34.4 mmol) was added. The mixture was heated at 70 °C in a sealed ampoule for 24 hours. The solvent was removed *in vacuo* to yield the product as a brown oil.



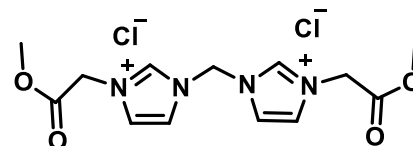
Yield: 0.21 g, 0.7 mmol (27%)

<sup>1</sup>H NMR (300 MHz, MeOD): δ 9.51 (s, 1H, NCHN), 8.07 (s, 1H, C=CH), 7.96 (s, 1H, HC=C), 5.83 (q, *J* = 4.4 Hz, 1H, CH), 4.28 (s, 3H, CH<sub>3</sub>), 4.07 (s, 3H, O-CH<sub>3</sub>), 2.14 (d, *J* = 4.4 Hz, 3H, CH<sub>3</sub>). <sup>1</sup>H NMR (300 MHz, CD<sub>3</sub>CN): δ 9.27 (s, 1H, NCHN), 7.68 (s, 1H, C=CH), 7.58 (s, 1H, HC=C), 5.59 (q, 1H, CH), 3.95 (s, 3H, CH<sub>3</sub>), 3.70 (s, 3H, O-CH<sub>3</sub>), 1.80 (d, 3H, CH<sub>3</sub>). <sup>13</sup>C{<sup>1</sup>H} NMR (75 MHz, MeOD): δ 170.8 (C=O), 139.4 (NCHN), 126.1 (C=C), 122.1 (C=C), 52.4 (N-C-CH<sub>3</sub>), 49.9 (O-CH<sub>3</sub>), 32.0 (N-CH<sub>3</sub>). HRMS (ESI<sup>+</sup>): calcd for C<sub>8</sub>H<sub>13</sub>IN<sub>2</sub>O<sub>2</sub> [M – I]<sup>+</sup>: 169.0972. Found: 169.0969. IR ν<sub>max</sub> / cm<sup>-1</sup>: 1742 (ester C=O), 1222 (ester C-O), 1173,

1076, 747, 658. Anal. Calcd for  $C_8H_{13}IN_2O_2 \cdot 3/2 H_2O$ : C, 29.74; H, 4.99; N, 8.79; found: C, 29.70; H, 4.70; N, 8.50.

### 8.2.43 Preparation of L29

1.1'-methylene-bis-1H-imidazole (0.2 g, 1.35 mmol) dissolved in MeCN (3 mL) and methyl chloroacetate (0.23 mL, 2.7 mmol) was added. The mixture heated at 90°C in a sealed ampoule for 20 hours. The solvent was removed from the solution *in vacuo* to yield a brown oil. Recrystallisation from MeOH / Et<sub>2</sub>O furnished the product as a sticky yellow solid (very hygroscopic).

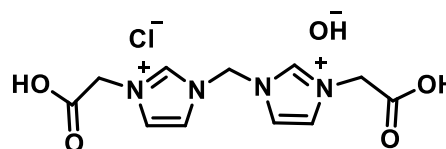


Yield: 0.35 g, 1.0 mmol (71%)

<sup>1</sup>H NMR (300 MHz, MeOD): δ 9.78 (s, 2H, NCHN), 8.20 (s, 2H, C=CH), 7.87 (s, 2H, HC=C), 7.03 (s, 2H, N-CH<sub>2</sub>-N), 5.50-5.25 (m, 4H, N-CH<sub>2</sub>-C=O), 3.85 (s, 6H, O-CH<sub>3</sub>). <sup>1</sup>H NMR (300 MHz, DMSO-d<sub>6</sub>): δ 9.87 (s, 2H, NCHN), 8.30 (s, 2H, C=CH), 7.91 (s, 2H, HC=C), 7.04 (s, 2H, N-CH<sub>2</sub>-N), 5.39 (s, 4H, N-CH<sub>2</sub>-C=O), 3.13 (s, 6H, O-CH<sub>3</sub>). <sup>13</sup>C{<sup>1</sup>H} NMR (75 MHz, MeOD): δ 170.0 (C=O), 140.9 (NCHN), 126.2, 123.2 (C=C), 63.2 (N-CH<sub>2</sub>-N), 53.5 (N-CH<sub>2</sub>-C=O), 49.9 (O-CH<sub>3</sub>). HRMS (ESI<sup>+</sup>): Calcd for C<sub>13</sub>H<sub>17</sub>N<sub>4</sub>O<sub>4</sub> [M - 2Cl]<sup>2+</sup>: 147.0659. Found: 147.0657. IR ν<sub>max</sub> / cm<sup>-1</sup>: 1746 (ester C=O), 1223 (ester C-O), 1167, 748, 619. Anal. Calcd for C<sub>13</sub>H<sub>18</sub>Cl<sub>2</sub>N<sub>4</sub>O<sub>4</sub>·3.5 H<sub>2</sub>O. MeCN: C, 38.39; H, 6.01; N, 14.92; found: C, 38.10; H, 5.60; N, 15.30.

### 8.2.44 Preparation of L30

1.1'-methylene-bis-1H-imidazole (0.3 g, 2.0 mmol) dissolved in MeCN (5 mL) and *tert*-butyl chloroacetate (0.58 mL, 4.0 mmol) added. The mixture was heated at 90°C in a sealed ampoule for 72 hours. Excess Et<sub>2</sub>O (80 mL) was added to the solution which had turned a bluish purple colour to yield a sticky light yellow solid. The Et<sub>2</sub>O was decanted and recrystallisation of the yellow solid from MeCN / Et<sub>2</sub>O furnishes a white solid that is hygroscopic and became sticky within a few minutes after being exposed to air.



Yield: 0.6 g, 1.9 mmol (93%)

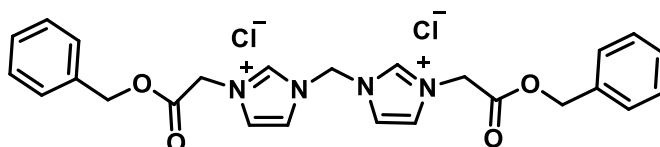
<sup>1</sup>H NMR (300 MHz, CD<sub>3</sub>CN): δ 10.65 (s, 2H, NCHN), 8.72 (s, 2H, C=CH), 7.51 (s, 2H, HC=C), 7.39 (s, 2H, N-CH<sub>2</sub>-N), 5.02 (s, 4H, N-CH<sub>2</sub>-C=O), 1.48 (s, 18H, CH<sub>3</sub>). <sup>13</sup>C{<sup>1</sup>H} NMR (125 MHz, CD<sub>3</sub>CN): δ 165.9 (C=O), 140.5 (NCHN),

125.0(C=C), 123.6 (C=C), 84.9(C-(CH<sub>3</sub>)<sub>3</sub>), 58.4 (N-CH<sub>2</sub>-N), 51.9 (N-CH<sub>2</sub>-C=O), 28.2 (C-(CH<sub>3</sub>)<sub>3</sub>). HRMS (ESI<sup>+</sup>): Calcd for C<sub>11</sub>H<sub>14</sub>N<sub>4</sub>O<sub>4</sub> [M – Cl-OH]<sup>2+</sup>: 133.0502. Found: 133.0534. IR  $\nu_{\max}$  / cm<sup>-1</sup>: 3080, 2977, 2930, (carboxylic acid OH), 1740(carboxylic acid C=O), 1153, 749, 615. Anal. Calcd for C<sub>11</sub>H<sub>15</sub>ClN<sub>4</sub>O<sub>5</sub>·<sup>3</sup>/<sub>2</sub>Et<sub>2</sub>O·<sup>1</sup>/<sub>2</sub> H<sub>2</sub>O: C, 46.52; H, 7.12; N, 12.77; found: C, 46.30; H, 7.30; N, 12.40.

### 8.2.45 Preparation of L31

1,1'-methylene-bis-1H-imidazole (0.3 g, 2.0 mmol) was dissolved in MeCN (5 mL) and benzyl chloroacetate (0.62 mL, 4.0 mmol) was added. The mixture was heated at 90°C in a sealed ampoule for 24 hours. Excess Et<sub>2</sub>O (80 mL) was added to the solution which had turned a bluish purple colour to yield a sticky light yellow solid.

Recrystallisation from MeCN / Et<sub>2</sub>O furnishes a white solid that is hygroscopic and becomes sticky within a few minutes after being exposed to air.

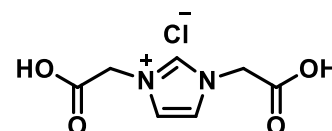


Yield: 0.62 g, 1.2 mmol (59%)

<sup>1</sup>H NMR (300 MHz, MeOD):  $\delta$  9.66 (s, 2H, NCHN), 8.07 (s, 2H, C=CH), 7.86 (s, 2H, HC=C), 7.43-7.40 (m, 10H, aromatic), 6.92 (s, 2H, N-CH<sub>2</sub>-N), 5.37 (s, 4H, N-CH<sub>2</sub>-C=O), 5.32 (s, 4H, CH<sub>2</sub>). <sup>13</sup>C{<sup>1</sup>H} NMR (125 MHz, MeOD):  $\delta$  167.4 (C=O), 136.3 (NCHN), 126.3(C=C), 123.1 (C=C), 69.3(N-CH<sub>2</sub>-N), 60.2 (N-CH<sub>2</sub>-C=O), 51.4 (CH<sub>2</sub>). HRMS (ESI<sup>+</sup>): Calcd for C<sub>16</sub>H<sub>17</sub>N<sub>4</sub>O<sub>2</sub> [M – benzyl acetate-2Cl]<sup>+</sup>: 297.1346. Found: 297.1347. IR  $\nu_{\max}$  / cm<sup>-1</sup>: 3060 (aromatic C=C), 1747 (ester C=O), 1638 (aromatic C-C), 1167 (ester C-O). Anal. Calcd for C<sub>25</sub>H<sub>26</sub>Cl<sub>2</sub>N<sub>4</sub>O<sub>4</sub>: C, 58.03; H, 5.07; N, 10.83; found: C, 58.40; H, 5.10; N, 10.80.

### 8.2.46 Preparation of L32

1H-imidazole (0.2 g, 2.9 mmol), potassium carbonate (0.66 g, 4.8 mmol) and chloroacetic acid (0.56 g, 5.88 mmol) were added. MeCN (30 mL) was added to the mixture and heated at 90°C for 48 hours in a sealed ampoule. The solution was filtered and the solid was washed with CH<sub>2</sub>Cl<sub>2</sub> (30 mL x 3) and MeOH (30 mL x 3). The filtrates were combined and the solvent was removed *in vacuo* to yield the product as a white solid (very hygroscopic).

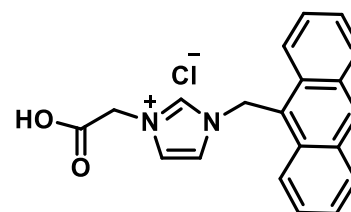


Yield: 0.46 g, 2.1 mmol (70%)

$^1\text{H}$  NMR (300 MHz, MeOD):  $\delta$  9.04 (s, 1H, NCHN), 8.44 (s, 2H, HC=CH), 7.43 (broad s, 4H, CH<sub>2</sub>).  $^{13}\text{C}\{^1\text{H}\}$  NMR (125 MHz, MeOD):  $\delta$  179.4, 174.9, 171.7, 124.0. HRMS (ESI<sup>+</sup>): Calcd for C<sub>7</sub>H<sub>9</sub>N<sub>2</sub>O<sub>4</sub> [M + H]<sup>+</sup>: 185.0557. Found: 185.0559. IR  $\nu_{\text{max}}$  / cm<sup>-1</sup>: 3009, 2923 (carboxylic acid OH), 1692 (carboxylic acid C=O), 1594, 1380. Anal Calcd for C<sub>7</sub>H<sub>9</sub>ClN<sub>2</sub>O<sub>4</sub>·<sup>5</sup>/<sub>2</sub>CH<sub>2</sub>Cl<sub>2</sub>: C, 26.36; H, 3.26; N, 6.47; found: C, 26.20; H, 3.10; N, 6.45.

### 8.2.47 Preparation of L33

**P33** (0.15 g, 0.58 mmol) and chloroacetic acid (0.06 g, 0.58 mmol) were dissolved in MeCN (30 mL) and the mixture was heated at 90°C for 24 hours in a sealed ampoule. A yellow solid precipitated out of solution after one hour of heating. The solution was filtered, and the yellow solid was washed with Et<sub>2</sub>O (90 mL) and dried *in vacuo*. Recrystallisation from CH<sub>2</sub>Cl<sub>2</sub> / Et<sub>2</sub>O and MeCN / Et<sub>2</sub>O precipitated the yellow solid which was filtered and dried *in vacuo* to furnish the product. The product is very hygroscopic and becomes sticky within a few minutes after being exposed to air.

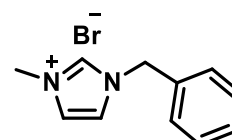


Yield: 0.09 g, 0.3 mmol (46%)

$^1\text{H}$  NMR (300 MHz, CDCl<sub>3</sub>):  $\delta$  11.30 (s, 1H, NCHN), 8.62 (s, 1H, aromatic), 8.31 (d,  $J$  = 8.9 Hz, 2H, aromatic), 8.08 (d,  $J$  = 8.9 Hz, 2H, aromatic), 7.69 (t,  $J$  = 6.6 Hz, 2H, aromatic), 7.69 (t,  $J$  = 6.6 Hz, 2H, aromatic), 6.60 (s, 2H, CH<sub>2</sub>), 5.23 (s, 4H, CH<sub>2</sub>).  $^{13}\text{C}\{^1\text{H}\}$  NMR (75 MHz, DMSO-*d*<sub>6</sub>):  $\delta$  129.9, 129.1, 129.0, 127.5, 127.0, 125.3, 125.1, 123.7, 123.4, 123.1, 122.3, 121.9, 49.9 (CH<sub>2</sub>), 44.8 (CH<sub>2</sub>). HRMS (ESI<sup>+</sup>): Calcd for C<sub>20</sub>H<sub>17</sub>N<sub>2</sub>O<sub>2</sub> [M - Cl]<sup>+</sup>: 317.1285. Found: 317.1288. IR  $\nu_{\text{max}}$  / cm<sup>-1</sup>: 3049, 2833 (carboxylic acid OH), 1711 (carboxylic acid C=O), 1256, 1156. Anal Calcd for C<sub>20</sub>H<sub>17</sub>ClN<sub>2</sub>O<sub>2</sub>·CH<sub>2</sub>Cl<sub>2</sub>·CH<sub>3</sub>CN·<sup>1</sup>/<sub>3</sub>H<sub>2</sub>O. C, 56.98; H, 4.71; N, 8.67; found: C, 56.90; H, 4.80; N, 8.70.

### 8.2.48 Preparation of L34<sup>12</sup>

1-Methyl imidazole (2.91 mL, 36.5 mmol) was dissolved in CH<sub>2</sub>Cl<sub>2</sub> (5 mL) and benzyl bromide (4.35 mL, 36.5 mmol), was added. The mixture was heated at reflux for 24 hours. Et<sub>2</sub>O (50 mL) was added to the solution to furnish a yellow oil. The Et<sub>2</sub>O was decanted and the yellow oil was dried *in vacuo*.

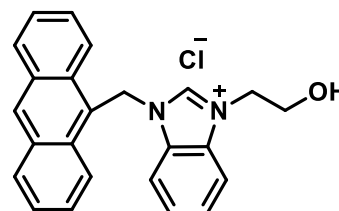


Yield: 7.0 g, 27.7 mmol (76%)

$^1\text{H}$  NMR (300 MHz,  $\text{CDCl}_3$ ):  $\delta$  9.61 (s, 1H, NCHN), 7.19 (s, 1H, C=CH), 7.14 (s, 1H, C=CH), 6.95 (m, 2H, aromatic), 6.70 (m, 3H, aromatic), 5.05 (s, 2H,  $\text{CH}_2$ ), 3.41 (s, 3H,  $\text{CH}_3$ ). HRMS (ESI $^+$ ): Calcd for  $\text{C}_{11}\text{H}_{13}\text{N}_2$  [M - Br] $^+$ : 174.1107. Found: 174.1111.

### 8.2.49 Preparation of L35

Anthracene-methylene benzimidazole (0.1 g, 0.32 mmol) and 2-chloroethanol (2.0 mL, 19.8 mmol) were heated at  $90^\circ\text{C}$  for 24 hours. Excess  $\text{Et}_2\text{O}$  was added to the mixture to yield a yellow solid which was dried *in vacuo*.

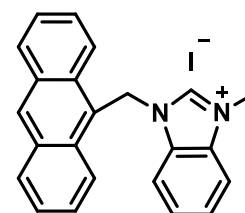


Yield: 0.05 g, 0.13 mmol (40 %)

$^1\text{H}$  NMR (300 MHz,  $\text{CDCl}_3$ ):  $\delta$  10.00 (s, 1H, NCHN), 8.65 (s, 1H, aromatic), 8.47 (m, 2H, aromatic), 8.11 (m, 2H, aromatic), 7.70-7.45 (m, 8H, aromatic), 6.69 (s, 2H,  $\text{CH}_2$ ), 4.55 (m, 2H,  $\text{CH}_2$ ), 4.05 (m, 2H,  $\text{CH}_2$ ). HRMS (ESI $^+$ ): Calcd for  $\text{C}_{24}\text{H}_{21}\text{N}_2\text{O}$  [M - Cl] $^+$ , calcd: 353.1654, found: 353.1681. Anal Calcd for  $\text{C}_{24}\text{H}_{21}\text{ClN}_2\text{O}$ ; C, 74.12; H, 5.44; N, 7.20, Found: C, 73.90; H, 5.60; N, 7.35.

### 8.2.50 Preparation of L36

Anthracene methylene benzimidazole (0.1g, 0.32 mmol) was dissolved in  $\text{CH}_2\text{Cl}_2$  (5 mL) and transferred to an ampoule. A large excess of methyl iodide (1 mL, 16 mmol) was added, and the mixture was heated at  $50^\circ\text{C}$  in the sealed ampoule for 24 hours. Excess  $\text{Et}_2\text{O}$  (100 mL) is added to the solution which had turned a clear orange colour yielding a yellow solid. The solution was filtered, and the solid recrystallised from  $\text{MeCN}/\text{Et}_2\text{O}$  to obtain the product as a bright yellow solid. The solvents were decanted and the solid dried *in vacuo*.

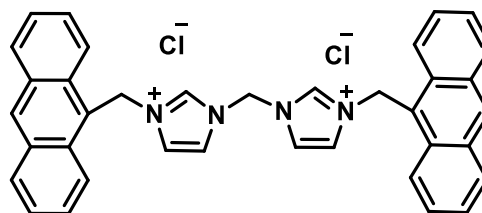


Yield: 0.1 g, 0.2 mmol (69%)

$^1\text{H}$  NMR (500 MHz,  $\text{CDCl}_3$ ):  $\delta$  10.40 (s, 1H, NCHN), 8.62 (s, 1H, aromatic), 8.49-8.46 (m, 2H, aromatic), 8.09-8.07 (m, 2H, aromatic), 7.51-7.41 (m, 8H, aromatic), 6.71 (s, 2H,  $\text{CH}_2$ ), 4.41 (s, 3H,  $\text{CH}_3$ ). HRMS (ESI $^+$ ): Calcd for  $\text{C}_{23}\text{H}_{19}\text{N}_2$  [M - I] $^+$  calcd: 323.1543 found: 323.1547. Anal Calcd for  $\text{C}_{23}\text{H}_{19}\text{IN}_2 \cdot 1/4\text{CH}_2\text{Cl}_2 \cdot 1/4\text{CH}_3\text{CN}$ , 59.21; H, 4.24; N, 6.54, Found: C, 59.00; H, 4.20; N, 6.70.

### 8.2.51 Preparation of L37

**P7** (0.1 g, 0.67 mmol) and 9-chloromethylantracene (0.305 g, 1.35 mmol) were dissolved in MeCN (30 mL). The mixture was heated at 90 °C for 24 hours in a sealed ampoule. A yellow solid precipitated out of solution after one hour of heating. The solution was filtered and the yellow solid was washed with Et<sub>2</sub>O (30 mL x 3) and dried *in vacuo*.

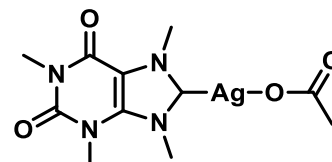


Yield : 0.62 g, 1.0 mmol (77%).

<sup>1</sup>H-NMR (300MHz, DMSO-d<sub>6</sub>): δ 8.94 (s, 2H, NCHN), 7.89 (s, 2H, HC=C), 7.55 (d, 4H, *J* = 8.0 Hz, aromatic), 7.40 (s, 2H, aromatic), 7.34 (d, 4H, , *J* = 8.0 Hz, aromatic), 6.85-6.72 (m, 10H, aromatic), 5.95 (s, 2H, CH<sub>2</sub>), 5.70 (s, 4H, CH<sub>2</sub>). HRMS (ESI<sup>+</sup>): calcd for C<sub>36</sub>H<sub>29</sub>N<sub>4</sub> [M - 2Cl]<sup>+</sup> calc : 530.2459; found: 530.2426. Anal Calcd for C<sub>37</sub>H<sub>30</sub>Cl<sub>2</sub>N<sub>2</sub>·<sup>2</sup>/<sub>3</sub>CH<sub>2</sub>Cl<sub>2</sub>·<sup>1</sup>/<sub>3</sub> CH<sub>3</sub>CN. C, 59.21; H, 4.24; N, 6.54, Found: C, 59.00; H, 4.20; N,6.70.

### 8.2.52 Preparation of C1<sup>8</sup>

**L1** (0.5 g, 2.4 mmol) was added to silver acetate (0.8 g, 4.8 mmol) in anhydrous MeOH (20 mL). The mixture was stirred for 40 minutes in the dark, at room temperature. The mixture was subsequently filtered and washed with MeOH, and the filtrate dried *in vacuo* to give the product as a white solid.

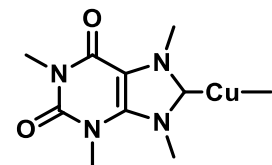


Yield: 0.5 g, 1.3 mmol (54%)

<sup>1</sup>H NMR (300 MHz, D<sub>2</sub>O): δ 4.23 (s, 3H, CH<sub>3</sub>), 4.17 (s, 3H, CH<sub>3</sub>), 3.85 (s, 3H, CH<sub>3</sub>), 3.41 (s, 3H, CH<sub>3</sub>), 1.94 (s, 3H, C=OCH<sub>3</sub>). <sup>13</sup>C{<sup>1</sup>H} NMR (75 MHz, DMSO-d<sub>6</sub>): δ 173.9(C=O), 153.2(C=O), 150.5(C=O), 140.4(C=C), 108.9(C=C), 33.5, 31.4, 30.4, 28.2(N-CH<sub>3</sub>), 23.0 (COCH<sub>3</sub>). HRMS (ESI<sup>+</sup>): Calcd for C<sub>11</sub>H<sub>15</sub>AgN<sub>4</sub>O<sub>4</sub> [M + H]<sup>+</sup> : 377.1453. Found: 377.2954. Anal. Calcd for C<sub>11</sub>H<sub>15</sub>AgN<sub>4</sub>O<sub>4</sub>: C, 35.13; H, 4.29; N, 14.90; found: C, 35.40; H, 4.00; N, 14.70.

### 8.2.53 Preparation of C1.Cu

**L1** (0.4 g, 1.2 mmol) was placed in a three-necked round bottomed flask and dried *in vacuo*. Two copper electrodes were inserted and anhydrous MeCN (50 mL) was cannula transferred into the flask and degassed for 1 hour. A voltage was applied to achieve a current of 30 mA that was maintained for a duration of 1 hour 20 mins by periodically altering the voltage. The product precipitated as a greyish yellow solid which was filtered, washed with MeCN and dried *in vacuo* to yield a pale green solid.

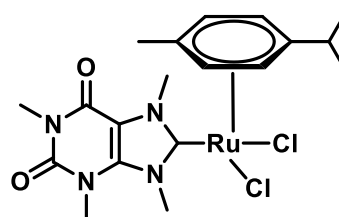


Yield: 0.23 g, 0.6 mmol (48%)

$^1\text{H}$  NMR (300 MHz, DMSO- $d_6$ ):  $\delta$  3.35, 3.18, 2.90, 2.41 (s, 3H, CH<sub>3</sub>).  $^{13}\text{C}\{^1\text{H}\}$  NMR (75 MHz, DMSO- $d_6$ ):  $\delta$  153.1(C=O), 150.3(C=O), 140.0(C=C), 108.3(C=C), 38.0, 36.7, 31.4, 28.1 (N-CH<sub>3</sub>). Anal. Calcd for C<sub>9</sub>H<sub>12</sub>CuIN<sub>4</sub>O<sub>2</sub>: C, 27.11; H, 3.03; N, 14.05. Found: C, 27.90; H, 3.10, N, 14.20.

### 8.2.54 Preparation of C1.Ru

**L1** (0.05 g, 0.15 mmol), silver oxide (0.018g, 0.075 mmol) and [Ru(*p*-cymene)Cl<sub>2</sub>]<sub>2</sub> (0.046 g, 0.075 mmol) were added to a Schlenk flask with activated 4Å molecular sieves and degassed. Anhydrous MeCN (8 mL) and CH<sub>2</sub>Cl<sub>2</sub> (10 mL) were transferred to the Schlenk flask and the mixture was heated at 40°C for 2 hours. The solution which had turned a clear orange colour was filtered through celite, and the solvent was removed *in vacuo* to yield the product as an orange solid.

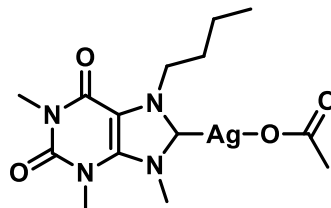


Yield: 0.025 g, 0.05 mmol (30%)

$^1\text{H}$  NMR (300 MHz, CDCl<sub>3</sub>):  $\delta$  5.48 (d,  $J$  = 6.0 Hz, 2H, aromatic), 5.24 (d,  $J$  = 6.0 Hz, 2H, aromatic), 4.34 (s, 3H, CH<sub>3</sub>), 4.29 (s, 3H, CH<sub>3</sub>), 3.78 (s, 3H, CH<sub>3</sub>), 3.40 (s, 3H, CH<sub>3</sub>), 2.15 (s, 3H, CH<sub>3</sub>), 2.97 (sept,  $J$  = 6.0 Hz, 1H, CH), 1.30 (d,  $J$  = 6.0 Hz, 6H, CH(CH<sub>3</sub>)<sub>3</sub>). HRMS (ESI<sup>+</sup>): Calcd for C<sub>19</sub>H<sub>26</sub>Cl<sub>2</sub>N<sub>4</sub>O<sub>2</sub>Ru [M - Cl]<sup>+</sup>: 479.0788. Found: 479.0810. Anal. Calcd for C<sub>19</sub>H<sub>26</sub>Cl<sub>2</sub>N<sub>4</sub>O<sub>2</sub>Ru·2H<sub>2</sub>O: C, 41.46; H, 5.49; N, 10.18. Found: C, 41.70; H, 5.10, N, 10.20.

### 8.2.55 Preparation of C2

**L2** (0.10 g, 0.26 mmol) and silver acetate (0.09 g, 1.54 mmol) were dissolved in a solvent mixture anhydrous MeOH (5 mL) and CH<sub>2</sub>Cl<sub>2</sub> (5 mL). The mixture was stirred for two hours in the dark. The solution was filtered and washed with CH<sub>2</sub>Cl<sub>2</sub>, and the filtrate dried *in vacuo* to give a white sticky solid. Recrystallisation from CH<sub>2</sub>Cl<sub>2</sub> / C<sub>5</sub>H<sub>9</sub> rendered the product as a white solid which was dried *in vacuo*.

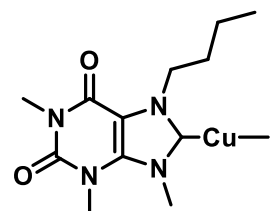


Yield: 0.06 g, 0.14 mmol (55%)

<sup>1</sup>H NMR (300 MHz, CDCl<sub>3</sub>): δ 4.44 (t, *J* = 7.4 Hz, 2H, CH<sub>2</sub>), 4.21 (s, 3H, CH<sub>3</sub>), 3.81 (s, 3H, CH<sub>3</sub>), 3.39 (s, 3H, CH<sub>3</sub>), 1.79 (quin, *J* = 7.35 Hz, 2H, CH<sub>2</sub>), 1.37 (sext, *J* = 7.4 Hz, 2H, CH<sub>2</sub>), 0.93 (t, 3H, CH<sub>3</sub>). <sup>13</sup>C{<sup>1</sup>H} NMR (75 MHz, CDCl<sub>3</sub>): δ 152.8(C=O), 150.4 (C=O), 140.2 (C), 109.2 (C), 53.2(C=O, acetate), 51.5(CH<sub>3</sub>), 39.6 (CH<sub>2</sub>), 33.5 (CH<sub>3</sub>), 32.0 (CH<sub>3</sub>), 28.4(CH<sub>2</sub>), 22.04(CH<sub>2</sub>), 19.4(CH<sub>3</sub>), 13.8(CH<sub>3</sub>). <sup>13</sup>C{<sup>1</sup>H} NMR (75 MHz, DMSO-*d*<sub>6</sub>): δ 185.2 (Ag-C), 152.7(C=O), 150.3 (C=O), 140.6 (C), 107.9 (C), 53.2(C=O, acetate), 50.0 (CH<sub>3</sub>), 39.6 (CH<sub>2</sub>), 32.9 (CH<sub>3</sub>), 31.3 (CH<sub>3</sub>), 28.4 (CH<sub>2</sub>), 22.04 (CH<sub>2</sub>), 18.9 (CH<sub>3</sub>), 13.4(CH<sub>3</sub>). ). HRMS (ESI<sup>+</sup>): Calcd for C<sub>24</sub>H<sub>36</sub>AgN<sub>8</sub>O<sub>4</sub> [2M + H]<sup>+</sup> : 608.1910. Found: 608.1939. Anal. Calcd for C<sub>14</sub>H<sub>22</sub>AgN<sub>4</sub>O<sub>4</sub>: C, 40.21; H, 5.30; N, 13.40. Found: C, 39.90; H, 5.30, N, 13.10.

### 8.2.56 Preparation of C2.Cu

**L2** (0.3g, 0.79 mmols) was placed in a 3 necked round bottomed flask. Two copper electrodes were inserted and anhydrous MeCN (15 mL) was cannula transferred into the flask and degassed for one hour. A voltage was applied to achieve a current of 30 mA that was maintained for a duration of 1 hour 20 mins by periodically altering the voltage. After one hour the complex started to precipitate out of solution. The solution filtered through celite and the solvent was removed from the filtrate *in vacuo* yielding the product a light grey solid.



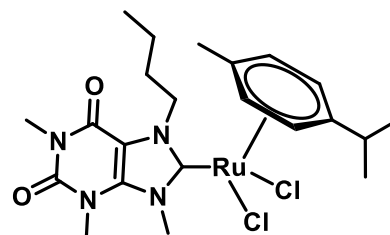
Yield: 0.07 g, 0.16 mmol (20%)

<sup>1</sup>H NMR (300 MHz, DMSO-*d*<sub>6</sub>): δ 4.42 (t, *J* = 7.5 Hz, 2H, CH<sub>2</sub>), 4.17(s, 3H, CH<sub>3</sub>), 3.73 (s, 3H, CH<sub>3</sub>), 3.24 (s, 3H, CH<sub>3</sub>), 1.75 (quin, *J* = 7.5 Hz, 2H, CH<sub>2</sub>), 1.35 (sext, *J* = 7.5 Hz, 2H, CH<sub>2</sub>), 0.91 (t, *J* = 7.5 Hz, 3H, CH<sub>3</sub>). <sup>13</sup>C{<sup>1</sup>H} NMR (75 MHz, DMSO-*d*<sub>6</sub>): δ 152.9(C=O), 152.4(C=O), 151.1(C=C), 150.2(C=C), 41.3, 38.1,

32.9, 27.7 (N-CH<sub>3</sub>), 31.3, 31.1, 29.9 (CH<sub>2</sub>) . HRMS (ESI<sup>+</sup>): calcd for C<sub>12</sub>H<sub>18</sub>CuN<sub>4</sub>O<sub>2</sub> [M - I + MeCN]<sup>+</sup> : 355.1070. Found: 355.0985. Anal. Calcd for C<sub>12</sub>H<sub>18</sub>CuIN<sub>4</sub>O<sub>2</sub>: C, 32.70; H, 4.12; N, 12.71. Found: C, 32.77; H, 4.12, N,12.40.

### 8.2.57 Preparation of C2.Ru

**L2** (0.1g, 0.26 mmol), silver oxide (0.031g, 0.135mmol) and [Ru(*p*-cymene)Cl<sub>2</sub>]<sub>2</sub> (0.081g, 0.135 mmol) were added to an ampoule with activated molecular sieves 4Å and degassed. Anhydrous CH<sub>2</sub>Cl<sub>2</sub> (20 mL) were transferred to the ampoule and the mixture was heated at 40°C for 1.5 hours. The solution which was a golden orange colour was filtered through celite, and the solvent was removed from filtrate *in vacuo* to yield the product as a golden orange solid.

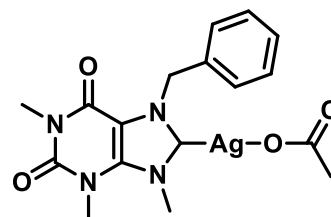


Yield: 0.065 g, 0.11 mmol (44%)

<sup>1</sup>H NMR (300 MHz, CDCl<sub>3</sub>): δ 5.45 (d, *J* = 6.0 Hz, 2H, aromatic), 5.17 (d, *J* = 6.0 Hz, 2H, aromatic), 4.57 (t, *J* = 7.5 Hz, CH<sub>2</sub>), 4.25(s, 3H, CH<sub>3</sub>), 3.73 (s, 3H, CH<sub>3</sub>), 3.37 (s, 3H, CH<sub>3</sub>), 2.94 (sept, *J* = 7.5 Hz, 1H, CH), 2.06 (s, 3H, CH<sub>3</sub>), 1.79 (broad s, 2H, CH<sub>2</sub>), 1.44 (broad s, 2H, CH<sub>2</sub>), 1.28 (d, *J* = 6.0 Hz, 6H, CH(CH<sub>3</sub>)<sub>3</sub>), 0.95 (t, *J* = 7.50 Hz, CH<sub>3</sub>) . HRMS (ESI<sup>+</sup>): calcd for C<sub>22</sub>H<sub>32</sub>ClN<sub>4</sub>O<sub>2</sub>Ru [M - Cl]<sup>+</sup> : 521.1257. Found: 521.1347. Anal. Calcd for C<sub>22</sub>H<sub>32</sub>Cl<sub>2</sub>N<sub>4</sub>O<sub>2</sub>Ru·H<sub>2</sub>O: C, 45.99; H, 5.97; N, 9.75. Found: C, 46.10; H, 5.70, N, 9.90.

### 8.2.58 Preparation of C3

**L3** (0.25 g, 0.61 mmol) was added to silver acetate (0.2 g, 1.2 mmol) in a solvent mixture of anhydrous CH<sub>2</sub>Cl<sub>2</sub> (5 mL) and MeOH (5 mL). The mixture was stirred at room temperature for two hours in the dark. The solution was filtered and the solid washed with CH<sub>2</sub>Cl<sub>2</sub> (30 mL). The solvent was removed from the filtrate *in vacuo* to give the product as a white solid.



Yield: 0.11 g, 0.25 mmol (40%)

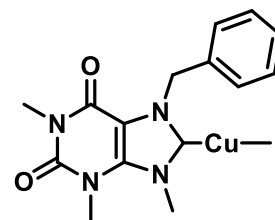
<sup>1</sup>H NMR (300 MHz, CDCl<sub>3</sub>): δ 7.45 (d, 2H, aromatic), 7.30-7.23 (m, 3H, aromatic), 5.63 (s, 2H, CH<sub>2</sub>), 4.18 (s, 3H, CH<sub>3</sub>), 3.76 (s, 3H, CH<sub>3</sub>), 3.34 (s, 3H, CH<sub>3</sub>). <sup>13</sup>C{<sup>1</sup>H} NMR (75 MHz, CDCl<sub>3</sub>): δ 185.5 (Ag-C), 178.2 (C=O), 153.1(C=O), 150.6 (C=O), 140.3 (C), 135.5(C-arom), 129.0, 128.7, 128.4, (CH, aromatic), 109.2 (C), 54.2(CH<sub>3</sub>), 40.0 (CH<sub>3</sub>), 32.0 (CH<sub>3</sub>), 28.8(CH<sub>2</sub>), 22.3 (CH<sub>3</sub>).

HRMS (ESI<sup>+</sup>): Calcd for C<sub>30</sub>H<sub>32</sub>AgN<sub>8</sub>O<sub>4</sub> [Ag(NHC)<sub>2</sub>]<sup>+</sup> : 675.1597. Found: 675.1616. Anal. Calcd for C<sub>17</sub>H<sub>20</sub>AgN<sub>4</sub>O<sub>4</sub>: C, 45.25; H, 4.24; N, 12.42. Found: C, 45.30; H, 4.20, N, 12.20

### 8.2.59 Preparation of C3.Cu

**L3** (0.2 g, 0.49 mmols) was placed in a three-necked round bottomed flask and degassed. Two copper electrodes were inserted and anhydrous MeCN (70 mL) was transferred into the flask and degassed for 1h.

A voltage was applied to achieve a current of 30 mA that was maintained for a duration of 1 hour 20 mins by periodically altering the voltage. After 1h the complex started to precipitate out of solution. The solution was filtered through celite and filtrate dried in *vacuo* yielding a pale grey solid.



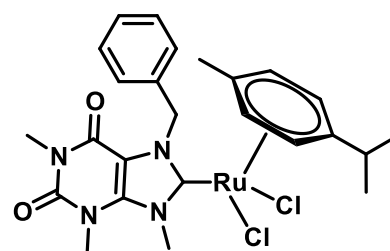
Yield: 0.16 g, 0.34 mmol (69%)

<sup>1</sup>H NMR (300 MHz, DMSO-d<sub>6</sub>): δ 7.39-7.27 (m, 5H, aromatic), 5.64 (s, 2H, CH<sub>2</sub>), 4.14 (s, 3H, CH<sub>3</sub>), 3.71 (s, 3H, CH<sub>3</sub>), 3.20 (s, 3H, CH<sub>3</sub>). <sup>13</sup>C{<sup>1</sup>H} NMR (75 MHz, DMSO-d<sub>6</sub>): δ 156.2(C=O), 153.0(C=O), 141.1(C=C), 137.0(C=C), 129.4, 128.4, 127.6, 117.9 (aromatic), 51.3(CH<sub>2</sub>), 38.3, 31.5, 28.1 (N-CH<sub>3</sub>). HRMS (ESI<sup>+</sup>): Calcd for C<sub>15</sub>H<sub>16</sub>CuN<sub>4</sub>O<sub>2</sub> [M – I + MeCN]<sup>+</sup> : 389.0913. Found: 389.0832. Anal. Calcd for C<sub>15</sub>H<sub>16</sub>CuN<sub>4</sub>O<sub>2</sub>: C, 37.95; H, 3.40; N, 11.80. Found: C, 38.00; H, 3.62, N, 11.79.

### 8.2.60 Preparation of C3.Ru

**L3** (0.05g, 0.12 mmol), silver oxide (0.014g, 0.062mmol) and [Ru(*p*-cymene)Cl<sub>2</sub>]<sub>2</sub> (0.038 g, 0.062 mmol) were added to an ampoule with activated molecular sieves 4Å and degassed.

Anhydrous CH<sub>2</sub>Cl<sub>2</sub> (10 mL) was transferred to the ampoule and the mixture was heated at 40°C for 1.5 hours. The solution which was a golden orange colour was filtered through celite, and the filtrate was dried in *vacuo* to yield the product as a golden orange solid.



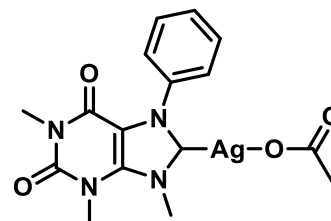
Yield: 0.021 g, 0.035 mmol (29%)

<sup>1</sup>H NMR (300 MHz, CDCl<sub>3</sub>): δ 7.40-7.01 (m, 5H, aromatic) 5.48 (d, *J* = 6.0 Hz, 2H, CH<sub>2</sub>), 5.28 (broad s, 4H, aromatic), 4.38 (s, 3H, CH<sub>3</sub>), 3.83 (s, 3H, CH<sub>3</sub>), 3.32 (s, 3H, CH<sub>3</sub>), 2.90 (sept, *J* = 6.0 Hz, 1H, CH), 2.04 (s, 3H, CH<sub>3</sub>), , 1.23 (d, *J* = 6.0 Hz, 6H, CH(CH<sub>3</sub>)<sub>3</sub>), 0.95 (t, *J* = 7.50 Hz, CH<sub>3</sub>) . HRMS (ESI<sup>+</sup>): calcd for

$C_{25}H_{30}ClN_4O_2Ru [M - Cl]^+$  : 555.1101. Found: 555.1358. Anal. Calcd for  $C_{19}H_{26}Cl_2N_4O_2Ru \cdot 2H_2O$ : C, 47.92; H, 5.47; N, 8.94. Found: C, 47.60; H, 5.10, N, 8.60.

### 8.2.61 Preparation of C4

**L4** (0.15 g, 0.38 mmol) was added to silver acetate (0.125 g, 0.75 mmol) in a solvent mixture of anhydrous MeCN (5 mL) and MeOH (5 mL). The mixture was stirred at room temperature for two hours in the dark. The mixture was filtered and the filtrate dried *in vacuo* to yield the product as a white solid.

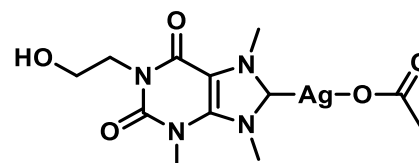


Yield: 0.115 g, 0.26 mmol (69%)

$^1H$  NMR (300 MHz, DMSO- $d_6$ ):  $\delta$  7.52-7.34 (m, 5H, aromatic), 4.28 (s, 3H, CH<sub>3</sub>), 3.81 (s, 3H, CH<sub>3</sub>), 3.71 (s, 3H, CH<sub>3</sub>), 3.62 (s, 3H, CH<sub>3</sub>).  $^{13}C\{^1H\}$  NMR (75 MHz, CDCl<sub>3</sub>):  $\delta$  186.1(Ag-C), 175.5 (C=O, acetate), 152.0(C=O), 150.0 (C=O), 141.1 (C=C), 137.6(C-aromatic), 129.3(CH-aromatic), 128.8 (CH-aromatic), 126.5(CH-aromatic), 109.2 (C=C), 31.6(CH<sub>3</sub>), 28.3(CH<sub>3</sub>), 23.2(CH<sub>3</sub>). HRMS (ESI<sup>+</sup>): Calcd for  $C_{28}H_{28}AgN_8O_4 [2M-Ag]^+$  : 647.1279. Found: 647.1297. Anal. Calcd for  $C_{16}H_{17}AgN_4O_4$  : C, 43.96; H,3.92; N,12.82. Found: C, 44.70; H, 4.40, N,12.60.

### 8.2.62 Preparation of C5

**L5** (0.1g, 0.27 mmol) was added to silver acetate (0.09g, 0.54 mmol) in a solvent mixture of anhydrous CH<sub>2</sub>Cl<sub>2</sub> (5 mL) and MeOH (5 mL). The mixture was stirred at room temperature for two hours in the dark. The mixture was filtered and washed with CH<sub>2</sub>Cl<sub>2</sub> and the filtrate dried *in vacuo* to give a white solid. Recrystallisation from MeOH / Et<sub>2</sub>O furnishes the product as a white solid.

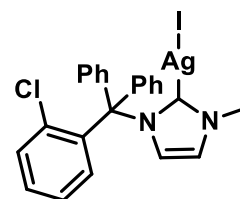


Yield: 0.03 g, 0.07 mmol (28%)

$^1H$  NMR (300 MHz, MeOD):  $\delta$  4.47 (broad s, 1H, OH), 4.18 (s, 3H, CH<sub>3</sub>), 4.15 (t,  $J$  = 6.0 Hz, 2H, CH<sub>2</sub>), 4.09 (s, 3H, CH<sub>3</sub>), 3.79 (s, 3H, CH<sub>3</sub>), 3.75 (t,  $J$  = 6.0 Hz, 2H, CH<sub>2</sub>), 3.53 (s, 3H, CH<sub>3</sub>).  $^{13}C$  NMR (75 MHz,  $d_4$ -MeOD):  $\delta$  179.7 (C=O, acetate), 143.9 (C), 123.8(C), 82.8 (CH<sub>2</sub>), 60.2 (CH<sub>2</sub>), 40.3 (CH<sub>3</sub>), 34.5(CH<sub>3</sub>), 32.9(CH<sub>3</sub>), 23.6 (CH<sub>3</sub>-acetate). HRMS (ESI<sup>+</sup>): Calcd for  $C_{20}H_{28}AgN_8O_6 [2M-Ag]^+$  Calc: 585.3625, found: 585.1187. Anal. Calcd for  $C_{11}H_{17}AgN_4O_5 \cdot \frac{1}{4} Et_2O$  : C, 36.85; H,4.64; N,13.22. Found: C,36.50; H,4.50, N,13.60.

### 8.2.63 Preparation of C6

**L6** (0.40 g, 0.84 mmol) and silver oxide (0.19g, 0.84 mmol) were dissolved in  $\text{CH}_2\text{Cl}_2$  (40 mL) and heated at reflux for 24 hours in the dark. The solution was filtered through celite, and the solid washed with  $\text{CH}_2\text{Cl}_2$  (30 mL). The filtrate was dried *in vacuo* to give the product as a white crystalline solid.

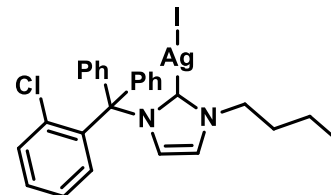


Yield: 0.21 g, 0.35 mmol (42%).

$^1\text{H}$  NMR (300 MHz,  $\text{CDCl}_3$ ):  $\delta$  7.34 – 6.95 (m, 16H, aromatic), 3.88 (s, 3H,  $\text{CH}_3$ ).  $^{13}\text{C}\{^1\text{H}\}$  NMR (75 MHz,  $\text{DMSO-d}_6$ ):  $\delta$  139.8 (C), 134.8 (C), 132.2 (C), 131.0 (CH), 130.2 (CH), 128.2 (CH), 128.1 (CH), 127.8 (CH), 123.2 (CH), 121.1 (CH), 118.5 (CH), 76.8 (CH), 40.1 ( $\text{CH}_3$ ). HRMS (ESI<sup>+</sup>): Calcd for  $\text{C}_{46}\text{H}_{38}\text{AgCl}_2\text{N}_4$  [2M –  $\text{AgI}_2$ ]<sup>+</sup> calcd: 825.1521 found: 825.1532. Anal. Calcd for  $\text{C}_{23}\text{H}_{19}\text{AgClIN}_2 \cdot 3/2 \text{CH}_2\text{Cl}_2$ : C, 40.81; H, 3.08; N, 3.89. Found: C, 40.90; H, 3.20; N, 4.10.

### 8.2.64 Preparation of C7

**L7** (0.15 g, 0.28 mmol) and silver oxide (0.07g, 0.28 mmol) were dissolved in  $\text{CH}_2\text{Cl}_2$  (15 mL) and heated at reflux for 24 hours in the dark. The solution was filtered through celite, and the solid washed with  $\text{CH}_2\text{Cl}_2$  (20 mL). The filtrate was dried *in vacuo* to give a yellow solid. The solid was recrystallised from  $\text{CH}_2\text{Cl}_2/\text{C}_5\text{H}_9$ , the solvent was decanted and the solid was dried *in vacuo* to yield the product as a yellow solid.

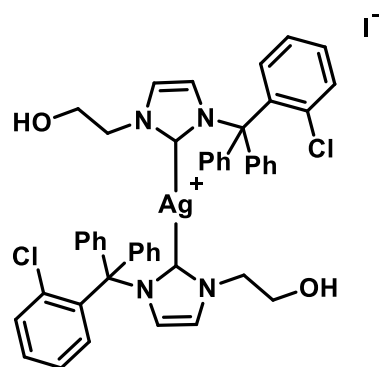


Yield: 0.08 g, 0.13 mmol (47%).

$^1\text{H}$  NMR (300 MHz,  $\text{CDCl}_3$ ):  $\delta$  7.45-7.09 (m, 15H, Ar + N-CH), 6.96 (s, 1H, N-CH), 4.15 (t,  $J = 7.5$  Hz, 2H, N- $\text{CH}_2\text{CH}_2\text{CH}_2\text{CH}_3$ ), 1.80 (quin,  $J = 7.5$  Hz, 7.3Hz, 2H,  $\text{CH}_2$ ), 1.32 (sext,  $J = 7.5$  Hz, 2H,  $\text{CH}_2$ ), 0.94 (t,  $J = 7.5$  Hz, 3H,  $\text{CH}_3$ ).  $^{13}\text{C}\{^1\text{H}\}$  NMR (75 MHz,  $\text{CDCl}_3$ ):  $\delta$  141.1 (C), 140.0 (C), 135.8 (C), 131.6 (CH), 130.7 (CH), 130.6 (CH), 128.5 (CH), 128.2 (CH), 128.1 (CH), 123.6 (CH), 118.2 (CH), 77.8 (C), 53.6 ( $\text{CH}_2$ ), 33.5 ( $\text{CH}_2$ ), 19.7 ( $\text{CH}_2$ ), 13.8 ( $\text{CH}_3$ ). HRMS (ESI<sup>+</sup>): calcd for  $\text{C}_{52}\text{H}_{50}\text{AgCl}_2\text{N}_4$  [2M- $\text{AgI}_2$ ]<sup>+</sup> calcd: 909.2460 found: 909.2609. Anal. Calcd for  $\text{C}_{26}\text{H}_{25}\text{AgClIN}_2 \cdot 2/3 \text{C}_5\text{H}_{12}$ : C, 51.52; H, 4.86; N, 4.10. Found: C, 51.90; H, 5.20; N, 4.00.

### 8.2.65 Preparation of C8

**L8** (0.32 g, 0.63 mmol) and silver oxide (0.14g, 0.63 mmol) were dissolved in CH<sub>2</sub>Cl<sub>2</sub> (30 mL) and heated at reflux for 24 hours in the dark. The solution was filtered through celite, and the solid washed with CH<sub>2</sub>Cl<sub>2</sub>. The solvent was removed from the filtrate *in vacuo* to yield the product as a white solid.

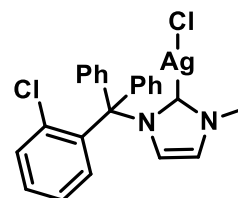


Yield: 0.12 g, 0.13 mmol (21%).

<sup>1</sup>H NMR (300 MHz, DMSO-d<sub>6</sub>): δ 8.63 (s, 1H, HC=CH) 7.59-6.96 (m, 15H, aromatic + HC=CH), 4.24 (t, *J* = 6.0 Hz, 2H, CH<sub>2</sub>), 3.67 (t, *J* = 6.0 Hz, 2H, CH<sub>2</sub>). <sup>13</sup>C{<sup>1</sup>H} NMR (75 MHz, CDCl<sub>3</sub>): δ 138.6 (C), 136.2 (C), 135.6 (C), 133.1 (CH), 131.3 (CH), 130.9 (CH), 129.9 (CH), 129.5 (CH), 129.0 (CH), 127.7 (CH), 122.9 (CH) 120.7 (CH), 78.4 (C), 61.0 (CH<sub>2</sub>), 54.4 (CH<sub>2</sub>). HRMS (ESI<sup>+</sup>): Calcd for C<sub>48</sub>H<sub>42</sub>AgCl<sub>2</sub>N<sub>4</sub>O<sub>2</sub> [2M-AgI<sub>2</sub>]<sup>+</sup> 887.1883. Found: 887.1864. Anal. Calcd for 3(C<sub>48</sub>H<sub>42</sub>AgCl<sub>2</sub>IN<sub>4</sub>O<sub>2</sub>)·1(C<sub>24</sub>H<sub>21</sub>AgClIN<sub>2</sub>O): C, 55.22; H, 4.11; N, 5.31; found: C, 55.11; H, 4.05; N, 5.36.

### 8.2.66 Preparation of C9

**L12** (0.50 g, 1.27 mmol) and silver oxide (0.29 g, 1.27 mmol) were dissolved in CH<sub>2</sub>Cl<sub>2</sub> (10 mL) and heated at reflux for 24 hours in the dark. The mixture was allowed to cool before it was filtered through celite, and the solid washed with CH<sub>2</sub>Cl<sub>2</sub>. The solvent was removed from the filtrate *in vacuo* to give the product as a white crystalline solid.

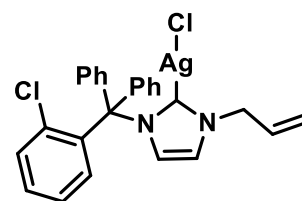


Yield: 0.40 g, 0.8 mmol (62%).

<sup>1</sup>H NMR (300 MHz, CDCl<sub>3</sub>): δ 7.44-7.42 (m, 2H, C=CH + aromatic), 7.36-7.09 (m, 14H, aromatic), 6.95 (m, 1H, HC=C), 3.88 (s, 3H, CH<sub>3</sub>). <sup>13</sup>C{<sup>1</sup>H} NMR (75MHz, CDCl<sub>3</sub>): δ 140.9 (C), 140.0 (C), 135.7 (C), 132.5 (CH), 131.5 (CH), 130.6 (CH), 130.5 (CH), 128.4 (CH), 128.1 (CH), 127.8 (CH), 123.6 (CH), 119.7 (CH), 77.7 (C), 40.2 (CH<sub>3</sub>). HRMS (ESI<sup>+</sup>): calcd for C<sub>46</sub>H<sub>38</sub>AgCl<sub>2</sub>N<sub>4</sub> [2M-AgCl<sub>2</sub>]<sup>+</sup> : 825.1521. Found: 825.1520. Anal. Calcd for C<sub>23</sub>H<sub>19</sub>AgClIN<sub>2</sub>·<sup>3</sup>/<sub>2</sub> H<sub>2</sub>O: C, 52.20; H, 4.19; N, 5.29; found: C, 52.00; H, 4.30; N, 4.90.

### 8.2.67 Preparation of C10

**L10** (0.30g, 0.71 mmol) and silver oxide (0.17 g, 0.71 mmol) were dissolved in  $\text{CH}_2\text{Cl}_2$  (8 mL) and heated at reflux for 24 hours in the dark. The mixture was allowed to cool before it was filtered through celite, and the solid washed with  $\text{CH}_2\text{Cl}_2$  (20 mL). The filtrate was dried *in vacuo* to give the product as a white solid.

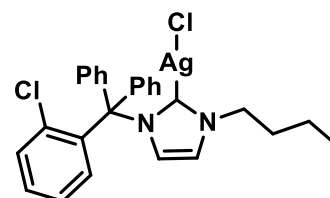


Yield: 0.14 g, 0.27 mmol (37%).

$^1\text{H}$  NMR (300 MHz,  $\text{CDCl}_3$ ):  $\delta$  7.36-7.04 (m, 15H, aromatic+ HC=C), 6.88 (s, 1H, C=CH), 5.87 (m, 1H, N- $\text{CH}_2\text{CHCH}_2$ ), 5.24-5.12 (m, 2H, N- $\text{CH}_2\text{CHCH}_2$ ), 4.7 (d,  $J$  = 4.7 Hz, 2H, N- $\text{CH}_2\text{CHCH}_2$ ).  $^{13}\text{C}\{^1\text{H}\}$  NMR (125 MHz,  $\text{CDCl}_3$ ):  $\delta$  139.9 (C), 135.8 (C), 132.7 (CH), 132.6 (CH), 131.7 (CH), 130.7 (CH), 130.6 (C), 128.5 (CH), 128.2 (CH), 128.0 (CH), 123.9 (CH), 119.5 (CH), 118.5 ( $\text{CH}_2$ ), 77.6 (C), 55.6 ( $\text{CH}_2$ ). HRMS (ESI<sup>+</sup>): Calcd for  $\text{C}_{50}\text{H}_{44}\text{AgCl}_2\text{N}_4$  [2M-AgCl<sub>2</sub>]<sup>+</sup>: 877.1834. Found: 877.1830. Anal. Calcd for  $\text{C}_{25}\text{H}_{21}\text{AgCl}_2\text{N}_2 \cdot \frac{1}{2} \text{H}_2\text{O}$ : C, 55.89; H, 4.13; N, 5.21; found: C, 55.50; H, 4.20; N, 5.00.

### 8.2.68 Preparation of C11

**L11** (0.02 g, 0.05 mmol) and silver oxide (0.006 g, 0.03 mmol) were dissolved in a solvent mixture of anhydrous MeOH (3 mL) and  $\text{CH}_2\text{Cl}_2$  (3 mL) in a Schlenk flask. The mixture was stirred at room temperature for 24 hours in the dark. The solution was filtered through celite, and the solvent was removed from the filtrate *in vacuo* to yield the product as a light yellow solid.

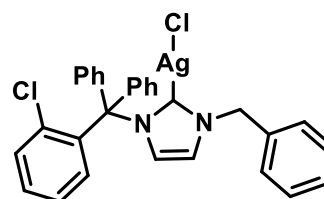


Yield: 0.005g, 0.001 mmol (20%).

$^1\text{H}$  NMR (300 MHz,  $\text{CDCl}_3$ ):  $\delta$  7.61-6.88 (m, 16H, aromatic + HC=CH), 4.15 (t,  $J$  = 7.2 Hz, 2H,  $\text{CH}_2$ ), 1.83 (dt,  $J$  = 14.4, 7.2 Hz, 2H,  $\text{CH}_2$ ), 1.57 (m, 2H,  $\text{CH}_2$ ), 0.92 (dd,  $J$  = 9.0, 5.7 Hz, 3H,  $\text{CH}_3$ ).  $^{13}\text{C}\{^1\text{H}\}$  NMR (75 MHz,  $\text{CDCl}_3$ ):  $\delta$  141.2, 139.6, 138.4, 135.4, 132.4, 131.4, 130.3, 129.7, 129.0, 128.4, 128.1, 127.8, 123.6, 118.2, 77.4, 53.2, 33.2, 19.5, 13.7. HRMS (ESI<sup>+</sup>): Calcd for  $\text{C}_{52}\text{H}_{50}\text{AgCl}_2\text{N}_4$  [2M-AgCl<sub>2</sub>]<sup>+</sup>: 909.2460. Found: 909.2609. Anal. Calcd for  $3(\text{C}_{26}\text{H}_{25}\text{AgCl}_2\text{N}_2) \cdot 1(\text{C}_{52}\text{H}_{50}\text{AgCl}_3\text{N}_4)$ : C, 60.57; H, 4.89; N, 5.43; found: C, 60.80; H, 4.80; N, 5.10.

### 8.2.69 Preparation of C12

**L12** (0.10 g, 0.21 mmol) and silver oxide (0.05 g, 0.21 mmol) were dissolved in  $\text{CH}_2\text{Cl}_2$  (8 mL) and heated at reflux for 24 hours in the dark. The mixture was filtered through celite and the solid washed with  $\text{CH}_2\text{Cl}_2$ . The solvent was removed from the filtrate *in vacuo* to give the product as an off white solid.

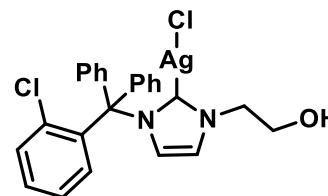


Yield : 0.06 g, 0.1 mmol (50 %).

$^1\text{H}$  NMR (300 MHz,  $\text{CDCl}_3$ ):  $\delta$  7.46-7.10 (m, 20H, Ar+ HC=C), 6.87 (s, 1H, C=CH), 5.35 (s, 2H,  $\text{CH}_2$ ).  $^{13}\text{C}\{^1\text{H}\}$  NMR (75 MHz,  $\text{CDCl}_3$ ):  $\delta$  141.0 (C), 139.9 (C), 135.8 (C), 135.6 (C), 132.7 (CH), 131.7 (CH), 130.7 (CH), 129.2 (CH), 128.8 (CH), 128.6 (CH), 128.2 (CH), 128.1 (CH), 127.8 (CH), 127.1 (CH), 78.0 (C), 57.2 ( $\text{CH}_2$ ). HRMS (ESI<sup>+</sup>): Calcd for  $\text{C}_{58}\text{H}_{46}\text{AgCl}_2\text{N}_4$  [2M-AgCl<sub>2</sub>]<sup>+</sup> : 977.2147. Found: 977.2170. Anal. Calcd for  $\text{C}_{29}\text{H}_{23}\text{AgCl}_2\text{N}_2 \cdot 2 \text{H}_2\text{O}$ : C, 56.70; H, 4.43; N, 4.56; found: C, 56.80; H, 4.60; N, 4.20.

### 8.2.70 Preparation of C13A

**L13** (0.2 g, 0.47 mmol) and silver oxide (0.13g, 0.47 mmol) were dissolved in  $\text{CH}_2\text{Cl}_2$  (20 mL). The mixture was stirred at room temperature for 24 hours in the dark. The mixture was filtered through celite, and the filtrate dried *in vacuo* to yield a orange solid. Recrystallisation from  $\text{CH}_2\text{Cl}_2$  /  $\text{Et}_2\text{O}$  yields the product as a white solid. The solvent was decanted and the solid dried *in vacuo*.

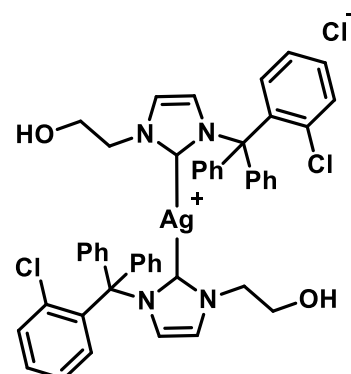


Yield: 0.23 g, 0.43 mmol (92 %).

$^1\text{H}$  NMR (300 MHz, MeOD):  $\delta$  7.41-7.04 (m, 14H, aromatic), 6.90-6.88 (m, 2H, HC=CH), 4.25 (t, 2H,  $J = 6.0$  Hz,  $\text{CH}_2$ ), 3.76 (t, 2H,  $J = 6.0$  Hz,  $\text{CH}_2$ ).  $^{13}\text{C}\{^1\text{H}\}$  NMR (75 MHz,  $d_4$ -MeOD):  $\delta$  187.9, 185.1 (Ag-C), 142.0, 141.6, 137.1 (C-Ar), 133.5, 132.4, 131.9, 130.3, 129.0, 128.0, 127.8 (CH-aromatic), 124.9, 120.6 (CH), 78.6 (C), 62.7, 56.6 ( $\text{CH}_2$ ). HRMS (ESI<sup>+</sup>): Calcd for  $\text{C}_{48}\text{H}_{42}\text{AgCl}_2\text{N}_4\text{O}_2$  [2M-AgCl<sub>2</sub>]<sup>+</sup>: 885.1732. Found: 885.1762. Anal. Calcd for  $\text{C}_{24}\text{H}_{21}\text{AgCl}_2\text{N}_2\text{O}$ : C, 54.16; H, 3.98; N, 5.26; found: C, 54.26; H, 4.16; N, 5.32.

### 8.2.71 Preparation of C13B

**L13** (0.2 g, 0.47 mmol) and silver oxide (0.065g, 0.28 mmol) were dissolved in solvent mixture of anhydrous MeOH (10 mL) and anhydrous CH<sub>2</sub>Cl<sub>2</sub> (5 mL) in a Schlenk flask with activated molecular sieves 4Å. The mixture was stirred at RT for 24 hours in the. The mixture was filtered through celite, and the solvent was removed from the filtrate in *vacuo*. The solid was recrystallised from CH<sub>2</sub>Cl<sub>2</sub> / Et<sub>2</sub>O yielding the product as a white solid. The solvents were decanted and the solid dried *in vacuo*.

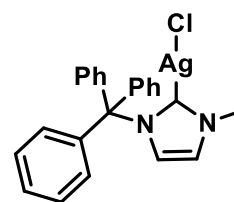


Yield: 0.13 g, 0.14 mmol (30 %).

<sup>1</sup>H NMR (300 MHz, d<sub>4</sub>-MeOD): δ 7.52-6.99 (m, 16H, Ar + HC=CH), 3.65-3.60 (m, 4H, CH<sub>2</sub>). <sup>13</sup>C{<sup>1</sup>H} NMR (75 MHz, d<sub>4</sub>-MeOD): δ 142.3, 141.6, 137.2 (C-Ar), 133.8, 132.5, 131.9, 131.6, 129.6, 129.1, 128.1, 124.9, 120.6 (CH), 78.7 (C), 62.5, 56.6 (CH<sub>2</sub>). HRMS (ESI<sup>+</sup>): Calcd for C<sub>48</sub>H<sub>42</sub>AgCl<sub>2</sub>N<sub>4</sub>O<sub>2</sub> [2M-AgCl<sub>2</sub>]<sup>+</sup>: 885.1732. Found: 885.1747. Anal. Calcd for C<sub>48</sub>H<sub>42</sub>AgCl<sub>3</sub>N<sub>4</sub>O<sub>2</sub>·½ Et<sub>2</sub>O: C, 62.59; H, 4.60; N, 6.08; found: C, 62.68; H, 4.94; N, 5.85.

### 8.2.72 Preparation of C14

**L14** (0.50 g, 1.38 mmol) and silver oxide (0.32 g, 1.38 mmol) were dissolved in CH<sub>2</sub>Cl<sub>2</sub> (30 mL) and heated at reflux for 18 hours in the dark. The mixture was filtered through celite, and the solvent was removed from the filtrate *in vacuo* to give a brown solid. Recrystallisation from CH<sub>2</sub>Cl<sub>2</sub> / Et<sub>2</sub>O yielded the product as a white solid. The solvents were decanted and the solid dried *in vacuo*.

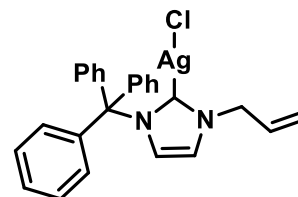


Yield: 0.4 g, 0.85 mmol (62%).

<sup>1</sup>H NMR (300 MHz, CDCl<sub>3</sub>): δ 7.34-7.20 (m, 15H, Ar), 7.04 (s, 1H, C=CH), 6.98 (s, 1H, HC=C), 3.84 (s, 3H, CH<sub>3</sub>). <sup>13</sup>C{<sup>1</sup>H} NMR (75MHz, CDCl<sub>3</sub>): δ 140.5 (C), 129.6, 128.5, 128.2, 127.9 (Ar), 122.0(HC=C), 119.8 (C=CH), 36.12 (CH<sub>3</sub>). HRMS (ESI<sup>+</sup>): Calcd for C<sub>46</sub>H<sub>40</sub>AgN<sub>4</sub> [2M-AgCl<sub>2</sub>]<sup>+</sup>: 757.2301. Found: 757.2314. Anal. Calcd for C<sub>23</sub>H<sub>20</sub>AgClN<sub>2</sub>·½ H<sub>2</sub>O: C, 57.94; H, 4.44; N, 5.88; found: C, 57.90; H, 4.60; N, 5.50.

### 8.2.73 Preparation of C15

**L15** (0.58 g, 1.49 mmol) and silver oxide (0.35 g, 1.49 mmol) were dissolved in  $\text{CH}_2\text{Cl}_2$  (30 mL) and heated at reflux for 18 hours in the dark. The mixture was filtered through celite, and the solvent was removed from the filtrate *in vacuo* to give a colourless oil. Recrystallisation from  $\text{CH}_2\text{Cl}_2$  /  $\text{Et}_2\text{O}$  yielded the product as a white solid. The solvents were decanted and the solid dried *in vacuo*.

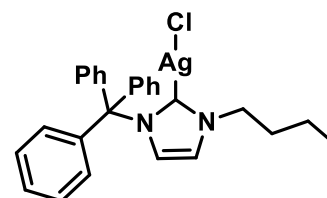


Yield: 0.41 g, 0.83 mmol (56 %).

$^1\text{H}$  NMR (300 MHz,  $\text{CDCl}_3$ ):  $\delta$  7.37-7.19 (m, 15H, Ar), 7.07 (s, 1H, C=CH), 6.95 (s, 1H, HC=C), 6.00 (m, 1H, N- $\text{CH}_2\text{CHCH}_2$ ), 5.24 (m, 2H, N- $\text{CH}_2\text{CHCH}_2$ ), 4.75 (dt,  $J$  = 5.8, 1.4 Hz, 2H, N- $\text{CH}_2\text{CHCH}_2$ ).  $^{13}\text{C}\{^1\text{H}\}$  NMR (75MHz,  $\text{CDCl}_3$ ):  $\delta$  142.1 (C), 132.6 (HC=C), 130.6(HC=C), 129.6, 128.9, 128.6, 127.7(aromatic), 119.5(HC=CH<sub>2</sub>), 117.5 (C=CH<sub>2</sub>), 55.6 (CH<sub>2</sub>). HRMS (ESI<sup>+</sup>): Calcd for  $\text{C}_{50}\text{H}_{44}\text{AgN}_4$  [2M-AgCl<sub>2</sub>]<sup>+</sup>: 809.2614. Found: 809.2616. Anal. Calcd for  $\text{C}_{25}\text{H}_{22}\text{AgClN}_2$ : C, 60.81; H, 4.49; N, 5.67; found: C, 60.61; H, 4.50; N, 5.60.

### 8.2.74 Preparation of C16

**L16** (0.62 g, 1.53 mmol) and silver oxide (0.36 g, 1.53 mmol) were dissolved in  $\text{CH}_2\text{Cl}_2$  (30 mL) and heated at reflux for 18 hours in the dark. The mixture was filtered through celite, and the solvent was removed from the filtrate *in vacuo* to give a colourless oil. Recrystallisation from  $\text{CH}_2\text{Cl}_2$  /  $\text{Et}_2\text{O}$  yielded the product as a white solid. The solvents were decanted and the solid dried *in vacuo*.

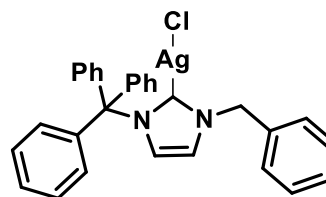


Yield: 0.21 g, 0.41 mmol (27 %).

$^1\text{H}$  NMR (300 MHz,  $\text{CDCl}_3$ ):  $\delta$  7.37-7.18 (m, 15H, aromatic), 7.05 (s, 1H, C=CH), 6.93 (s, 1H, HC=C), 4.13 (t,  $J$  = 7.3 Hz, 2H, CH<sub>2</sub>), 1.80 (quin,  $J$  = 7.3 Hz, 2H, CH<sub>2</sub>), 1.31 (sext,  $J$  = 7.3 Hz, 2H, CH<sub>2</sub>), 0.93 (t,  $J$  = 7.3 Hz, 2H, CH<sub>3</sub>).  $^{13}\text{C}\{^1\text{H}\}$  NMR (75 MHz,  $\text{CDCl}_3$ ):  $\delta$  147.0 (C), 137.2, 129.7, 129.4, 129.1, 128.0, 127.8, 124.0, 122.6 (CH), 79.7 (C) 50.6, 32.4, 19.6 (CH<sub>2</sub>), 13.6 (CH<sub>3</sub>). HRMS (ESI<sup>+</sup>): Calcd for  $\text{C}_{52}\text{H}_{52}\text{AgN}_4$  [2M-AgCl<sub>2</sub>]<sup>+</sup>: 841.3240. Found: 841.3245. Anal. Calcd for  $\text{C}_{26}\text{H}_{26}\text{AgClN}_2$ : C, 61.25; H, 5.14; N, 5.49; found: C, 61.60; H, 5.15; N, 5.40.

### 8.2.75 Preparation of C17

**L17** (0.086 g, 0.19 mmol) and silver oxide (0.027g, 0.12mmol) were dissolved in a mixture of anhydrous MeOH (5 mL) and CH<sub>2</sub>Cl<sub>2</sub> (5 mL) in a Schlenk flask with activated molecular sieves 4Å. The mixture was stirred at room temperature for 24 hours in the dark. The solution was filtered through celite, and the solvents were removed from the filtrate dried in *vacuo* to yield the product as a light yellow solid.

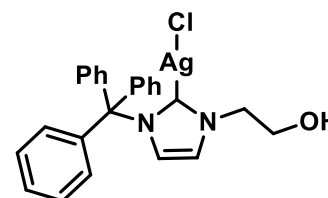


Yield : 0.01g, 0.013 mmol (7 %).

<sup>1</sup>H NMR (300 MHz, CDCl<sub>3</sub>): δ 7.45-6.88 (m, 22H, Ar + HC=CH), 4.54 (s, 2H, CH<sub>2</sub>). <sup>13</sup>C{<sup>1</sup>H} NMR (125 MHz, CDCl<sub>3</sub>): δ 186.6, 184.1 (Ag-C), 142.3, 135.8 (C-Ar), 130.1, 129.9, 129.0, 128.5, 128.3, 127.4, (CH- Ar), 124.3, 119.6 (CH), 77.4 (C), 65.9 (CH<sub>2</sub>). HRMS (ESI<sup>+</sup>): Calcd for C<sub>58</sub>H<sub>48</sub>AgN<sub>4</sub> [2M-AgCl<sub>2</sub>]<sup>+</sup>: 909.2927. Found: 909.2964. Anal. Calcd for (C<sub>29</sub>H<sub>24</sub>AgClN<sub>2</sub>)·(C<sub>58</sub>H<sub>48</sub>AgClN<sub>4</sub>): C, 70.22; H, 4.88; N, 5.65; found: C, 70.30; H, 5.30; N, 5.60.

### 8.2.76 Preparation of C18A

**L18** (0.2 g, 0.26 mmol) and silver oxide (0.08 g, 0.26 mmol) were dissolved in CH<sub>2</sub>Cl<sub>2</sub> (20 mL). The mixture was stirred at room temperature for 24 hours in the dark. The mixture was filtered through celite, and the solvent was removed from the filtrate *in vacuo* to yield a white solid. Recrystallisation from CH<sub>2</sub>Cl<sub>2</sub> / Et<sub>2</sub>O yields the product as a white solid. The solvents were decanted and the solid dried *in vacuo*.

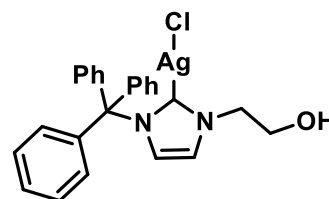


Yield: 0.09g, 0.18 mmol (70%).

<sup>1</sup>H NMR (300 MHz, CDCl<sub>3</sub>): δ 7.23-7.08 (m, 15H, aromatic), 6.94 (broad s, 2H, HC=CH), 4.23-4.18 (m, 2H, CH<sub>2</sub>), 3.77-3.61(m, 2H, CH<sub>2</sub>). <sup>13</sup>C{<sup>1</sup>H} NMR (75 MHz, CDCl<sub>3</sub>): δ 141.5 (C-Ar), 130.1, 128.1, 127.8 (CH-Ar), 122.6, 120.7 (CH), 77.4 (C), 55.3, 53.2 (CH<sub>2</sub>). HRMS (ESI<sup>+</sup>): Calcd for C<sub>48</sub>H<sub>44</sub>AgN<sub>4</sub>O<sub>2</sub> [2M-AgCl<sub>2</sub>]<sup>+</sup> calcd: 817.2512. Found: 817.2544. Anal. Calcd for C<sub>24</sub>H<sub>22</sub>AgClN<sub>2</sub>O: C, 57.91; H, 4.46; N, 5.63; found: C, 58.22; H, 4.23; N, 5.75.

### 8.2.77 Preparation of C18B

**L18** (0.1 g, 0.26 mmol) and silver oxide (0.04 g, 0.15 mmol) were dissolved in a solvent mixture of anhydrous MeOH (10 mL) and anhydrous CH<sub>2</sub>Cl<sub>2</sub> (5 mL) in a Schlenk flask. The mixture was stirred at room temperature for 24 hours in the dark under anhydrous conditions. The solution was filtered through celite, and the solvent was removed from the filtrate in *vacuo* yielding the product as a white solid.

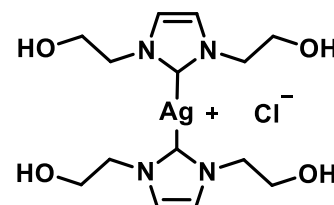


Yield: 0.018g, 0.031 (12%).

<sup>1</sup>H NMR (300 MHz, MeOD): δ 7.63 (broad s, 1H, C=CH), 7.48-7.00 (m, 15H, Ar), 6.86 (broad s, 1H, HC=C), 4.12 (t, *J* = 5.10 Hz, 2H, CH<sub>2</sub>), 3.81 (t, *J* = 5.10 Hz, 2H, CH<sub>2</sub>). <sup>13</sup>C{<sup>1</sup>H} NMR (75 MHz, MeOD): δ 144.0 (C-Ar), 131.4, 129.4, 129.2 (CH-Ar), 124.5, 120.8 (CH), 78.6 (C), 62.4, 56.3 (CH<sub>2</sub>). HRMS (ESI<sup>+</sup>): Calcd for C<sub>48</sub>H<sub>44</sub>AgN<sub>4</sub>O<sub>2</sub> [2M-AgCl<sub>2</sub>]<sup>+</sup> calcd: 817.2512. Found: 817.2529. Anal. Calcd for 4(C<sub>24</sub>H<sub>22</sub>AgClN<sub>2</sub>O)·1(C<sub>48</sub>H<sub>44</sub>AgClN<sub>4</sub>O<sub>2</sub>): C, 60.83; H, 4.68; N, 5.91; found: C, 60.80; H, 4.50; N, 5.80.

### 8.2.78 Preparation of C19

**L19** (0.1g, 0.52 mmol), silver oxide (0.12g, 0.52 mmol) were dissolved in MeOH (10 mL) were stirred at room temperature, in the dark for 4 hours. The mixture was filtered through celite and Et<sub>2</sub>O (50 mL) was added to the filtrate precipitating a light brown solid. The solvent was decanted and the solid dried *in vacuo*.

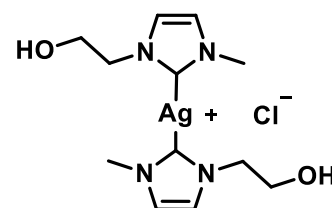


Yield: 0.115 g, 0.25 mmol (49%)

<sup>1</sup>H NMR (300 MHz, MeOD): δ 7.23 (s, 4H, HC=CH), 4.16 (t, *J* = 5.4, 8H, CH<sub>2</sub>), 3.79 (t, *J* = 5.4, 8H, CH<sub>2</sub>). <sup>13</sup>C{<sup>1</sup>H} NMR (75 MHz, MeOD): δ 123.0 (HC=CH), 63.0, 55.4 (CH<sub>2</sub>). HRMS (ESI<sup>+</sup>): calcd for C<sub>14</sub>H<sub>24</sub>AgN<sub>4</sub>O<sub>4</sub> [M - Cl]<sup>+</sup>: calcd: 419.0843. Found: 419.0845. Anal. Calcd for C<sub>14</sub>H<sub>24</sub>AgClN<sub>4</sub>O<sub>4</sub>: C, 36.90; H, 5.31; N, 12.30; found: C, 37.20; H, 5.40; N, 12.15.

**8.2.79 Preparation of C20<sup>10, 11</sup>**

**L20** (0.8 g, 4.9 mmols) was dissolved in MeOH (30 mL) and silver oxide (0.87 g, 3.8 mmols) was added. The mixture was heated at reflux for 8 hours. The solution was filtered through celite, and the solvent was removed from the filtrate *in vacuo* to yield a brown solid. Recrystallisation from MeOH / Et<sub>2</sub>O furnished the product as a light yellow solid. The solvents were decanted and the solid dried *in vacuo*.

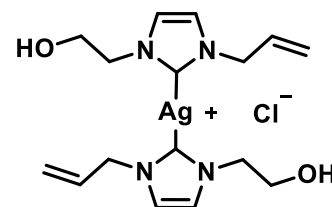


Yield: 0.42 g, 1.06 mmol (22 %)

<sup>1</sup>H NMR (300 MHz, DMSO-d<sub>6</sub>): δ 7.40 (s, 1H, C=CH), 7.36 (s, 1H, C=CH), 4.07 (t, *J* = 6.0 Hz, 2H, CH<sub>2</sub>), 3.66 (t, *J* = 6.0 Hz, 2H, CH<sub>2</sub>), 3.13 (s, 3H, CH<sub>3</sub>). <sup>13</sup>C{<sup>1</sup>H} NMR (125 MHz, DMSO-d<sub>6</sub>): δ 122.0, 121.8 (HC=CH), 61.5 (CH<sub>2</sub>), 54.0 (CH<sub>2</sub>), 37.8 (CH<sub>3</sub>). HRMS (ESI<sup>+</sup>): calcd for C<sub>12</sub>H<sub>21</sub>AgN<sub>4</sub>O<sub>2</sub> [M - Cl]<sup>+</sup> calcd: 360.071 found: 360.066. Anal. Calcd for C<sub>12</sub>H<sub>20</sub>AgClN<sub>4</sub>O<sub>2</sub>: C, 36.43; H, 5.10; N, 14.16. Found: C, 36.80; H, 5.30; N, 13.80.

**8.2.80 Preparation of C21**

**L21** (0.1g, 0.52 mmols) was dissolved in MeOH (10 mL) and silver oxide (0.13g, 0.52 mmols) was added and the mixture was heated at reflux for 4 hours. The solution which had turned a grey colour was filtered through celite and the solvent was removed from the filtrate *in vacuo* to yield a brown oil, which decomposes to a dark grey colour when upon recrystallisation from MeOH / Et<sub>2</sub>O and further drying *in vacuo*.

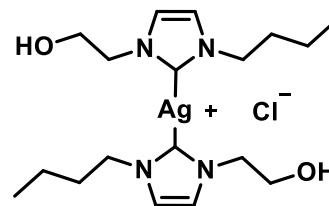


Challenging to analyse due to fast decomposition.

<sup>1</sup>H NMR (300 MHz, MeOD): δ 7.38 (d, 2H, C=CH), 7.30 (d, 2H, C=CH), 6.15-6.03 (m, 2H, C=CH-CH<sub>2</sub>), 5.33-5.19 (m, 4H, HC=CH<sub>2</sub>), 4.82 (m, 4H, CH<sub>2</sub>), 4.30-4.27 (m, 4H, CH<sub>2</sub>), 3.92-3.89 (m, 4H, CH<sub>2</sub>).

**8.2.81 Preparation of C22**

**L22** (0.1g, 0.49 mmol), silver oxide (0.11 mg, 0.49 mmol) and MeOH (10 mL) were stirred at room temperature, in the dark for 4 hours. The mixture was filtered through celite, and the solvent was removed from the filtrate *in vacuo* to yield a yellow oil. Recrystallisation from MeOH / Et<sub>2</sub>O furnishes the product as a yellow solid.

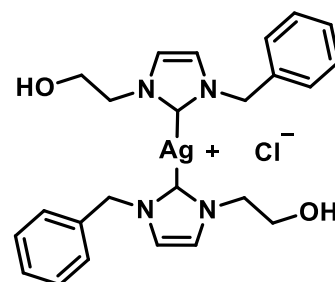


Yield: 0.20 g, 0.44 mmol (88 %)

<sup>1</sup>H NMR (300 MHz, MeOD): δ 7.25 (m, 4H, HC=CH), 4.18 (t, *J* = 5.1 Hz, 4H, CH<sub>2</sub>), 4.10 (t, *J* = 7.2 Hz, 4H, CH<sub>2</sub>), 3.79 (t, *J* = 5.1 Hz, 4H, CH<sub>2</sub>), 1.78 (m, 4H, CH<sub>2</sub>), 1.29 (m, 4H, CH<sub>2</sub>), 0.83 (t, *J* = 7.2, 6H, CH<sub>3</sub>). <sup>13</sup>C{<sup>1</sup>H} NMR (75 MHz, MeOD): δ 123.2, 122.6 (HC=CH), 62.9, 55.4 (CH<sub>2</sub>), 52.6 (CH<sub>2</sub>), 34.9 (CH<sub>2</sub>), 20.9 (CH<sub>2</sub>), 14.1 (CH<sub>3</sub>). HRMS (ESI<sup>+</sup>): calcd for C<sub>18</sub>H<sub>32</sub>AgN<sub>4</sub>O<sub>2</sub> [M - Cl]<sup>+</sup> calcd: 443.1571, found:443.1576. Anal. Calcd for C<sub>18</sub>H<sub>32</sub>AgClN<sub>4</sub>O<sub>2</sub>·<sup>4</sup>/<sub>5</sub>MeOH: C, 44.68; H, 7.01; N, 11.09. Found: C, 44.30; H, 7.20; N, 10.70.

**8.2.82 Preparation of C23**

**L23** (0.1g, 0.42mmol) was dissolved in MeOH (10 mL) and silver oxide (0.097g, 0.42mmol) was added. The mixture heated to reflux for 24 hours in the dark. The solution was filtered through celite, and the solvent was removed from the filtrate *in vacuo* to yield the product as a brown solid.

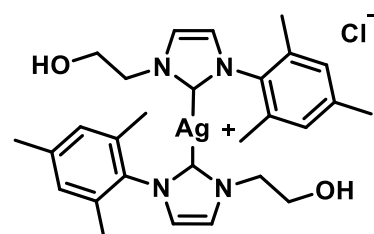


Yield: 0.15 g, 0.27 mmol (65 %)

<sup>1</sup>H NMR (300 MHz, MeOD): δ 7.27 -7.12 (m, 14H, Ar, HC=CH), 5.18 (s, 4H, CH<sub>2</sub>), 4.10 (t, *J* = 5.4 Hz, 4H, CH<sub>2</sub>), 3.74 (t, *J* = 5.4 Hz, 4H, CH<sub>2</sub>). <sup>13</sup>C{<sup>1</sup>H} NMR (125 MHz, MeOD): 182.3 (Ag-C), 138.4 (C-Ar), 130.0, 129.3, 128.7 (HC-Ar), 123.5, 123.2 (HC=CH), 62.4, 56.0 (CH<sub>2</sub>), 55.5 (CH<sub>2</sub>). HRMS (ESI<sup>+</sup>): Calcd for C<sub>24</sub>H<sub>28</sub>AgN<sub>4</sub>O<sub>2</sub> [M - Cl]<sup>+</sup> calcd: 511.1258, found: 511.1257. Anal. Calcd for C<sub>24</sub>H<sub>28</sub>AgClN<sub>4</sub>O<sub>2</sub>: C, 52.62; H, 5.15; N, 10.23. Found: C, 52.90; H, 5.55; N, 9.85.

### 8.2.83 Preparation of C24<sup>10</sup>

**L24** (0.1 g, 0.38 mmol) was dissolved in MeOH (15 mL) and silver oxide (0.09 g, 0.38 mmol) was added. The mixture was stirred for 6 hours at room temperature. The solution was filtered through celite and the solvent was removed from the filtrate *in vacuo* to obtain a brown solid. The solid was recrystallised from MeOH / Et<sub>2</sub>O, the solvents decanted and the solid was dried *in vacuo*.

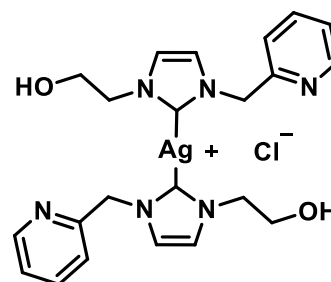


Yield: 0.16 g, 0.26 mmol (70%)

<sup>1</sup>H NMR (300 MHz, MeOD): δ 7.51 (s, 1H, C=CH), 7.21 (s, 1H, C=CH), 7.01 (s, 2H, aromatic), 4.21 (t, *J* = 5.4 Hz, 2H, CH<sub>2</sub>), 3.84 (t, *J* = 5.4 Hz, 2H, CH<sub>2</sub>), 2.43 (s, 3H, CH<sub>3</sub>), 1.85 (s, 6H, CH<sub>3</sub>). <sup>13</sup>C{<sup>1</sup>H} NMR (75 MHz, CDCl<sub>3</sub>): δ 138.7, 135.7, 135.0 (C-arom), 129.0 (CH-arom), 122.7, 121.9 (HC=CH), 61.6, 54.6 (CH<sub>2</sub>), 21.1 (*p*-CH<sub>3</sub>), 17.4 (*o*-CH<sub>3</sub>). HRMS (ESI<sup>+</sup>): calcd for C<sub>28</sub>H<sub>36</sub>AgN<sub>4</sub>O<sub>2</sub> [M - Cl]<sup>+</sup> calcd: 567.1884 found: 567.1889. Anal. Calcd for C<sub>28</sub>H<sub>36</sub>AgClN<sub>4</sub>O<sub>2</sub>·<sup>3</sup>/<sub>2</sub>H<sub>2</sub>O: C, 53.39; H, 6.08; N, 8.89. Found: C, 53.00; H, 6.10; N, 8.50.

### 8.2.84 Preparation of C25

**L25** (0.1 g, 0.42 mmol) and silver oxide (0.097 g, 0.42 mmol) were dissolved in MeOH (10 mL) and the mixture was stirred at room temperature for 4 hours, in the dark. The solution was filtered through celite, and excess Et<sub>2</sub>O was added to precipitate a brown oil. The brown oil was recrystallised from MeOH / Et<sub>2</sub>O to furnish the product as a brown solid. The solvent was decanted and the solid dried *in vacuo*.

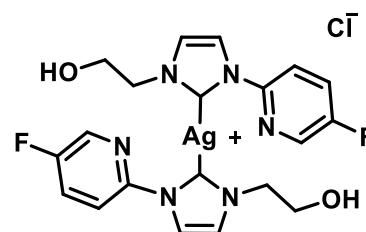


Yield: 0.15 g, 0.27 mmol (64%)

<sup>1</sup>H NMR (300 MHz, MeOD): δ 8.43-8.41 (m, 2H, HCN-Ar), 7.72 (td, *J* = 7.7 Hz, 2H, HC=CH), 7.59-7.57 (m, 2H, Ar), 7.31 (q, *J* = 7.7 Hz, 4H, Ar), 5.38 (s, 4H, CH<sub>2</sub>), 4.28-4.22 (m, 4H, CH<sub>2</sub>), 3.82-3.78 (m, 4H, CH<sub>2</sub>); <sup>13</sup>C{<sup>1</sup>H} NMR (125 MHz, MeOD): δ 182.9 (Ag-C), 150.5 (HC-Ar), 139.1 (HC-Ar), 125.2, 124.8 (HC=CH), 123.7 (HC-Ar), 123.4 (HC-Ar), 62.7 (CH<sub>2</sub>), 57.2 (CH<sub>2</sub>), 55.4 (CH<sub>2</sub>); HRMS (ESI<sup>+</sup>): calcd for C<sub>22</sub>H<sub>26</sub>AgN<sub>6</sub>O<sub>2</sub> [M - Cl]<sup>+</sup>: 513.1163, found 513.1167. Anal. Calcd for C<sub>22</sub>H<sub>26</sub>AgN<sub>6</sub>O<sub>2</sub>·H<sub>2</sub>O·MeOH: C, 46.05; H, 5.38; N, 14.01, Found: C, 46.30; H, 5.60; N, 13.70.

### 8.2.85 Preparation of C26

**L26** (0.08g, 0.33 mmol), silver oxide (0.076 g, 0.33 mmol) were dissolved in MeOH (10 mL), and the mixture was stirred at room temperature for 4 hours, in the dark. The mixture was filtered through celite and Et<sub>2</sub>O (80 mL) was added to precipitate the product as an off-white solid. The solvent was decanted and the solid was dried *in vacuo*.

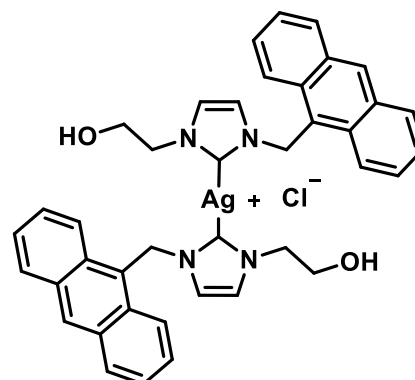


Yield: 0.03g, 0.06 mmol (17 %)

<sup>1</sup>H NMR (300 MHz, MeOD): δ 8.22 (broad s, 2H, C=CH), 7.94-7.87 (m, 4H, Ar), 7.71-7.63 (m, 2H, Ar), 7.51 (broad s, 2H, C=CH), 4.32 (t, *J* = 5.2 Hz, 2H, CH<sub>2</sub>), 3.88 (t, *J* = 5.2 Hz, 2H, CH<sub>2</sub>); <sup>13</sup>C{<sup>1</sup>H} NMR (75 MHz, MeOD): δ 137.9, 137.6, 127.8, 127.5, 124.4, 121.3, 118.3, 62.8 (CH<sub>2</sub>), 56.10 (CH<sub>2</sub>); HRMS (ESI<sup>+</sup>): Calcd for C<sub>20</sub>H<sub>20</sub>AgN<sub>6</sub>O<sub>2</sub>F<sub>2</sub> [M – Cl]<sup>+</sup>, 521.0667, Found 521.0656. Anal. Calcd for C<sub>20</sub>H<sub>20</sub>AgF<sub>2</sub>N<sub>6</sub>O<sub>2</sub>·<sup>2</sup>/<sub>3</sub> H<sub>2</sub>O: C, 42.47; H, 3.97; N, 14.61, Found: C, 42.80; H, 3.85; N, 14.30.

### 8.2.86 Preparation of C27

**L27** (0.3 g, 0.89 mmol) and silver oxide (0.12 g, 0.53 mmol) were added to a Schlenk flask with activated 4Å molecular sieves and degassed. Anhydrous MeCN (20 mL) and MeOH (14 mL) were transferred to the Schlenk flask, and the mixture was stirred at RT for 18 hours. The solution was filtered through celite and the solvents removed *in vacuo* rendering the product as a light yellow solid.



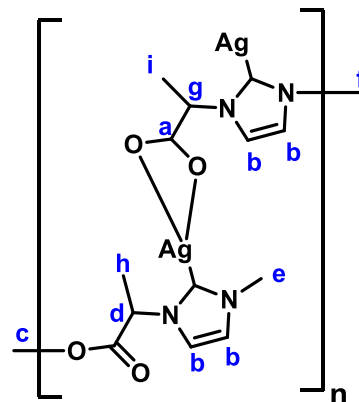
Yield: 0.24 g, 0.32 mmol (36%)

<sup>1</sup>H NMR (300 MHz, CDCl<sub>3</sub>): δ 8.53(s, 1H, aromatic), 8.32 (d, 2H, *J* = 8.4 Hz, aromatic), 8.05 (d, 2H, *J* = 8.4 Hz, aromatic), 7.54-7.44 (m, 4H, aromatic), 6.89 (s, 1H, C=CH), 6.50 (s, 1H, HC=C), 6.24 (s, 2H, CH<sub>2</sub>), 4.33 (m, 2H, CH<sub>2</sub>), 3.94 (m, 2H, CH<sub>2</sub>). <sup>13</sup>C{<sup>1</sup>H} NMR (75 MHz, CDCl<sub>3</sub>): δ 134.1 (C), 131.4 (C), 131.0 (C), 129.7 (CH), 129.5 (CH), 129.5 (CH), 127.6 (CH), 122.9 (CH), 125.5 (CH), 123.3 (CH), 121.7(CH), 61.6 (CH<sub>2</sub>), 55.0 (CH<sub>2</sub>), 47.6 (CH<sub>2</sub>). HRMS (ESI<sup>+</sup>): Calcd for C<sub>40</sub>H<sub>36</sub>AgN<sub>4</sub>O<sub>2</sub> [M-Cl]<sup>+</sup>, calcd: 711.1884, found: 711.1879. Anal. Calcd for

$C_{40}H_{36}AgClN_4O_2 \cdot 2H_2O$ : C, 61.27; H, 5.14; N, 7.15, Found: C, 60.90; H, 5.00; N, 7.50.

### 8.2.87 Preparation of C28

**L28** (0.15 g, 0.53 mmol) and silver oxide (0.12g, 0.51mmol) were added to activated molecular sieves 4Å in a Schlenk flask and dried in *vacuo*. Anhydrous MeOH (10 mL) were transferred to the Schlenk flask and the mixture was stirred at room temperature for 24 hours. The solution was filtered through celite, and the solvents removed from the filtrate *in vacuo* to yield the product as an off-white solid.

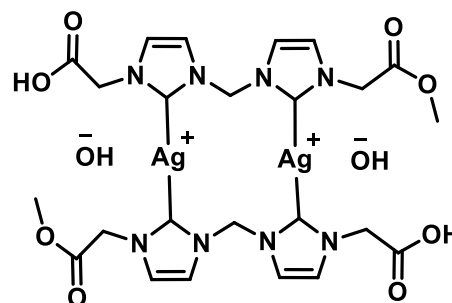


Yield: 0.025g, 0.06 mmol (11 %).

$^1H$  NMR (300 MHz, MeOD):  $\delta$  7.99 (s, 1H, **a**), 7.72 (s, 5H, **a**), 7.58 (s, 5H, **b**), 7.18 (s, 6H, **b**), 6.93 (s, 6H, **b**), 4.94-4.89 (m, 9H, **d**), 4.72 (q,  $J = 4.30$  Hz, 6H, **g**), 3.93 (s, 3H, **c**), 3.70 (s, 1H, **e**), 3.00 (s, 3H, **e**), 2.87 (s, 3H, **f**), 1.81-1.79 (m, 23H, **h/i**), 1.69 (d,  $J = 4.3$  Hz, 18H, **h**), 1.30 (d,  $J = 4.3$  Hz, 18H, **i**).  $^{13}C\{^1H\}$  NMR (125 MHz, MeOD):  $\delta$  183.2 (Ag-C), 177.4 (C=O), 174.7(C=O), 137.8(C=C), 128.3 (C=C), 122.3 (C=C), 120.0 (C=C), 61.9 (N-CH-CH<sub>3</sub>), 59.7 (N-CH-CH<sub>3</sub>), 53.0(CH), 36.8 (O-CH<sub>3</sub>), 21.8 (N-CH<sub>3</sub>), 19.9 (CH<sub>3</sub>), 19.2 (CH<sub>3</sub>). HRMS (ESI<sup>+</sup>): calcd for  $C_{14}H_{22}AgN_4O_4 [M - Ag + H]^+$  calcd: 419.0684, found: 419.0914. Anal. Calcd for  $C_{21}H_{30}Ag_2N_6O_6 \cdot 3/4MeOH$ : C, 33.99; H, 5.30; N, 11.19. Found: C, 34.10; H, 4.96; N, 10.80.

### 8.2.88 Preparation of C29

**L29** (0.075 g, 0.25 mmol) and silver oxide (0.12 g, 0.51 mmol) were added to a Schlenk flask and dried in *vacuo*. Anhydrous MeOH (15 mL) was transferred to the Schlenk flask and the mixture was stirred at room temperature for 18 hours. The solution, which had turned grey, was filtered through celite, and the solvent removed from the filtrate *in vacuo* to yield the product as a white solid.



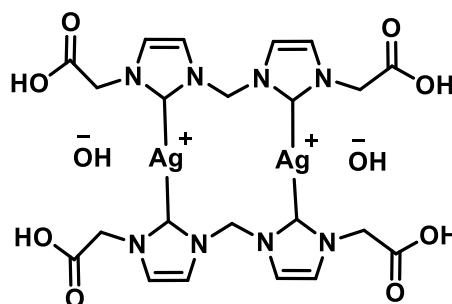
Yield: 0.05 g, 0.06 mmol (24 %)

$^1H$  NMR (300 MHz, MeOD):  $\delta$  7.59 (s, 4H, C=CH), 7.33 (s, 4H, HC=C), 7.24 (s, 4H, N-CH<sub>2</sub>-N), 5.02-4.58 (m, 8H, N-CH<sub>2</sub>-C=O), 3.22 (s, 6H, O-CH<sub>3</sub>).  $^{13}C\{^1H\}$

NMR (125 MHz, MeOD):  $\delta$  125.1(C=O), 122.2, 121.7(C=C), 65.1, 56.4 (CH<sub>2</sub>), 49.6 (CH<sub>3</sub>). HRMS (ESI<sup>+</sup>): calcd for C<sub>25</sub>H<sub>31</sub>Ag<sub>2</sub>N<sub>8</sub>O<sub>9</sub> [M-2OH]<sup>2+</sup> calcd: 388.0215, found: 388.0258. IR  $\nu_{\text{max}}$  / cm<sup>-1</sup>: 3371(OH), 3100, 2966 (carboxylic acid OH), 1741(ester C=O), 1368, 1230, 727. Anal. Calcd for C<sub>24</sub>H<sub>36</sub>Ag<sub>2</sub>N<sub>8</sub>O<sub>11</sub>·<sup>3</sup>/<sub>2</sub>H<sub>2</sub>O: C, 34.59; H, 4.00; N, 13.45. Found: C, 34.70; H, 4.40; N, 13.60.

### 8.2.89 Preparation of C30

**L30** (0.2 g, 0.42 mmol) and Silver oxide (0.19 g, 0.84 mmol) were added to activated molecular sieves 4Å in a Schlenk flask and dried *in vacuo*. Anhydrous MeCN (10 mL) and anhydrous MeOH (10 mL) were transferred to the Schlenk flask and the mixture was stirred at room temperature for 24 hours. The solution, which had turned grey, was filtered through celite, and the solvent removed from the filtrate *in vacuo* to yield the product as a white solid.

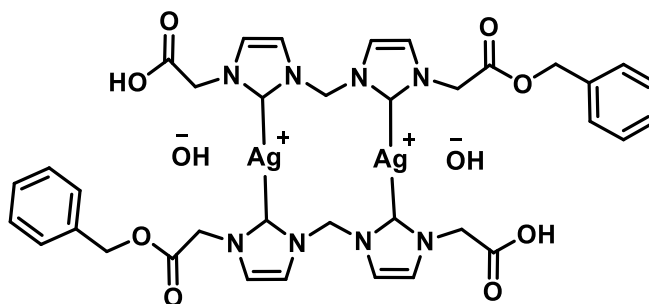


Yield: 0.15 g, 0.2 mmol (46 %)

<sup>1</sup>H NMR (300 MHz, MeOD):  $\delta$  7.60 (s, 4H, C=CH), 7.33 (s, 4H, HC=C), 7.24 (s, 4H, N-CH<sub>2</sub>-N), 6.48(broad s, 6H, OH), 4.60 (s, 8H, N-CH<sub>2</sub>-C=O). <sup>13</sup>C{<sup>1</sup>H} NMR (125 MHz, MeOD):  $\delta$  124.1(C=O), 121.3, 120.4 (C=C), 55.5, 51.8 (CH<sub>2</sub>). HRMS (ESI<sup>+</sup>): calcd for C<sub>23</sub>H<sub>29</sub>Ag<sub>2</sub>N<sub>8</sub>NaO<sub>9</sub> [M-2OH+H<sub>2</sub>O +MeCN]<sup>2+</sup>, calc: 399.4982, found: 399.5605. IR  $\nu_{\text{max}}$  / cm<sup>-1</sup> : 3366(OH), 3099, 2966(carboxylic acid OH), 1742(carboxylic acid C=O), 1368, 1170, , 727. Anal. Calcd for C<sub>22</sub>H<sub>30</sub>Ag<sub>2</sub>N<sub>8</sub>O<sub>10</sub>·CH<sub>3</sub>OH: C, 34.04; H, 3.73; N, 13.83. Found: C, 34.20; H, 3.90; N, 13.50.

### 8.2.90 Preparation of C31

**L31** (0.3 g, 0.58 mmol) and silver oxide (0.27 g, 1.16 mmol) were added to activated molecular sieves 4Å in a Schlenk flask and dried *in vacuo*. Anhydrous MeOH (10 mL) was transferred to the Schlenk flask and the mixture was stirred at room temperature for 24 hours. The solution, which had turned grey, was filtered through celite. Et<sub>2</sub>O (60 mL) was added to the filtrate to precipitate the



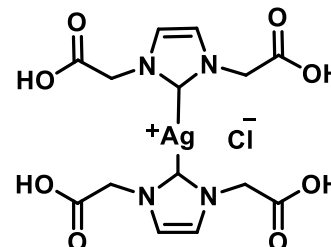
product as a white solid. The solvent was decanted and the solid was dried *in vacuo*.

Yield : 0.1 g, 0.1 mmol (18%)

$^1\text{H}$  NMR (300 MHz, MeOD):  $\delta$  7.69 (s, 2H, C=CH), 7.59 (s, 2H, HC=C), 7.49-7.23(m, 10H, aromatic), 4.71 (s, 2H, N-CH<sub>2</sub>-N), 4.62 (s, 4H, N-CH<sub>2</sub>-C=O), 3.37 (s, 4H, CH<sub>2</sub>).  $^{13}\text{C}\{^1\text{H}\}$  NMR (125 MHz, MeOD):  $\delta$  173.6, 170.1 (Ag-C), 142.6 (C=O), 129.3, 125.2, 127.9, 125.2 (aromatic), 123.9 (C=C), 122.2 (C=C), 65.1 (N-CH<sub>2</sub>-N), 56.6 (N-CH<sub>2</sub>-C=O), 53.3 (CH<sub>2</sub>). HRMS (ESI<sup>+</sup>): calcd for C<sub>36</sub>H<sub>35</sub>Ag<sub>2</sub>N<sub>8</sub>O<sub>8</sub> [M-2OH-H]<sup>+</sup>, Calcd: 923.0671, found : 923.0701. IR  $\nu_{\text{max}}$  / cm<sup>-1</sup> : 3254 (OH), 3092, 3001 (carboxylic acid OH) , 1745 (ester), 1604 (C-C benzene). Anal. Calcd for C<sub>40</sub>H<sub>48</sub>Ag<sub>2</sub>N<sub>8</sub>O<sub>11</sub> · Et<sub>2</sub>O: C: 46.53 H: 4.69 N: 10.85, found: C: 46.50 H: 4.30 N: 10.70

### 8.2.91 Preparation of C32

**L32** (0.10g, 0.45 mmol) and silver oxide (0.11g, 0.45 mmol) were added to an ampoule with activated molecular sieves 4Å and dried *in vacuo*. Anhydrous CH<sub>3</sub>CN (12 mL) and MeOH (15 mL) were transferred to the ampoule and the mixture was stirred at room temperature for 24 hours. The solution was filtered through celite, and the solvents were removed from the filtrate *in vacuo* to yield the product as a sticky white solid. Recrystallisation from MeOH / C<sub>5</sub>H<sub>12</sub> and MeCN/ C<sub>5</sub>H<sub>12</sub>, decantation of the solvents and drying of the solid *in vacuo* renders a sticky white solid (very hygroscopic).

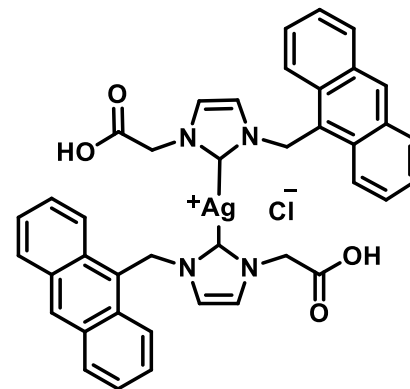


Yield: 0.08 g, 0.13 mmol (30 %)

$^1\text{H}$ -NMR (300MHz, MeOD):  $\delta$  8.44 (s, 1H, CH), 7.49 (s, 2H, CH), 6.95 (s, 2H, CH), 6.81 (s, 2H, CH), 4.45 (s, 4H, CH<sub>2</sub>).  $^{13}\text{C}\{^1\text{H}\}$ -NMR (75MHz, MeOD):  $\delta$  179.9 (Ag-C), 171.7 (C=O), 124.0 (CH), 63.0 (CH<sub>2</sub>). HRMS (ESI<sup>+</sup>): calcd for C<sub>16</sub>H<sub>18</sub>AgN<sub>5</sub>NaO<sub>8</sub> [M-H+MeCN+Na]<sup>+</sup>: 539.2044, Found: 539.3042. Anal. Calcd for C<sub>14</sub>H<sub>16</sub>AgClN<sub>4</sub>O<sub>8</sub> · 3 MeCN · 2/3 C<sub>5</sub>H<sub>12</sub>: C: 41.04 H: 4.80 N: 14.36, found: C: 41.40 H: 4.80 N: 14.70.

### 8.2.92 Preparation of C33

**L33** (0.05 g, 0.14 mmol) and silver oxide (0.42 g, 1.81 mmol) were added to an ampoule with 4Å activated molecular sieves, and dried *in vacuo*. Dry CH<sub>2</sub>Cl<sub>2</sub> (7 mL) and MeOH (7 mL) were transferred to the ampoule and the mixture was stirred at RT for 24 hours. The solution which had turned an orange colour was filtered through celite, and the solvents were removed from the filtrate *in vacuo* to yield the product as a red/orange solid. The solid is very hygroscopic and turns to an oil when exposed to air. Recrystallisation from MeCN / Et<sub>2</sub>O yields the product as an orange solid. The solvents were decanted and the solid dried *in vacuo*.

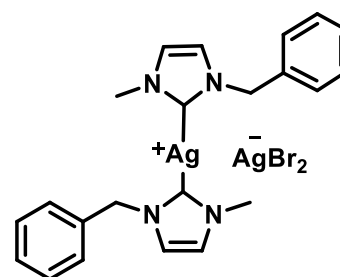


Yield: 0.02 g, 0.024 mmol (18 %)

<sup>1</sup>H-NMR (300 MHz, MeOD): δ 8.34 (m, 4H, aromatic), 8.20 (m, 4H, aromatic), 7.77-7.25 (m, 10H, aromatic), 6.46 (broad s, 4H, CH<sub>2</sub>), 6.11 (broad s, 4H, CH<sub>2</sub>). <sup>13</sup>C{<sup>1</sup>H}-NMR (75 MHz, MeOD): δ 132.1, 131.5, 130.3, 130.1, 128.8, 128.3, 126.1, 126.0 (aromatic), 123.5, 122.7 (HC=CH), 69.4 (CH<sub>2</sub>), 30.9 (CH<sub>2</sub>). HRMS (ESI<sup>+</sup>): calcd for C<sub>40</sub>H<sub>32</sub>AgN<sub>4</sub>O<sub>4</sub> [M - Cl]<sup>+</sup> calc : 741.1466; found: 741.1474. Anal. Calcd for C<sub>40</sub>H<sub>32</sub>AgClN<sub>4</sub>O<sub>4</sub> ·<sup>3</sup>/<sub>2</sub> MeCN ·<sup>3</sup>/<sub>2</sub> CH<sub>2</sub>Cl<sub>2</sub>: C: 55.27 H: 4.33 N: 7.97, found: C: 55.50 H: 4.40 N: 8.35.

### 8.2.93 Preparation of C34<sup>12</sup>

**L34** (0.58 g, 2.29 mmols) was dissolved in CH<sub>2</sub>Cl<sub>2</sub> (7 mL), and silver oxide (0.27g, 1.15 mmol) was added. The mixture was stirred at room temperature for 18 hours. Filter solution over celite, dried *in vacuo* to give a white solid. Recrystallisation from CH<sub>2</sub>Cl<sub>2</sub> / Et<sub>2</sub>O yields the product as a white solid.



Yield: 0.76 g, 1.06 mmol (46 %)

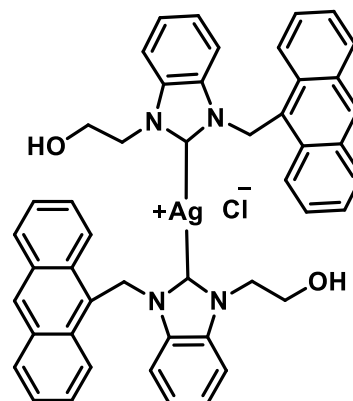
<sup>1</sup>H NMR (300 MHz, CDCl<sub>3</sub>): δ 7.28-7.17 (m, 10H, aromatic), 6.91 (s, 2H, C=CH), 6.86 (s, 2H, C=CH), 5.22 (s, 4H, CH<sub>2</sub>), 3.41 (s, 6H, CH<sub>3</sub>). <sup>13</sup>C{<sup>1</sup>H} NMR (500 MHz, CDCl<sub>3</sub>): δ 182.4 (Ag-C), 135.8 (C), 129.1 (CH), 128.5 (CH), 127.9 (CH), 122.6 (CH), 121.2 (CH), 55.6 (CH<sub>2</sub>), 38.9 (CH<sub>3</sub>). HRMS (ESI<sup>+</sup>): Calcd for [M-AgBr<sub>2</sub>]<sup>+</sup>, calc: 453.1043, found: 453.1031. Anal. Calcd for C<sub>22</sub>H<sub>24</sub>Ag<sub>2</sub>BrN<sub>4</sub> ·<sup>1</sup>/<sub>4</sub> Et<sub>2</sub>O: C, 37.41; H, 3.62; N, 7.59. Found: C, 37.65; H, 3.50, N, 7.90.

## 8.2.94 Preparation of C35

**L35** (0.01 g, 0.026 mmol) and silver oxide (0.006 g, 0.026 mmol) were dissolved in a solvent mixture of MeOD (0.5 mL) and  $\text{CDCl}_3$  (0.5 mL). The mixture was stirred at RT for 4 hours. The solution was filtered through celite and the solvents were removed *in vacuo* to yield a yellow solid.

Yield: 0.015 g, 0.018 mmol (68 %)

$^1\text{H}$  NMR (300 MHz,  $\text{CDCl}_3$ ):  $\delta$  8.45-7.16(m, 13H, CH-aromatic), 6.19(s, 2H,  $\text{CH}_2$ ), 4.40 (broad s, 2H,  $\text{CH}_2$ ), 3.91 (broad s, 2H,  $\text{CH}_2$ ).  $^{13}\text{C}\{^1\text{H}\}$  NMR (75 MHz,  $\text{CDCl}_3$ ):  $\delta$  131.5, 129.6, 127.7, 125.5, 124.0, 123.7, 111.7(CH-aromatic), 53.5, (CH<sub>2</sub>), 30.4 (CH<sub>3</sub>). HRMS (ESI<sup>+</sup>): Calcd for  $\text{C}_{48}\text{H}_{40}\text{AgN}_4\text{O}_2$  [2M - Cl]<sup>+</sup>, calcd: 813.2199, found: 813.2180. Anal. Calcd for  $\text{C}_{48}\text{H}_{40}\text{AgClN}_4\text{O}_2$ : C, 67.97; H, 4.75; N, 6.61. Found: C, 67.80; H, 4.85, N, 6.80.

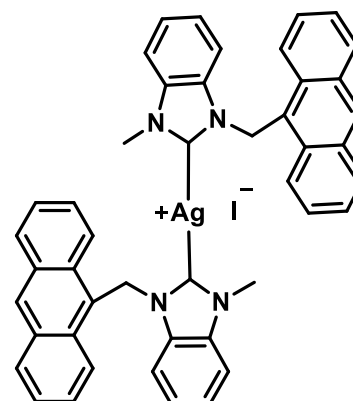


## 8.2.95 Preparation of C36

**L36** (0.09g, 0.20 mmol) and silver oxide (0.046g, 0.20mmol) were added to a Schlenk flask with activated 4Å molecular sieves and dried *in vacuo*. Anhydrous  $\text{CH}_2\text{Cl}_2$  (10 mL) and MeOH (10 mL) were transferred to the Schlenk flask. The mixture was stirred at RT for 24 hours. The solution was filtered through celite and the solvents were removed *in vacuo* to yield a dark orange solid.

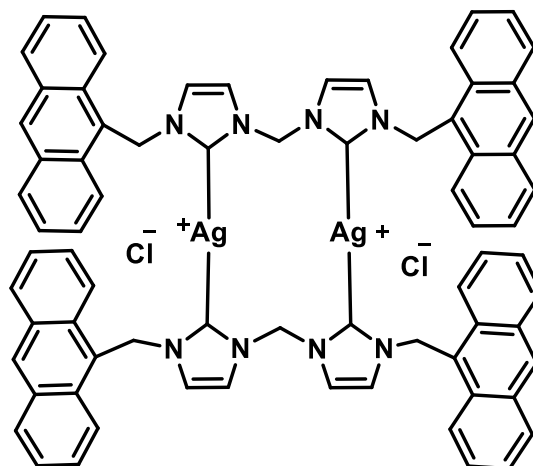
Yield: 0.01 g, 0.011 mmol (6%)

$^1\text{H}$  NMR (300 MHz,  $\text{CDCl}_3$ ):  $\delta$  8.46 (s, 1H, aromatic), 8.18-7.93 (m, 4H, aromatic), 7.47-7.31 (m, 8H, aromatic), 6.26 (s, 2H,  $\text{CH}_2$ ), 4.96 (s, 3H,  $\text{CH}_3$ ).  $^{13}\text{C}\{^1\text{H}\}$  NMR (75 MHz, DMSO- $d_6$ ):  $\delta$  HRMS (ESI<sup>+</sup>): Calcd for  $\text{C}_{46}\text{H}_{36}\text{AgN}_4$  [2M - I]<sup>+</sup> calcd: 751.1991 found: 751.1985. Anal. Calcd for  $\text{C}_{46}\text{H}_{36}\text{AgIN}_4$ : C, 62.81; H, 4.13; N, 6.37. Found: C, 62.60; H, 4.75, N, 6.50.



### 8.2.96 Preparation of C37

**L37** (0.1g, 0.16 mmol) and silver oxide (0.036g, 0.16mmol) were added to an ampoule dried *in vacuo*, evacuated and purged with Argon (x3). Dry CH<sub>2</sub>Cl<sub>2</sub> (10 mL) was transferred to the ampoule and the mixture was heated at 50°C for 24 hours. To improve the solubility of the mixture, dry MeOH (10 mL) was added after 24 hours and the mixture was heated for an additional 24 hours. The solution was filtered through celite; excess Et<sub>2</sub>O (300 mL) was added to the filtrate and the product precipitated out of solution as a yellow solid which was filtered and dried *in vacuo*.

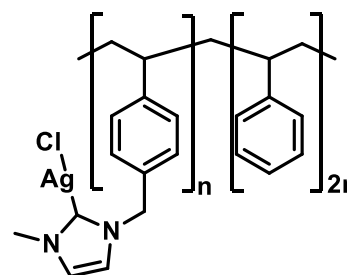


Yield: 0.05 g, 0.04 mmol (22 %).

<sup>1</sup>H NMR (300 MHz, DMSO-d<sub>6</sub>): δ 8.75 (s, 2H, C=CH), 8.11-7.18(m, 20H, aromatic + HC=C), 6.04-5.76 (broad m, 4H, CH<sub>2</sub>), 4.04 (broad s, 2H, CH<sub>2</sub>). <sup>13</sup>C{<sup>1</sup>H} NMR (75 MHz, DMSO-d<sub>6</sub>): δ 131.8, 131.0, 129.9, 127.7, 126.0 (CH, aromatic), 124.8, 123.7 (CH=CH), 65.8, 15.1 (CH<sub>2</sub>). HRMS (ESI<sup>+</sup>): Calcd for C<sub>74</sub>H<sub>56</sub>Ag<sub>2</sub>N<sub>8</sub> [M - 2Cl]<sup>2+</sup> calc : 636.1358; found: 636.1376. Anal. Calcd for C<sub>74</sub>H<sub>56</sub>Ag<sub>2</sub>Cl<sub>2</sub>N<sub>8</sub> · <sup>2</sup>/<sub>3</sub> CH<sub>2</sub>Cl<sub>2</sub>: C: 61.63; H: 4.04; N: 7.62, found: C: 61.60; H: 4.40; N: 7.80

### 8.2.97 Preparation of PDC1

**PM1** (0.3 g, 0.78 mmol) and silver oxide (0.5g, 2.16 mmol) were added to a Schlenk flask and dried in *vacuo* for one hour. Anhydrous MeOH (14 mL) was cannula transferred to the Schlenk flask and the mixture was stirred at RT for 24 hours. The solution, which had turned brown, was cannula filtered through celite, and the solvent removed from the filtrate in *vacuo* to furnish a brown solid.



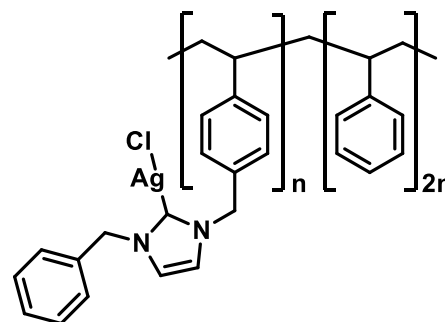
Yield: 0.21g, 0.37 mmol (48 %)

<sup>1</sup>H NMR (300 MHz, MeOD): δ 7.39-6.62 (broad m, aromatic + CH), 5.12 (broad s, CH<sub>2</sub>), 3.88 (broad s, CH<sub>3</sub>). <sup>13</sup>C{<sup>1</sup>H} NMR (125 MHz, MeOD): δ 170.2, 164.9, 146.8(broad), 139.1 137.3, 135.7, 135.6, 129.3 (broad), 127.1(broad), 124.3,

123.3(broad), 55.6, 41.9, 38.9, 37.1, 35.2, 31.9, 23.3, 14.8. Anal. Calcd for  $C_{30}H_{34}AgClN_2$ : C: 63.67; H: 6.06; N: 4.95, found: C: 63.40; H: 6.00; N: 5.00

### 8.2.98 Preparation of PDC2

**PM2** (0.3 g, 0.66 mmol) and silver oxide (0.46 g, 1.96 mmol) were added to a Schlenk flask and dried in *vacuo* for one hour, evacuated and purged with  $N_2$  (x3). Anhydrous MeOH (15 mL) was cannula transferred to the Schlenk flask and the mixture was stirred at room temperature for 72 hours. The solution, which had turned brown, was cannula filtered through celite, and the solvent removed from the filtrate in *vacuo* to yield a brown solid.

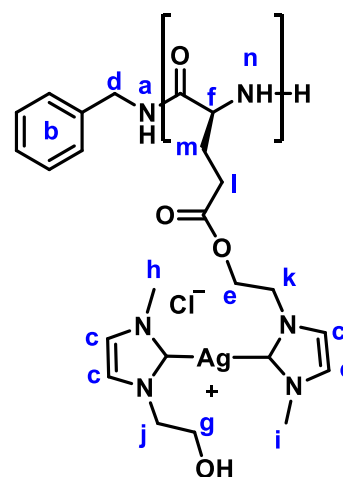


Yield: 0.18 g, 0.28 mmol (43%)

$^1H$  NMR (300 MHz, MeOD):  $\delta$  7.43-6.59 (broad m, aromatic + CH), 5.28 (broad s  $CH_2$ ).  $^{13}C\{^1H\}$  NMR (125 MHz, MeOD):  $\delta$  170.3, 138.4, 137.3, 130.2(broad), 129.5(broad), 128.7(broad), 127.0(broad), 123.6(broad), 56.1(broad), 41.9(broad), 35.5, 23.6, 14.5. Anal. Calcd for  $C_{37}H_{40}AgClN_2$ : C: 67.74; H: 6.15; N: 4.27, found: C: 68.10; H: 6.00; N: 4.60

### 8.2.99 Preparation of PDC3

Poly- (L)-glutamic acid **PM3** (0.05g, 0.21mmol), **C20** (0.11g, 0.21mmol) and 4-Dimethylaminopyridine (DMAP) (0.0026g, 0.021mmol) were added to a Schlenk flask and dried in *vacuo* for one hour. Anhydrous DMF (10 mL) was transferred to the Schlenk flask and the mixture was cooled to  $0^\circ C$  in an ice bath, at which point Dicyclohexylcardodiimide (DCC, 0.044 g, 0.21 mmol) was added. The mixture was stirred for 5 minutes at  $0^\circ C$ , warmed to room temperature and stirred for 5 hours. The solution was cannula filtered, and the the solvents were removed from the filtrate *in vacuo* to yield a sticky brown solid.



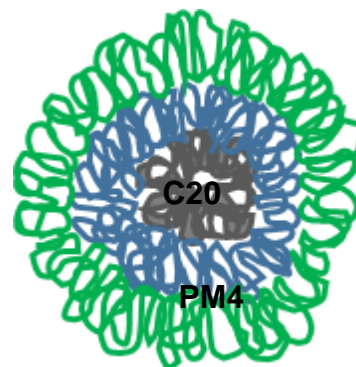
Yield : 0.06 g, 0.1 mmol (45 %)

$^1H$  NMR (300 MHz, DMSO- $d_6$ ):  $\delta$  8.50 (s, NH, **a**), 8.08-7.83 (m, aromatic, **b**), 7.48 , 7.43 (s, HC=CH, **c**), 4.96 (d,  $J = 8.3$  Hz, arom- $CH_2$ -NH, **d**), 4.41(broad t,  $CH_2$ , **e**), 4.21 (broad q, CH, **f**), 3.73 (t,  $J = 5.1$  Hz,  $CH_2$ , **g**), 2.89, 2.73 (s,  $CH_3$ , **h**)

& i), 1.63-1.52 (broad m, CH<sub>2</sub>, j, k & l), 1.26-1.09 (broad m, CH<sub>2</sub> + NH, m + n). HRMS (ESI<sup>+</sup>): calcd for C<sub>24</sub>H<sub>33</sub>AgN<sub>5</sub>O<sub>4</sub> [M-Cl-NH<sub>2</sub>]<sup>+</sup> calc: 565.1653; found: 565.2416. Anal. Calcd for C<sub>29</sub>H<sub>43</sub>AgClN<sub>7</sub>O<sub>6</sub> · 2/3 Et<sub>2</sub>O: C: 48.86; H: 6.43; N: 12.60, found: C: 48.90; H: 6.80; N: 13.00.

### 8.2.100 Preparation of PDM4a

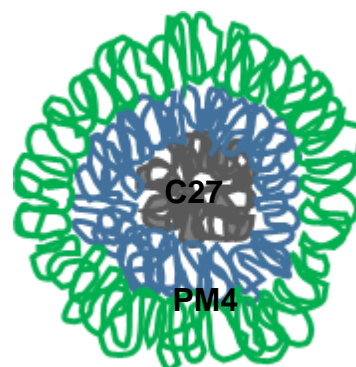
Two stock solutions of **PM4** (mPEG<sub>5000</sub>P(Phe)) (1mg/mL) in DMF, and of **C20** (0.25mg/mL) in H<sub>2</sub>O, were prepared by serial dilution. 20, 40, 200 and 400µl of the **PM4** solution (1mg/mL) were added to 2mL of the solution of **C20** using a micropipette. The solutions were shaken on a vibrax machine, and the average particle size and polydispersity index (PDI) were measured using dynamic light scattering (DLS).



|                                     | (1) 20µL  | (2) 40µL  | (3) 200µL  | (4) 400 µL   |
|-------------------------------------|---|---|--|--|
| <b>C23</b><br>conc<br>0.25<br>mg/mL | <b>PM4</b> conc:<br>0.01mg/mL<br>Particle size:<br>301.7 d.nm<br>PDI: 0.884 | <b>PM4</b> conc:<br>0.02mg/mL<br>Particle size:<br>277.4 d.nm<br>PDI: 0.983 | <b>PM4</b> conc:<br>0.1mg/mL<br>Particle size:<br>260.1 d.nm<br>PDI: 0.984 | <b>PM4</b> conc:<br>0.2mg/mL<br>Particle size:<br>151.7 d.nm<br>PDI: 0.307 |

### 8.2.101 Preparation of PDM4b

Two stock solutions of **PM4** (mPEG<sub>5000</sub>P(Phe)) (1mg/mL) in CH<sub>2</sub>Cl<sub>2</sub>, and of **C27** (1mg/mL) in CH<sub>2</sub>Cl<sub>2</sub>, were prepared with the aid of sonication. Equal volumes (2.9 mL) of the two solutions were combined, and an equivalent volume of nanopure H<sub>2</sub>O (5.8 mL) was added to the mixture. The solutions were shaken on a vibrax machine for 15 minutes, left to stand for 4 hours before the organic layer was removed *in vacuo*. The average particle size and polydispersity index (PDI) were measured using dynamic light scattering (DLS).



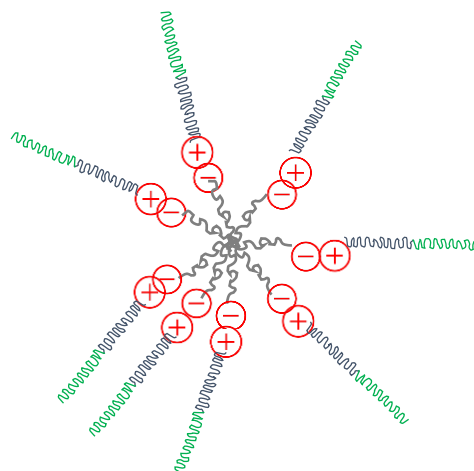
**C27:PM4** = 1:1

Average particle size: 134.3 d.nm

PDI: 0.665

### 8.2.102 Preparation of PDM5

Solutions in HPLC grade water of concentration 1mg/mL were prepared of **PM5A-C, L30, L32, L33, C30, C32** and **C33**. The solutions of the three polymers, ligands and complexes were filtered through 0.45µm and 0.2µm filters and analysed using DLS to confirm no particles were present before encapsulation. Equal volumes of solutions (1mL) of polymer and of ligand or complex were mixed to form solutions of 1:1 ratio, and agitated on vibrax machine. The particles in solution were analysed using DLS at 37°C to mimic the body temperature.



**PM5 A** : mPEG5000: poly(lysine) = 1:39

**1: L30 3: L32 5: L33**

**PM5 B** : mPEG5000: poly(lysine) = 1:50

**2: C30 4: C32 6: C33**

**PM5 C** : mPEG5000: poly(lysine) = 1:140

|   |   |   |
|---|---|---|
| <b>PDM5A.L30</b><br>PDI: 1.000<br>APS: <b>146.0nm</b> | <b>PDM5B.L30</b><br>PDI: 0.754<br>APS: <b>173.1nm</b> | <b>PDM5C.L30</b><br>PDI: 0.292<br>APS: <b>224.2nm</b> |
| <b>PDM5A.C30</b><br>PDI: 0.188<br>APS: <b>159.7nm</b> | <b>PDM5B.C30</b><br>PDI: 0.173<br>APS: <b>175.6nm</b> | <b>PDM5C.C30</b><br>PDI: 0.153<br>APS: <b>176.5nm</b> |
| <b>PDM5A.L32</b><br>PDI: 0.545<br>APS: <b>130.0nm</b> | <b>PDM5B.L32</b><br>PDI: 0.632<br>APS: <b>162.2nm</b> | <b>PDM5C.L32</b><br>PDI: 0.270<br>APS: <b>252.1nm</b> |
| <b>PDM5A.C32</b><br>PDI: 0.769<br>APS: <b>101.1nm</b> | <b>PDM5B.C32</b><br>PDI: 0.277<br>APS: <b>178.2nm</b> | <b>PDM5C.C32</b><br>PDI: 0.378<br>APS: <b>199.5nm</b> |
| <b>PDM5A.L33</b><br>PDI: 1.000<br>APS: <b>121.8nm</b> | -   | <b>PDM5C.L33</b><br>PDI: 0.484<br>APS: <b>253.2nm</b> |
| <b>PDM5A.C33</b><br>PDI: 0.249<br>APS: <b>160.8nm</b> | <b>PDM5B.C33</b><br>PDI: 0.173<br>APS: <b>452.7nm</b> | <b>PDM5C.C33</b><br>PDI: 0.449<br>APS: <b>221.8nm</b> |

### 8.3. References

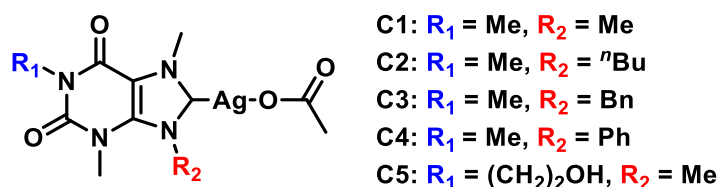
1. V. Vichai and K. Kirtikara, *Nature Protocols*, 2006, **1**, 1112-1116.
2. M. J. Panzner, K. M. Hindi, B. D. Wright, J. B. Taylor, D. S. Han, W. J. Youngs and C. L. Cannon, *Dalton Transactions*, 2009, 7308-7313.
3. A. Meyer, M. A. Taige and T. Strassner, *Journal of Organometallic Chemistry*, 2009, **694**, 1861-1868.
4. W. Zauner, M. Ogris and E. Wagner, *Advanced Drug Delivery Reviews*, 1998, **30**, 97-113.
5. K. Zatloukal, E. Wagner, M. Cotten, S. Phillips, C. Plank, P. Steinlein, D. T. Curiel and M. L. Birnstiel, *Annals of the New York Academy of Sciences*, 1992, **660**, 136-153.
6. A. C. Farthing and R. J. W. Reynolds, *Nature*, 1950, **165**, 647-647.
7. C. Deng, J. Wu, R. Cheng, F. Meng, H.-A. Klok and Z. Zhong, *Progress in Polymer Science*, 2014, **39**, 330-364.
8. A. Kascatan-Nebioglu, A. Melaiye, K. Hindi, S. Durmus, M. J. Panzner, L. A. Hogue, R. J. Mallett, C. E. Hovis, M. Coughenour, S. D. Crosby, A. Milsted, D. L. Ely, C. A. Tessier, C. L. Cannon and W. J. Youngs, *Journal of Medicinal Chemistry*, 2006, **49**, 6811-6818.
9. A. Kascatan-Nebioglu, M. J. Panzner, J. C. Garrison, C. A. Tessier and W. J. Youngs, *Organometallics*, 2004, **23**, 1928-1931.
10. S. Hameury, P. de Fremont, P.-A. R. Breuil, H. Olivier-Bourbigou and P. Braunstein, *Dalton Transactions*, 2014, **43**, 4700-4710.
11. B. Jacques, D. Hueber, S. Hameury, P. Braunstein, P. Pale, A. Blanc and P. de Fremont, *Organometallics*, 2014, **33**, 2326-2335.
12. D. C. F. Monteiro, R. M. Phillips, B. D. Crossley, J. Fielden and C. E. Willans, *Dalton Transactions*, 2012, **41**, 3720-3725.

## Chapter 9

### Summary, conclusions and future work

Thirty seven Ag(I)-NHC complexes were designed and synthesised for chemotherapeutic purposes. The complexes are categorised into three classes according to their precursors, which are either naturally derived or biologically relevant. The three classes are: 1, xanthine-derived, 2, clotrimazole-derived, and 3, water-soluble Ag(I)-NHC complexes. Full characterisation of the complexes included NMR spectroscopy, HRMS, elemental analysis and X-ray diffraction analysis. The Log *P* values of the complexes were determined, followed by *in vitro* cytotoxicity testing against various cancerous and non-cancerous cells. Structure-activity relationships were determined for each individual class from the IC<sub>50</sub> and Log *P* values, from which a general SAR was observed across the classes. It was clear that combining a hydrophilic N-substituent and a hydrophobic N-substituent in the same complex which renders 'intermediate lipophilicity', increases the antiproliferative activity.

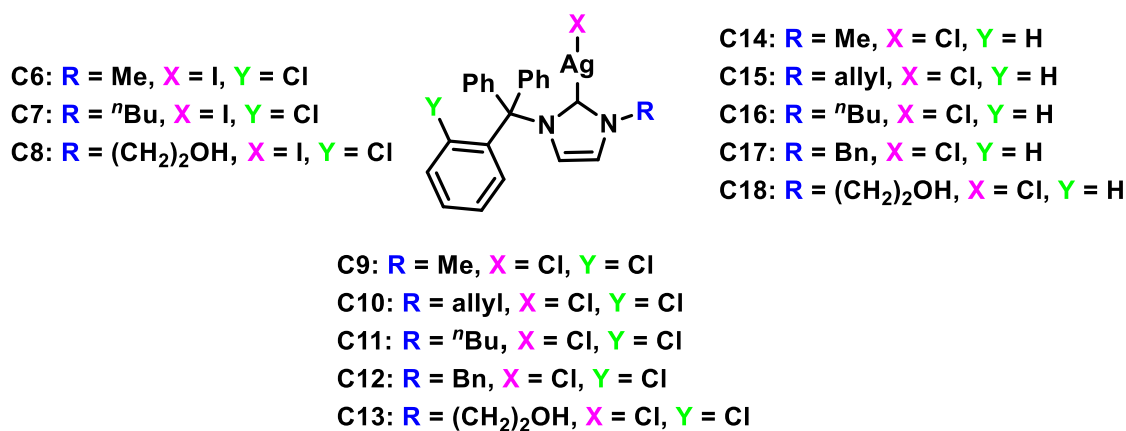
#### 1. Xanthine-derived (Chapter 2):



Lipophilicity trend: C2 > C3 > C4 > C1 > C5

Most cytotoxic: C4 & C5 (C4 > C5, C4 Log *P* = 0.15)

#### 2. Clotrimazole-derived (Chapter 4):

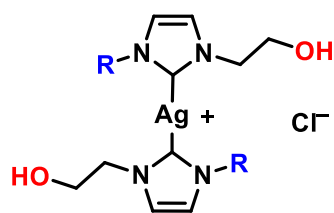


Lipophilicity trend: R: Bn > <sup>n</sup>Bu > allyl > Me > (CH<sub>2</sub>)<sub>2</sub>OH, X: I > Cl, Y: Cl > H

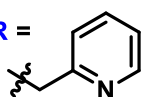
Most cytotoxic: **C13** & **C18** (Log *P* values between 0.25 - 0.30)

## 3. Water-soluble complexes (Chapter 5):

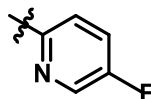
A.

C19: R = (CH<sub>2</sub>)<sub>2</sub>OH    C20: R = Me    C21: R = allylC22: R = <sup>n</sup>Bu    C23: R = Bn    C24: R = Mes

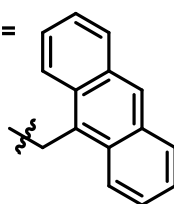
C25: R =



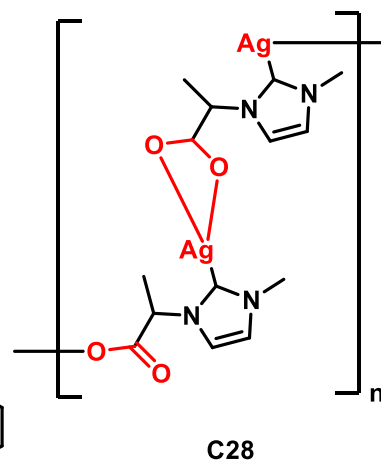
C26: R =



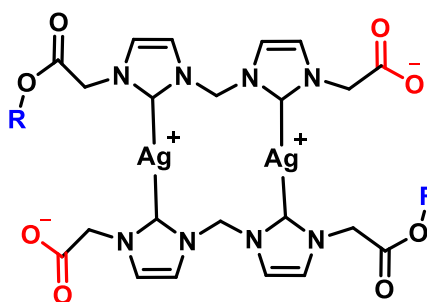
C27: R =



B.



C.

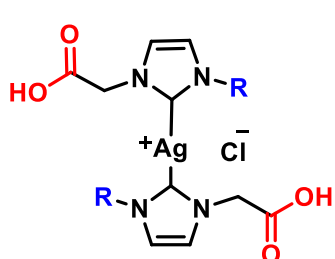


C29: R = Me

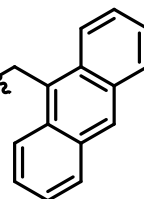
C30: R = H

C31: R = Bn

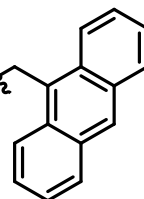
D.



C32: R =



C33: R =



Most cytotoxic: **C23** & **C27** & **C31** (**C23** > **C27** > **C31**, Log *P* values between 0.02 - 0.50)

**Figure 9.1:** Summary of Ag(I)-NHC complexes investigated for anticancer properties

The steric bulk provided by the hydrophobic N-substituent appears to improve anticancer activity, i.e. the bulkier the hydrophobic N-substituent the lower the IC<sub>50</sub> value. This can be observed with groups like phenyl group in **C4** and the triphenyl group in **C13** and **C18**. The steric bulk possibly leads to a slower release of the Ag<sup>+</sup> ions, leading to a prolonged duration of action. The bulky N-triphenyl substituent present in the clotrimazole-derived complexes is possibly behind the overall general higher cytotoxicity results of this class of complexes over the other classes. In particular, the N-hydroxyethyl containing complexes **C13** and **C18** are very promising anticancer drugs as they revealed IC<sub>50</sub> values

similar to those obtained for cisplatin, with a higher selectivity to a number of cancerous cell lines over a non-cancerous cell line (Chapter 4).

Xanthine-derived Cu(I)- and Ru(II)-NHC complexes were synthesised and the results from *in vitro* studies revealed minimal or non-existent anticancer activity of these complexes ( $IC_{50} > 100\mu M$ , Chapter 3). The corresponding Ag(I)-NHC complexes (Chapter 2) are therefore superior as potential anticancer drugs, possibly due to the weaker Ag-C bond that can release  $Ag^+$  ions in solution responsible for cytotoxicity.

Anticancer activity:

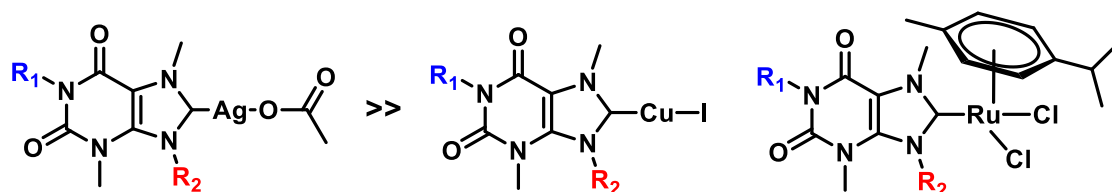


**Figure 9.2:** Xanthine-derived Cu(I)- & Ru(II)-NHC showed low or no cytotoxicity

*In vivo* delivery of the complexes to the cancerous tissue without enzymatic degradation and with high selectivity were major concerns that had to be addressed. Tacke and co-workers reported poor selectivity of a Ag(I)-NHC complex (with previously reported promising *in vitro* results) to cancerous tissue *in vivo* animal models, as the complex revealed toxicity to non-tumour bearing mice.<sup>1</sup> Therefore, developing polymer-based carriers was rationalised for the delivery of the Ag(I)-NHC complexes to cancerous tissue *in vivo* by avoiding enzymatic inactivation and by selectivity to cancerous tissue (Chapter 6). Polymer-drug conjugates (PDCs) of various polymers conjugated to Ag(I)-NHC complexes were chemically synthesised, however, the linear nature of the PDCs does not eliminate the possibility of enzymatic attack and inactivation of the Ag(I)-NHC complex. Formation of polymer-drug micelles (PDMs) with physically encapsulated Ag(I)-NHC complexes was performed through two methods, the first being the self-assembly of polymer when a solution of the polymer in DMF is added to a solution of the Ag(I)-NHC complex in water and the second by electrostatic interaction of negatively charged Ag(I)-NHC complex to a positively charged polymer. The particles were analysed using Dynamic light scattering (DLS) to determine the average particle size and Polydispersity index (PDI) of the particles. Scanning electron microscopy (SEM) was used to image the particles and Energy dispersive X-ray spectroscopy (EDX) was used to map the position of Ag ions in the sample, suggesting successful encapsulation of the

complexes. Confocal fluorescence microscopy was used to locate the position of the fluorescent complex **C27** in the PDM.

A unique bio-membrane sensing device was used to screen the effect of the Ag(I)-NHC complexes on a phospholipid monolayer (Chapter 7). Interactions with the membrane reflects potential interactions with cellular membranes *in vivo*. The monolayer is deposited on a Hg coated Pt electrode, which is connected to a flow cell, and the interactions with the monolayer are detected using rapid cyclic voltammetry (RCV). Complexes that are membrane-active can pass biological membranes via passive diffusion, while complexes which do not interact with the membrane enter cells *via* active transport. Cisplatin and xanthine-derived Ag(I)-NHC complexes did not interact with the monolayer, only water-soluble Ag(I)-NHC complexes with bulky N-aromatic groups, N-mesityl and N-anthracenyl were membrane active, and all clotrimazole-derived complexes were able to interact with the membrane in varying degrees according to the N-substituents, counterions and phenyl substituents.

For the clotrimazole-derived membrane-active complexes, a correlation between the limit of detection (LoD) calculated using this technique and IC<sub>50</sub> values was observed. This result displays the potential of using this technique as a 'prescreening' tool to reduce or eliminate the use of expensive *in vitro* cytotoxicity testing. The role of each portion of the Ag(I)-NHC complex in cell entry was investigated using this device, by testing the ability of each portion to interact with the membrane, and the membranes ability to recover. The imidazolium salts displayed membrane-interactions similar to those observed for the Ag(I)-NHCs, however, the unlike with Ag(I)-NHCs, the membrane was able to recover to its normal state after exposure to the imidazolium salts. Silver salts did not interact with the membrane, supporting the hypothesis that the role of the NHC moiety is to carry Ag to the cancerous tissue and for the interaction with the membrane, while the role of the Ag portion is to damage the membrane. Future work regarding this technique may involve developing a procedure for deposition of cancerous cells or tissue on the microfabricated chip and using RCV to detect changes/damage caused by compounds.

The promising cytotoxicity results of the clotrimazole-derived Ag(I)-NHC complexes, including promising selectivity to cancerous cells, may encourage the future use of other imidazole- and triazole-based antifungal agents such as Ketoconazole and Fluconazole. It will be interesting to investigate the effect of the presence of dihalides in both compounds on the anticancer activity, in addition to the effects of other groups such as ether, ketone and alcohol that were not present in clotrimazole. Mechanistic studies are currently being conducted at the University of Huddersfield to help determine the biological targets of the Ag(I)-NHC complexes, such as thioredoxin reductase and topoisomerase. Future work will possibly include *in vivo* animal testing of the Ag(I)-NHC complexes, and the PDCs and PDMs formed, in order to evaluate the effect of encapsulation on the delivery of the complexes to the cancerous tissue. Tacke and co-workers reported the selective antibacterial activity of a benzyl-substituted Ag(I)-NHC complex *in vivo* using *Galleria mellonella larvae*, observed through the high survival rate of the *larvae* after treatment.<sup>2</sup> Hence, future work can also include antibacterial testing of the complexes, especially antifungal-derived complexes, e.g. clotrimazole-derived Ag(I)-NHC complexes, as the antibacterial properties of both the silver and the antifungal precursor may combine to give a synergistic antibacterial effect.

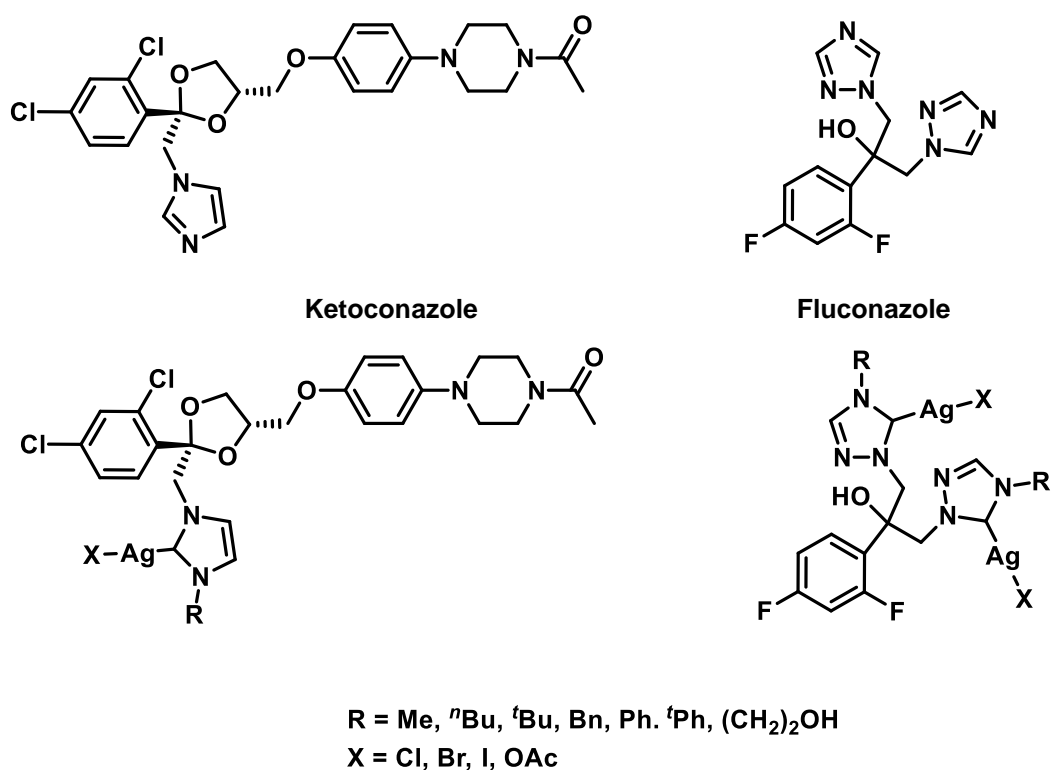


**Figure 9.3:** Ag(I)-NHC complexes derived from antifungal agents for future work

## 9.1 References

1. I. Fichtner, J. Cinatl, M. Michaelis, L. C. Sanders, R. Hilger, B. N. Kennedy, A. L. Reynolds, F. Hackenberg, G. Lally, S. J. Quinn, I. McRae and M. Tacke, *Letters in Drug Design & Discovery*, 2012, **9**, 815-822.
2. N. Browne, F. Hackenberg, W. Streciwilk, M. Tacke and K. Kavanagh, *Biometals*, 2014, **27**, 745-752.

## Appendix

### Crystal data and structure refinement for L2

|   |   |
|---|---|
| Empirical formula                           | C <sub>12</sub> H <sub>19</sub> N <sub>4</sub> O <sub>2</sub> I |
| Formula weight                              | 378.21  |
| Temperature/K                               | 99.98(14)   |
| Crystal system                              | monoclinic  |
| Space group                                 | Cc  |
| a/Å   | 9.4007(7)   |
| b/Å   | 22.7653(11)   |
| c/Å   | 7.1881(5)   |
| α/°   | 90.00   |
| β/°   | 90.244(6)   |
| γ/°   | 90.00   |
| Volume/Å <sup>3</sup>                       | 1538.31(17)   |
| Z   | 4   |
| ρ <sub>calc</sub> /mg/mm <sup>3</sup>       | 1.633   |
| m/mm <sup>-1</sup>                          | 2.086   |
| F(000)                                      | 752.0   |
| Crystal size/mm <sup>3</sup>                | 0.21 × 0.17 × 0.06  |
| 2θ range for data collection                | 6.7 to 54.2°  |
| Index ranges                                | -8 ≤ h ≤ 12, -24 ≤ k ≤ 29, -9 ≤ l ≤ 8                           |
| Reflections collected                       | 4777  |
| Independent reflections                     | 2369[R(int) = 0.0372]   |
| Data/restraints/parameters                  | 2369/289/159  |
| Goodness-of-fit on F <sup>2</sup>           | 1.085   |
| Final R indexes [I ≥ 2σ (I)]                | R <sub>1</sub> = 0.0564, wR <sub>2</sub> = 0.1407               |
| Final R indexes [all data]                  | R <sub>1</sub> = 0.0593, wR <sub>2</sub> = 0.1439               |
| Largest diff. peak/hole / e Å <sup>-3</sup> | 2.11/-1.31  |
| Flack parameter                             | 0.28(8)   |

**Crystal data and structure refinement for L3**

|   |   |
|---|---|
| Empirical formula                           | C <sub>15</sub> H <sub>17</sub> N <sub>4</sub> O <sub>2</sub> l |
| Formula weight                              | 412.23  |
| Temperature/K                               | 100.00(10)  |
| Crystal system                              | orthorhombic  |
| Space group                                 | Pna2 <sub>1</sub>   |
| a/Å   | 16.8371(11)   |
| b/Å   | 10.7293(6)  |
| c/Å   | 9.0448(6)   |
| α/°   | 90.00   |
| β/°   | 90.00   |
| γ/°   | 90.00   |
| Volume/Å <sup>3</sup>                       | 1633.95(18)   |
| Z   | 4   |
| ρ <sub>calc</sub> /mg/mm <sup>3</sup>       | 1.676   |
| m/mm <sup>-1</sup>                          | 15.511  |
| F(000)                                      | 816.0   |
| Crystal size/mm <sup>3</sup>                | 0.05 × 0.03 × 0.02  |
| 2θ range for data collection                | 9.78 to 133.18°   |
| Index ranges                                | -20 ≤ h ≤ 20, -12 ≤ k ≤ 10, -9 ≤ l ≤ 10                         |
| Reflections collected                       | 9250  |
| Independent reflections                     | 2736[R(int) = 0.0828]   |
| Data/restraints/parameters                  | 2736/1/202  |
| Goodness-of-fit on F <sup>2</sup>           | 1.017   |
| Final R indexes [I ≥ 2σ (I)]                | R <sub>1</sub> = 0.0491, wR <sub>2</sub> = 0.1024               |
| Final R indexes [all data]                  | R <sub>1</sub> = 0.0921, wR <sub>2</sub> = 0.1211               |
| Largest diff. peak/hole / e Å <sup>-3</sup> | 0.84/-0.83  |
| Flack parameter                             | 0.084(14)   |

**Crystal data and structure refinement for L3.1**

|   |   |
|---|---|
| Empirical formula                           | C <sub>44</sub> H <sub>48</sub> N <sub>8</sub> S <sub>2</sub> O <sub>10</sub> |
| Formula weight                              | 913.02  |
| Temperature/K                               | 99.99(10)   |
| Crystal system                              | triclinic   |
| Space group                                 | P1  |
| a/Å   | 7.5899(4)   |
| b/Å   | 9.5719(6)   |
| c/Å   | 14.6977(8)  |
| α/°   | 96.675(5)   |
| β/°   | 96.534(4)   |
| γ/°   | 91.422(4)   |
| Volume/Å <sup>3</sup>                       | 1052.87(10)   |
| Z   | 1   |
| ρ <sub>calc</sub> /mg/mm <sup>3</sup>       | 1.440   |
| m/mm <sup>-1</sup>                          | 0.198   |
| F(000)                                      | 480.0   |
| Crystal size/mm <sup>3</sup>                | 0.12 × 0.05 × 0.04  |
| 2θ range for data collection                | 4.28 to 52.74°  |
| Index ranges                                | -9 ≤ h ≤ 9, -11 ≤ k ≤ 11, -18 ≤ l ≤ 13  |
| Reflections collected                       | 7315  |
| Independent reflections                     | 5769[R(int) = 0.0278]   |
| Data/restraints/parameters                  | 5769/3/586  |
| Goodness-of-fit on F <sup>2</sup>           | 1.064   |
| Final R indexes [I ≥ 2σ (I)]                | R <sub>1</sub> = 0.0418, wR <sub>2</sub> = 0.0903                             |
| Final R indexes [all data]                  | R <sub>1</sub> = 0.0492, wR <sub>2</sub> = 0.0950                             |
| Largest diff. peak/hole / e Å <sup>-3</sup> | 0.24/-0.30  |
| Flack parameter                             | 0.59(7)   |

**Crystal data and structure refinement for L4**

|   |   |
|---|---|
| Empirical formula                           | C <sub>14</sub> H <sub>19</sub> N <sub>4</sub> O <sub>4</sub> l |
| Formula weight                              | 434.23  |
| Temperature/K                               | 99.97(11)   |
| Crystal system                              | monoclinic  |
| Space group                                 | P2 <sub>1</sub> /n  |
| a/Å   | 10.4060(11)   |
| b/Å   | 7.2140(7)   |
| c/Å   | 21.938(2)   |
| α/°   | 90.00   |
| β/°   | 89.954(9)   |
| γ/°   | 90.00   |
| Volume/Å <sup>3</sup>                       | 1646.9(3)   |
| Z   | 4   |
| ρ <sub>calc</sub> /mg/mm <sup>3</sup>       | 1.751   |
| m/mm <sup>-1</sup>                          | 1.970   |
| F(000)                                      | 864.0   |
| Crystal size/mm <sup>3</sup>                | 0.17 × 0.06 × 0.04  |
| 2θ range for data collection                | 6.76 to 54.2°   |
| Index ranges                                | -13 ≤ h ≤ 13, -9 ≤ k ≤ 9, -28 ≤ l ≤ 28                          |
| Reflections collected                       | 8263  |
| Independent reflections                     | 3604[R(int) = 0.0537]   |
| Data/restraints/parameters                  | 3604/6/225  |
| Goodness-of-fit on F <sup>2</sup>           | 1.016   |
| Final R indexes [I ≥ 2σ (I)]                | R <sub>1</sub> = 0.0424, wR <sub>2</sub> = 0.0689               |
| Final R indexes [all data]                  | R <sub>1</sub> = 0.0668, wR <sub>2</sub> = 0.0775               |
| Largest diff. peak/hole / e Å <sup>-3</sup> | 0.85/-0.86  |

**Crystal data and structure refinement for L6**

|   |   |
|---|---|
| Empirical formula                           | C <sub>23</sub> H <sub>20</sub> ClIN <sub>2</sub> |
| Formula weight                              | 486.76  |
| Temperature/K                               | 99.98(10)   |
| Crystal system                              | orthorhombic                                      |
| Space group                                 | Pbca  |
| a/Å   | 11.1938(5)  |
| b/Å   | 14.6954(5)  |
| c/Å   | 25.1005(10)                                       |
| α/°   | 90.00   |
| β/°   | 90.00   |
| γ/°   | 90.00   |
| Volume/Å <sup>3</sup>                       | 4129.0(3)   |
| Z   | 8   |
| ρ <sub>calc</sub> /mg/mm <sup>3</sup>       | 1.566   |
| m/mm <sup>-1</sup>                          | 1.690   |
| F(000)                                      | 1936.0  |
| Crystal size/mm <sup>3</sup>                | 0.21 × 0.11 × 0.07                                |
| 2θ range for data collection                | 6.5 to 56.56°                                     |
| Index ranges                                | -14 ≤ h ≤ 9, -19 ≤ k ≤ 18, -33 ≤ l ≤ 27           |
| Reflections collected                       | 13104   |
| Independent reflections                     | 5081[R(int) = 0.0410]                             |
| Data/restraints/parameters                  | 5081/0/245  |
| Goodness-of-fit on F <sup>2</sup>           | 1.032   |
| Final R indexes [I ≥ 2σ (I)]                | R <sub>1</sub> = 0.0414, wR <sub>2</sub> = 0.0820 |
| Final R indexes [all data]                  | R <sub>1</sub> = 0.0662, wR <sub>2</sub> = 0.0924 |
| Largest diff. peak/hole / e Å <sup>-3</sup> | 2.02/-1.09  |

**Crystal data and structure refinement for L7**

|   |  |
|---|--|
| Empirical formula                           | C <sub>26</sub> H <sub>26</sub> N <sub>2</sub> ClI |
| Formula weight                              | 528.84   |
| Temperature/K                               | 99.8(6)  |
| Crystal system                              | triclinic  |
| Space group                                 | P-1  |
| a/Å   | 9.0800(4)  |
| b/Å   | 10.6879(6)   |
| c/Å   | 12.7305(6)   |
| α/°   | 79.385(4)  |
| β/°   | 70.251(4)  |
| γ/°   | 79.962(4)  |
| Volume/Å <sup>3</sup>                       | 1134.47(10)  |
| Z   | 2  |
| ρ <sub>calc</sub> /mg/mm <sup>3</sup>       | 1.548  |
| m/mm <sup>-1</sup>                          | 1.545  |
| F(000)                                      | 532.0  |
| Crystal size/mm <sup>3</sup>                | 0.28 × 0.16 × 0.11                                 |
| 2θ range for data collection                | 5.62 to 56.56°                                     |
| Index ranges                                | -12 ≤ h ≤ 10, -9 ≤ k ≤ 14, -14 ≤ l ≤ 16            |
| Reflections collected                       | 8893   |
| Independent reflections                     | 5543[R(int) = 0.0353]                              |
| Data/restraints/parameters                  | 5543/0/300   |
| Goodness-of-fit on F <sup>2</sup>           | 1.049  |
| Final R indexes [I ≥ 2σ (I)]                | R <sub>1</sub> = 0.0362, wR <sub>2</sub> = 0.0723  |
| Final R indexes [all data]                  | R <sub>1</sub> = 0.0450, wR <sub>2</sub> = 0.0780  |
| Largest diff. peak/hole / e Å <sup>-3</sup> | 0.73/-0.49   |

**Crystal data and structure refinement for L8**

|   |   |
|---|---|
| Empirical formula                           | $C_{24}H_{22}N_2OCl_{1.26}I_{0.74}$               |
| Formula weight                              | 493.01  |
| Temperature/K                               | 100.0(2)  |
| Crystal system                              | triclinic   |
| Space group                                 | P-1   |
| a/Å   | 8.7680(5)   |
| b/Å   | 10.5147(6)  |
| c/Å   | 12.2516(7)  |
| $\alpha/^\circ$                             | 77.789(5)   |
| $\beta/^\circ$                              | 72.958(5)   |
| $\gamma/^\circ$                             | 79.794(4)   |
| Volume/Å <sup>3</sup>                       | 1047.43(10)                                       |
| Z   | 2   |
| $\rho_{\text{calc}}/\text{mg}/\text{mm}^3$  | 1.563   |
| $m/\text{mm}^{-1}$                          | 1.324   |
| F(000)                                      | 497.3   |
| Crystal size/ $\text{mm}^3$                 | 0.26 × 0.14 × 0.1                                 |
| 2 $\Theta$ range for data collection        | 5.92 to 56.56°                                    |
| Index ranges                                | -11 ≤ h ≤ 10, -13 ≤ k ≤ 14, -16 ≤ l ≤ 12          |
| Reflections collected                       | 8180  |
| Independent reflections                     | 5163[R(int) = 0.0315]                             |
| Data/restraints/parameters                  | 5163/2/270  |
| Goodness-of-fit on F <sup>2</sup>           | 1.240   |
| Final R indexes [ $I \geq 2\sigma(I)$ ]     | R <sub>1</sub> = 0.0585, wR <sub>2</sub> = 0.1120 |
| Final R indexes [all data]                  | R <sub>1</sub> = 0.0679, wR <sub>2</sub> = 0.1165 |
| Largest diff. peak/hole / e Å <sup>-3</sup> | 1.14/-0.84  |

**Crystal data and structure refinement for L9**

|   |  |
|---|--|
| Empirical formula                           | C <sub>23</sub> H <sub>20</sub> N <sub>2</sub> Cl <sub>2</sub> |
| Formula weight                              | 395.31   |
| Temperature/K                               | 100.0(3)   |
| Crystal system                              | monoclinic   |
| Space group                                 | P2 <sub>1</sub>  |
| a/Å   | 8.2285(3)  |
| b/Å   | 14.0099(5)   |
| c/Å   | 8.8801(3)  |
| α/°   | 90.00  |
| β/°   | 105.303(4)   |
| γ/°   | 90.00  |
| Volume/Å <sup>3</sup>                       | 987.41(6)  |
| Z   | 2  |
| ρ <sub>calc</sub> /mg/mm <sup>3</sup>       | 1.330  |
| m/mm <sup>-1</sup>                          | 3.019  |
| F(000)                                      | 412.0  |
| Crystal size/mm <sup>3</sup>                | 0.09 × 0.05 × 0.04   |
| 2θ range for data collection                | 10.32 to 133.04°   |
| Index ranges                                | -9 ≤ h ≤ 6, -16 ≤ k ≤ 14, -10 ≤ l ≤ 9                          |
| Reflections collected                       | 3657   |
| Independent reflections                     | 2561[R(int) = 0.0318]  |
| Data/restraints/parameters                  | 2561/1/254   |
| Goodness-of-fit on F <sup>2</sup>           | 1.116  |
| Final R indexes [I ≥ 2σ (I)]                | R <sub>1</sub> = 0.0363, wR <sub>2</sub> = 0.0864              |
| Final R indexes [all data]                  | R <sub>1</sub> = 0.0392, wR <sub>2</sub> = 0.0875              |
| Largest diff. peak/hole / e Å <sup>-3</sup> | 0.32/-0.19   |
| Flack parameter                             | -0.001(16)   |

**Crystal data and structure refinement for L10**

|   |   |
|---|---|
| Empirical formula                           | C <sub>25</sub> H <sub>24</sub> N <sub>2</sub> OCl <sub>2</sub> |
| Formula weight                              | 439.36  |
| Temperature/K                               | 99.9(4)   |
| Crystal system                              | orthorhombic  |
| Space group                                 | Pbca  |
| a/Å   | 8.7356(5)   |
| b/Å   | 19.9479(8)  |
| c/Å   | 24.8334(12)   |
| α/°   | 90.00   |
| β/°   | 90.00   |
| γ/°   | 90.00   |
| Volume/Å <sup>3</sup>                       | 4327.4(4)   |
| Z   | 8   |
| ρ <sub>calc</sub> /mg/mm <sup>3</sup>       | 1.349   |
| m/mm <sup>-1</sup>                          | 0.320   |
| F(000)                                      | 1840.0  |
| Crystal size/mm <sup>3</sup>                | 0.31 × 0.2 × 0.15   |
| 2θ range for data collection                | 6.4 to 56.56°   |
| Index ranges                                | -9 ≤ h ≤ 11, -14 ≤ k ≤ 26, -26 ≤ l ≤ 32                         |
| Reflections collected                       | 15101   |
| Independent reflections                     | 5342[R(int) = 0.0497]   |
| Data/restraints/parameters                  | 5342/3/277  |
| Goodness-of-fit on F <sup>2</sup>           | 1.029   |
| Final R indexes [I ≥ 2σ (I)]                | R <sub>1</sub> = 0.0479, wR <sub>2</sub> = 0.0909               |
| Final R indexes [all data]                  | R <sub>1</sub> = 0.0727, wR <sub>2</sub> = 0.1023               |
| Largest diff. peak/hole / e Å <sup>-3</sup> | 0.37/-0.39  |

**Crystal data and structure refinement for L12**

|   |   |
|---|---|
| Empirical formula                           | C <sub>29</sub> H <sub>26</sub> N <sub>2</sub> OCl <sub>2</sub> |
| Formula weight                              | 489.42  |
| Temperature/K                               | 99.9(4)   |
| Crystal system                              | monoclinic  |
| Space group                                 | P2 <sub>1</sub> /c  |
| a/Å   | 10.7546(7)  |
| b/Å   | 25.2780(12)   |
| c/Å   | 10.1699(7)  |
| α/°   | 90.00   |
| β/°   | 115.850(8)  |
| γ/°   | 90.00   |
| Volume/Å <sup>3</sup>                       | 2488.1(3)   |
| Z   | 4   |
| ρ <sub>calc</sub> /mg/mm <sup>3</sup>       | 1.307   |
| m/mm <sup>-1</sup>                          | 0.286   |
| F(000)                                      | 1024.0  |
| Crystal size/mm <sup>3</sup>                | 0.33 × 0.15 × 0.12  |
| 2θ range for data collection                | 6.58 to 56.56°  |
| Index ranges                                | -14 ≤ h ≤ 14, -27 ≤ k ≤ 33, -10 ≤ l ≤ 13                        |
| Reflections collected                       | 11440   |
| Independent reflections                     | 6126[R(int) = 0.0397]   |
| Data/restraints/parameters                  | 6126/3/307  |
| Goodness-of-fit on F <sup>2</sup>           | 1.042   |
| Final R indexes [I ≥ 2σ (I)]                | R <sub>1</sub> = 0.0493, wR <sub>2</sub> = 0.1045               |
| Final R indexes [all data]                  | R <sub>1</sub> = 0.0679, wR <sub>2</sub> = 0.1174               |
| Largest diff. peak/hole / e Å <sup>-3</sup> | 0.81/-0.43  |

**Crystal data and structure refinement for L13**

|   |  |
|---|--|
| Empirical formula                           | C <sub>24</sub> H <sub>22</sub> Cl <sub>2</sub> N <sub>2</sub> O |
| Formula weight                              | 425.33   |
| Temperature/K                               | 120.0(2)   |
| Crystal system                              | triclinic  |
| Space group                                 | P-1  |
| a/Å   | 8.6119(7)  |
| b/Å   | 10.5213(8)   |
| c/Å   | 11.8588(7)   |
| α/°   | 79.723(6)  |
| β/°   | 73.537(6)  |
| γ/°   | 80.616(6)  |
| Volume/Å <sup>3</sup>                       | 1006.70(13)  |
| Z   | 2  |
| ρ <sub>calc</sub> /mg/mm <sup>3</sup>       | 1.403  |
| m/mm <sup>-1</sup>                          | 0.341  |
| F(000)                                      | 444.0  |
| Crystal size/mm <sup>3</sup>                | 0.11 × 0.06 × 0.03   |
| 2θ range for data collection                | 5.946 to 56.564°   |
| Index ranges                                | -10 ≤ h ≤ 11, -14 ≤ k ≤ 14, -15 ≤ l ≤ 15                         |
| Reflections collected                       | 15179  |
| Independent reflections                     | 4984[R(int) = 0.0403]  |
| Data/restraints/parameters                  | 4984/0/282   |
| Goodness-of-fit on F <sup>2</sup>           | 1.039  |
| Final R indexes [I ≥ 2σ (I)]                | R <sub>1</sub> = 0.0439, wR <sub>2</sub> = 0.0871                |
| Final R indexes [all data]                  | R <sub>1</sub> = 0.0616, wR <sub>2</sub> = 0.0947                |
| Largest diff. peak/hole / e Å <sup>-3</sup> | 0.39/-0.52   |

**Crystal data and structure refinement for L18**

|   |  |
|---|--|
| Empirical formula                           | C <sub>24</sub> H <sub>23</sub> N <sub>2</sub> OCl |
| Formula weight                              | 390.89   |
| Temperature/K                               | 120.15   |
| Crystal system                              | monoclinic   |
| Space group                                 | P2 <sub>1</sub> /c                                 |
| a/Å   | 12.6173(5)   |
| b/Å   | 13.0098(5)   |
| c/Å   | 12.7200(5)   |
| α/°   | 90   |
| β/°   | 107.183(5)   |
| γ/°   | 90   |
| Volume/Å <sup>3</sup>                       | 1994.76(15)  |
| Z   | 4  |
| ρ <sub>calc</sub> /mg/mm <sup>3</sup>       | 1.302  |
| m/mm <sup>-1</sup>                          | 0.209  |
| F(000)                                      | 824.0  |
| Crystal size/mm <sup>3</sup>                | 0.46 × 0.35 × 0.19                                 |
| 2θ range for data collection                | 6.558 to 56.564°                                   |
| Index ranges                                | -16 ≤ h ≤ 12, -17 ≤ k ≤ 11, -16 ≤ l ≤ 15           |
| Reflections collected                       | 9414   |
| Independent reflections                     | 4908[R(int) = 0.0382]                              |
| Data/restraints/parameters                  | 4908/1/257   |
| Goodness-of-fit on F <sup>2</sup>           | 1.071  |
| Final R indexes [I ≥ 2σ (I)]                | R <sub>1</sub> = 0.0446, wR <sub>2</sub> = 0.0972  |
| Final R indexes [all data]                  | R <sub>1</sub> = 0.0583, wR <sub>2</sub> = 0.1096  |
| Largest diff. peak/hole / e Å <sup>-3</sup> | 0.26/-0.27   |

**Crystal data and structure refinement for PM3-L20**

|   |  |
|---|--|
| Empirical formula                           | C <sub>6</sub> H <sub>10</sub> N <sub>2</sub> O <sub>4</sub> S |
| Formula weight                              | 206.22   |
| Temperature/K                               | 119.98(16)   |
| Crystal system                              | orthorhombic   |
| Space group                                 | Pbca   |
| a/Å   | 9.9422(6)  |
| b/Å   | 12.5114(8)   |
| c/Å   | 14.2894(10)  |
| α/°   | 90.00  |
| β/°   | 90.00  |
| γ/°   | 90.00  |
| Volume/Å <sup>3</sup>                       | 1777.48(19)  |
| Z   | 8  |
| ρ <sub>calc</sub> /mg/mm <sup>3</sup>       | 1.541  |
| m/mm <sup>-1</sup>                          | 3.186  |
| F(000)                                      | 864.0  |
| Crystal size/mm <sup>3</sup>                | 0.25 × 0.11 × 0.3  |
| 2θ range for data collection                | 12.38 to 146.5°  |
| Index ranges                                | -9 ≤ h ≤ 9, -8 ≤ k ≤ 13, -12 ≤ l ≤ 17                          |
| Reflections collected                       | 2054   |
| Independent reflections                     | 1084[R(int) = 0.0356]  |
| Data/restraints/parameters                  | 1084/0/119   |
| Goodness-of-fit on F <sup>2</sup>           | 1.048  |
| Final R indexes [I ≥ 2σ (I)]                | R <sub>1</sub> = 0.0496, wR <sub>2</sub> = 0.1227              |
| Final R indexes [all data]                  | R <sub>1</sub> = 0.0674, wR <sub>2</sub> = 0.1347              |
| Largest diff. peak/hole / e Å <sup>-3</sup> | 0.30/-0.47   |

**Crystal data and structure refinement for C1**

|   |  |
|---|--|
| Empirical formula                           | C <sub>11</sub> H <sub>19</sub> N <sub>4</sub> O <sub>6</sub> Ag |
| Formula weight                              | 411.17   |
| Temperature/K                               | 100.00(10)   |
| Crystal system                              | monoclinic   |
| Space group                                 | P2 <sub>1</sub> /m   |
| a/Å   | 8.4188(3)  |
| b/Å   | 6.2963(2)  |
| c/Å   | 14.1810(4)   |
| α/°   | 90.00  |
| β/°   | 98.199(3)  |
| γ/°   | 90.00  |
| Volume/Å <sup>3</sup>                       | 744.01(4)  |
| Z   | 2  |
| ρ <sub>calc</sub> /mg/mm <sup>3</sup>       | 1.835  |
| m/mm <sup>-1</sup>                          | 1.390  |
| F(000)                                      | 416.0  |
| Crystal size/mm <sup>3</sup>                | 0.18 × 0.16 × 0.08   |
| 2θ range for data collection                | 5.32 to 56.56°   |
| Index ranges                                | -11 ≤ h ≤ 8, -6 ≤ k ≤ 8, -12 ≤ l ≤ 18                            |
| Reflections collected                       | 3462   |
| Independent reflections                     | 1985[R(int) = 0.0260]  |
| Data/restraints/parameters                  | 1985/6/149   |
| Goodness-of-fit on F <sup>2</sup>           | 1.035  |
| Final R indexes [I >= 2σ (I)]               | R <sub>1</sub> = 0.0279, wR <sub>2</sub> = 0.0665                |
| Final R indexes [all data]                  | R <sub>1</sub> = 0.0310, wR <sub>2</sub> = 0.0687                |
| Largest diff. peak/hole / e Å <sup>-3</sup> | 0.67/-0.49   |

**Crystal data and structure refinement for C1.Cu**

|   |  |
|---|--|
| Empirical formula                           | C <sub>18</sub> H <sub>24</sub> Cu <sub>2</sub> I <sub>2</sub> N <sub>8</sub> O <sub>4</sub> |
| Formula weight                              | 797.33   |
| Temperature/K                               | 120.02(10)   |
| Crystal system                              | triclinic  |
| Space group                                 | P-1  |
| a/Å   | 7.9096(10)   |
| b/Å   | 8.1576(10)   |
| c/Å   | 10.2410(9)   |
| α/°   | 71.654(9)  |
| β/°   | 82.622(9)  |
| γ/°   | 72.967(11)   |
| Volume/Å <sup>3</sup>                       | 599.20(12)   |
| Z   | 1  |
| ρ <sub>calc</sub> /mg/mm <sup>3</sup>       | 2.210  |
| m/mm <sup>-1</sup>                          | 4.394  |
| F(000)                                      | 384.0  |
| Crystal size/mm <sup>3</sup>                | 0.18 × 0.15 × 0.03   |
| 2θ range for data collection                | 6.56 to 59.4°  |
| Index ranges                                | -10 ≤ h ≤ 10, -10 ≤ k ≤ 11, -14 ≤ l ≤ 13   |
| Reflections collected                       | 5468   |
| Independent reflections                     | 2820[R(int) = 0.0457]  |
| Data/restraints/parameters                  | 2820/0/158   |
| Goodness-of-fit on F <sup>2</sup>           | 1.055  |
| Final R indexes [I ≥ 2σ (I)]                | R <sub>1</sub> = 0.0470, wR <sub>2</sub> = 0.0777  |
| Final R indexes [all data]                  | R <sub>1</sub> = 0.0672, wR <sub>2</sub> = 0.0883  |
| Largest diff. peak/hole / e Å <sup>-3</sup> | 1.37/-1.18   |

**Crystal data and structure refinement for C2**

|   |   |
|---|---|
| Empirical formula                           | C <sub>28</sub> H <sub>44</sub> N <sub>8</sub> O <sub>9</sub> Ag <sub>2</sub> |
| Formula weight                              | 852.45  |
| Temperature/K                               | 100.0(2)  |
| Crystal system                              | triclinic   |
| Space group                                 | P-1   |
| a/Å   | 9.0608(4)   |
| b/Å   | 9.5485(5)   |
| c/Å   | 19.4525(9)  |
| α/°   | 87.707(4)   |
| β/°   | 84.198(4)   |
| γ/°   | 82.717(4)   |
| Volume/Å <sup>3</sup>                       | 1660.21(14)   |
| Z   | 2   |
| ρ <sub>calc</sub> /mg/mm <sup>3</sup>       | 1.705   |
| m/mm <sup>-1</sup>                          | 1.243   |
| F(000)                                      | 868.0   |
| Crystal size/mm <sup>3</sup>                | 0.21 × 0.1 × 0.03   |
| 2θ range for data collection                | 5.86 to 56.56°  |
| Index ranges                                | -12 ≤ h ≤ 12, -12 ≤ k ≤ 12, -25 ≤ l ≤ 25                                      |
| Reflections collected                       | 24918   |
| Independent reflections                     | 8239[R(int) = 0.0369]   |
| Data/restraints/parameters                  | 8239/0/395  |
| Goodness-of-fit on F <sup>2</sup>           | 1.022   |
| Final R indexes [I ≥ 2σ (I)]                | R <sub>1</sub> = 0.0331, wR <sub>2</sub> = 0.0712                             |
| Final R indexes [all data]                  | R <sub>1</sub> = 0.0447, wR <sub>2</sub> = 0.0764                             |
| Largest diff. peak/hole / e Å <sup>-3</sup> | 1.22/-0.57  |

**Crystal data and structure refinement for C2.Ru**

|   |  |
|---|--|
| Empirical formula                           | C <sub>25</sub> H <sub>30</sub> N <sub>4</sub> O <sub>2</sub> Cl <sub>2</sub> Ru |
| Formula weight                              | 590.50   |
| Temperature/K                               | 293(2)   |
| Crystal system                              | orthorhombic   |
| Space group                                 | P2 <sub>1</sub> 2 <sub>1</sub> 2 <sub>1</sub>                                    |
| a/Å   | 6.9286(2)  |
| b/Å   | 13.2717(4)   |
| c/Å   | 26.4095(7)   |
| α/°   | 90.00  |
| β/°   | 90.00  |
| γ/°   | 90.00  |
| Volume/Å <sup>3</sup>                       | 2428.47(12)  |
| Z   | 4  |
| ρ <sub>calc</sub> /mg/mm <sup>3</sup>       | 1.615  |
| m/mm <sup>-1</sup>                          | 0.830  |
| F(000)                                      | 1208.0   |
| Crystal size/mm <sup>3</sup>                | 0.30 × 0.26 × 0.11   |
| 2θ range for data collection                | 5.38 to 63.82°   |
| Index ranges                                | -10 ≤ h ≤ 9, -20 ≤ k ≤ 20, -39 ≤ l ≤ 39  |
| Reflections collected                       | 30747  |
| Independent reflections                     | 8440[R(int) = 0.0521]  |
| Data/restraints/parameters                  | 8440/0/140   |
| Goodness-of-fit on F <sup>2</sup>           | 1.721  |
| Final R indexes [I ≥ 2σ (I)]                | R <sub>1</sub> = 0.0503, wR <sub>2</sub> = 0.1598                                |
| Final R indexes [all data]                  | R <sub>1</sub> = 0.0558, wR <sub>2</sub> = 0.2092                                |
| Largest diff. peak/hole / e Å <sup>-3</sup> | 1.57/-2.09   |
| Flack parameter                             | -0.10(5)   |

**Crystal data and structure refinement for C3**

|   |  |
|---|--|
| Empirical formula                           | C <sub>17</sub> H <sub>19</sub> N <sub>4</sub> O <sub>4</sub> Ag |
| Formula weight                              | 451.23   |
| Temperature/K                               | 200.15   |
| Crystal system                              | triclinic  |
| Space group                                 | P-1  |
| a/Å   | 7.9222(8)  |
| b/Å   | 9.4296(18)   |
| c/Å   | 12.3121(19)  |
| α/°   | 105.139(15)  |
| β/°   | 96.986(10)   |
| γ/°   | 92.438(11)   |
| Volume/Å <sup>3</sup>                       | 878.6(2)   |
| Z   | 2  |
| ρ <sub>calc</sub> /mg/mm <sup>3</sup>       | 1.706  |
| m/mm <sup>-1</sup>                          | 1.178  |
| F(000)                                      | 456.0  |
| Crystal size/mm <sup>3</sup>                | 0.24 × 0.08 × 0.05   |
| 2θ range for data collection                | 6.6 to 56.76°  |
| Index ranges                                | -7 ≤ h ≤ 10, -12 ≤ k ≤ 12, -16 ≤ l ≤ 16                          |
| Reflections collected                       | 13274  |
| Independent reflections                     | 4315[R(int) = 0.1124]  |
| Data/restraints/parameters                  | 4315/0/240   |
| Goodness-of-fit on F <sup>2</sup>           | 1.061  |
| Final R indexes [I ≥ 2σ (I)]                | R <sub>1</sub> = 0.0774, wR <sub>2</sub> = 0.1653                |
| Final R indexes [all data]                  | R <sub>1</sub> = 0.1181, wR <sub>2</sub> = 0.1792                |
| Largest diff. peak/hole / e Å <sup>-3</sup> | 1.86/-0.92   |

**Crystal data and structure refinement for C3.Ru**

|   |  |
|---|--|
| Empirical formula                           | C <sub>25</sub> H <sub>30</sub> N <sub>4</sub> O <sub>2</sub> Cl <sub>2</sub> Ru |
| Formula weight                              | 590.50   |
| Temperature/K                               | 120.00(10)   |
| Crystal system                              | orthorhombic   |
| Space group                                 | P2 <sub>1</sub> 2 <sub>1</sub> 2 <sub>1</sub>                                    |
| a/Å   | 6.6604(5)  |
| b/Å   | 18.959(2)  |
| c/Å   | 19.833(3)  |
| α/°   | 90.00  |
| β/°   | 90.00  |
| γ/°   | 90.00  |
| Volume/Å <sup>3</sup>                       | 2504.4(5)  |
| Z   | 4  |
| ρ <sub>calc</sub> /mg/mm <sup>3</sup>       | 1.566  |
| m/mm <sup>-1</sup>                          | 0.870  |
| F(000)                                      | 1208.0   |
| Crystal size/mm <sup>3</sup>                | 0.23 × 0.15 × 0.08   |
| 2θ range for data collection                | 6.46 to 59.42°   |
| Index ranges                                | -9 ≤ h ≤ 7, -25 ≤ k ≤ 26, -21 ≤ l ≤ 27   |
| Reflections collected                       | 16203  |
| Independent reflections                     | 5939[R(int) = 0.1042]  |
| Data/restraints/parameters                  | 5939/0/313   |
| Goodness-of-fit on F <sup>2</sup>           | 0.942  |
| Final R indexes [I ≥ 2σ (I)]                | R <sub>1</sub> = 0.0758, wR <sub>2</sub> = 0.1578                                |
| Final R indexes [all data]                  | R <sub>1</sub> = 0.1140, wR <sub>2</sub> = 0.1837                                |
| Largest diff. peak/hole / e Å <sup>-3</sup> | 1.27/-1.10   |
| Flack parameter                             | 0.05(7)  |

**Crystal data and structure refinement for C4**

|   |  |
|---|--|
| Empirical formula                           | C <sub>16</sub> H <sub>17</sub> N <sub>4</sub> O <sub>4</sub> Ag |
| Formula weight                              | 437.21   |
| Temperature/K                               | 99.9(5)  |
| Crystal system                              | triclinic  |
| Space group                                 | P-1  |
| a/Å   | 8.7170(6)  |
| b/Å   | 9.9462(6)  |
| c/Å   | 10.2712(9)   |
| α/°   | 82.181(6)  |
| β/°   | 86.063(6)  |
| γ/°   | 67.816(6)  |
| Volume/Å <sup>3</sup>                       | 816.79(10)   |
| Z   | 2  |
| ρ <sub>calc</sub> /mg/mm <sup>3</sup>       | 1.778  |
| m/mm <sup>-1</sup>                          | 1.264  |
| F(000)                                      | 440.0  |
| Crystal size/mm <sup>3</sup>                | 0.2 × 0.12 × 0.06  |
| 2θ range for data collection                | 6.34 to 56.56°   |
| Index ranges                                | -11 ≤ h ≤ 11, -13 ≤ k ≤ 10, -9 ≤ l ≤ 13                          |
| Reflections collected                       | 6438   |
| Independent reflections                     | 4023[R(int) = 0.0405]  |
| Data/restraints/parameters                  | 4023/0/230   |
| Goodness-of-fit on F <sup>2</sup>           | 1.043  |
| Final R indexes [I ≥ 2σ (I)]                | R <sub>1</sub> = 0.0430, wR <sub>2</sub> = 0.0756                |
| Final R indexes [all data]                  | R <sub>1</sub> = 0.0531, wR <sub>2</sub> = 0.0836                |
| Largest diff. peak/hole / e Å <sup>-3</sup> | 0.74/-0.78   |

**Crystal data and structure refinement for C7**

|   |  |
|---|--|
| Empirical formula                             | $C_{106.5}H_{106}N_8Cl_6Ag_4I_2$         |
| Formula weight                                | 2395.97                                  |
| Temperature/K                                 | 99.93(16)                                |
| Crystal system                                | monoclinic                               |
| Space group                                   | $P2_1/n$                                 |
| $a/\text{\AA}$                                | 19.1036(18)                              |
| $b/\text{\AA}$                                | 23.4773(18)                              |
| $c/\text{\AA}$                                | 24.0473(14)                              |
| $\alpha/^\circ$                               | 90.00                                    |
| $\beta/^\circ$                                | 102.591(7)                               |
| $\gamma/^\circ$                               | 90.00                                    |
| Volume/ $\text{\AA}^3$                        | 10525.9(14)                              |
| Z   | 4  |
| $\rho_{\text{calc}}/\text{mg}/\text{mm}^3$    | 1.512                                    |
| $m/\text{mm}^{-1}$                            | 12.262                                   |
| F(000)  | 4788.0                                   |
| Crystal size/ $\text{mm}^3$                   | 0.14 × 0.06 × 0.04                       |
| 2 $\Theta$ range for data collection          | 6.56 to 113.84°                          |
| Index ranges                                  | -20 ≤ h ≤ 19, -18 ≤ k ≤ 25, -26 ≤ l ≤ 21 |
| Reflections collected                         | 27795                                    |
| Independent reflections                       | 14093[R(int) = 0.1021]                   |
| Data/restraints/parameters                    | 14093/8/1160                             |
| Goodness-of-fit on $F^2$                      | 0.976                                    |
| Final R indexes [ $I \geq 2\sigma(I)$ ]       | $R_1 = 0.1000$ , $wR_2 = 0.2512$         |
| Final R indexes [all data]                    | $R_1 = 0.1859$ , $wR_2 = 0.3281$         |
| Largest diff. peak/hole / $e \text{\AA}^{-3}$ | 1.92/-2.21                               |

**Crystal data and structure refinement for C13B**

|   |   |
|---|---|
| Empirical formula                           | C <sub>48</sub> H <sub>40</sub> AgCl <sub>3</sub> N <sub>4</sub> O <sub>2</sub> |
| Formula weight                              | 919.06  |
| Temperature/K                               | 119.98(18)  |
| Crystal system                              | monoclinic  |
| Space group                                 | C2/c  |
| a/Å   | 21.311(2)   |
| b/Å   | 15.0537(13)   |
| c/Å   | 14.0953(13)   |
| α/°   | 90.00   |
| β/°   | 90.886(10)  |
| γ/°   | 90.00   |
| Volume/Å <sup>3</sup>                       | 4521.3(7)   |
| Z   | 4   |
| ρ <sub>calc</sub> /mg/mm <sup>3</sup>       | 1.350   |
| m/mm <sup>-1</sup>                          | 0.665   |
| F(000)                                      | 1880.0  |
| Crystal size/mm <sup>3</sup>                | 0.12 × 0.08 × 0.06  |
| 2θ range for data collection                | 6.14 to 50.06°  |
| Index ranges                                | -24 ≤ h ≤ 25, -17 ≤ k ≤ 17, -16 ≤ l ≤ 16  |
| Reflections collected                       | 13428   |
| Independent reflections                     | 3919[R(int) = 0.0858]   |
| Data/restraints/parameters                  | 3919/1/275  |
| Goodness-of-fit on F <sup>2</sup>           | 1.042   |
| Final R indexes [I ≥ 2σ (I)]                | R <sub>1</sub> = 0.1018, wR <sub>2</sub> = 0.2844                               |
| Final R indexes [all data]                  | R <sub>1</sub> = 0.1554, wR <sub>2</sub> = 0.3228                               |
| Largest diff. peak/hole / e Å <sup>-3</sup> | 1.49/-0.64  |

**Crystal data and structure refinement for C14**

|   |   |
|---|---|
| Empirical formula                           | C <sub>23</sub> H <sub>20</sub> N <sub>2</sub> ClAg |
| Formula weight                              | 467.73  |
| Temperature/K                               | 110.01(10)  |
| Crystal system                              | monoclinic  |
| Space group                                 | P2 <sub>1</sub> /n                                  |
| a/Å   | 13.5174(5)  |
| b/Å   | 9.9426(3)   |
| c/Å   | 15.6082(6)  |
| α/°   | 90.00   |
| β/°   | 106.551(4)  |
| γ/°   | 90.00   |
| Volume/Å <sup>3</sup>                       | 2010.80(12)   |
| Z   | 4   |
| ρ <sub>calc</sub> /mg/mm <sup>3</sup>       | 1.545   |
| m/mm <sup>-1</sup>                          | 1.145   |
| F(000)                                      | 944.0   |
| Crystal size/mm <sup>3</sup>                | 0.41 × 0.16 × 0.14                                  |
| 2θ range for data collection                | 6.24 to 56.56°                                      |
| Index ranges                                | -18 ≤ h ≤ 17, -9 ≤ k ≤ 13, -20 ≤ l ≤ 20             |
| Reflections collected                       | 15088   |
| Independent reflections                     | 4992[R(int) = 0.0523]                               |
| Data/restraints/parameters                  | 4992/0/245  |
| Goodness-of-fit on F <sup>2</sup>           | 1.253   |
| Final R indexes [I ≥ 2σ (I)]                | R <sub>1</sub> = 0.0757, wR <sub>2</sub> = 0.1738   |
| Final R indexes [all data]                  | R <sub>1</sub> = 0.0850, wR <sub>2</sub> = 0.1784   |
| Largest diff. peak/hole / e Å <sup>-3</sup> | 4.70/-0.82  |

**Crystal data and structure refinement for C15**

|   |   |
|---|---|
| Empirical formula                           | C <sub>25</sub> H <sub>22</sub> N <sub>2</sub> ClAg |
| Formula weight                              | 493.77  |
| Temperature/K                               | 120.01(10)  |
| Crystal system                              | monoclinic  |
| Space group                                 | P2 <sub>1</sub>                                     |
| a/Å   | 7.2098(3)   |
| b/Å   | 10.3663(5)  |
| c/Å   | 13.7678(6)  |
| α/°   | 90.00   |
| β/°   | 92.764(4)   |
| γ/°   | 90.00   |
| Volume/Å <sup>3</sup>                       | 1027.79(8)  |
| Z   | 2   |
| ρ <sub>calc</sub> /mg/mm <sup>3</sup>       | 1.595   |
| m/mm <sup>-1</sup>                          | 1.124   |
| F(000)                                      | 500.0   |
| Crystal size/mm <sup>3</sup>                | 0.5 × 0.39 × 0.29                                   |
| 2θ range for data collection                | 5.92 to 61°   |
| Index ranges                                | -8 ≤ h ≤ 10, -12 ≤ k ≤ 14, -19 ≤ l ≤ 19             |
| Reflections collected                       | 10205   |
| Independent reflections                     | 5255[R(int) = 0.0591]                               |
| Data/restraints/parameters                  | 5255/1/262  |
| Goodness-of-fit on F <sup>2</sup>           | 1.081   |
| Final R indexes [I ≥ 2σ (I)]                | R <sub>1</sub> = 0.0377, wR <sub>2</sub> = 0.0926   |
| Final R indexes [all data]                  | R <sub>1</sub> = 0.0387, wR <sub>2</sub> = 0.0939   |
| Largest diff. peak/hole / e Å <sup>-3</sup> | 0.55/-0.69  |
| Flack parameter                             | 0.00(3)   |

**Crystal data and structure refinement for C17**

|   |  |
|---|--|
| Empirical formula                           | $C_{58.75}H_{49.5}AgCl_{2.5}N_4O_{0.25}$ |
| Formula weight                              | 1012.02                                  |
| Temperature/K                               | 120.0(2)                                 |
| Crystal system                              | monoclinic                               |
| Space group                                 | $P2_1/n$                                 |
| a/Å   | 13.3752(3)                               |
| b/Å   | 18.7972(4)                               |
| c/Å   | 19.9989(6)                               |
| $\alpha/^\circ$                             | 90.00                                    |
| $\beta/^\circ$                              | 103.388(3)                               |
| $\gamma/^\circ$                             | 90.00                                    |
| Volume/Å <sup>3</sup>                       | 4891.4(2)                                |
| Z   | 4  |
| $\rho_{\text{calc}}/\text{mg}/\text{mm}^3$  | 1.374                                    |
| $m/\text{mm}^{-1}$                          | 0.593                                    |
| F(000)                                      | 2086.0                                   |
| Crystal size/mm <sup>3</sup>                | 0.2166 × 0.1046 × 0.0771                 |
| 2 $\Theta$ range for data collection        | 6.02 to 56.56°                           |
| Index ranges                                | -17 ≤ h ≤ 17, -23 ≤ k ≤ 25, -26 ≤ l ≤ 26 |
| Reflections collected                       | 55175                                    |
| Independent reflections                     | 12129[R(int) = 0.0473]                   |
| Data/restraints/parameters                  | 12129/2/620                              |
| Goodness-of-fit on F <sup>2</sup>           | 1.051                                    |
| Final R indexes [ $I \geq 2\sigma(I)$ ]     | $R_1 = 0.0564$ , $wR_2 = 0.1381$         |
| Final R indexes [all data]                  | $R_1 = 0.0728$ , $wR_2 = 0.1493$         |
| Largest diff. peak/hole / e Å <sup>-3</sup> | 1.21/-1.70                               |

**Crystal data and structure refinement for C28**

|   |   |
|---|---|
| Empirical formula                           | C <sub>7</sub> H <sub>9</sub> AgN <sub>2</sub> O <sub>2</sub> |
| Formula weight                              | 261.03  |
| Temperature/K                               | 120.00(10)  |
| Crystal system                              | monoclinic  |
| Space group                                 | P2 <sub>1</sub> /n  |
| a/Å   | 9.1676(16)  |
| b/Å   | 9.8932(6)   |
| c/Å   | 9.4004(9)   |
| α/°   | 90.00   |
| β/°   | 97.675(12)  |
| γ/°   | 90.00   |
| Volume/Å <sup>3</sup>                       | 844.95(17)  |
| Z   | 4   |
| ρ <sub>calc</sub> /mg/mm <sup>3</sup>       | 2.052   |
| m/mm <sup>-1</sup>                          | 2.343   |
| F(000)                                      | 512.0   |
| Crystal size/mm <sup>3</sup>                | 0.09 × 0.04 × 0.03  |
| 2θ range for data collection                | 6.08 to 52.74°  |
| Index ranges                                | -11 ≤ h ≤ 10, -12 ≤ k ≤ 12, -11 ≤ l ≤ 9                       |
| Reflections collected                       | 4909  |
| Independent reflections                     | 1719[R(int) = 0.0502]   |
| Data/restraints/parameters                  | 1719/0/111  |
| Goodness-of-fit on F <sup>2</sup>           | 1.076   |
| Final R indexes [I ≥ 2σ (I)]                | R <sub>1</sub> = 0.0711, wR <sub>2</sub> = 0.1356             |
| Final R indexes [all data]                  | R <sub>1</sub> = 0.1285, wR <sub>2</sub> = 0.1620             |
| Largest diff. peak/hole / e Å <sup>-3</sup> | 1.27/-2.00  |